PH

VOLUM

THE PHYSICAL REVIEW

A journal [illegible] *and theoretical physics established by E. L. Nichols in 1893*

Published by the American [illegible] for the

AMERICAN PHYSICAL [illegible]

Office [illegible]

President

C. C. LAURITSEN
California Institute of Technology
Pasadena, California

Vice-President

J. H. VAN VLECK
Harvard University
Cambridge, Massachusetts

Secretary

K. K. DARROW
Bell Telephone Laboratories
Office:
Columbia University
New York 27, New York

Treasurer

G. P. HARNWELL
Columbia University
New York 27, New York

Assistant Secretary
for the Pacific Coast

J. KAPLAN
University of California
Los Angeles
Los Angeles, California

Managing Editor

S. A. GOUDSMIT
Brookhaven National Laboratory
Upton, Long Island
New York

BOARD OF EDITORS

Editor

S. A. Goudsmit

Assistant Editor

S. Pasternack

Associate Editors

J. Barnes
T. Bonner
R. G. Herb
W. E. Lamb, Jr.
A. J. F. Siegert
W. E. Stephens

Harvey Brooks
R. F. Christy
C. L. Critchfield
M. Deutsch
T. H. Johnson
Bruno Rossi

M. Goldh
E. Hutch
A. W. Lu
A. Pais
R. Serber
H. S. W. M

Manuscripts for publication should be submitted to S. A. Goudsmit, Brookhaven National Laboratory, Upton, Long Island, New York. Authors' institutions are requested to pay a publication charge of $[illegible] per page which, if honored, entitles them to 100 free reprints. Instructions will be sent with galley proofs.

Proof and all correspondence concerning papers in the process of publication should be addressed to the Publication Manager, American Institute of Physics, 57 East 55 Street, New York 22, New York.

Subscription Price

United States and Canada ..... $[illegible]
Elsewhere ..... [illegible]

Back Numbers[1]

Yearly [illegible] *number rate when complete year is available:*
Prior to 1949: $20.00
Thereafter: $27.00

Single numbers: $2.50 each, prior to July, 1929;
$1.00 each, July, 1929–December, 1941;
$2.00 each, January, 1942–December, 1946;
$1.00 each, January, 1947–December, 1948;
$1.25 each, thereafter.

General Index, 1893–1920: $4.00.

Subscriptions, renewals, and orders for back numbers should be addressed to the American Institute of Physics, 57 East 55 Street, New York 22, New York.

Changes of address in the case of members of the American Physical Society should be addressed to the Treasurer; in the case of other subscribers to the American Institute of Physics.

[1]For single copies of Physics Department, Cornell University, Ithaca, New York.

Published monthly by the [illegible] at Prince and Lemon Streets, Lancaster, Pennsylvania.

Entered as second-class matter [illegible] at the Post Office at Lancaster, Pennsylvania, under the Act of March 3, 1879.

Acceptance for mailing at special rate of postage provided for in paragraph (d-2), section 34.40, P. L. & R. of 1948, authorized [illegible]

THE
PHYSICAL REVIEW

A journal of experimental and theoretical physics established by E. L. Nichols in 1893

SECOND SERIES, VOL. 81, NO. 6 MARCH 15, 1951

The Altitude and Latitude Variation in the Rate of Occurrence of Nuclear Disintegrations Produced in the Stratosphere by Cosmic Rays*

J. J. LORD
Department of Physics, University of Chicago, Chicago, Illinois
(Received October 19, 1950)

The variation with altitude of the rate of production of stars in photographic plates was measured from mountain elevations to 94,000 feet at geomagnetic latitude $\lambda \simeq 54°$N. The type of particle initiating each star was determined and showed that the total flux of star-producing protons decreased rapidly from 94,000 feet to 11,500 feet and was compatible with an absorption mean free path (m.f.p.) of 145 g/cm². The total flux of star-producing neutrons showed a maximum near 70,000 feet and then decreased with altitude with an absorption mean free path of 170 g/cm². Similar altitude dependence measurements were made at $\lambda \simeq 28°$N and showed that the rate of production by neutrons of stars of 3 to 9 prongs at 94,000 feet was 0.19 of the corresponding value at $\lambda \simeq 54°$. This demonstrates that 81 percent of the small stars at $\lambda \simeq 54°$ must be due to the primary particles of the cosmic radiation in the energy intervals given by the geomagnetic cut-off at $\lambda \simeq 28°$ and $\lambda \simeq 54°$ (1 to 8 Bev for protons, and for α-particles and heavy nuclei 0.35 to 3.5 Bev per nucleon). The total flux of star-producing protons varies by a factor of 3.0 between these two latitudes at 94,000 feet and shows that 67 percent of the proton-initiated stars at $\lambda \simeq 54°$ are due to primary particles of the energies given above.

I. INTRODUCTION

A CONSIDERABLE insight into the nature and interactions of high energy cosmic-ray particles can be obtained from the variation with altitude and latitude of the rate of production of nuclear disintegrations. A large number of investigations have been conducted in the lower atmosphere from sea level to mountain elevations by means of photographic emulsion techniques.[1] In addition, some experiments, were also performed in airplanes up to altitudes of about 35,000 feet at northern latitudes.[2]

In the stratosphere, at northern latitudes, preliminary measurements of the total nuclear disintegration intensity, using plates of low sensitivity, have been made at four different altitudes.[3] Many other measurements,[4,5] mostly with low sensitivity plates, have been made at only single altitudes. However, in some of these cases the general trend in the altitude variation of nuclear disintegrations in the stratosphere could be deduced.[3,5] The rate of production of nuclear disintegrations in photographic emulsions has been measured at a number of different latitudes from sea level to mountain elevations.[6] In the stratosphere measurements have been carried out at only two different latitudes.[7]

The majority of the above investigations have been conducted with photographic plates of low sensitivity which record only particles of moderate energies. In the investigations reported in the following paper, photographic plates sensitive to charged particles of all energies were used to measure the latitude and altitude dependence of the rate of production of stars. The altitude variation in the stratosphere of stars produced by neutrons, protons, alpha-particles, and heavy nuclei yields information as to the type of interactions pro-

* Assisted by the joint program of the ONR and AEC.

[1] Lattes, Occhialini, and Powell, Nature **160**, 453 (1947); D. H. Perkins, Nature **160**, 707 (1947); Bernardini, Cortini, and Manfredini, Nuovo cimento **5**, 511 (1948); G. E. Belovitskii, and L. V. Sukhov, Doklady Akad., Nauk SSSR **62**, No. 2, 207 (1948); E. P. George, and A. C. Jason, Proc. Phys. Soc. (London) **A62**, 243 (1949); Brown, Camerini, Fowler, Heitler, King, and Powell, Phil. Mag. **40**, 862 (1949).

[2] Nora Page, Proc. Phys. Soc. (London) **A63**, 250 (1950); H. H. Foster, Phys. Rev. **78**, 247 (1950).

[3] M. Schein and J. J. Lord, Phys. Rev. **73**, 189 (1948); J. J. Lord and M. Schein, Phys. Rev. **75**, 1957 (1949).

[4] Salant, Hornbostel, and Dollmann, Phys. Rev. **74**, 694 (1948); M. Addario and S. Tamburino, Phys. Rev. **76**, 983 (1949); Yagoda, Kaplan, and Conner, Phys. Rev. **76**, 171 (1949); Camerini, Coor, Davies, Fowler, Lock, Muirhead, and Tobin, Phil. Mag. **40**, 1073 (1949).

[5] Freier, Ney, and Oppenheimer, Phys. Rev. **75**, 1451 (1949).

[6] Beets, Morand, and Winand, Compt. rend. **229**, 1227 (1949); H. Yagoda, *Echo Lake Cosmic-Ray Symposium* (1949), unpublished.

[7] E. O. Salant, *Echo Lake Cosmic-Ray Symposium* (1949), unpublished.

duced by the primary cosmic-ray particles. Further, the stars produced by neutrons show both the manner in which primary particles produce secondary nucleons in the atmosphere and the manner in which these secondary particles lose their energy. The variation with latitude of these phenomena then shows the dependence of the nuclear disintegrations and the production of secondary particles on the energy of the primary particles.

II. EXPERIMENTAL PROCEDURES

(A) Apparatus

All investigations described in this paper were carried out with Ilford G-5 emulsions in order to avoid, as much as possible, any difference in measurement which may occur in using emulsions of various types. For each measurement a sandwich of 6 to 12 plates, two inches by two inches, were employed with the emulsions of adjacent plates in direct contact. Each group of plates was then covered with a single layer of Cellophane, and

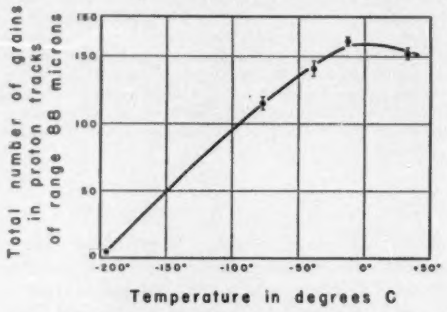

FIG. 1. Temperature sensitivity of photographic emulsions.

then about four layers of 0.002-inch thick aluminum foil to protect the emulsions from visible radiation. The plates were always located with the surfaces of the emulsions parallel to the zenith direction.

Near-by matter in sufficient quantities can effect the rate of star production by a factor as large as 50 percent. For this reason each group of plates was placed in a small cubical celluloid-covered Dow metal balloon gondola of the dimension of 10 inches on each edge. The total mass of the gondola and the plates was close to 300 grams. About 50 percent of the area of the balloon gondola was covered with aluminum foil in order to eliminate the excessive heating effect of the sunlight. With the arrangement just mentioned the temperature of the plates was kept between $-5°$ and $+10°$C on each individual flight. The sensitivity of the plates is not appreciably affected by temperature under the above conditions of exposure. This can be seen from the graph in Fig. 1, showing the variation of grain density with temperature of 3-Mev proton tracks. These results are in essential agreement with the measurements of Dilworth and Dollmann.[9] Measurements of the grain density of minimum ionization tracks show that the grain density decreases by less than 10 percent for a decrease of temperature from $+20°$ to approximately $-50°$C, which is considerably less than for heavily ionizing tracks as shown in Fig. 1.

[8] J. J. Lord and M. Schein, Phys. Rev. **73**, 1956 (1949).

(B) Method of Exposure in the Stratosphere

The small balloon gondolas described above were attached to the rigging from either a cluster of K2000-type balloons or a single large plastic balloon.[10] In each case the gondola with plates was located at least 15 feet above any material being used for other experiments on the same balloon flight. The constancy of the measured intensity of stars at 1.1-cm Hg pressure-altitude for a number of separate flights demonstrated that the above arrangement of plates was free of any influence of material when kept at least 15 feet below the plates.

The pressure-altitude for the cluster balloon flights was determined with both a recording aneroid type barometer and, for greater accuracy at less than 15-cm Hg pressure, a recording Hg U-tube pressure gage. In the aneroid barometer, expansion of the bellows moved a small lever arm at the end of which was attached a pen. The pen produced a line on a clock-driven paper disk, and the amplitude of this line was proportional to the pressure. The most serious source of error in pressure readings, measured with aneroid type barometers, is due to variations of temperature. To avoid this difficulty only standard radiosonde bellows and lever arms made up with bimetal elements were employed. Those barometers which were selected for use showed less than three millimeters change in pressure for a temperature change of at least 20°C.

The Hg U-tube barometer utilized a beam of light, falling on one arm of a U-tube placed before a slit. Behind the slit a clock-driven drum, covered with a piece of photographic paper, revolved slowly. As pressure changes altered the level of the mercury in the

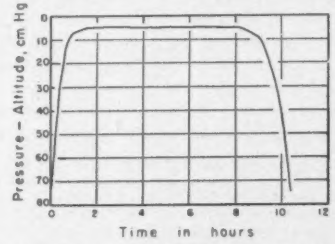

FIG. 2. A typical free balloon flight time *versus* pressure-altitude curve.

[9] C. C. Dilworth, *Cosmic Radiation* (Interscience Publishers, Inc., New York, 1949), p. 157. E. M. Dollmann, Rev. Sci. Instr. **21**, 118 (1950).

[10] These balloon flights were made possible through the courtesy of the ONR and the General Mills Company.

tube, the length of the section of the slit under illumination was changed by a corresponding amount. The Hg U-tube barometer, owing to the short column of Hg (about 10 cm), is not affected appreciably by temperature changes occurring on any of the balloon flights. The pressure readings obtained from this barometer are accurate to 0.5 mm.

The pressure-altitude *vs* time curve for a typical flight at low altitude is given in Fig. 2. In this flight a cluster of 12 balloons was used, which reached their ceiling pressure-altitude of 4.7 cm Hg 1.5 hours after release. After a number of balloons had burst, the equipment remained almost at a fixed pressure-altitude for 8.6 hours. Then a few more balloons burst and the equipment descended slowly to earth with 4 balloons still inflated. The essential data regarding the other flights used in this investigation are given in Table I.

(C) Determination of the Volume of Emulsions

The plates employed in these measurements were all developed by the temperature variation method. In order to determine the rate of production of nuclear disintegrations in the photographic emulsions, it was necessary to know, prior to processing the volume, the composition and density of the portions of each emulsion examined. The composition of the emulsion is given by Ilford in a small information circular attached to each box of plates. The composition and related relevant data are given in Table II. The plates delivered had a very uniform composition; however, the figures given for the composition in Table II are at best only approximate. For this reason it was found that the most accurate method for finding the frequency of nuclear events in the emulsion would be in terms of the rate per gram of emulsion. As can be seen in Table II, the heavy elements, silver and bromine, account for about 70 percent of the total geometrical cross section for nuclear events occurring in the emulsion. The measurements of Perkins and Harding[11] show that this is actually the case.

TABLE I. Balloon flights.

Date of flight	Average ceiling pressure-altitude in cm of Hg	Time in hours at ceiling pressure-altitude	Geomagnetic latitude
April 2, 1949	1.0	5.8	55°N
May 26, 1949	1.0	4.1	55°N
July 22, 1949	1.0	6.8	55°N
September 15, 1949	1.1	7.1	55°N
August 3, 1949	3.5	6.5	55°N
March 30, 1950	4.7	8.6	53°N
August 30, 1949	6.0	1.8	55°N
May 29, 1949	8.0	2.8	53°N
November 15, 1949	1.1	6.6	28°N
November 14, 1949	3.5	8.4	28°N

TABLE II. Compositions and cross sections of Ilford G-5 emulsion.

Element	Atomic weight A_i	Density of emulsion components in g/cc ρ_i	Number of atoms per cc N_i	cross section per nucleus in cm² σ_i	Cross section of N_i nuclei per cc $N_i\times\sigma_i$
$_{47}$Ag	107.9	1.85	1.056×10^{22}	1.338×10^{-24}	1.411×10^{-2}
$_{35}$Br	79.9	1.36	1.025×10^{22}	1.094×10^{-24}	1.121×10^{-2}
$_{53}$I	126.9	0.024	0.01139×10^{22}	1.49×10^{-24}	1.698×10^{-4}
$_{6}$C	12.0	0.27	1.3545×10^{22}	0.309×10^{-24}	4.18×10^{-2}
$_{1}$H	1.01	0.056	3.34×10^{22}	0.0594×10^{-24}	19.8×10^{-4}
$_{8}$O	16.0	0.27	0.939×10^{22}	0.3745×10^{-24}	3.52×10^{-2}
$_{16}$S	32.1	0.010	0.01873×10^{22}	0.596×10^{-24}	11.18×10^{-4}
$_{7}$N	14.0	0.067	0.2875×10^{22}	0.343×10^{-24}	9.86×10^{-4}
Total		3.907	8.032×10^{22}		361.67×10^{-4}

The total nuclear cross section per gram of emulsion is given in terms of the symbols in Table II by the following equation:

$$\sigma_T/\rho_T=[N_0\textstyle\sum_i(\rho_i/A_i)\sigma_i]/(\sum_i\rho_i), \qquad (1)$$

where N_0=Avogadro's number, A_i=atomic weight of component i of emulsion, ρ_i=density of component i of emulsion, σ_i=geometrical cross section of nucleus of component i, σ_T=cross section per cc of emulsion, ρ_T=density of emulsion. From the approximate values of the composition given in Table II in the above formula it follows directly that a given percentage change in the composition of silver or bromine results in a change of one-fourth of this amount in the cross section per gram. Thus, the frequency of nuclear collisions per gram will be quite insensitive even to quite appreciable changes in the composition of the emulsion.

While the plates for each balloon flight were being chosen, several sample plates were selected at random and set aside for the purpose of determining the mass of the emulsion per square centimeter. The sample plates selected were carefully divided into two sections, and one-half of each was processed in the same manner as those used for the balloon flight. Measurements of mass, thickness,[12] and area of emulsion were then made

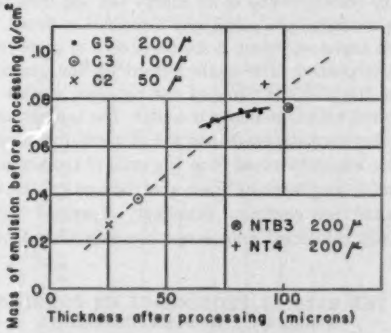

FIG. 3. The mass per square centimeter of emulsions before processing in terms of the thickness after processing.

[11] J. B. Harding, Nature **163**, 440 (1949).

[12] The emulsion and glass backing of the plate were weighed together first; and then, after the emulsion had been removed completely with acid, the weight of the glass backing alone was subtracted from the total to give the weight of the emulsion.

on both the processed and the unprocessed portions. The relation, as obtained from the sample plates, between the mass per square centimeter of the emulsion, before processing, to the thickness after processing is given in Fig. 3 and compared with several other types and thicknesses of plates. It can be seen, Fig. 3, that for the 200-micron thick plates, used in this investigation, the thickness, after processing, provides a very accurate measure of the original mass per square centimeter. The average thickness of each emulsion examined was measured with an accuracy of 2 percent, and from the curve in Fig. 3 it follows directly that the mass of the emulsion before processing is then known to an accuracy of 1 percent. The area of each emulsion examined was measured to 0.5 percent with a standard microscope stage.

The intensities of stars determined per gram of emulsion were multiplied by 3.91, the average density of the emulsion, so that the measurements could be compared directly with those data of other investigations in which the intensities are given per cubic centimeter.

(D) Scanning and Examination of Plates

All of the emulsions used were scanned carefully with a binocular microscope employing a total magnification of 210. This power is higher than is needed for the detection of most events, but is quite necessary for good efficiency[13] in locating small stars and mesons. The detection efficiency of large stars was always greater than 99 percent, but many of the plates had to be scanned several times in order for an efficiency greater than 97 percent to be obtained for the detection of all stars.

After the events had been located in the scanning operation, each was re-examined using a 90-power oil immersion objective, thus obtaining the exact number of tracks per star. All tracks from stars having a grain density corresponding to an energy loss less than seven times the minimum value were examined in detail. The spatial angles and grain densities of each of these tracks was determined. The angle formed by the projection of the track in the plane of the emulsion surface was measured with a goniometer ocular. The tangent of the angle between the track and the plane of the emulsion surface was determined from the ratio of the horizontal projected length of the track and the vertical distance, corrected for emulsion shrinkage, measured with a specially calibrated microscope fine adjustment movement.

III. THE RATE OF PRODUCTION OF COSMIC-RAY STARS IN THE STRATOSPHERE

(A) Determination of the Frequency of Stars

This investigation contains the determination of the rate of production of stars at a number of specific altitudes in the stratosphere. As can be seen from the pressure *versus* time curves for typical flights[3] (Fig. 2), corrections have to be made for those stars which occurred during the period of ascent and descent of the balloon. In addition, the photographic plates were exposed at sea level for a few days; and, since they were transported by air from London to Chicago, some of the cosmic-ray stars were produced during this time. All of the above factors were carefully taken into consideration; and it was found that, depending upon the altitude and length of the balloon flight, the corrections were between 2 and 7 percent of the total number of stars. The number of stars per gram of emulsion which were produced prior to the balloon flight was determined from several sample plates developed just before the flight. The corrections for the time of ascent and descent were obtained in two different ways. (a) For the balloon flights at geomagnetic latitudes of $\lambda=27°$N to $\lambda=29°$N, several plates placed in a separate gondola were released on the ascent at a pressure-altitude of 3.5 cm Hg (70,000 feet). This made it possible to subtract from the total all stars which were produced below this altitude. (b) At geomagnetic latitudes $\lambda=52°$N to $\lambda=56°$N the corrections during the time of ascent and descent were made by carrying out a numerical integration of the following expression:

$$N(x)=I_P(x)\int_0^T f_x(p-P)dt,$$

where $N(x)$=total number of stars per cc having x prongs as measured in the emulsion, P=average pressure-altitude at which balloon flight leveled off, $I_P(x)$ =rate of production of stars with x prongs per cc per day at pressure-altitude P, $f_x(p-P)$=variation with pressure-altitude of rate of production of stars having x prongs and normalized to unity at $p=P$, t=time in hours, and T=total length of flight in hours. The approximate value of $f_x(p-P)$ was taken from previous measurements[3] and $I_P(x)$, the rate of production of stars with x prongs for each balloon flight leveling off at the

TABLE III. Rate of production of stars.

Type of star (number of prongs)	Rate of production of stars per cc per day: Geomagnetic latitude $\lambda=52°$N–56°N, Pressure-altitude in cm Hg: 1.1	3.5	4.7	6.0	8.9	50.0	Geomagnetic latitude $\lambda\simeq27°$N –29°N, Pressure-altitude in cm Hg: 1.1	3.5
greater than 2	2390	2030	2150	2040	1610	22.0	575	425
3, 4, and 5	1030	1059	1162	1210	820	18.2	215	187
6, 7, 8, and 9	742	619	616	520	422	2.6	127	106
greater than 9	618	352	372	235	290	1.2	238	132
greater than 16	223	122	128	27	116	0.29	105	61

[13] G. Cortini and A. Manfredini, Nature **163**, 991 (1949).

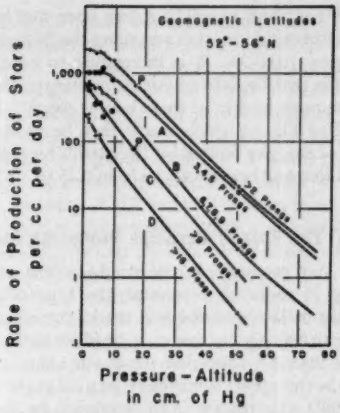

FIG. 4. Rate of production of stars as a function of pressure-altitude at $\lambda \simeq 54°$N.

pressure altitude P, was calculated. With these values of $I_P(x)$, more accurate values of $f_s(p-P)$ were calculated. This method of successive approximations was repeated until a value of $f_s(p-P)$ was found within the same limit of error as the actually measured values of $I_P(x)$.

(B) Altitude Variation ($\lambda = 52°$–$56°$N and $\lambda = 27°$–$29°$N)

In Table III the results of the star intensity measurements at $\lambda = 52°$–$56°$N are given as based on 8 balloon flights and plates exposed at Climax, Colorado (50 cm Hg pressure $\lambda = 48°$N). The data in the table is plotted in Fig. 4, and the slope of the portions of the curves extending to sea level were obtained from the measurements of George and Jason.[1] The two points marked P in Fig. 4 were taken from the measurements of Page[2] and normalized to the intensities at Climax, Colorado. The altitude variation of stars according to prongs showed sufficient regularity that the stars were grouped as indicated on each curve in Fig. 4.

It can be seen from curve A, Fig. 4, that the rate of production of stars of 3, 4, and 5 prongs increases very nearly exponentially with atmospheric pressure from sea level to about 6 cm Hg. Near 6 cm Hg this rate of star production then quickly ceases to increase and remains almost constant up to the highest elevations reached in this investigation, 1.1 cm Hg (94,000 feet). Curve B, the rate of production of stars of 6, 7, 8, and 9 prongs is similar to curve A except that there is a slow increase in the rate of star production in the interval from 6.0 to 1.1 cm Hg. Both curves 3 and D differ markedly from A and B in that they show that the rate of production of larger stars of, respectively, more than 9 and more than 16 prongs increases rapidly with elevation from sea level to 1.1 cm Hg.

Considerable information as to the manner in which star-producing particles are absorbed in air can be obtained if the simplifying but reasonable assumption is made that each particle causes a nuclear disintegration in which either (a) no further star-producing particles are emitted or (b) the emitted star-producing particles are produced in the same direction as the incident particle. The rate of production of stars in a thin photographic emulsion is proportional to the integrated flux of star-producing particles, J (number of particles per second passing through a sphere of 1 cm² cross-sectional area). If the intensity, I_θ, of incident particles per cm² per sec per steradian at the top of the atmosphere is taken to be independent of zenith angle, it can easily be shown that the integrated flux $J(y)$ at any depth in the atmosphere y is given by:

$$J(y) = \int_0^{90°} I_\theta \exp(-y/L_0 \cos\theta) \sin\theta d\theta, \qquad (2)$$

where θ = zenith angle, y = depth in the atmosphere in g/cm², L_0 = absorption mean free path for nuclear collisions per cm².

The slope of the curves $J(y)$ *vs* y can be made equal to that of any portion of the rate of star production curves in Fig. 4 by adjustment of L_0, the absorption mean free path for nuclear collisions. This gives a value of $L_0 = 165$ g/cm² for particles producing the stars of 3, 4, and 5 prongs at pressures greater than 15 cm Hg. The curve $J(y)$ can be made to fit quite well all of the measured values of the rate of production of stars of more than 16 prongs for $L_0 = 120$ g/cm². It is obvious from the curves in Fig. 4 that the absorption mean free path for particles producing small stars has no meaning in the region between 1.1- and 10-cm Hg pressure, since in this region star-producing secondary particles are being produced by the primaries very abundantly.

In Table III data are given for the rate of star production at two different balloon altitudes at $\lambda = 27°$–

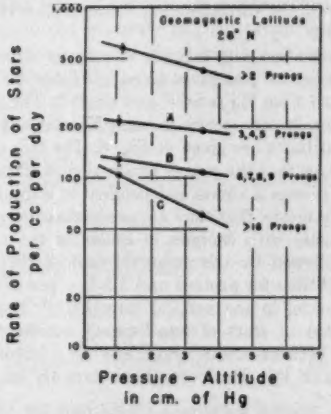

FIG. 5. Rate of production of stars as a function of pressure-altitude at $\lambda \simeq 28°$N.

TABLE IV. Variation in the rate of star production between $\lambda \simeq 28°$ and $\lambda \simeq 54°$.

Type of star (number of prongs)	Rate of production per cc per day $\lambda \simeq 54°$	$\lambda \simeq 28°$	Ratio: rate at 54°N divided by rate at 28°N
>3	1950±100	530±38	3.7±0.3
3, 4, 5	1030±100	215±17	4.8±0.6
6, 7, 8, 9	742±50	127±20	5.8±0.9
>9	618±50	238±15	2.6±0.2
>16	223±25	105±20	2.1±0.4

29°N. These data are plotted in Fig. 5, where it can be seen from curve A that the rate of production of stars of 3, 4, and 5 prongs undergoes a slight decrease from 1.1- to 3.5-cm Hg pressure, while the stars of 6, 7, 8, and 9 prongs, curve B, show a somewhat larger decrease in the same interval. In contrast to this, the rate of production of the larger stars of more than 16 prongs, curve C, shows a very large decrease by a factor of 1.7 in the interval from 1.1 to 3.5 cm Hg. Applying expression (2) to curve C (Fig. 5) the rate of production of stars of more than 16 prongs gives a value of the absorption mean free path L_0 equal to 130 g/cm², which is approximately the same as the corresponding value of 125 g/cm² at $\lambda \simeq 54°$N.

Although few data are available for the rate of star production at mountain elevations near $\lambda \simeq 28°$N, a good estimate of the total rate of star production at 43 cm Hg can be obtained from the general latitude variation measurements of Beets, Morand, and Winand,[14] which are in general agreement with the nuclear disintegration measurements of Simpson and Uretz.[14] From the former data,[14] the rate of production of stars of more than 3 prongs was calculated to be 15.5 per cc per day at 43 cm Hg and at $\lambda \simeq 28°$N. The above rate at 43 cm Hg and the rate of 3.5 cm Hg from Table III can be used in expression (2) and gives an absorption mean free path of $L_0 = 220$ g/cm², which is to be compared with the corresponding value of $L_0 = 165$ g/cm² at $\lambda \simeq 54°$N.

The variation with latitude of stars as a function of the number of prongs is given in Table IV for the flights at 1.1 cm Hg ($\lambda \simeq 54°$ and $\lambda \simeq 28°$). The complete curves for star frequency *vs* prong numbers at two different latitudes are given in Fig. 6. The two curves in Fig. 6 show that the rate of production of stars of more than 25 prongs is almost independent of latitude, which definitely means that they are predominantly produced by particles with energies in excess of the minimum values allowed by the magnetic field of the earth at $\lambda \simeq 28°$ (8 Bev for protons and 3.5 Bev per nucleon for heavy nuclei in the vertical direction).[15] The rate of production of stars of small prong number up to 9 changes between $\lambda \simeq 28°$ and $\lambda \simeq 54°$ by a factor as large as 5 (Table IV). However, these stars are largely produced by neutrons, as will be shown later, and hence do not give direct information regarding the latitude effect for primary particles. It is interesting to note in this connection that the latitude-sensitive stars produced by primaries must largely be those having roughly 10 to 25 prongs (see Fig. 6) which would then be produced by protons of energies limited by the earth's magnetic field of 1 to 8 Bev and heavier nuclei from 0.35 to 3.5 Bev per nucleon.

[14] Beets, Morand, and Winand, Compt. rend. **229**, 1227 (1949). J. A. Simpson and R. B. Uretz, Phys. Rev. **76**, 569 (1949).
[15] M. S. Vallarta, Phys. Rev. **74**, 1837 (1948).

(C) The Flux of Particles Producing Stars

Each star produced in the emulsion was examined carefully in order to determine the type of particle producing it. If one of the star tracks corresponded to that due to a singly charged particle of ionization energy loss less than 1.4 times the minimum value, and was located in the upper hemisphere (zenith angle between 0° and 90°), this track was considered to be due to the incident particle. The zenith angle distribution of singly

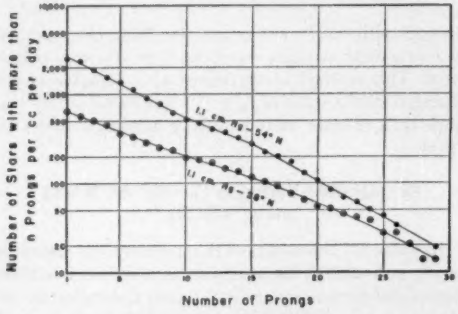

FIG. 6. Rate of production of stars with more than n prongs per cc per day at 94,000 feet as a function of the number of prongs n. The upper curve refers to $\lambda \simeq 54°$ and the lower $\lambda \simeq 28°$.

charged particles producing stars at 1.1 cm Hg, as will be discussed later (Fig. 7), shows that the tracks are sufficiently collimated about the vertical direction that an error of only a few percent would be made by the above method of selection of incident singly charged particles. π-mesons are known to decay in such a short time that their contribution to the production of stars in the rarified atmosphere at balloon elevations can be shown to be less than about 2 percent of the total stars. Thus, all singly charged particles producing stars will be considered to be protons.

Since tracks of minimum ionization of very short lengths are often difficult to find, only stars which were at least 15 microns from either surface of the processed emulsion were included in the measurements made to determine the types of particles producing stars. The average shrinkage factor for these emulsions was about 2.4, so that the minimum track length examined was about 35 microns; and owing to the collimation about the vertical direction of incident tracks, the average length was considerably longer. Measurements of the

decay electron tracks from μ-mesons showed that the detection efficiency was almost constant for angles ψ between the track and the surface of the emulsion, but fell off rapidly for angles ψ larger than 80°. Since positive μ-mesons from π–μ-disintegrations in the emulsion always decay with the emulsion of an electron, the absolute detection efficiency of these minimum ionization tracks was measured to be nearly 90 percent. For the majority of the incident protons close to minimum ionization which produce stars, the angle ψ is small (less than 50°), so that the detection efficiency for these protons must be greater than 95 percent.

Those stars in which a track was located in the upper hemisphere which corresponded to an ionization between 3 and 5 times the minimum value were examined to see if the star could have been produced by an alpha-particle because an alpha-particle with sufficient energy to produce a star would have an ionization in this range. That such a possibility exists was demonstrated by the fact that the distribution of ionization of all star tracks in the upper hemisphere which would be incident tracks showed a small peak at 4 times the minimum value. After subtraction of the background, the tracks located in this peak represented the number of alpha-particles which produced stars in the emulsion. The stars produced by nuclei heavier than boron were detected directly by the high delta-ray density on the incident track. The remaining stars in which no charged incident track could be identified were assumed to be produced by neutrons.

The rate of production of stars per cc per day by protons, neutrons, alpha-particles, and heavy nuclei is given in Table V at 1.1-cm Hg pressure for $\lambda \simeq 54°$ and $\lambda \simeq 28°$. The integrated flux of particles J_a per sec can be determined if the interaction mean free path is known for each type of particle producing stars. For an emulsion thin compared with the interaction mean free path, it can be shown that:

$$J_a = (L_a/3.91) \times (N_a/86{,}400), \qquad (3)$$

where J_a = flux of particles of type a per sec passing through a sphere of 1-cm² cross-sectional area, L_a = the collision mean free path in g/cm² for an emulsion of average density 3.91, N_a = the rate of production of

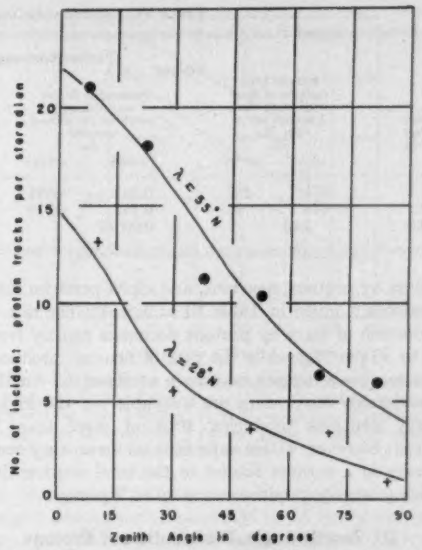

FIG. 7. Zenith angle dependence of all protons producing stars at 94,000 feet and $\lambda \simeq 54°$ and $\lambda \simeq 28°$.

stars by particles of type a per cc per day. Camerini, *et al.*[16] have shown that the collision mean free paths, L_a, correspond very nearly to values equal to the average geometrical cross-sectional area of nuclei in the emulsion. Using this mean free path gives the values of the flux of particles initiating stars at $\lambda \simeq 54°$ and $\lambda \simeq 28°$ in Table V.

The flux of the total star-producing protons at 1.1-cm Hg pressure varies by a factor of 3.0 between $\lambda \simeq 28°$ and $\lambda \simeq 54°$, while the total neutrons which predominantly produce stars of 3 to 9 prongs vary by a factor of 5.2. The large change in the neutron flux is most likely due to the relatively efficient production of low energy neutrons by the great number of low energy primary protons, alpha-particles, and heavy nuclei at $\lambda \simeq 54°$N.

The variation with altitude of the rate of production

TABLE V. Flux of particles producing stars.

1	2		3	4		5
Incident particles	Rate of production of stars of 3 or more prongs per cc per day at 1.1-cm Hg pressure-altitude		Emulsion interaction mean free path in grams/cm² L_a	Integrated flux of particles per second per cm² at 1.1-cm Hg pressure J_a		Latitude effect flux at $\lambda \simeq 54°$N / flux at $\lambda \simeq 28°$N
	$\lambda \simeq 54°$N	$\lambda \simeq 28°$N		$\lambda \simeq 54°$N	$\lambda \simeq 28°$N	
Protons	873	287	100	0.259±0.02	0.085±0.01	3.04±0.4
Neutrons	1400	266	100	0.414±0.03	0.079±0.01	5.2±0.5
Alpha-particles	107	25	39	0.012±0.003	0.0028±0.007	4.3±0.9
Heavy nuclei $Z \geqslant 6$	7.2	2.1				~3.4
Total	2390	575		0.68	0.17	4.0

[16] Camerini, Fowler, Lock, and Muirhead, Phil. Mag. **41**, 413 (1950).

TABLE VI. Altitude variation of flux of particles producing stars.

Pressure-altitude (cm Hg)	Particles producing stars: Protons — Rate of production of stars with more than 2 prongs per cc per day N_s		Protons — Integrated flux of star producing particles per second per cm² J_s		Neutrons N_s		Neutrons J_s		Alpha-particles N_s	Alpha-particles N_s
	$\lambda \simeq 54°$	$\lambda \simeq 28°$	$\lambda \simeq 54°$	$\lambda \simeq 28°$	$\lambda \simeq 54°$	$\lambda \simeq 28°$	$\lambda \simeq 54°$	$\lambda \simeq 28°$	$\lambda \simeq 54°$	$\lambda \simeq 28°$
1.1	873	287	0.26	0.085	1400	266	0.41	0.079	107	25
3.5	446	96	0.132	0.029	1660	275	0.49	0.081	54	12
50.0	2.46		0.00070		23.14		0.0068			

of stars by protons, neutrons, and alpha-particles for 3 elevations is given in Table VI at $\lambda \simeq 54°$. The rate of production of stars by protons decreases rapidly from 1.1 to 50 cm Hg, while the rate of neutron produced stars reaches a definite maximum at about 3.5 cm Hg. Considerably fewer data are available for the higher energy neutrons producing stars of more than 16 prongs; however, within experimental error, they seem to vary in a manner similar to the total neutron flux which primarily produces stars up to 9 prongs.

(D) Zenith Angle Distribution of Protons Producing Stars

The zenith angle distribution was given previously[17] for higher energy protons which produced at least two minimum ionization tracks in a nuclear interaction. In this case the incident energy was sufficiently higher than the magnetic cut-off, so that the protons entered the earth's atmosphere, isotropically distributed in the upper hemisphere. The observed distribution at 1.1-cm Hg pressure showed comparable numbers of incident protons for all zenith angles up to about 70°, and then the number decreased rapidly for larger angles. This distribution is in good agreement with that to be expected for high energy protons absorbed with a cross section slightly larger than the nuclear area.

The zenith angle distribution has now been determined for all protons, including those of lower energies, which produce stars. Plates from four different balloon flights at $\lambda \simeq 54°$ and from one at $\lambda \simeq 28°$ were employed. The zenith angles were measured for all incident protons and were grouped according to the number of tracks per unit solid angle at the zenith angle, θ. These data are given in Fig. 7 for the measurements at $\lambda \simeq 54°$ and $\lambda \simeq 28°$. The zenith angle distribution curve for the total number of protons is quite different from that for only those of very high energy. This is to be expected, since the cross section for energy loss due to ionization of low energy protons becomes comparable to that due to nuclear collisions, which would tend to make the curve steeper. It is to be noted that the curve at $\lambda \simeq 54°$, Fig. 7 falls to half-intensity at an angle of $\theta = 47°$, while the corresponding curve at $\lambda \simeq 28°$ reaches half-intensity at $\theta = 26°$. This is probably owing to the larger influence of the azimuthal variation of the magnetic cutoff of the earth[18] at $\lambda \simeq 28°$ and the greater fraction of the secondary protons produced by primary alpha particles and heavy nuclei at $\lambda \simeq 28°$ than at $\lambda \simeq 54°$.

[17] J. J. Lord and M. Schein, Phys. Rev. **77**, 25 (1950).

IV. CONCLUSIONS

The altitude dependence of nuclear disintegrations extending from 1.1 cm Hg down to sea level and the flux of star producing radiation give a considerable amount of information concerning the nature of the nuclear interactions of primary cosmic-ray particles and the energies of the particles initiating stars in the atmosphere.

From the data presented in this paper the following conclusions can be drawn.

(1) Neutrons at $\lambda \simeq 54°$ account for 56, 76, and 91 percent of the total stars at, respectively, 1.1-, 3.5-, and 50-cm Hg pressure. The flux of neutrons producing stars of more than two prongs reaches a broad maximum near 3.5 cm Hg (Fig. 8). The calculation of Bethe, Korff, and Placzek[18] showed that the slowing down process for fast neutrons would result in a maximum in the intensity of slow neutrons at a distance of about 1 meter of water equivalent from the top of the atmosphere. Yuan[19] has found a maximum in the slow neutron intensity at about 8 to 9 cm Hg, which is in good agreement with both the calculations of these authors[18] and the maximum in the intensity of star producing neutrons near 3.5 cm Hg as given in this paper.

It remains as an interesting problem to determine the intensity of star-producing neutrons at altitudes greater than 1.1 cm Hg, where it is only 15 percent lower than at the maximum. At still higher altitudes it should then decrease very rapidly, since the neutrons must be secondary in origin.

(2) At 1.1-cm Hg pressure ($\lambda \simeq 54°$N) only about 23 percent of the stars with more than 16 prongs are produced by high energy neutrons; the remaining 69 percent and 8 percent are produced, respectively, by protons and α-particles. The corresponding figures for neutrons are 45 percent at 3.5 cm Hg and 50 percent at 50 cm Hg. Considering that stars of more than 16 prongs are only moderately sensitive to latitude (Fig. 6),

[18] Bethe, Korff, and Placzek, Phys. Rev. **57**, 573 (1940).
[19] L. C. L. Yuan, Phys. Rev. **77**, 728 (1950).

it follows that 43 percent of them must be produced by particles of energies in excess of that given by the magnetic cut-off of the earth[18] at $\lambda \simeq 28°$N (8 Bev for protons and 3.5 Bev per nucleon for α-particles and heavier nuclei). The variation with altitude of the flux of these high energy star-producing neutrons, Fig. 8, shows little change between 1.1 and 3.5 cm of Hg, which demonstrates that a large fraction of them are of secondary origin.

(3) Measurements of the rate of production of stars by ionizing incident particles shows that at 1.1-, 3.5-, and 50-cm Hg pressure protons produce, respectively, 69, 55, and 50 percent of the total stars of more than 16 prongs. This, in contrast to the high energy star producing neutrons, shows (Fig. 4) that the number of high energy protons initiating stars decreases rapidly with altitude at the highest elevations (1.1 cm Hg). This shows that a part of these stars must be produced by primaries of even stronger absorption close to the top of the atmosphere.

The variation with altitude of the flux of protons producing all stars of more than 2 prongs is given in Fig. 8 and is in good agreement with an absorption mean free path of 145 g/cm^2.

(4) The rate of production of stars by alpha-particles at 1.1-cm Hg pressure amounts to approximately 5 percent of the total star production at both $\lambda \simeq 54°$ and $\lambda \simeq 28°$. This figure, which is low compared to the known primary flux,[20] is apparently due to the rapid absorption of the α-particles incident isotropically in the upper hemisphere at the top of the atmosphere.

(5) The total rate of production of stars with two or more prongs at $\lambda \simeq 54°$ and 1.1-cm Hg pressure is 3.85 times the corresponding value at $\lambda \simeq 28°$. Most of this increase is due to the large rate of production of small stars by neutrons, which varies by a factor of 5.2 between the above-mentioned latitudes and which is the largest latitude effect which has been observed for any component of the cosmic radiation so far. Taking into account the magnetic cut-off for 54°N and 28°N this shows that 81 percent of the neutrons initiating stars

[20] H. L. Bradt and B. Peters, Phys. Rev. 77, 54 (1950).

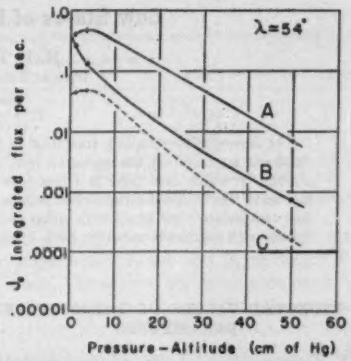

FIG. 8. Integrated flux of star-producing particles as a function of pressure-altitude. Curve *A*—total flux of neutrons producing stars of more than 2 prongs; curve *B*—total flux of protons producing stars of more than 2 prongs; curve *C*—flux of neutrons producing stars of more than 16 prongs.

are produced by primary particles of energies between 1 and 8 Bev for protons and 0.35 to 3.5 Bev per nucleon for α-particles and heavier nuclei. Since within these energy limits meson production is small, most of the primary energy in collisions with air nuclei goes into the production of secondary nucleons.

The variation of the star-producing proton flux between the above latitudes was 3.0 (Table V), which within statistical error is in agreement with the measurements of other authors.[21] This shows that 67 percent of the proton-initiated stars at $\lambda \simeq 54°$ arise from primary particles in the above-mentioned energy intervals imposed by the magnetic cutoff of the magnetic field of the earth.

It is a pleasure to acknowledge the advice and encouragement of Professor Marcel Schein who suggested this work. I should also like to thank Professor Metcalf, director of the Athletic Department, for his competent assistance in making the athletic field available for balloon flights.

[21] Salant, Hornbostel, Fisk, and Smith, Phys. Rev. 79, 184 (1950); Winckler, Stix, Dwight, and Sabin, Phys. Rev. 79, 656 (1950).

Low States of Li^7 in Intermediate Coupling

H. H. Hummel and D. R. Inglis
Argonne National Laboratory, Chicago, Illinois
(Received October 9, 1950)

The intermediate-coupling transition of the five lowest levels of Li^7—Be^7 is discussed. Some analytical emphasis is placed on the approach from the (jj) coupling extreme with ordinary (nonexchange) interactions, in which case there is a first-order degeneracy which might have helped explain the scarcity of low levels, but second-order perturbations are shown to be too large. The only possibility of obtaining just two isolated low levels with either ordinary or Majorana interactions lies near the (LS) coupling extreme, with angular momentum $I=1/2$ for the excited state.

I. EXPECTED VALUES OF THE COUPLING PARAMETERS

THE determination of the relative magnitude of the spin-orbit energy parameter a and the parameter K representing the specific nuclear interaction in light nuclei remains one of the unsolved problems in the formulation of nuclear structure in terms of two-nucleon interactions. The dynamical theory[1] of spin-orbit coupling which treats a nucleon spin in direct analogy to the spin of an atomic electron suggests a single-nucleon spin-orbit parameter of the order of magnitude 100 kev in a light nucleus like Li^7, which, especially after being reduced by a factor 1/3 corresponding to the three p-nucleons of Li^7, leaves a splitting considerably too small to account alone for the 480-kev excitation of the first known excited state of Li^7 as the splitting of a ^2P. The successful interpretation[2] of extensive regularities among the heavier nuclei in terms of a (jj) coupling scheme which depends on relatively large spin-orbit energy for its realization and also the recent interpretation of the charge dependence of high energy nucleon-nucleon scattering[3] suggest that there must be another origin[4,5] of spin-orbit energy beyond the dynamical relativistic Thomas term, strong enough to make the single-nucleon doublet splitting about 2 Mev or more in heavy nuclei ($A \geqslant 120$) for nucleons having large orbital angular momentum lh, say $l \geqslant 4$. The Thomas term varies with orbital angular momentum and radius as l^2/r^4 [or, more exactly, as $l(l+\frac{1}{2})(l+1)/r^4$], as does also the theory of Gaus[6] and probably other theories arising from the detailed demands of relativistic invariance. If we thus assume that the single-nucleon doublet splitting varies with l and with mass number A as $l(l+\frac{1}{2})(l+1)/A^{4/3}$, we would expect a splitting of about 3 Mev or more for a single nucleon in Li^7, or a nuclear ^2P splitting of about 1 Mev. This is larger than the observed 480-kev splitting of the two low states by a factor of two, but such an estimate must be considered quite uncertain. The 480-kev splitting thus seems compatible with (jj) coupling in heavy nuclei. Observations of the reaction $Be^9(d,\alpha)Li^7$ at two bombarding energies[6,7] indicate a spectrum of Li^7 devoid of sharply defined[8] levels from 480 kev up to beyond 3.6 Mev, as would be characteristic of rather extreme (LS) coupling with a 480-kev wide ^2P well removed from the next multiplet, if no states have been missed by this reaction.

Although the single-nucleon doublet splitting does not differ greatly between light and heavy nuclei, the competing parameters do vary in the right direction to make it possible to have (LS) coupling in light nuclei and (jj) coupling in heavy nuclei. The occurrence of (LS) coupling requires that the parameters representing the two-nucleon interaction be much larger than the spin-orbit parameter a, and they are, indeed, larger for light than for heavy nuclei because they depend on the probability of finding two given nucleons within the interaction range of each other. For p-nucleons there are two such parameters,[9] K and L, and their magnitudes may be estimated by means of the three-dimensional harmonic-oscillator approximation.[9,10]

$$K=B\sigma^{3/2}/\tau^{7/2}, \quad L=(\tau^2-2\tau+3)K, \quad \tau\equiv\sigma+2. \quad (1)$$

[1] D. R. Inglis, Phys. Rev. **50**, 783 (1936); G. Breit and J. R. Stehn, Phys. Rev. **53**, 459 (1938).
[2] M. G. Mayer, Phys. Rev. **75**, 1969 (1949); **78**, 16 (1950); Haxel, Jensen, and Suess, Phys. Rev. **75**, 1766 (1949); Naturwissenschaften **36**, 155 (1949). See, however, E. Feenberg, Phys. Rev. **76**, 1275 (1949) and G. Racah, Phys. Rev. **78**, 622 (1950), where it is suggested that at least some of the Mayer-Jensen results may be obtained without such large spin-orbit coupling as assumed in the text.
[3] K. M. Case and A. Pais, Phys. Rev. **80**, 138 (1950).
[4] H. Gaus, communication from W. F. Weizsacher.
[5] A. M. Feingold and E. P. Wigner, Phys. Rev. **79**, 221 (1950).
[6] W. W. Buechner and E. N. Strait, Phys. Rev. **76**, 1547 (1949).
[7] D. R. Inglis, Phys. Rev. **78**, 104 (1950).
[8] With B^9+d, in addition to the sharply-defined alpha-energies corresponding to the two low levels of Li^7, a continuum of alpha-energies is observed in reference 7 and attributed to the formation of two alphas and a triton. These alpha-energies would correspond to Li^7 excitation energies between 2.5 Mev and 3.6 Mev (the limit of the observations). If one should choose instead to attribute these alphas to a broad state of Li^7, its lifetime would be not much more than the time for an alpha and a triton to fly apart beyond a reasonable range of interaction, and the existence of a state described in these terms would not be expected to interfere with the existence of sharp states describable more nearly by the shell model. These could be alternative modes of excitation with very small matrix elements between them.
[9] E. Feenberg and E. Wigner, Phys. Rev. **51**, 95 (1937), Eq. (23).
[10] D. R. Inglis, Phys. Rev. **51**, 531 (1937). In the notation of this paper,

$$K=\int x_1x_2y_1y_2R^2(r_1)R^2(r_2)R\exp(-\alpha r_{12}^2)dr_1dr_2=f_{1100}{}^2f_{0000}(\sigma/r)^{3/2}B;$$

$$L=\int x_1^2x_2^2R^2(r_1)R^2(r_2)B\exp(-\alpha r_{12}^2)dr_1dr_2=f_{1111}f_{0000}{}^2(\sigma/r)^{3/2}B.$$

TABLE I. First-order energies, (jj) coupling.

I of state	Ordinary interaction $p-p$	Ordinary interaction $p-n$	Ordinary interaction Total	Majorana interaction $p-p$	Majorana interaction $p-n$	Majorana interaction Total	Total, $L=6K$
7/2	$L-7K/3$	$2L-8K/3$	$3L-5K$	$\frac{1}{4}(-L+5K)$	$\frac{1}{4}(2L-K)$	$L+K$	$7K$
5/2	$L-7K/3$	$2L-8K/3$	$3L-5K$	$\frac{1}{4}(-L+5K)$	$2(4L-3K)/9$	$(5L+21K)/9$	$17K/3$
$3/2(J_p=2)$	$L-7K/3$	$2L-8K/3$	$3L-5K$	$\frac{1}{4}(-L+5K)$	$\frac{1}{4}(L+17K)$	$(-L+27K)/6$	$7K/2$
1/2	$L-7K/3$	$2L-8K/3$	$3L-5K$	$\frac{1}{4}(-L+5K)$	$10K/3$	$-\frac{1}{4}L+5K$	$3K$
$3/2(J_p=0)$	$L+\frac{1}{4}K$	$2L-8K/3$	$3L-7K/3$	$\frac{1}{4}(L+7K)$	$\frac{1}{4}(L+2K)$	$L+11K/3$	$29K/3$
3/2(First excited)			$3L-17K/3$			$[5L+49K-(129L^2-230LK+105K^2)^{\frac{1}{2}}]/12$	$1.75K$
3/2(Ground)			$3L-5K/3$			$[5L+49K+(129L^2-230LK+105K^2)^{\frac{1}{2}}]/12$	$11.42K$

Here B is the effective depth of the interaction, say, $50mc^2$, and $\sigma^{\frac{1}{2}}$ is the ratio of the range of the interactions to the radius of the nucleon distribution. That is, $\exp(-\alpha r^2)$ appears in the interaction and $\exp(-\sigma\alpha r^2/2)$ in the wave function. For lithium a value of σ about 1 is appropriate[9] (which means that a nucleon at the center of the nucleus can just interact with one at the edge), and the nuclear volume is proportional to $\sigma^{-3/2}$, which is proportional to mass number A, so for a moderately heavy nucleus with $A=120$, a corresponding value would be $\sigma=0.15$. For Li⁷ we thus estimate that K is five times and L nine times as great as in a moderately heavy nucleus. While one is actually not much interested in p-nucleons in the empirical study of spin-orbit coupling in moderately heavy nuclei, the trend suggested by this estimate (as compared with a 50 percent increase in the spin-orbit parameter a) is about strong enough to reconcile, if necessary, the occurrence of (LS) coupling in light nuclei with (jj) in heavy. It seems to be somewhat more likely from this rough evaluation of the integrals that Li⁷ and Be⁷ might be in a coupling condition intermediate between the (LS) and (jj) extremes, but nearer to (LS) coupling than are heavy nuclei.

It is to be anticipated that further states of Li⁷ and Be⁷ will be observed beyond the two low states which have as yet been observed with certainty in each, and it will be of interest to try to interpret their spacing in terms of coupling schemes and assumed interactions. We here study energies of the five lowest states as they approach intermediate coupling from both extremes, and then infer the intermediate-coupling transition between them by interpolation.

II. EXTREME (jj) COUPLING

In addition to the usual binding forces approximated by a central potential well, the hamiltonian is, for the sake of obtaining the (jj) coupling scheme, assumed to contain the zero-order term $\Sigma a\mathbf{l}_i\cdot\mathbf{s}_i$ coupling the nucleon spins to their individual orbits. With the sign of a determined by the usual rule, the p-shell of Li⁷ then contains the lowest "jj-configuration" $(P_{3/2})^2_{neut}(P_{3/2})_{prot}$. As the first-order term in the hamiltonian one introduces the symmetric (that is, charge-independent) interaction between all pairs of particles. The evaluation of the neutron-neutron part is strongly dependent on the antisymmetry of the wave function in the two neutrons, and as a first step may be said to give rise to the neutron states with total angular momentum $J_n=0$ and 2, of which 0 is the ground state. The excited states may be described first in terms of a coupling of this $J_n=2$ to the proton vector $j_p=3/2$, giving rise, with the ground state, to a set of states in which the energy is not yet diagonal because of the existence of two states with $I=3/2$. The diagonal elements are given in Table I, and the nondiagonal elements for ordinary and Majorana interactions are $(2/3)5^{\frac{1}{2}}K$ and $(5^{\frac{1}{2}}/3)(L-K)$, respectively. The signs are here consistent with the choice of phase made by Condon and Shortley.[11] The proper values after diagonalization are given in the last two rows of Table I. Both K and L appear for Majorana interactions, and the specialization is made $L/K=6$. This corresponds to the reasonable value $\sigma=1$, and the ratio is not very sensitive to variation of σ. With ordinary interactions the states with $I=1/2$, 5/2, and 7/2 are degenerate, and there is some interest in investigating the extent to which the second-order perturbations lift this degeneracy.[12]

III. (jj) COUPLING IN SECOND ORDER WITH ORDINARY INTERACTIONS

The zero-order excited states within the p-shell, of which the perturbing effect has been considered, may be grouped in "jj-configurations" according to whether the proton has been excited to the $p_{\frac{1}{2}}$ single-nucleon state, or a neutron, or both, or both neutrons. (The excitation of all three leads to zero matrix elements because of the two-body interactions assumed.) These are listed across the top of Table II, and below them are tabulated their approximate contributions to the energy of the various states of the lowest "jj-configu-

TABLE II. Depression of $(P_{3/2})_p{}^3(P_{3/2})_n$ levels by higher levels, ordinary interaction. ΔE in units of K^2/a.

I of low state \ Perturbing configuration	$(P_{3/2})_p{}^3\times[P_{1/2}]_n$	$(P_{3/2})_p\times[P_{1/2}]_p\times(P_{3/2})_n^2$	$(P_{3/2})_p\times[P_{1/2}]_p\times[P_{1/2}]_n$	$[P_{1/2}]_p{}^2\times(P_{3/2})_n^2$	Total
7/2	···	4/3	···	···	4/3
5/3	···	8/27	7/27	···	5/9
3/2	20/81	40/27	40/27	25/81	95/27
1/2	256/135	1024/405	16/45	···	1936/405
3/2(Ground)	100/81	8/27	2/27	125/81	85/27

[11] E. U. Condon and G. H. Shortley, *Theory of Atomic Spectra* (The Cambridge University Press, New York, 1936).
[12] D. R. Inglis, Phys. Rev. 77, 724 (1949).

ration," calculated with ordinary (nonexchange) interactions.

IV. (*LS*) COUPLING

Since the number of states in the configuration $p^2_{neut}p_{prot}$ with a given value of I ranges up to eight for $I=3/2$, the secular determinants whose solution would be required for a complete description of the intermediate-coupling transition are of rather high order. In order to avoid handling them, it is desirable to approximate the intermediate-coupling transition for the low states which have most potential experimental interest by interpolation between the two extreme coupling schemes.

The level scheme for extreme (*LS*) coupling has been given by Feenberg and Wigner[13] and by Feenberg and Phillips[14] for the various phenomenological exchange interactions. Their results for Li^7 for ordinary and Majorana interactions are given in Table III. In the above discussion of (*jj*) coupling, we have departed

TABLE III. Energy in (*LS*) coupling.

(*LS*) state	(*LS*) energy ord. int. (maj. $L=6K$)	Spin-orbit energy (A) (*LS*)	Spin-orbit energy (diagonalized)
$^4D_{1/2}$		$(a/3)(-9/2)=-3/2a$	
$^4D_{3/2}$		$(a/3)(-3) =-a$	
$^2D_{3/2}$, $^2D_{3/2}$	$3L-6K$	$(a/6)(-3/2)=-a/4$	
$^4D_{5/2}$	$(3K)$	$(a/3)(-1/2)=-a/6$	
$^2D_{5/2}$, $^2D_{5/2}$		$(a/6)(1) = a/6$	
$^4D_{7/2}$		$(a/3)(3) = a$	
$^4P_{1/2}$		$(a/3)(-5/2)=-5/6a$	
$^4P_{3/2}$		$(a/3)(-1) =-a/3$	$-0.447a$
$^2P_{1/2}$, $^2P_{1/2}$	$3L-4K$	$(a/6)(-1) =-a/6$	0
$^2P_{3/2}$, $^2P_{3/2}$	$(5K)$	$(a/6)(1/2) = a/12$	$0.280a$
$^4P_{5/2}$		$(a/3)(3/2) = a/2$	
$^2F_{5/2}$	$3L-3K$	$(a/3)(-2) =-2a/3$	
$^2F_{7/2}$	$(15K)$	$(a/3)(3/2) = a/2$	
$^2P_{1/2}$	$3L+2K$	$(a/3)(-1) =-a/3$	
$^2P_{3/2}$	$(20K)$	$(a/3)(1/2) = a/6$	

from the extreme coupling scheme and have taken a first step towards intermediate coupling, which in that case involved the second-order influence of higher states. The corresponding first step from extreme (*LS*) coupling towards intermediate coupling consists in the introduction of the spin-orbit energy in the hamiltonian and the inclusion of its diagonal elements in the energy. These are given in Table III. It happens that the extreme (*LS*) coupling scheme leaves degeneracies of levels with the same value of I, which must also be lifted in this step. For the low states whose intermediate-coupling transition we wish to consider here, this involves the diagonalization of a three-row matrix for $I=3/2$. The results of this step are given in Table III.

V. INTERPOLATED INTERMEDIATE COUPLING

Interpolation between extreme coupling schemes is a familiar device in atomic spectroscopy, both in the intermediate coupling transition from (*LS*) to (*jj*) coupling and in the Paschen-Back transition so important to modern magnetic resonance methods of determining molecular and nuclear moments. In such interpolation the rule[15] is employed which forbids crossing of the energies of states having the same value of I (and M_I). The intermediate-coupling transition for the five low states of Li^7 is shown in Fig. 1, in which the energies of the states are represented as functions of the spin-orbit coupling parameter, a. The transition for these five states is, of course, only part of a larger transition scheme which is indicated schematically in the small insert in Fig. 1, involving many more states for which the details have not been worked out. In order to provide a graph which is more convenient for studying the behavior of the levels near (*jj*) coupling, the same energies are plotted in Fig. 2 after subtraction of the term $(3a/2)$. In drawing the interpolations involved in these curves, there is some arbitrariness but relatively little because one step has been calculated approaching intermediate coupling from each extreme (giving the slope on the left side and the departure of the curve from an asymptote on the right side). The curves are thus not quantitatively reliable in the intermediate region and are these drawn with broken lines.

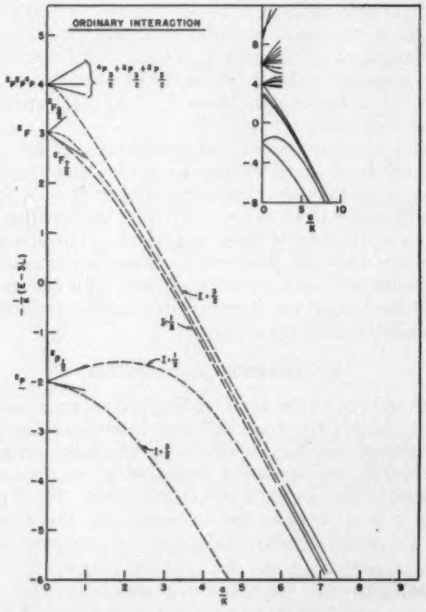

FIG. 1. Energy level diagram of the five low states of Li^7 with intermediate coupling (ordinary interactions).

[13] E. Feenberg and E. P. Wigner, Phys. Rev. **51**, 95 (1937).
[14] E. Feenberg and M. Phillips, Phys. Rev. **51**, 597 (1937).
[15] J. Von Neumann and E. Wigner, Physik. Z. **30**, 467 (1929).

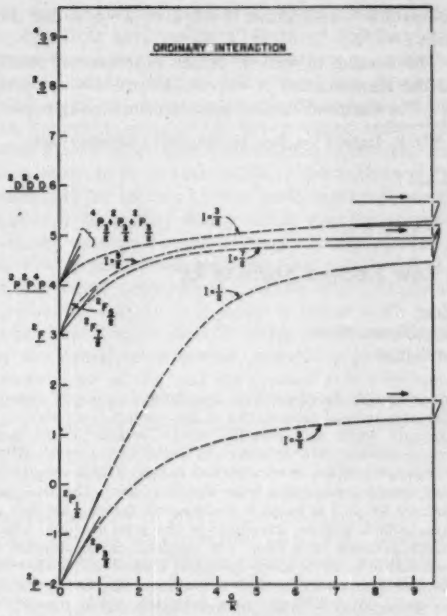

FIG. 2. Revised form of the energy level diagram of Fig. 1. The variation of $-(E-3L+3a/2)/K$ with a/K is shown.

VI. INTERMEDIATE COUPLING WITH SPACE-EXCHANGE INTERACTIONS

The estimated variation of the energies with Majorana (space-exchange) interactions, rather than ordinary (nonexchange) interactions is given in Fig. 3, plotted in the same way as in Fig. 2. With these exchange interactions the second-order departure from (jj) coupling has not been carried out, so that only the asymptote is known on the right side; and the interpolation is considerably less reliable than in the preceding curves, but is presented as a schematic indication of the sort of modification that may be introduced by exchange. The slope on the left side is given by the same calculation as before.

VII. DISCUSSION

One sees from Figs. 2 and 3 that a great variety of patterns for the excited states of Li^7-Be^7 is possible. In Fig. 2, the states with $I=\frac{1}{2}$, 5/2, and 7/2 approach the same asymptote in extreme (jj) coupling. The suggestion has been made[12] that one might resort to this first-order degeneracy to try to understand the scarcity of low states of Li^7 in the face of the enigmatic intensity ratio of the reaction $B^{10}(n,\alpha)Li^7$ which seems to require the inclusion of a state with $I=5/2$ in the 480-kev level, rather than just $I=1/2$, for a rational explanation. The second-order splitting of these states indicated on the right side of Fig. 2 is, however, so great that an implausibly large ratio a/K would be required to keep within the experimental resolution (perhaps 15 kev) of the 480-kev level; and, furthermore, a higher level to correspond to $I=3/2$ has failed to appear in most of the observations. Within the scope of Figs. 2 and 3, there is no other way to assign $I=5/2$ to the 480-kev level. If one chooses to ignore the $B^{10}(n,\alpha)$ intensity ratio as fortuitous, an otherwise natural explanation of the scarcity of states is had by selecting a pattern on the left side of Fig. 2 or Fig. 3, with $a/K\leqslant 1$, near (LS) coupling with the ground state and 480-kev state as the two states of a low ^2P as in the original assignment. Somewhere above 3.6 Mev, to which available observations extend, further excited states are expected, the pattern of which depends strongly on the exchange nature of the interactions. Although the apparently most reliable and extensive experiments reveal only two low states of Li^7 (or Be^7), a pattern of four states below 1 Mev in Be^7 has been reported by Grosskreutz and Mather[16] on the basis of cyclotron observations, of $Li^7(p,n)Be^7$ at 5 Mev, and in Fig. 3 with $a/K\approx 3$ one can find a pattern similar to theirs. Because of their 200-kev state, this would make the assignment $I=7/2$ to the 430-kev state in Be^7 (or

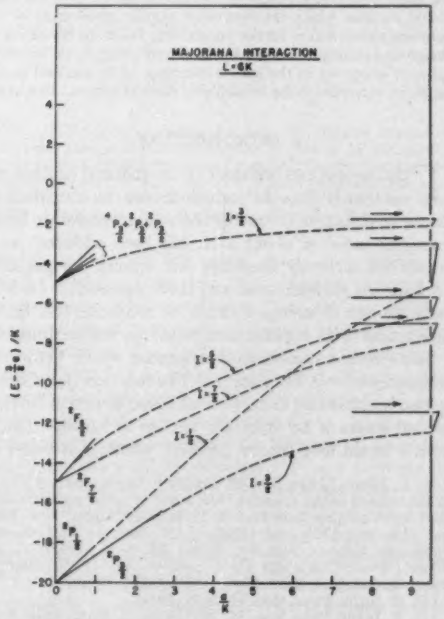

FIG. 3. Energy level diagram of Li^7 with Majorana interactions.

[16] J. C. Grosskreutz and K. B. Mather, Phys. Rev. 77, 580 (1950).

480 kev in Li^7) as would be satisfactory for the $B^{10}(n,\alpha)$ intensity ratio, but not for that[8,17] of Be^7 K—capture nor for the observed lifetime[8,18] of the 480-kev state. The K-capture and lifetime data are at least roughly compatible[12] with either $I=1/2$ or $I=5/2$, but not with $I=7/2$.

The bearing of various recent experimental results on the identification of the well-known 480-kev state in Li^7 is discussed further in an accompanying paper.[19]

[17] B. Rose and A. R. W. Wilson, Phys. Rev. **78**, 68 (1950).
[18] B. T. Feld, Phys. Rev. **75**, 1618 (1949).
[19] D. R. Inglis, Phys. Rev. **81**, 914 (1951), following paper.

PHYSICAL REVIEW VOLUME 81, NUMBER 6 MARCH 15, 1951

The $B^{10}(n,\alpha)$ Reaction and the Low Excited State of Li^7

D. R. INGLIS
Argonne National Laboratory, Chicago, Illinois
(Received October 9, 1950)

Conflicting evidence concerning the nuclear spin I of the low excited state of Li^7 is discussed. By comparison of the apparent likelihood of sufficiently unexpected behavior of the matrix elements involved in the interpretation of the various experiments, it is concluded that the original assignment $I=\frac{1}{2}$ is almost certainly correct, although the experiments are unfortunately not completely decisive. One is prejudiced toward this conclusion by theoretical expectations from nuclear models such as discussed in the preceding paper. The only evidence against $I=\frac{1}{2}$ is the strong preference of the thermal-neutron reaction $B^{10}(n,\alpha)Li^7$ for the transition to the excited state. This anomalous intensity ratio is about what would be expected with $I=5/2$; but with $I=\frac{1}{2}$, even the most favorable assumption concerning the state of the compound nucleus, which involves large angular momentum of the outgoing alpha, makes barrier pentrability favor the transition to the ground state and leaves a factor of over thirty in the intensity ratio, or about six in the matrix elements, to be ascribed to unexpected behavior of the incalculable nuclear factors. This could and apparently does happen by cancellation in a matrix element. The large thermal cross section of the reaction is ascribed to a resonance which is abnormally narrow because of the large angular momentum of the alpha, and it must by chance fall within an estimated 30 kev of zero neutron energy. This is compatible with observed deviations from the "1/v law." The strongest evidence for $I=\frac{1}{2}$ is found in the observed approximate lack of alpha-gamma angular correlation in the same reaction, which follows naturally with $I=\frac{1}{2}$. The magnetic dipole radiation is estimated to be about strong enough to account for the observed lifetime. With $I=5/2$, a small admixture of electric quadrupole radiation, but still larger than estimated, would permit the approximate lack of correlation to occur fortuitously. Another experimental result which seems natural with $I=\frac{1}{2}$, the isotropy of the gammas accompanying inelastic scattering of protons from Li^7, could be ascribed to chance properties of the compound nucleus; but it is unlikely that both of these results, each of which favors $I=\frac{1}{2}$, should occur fortuitously.

I. INTRODUCTION

THE anomalous behavior of the thermal neutron reaction $B^{10}(n,\alpha)Li^7$, which favors the transition to the excited state of Li^7 rather than the ground state by an intensity ratio[1] of about 17:1, has been adduced[2] as a reason for seriously doubting the original assignment[3] $I=\frac{1}{2}$ for the excited state, and favoring instead[4] $I=5/2$, even though it seems difficult to reconcile this latter assignment with expectations based on nuclear models.

Some recent results have appeared which favor the assignment $I=\frac{1}{2}$. They are: (1) The reaction $Be^9(d,\alpha)Li^7$ at two bombarding energies[5] has failed to detect further excited states of Li^7 from 480 kev up to 5.6 Mev (aside from a broad level above 2.5 Mev which, if it exists at all, breaks up into a trition plus an alpha almost during the reaction). This isolation of the two low levels makes them look like a doublet, and a study of intermediate coupling[6] makes it difficult to interpret them as anything but a doublet. (2) An investigation of the possibility of angular correlation between the alphas leading to the excited state and the subsequent gammas in the thermal reaction $B^{10}(n,\alpha)Li^{7*}$, as suggested by Feld and by Devons,[7] has been carried out by Rose and Wilson[8] and they observe spherical symmetry (within one or two percent) which strongly favors the assignment $I=\frac{1}{2}$, because with any other value of I a correlation would, in general, be expected; and its fortuitous disappearance (to this accuracy) seems quite unlikely, as is discussed further below. (3) The spherical symmetry of the gammas resulting from the inelastic scattering $Li^7(p,p')Li^{7*}$ observed by Littauer[9] has been interpreted by him as indicating $I=\frac{1}{2}$ for the excited state of Li^7, although it could instead mean merely that the relevant state of the compound nucleus Be^8 has $I_{Be^8}=0$, since the rather difficult measurement could be made

[1] G. C. Hanna [Phys. Rev. **80**, 530 (1950)] finds a ratio of 17.1:1 on the basis of better statistics than found in earlier papers, which gave ratios ranging from 12:1 to 15:1; R. S. Wilson, Proc. Roy. Soc. (London) **177A**, 382 (1941); J. K. Bøggild, Kgl. Danske Videnskab. Selskab. Mat.-fys. Medd. **23**, 4, 26 (1945); C. W. Gilbert, Proc. Cambridge Phys. Soc. **44**, 447 (1948); Stebler, Huber, and Bicksel, Helv. Phys. Acta **22**, 372 (1949).
[2] D. R. Inglis, Phys. Rev. **74**, 1876 (1948).
[3] D. R. Inglis, Phys. Rev. **50**, 783 (1936); G. Breit, Phys. Rev. **51**, 248 (1937).
[4] S. S. Hanna and D. R. Inglis, Phys. Rev. **75**, 1767 (1949).
[5] W. W. Buechner and E. N. Strait, Phys. Rev. **76**, 1547 (1949); D. R. Inglis, Phys. Rev. **78**, 104 (1950); R. W. Gelinas and S. S. Hanna, Bull. Am. Phys. Soc. **26**, No. 1, Abstract C3 (1951).
[6] H. H. Hummel and D. R. Inglis, Phys. Rev. **81**, 910 (1951).
[7] B. T. Feld, Phys. Rev. **75**, 1618 (1949); S. Devons, Proc. Phys. Soc. (London) **62A**, 580 (1949).
[8] B. Rose and A. R. W. Wilson, Phys. Rev. **78**, 68 (1950).
[9] R. M. Littauer, Proc. Phys. Soc. (London) **63A**, 294 (1950).

only in the neighborhood of a prominent resonance[10] at $E_p=1030$ kev, having a width of 168 kev. The measurement was indeed made at as low an energy as possible, 800 kev, on the lower edge of this resonance; but it is still not clear to what extent this might reduce the dominant influence of the resonant state. The value $I_{n_0}=0$ is possible with entering p-protons, and there seems to be no clear reason in the analysis of the resonances for making another assignment.[11] If repetition at quite another energy should give the same result, the conclusion would be greatly strengthened; but no further convenient resonances have been found.[12] It thus seems premature to conclude from this experiment alone that $I=\frac{1}{2}$: it leaves a rather small probability that I might be 5/2, which is to be multiplied by the considerably smaller probability provided by the evidence of (2), and the product is a very small probability that I might be 5/2. Similar measurements of the angular distributions of the gammas from $Li^6(d,p)Li^{7*}$, as has been discussed by Hanna,[13] and of $B^{10}(p,\alpha)Be^{7*}$, particularly at the 1.5-Mev resonance, would also serve to verify this conclusion. Since $I=\frac{1}{2}$ has the property of giving spherical symmetry, which might, in such an experiment at a single resonance, arise from some other circumstance, several verifications of the identification $I=\frac{1}{2}$ would not seem superfluous.

There are other experimental results concerning the excited state which seem to be about equally compatible[4] with $I=\frac{1}{2}$ or 5/2, such as the intensity ratio[14] in Be^7 K-capture (11 percent to the excited state) and the lifetime[15] of the excited state (10^{-13} sec, magnetic dipole). These depend mainly on ΔI between the excited and ground state, which is 1 in either case. Comparison of the angular distributions of the two proton groups in $Li^6(d,p)Li^7$ is another possible indication; but cannot be considered very significant at present, because there is some disagreement in detail between data from two laboratories.[16]

The two aspects of the reaction $B^{10}(n,\alpha)Li^7$, the intensity ratio on the one hand and the alpha-gamma angular correlation (supported by the $Li^7(p,p')$ gammas) on the other, are thus considered to be opposing bits of evidence, the former favoring $I=5/2$ and the latter $\frac{1}{2}$; but the theoretical considerations on which these conclusions are based are essentially incomplete in both cases. One calculates the obvious factors, such as barrier penetrability and orientation coefficients, but is in each case left with the essentially nuclear factors of the matrix elements which are not calculated. On the basis of estimates or plausible surmises concerning these factors, one arrives at conclusions which are not rigorous but subject to the vagaries of chance within the latitude of the estimate, such as chance cancellation of positive and negative parts of an integration to change an order of magnitude. Whichever value of I is correct, there must have been an unexpected fortuitous behavior of the matrix elements operating in one or the other of these experiments. We therefore here examine the interpretations of both $B^{10}(n,\alpha)$ experiments a little more closely, from the point of view of trying to compare the probabilities that sufficiently unexpected behavior of the matrix elements might occur in one or the other.

II. THE INTENSITY-RATIO ARGUMENT AGAINST $I=\frac{1}{2}$ FOR THE 480-kev STATE

B^{10} has the large nuclear spin $I=3$, and the strong preference of the thermal reaction $B^{10}(n,\alpha)Li^7$ for the 480-kev state of Li^7 suggests a larger angular momentum I for this excited state than for the ground state, because the compound state formed by a thermal neutron also has large I, and the excited state with large I may then be formed with a smaller angular momentum L_α of the alpha (and, consequently, a smaller centrifugal barrier) than required to form the ground state. More specifically, there are four relevant combinations of choices of compound and final states, as presented in Fig. 1. The compound nucleus has I either 5/2 or 7/2 or both, depending on chance placement of the high levels of B^{11}. We assume it to have even parity, indicated by superscript $+$, on the basis of the only reasonable models for B^{10} plus an s-neutron, and thus have a choice between $5/2^+$ and $7/2^+$ for the compound nucleus. There can be very little doubt about this, or about the assignment $3/2^-$ to the ground state of Li^7; and it seems almost as certain that the 480-kev state of Li^7 also has odd parity. Only odd values of L_α are thus considered, and only the lowest value permissible in each transition. The transition scheme (a) in Fig. 1 is the one which provides a natural explanation of the observed intensity ratio on the basis of the assumption $I=5/2$ for the 480-kev state. With $7/2^+$ for the compound state, the parity and angular

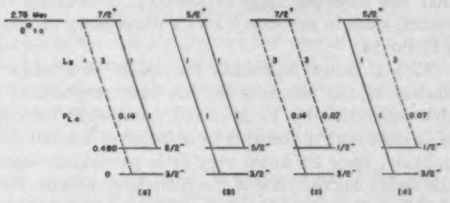

FIG. 1. Transition schemes for the two possible choices of compound state and the two relevant choices of Li^7 states. The lowest alpha-angular momentum L_α and the barrier penetrability P_{L_α} are indicated for each transition. Barrier penetrabilities, when the energy is not over the barrier, are estimated by the usual WKB approximation with the nuclear radius $R=(7^{\frac{1}{3}}+4^{\frac{1}{3}})e^2/2\ mc^2$.

[10] Fowler, Lauritsen, and Rubin, Phys. Rev. 75, 1463 (1949); W. A. Fowler and C. C. Lauritsen, Phys. Rev. 76, 314 (1949).
[11] E. R. Cohen, Phys. Rev. 75, 1473 (1949).
[12] Richards, Bashkin, Craig, Donahue, Johnson, and Martin, Phys. Rev. 79, 239 (1950).
[13] S. S. Hanna, Phys. Rev. 76, 686 (1949).
[14] R. M. Williamson and H. T. Richards, Phys. Rev. 76, 614 (1949).
[15] L. C. Elliott and R. E. Bell, Phys. Rev. 74, 1869 (1948); Rasmussen, Lauritsen, and Lauritsen, Phys. Rev. 75, 199 (1948).
[16] Krone, Hanna, and Inglis, Phys. Rev. 80, 603 (1950); W. Whaling and T. W. Bonner, Phys. Rev. 79, 258 (1950).

momentum differences permit $L_\alpha=1$ for the excited state but require $L_\alpha=3$ for the ground-state transition, and the estimated penetration factors provide a ratio 7:1 in favor of the excited state, leaving only a little more than a factor 2 in the observed ratio 17:1 to be attributed to the nuclear matrix elements. The scheme (b) has no particular virtue. With the original assignment $I=\frac{1}{2}$ for the excited state of Li^7, one must choose between schemes (c) and (d); and scheme (d), with a compound state $5/2^+$, is to be rejected because the centrifugal barrier favors the transition to the ground state by a factor of about 14, thus making a discrepancy with the observed intensity ratio by a factor of over two hundred.

With the scheme (c) in Fig. 1, the discrepancy is not so extreme, and it is in terms of this scheme that one may most reasonably hope to reconcile the observed intensity ratio with the evidence favoring $I=\frac{1}{2}$. In this scheme one has the compound state $7/2^+$ and a rather large centrifugal barrier, with $L_\alpha=3$, for both transitions. There is still a preference for the transition to the ground state arising from the energy dependence of the barrier penetrability, but only by about a factor 2, so that the observed ratio of about 17:1 favoring the excited state in this case leaves a discrepancy of about a factor 34.

Such a factor represents the *square* of a ratio of nuclear matrix elements (as has been emphasized in this connection by Fermi); and unexpected behavior of nuclear matrix elements by a factor of 6 is not very unlikely, since we know very little particularly about the highly excited state of the compound nucleus. With (LS)-coupling wave functions, which are simpler than one has a right to expect, one does not obtain so large a factor. For example, with the compound state c assumed to be a $^2G_{7/2}$, and with the wave function ψ_g of the final ground state of the system compounded with the usual coefficients of $L_\alpha=3$ for the alpha and $^2P_{3/2}$ for Li^7, and similarly with $^2P_{\frac{1}{2}}$ for ψ_e of the excited state, one finds for the transition matrix elements $(c|H|g)=G$, $(c|H|e)=1.9G$, where the spin-orbit coupling in the hamiltonian H is neglected and G is an integral involving the $^2G_{7/2}$ (with projection $M=7/2$) and that linear combination of ψ_g and ψ_e which most closely corresponds to it. The nuclear factor in the intensity ratio in this case favors the excited state, but only by a factor 3.6, which is not enough to account for the "anomalous" ratio 34. A compound state c' consisting simply of a $^2F_{7/2}$ gives similarly $(c'|H|g)=3^{\frac{1}{2}}F$, $(c'|H|e)=-F$, where F is a parameter similar to G. This contributes to the intensity ratio a factor 3 in favor of the ground state. But a less simple compound state c'' consisting of an arbitrary linear combination of c and c' would have a matrix element to the ground state $(c''|H|g)$ which is an arbitrary linear combination of F and G (subject to normalization), which might even be zero; and the *a priori* chance that this be as small as one-sixth of another such combination $(c''|H|e)$ is of the order of magnitude one-tenth, not really very small at all. This illustrates the danger of estimates ignoring nuclear matrix factors where superpositions are involved and suggests why their success in simpler problems, such as the relation between parities and the asymptotic low energy behavior of the lithium-two-alpha-reactions,[17] does not imply their safe applicability elsewhere. Because of the expected complexity of the compound state, it is not even necessary to superpose a small amount of another compound state with $I=5/2$, or to invoke a more complicated ^2P in Li^7, such as suggested by the possibility of a positive quadrupole moment.[18]

III. RESONANCES IN THE REACTION $B^{10}(n,\alpha)Li^7$

Whether we can thus perforce escape from the intensity-ratio difficulty by use of the transition scheme shown in Fig. 1(c) depends further on whether the absolute intensity of the reaction is compatible with $L_\alpha=3$. Since matrix elements may be expected to have a natural maximum value corresponding to little orthogonality, they may more easily be fortuitously small than fortuitously large, so we would prefer to assume that the matrix element to the excited state is the normal one and that the ground-state transition is abnormally weak. At first sight, it might seem unlikely that this otherwise normal matrix element could include the unfavorable penetration factor associated with $L_\alpha=3$, because this reaction is so exceptionally strong that it, although in the rarer isotope, leads to the prevalent use of boron as a slow-neutron absorber. This may, however, also be ascribed to a fortuitous circumstance, namely, that a fairly normal resonance for incident neutrons on this particular light nucleus happens to fall almost exactly at thermal energy. An examination of the energy variation of the cross section shows that no further strange behavior of the matrix elements is required.

The Breit-Wigner one-level dispersion formula for the cross section σ of the transition to one state of the final nucleus is

$$\sigma=4\pi\lambda\lambda_R\Gamma_{n,R}\Gamma_\alpha/(\Gamma^2+\Delta E^2); \qquad (1)$$

and when the deviation ΔE of the energy from exact resonance is considerably less than the resonance width Γ, it may, of course, be written

$$\sigma=4\pi\lambda\lambda_R\Gamma_{n,R}\Gamma_\alpha/\Gamma^2$$
$$=2.6(EE_R)^{-\frac{1}{2}}\Gamma_{n,R}\Gamma_\alpha/\Gamma^2 \text{ Mev-barns}, \qquad (2)$$

where $\lambda=(\text{neutron wavelength})/2\pi=\hbar/Mv_n$, the subscript R means "at resonance," Γ_n is the neutron width, and Γ_α the partial width for alpha-emission leading to,

[17] R. Resnick and D. R. Inglis, Phys. Rev. **76**, 1318 (1949).

[18] P. Kusch, Phys. Rev. **76**, 138 (1949); R. E. Present, Phys. Rev. **80**, 43 (1950); R. Avery and C. H. Blanchard, Phys. Rev. **78**, 704 (1950). The positive sign is deduced from available estimates of the sign of the quadrupole coupling q, which should probably be doubted at least as much as the simple nuclear models until the evidence becomes more complete. Thanks are due to Dr. H. M. Foley and Dr. E. Eisner for discussions of this point.

let us say, the 480-kev state of Li^7. We then have a similar formula for σ_0, containing Γ_{a0}, for the transition to the ground state, and $\Gamma=\Gamma_n+\Gamma_a+\Gamma_{a0}$. Experimentally $\sigma_0 \ll \sigma$ and thus $\Gamma_{a0} \ll \Gamma_a$ and may be neglected. If the two Γ's are equal, the factor $\Gamma_n\Gamma_a/\Gamma^2$ in Eq. (2) has its maximum value $\frac{1}{4}$, whereas if the two Γ's are quite different, it is, of course, approximated by the ratio of the smaller Γ to the larger.

Equation (2), which is written explicitly for an (n,α) reaction, applies also to other reactions; but the numerical factor 2.6 becomes 1.3 for deuteron-induced reactions and 0.65 for alpha-reactions. (The reduced-mass correction has been omitted.) The few cross sections which are known for resonances in light nuclei, such as those in $Li^6(n,\alpha)H^3(?)$, $C^{12}(d,p)C^{13*}$, $N^{15}(p,\alpha)$, and $Be^9(\alpha,n)$, seem to fall preponderantly within a factor of about 2 of the upper limit (with some of them a bit above the upper limit as though neighboring resonances contribute at a peak, and one or two of them a factor of 10 or 20 below the upper limit), suggesting that there is frequently no great difference between the two Γ's.

There is thus no general indication as to which of the Γ's is expected to be the larger; but we wish to show that the situation may be the same in the thermal resonance and in another typical resonance, without special behavior of the matrix elements. As the most appropriate typical resonance we take the one in the mirror reaction $B^{10}(n,\alpha)Be^{7*}$ at about 1.5 Mev, with a half-width of about 100 kev and a cross section at resonance about 0.14 barn (this value being based on assumed spherical symmetry). This is probably not the mirror resonance, since the corresponding proton energy would be at about 3 Mev, in a region which has not been explored. The width of this resonance is rather typical of such resonances (although they vary considerably), and we assume that it is not narrowed by unfavorable penetration factors arising from high angular momenta. It has a value $\sigma E_R \approx 0.2$ Mev-barns, a factor 3 below the maximum allowed by Eq. (2) (with $E=E_R$); and this factor we attribute to inequality of the Γ's by about a factor 10. We can compare the mirror reactions roughly by noting that a width Γ for a particle with (reduced) mass M and energy E varies as

$$\Gamma \sim M^{\frac{1}{2}}E^{\frac{1}{2}}|H_{ik}|^2,$$

where the matrix element H_{ik} when squared contains a penetration factor φ. If in the $B^{10}(p,\alpha)Be^{7*}$ reaction we have $\Gamma_a > \Gamma_p$, then $\Gamma_a \approx 100$ kev, $\Gamma_p \approx 10$ kev. These include a penetration factor $\varphi_a=1$ for the alphas if $L_a=0$ or 1, and for the protons it is either about $\frac{1}{4}$ or $\frac{1}{3}$, depending on whether $L_p=0$ or 1, which depends on the parity of the resonant level; let us say roughly, $\varphi_p=\frac{1}{3}$. (With these numbers, and $E_a=2.1$ Mev, the proton and alpha-matrix elements without barrier would be about equal.) For the reaction $B^{10}(n,\alpha)Li^{7*}$, with $L_a=3$, we have $E_a^{\frac{1}{2}}$ only 15 percent greater and the unfavorable penetration factor $\varphi_a=0.07$. If we assume that the matrix elements are otherwise roughly equal, we may thus estimate $\Gamma_a=8$ kev for the neutron reaction. Comparing the neutron width with the proton width without barrier, roughly 20 kev, the matrix elements again being taken otherwise equal, we have

$$\Gamma_n \approx (E_R/1.5\ \text{Mev})^{\frac{1}{2}}\ 20\ \text{kev}.$$

If this were about equal to (or greater than) the alpha-width, 8 kev, we would have the resonant neutron energy $E=\frac{1}{4}$ Mev (or more) with a total half-width of only 16 kev (or slightly more), so zero-energy would be far out of the resonant region, and we would have a high resonance above the $1/v$ dependence, which is not observed. Thus, we are led to assume that $\Gamma_n < \Gamma_a$, so that

$$\sigma(EE_R)^{\frac{1}{2}} \approx 2.6(\Gamma_n/\Gamma_a)\ \text{Mev barns},$$

and that thermal energy is approximately in the resonant region. The large experimental thermal cross section, 3700 barns, gives us for all energies approximately in the resonant region, including thermal,

$$\sigma E^{\frac{1}{2}} = 3700(4\times 10^7)^{-\frac{1}{2}}(\text{Mev})^{\frac{1}{2}}\ \text{barns} = 0.6(\text{Mev})^{\frac{1}{2}}\ \text{barns}.$$

From these we have

$$E_R = 20(\Gamma_n/\Gamma_a)\ \text{Mev} < 8\ \text{kev},$$

the latter because E_R must be low enouth to leave zero energy in the resonant region; and thus Γ_n is very small, corresponding to the low resonant energy, without requiring any special behavior of the matrix element, and the total width is the alpha-width, which is made small by φ_a.

If, on the other hand, in the reaction $B^{10}(p,\alpha)Be^{7*}$ we have $\Gamma_p > \Gamma_a$, then $\Gamma_p \approx 100$ kev and $\Gamma_a \approx 10$ kev. In the neutron reaction $\Gamma_a \approx 1$ kev because of φ_a, $\Gamma_n \approx (E_R/1.5\ \text{Mev})^{\frac{1}{2}}\ 100\ \text{kev} > E_R$, which means that E_R and Γ_n are both less than about 7 kev. Because of uncertainties concerning the matrix elements, it would not be surprising to find this limit exceeded by a factor of five or so.

We see thus that no unusual behavior of the matrix elements is required to make boron an exceptionally good slow-neutron absorber, in spite of the assumption $L_a=3$, provided that the resonant level happens to be placed within about 30 kev (or perhaps even 50 kev) of zero energy. (This energy corresponds to a proton bombarding energy of about 3 Mev in the mirror reaction, in a region which has not been explored.) That this does not seem like an improbable occurrence may be seen by examining the variation of σ with energy, so far as it is known. The agreement with the "$1/v$ law" is good up to several hundred electron volts, but not very good, especially beyond that region, as is seen by examination of Fig. 2. There is a gap between 1 and 4 kev, which separates the regions of applicability of two methods of obtaining monoenergetic neutrons, in which there are no data available, and the points bordering this region on either side are more doubtful than the rest, so that one may draw no firm conclusions from

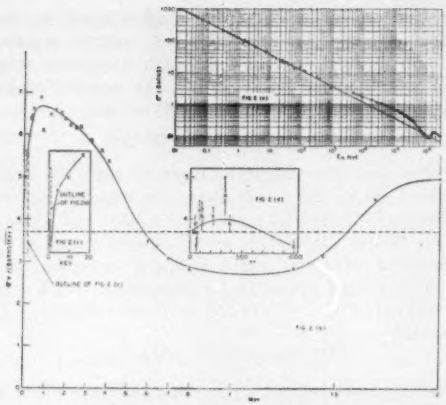

FIG. 2. Energy variation of the cross section for the reaction $B^{10}(n,\alpha)Li^7$. Note that (c) and (d) are successive expansions of the energy scale of the low energy end of (b), displaying the apparent narrow low energy resonance. The bulk of the data in the velocity selector range (0.02 to 1000 ev) are from the work of Sutton, McDaniel, Anderson, and Lavatelli, Phys. Rev. **71**, 272 (1947), which covers a wider range of energy than the similar work of J. Rainwater and W. W. Havens, Jr., Phys. Rev. **70**, 136 (1946), and in the statitron range (5 kev to 2 Mev) from the work of Bailey, *et al.* (Los Alamos, unpublished), though important check points have been obtained by others (see Goldsmith, Ibser, and Feld, Revs. Modern Phys. **19**, 265 (1947), from which the logarithmic plot is taken). *Note added in proof:* Very recent data of Barshall, *et al.* (private communication) show σv only about $\frac{1}{3}$ to $\frac{1}{4}$ as great as here plotted in the region $\frac{1}{2}$ to 2 Mev, with the 2-Mev resonance more prominent than here. This disagreement casts some doubt on even the existence of a maximum near 100 kev. The main point remains that there is no evidence for a strict $1/v$ dependence beyond 100 ev.

them. It appears quite possible that there is rather sharp resonance, only about 1 kev wide and with $E_R \approx \frac{1}{2}$ kev, responsible for the $1/v$ dependence at low energies. This would probably correspond to the first case discussed above, with the total width equal to the alpha-width, which may be made so narrow partly by the penetration factor arising from $L_a=3$ and partly by variations among the matrix elements. The experimental appearance of such a very narrow resonance depends solely on the low point near 1 kev, which is not considered reliable enough to establish the existence of the resonance. There is a very sharp rise in the region 5 to 30 kev, and then a peak too broad to be attributed to a single level. It is possible either that the sharp level below 1 kev exists and the sharp rise indicates an angular momentum greater than zero for the neutrons in the higher resonances, preventing their contributing to the thermal reaction, or more likely, that the point at 1 kev is erroneous and the thermal cross section arises mainly from a resonance perhaps 50 kev wide in the neighborhood of 30 kev, one of two or more responsible for the peak near 100 kev. The resonance denominator would change very little over the 1-kev region in which the $1/v$ variation has been observed, in spite of the apparent sharpness of the rise on a contracted energy scale. This possibility does not require any very exact fortuitous placement of a level, and either pattern of the deviations from a $1/v$ variation is consistent with a resonance width compatible with $L_a=3$.

We conclude that no second unlikely circumstance, but only the one associated with the intensity ratio itself, is required to permit the interpretation represented by Fig. 1(c).

Recent measurements[19] at various rather widely-spaced energies up to about 4 Mev show that the $B^{10}(n,\alpha)Li^7$ intensity ratio strongly favors the excited-state transition only at energies well below $\frac{1}{2}$ Mev. This new information is not surprising, and does not alter the dilemma, since the participation of p and d neutrons becomes possible at the higher neutron energies. The deviations from the "$1/v$ law" suggest two or more states in the region 50 to 400 kev, not necessarily formed by s neutrons, and it is not expected that the narrow state chiefly responsible for the thermal behavior should be dominant at higher energies.

IV. THE ALPHA-GAMMA ANGULAR CORRELATION IN $B^{10}(n,\alpha)Li^{7*}(\gamma)Li^7$

With $I=\frac{1}{2}$ for the excited state of Li^7 one would have no angular correlation between the alphas and the subsequent gammas from the reaction $B^{10}(n,\alpha)Li^{7*}$ (just as spin $\frac{1}{2}$ can carry no quadrupole moment); but with $I=5/2$ for Li^{7*} and $7/2$ for the compound nucleus B^{11}, as in Fig. 1(a), one expects a correlation of the form $(1+A\cos^2\theta)$, and Devons[7] has calculated

$$A=(a^2-0.4b^2-4.5ab\sin\delta)/(7a^2+5.1b^2-1.5ab\sin\delta),$$

where a^2 is the probability of magnetic dipole radiation, b^2 that of electric quadrupole, with $a^2+b^2=1$, and δ is a relative phase which is arbitrary[19a] because of the possible complexity of the compound state and the different nature of the electric and magnetic operators. It is to be noted that $|A|\ll 1$ for both of the extreme cases of unmixed radiation:

$A=$ 0.079 for magnetic dipole radiation ($b=0$);
$A=-0.143$ for electric quadrupole radiation ($a=0$),

as was calculated also by Feld,[7] and the uncertainty[8] in the observation $A\approx 0$ covers about one-seventh of the range between them. The lifetime for magnetic dipole radiation may be estimated[20] as

$$\tau \approx [(4/3\hbar)(\omega/c)^3\mu^2\sigma_{mn}{}^2]^{-1}$$
$$\approx (3/8)1837^2\ 137^2(3\times 10^{-13}/3\times 10^{10})\ \text{sec} \approx 2\times 10^{-12}\ \text{sec},$$

where we have put $\hbar\omega=mc^2$, the spin magnetic moment $\mu=1.4e\hbar/Mc$, and the nondiagonal matrix element of the spin operator, $\sigma_{mn}\approx 1$. It appears that the matrix

[19] P. Huber, personal conversation; also, Petree and Barschall.

[19a] *Note added in proof:* See, however, S. P. Lloyd, Phys. Rev. **81**, 161 (1951), whose result, $\sin\delta=\pm 1$, which was also derived independently by E. N. Adams, II, shows that the cancellation would have a probability $\frac{1}{2}$ if b should be just large enough.

[20] L. I. Schiff, *Quantum Mechanics* (McGraw-Hill Book Company, Inc., New York, 1949), p. 251; Fermi, Orear, Rosenfeld, and Schluter, *Nuclear Physics* (University of Pennsylvania Press, Philadelphia, 1941), Chapter V.

element is about 50 percent larger than here estimated (as could perhaps happen for example by superposition of spin and orbital effects), since this should be the large term and the observed lifetime[15] is 0.75×10^{-13} sec. For electric quadrupole radiation, we assume that the charge is, in effect, associated with the protons, in keeping with Siegert's theorem extended to higher electric multipoles,[21] and then have as a similar rough estimate of the lifetime

$$\tau>[(2/\hbar)(\omega/c)^5e^2(r_{11}r_\perp)_{mn}^2]^{-1}$$
$$\approx[(137)^6/2\times10^{23}]\text{ sec}=4\times10^{-11}\text{ sec.}$$

(For heavy nuclei, the magnetic moments μ are about the same because of the suppressing effect of shell structure, and the electric quadrupole reciprocal lifetime grows relative to magnetic dipole by a factor $\omega^2A^{4/3}$, making the two about equal for $\hbar\omega=5mc^2$, $A=100$, in keeping with the customary classification of degrees of forbiddenness.) For this rather soft radiation from a light nucleus one thus expects the electric quadrupole radiation to be something like 200 times weaker than the magnetic dipole radiation, implying $b/a\leqslant1/15$. The numerical coefficient 4.5 in the expression for A is, however, so large that the rather small value $b/a\approx1/5$ would make it possible for A to be zero (as was pointed out by Adams). Thus, an electric quadrupole matrix element three times larger than this rough upper limit[21a] would make it possible for A to vanish fortuitously. For $I=5/2$, this would require either a failure of Siegert's theorem to hold to this accuracy, or a concerted action of more than one proton in spite of the stability of the s-shell, or a considerably larger nucleus than estimated, as might be associated with the weak stability of Li^7 relative to $\alpha+T$, or a combination of these effects and a surprising lack of cancellation in the matrix element, but in any case with the simultaneous circumstance that $\sin\delta$ have the right sign, this seems much less likely than that one matrix element in the intensity ratio should be small because of cancellation by a factor 6.

The observed approximate lack of alpha-gamma angular correlation, together with the expectation of predominantly magnetic dipole radiation and the isotropy of the $Li^7(p,p')$ gammas, thus seem to demonstrate[22] that $I=\frac{1}{2}$ considerably more conclusively than does the thermal intensity ratio suggest that $I=5/2$, and thus practically forces one to ascribe the anomalous intensity ratio to chance misbehavior of a matrix element. This conclusion is happily in keeping with theoretical expectations based on nuclear models, that $I=\frac{1}{2}$ with odd parity.

Gratitude is expressed to Professor E. Fermi and Dr. E. N. Adams, II, of the University of Chicago and to Professor S. Devons of Imperial College, London, for discussion of these and related topics.

[21] A. Seigert, Phys. Rev. **52**, 727, (1937), and recent discussions of R. G. Sachs.

[21a] *Note added in proof:* An empirical tendency of electric multipole matrix elements to be much smaller than such a roughly estimated upper limit, especially when compared with magnetic multipoles to which meson exchange currents may contribute, has been pointed out by M. Goldhaber, Bull. Am. Phys. Soc. **26**, No. 1, M4 (title only) (1951).

[22] There is another possibility not represented in Fig. 1 which would give no angular correlation (Reference 7) and require the unexpected behavior to provide only a factor 17 instead of 34, namely, $5/2^+$ for both the compound state and the 480-Kev state; but this parity for Li^7 seems too unlikely, on the basis of models and the observed isolation of the two low states, to merit further consideration.

PHYSICAL REVIEW VOLUME 81, NUMBER 6 MARCH 15, 1951

Variation with Energy of Nuclear Collision Cross Sections for High Energy Neutrons

J. DeJuren* and B. J. Moyer
Radiation Laboratory, Department of Physics,† University of California, Berkeley, California

(Received November 20, 1950)

Nuclear total cross sections for high energy neutrons have been measured for approximately known neutron energies in the range 90 to 270 Mev. It is observed that cross sections in every case drop rather rapidly between 100 and 180 Mev to a level which continues with little further variation up to the highest neutron energies available in the experiment. Comparisons are made with nuclear attenuation data for cosmic rays.

I. INTRODUCTION

NUCLEAR collision cross sections for high energy neutrons have been measured at three different energy regions for neutrons produced by the University of California 184-inch cyclotron. Stripping of 90-, and 190-Mev deuterons by beryllium targets produced neutrons[1,2] of mean energies 40 and 90 Mev, respectively. Measurements[3,4] utilizing the $C^{12}(n,2n)C^{11}$ reaction for detection provided total nuclear cross sections at estimated mean neutron detection energies of 42 and

* This paper is based on material submitted to the University of California in partial satisfaction of the requirements for the Ph.D. degree.

† This work was performed under the auspices of the AEC.

[1] Helmholz, McMillan, and Sewell, Phys. Rev. **72**, 1003 (1947).
[2] R. Serber, Phys. Rev. **72**, 1008 (1947).
[3] R. Hildebrand and C. Leith, in preparation for publication.
[4] Cook, McMillan, Peterson, and Sewell, Phys. Rev. **75**, 7 (1949).

84 Mev, respectively. Bismuth fission, which has a threshold at about 50 Mev, was used for detection of the 90-Mev neutrons; and both inelastic and total cross sections of nuclei were measured[5] at an estimated mean detection energy of 95 Mev.

The bombardment of a 2-inch Be target with 350-Mev protons produces high energy neutrons with a broad energy distribution possessing a maximum at about 270 Mev. Total cross sections were measured for various nuclei using both bismuth fission[6] detection and a scintillation counter recoil proton telescope[7] possessing an equivalent neutron threshold of 250 Mev. The two methods gave values which agreed well with each other.

However, the model of the transparent nucleus developed by Fernbach, Serber, and Taylor,[8] which described the inelastic and total cross-section measurements adequately in the region of 90 Mev, could not fit the 270-Mev data if expected values independent of the atomic number were employed for the two parameters of their theory. The two parameters are k_1, the change in propagation vector of the neutron upon entering nuclear matter; and K, the absorption coefficient for the neutron wave in nuclear matter.

Indeed, the 270-Mev data would require that an impinging neutron experience no change in potential on entering a nucleus, if this theory were to be retained.

As the energy interval between the 95- and 270-Mev measurements was wide, it was felt necessary to investigate the variation of neutron total cross sections of a representative number of nuclei within this energy region.

II. PARTICLE ENERGIES AND EFFECTIVE DETECTION ENERGIES

In connection with various experimental programs with the 184-inch cyclotron the energy distribution of the neutrons knocked out of a 2-inch Be target by the 350-Mev protons has been measured by Cladis and Hadley, by Fox, *et al.*,[7] and by Kelly, Wiegand, and Segrè. All three measurements show a broad distribution peaked around 270 Mev, a composite result of which is shown in Fig. 1 as $N(E)$.

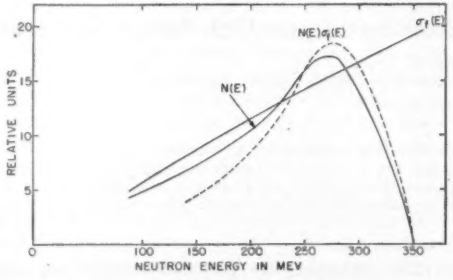

FIG. 1. Estimation of detection efficiency *vs* neutron energy in the case of 350-Mev protons. $N(E)$ is the neutron energy spectrum from a two-inch Be target bombarded by 350-Mev protons. $\sigma_f(E)$ is the approximate excitation function for Bi fission by neutrons. The dashed curve is then the detection efficiency *vs* energy.

In order to obtain information concerning the variation with neutron energy of the bismuth fission counter, the ratio of Bi fission to the $C^{12}(n,2n)C^{11}$ reaction was studied for neutrons with mean energies at 90 Mev, at 270 Mev, and for several intermediate values. This ratio increased uniformly by a factor of 3.56 ± 0.11 as the mean neutron energy changed from 90 to 270 Mev. According to theoretical calculations by Baumhoff at this laboratory, the $(n,2n)$ reaction yield in carbon should decrease slowly over this region to a value of about 0.8 of the 90-Mev yield. Similar theoretical calculations for the (p,pn) reaction[9] in carbon have proved to be quite valid. It may be presumed therefore that the efficiency of the Bi fission reaction increases uniformly by a factor of about three in the neutron energy interval in question.

The selection of neutrons with different mean energies was accomplished by the use of a ½-inch Be target at various radii in the cyclotron, with appropriate adjustments of the counters for each target position. It is necessary then to estimate the neutron spectra produced by the various proton energies employed. The following data are pertinent:

(1) The neutron spectra from ½-inch and 2-inch Be targets are very nearly identical at these energies, because of multiple passages of the circulating beam through the targets.

(2) The neutron spectrum from a Be target bombarded by 180-Mev protons has been observed by Fox and Wouters[10] to have its maximum in the vicinity of 110 Mev.

(3) The neutron spectrum from a 2-inch Be target bombarded by 350-Mev protons has its maximum at about 270 Mev.

(4) The ratio of Bi fission cross section to the $C^{12}(n,2n)C^{11}$ cross section for neutrons from 165-Mev protons was equal to that for the neutrons of 90-Mev mean energy from the stripping of 190-Mev deuterons.

In the light of these observations it will be assumed that the mean energy of the neutron spectrum falls 70 Mev lower than the energy of the bombarding protons for a ½-inch Be target.

The comparison of Bi fission with the $C^{12}(n,2n)C^{11}$ reaction was accomplished by exposing a fission counter and a polystyrene foil simultaneously in the proper location relative to the proton target. Measurements were made at 40-Mev intervals of proton energy ranging from 150 to 350 Mev. Sufficient absorbing material was placed before the detectors to stop protons scattered out through the tank wall from the target.

The effective neutron detection energy is estimated by plotting the product of the neutron energy distribution and the Bi fission cross section *vs* energy. In Fig. 1 this is illustrated for the case of neutrons from the 350-Mev protons. The effective detection energy is not

[5] J. DeJuren and N. Knable, Phys. Rev. **77**, 606 (1950).
[6] J. DeJuren, Phys. Rev. **80**, 27 (1950).
[7] Fox, Leith, Wouters, and MacKenzie, Phys. Rev. **80**, 23 (1950).
[8] Fernbach, Serber, and Taylor, Phys. Rev. **75**, 1352 (1949).
[9] W. Heckrotte and P. Wolff, Phys. Rev. **73**, 264 (1948).
[10] R. Fox and L. Wouters (private communication).

significantly different from the mean energy of the neutrons.

III. EXPERIMENTAL ARRANGEMENT

The neutrons produced by the bombardment of the 2-inch Be target by 345-Mev protons have a wide angular distribution with a half-width at half-maximum of 25° (as measured with bismuth fission). Since only two collimators are present in the concrete shielding, corresponding to proton energies of 180 and 350 Mev, the detector must be placed inside the shielding for intermediate energies (Fig. 2). Most of the neutron flux passes through an inch of steel tank wall as well as other tank fixtures, so that the elastically scattered flux from these could constitute a background of perhaps 10 to 20 percent of the undeviated flux in the absence of any collimation. To reduce the detector background the chamber was placed behind a 7-foot thick concrete block with an adjustable collimating arrangement through its central region admitting a neutron beam slightly less than 2 inches in diameter. As the target position was varied from 81 inches to 54 inches to obtain the desired proton energy settings, the collimating apparatus was swiveled into alignment for the various target positions. The detector was placed six feet to the rear of the concrete block, and the attenuating materials were aligned immediately in front of the block on a wooden holder as shown in Fig. 2. The distance from absorbers to detector was about 13 feet, so the geometry was "good" with only small angular scattering corrections necessary.

To monitor the neutron beam a bismuth fission chamber was placed to one side of the concrete block where the contribution of neutrons scattered from the absorbers to its counting rate was negligible. Background was determined by placing approximately seven mean free paths of absorbers on the holder. For most measurements the background was of the order of 5 percent of the detector counting rate with no absorbers present. The geometry was tested by comparison of the attenuation of the 270-Mev neutrons using the above geometry with the previous[6] setup in which the detector was placed outside the 10-foot concrete shielding in the collimated neutron beam. With the detector outside the shielding the background was completely negligible and the angular scattering correction smaller by a factor of two than in the present case.

To test the new geometry the length of copper absorber was increased by 3-inch steps to 12 inches, and the resulting attenuation when corrected for background was found to be linear as a function of absorber length when plotted on semilogarithmic paper.

If N_0 is the number of neutrons per second reaching the detector with no absorber present and N is the number when absorber of length L is present, then

$$(N-b)/(N_0-b)=e^{-n\sigma_t L}, \qquad (1)$$

where b is the background counting rate when an absorber that absorbs essentially all the neutrons is placed in position, n is the number of nuclei per cubic centimeter, and σ_t is the total nuclear cross section. A value of $1.14\pm0.02\times10^{-24}$ cm² was obtained with the present arrangement, as compared with the result outside the shielding of $1.15\pm0.02\times10^{-24}$ cm² for the copper total cross section.[6] Linear semilog plots were obtained at other probe positions to check the geometry. Most of the measurements were made with between one and two mean free paths of absorber present in order to obtain optimum statistics for a minimum time of cyclotron operation.

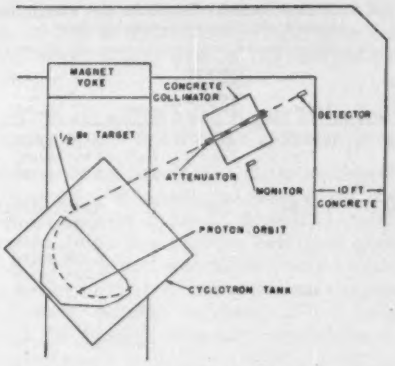

FIG. 2. Plan view of experimental arrangement.

IV. ATTENUATOR MATERIALS

The metals used in the experiments were usually machined cylinders, three or four inches in diameter with negligible chemical impurities. Densities were obtained from measurements of the physical volumes with micrometer and vernier calipers and accurate weights of the cylinders.

The total cross section of hydrogen was measured using pentane-carbon differences. A brass cylindrical holder 48 inches long with $\frac{1}{32}$-inch thick walls and bases held the pentane. An array of seven machined, 3-inch diameter graphite cylinders, with total mass per unit area equal to that of the carbon in the 48-inch length of pentane, plus a $\frac{1}{16}$-inch thick brass disk, were alternately used with the pentane to attenuate the neutron beam. The decrease in the detector counting rate when the graphite was replaced by pentane is from the attenuation of the neutrons due to the hydrogen alone. Since only 0.3 to 0.4 mean free path of hydrogen is present (depending on the neutron energy), repeated cycles were made at a given probe setting to obtain good statistics. The percent statistical error of the cross-section measurement is equal to the percent statistical error in counting divided by the number of mean free paths of hydrogen present. Short blank cycles were taken with an empty holder to obtain the carbon cross section.

TABLE I. Total cross sections of nuclei for high energy neutrons measured with bismuth fission chambers.

Proton energy (Mev)	Target	Estimated neutron energy (Mev)	Element	σ_t (barns)
310	0.5″ Be	240	Al	0.576 ±0.012
			Cu	1.15 ±0.02
			Pb	2.88 ±0.05
290	0.5″ Be	220	H	0.0410±0.0041
				0.0410±0.0029
				0.041 ±0.0024 (av)
			C	0.288 ±0.10
				0.283 ±0.08
				0.285 ±0.06 (av)
			Al	0.576 ±0.021
			Cu	1.15 ±0.035
			Pb	2.99 ±0.14
270	2″ Be	190	C	0.291 ±0.009
			Al	0.540 ±0.028
			Cu	1.15 ±0.04
			Sn	1.90 ±0.07
			Pb	2.85 ±0.10
			U	3.28 ±0.13
250	0.5″ Be	180	Al	0.575 ±0.013
			Cu	1.25 ±0.03
			Pb	3.06 ±0.06
230	0.5″ Be	160	H	0.0548±0.0060
				0.0504±0.0029
				0.0512±0.0026 (av)
			C	0.298 ±0.012
				0.295 ±0.0075
				0.296 ±0.006 (av)
225	2″ Be	145	Cu	1.31 ±0.04
	0.5″ Be	155	Cu	1.30 ±0.04
185	0.5″ Be	115	Cu	1.52 ±0.06
180–190[a]	0.5″ Be	110–120	Al	0.733 ±0.012
			Cu	1.49 ±0.02
			Pb	3.71 ±0.06

[a] Probe position not accurately known.

V. RESULTS

The data obtained are given in Table I. Pertinent results from the previous studies[5,6] at 95 and 270-Mev are given in Table II. Copper, tin, lead, and uranium have small diffraction scattering corrections (<1 percent) incorporated into their cross-section values. The variations of the cross sections with energy are shown in graphical form for carbon, aluminum, copper, and lead in Fig. 3. The variation of the hydrogen cross section is illustrated in Fig. 4. Data from previous studies[3–6] are included in these curves, and in Fig. 3, published results at[11] 14 Mev and[12] 25 Mev have been also plotted. The errors given are the statistical fluctuations from counting alone expressed in standard deviations.

TABLE II. Total cross sections for 95- and 270-Mev neutrons measured previously with bismuth fission chambers.[a]

Element	σ_t(95 Mev) $\times 10^{24}$ cm^2	σ_t(270 Mev) $\times 10^{24}$ cm^2
Hydrogen	0.073±0.0015	0.038±0.0015
Carbon	0.498±0.003	0.288±0.003
Aluminum	0.993±0.011	0.555±0.008
Copper	2.00 ±0.02	1.15 ±0.02
Lead	4.48 ±0.03	2.84 ±0.03

[a] References 5 and 6.

VI. DISCUSSION OF RESULTS

Carbon, aluminum, copper, and lead all exhibit little variation in their total cross-section values from about 180-Mev to 270-Mev mean neutron energy, as Fig. 3 indicates. The neutron energy distribution detected by the fission chambers is rather broad for the measurements undertaken and the resulting cross sections may

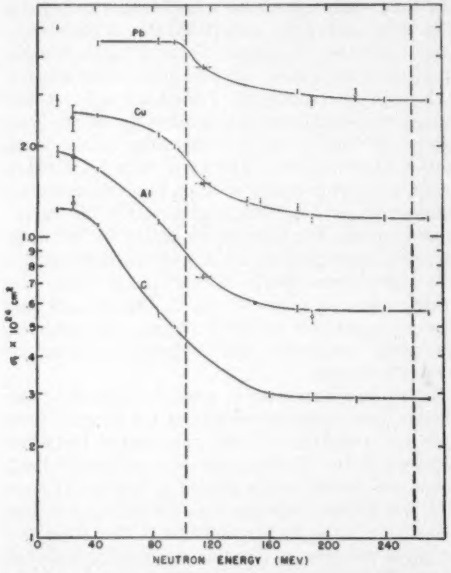

FIG. 3. Total cross sections vs neutron energy. The region between dashed lines contains the data from the present experiment. On either side of this region are data from earlier experiments by the same authors and by others mentioned in text.

not correspond exactly to the true cross section at the mean detected energy of the unattenuated distribution. If the detected energy distribution is given by $f(E)$, where $f(E)$ is normalized so that

$$\int_{E_{\min}}^{E_{\max}} f(E)dE=1,$$

the measured value of the cross section is from Eq. (1):

$$nL\sigma_m=\ln\left(\frac{N_0-b}{N-b}\right)=-\ln\int_{E_{\min}}^{E_{\max}} f(E)e^{-n\sigma_t(E)L}dE,$$

[11] Amaldi, Bocciarelli, Cacciapuoti, and Trabachi, Nuovo cimento 3, 203 (1946).

[12] R. Sherr, Phys. Rev. 68, 240 (1945).

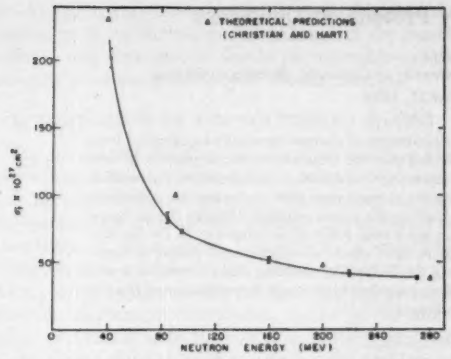

FIG. 4. Total n–p cross section vs neutron energy. Triangles represent theoretical predictions of Christian and Hart (reference 13).

or

$$\sigma_m = \frac{-1}{nL} \ln \int_{E_{\min}}^{E_{\max}} f(E) e^{-n\sigma_t(E)L} dE. \qquad (2)$$

If σ_m is examined for the energy intervals where measurements were made, the following statements may be made for the four nuclei above:

(1) For mean energies of 240 Mev or above, the variation of $\sigma_t(E)$ over the distribution is slight and σ_m agrees with $\sigma(\bar{E})$ at the mean energy

$$\bar{E} = \int_{E_{\min}}^{E_{\max}} Ef(E) dE.$$

(2) As the mean energy of the distribution is lowered to 160 Mev, $\sigma_t(E)$ begins to increase on the low energy side of the distribution from its level value, and the measured value σ_m will be higher than $\sigma(\bar{E})$.

In general the broad neutron distribution tends to round off the shape of the curves of Fig. 3. The plateaus are possibly slightly flatter and longer in extent than shown.

No attempt has been made to correct the present data for the spread in the neutron energies, since the detected neutron distribution is hardly known with sufficient accuracy. A measurement of cross sections for a small neutron energy interval centered about 140 Mev would define the cross-section variations in this region more precisely. Faster electronic circuits under development in connection with scintillation counters may make this measurement feasible.

The theoretical predictions of Christian and Hart[13] for a Yukawa potential with tensor interaction are also shown in Fig. 4. Experimentally, the cross section deviates more markedly from an $1/E$ variation than it does theoretically.

[13] R. Christian and E. Hart, Phys. Rev. **77**, 441 (1950).

VII. COMPARISON WITH CROSS SECTIONS OBSERVED IN COSMIC-RAY ATTENUATION

Estimates of the attenuation in the atmosphere of the components of cosmic radiation giving rise to penetrating showers, bursts in thin-walled chambers, nuclear stars, and slow neutrons have been given by Rossi.[14,15] It is shown that these events are almost certainly due to the high energy nucleon components of the cosmic radiation, consisting of both primary nucleons and energetic secondary nucleons formed in the atmosphere.

A summary of the data in references 14 and 15 is given in Table III. The attenuation lengths listed apply to integrated intensities, i.e., intensities measured without close angular or energy definition.

In some previous measurements by DeJuren[6] of poor geometry attenuation of the 270-Mev neutrons, it was found that the cross sections for inelastic collision were at least one-half the total collision cross sections. For 90-Mev neutrons the inelastic cross section is slightly less[5,16] than $\frac{1}{2}\sigma_t$.

TABLE III. Attenuation lengths for reduction of integrated intensity by factor of $1/e$.

Type of event	Attenuation length in atmosphere	Attenuation length in Pb
Penetrating showers	110–125 g/cm²	
Bursts	120–140 g/cm²	250–450 g/cm²
Stars	135–150 g/cm²	<250 g/cm²
Slow neutrons	160–190 g/cm²	

If, for comparison with the cosmic-ray data, absorption cross sections of one-half the total cross sections measured for 270-Mev neutrons[6] are used, the calculated attenuation lengths are 138 g/cm² in air, and 250 g/cm² in Pb. Rossi[15] quotes an attenuation length for "neutral N-rays" (supposedly high energy neutrons) in air of 130 g/cm².

It appears that cross sections for high energy neutron absorption fall rather abruptly to a broad, slowly-varying or flat region at approximately the minimum level demonstrated in cosmic rays, and that this flat region is entered at energies as low as approximately 200 Mev.

[14] B. Rossi, Revs. Modern Phys. **20**, 537 (1948).
[15] B. Rossi, ONR Technical Report No. 26 (Massachusetts Institute of Technology) April 4, 1949; AEC Index No. NP-891.
[16] Bratenahl, Fernbach, Hildebrand, Leith, and Moyer, Phys. Rev. **77**, 597 (1950).

The Production of Mesons by Protons on Deuterons*

H. P. Noyes
Radiation Laboratory, Department of Physics, University of California, Berkeley, California
(Received September 25, 1950)

An attempt is made to predict the energy and angular distribution of charged mesons to be expected from the bombardment of deuterium by 345-Mev protons assuming that the cross section for production in two-nucleon collisions is known. The problem is simplified by assuming that the third particle enters the reaction only by giving to the struck particle a momentum distribution at some time prior to the meson production, by carrying off the complementary momentum, and by limiting the states available through the exclusion principle. The possibility of the reformation of a deuteron more than doubles the cross section for the production of positive if it occurs. Hence the positive-negative ratio offers an experimental means of determining the spin dependence of positive meson production in the final state, assuming that the ratio of p–n to p–p production is known. Alternatively, this approach offers a method for a rough determination of the p–n meson production cross section using high energy proton beams.

I. INTRODUCTION

THE purpose of this paper is to attempt to predict the energy and angular distribution of mesons resulting from the bombardment of deuterium by 345-Mev protons, under the assumption that the cross section for the production of mesons in two-nucleon collisions is known. Alternatively, since high energy neutron sources of sufficient intensity and energy resolution for an accurate, direct study of meson production in n–p collisions have not yet been achieved, this analysis can offer a method for learning something of this n–p cross section. The production of mesons in proton-proton collisions in being investigated experimentally by Richman, Wilcox, Whitehead, Cartwright, and Peterson;[1] and Brueckner has conducted a theoretical investigation of the problem in the light of these experiments.[2]

The general method of attacking the problem was suggested to the author by Chew, in analogy with an approach he is using in the study of n–d inelastic scattering.[3] It rests upon two assumptions, of which the first is probably justified, while the second is open to considerable question. The first assumption is that the production takes place in a time so short compared with the period of the deuteron that the impulse approximation may be used. Since for the incident proton $v/c = 0.682$, the time for it to cross a meson Compton wavelength is only two percent of the deuteron period. Hence it seems to be reasonable to assume that the problem can be treated in terms of the production of mesons by two nucleons, one of which has the momentum distribution of a particle in the deuteron, while the third particle simply carries off the complementary momentum without otherwise entering the reaction. The general examination of the errors made in impulse approximations of this type is to be discussed in a forthcoming paper by Wick and Chew.

The more dubious assumption is that the particles which produce the meson do not then interact with the third particle except insofar as the exclusion principle limits the states available to them. This is essentially the same approximation as the neglect of double scattering from alternate particles in the inelastic scattering of nucleons by deuterons. In the latter problem one of the three particles must have a large momentum relative to a pair of particles that are interacting strongly. As Chew has shown, this allows a straightforward treatment in terms of two-body interactions. When a meson is formed, however, it is quite possible for all three nucleons to have comparable momenta, so that exact treatment would require a solution of the three-body problem.

Still, it can be argued that the situation is not so desperate as to invalidate the method used below. Firstly, when the three momenta are comparable, the exclusion principle causes a compensating reduction in the cross section. A further limitation occurs in that the phase space available to the three particles in this energy region (i.e., the region of high meson energy) is small. Outside of this region the effect is small. In fact, if the third particle has a relative energy of 40 Mev or greater, as is true on the average for most of the distribution except the high energy tail already discussed, its cross section at the average distance from the two interacting particles (4 or 5 wavelengths at this energy) covers less than six percent of the solid angle into which these particles may go. Moreover, the interaction between the two particles which produce the meson can be taken into account to the same extent as was done by Brueckner. This interaction completely alters the two nucleon distribution both in magnitude and shape; it increases the magnitude of the p–d cross section by a corresponding amount but has much less influence on the shape. Thus, the results given below should be at least qualitatively correct, except possibly

* The work described in this paper was performed under the auspices of the AEC.
[1] Wilcox, Cartwright, Richman, and Whitehead, Phys. Rev. **79**, 198 (1950). C. Richman and H. A. Wilcox, private communication. V. Peterson, Phys. Rev. **79**, 407 (1950), and private communication.
[2] K. Brueckner, Phys. Rev. **79**, 641 (1950), and private communication.
[3] G. F. Chew, Phys. Rev. **80**, 196 (1950).

for the high energy tail. Clearly this method ignores the possibility of the formation of a triton, but the results indicate that this process should be separable experimentally from the main body of the distribution.

II. DERIVATION OF THE SCATTERING MATRIX

The formal statement of the above assumptions and derivation of the scattering matrix will be carried out in terms of the R matrix notation.[4] The assumption that the two-nucleon cross section is known can be stated as knowledge of appropriate two-particle R matrices. These are then combined with the assumption that the third particle influences the reaction only by giving a deuteron momentum distribution to one of the interaction particles at some time previous to the production of the meson, to give an R matrix for the problem at hand.

In order to clarify the notation, consider the two-particle case briefly. Let the momentum and spin variables of the incident proton and struck neutron be denoted by ξ_0 and ξ_n, respectively, the final neutron variables by ξ_1 and ξ_2, and the positive meson variables by η^+. Then $R_{np}{}^+$, which describes the transformation of a proton ξ_0 and a neutron ξ_n into two neutrons ξ_1 and ξ_2 and a positive meson η^+, can be written as $(\xi_1\xi_2\eta^+|R_{np}{}^+|\xi_0\xi_n)$. Momentum conservation may be factored out giving

$$(\xi_1\xi_2\eta^+|R_{np}{}^+|\xi_0\xi_n)=\delta(\mathbf{k}_1+\mathbf{k}_2+\mathbf{q}-\mathbf{K}_0-\mathbf{K}_n)\times(\tfrac{1}{2}(\mathbf{k}_1-\mathbf{k}_2),\sigma_1,\sigma_2,\mathbf{q}|r_{np}{}^+|\tfrac{1}{2}(\mathbf{k}_0-\mathbf{k}_n),\sigma_0,\sigma_n), \quad (1)$$

where the spin and momentum variables of the nucleons have been introduced explicitly. Note that this separation restricts us to treating the nucleons nonrelativistically throughout (except that the incident proton may be treated relativistically in calculating the energy and momentum available for the reaction; the treatment of the final nucleons can be shown to be a good approximation). The cross section for the production of positive mesons in an n–p collision is then to be written as

$$d\sigma_{np}{}^+=(2\pi/\hbar v_0)|r_{np}{}^+|^2\delta(E_1+E_2+E_q-E_0-E_n)\times[d\mathbf{k}'/(2\pi)^3][d\mathbf{q}/(2\pi)^3], \quad (2)$$

where $\mathbf{k}'=\frac{1}{2}(\mathbf{k}_1-\mathbf{k}_2)$ and all other variables in $r_{np}{}^+$ are to be expressed in terms of $\mathbf{k}'$, $\mathbf{q}$ (and $\mathbf{k}_0$) by means of momentum conservation. That is, formally, $r_{np}{}^+$ appears in the cross section in the same way as a matrix element for the transition calculated in Born approximation; this analogy is useful in practice. In fact, the whole calculation is formally equivalent to a second-order perturbation calculation assuming that the nuclear forces and meson production arise from separate interaction terms in the hamiltonian and that the corresponding second-order calculation for the two-particle case gives the correct answer.

[4] C. Möller, Det. Kgl. Danske Vidensk. XIII, No. 1 (1946).

In terms of this notation the (unsymmetrized) R matrices for the deuteron problem under our assumptions may be written, for negatives:

$$(\xi_1\xi_2\xi_3\eta^-|R_{pd}{}^-|\xi_0\xi_D)=\sum_{\xi_3'\xi_n\xi_p}(\xi_1\xi_2\eta^-|R_{np}{}^-|\xi_0\xi_n)\delta_{\xi_3\xi_3'}\times\psi_D(\xi_n\xi_p)\psi_{\mathbf{t}0}(\xi_0') \quad (3)$$

and for positives:

$$(\xi_1{}^{(n)}\xi_2{}^{(n)}\xi_3{}^{(p)}\eta^+|R_{pd}{}^+|\xi_0\xi_D)=\sum_{\xi_3'\xi_n\xi_p}\{\exp(i\delta_{np})\cdot(\xi_1\xi_2\eta^+|R_{np}{}^+|\xi_0\xi_n)\delta_{\xi_3\xi_3'}+\exp(i\delta_{pp})\cdot(\xi_1{}^{(n)}\xi_2{}^{(p)}\eta^+|R_{pp}{}^+|\xi_0\xi_n)\delta_{\xi_n\xi_3'}\}\times\psi_D(\xi_n\xi_p)\psi_{\mathbf{t}0}(\xi_0'), \quad (4)$$

where $\psi_{\mathbf{t}0}(\xi_0')$ is the incident plane wave $\delta_{\mathbf{t}_0\mathbf{t}_0'}$, $\psi_D(\xi_n\xi_p)$ is the deuteron function $\chi_D(\sigma_n\sigma_p)g_0(\frac{1}{2}\mathbf{k}_n-\frac{1}{2}\mathbf{k}_p)\delta(\mathbf{k}_n+\mathbf{k}_p-2\mathbf{k}_c)$, and $2\mathbf{k}_c$ is the momentum of the deuteron in whatever coordinate system is chosen. These two equations contain the formal statement of the assumptions (a) that the third particle influences the production of the meson only through giving to the struck particle a deuteron momentum distribution at some time previous to the collision, and (b) that the three nucleons go directly into the final state $\xi_1\xi_2\xi_3$ without further interaction not contained in the two-nucleon $R_{np}{}^\pm$ and $R_{pp}{}^+$. According to the argument given in the introduction the interaction thus included should contain most of the influence of forces between the particles in the final state. Equation (3) is to be antisymmetrized in the three final neutrons $\xi_1\xi_2\xi_3$, and (4) in the two final neutrons; the corresponding r matrices are then to be squared, averaged over the initial proton and deuteron spin states, and summed over the final spin states. Note that the phase in the production of positives can be determined only from a specific meson theory so that the results will be uncertain by the amount of the interference term if empirical R matrices are used. The cross section is then given by

$$d\sigma_{pd}=(2\pi/\hbar v_0)|r_{pd}|^2\delta(E_1+E_2+E_3+E_q-E_0-E_D)\rho_f,$$

where the variables appearing in r_{pd} and in the density of final states ρ_f are to be interpreted in terms of the new momentum conservation condition $\mathbf{k}_1+\mathbf{k}_2+\mathbf{k}_3+\mathbf{q}-\mathbf{k}_0-2\mathbf{k}_c=0$ that arises from integrating the original $\delta(\mathbf{k}_1+\mathbf{k}_2+\mathbf{q}-\mathbf{k}_0-\mathbf{k}_n)$ over $\mathbf{k}_n$ and $\mathbf{k}_p$.

Positive mesons can also be formed with the final nucleons coming off as a neutron and a deuteron instead of as two neutrons and a proton. According to the approximation being used here, this process will occur mainly when the positive meson is produced from the proton in the deuteron. This is the same process as that considered by Brueckner, Chew, and Hart[5] in proton-proton collisions, and can be included by calculating

$$(\xi_1\xi_{D'}\eta^+|R_{pd}{}^{+(d)}|\xi_0\xi_D)=\sum_{\xi_3'\xi_n\xi_p}(\xi_{D'}\eta^+|R_{pp}{}^{+(d)}|\xi_0\xi_p)\delta_{\xi_n\xi_1}\times\psi_D(\xi_n\xi_p)\psi_{\mathbf{t}0}(\xi_0'). \quad (5)$$

[5] Brueckner, Chew, and Hart, Phys. Rev. (to be published).

Clearly this term is incoherent with processes that lead to one proton and two neutrons. The alternative case when one of the two neutrons produced in the n–p collisions picks up the original proton in the deuteron is neglected in this approximation. Equations (3)–(5) are the formal solution of the problem posed; given the R matrices for the production of mesons in two-nucleon collisions, which except for phase can be found empirically, they enable us to calculate the production of mesons by proton-deuteron collisions under the assumptions (a) and (b) above, and subject to the uncertainty in the sign and magnitude of the coefficient of the interference term in the production of positives introduced by the unknown phase $\exp[i(\delta_{pn}-\delta_{pp})]$.

III. RESULTS

The calculation of the matrix elements and phase space integrals is discussed in the appendix. Clearly (3), (4), and (5) imply a much more detailed knowledge of the production process than is at present available, so that simplifying assumptions have been introduced. These are general features found to hold for the four meson theories considered by Brueckner; namely, scalar, vector, and pseudoscalar with pseudoscalar and pseudovector coupling. These are that, near threshold, the two-particle matrix elements depend principally on the meson variables, the initial and final spins of the nucleons, and the magnitude of their relative momenta, and only weakly on the absolute magnitude or direction of the momenta. Consequently, when the two final nucleons are identical, their final state must be a singlet spin state. These restrictions arise from neglect of the final nucleon momenta relative to the initial momenta of the nucleons and neglecting the recoil of the nucleons due to the emission of the meson. The answers obtained by this approximation are in agreement with preliminary experiments, so these assumptions will be used here as a semi-empirical result.

Under these restrictions, the transition rate for the production of negative mesons in p–d collisions is given by

$$\begin{aligned} w_{pd}^{-} = (2\pi/\hbar)\rho_f \times 1/6\{ & |M_{pn}^{-}(|\mathbf{k}_1-\mathbf{k}_2|^2,\eta^-)|^2 g_0^2(\mathbf{k}_2+\mathbf{k}_c) \\ & - M_{pn}^{-}(|\mathbf{k}_1-\mathbf{k}_2|^2,\eta^-)^* M_{pn}^{-}(|\mathbf{k}_2-\mathbf{k}_3|^2,\eta^-) \\ & \times g_0^*(\mathbf{k}_3+\mathbf{k}_c) g_0(\mathbf{k}_1+\mathbf{k}_c) \\ & + |M_{pn}^{-}(|\mathbf{k}_2-\mathbf{k}_3|^2,\eta^-)|^2 g_0^2(\mathbf{k}_1+\mathbf{k}_c) \\ & - M_{pn}^{-}(|\mathbf{k}_2-\mathbf{k}_2|^2,\eta^-)^* M_{pn}^{-}(|\mathbf{k}_3-\mathbf{k}_1|^2,\eta^-) \\ & \times g_0^*(\mathbf{k}_1+\mathbf{k}_c) g_0(\mathbf{k}_2+\mathbf{k}_c) \\ & + |M_{pn}^{-}(|\mathbf{k}_3-\mathbf{k}_1|^2,\eta^-)|^2 g_0^2(\mathbf{k}_2+\mathbf{k}_c) \\ & - M_{pn}^{-}(|\mathbf{k}_3-\mathbf{k}_1|^2,\eta^-)^* M_{pn}^{-}(|\mathbf{k}_1-\mathbf{k}_2|^2,\eta^-) \\ & \times g_0^*(\mathbf{k}_2+\mathbf{k}_c) g_0(\mathbf{k}_3+\mathbf{k}_c)\}, \quad (6) \end{aligned}$$

where M_{pn}^{-} is the two-nucleon matrix element for the production of negatives and g_0 is the momentum amplitude in the deuteron. The three positive terms give the distribution that would be produced in an n–p collision where the neutron had the momentum distribution in the deuteron. The negative terms are a correction taking account of those states which are excluded by the presence of the third particle. The assumption that M_{pn}^{-} is a constant gives the phase space for the problem less the exclusion principle correction. The meson distribution in the forward direction under this assumption is plotted in Fig. 1 to the same scale as the production of negative mesons in n–p collisions under the same assumption. The general character of this distribution persists when the forces between the two interacting nucleons in their final state are taken into account.

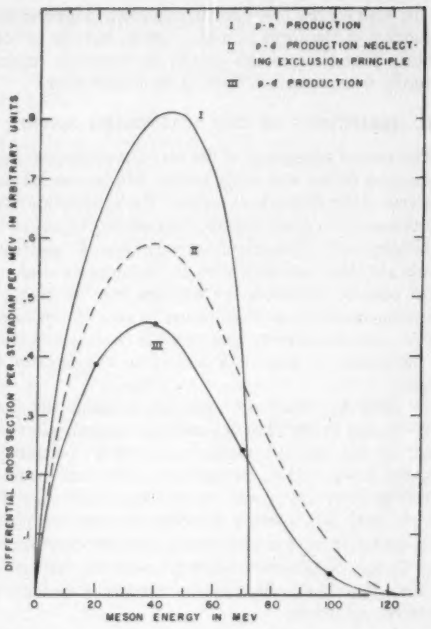

FIG. 1. Production of negative mesons in the forward direction by 345-Mev protons assuming a constant matrix element; coulomb forces neglected.

The experimental results on the production of positive mesons in proton-proton collisions[1] are clearly incompatible with the assumption that the matrix element is a constant. Brueckner, Chew, and Hart[5] have shown that the discrepancy can be removed by taking into account the interaction of the nucleons after the production of the meson. Essentially, this is found to introduce into the R matrix a factor $K_0/(\alpha_t^2+k_r^2)^{\frac{1}{2}}$ if the final state is a triplet, and $0.876\ K_0/(\alpha_s^2+k_r^2)^{\frac{1}{2}}$ if the final state is a singlet. [$\alpha^2=M|\epsilon|/\hbar^2$, where ϵ is the binding energy of the deuteron or of the virtual singlet

level for triplet and singlet states, respectively, $\mathbf{k}_r=\frac{1}{2}(\mathbf{k}_1-\mathbf{k}_2)$ is the relative momentum of the final nucleons, and K_0 is the inverse Compton wavelength of the meson $\mu c/\hbar$.] Since under our assumptions the final state in the production of negatives in a singlet, the result (relative to the two-nucleon production) is the same for all four theories and is given in Fig. 2. The chief effect on the deuteron spectrum (outside of the change in magnitude) of taking this effect into account is to shift the peak of the distribution from 40 Mev to 60 Mev. Coulomb forces between the two protons in the final state might be expected to wipe out the sharp peak in the two-particle distribution; but since little area is included under the peak, the smoothed-out deuteron distribution should be little affected by this correction.[6] Further, α_s is well known from p–p scattering, so that this result should be relatively trustworthy. In particular, it is not subject to the interference correction that appears in the production of positive mesons.

The production of positives is more complicated in that a deuteron may appear as one of the final particles, that the final state may be singlet, triplet, or a mixture depending upon the theory, and that positives produced from the neutron may interfere with positives produced from the proton with an undetermined phase. The general formula for the case of a deuteron appearing as a final particle has already been given; the calculation is straightforward and leads to the result given in the Appendix. For the rest of the cross section the transition probability is

$$\begin{aligned} w_{pd}{}^{+}=(2\pi/\hbar)\rho_f\{&|M_{pn}{}^{+}(|\mathbf{k}_1-\mathbf{k}_2|^2,\eta^+)|^2 g_0{}^2(\mathbf{k}_3+\mathbf{k}_c)\\ &+|M_{pp}{}^{+}(|\mathbf{k}_1-\mathbf{k}_3|^2,\eta^+)|^2 g_0{}^2(\mathbf{k}_2+\mathbf{k}_c)\\ &+|M_{pp}{}^{+}(|\mathbf{k}_2-\mathbf{k}_3|^2,\eta^+)|^2 g_0{}^2(\mathbf{k}_1+\mathbf{k}_c)\\ &-M_{pp}{}^{+}(|\mathbf{k}_1-\mathbf{k}_3|^2,\eta^+)^* M_{pp}(|\mathbf{k}_2-\mathbf{k}_3|^2,\eta^+)\\ &\quad\times g_0{}^*(\mathbf{k}_2+\mathbf{k}_c) g_0(\mathbf{k}_1+\mathbf{k}_c)\\ &+A\cos(\delta_{pn}-\delta_{pp})M_{pn}{}^{+}\\ &\quad\times(|\mathbf{k}_1-\mathbf{k}_2|^2,\eta^+)^* g_0{}^*(\mathbf{k}_3+\mathbf{k}_c)\\ &\quad\times[M_{pp}{}^{+}(|\mathbf{k}_1-\mathbf{k}_3|^2,\eta^+) g_0(\mathbf{k}_2+\mathbf{k}_c)\\ &\quad+M_{pp}{}^{+}(|\mathbf{k}_2-\mathbf{k}_3|^2,\eta^+)] g_0(\mathbf{k}_1+\mathbf{k}_c)]\}, \quad (7) \end{aligned}$$

where $A\cos(\delta_{pn}-\delta_{pp})$ depends upon the theory. Note that for equal p–n and p–p matrix elements the exclusion correction is one-third the correction in the case of negatives. This is a specific example of a general argument given by Chew and Steinberger[7] to show that the exclusion correction will increase the positive negative ratio for the production of positive mesons by protons in complex nuclei.

For the final state a singlet spin state (scalar or vector mesons, $A=1$), under the usual assumption that the n–p and p–p scattering lengths are equal, the production of positives is also given in Fig. 2. This curve (II) is made up of three parts, which can be determined from the curves already given for the production of negative mesons (IV and V). The distribution of positives produced by a collision of the incident proton with the neutron will be the same as the distribution of negative (V) times the ratio of $n+p\to\pi^+$ to $n+p\to\pi^-$ cross sections. The distribution of positives produced in collisions between the incident proton and the proton in the deuteron will again have the same form but will be multiplied by the ratio of $p+p\to\pi^+$ to $p+n\to\pi^+$ cross sections. (If the p–n and p–p matrix elements are equal this ratio will be two, since either proton can give a positive meson in the p–p case.) The exclusion principle correction is the same as that taking (V) into (IV) times one-half the ratio of p–p to p–n cross sections. Note that in the case plotted, $(\sigma_{pn}{}^{+}/\sigma_{pn}{}^{-}=1$ and $\sigma_{pp}{}^{+}/\sigma_{pn}{}^{+}=2)$, this exclusion correction is only one-third as large compared to the total cross section as is the exclusion correction in the production of negatives. Under this assumption that the p–n and p–p matrix elements are equal, the positive-negative ratio for mesons of 60 Mev in the forward direction is 3.84 ± 0.84. The uncertainty

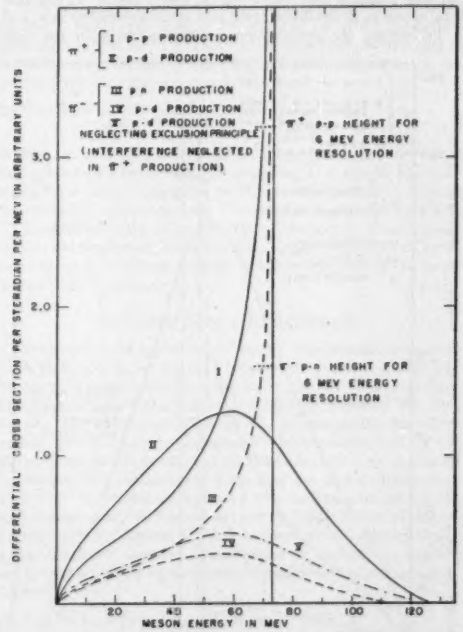

FIG. 2. Production of negative and positive mesons in the forward direction by 345-Mev protons leading to a singlet final state; interference term neglected; p–n and p–p matrix elements assumed equal.

[6] This correction has been calculated by K. Watson and is indeed small.

[7] G. F. Chew and J. Steinberger, Phys. Rev. 78, 497 (1950).

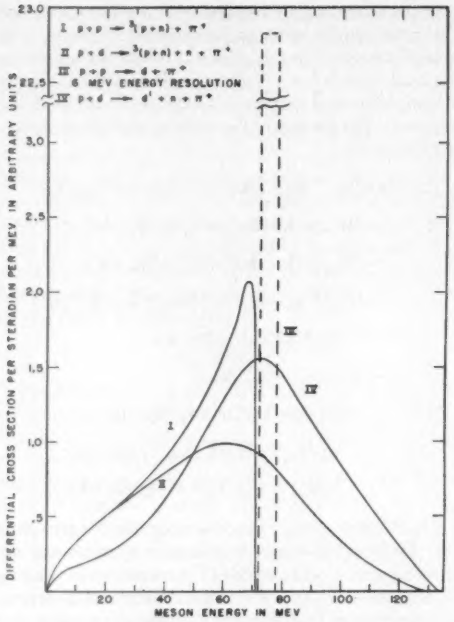
I p+p → ³(p+n)+π⁺
II p+d → ³(p+n)+n+π⁺
III p+p → d+π⁺
6 MEV ENERGY RESOLUTION
IV p+d → d'+n+π⁺
DIFFERENTIAL CROSS SECTION PER STERADIAN PER MEV IN ARBITRARY UNITS
MESON ENERGY IN MEV

FIG. 3. Production of positive mesons in the forward direction by 345-Mev protons striking free protons or protons bound in deuterons leading to a triplet final state.

is due to the possible interference between positives produced from the neutron and those produced from the proton in the deuteron.

For the final state a triplet (pseudoscalar theory with pseudovector coupling or $\frac{2}{3}$ of the time with pseudoscalar coupling) the cross section is greatly increased by the reformation of a deuteron in the final state. The distribution of positives produced from the proton is much the same as when the final state is a singlet, but the case when the deuteron reappears as one of the final particles has comparable cross section. The comparison of these two parts of the cross section is given in Fig. 3. Note that the value of the measured p–d cross section relative to the cross section measured for the production of positives in p–p collisions will depend critically on the energy resolution of the apparatus used in the latter experiment. (The ratio of the deuteron peak to the peak of the continuum distribution is given by $4\pi E_d/\Delta E$ where E_d is the binding energy of the deuteron and ΔE is the energy resolution in the center of mass system.) The total cross section in the forward direction (again assuming n–p and p–p matrix elements equal, and neglecting interference) is plotted in Fig. 4. The positive-negative ratio in the forward direction at 60 Mev is 8.22 ± 0.84. This large increase in the positive-negative ratio when the final state is a triplet is, of course, due to the added cross section resulting from the reformation of the deuteron. This increase is clearly much larger than the uncertainty due to the interference term. Hence, if the matrix element for p–n production were known to be approximately equal to that for p–p production, the experimental value for this positive-negative ratio would determine fairly clearly whether or not the reformation of a deuteron occurs appreciably in p–p meson production. Conversely, if the formation of a deuteron could be demonstrated in meson production from hydrogen, this ratio would give a fair idea as to the ratio of p–n to p–p matrix elements (assuming the p–n matrix element the same for both positive and negative meson production).

This problem was suggested to me by Professor Chew, and he has been most liberal with advice and help during the investigation. Keith Brueckner's parallel investigation of the fundamental two-nucleon problem has been drawn on throughout, and his advice was most helpful. Much is owed to the criticism and encouragement of Professor Robert Serber.

APPENDIX

A. Calculation of the Matrix Elements

The general expression (3) is specialized by the assumption that $R_{np}{}^{-}$ depends only on σ_1, σ_2, $|\mathbf{k}_1-\mathbf{k}_2|^2$, and η^- in the final state, σ_0 and σ_n in the initial state, and is antisymmetric in σ_1 and σ_2. Performing the integrations, antisymmetrizing in the final

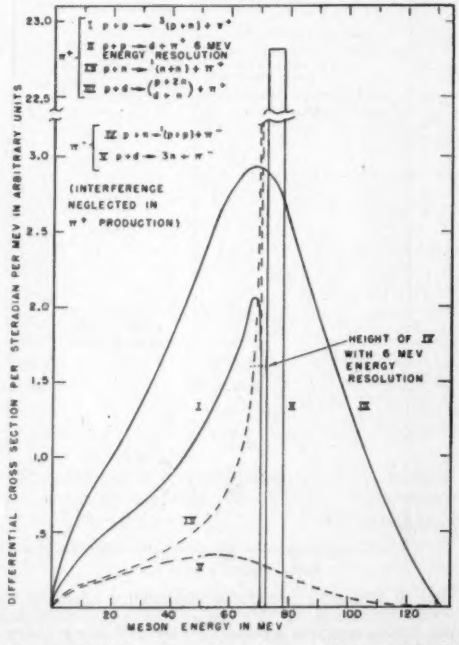
I p+p → ³(p+n)+π⁺
II p+p → d+π⁺ 6 MEV ENERGY RESOLUTION
III p+n → (n+n)+π⁺
IV p+d → (p+2n / d+n)+π⁺
V p+n → ³(p+p)+π⁻
VI p+d → 3n+π⁻
(INTERFERENCE NEGLECTED IN π⁺ PRODUCTION)
HEIGHT OF II WITH 6 MEV ENERGY RESOLUTION
DIFFERENTIAL CROSS SECTION PER STERADIAN PER MEV IN ARBITRARY UNITS
MESON ENERGY IN MEV

FIG. 4. Production of positive and negative mesons in the forward direction by 345-Mev protons leading to a triplet final state when the two final particles are not identical; interference term neglected.

three protons, and taking out the delta-function giving momentum conservation gives

$$r_{pd}^{-}=\sum_{\sigma_n}(\sigma_1\sigma_2|\mathbf{k}_1-\mathbf{k}_2|^2\eta^-|r_{np}^-|\sigma_3\sigma_n)\chi_D(\sigma_n\sigma_4)g_0(\mathbf{k}_3+\mathbf{k}_4)$$
$$-(\sigma_1\sigma_3|\mathbf{k}_1-\mathbf{k}_2|^2\eta^-|r_{np}^-|\sigma_2\sigma_n)\chi_D(\sigma_n\sigma_2)g_0(\mathbf{k}_2+\mathbf{k}_4)$$
$$-(\sigma_2\sigma_2|\mathbf{k}_2-\mathbf{k}_3|^2\eta^-|r_{np}^-|\sigma_1\sigma_n)\chi_D(\sigma_n\sigma_1)g_0(\mathbf{k}_1+\mathbf{k}_4). \quad (8)$$

Since we are interested only in the meson distribution, the result will be integrated over all nucleon momenta; hence the matrix element that will appear in the cross section may be written

$$|r_{pd}^{-}|^2=\left(\frac{1}{3!}\right)\times\left(\frac{1}{6}\right)\times 3\sum_{\substack{\sigma_1\sigma_2\sigma_3\\ \sigma_1'\sigma_2'\sigma_3'}} g_0^*(\mathbf{k}_3+\mathbf{k}_4)F^*(|\mathbf{k}_1-\mathbf{k}_2|^2,\eta^-)$$
$$\times\chi_D^{*2}(\sigma_n'\sigma_3')(\sigma_1\sigma_3|r_{np}^-|\sigma_2\sigma_n')^*[(\sigma_1\sigma_3|r_{np}^-|\sigma_2\sigma_n)$$
$$\times\chi_D(\sigma_n\sigma_2)F(|\mathbf{k}_1-\mathbf{k}_2|^2,\eta^-)g_0(\mathbf{k}_3+\mathbf{k}_4)$$
$$-2(\sigma_2\sigma_2|r_{np}^-|\sigma_3\sigma_n)\chi_D(\sigma_n\sigma_1)$$
$$\times F(|\mathbf{k}_2-\mathbf{k}_3|^2,\eta^-)g_0(\mathbf{k}_1+\mathbf{k}_4)\}, \quad (9)$$

where (as in the case in the theories considered by Brueckner) the momentum dependence can be factored out as $F(|\mathbf{k}_i-\mathbf{k}_j|^2,\eta^-)$, the $1/3!$ is the phase space factor for three identical particles, and the $\frac{1}{6}$ comes from the average over the six initial spin states. Since

$$\sum_{D,\,\sigma_1}\chi_D^*(\sigma_n'\sigma_3)\chi_D(\sigma_n\sigma_3)=\tfrac{1}{2}\delta_{\sigma_n\sigma_n'} \quad (10)$$

the diagonal term reduces to

$$\tfrac{1}{2}g_0^2(\mathbf{k}_3+\mathbf{k}_4)\times\tfrac{1}{2}\sum_{\substack{\sigma_3\sigma_n\\ \sigma_1\sigma_2}}|F(|\mathbf{k}_1-\mathbf{k}_2|^2,\eta^-)(\sigma_1\sigma_2|r_{np}^-|\sigma_3\sigma_n)|^2$$
$$=\tfrac{1}{2}g_0^2(\mathbf{k}_3+\mathbf{k}_4)|M_{np}^-(|\mathbf{k}_1-\mathbf{k}_2|^2,\eta^-)|^2, \quad (11)$$

i.e., simply to $\frac{1}{2}$ the matrix element (squared) for negative production in p–n collisions times the momentum distribution in the deuteron. This is the term to be expected for direct production from the neutron. (The $\frac{1}{2}$ occurs in the two particle case also as the phase space factor for two identical particles.) Similarly, the spin sum for the exclusion correction gives

$$\tfrac{1}{2}g_0^*(\mathbf{k}_3+\mathbf{k}_4)M_{pn}^-(|\mathbf{k}_1-\mathbf{k}_2|^2,\eta^-)$$
$$\times M_{pn}^-(|\mathbf{k}_2-\mathbf{k}_3|^2,\eta^-)^*M_{pn}^-(|\mathbf{k}_3-\mathbf{k}_1|^2,\eta^-), \quad (12)$$

so that the exclusion correction is 100 percent when the three final particles all have the same momenta, as it should be. Combining these and including the cyclic permutations of 1, 2, 3 gives the result (6) already quoted. The matrix element for positives, (7), is obtained in the same way. Here, however, no simplification such as the final state being always a singlet occurs and different theories can give different results for the coefficient of the interference term $A\cos(\delta_{pn}-\delta_{pp})$.

B. Phase Space Integrations

The canonical variables picked were r, the internal coordinate of the deuteron, y, the distance between the incident proton and the center of mass of the deuteron, and x, the center-of-mass coordinate for the three particles, with conjugate momenta $\hbar k_r$, $\hbar k_y$, and $\hbar k_x$. The initial kinetic energy T_0 and momentum $\hbar k_0$ of the incident proton must be calculated relativistically, but in the deuteron case it was found that the final nucleons may be treated as nonrelativistic without greatly altering the meson distribution. (This is to be contrasted with the two-nucleon case where the final nucleons may be treated as nonrelativistic in the center-of-mass system, but the result must be transformed relativistically to the laboratory system.) Conservation of momentum requires that $\mathbf{k}_x+\mathbf{q}=\mathbf{k}_0$, where $\hbar\mathbf{q}$ is the meson momentum and conservation of energy gives

$$k_r=\hbar^{-1}[MT_0-ME_d-ME_q-\tfrac{1}{4}\hbar^2|\mathbf{k}_0-\mathbf{q}|^2-\tfrac{1}{3}\hbar^2k_y^2]^{\frac{1}{2}}$$
$$=[g-\tfrac{1}{3}k_y^2]^{\frac{1}{2}}, \quad (13)$$

where $E_q=(\mu^2c^4+\hbar^2q^2c^2)^{\frac{1}{2}}$ is the meson energy and E_d the deuteron binding energy. For a constant matrix element the diagonal term leads to the integral

$$\int\rho_f g_0^2(k_1)=\frac{dq}{(2\pi)^3}\int_0^{(4q/3)^{\frac{1}{2}}}\frac{M[g-\frac{1}{3}k_y^2]^{\frac{1}{2}}k_y^2dk_y}{2\hbar^3(2\pi)^3}$$
$$\times\int_{-1}^{1}\frac{d\mu_y}{(2\pi)^3}8\pi^2\frac{8\pi\alpha N^2}{(\alpha^2+\frac{1}{3}k_y^2+k_r^2+\frac{2}{3}k_yk_y\mu_y)^2}, \quad (14)$$

where the deuteron momentum distribution has been taken to be $(8\pi\alpha N^2)^{\frac{1}{2}}/(\alpha^2+k^2)$. The calculation has also been carried through for the more reasonable deuteron wave function $[\exp(-\alpha r)-\exp(-\beta r)]/r$ with $\beta/\alpha=6$. The only important change this makes over the wave function $\exp(-\alpha r)/r$ is that N^2 changes from unity to $6(6+1)/(6-1)^2=1.68$. The angular integration is elementary and the branch points of the final integral allow it to be replaced by a contour and done by residues giving

$$\int\rho_f g_0^2(k_1)=\frac{dq}{(2\pi)^3}\left(\frac{3^{\frac{1}{2}}MN^2\alpha}{\hbar^3}\right)\left\{\frac{A[r-\rho]^{\frac{1}{2}}+B[r+\rho]^{\frac{1}{2}}}{2^{\frac{1}{2}}AB}-1\right\}, \quad (15)$$

where

$$A^2=3\alpha^2/4K_0^2;\quad B^2=k_x^2/12K_0^2;\quad G=g/K_0^2;$$
$$\rho=G+A^2-B^2;\quad r=[\rho^2+4A^2B^2]^{\frac{1}{2}}$$

and K_0 is the meson inverse Compton wavelength. The exclusion principle correction reduces to

$$\frac{dq}{(2\pi)^3}\left(\frac{3MN^2\alpha}{2\pi\hbar^2}\right)\left(\frac{K_0}{k_x}\right)\int_0^{(4G/3)^{\frac{1}{2}}}\pi dx\int_{\frac{1}{2}(k_x/K_0)-\frac{1}{2}x}^{\frac{1}{2}(k_x/K_0)+\frac{1}{2}x}dy$$
$$\times\frac{K_0^2\ln\left[\dfrac{\alpha^2+(K_0y+k_r)^2}{\alpha^2+(K_0y-k_r)^2}\right]}{\alpha^2+K_0^2y^2+k_r^2}, \quad (16)$$

where $k_r^2=K_0^2(4/3G-x)$. This integral was evaluated numerically.

The diagonal term integral that occurs when the forces between the particles in the final state are taken into account differs only by the factor $K_0^2/(\alpha^2+k_r^2)$ in the final integration, so that this integral may again be done by residues giving

$$\int\frac{\rho_f g_0^2(k_1)K_0^2}{\alpha_i^2+\frac{1}{4}|\mathbf{k}_2-\mathbf{k}_3|^2}=\frac{dq}{(2\pi)^3}\left(\frac{3^{\frac{1}{2}}MN^2\alpha K_0^2}{\hbar^3[(\rho+A_i^2)^2+4A^2B^2]}\right)$$
$$\times\{(\rho+A_i^2/2^{\frac{1}{2}}AB)[A(r-\rho)^{\frac{1}{2}}+B(r+\rho)^{\frac{1}{2}}]$$
$$+(1/2^{\frac{1}{2}})[B(r-\rho)^{\frac{1}{2}}-A(r+\rho)^{\frac{1}{2}}]-A_i(G+A_i^2)^{\frac{1}{2}}\}, \quad (17)$$

where $A_i^2=\alpha_s^2/K_0^2$ or α_t^2/K_0^2 depending upon whether the final state is a singlet or a triplet. The corresponding exclusion principle correction was not calculated but was estimated to be approximately the same percent of the diagonal term at the same meson energy as the corresponding correction for the constant matrix element case.

When one of the final particles is a deuteron, energy and momentum conservation give for the density of final states

$$\rho_f=\left(\frac{2M}{3\hbar^2}\right)k_y\frac{d\Omega_y}{(2\pi)^3}\frac{dq}{(2\pi)^3},\ \text{where } k_y=(2/3^{\frac{1}{2}})(g+\alpha_i^2)^{\frac{1}{2}}. \quad (18)$$

The angular integration is elementary, giving

$$\int d\Omega_y g_0^2(k_1)=9\pi N^2/4[(\rho+A_i^2)^2+4A^2B^2]^{\frac{1}{2}}. \quad (19)$$

The ratio of matrix elements for the two-particle case is given by Bruckner as

$$\left|\frac{M_{pp}^{+(d)}}{M_{pp}^{+}(\alpha^2+k_r^2)^{\frac{1}{2}}}\right|^2=\frac{(2\pi)^3[(\alpha/2\pi)^{\frac{1}{2}}K_0]^3}{K_0^3}=4\pi^2\alpha, \quad (20)$$

so that this result can be immediately related to our previous formulas.

The Angular Distribution of Photo-Protons from Deuterium*†

GERSON GOLDHABER‡
University of Wisconsin, Madison, Wisconsin
(Received November 3, 1950)

The angular distribution of the photo-protons from the photo-disintegration of deuterium was measured. The 6- and 7-Mev gamma-rays from the $F^{19}+H^1$ reaction were used as a gamma-ray source. Photographic emulsions loaded with deuterium were used to record the photo-proton tracks.

The angular distribution is best fitted by the expression $a+b\sin^2\theta(1+\kappa\cos\theta)$ with values of a/b of 0.09 ± 0.07, 0.17 ± 0.07, 0.15 ± 0.06 for $E_\gamma=6$, 7, and 6 and 7 Mev combined, respectively. For 6 and 7 Mev combined, $\kappa=0.4^{+0.2}_{-0.3}$. Using the 6-Mev gamma-ray line as a calibration point, a value $E_\gamma=7.1\pm0.1$ was obtained for the 7-Mev line.

I. INTRODUCTION

SEVERAL experiments have been performed recently to determine the angular distribution of the products from the photo-disintegration of deuterium. The various observers measured either the angular distribution of the photo-neutrons[1–4] or that of the photo-protons.[5–9] The radiation sources used were ThC'',[1] Na^{24},[2–4,6] gamma-rays from the $F^{19}+H^1$ reaction,[5] gamma-rays from the Li^7+H^1 reaction,[7] x-rays from an electron electrostatic generator ($Ex\leq3.2$ Mev),[8] and x-rays from a betatron[9] ($Ex\leq20.3$ Mev).

Theoretical predictions have been[10] that for low gamma-ray energies, say $E_\gamma<20$ Mev, the angular distribution in the CM system should be of the form $(a+b\sin^2\theta)$, where θ is the angle of the photo-proton or photo-neutron relative to the gamma-ray direction. For higher energy gamma-rays[11–13] theoretical calculations predict a departure from the $(a+b\sin^2\theta)$ distribution. In particular, a fore and aft asymmetry with a shift of the photo-protons in the forward direction is predicted.

Marshall and Guth[13,14] and Blair[15] calculated a fore and aft asymmetry for the electric component of the photo-disintegration cross section of deuterium. The effect is analogous to the one calculated by Sommerfeld and Schur[16] for photo-electrons from x-rays on hydrogen. Marshall and Guth obtained an angular distribution for the photo-protons in the CM system of the form

$$[a+b\sin^2\theta(1+2\beta\cos\theta)],$$

where $\beta=v/c=(E_\gamma-W/Mc^2)^{\frac{1}{2}}$. W is the binding energy of the deuteron and M is the proton mass. Such an asymmetry effect was observed experimentally by Fuller.[9]

In the present investigation another attempt was made to use the gamma-rays from the $F^{19}+H^1$ reaction as a gamma-ray source for the photo-disintegration of deuterium. The $F^{19}+H^1$ gamma-rays consist of two monochromatic lines[17–19] at roughly 6 and 7 Mev. Recent evidence indicates that the 7-Mev line is probably a close doublet with components at 6.91 and 7.11 Mev.[20,21] The gamma-rays are considered to be due to the reaction:[22]

$$F^{19}+H^1\rightarrow Ne^{20*}\rightarrow O^{16*}+He^4,$$
$$O^{16*}\rightarrow O^{16}+h\nu,$$

which also leads to a pair-emitting level[18] at 6.05 Mev.

The gamma-ray yield from this $(p\alpha',\gamma)$ reaction is very copious compared with (p,γ) reactions.[23,24] Also, the gamma-ray energy appears to be essentially independent of the proton energy[19] up to $E_p=5$ Mev. The $F^{19}+H^1$ reaction is thus a convenient gamma-ray source when protons with an energy of several Mev are available.

Nuclear emulsions loaded with deuterium[24a] were used

---

* Part of a thesis submitted to the Graduate School of the University of Wisconsin in partial fulfilment of the requirements for the Ph.D. A preliminary report was presented at the 1949 Chicago Meeting of the A.P.S., Phys. Rev. **77**, 753 (1950).

† This work was supported by the Wisconsin Alumni Research Foundation and the U. S. AEC.

‡ Now at Department of Physics, Columbia University, New York.

[1] G. Graham and H. Halban, Revs. Modern Phys. **17**, 297 (1945) (contains references to earlier work).
[2] E. P. Meiners, Jr., Phys. Rev. **76**, 259 (1949).
[3] B. Hamermesh and A. Wattenberg, Phys. Rev. **76**, 1408 (1949).
[4] F. Genevese, Phys. Rev. **76**, 1288 (1949).
[5] Gibson, Green, and Livesey, Nature **160**, 534 (1949).
[6] N. O. Lassen, Phys. Rev. **74**, 1533 (1948); **75**, 1099 (1949).
[7] H. Wäffler and S. Younis, Helv. Phys. Acta **22**, 414 (1949); **22**, 614 (1949); **23**, 206 (1950).
[8] W. M. Woodward and I. Halpern, Phys. Rev. **76**, 107 (1949).
[9] E. G. Fuller, Phys. Rev. **76**, 576 (1949); **79**, 303 (1950).
[10] H. A. Bethe and R. F. Bacher, Revs. Modern Phys. **8**, 122 (1936).
[11] M. E. Rose and G. Goertzel, Phys. Rev. **72**, 749 (1947).
[12] L. I. Schiff, Phys. Rev. **78**, 733 (1950).
[13] J. F. Marshall and E. Guth, Phys. Rev. **78**, 738 (1950).
[14] J. F. Marshall and E. Guth, Phys. Rev. **76**, 1879 (1949).
[15] J. S. Blair, private communication.
[16] A. Sommerfeld and G. Schur, Ann. Physik **4**, 409 (1930).
[17] R. L. Walker and B. D. McDaniel, Phys. Rev. **74**, 315 (1948).
[18] Rasmussen, Hornyak, and Lauritsen, Phys. Rev. **75**, 1462 (1949).
[19] J. A. Phillips and P. G. Kruger, Phys. Rev. **76**, 1471 (1949).
[20] W. E. Burcham and J. M. Freeman, Phys. Rev. **75**, 1756 (1949).
[21] Chao, Tollesterup, Fowler, and Lauritsen, Phys. Rev. **79**, 108 (1950).
[22] Streib, Fowler, and Lauritsen, Phys. Rev. **59**, 253 (1941).
[23] Fowler, Lauritsen, and Lauritsen, Revs. Modern Phys. **20**, 236 (1948).
[24] W. A. Fowler and C. C. Lauritsen, Phys. Rev. **76**, 314 (1949).
[24a] The D_2O used was supplied by the Stuart Oxygen Company, San Francisco, California, and was obtained on allocation from the Isotopes Division of the AEC.

to record the photo-protons from the photo-disintegration of deuterium. When these emulsions are exposed to the $F^{19}+H^1$ gamma-rays, photo-disintegration takes place within the emulsion; and a single emulsion can be used to record all of the photo-proton tracks.§

II. EXPERIMENTAL PROCEDURE

The photographic emulsions (Eastman NTA, 100 micron) were loaded with deuterium by soaking them in D_2O[7,25–27] for 5 min at 9°C. About 20 mg/cm² of D_2O were thus introduced into the emulsions. A similar control emulsion was prepared by soaking it in H_2O. The emulsions swell on the above treatment by a factor of 1.7 (as measured with a micrometer). The total shrinkage of the emulsions (from the wet state to the dry developed state, as measured in the microscope) is $K=4\pm0.6$.[27a]

Immediately after loading the emulsions were exposed in an air-tight camera to the $F^{19}+H^1$ gamma-rays. The two emulsions, one containing D_2O and the other H_2O, were placed in a horizontal plane with the emulsion side up[27b] and with the long side of the emulsion parallel to the proton beam (Fig. 1). The plane of the emulsion thus contained the proton beam direction. The shape of the area scanned was so chosen that the variation in direction of the incident gamma-ray beam over that area was ~1° and could thus be neglected. The position of that area afforded a reasonable ratio of fogging to track density. A 2.6-Mev proton beam from the Wisconsin electrostatic generator was used to bombard a thick CaF_2 target for a 35-μamp-hr exposure. The proton beam was focused on a spot 4×6 mm with the short axis in the horizontal plane. It was found necessary in order to reduce the fogging of the emulsions to introduce a 10-mm aluminum absorber. This absorber is thick enough to absorb the electrons and positrons from the internal pair production[18,22] from the $F^{19}+H^1$ reaction. The emulsions were processed immediately after the exposure.

III. THE SCANNING

The scanning was performed independently by two observers. A binocular Bausch and Lomb microscope was used at a magnification of 980X. The microscope was fitted with a protractor eye-piece and an eye-piece scale.

(A) Measurements

The measurements performed on each acceptable track were:[28] (1) projected length L', (2) dip d', and (3) projected angle α' with gamma-ray direction. The measurements were performed with the eye-piece scale, the fine focus scale, and the protractor eye-piece, respectively. Individual measurements could generally be repeated independently to within $\pm1\mu$, $\pm1\mu$, and $\pm2°$, respectively.

It was not always possible to decide uniquely on the length or sense of tracks. This was owing to the lowering of the quality of the tracks because of the dilution with D_2O and the slight fogging by gamma-rays. Out of all the tracks measured, 6 percent were uncertain in length and 20 percent uncertain in sense.

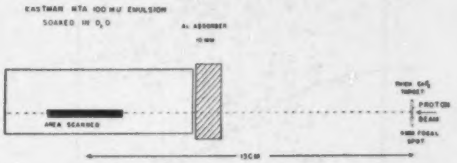

FIG. 1. Exposure geometry. The photographic emulsions were exposed in a horizontal plane with the long axis parallel to the proton beam direction. Two emulsions, one soaked in D_2O and one in H_2O, were exposed.

(B) Criteria for Acceptable Tracks

(1) The center of the track must lie within the field of view when detected.

(2) The track must have an "apparent" angle of dip $\beta'\leq11.8°$ in the developed emulsion. This corresponds to an "original angle of dip" of $\beta\leq40°$ in the wet emulsion.

(3) The track must not leave the emulsion.

(4) The track must not be scattered through an angle larger than 10° in the plane of the emulsion except where that scattering occurs close to one end of the track (i.e., within a segment about ⅓ the length of the track from one end).

Criterion (1) was adopted as it is independent of the sense of the tracks. Criterion (4) was adopted to eliminate tracks with large scattering angles. Their elimination was considered necessary because uncertainty in sense in such tracks would introduce a corresponding

§ *Note added in proof:*—Since the present paper was submitted for publication two further papers, dealing with the angular distribution of the $D^2(\gamma,n)H^1$ reaction by $F^{19}+H^1$ gamma-rays, have been published. Phillips, Lawson, and Kruger [Phys. Rev. **80**, 1069 (1950)] measured the angular distribution of photo-protons in a cloud chamber containing heavy methane (CD_4). Their experimental angular distribution curve indicates a comparable forward asymmetry but a smaller isotropic component than the present work. P. V. C. Hough [Phys. Rev. **80**, 1069 (1950)] performed an experiment very similar to the one reported here. Owing to his lower bombarding energy (E_p=1.1 Mev) the gamma-rays used consisted mainly of the 6-Mev line. Hough quotes an isotropic component of $a/b=0.02\ ^{+0.04}_{-0.02}$, which is smaller than the values found in the present work.

[25] G. Goldhaber, Phys. Rev. **74**, 1725 (1948).

[26] B. Hamermesh, Phys. Rev. **76**, 182A (1949); **80**, 131 (1950).

[27] P. K. S. Wang and M. Wiener, Phys. Rev. **76**, 1724 (1949).

[27a] The Eastman NTA emulsions are coated on a thin gelatin base (~5μ). This swells considerably on soaking in water. The uncertainty as to what fraction of K is due to the swelling of this gelatin base contributes strongly to the error in K.

[27b] In earlier experiments emulsions were placed in a vertical plane, but it was found that D_2O collected in the lower region of the emulsion owing to the action of gravity. This gave rise to a non-uniform D_2O concentration and presumably non-uniform stopping power and swelling.

[28] F. C. Champion and C. F. Powell, Proc. Roy. Soc. (London) **183**, 64 (1944–1945).

uncertainty in the angular distribution. The number of tracks eliminated on the basis of Criterion (4) amounted to 3 percent of the total number measured.

(C) Background

An area of 70 mm² was scanned on the D_2O emulsion, and a total of 1082 acceptable tracks were found. In the H_2O emulsion, $\frac{1}{4}$ of that area was scanned, and 24 tracks were found. All of the tracks found in the H_2O emulsion were less than 30 microns long, which is shorter than the range of the photo-protons from the

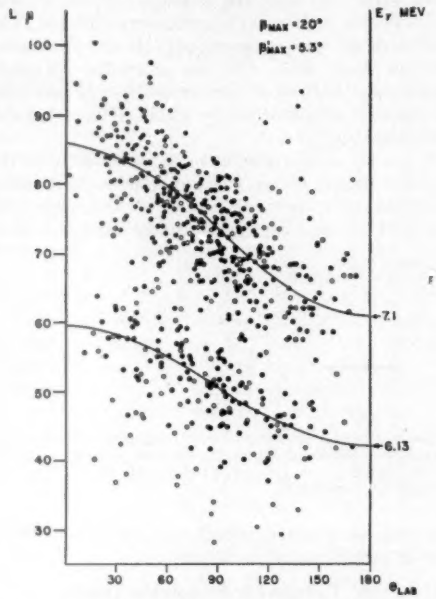

FIG. 2. All the tracks observed with $\beta \leq 20°$ are plotted on an L, θ_{lab} plot (607 tracks). L is the length of the tracks in microns and θ_{lab} the angle between the gamma-ray beam and the photo-proton. The two curves shown give the calculated positions of the photo-protons due to the 6.13- and 7.1-Mev gamma rays. Calibration point $E_\gamma = 6.13$ Mev. The full circles represent tracks about which the observers felt certain as to length and sense. The open circles represent tracks for which there was an uncertainty either in length or in sense. Note that the ordinate scale starts at 25μ.

6- and 7-Mev gamma-ray lines. It was thus possible to ascribe to background 60 tracks found in the D_2O emulsion of length less than 30 microns, leaving 1022 tracks due to the 6- and 7-Mev radiation.

IV. ANALYSIS OF TRACKS

(A) The Original Photo-Proton Tracks

On making the usual assumptions[28] that the emulsions shrink only in the z direction, one obtains L and θ_{lab}, the original length and angle coordinates of a track, from

$$\beta = \tan^{-1}(Kd'/L'), \quad L = L' \sec\beta, \quad \alpha = \alpha',$$
$$\cos\theta_{lab} = \cos\alpha \cos\beta.$$

Here the primed letters correspond to measurements in the developed (shrunk) emulsion and the unprimed letters correspond to the original values in the wet (D_2O) emulsion during exposure. L' is the projected length as measured, d' is the dip, α' is the projected angle with the gamma-ray direction, K the shrinkage factor ($K = 4 \pm 0.6$), and β is the original angle of dip.

(B) Correction for Tracks Leaving the Emulsion

The correction factor for the tracks found in the interval θ and $\theta + \Delta\theta$ is given by $[1 - f(E_\gamma, \theta)]^{-1}$, where $f(E_\gamma, \theta)$ is the fraction of tracks with $\beta \leq \beta_{max}$ (i.e., satisfying Criterion (2) for the acceptance of tracks) which leave the emulsion.

$$f(E_\gamma, \theta) = L(E_\gamma, \theta) \sin\theta (1 - \cos\gamma_m)/D\gamma_m,$$
$$\gamma_m = \pi/2 \text{ for } \theta \leq \beta_{max} \text{ and } \theta \geq \pi - \beta_{max}$$
$$= \sin^{-1}(\sin\beta_{max}/\sin\theta) \text{ for } \beta_{max} < \theta < \pi - \beta_{max}.$$

Here β_{max} is the maximum value of β (the angle of dip) considered in a particular analysis. γ_m is the angle obtained by projecting β_{max} onto the plane perpendicular to the gamma-ray beam. D is the thickness of the wet emulsion. $L(E_\gamma, \theta)$ is the average track length for a given gamma-ray line E_γ at the angle θ. This quantity is obtained from the experimental L, θ plot (Fig. 2).

(C) Conversion to Unit Solid Angle in the CM System

The factor for conversion to unit solid angle in the CM system is

$$(\Delta\Omega_{CM})^{-1} = (\Delta\Omega_{lab} d\Omega_{CM}/d\Omega_{lab})^{-1},$$

where $\Delta\Omega_{lab} = 4\gamma_m \langle \sin\theta_{lab} \rangle_{Av} \Delta\theta_{lab}$ and

$$d\Omega_{CM}/d\Omega_{lab} \approx 1 + E_\gamma \cos\theta_{lab} / [(E_\gamma - W)Mc^2]^{\frac{1}{2}} \times \cos(\theta_{CM} - \theta_{lab})$$
$$\approx 1 + E_\gamma \cos\theta_{lab} / [(E_\gamma - W)Mc^2]^{\frac{1}{2}}.$$

Here γ_m takes up the same values as above. $\langle \mathrm{Sin}\theta_{lab} \rangle_{Av}$ is the average value of $\sin\theta_{lab}$ in the interval $\Delta\theta_{lab}$. W is the binding energy of the deuteron and M is the proton mass. The factor $\cos(\theta_{CM} - \theta_{lab}) \approx 1$, as the maximum difference $\theta_{CM} - \theta_{lab} \approx 3°$ for the gamma-ray energies under consideration here.

V. THE SPECTRAL ANALYSIS

(A) The Analysis

For the spectral analysis only those tracks with $\beta \leq 20°$ were used (607 tracks). For these tracks the number of tracks uncertain in sense or length was percentagewise less than for the tracks with larger angles of dip. Also, the error in K, the shrinkage factor, is of smaller importance. A plot of the raw data is shown in Fig. 2. It can be seen that the points fall into two

distinct groups corresponding to the 6- and 7-Mev gamma-rays from the $F^{19}+H^1$ reaction.[17-19] The curves of equal gamma-ray energy were constructed by calculating E_p', the photo-proton energy,[28a] and then converting E_p' into R_p', the photo-proton range in air, by using the range-energy curves given by Livingston and Bethe.[29] The 6.13-Mev gamma-ray was then used as a calibration point, which gave a relative stopping power for the wet emulsion of $S=1350$. This value is 28 percent lower than the value given by Webb[30] for dry Eastman emulsions. The variation of the relative stopping power with energy over the photo-proton energies under consideration was neglected.

The spectrum (Fig. 3) was then obtained by counting the number of tracks lying between two such equi-energetic curves, drawn at intervals $\Delta E_\gamma=0.1$ Mev apart. In Fig. 2, for clarity only two such curves are shown. In the correction factor for tracks leaving the emulsion, no θ dependence enters in for the spectral analysis. The factor then becomes $[1-f(E_\gamma)]^{-1}$, where

$$f(E_\gamma)=L(E_\gamma)(1-\cos\beta_{\max})/D\beta_{\max}.$$

Here $L(E_\gamma)$ is the average range in the wet emulsion of photo-protons corresponding to the gamma-ray energy E_γ. D is the thickness of the wet emulsion and $\beta_{\max}$ is the maximum original angle of dip accepted in this analysis, *viz.*, $\beta_{\max}=20°$.

(B) The Gamma-Ray Energies and Relative Intensities

An energy of 7.1 ± 0.1 Mev was found for the energy of the 7-Mev line from $F^{19}+H^1$ when 6.13 Mev[17-19] was used as the energy of the 6-Mev line in the calibration of the photo-proton range in the wet (D_2O) emulsion. No splitting of the 7-Mev line[20,21] could be observed with the resolution obtained here. The intensity ratio observed for the two gamma-ray yields (in the forward direction, for $E_p=2.6$ Mev, on a thick CaF_2 target) gives:[30a]

$$I(7)\sigma_{ph}(7)/I(6)\sigma_{ph}(6)=2.2\pm0.2,$$

where $I(E_\gamma)$ is the intensity of the gamma-ray of energy E_γ and $\sigma_{ph}(E_\gamma)$ is the cross section for photo-disintegration. A probable upper limit for the intensity of the 13-Mev gamma-ray from the $F^{19}(p,\gamma)Ne^{20}$ reaction can also be estimated.[31] As not a single track was found that could be ascribed to that reaction, it is concluded that there is a 50:50 chance that

$$I(13)/I(6 \text{ and } 7)<0.002 \text{ at } E_p=2.6 \text{ Mev},$$

for a thick CaF_2 target. Here use was made of the variation of σ_{ph} with energy as measured by Fuller.[9]

[28a] $E_p'\approx\frac{1}{2}(E_\gamma-W)+\frac{1}{2}E_\gamma\cos\theta[(E-W)/Mc^2]^{\frac{1}{2}}$.
[29] M. S. Livingston and H. A. Bethe, Revs. Modern Phys. **9**, 268 (1937).
[30] J. H. Webb, Phys. Rev. **74**, 511 (1948).
[30a] This value differs appreciably from the estimate given earlier (reference 25) by the author, based on only 109 tracks.
[31] S. Devons and H. G. Hereward, Nature **162**, 331 (1948).

VI. ANGULAR DISTRIBUTION

(A) The Analysis

The angular distribution analysis was performed for the 6-Mev, the 7-Mev, and the 6- and 7-Mev radiation combined for various values of $\beta_{\max}$, the maximum angle of dip accepted in an analysis of the data. As the number of tracks uncertain in sense increased with increasing β, only the data with $\beta\leq30°$ was used in an analysis of the form $[a+b\sin^2\theta(1+\kappa\cos\theta)]$. For $\beta\leq30°$ (849 tracks) the number of tracks uncertain in sense amounted to 18 percent. The total data $\beta\leq40°$ (1022 tracks) was used in an analysis of the form $(a+b\sin^2\theta)$.

The analysis of the tracks with $\beta\leq30°$ is shown in Figs. 4 and 5. The histograms represent the experimental angular distribution. The circles represent the angular distribution corrected for tracks leaving the emulsion and converted to unit solid angle in the CM system, plotted against θ_{CM}. The full and dotted curves

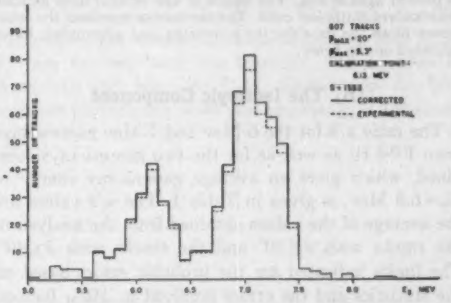

FIG. 3. The spectral distribution of the gamma-rays. The experimental histogram and the histogram corrected for tracks leaving the emulsion are shown. Using $E_\gamma=6.13$ Mev as a calibration point $E_\gamma=7.1\pm0.1$ Mev is the value obtained for the 7-Mev gamma-ray from $F^{19}+H^1$.

represent the least-square fit in the forms $[a+b\sin^2\theta\times(1+\kappa\cos\theta)]$ and $(a+b\sin^2\theta)$, respectively.

To carry out the $(a+b\sin^2\theta)$ analysis on the total data ($\beta\leq40°$), the experimental data was first folded around 90° lab; correction was made for tracks leaving; the conversion to unit solid angle (lab) was then performed; and the results was plotted against $\sin^2\theta$ (Fig. 6). In this fashion any asymmetry of the form $(1+\kappa\cos\theta)$ cancels out. Also, as has been pointed out by Hansson and Hulthén,[32] the $\theta_{lab}\rightarrow\theta_{CM}$ shift and the CM solid angle factor have no appreciable effect when the experimental angular distribution is folded around 90°. The result of such an analysis is a straight line whose intercept with the abscissa gives $-a/b$.

The separation into the 6- and 7-Mev lines for $\beta\leq40°$ could be made with an uncertainty of about 20 tracks. This contributes to the larger uncertainty in the a/b value for the 6- and 7-Mev radiation separately.

[32] I. F. E. Hansson and L. Hulthén, Phys. Rev. **76**, 1163 (1949).

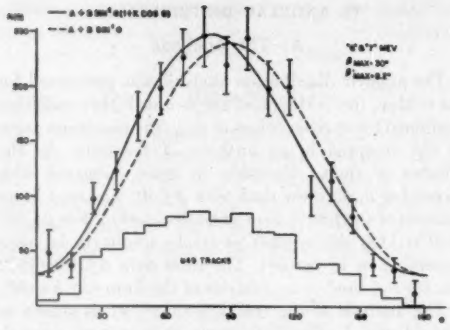

FIG. 4. The histogram represents the experimental angular distribution for the 6- and 7-Mev gamma-rays combined and $\beta \leq 30°$. $N(\theta)$ is the number of tracks observed per 10° interval as plotted against θ_{lab}. The circles represent the angular distribution corrected for tracks leaving the emulsion per unit solid angle in the CM system as plotted against θ_{CM}. $N(\theta)$ thus corresponds in this case to the number of tracks per unit solid angle in the CM system as plotted against θ_{CM}. The length of the vertical lines indicate the standard statistical error. The two curves represent the least-square fit to the data for the symmetric and asymmetric forms indicated on the figure.

(B) The Isotropic Component

The ratio a/b for the 6-Mev and 7-Mev gamma-rays from $F^{19}+H^1$ as well as for the two gamma-rays combined, which gives an average gamma-ray energy of $E_\gamma = 6.8$ Mev, is given in Table I. The a/b values are the average of the values obtained from the analysis of the tracks with $\beta \leq 30°$ and the tracks with $\beta \leq 40°$. The limits indicated are the probable errors based on the statistics and the errors involved in $\Delta\Omega_{CM}$ factors.

To check the internal consistency of the a/b values,

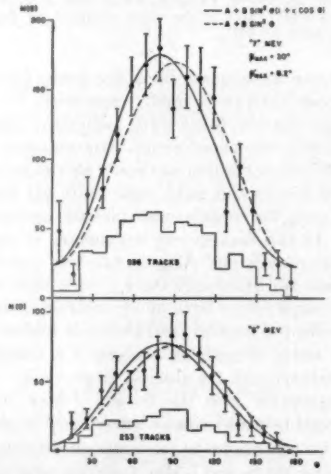

FIG. 5. The same as Fig. 4, except that the 6- and 7-Mev gamma-ray lines are here shown plotted separately.

analyses were made, for the 6- and 7-Mev radiation combined, of the following parts of the complete data: the data of each observer separately; all the tracks in the left-hand and right-hand quadrant separately; all the tracks with $\beta_{max} = 10°, 20°, 30°, 40°$ separately. In each of these analyses the value of a/b obtained fell within ± 0.03 of the value 0.15 as given in Table I. These internal consistency checks would not of course exclude other possible systematic errors.

From theoretical considerations the isotropic term is composed of two separate components. These are, (1) the magnetic transitions to the final S state, and

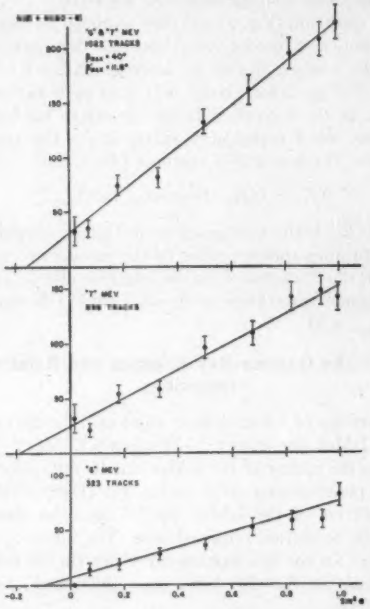

FIG. 6. In the construction of this figure the experimental angular distribution for $\beta \leq 40°$ was folded around an axis at 90°. Corrections for tracks leaving the emulsion and conversion to unit solid angle in the lab system were then carried out. The conversion factor to unit solid angle was here so chosen that $N(\theta)+N(180°-\theta)$ represents the average number of tracks at θ and $180°-\theta$ per unit solid angle (lab). In such a plot the intercept with the abscissa is equal to $-a/b$.

(2) a contribution from the interference among the final ^3P_J states. These two components are additive.

The magnetic transitions, which give rise to σ_m the magnetic cross section for photo-disintegration, have been dealt with fairly extensively in the recent literature. Hansson and Hulthen[22] calculated values for σ_m and σ_e, the electric cross section for photo-disintegration at $E_\gamma = 6.2$ Mev for various theoretical assumptions. Bethe and Longmire[23] give formulas for σ_m and σ_e which hold at low gamma-ray energies. One can then compute

[23] H. A. Bethe and C. Longmire, Phys. Rev. 77. 647 (1950).

$(a/b)_{mag}$ from

$$\sigma_m/(\tfrac{3}{2}\sigma_e+\sigma_m)=[\sigma(0)/\sigma(\tfrac{1}{2}\pi)]_{CM}=a/(a+b),$$

and the result in both cases is approximately[34] $(a/b)_{mag}=0.02$.

For the component due to the ^3P_J state interference, which is characteristic of the presence of a noncentral nuclear interaction, it is difficult to make a reasonable estimate, inasmuch as the detailed nature of the P state interaction potential is currently unsettled. Rough estimates[35] based on current theories[36–38] indicate that $(a/b)_{exp}-(a/b)_{mag}$ is larger than can be explained on such a basis.

(C) The Asymmetry Effect

For the 7-Mev radiation and for the 6- and 7-Mev radiation combined, the experimental points give a closer fit to the asymmetric curve $[a+b\sin^2\theta(1+\kappa\cos\theta)]$ than to the symmetric curve $(a+b\sin^2\theta)$ (Figs. 4 and 5). As 18 percent of the tracks with $\beta\leq 30°$ are uncertain in sense, only an estimate of κ, the asymmetry coefficient, can be given. The value obtained from the direct analysis of the 6- and 7-Mev radiation combined (Fig. 4) is $\kappa=0.4$. Similar analyses were carried out in which all the tracks uncertain in sense were shifted from the interval $0°\leq\theta_{CM}\leq 90°$ to the interval $90°\leq\theta_{CM}\leq 180°$ and vice versa. Under such circumstances κ can be made to vary between $0.1<\kappa<0.6$. κ was thus estimated as $\kappa=0.4^{+0.2}_{-0.3}$. The lower limit of uncertainty is just compatible with the theoretical value $\kappa_{th}=2\beta=0.14$ for $E_\gamma=6.8$ Mev, the average gamma-ray energy.

TABLE I. Values of a/b where the angular distribution of photo-protons is given by $[a+b\sin^2\theta(1+\kappa\cos\theta)]$.

E_γ(Mev)	6	7	6 and 7
a/b	0.09±0.07	0.17±0.07	0.15±0.06

The author is greatly indebted to Professor H. T. Richards for his guidance and continued interest in this work. Thanks are also due to Mr. N. Austern for discussions on the theoretical implications, to Mr. E. D. Berners for help with the scanning, and to Miss F. Ajzenberg and Mrs. M. J. W. Laubenstein for help with the preparatory work and processing of the emulsions.

[34] This number is probably increased by 10 percent, as is found to be implied by the magnetic moment anomaly of the three-body system. N. Austern and R. G. Sachs, Phys. Rev. 81, 710 (1951).
[35] N. Austern (private communication).
[36] W. Rarita and J. Schwinger, Phys. Rev. 59, 436, 556 (1941).
[37] T. M. Hu and H. S. W. Massey, Proc. Roy. Soc. (London) 196, 135 (1949).
[38] R. S. Christian and E. W. Hart, Phys. Rev. 77, 441 (1950).

Renormalization of Neutral Mesons in Three-Field Problems

P. T. MATTHEWS
Institute for Advanced Study, Princeton, New Jersey
(Received October 27, 1950)

It is shown that a finite S-matrix can be obtained to low orders by renormalization if neutral spin zero mesons with (pseudo) scalar coupling are added to the mixture of nucleons, photons, and charged spin zero mesons previously considered, provided that a limited number of contact interactions are introduced. A general proof for any order is not given; but it is shown that at no stage can divergences of a new form appear, requiring the introduction of additional contact terms.

Renormalization certainly fails for the pseudovector interaction and the possibility of defining a finite S-matrix, formally, with the use of regulators, is considered. It is shown that it is not possible to do this in a manner which is both self-consistent and consistent with the renormalization of the pseudoscalar coupling. This result is related to the "ambiguities" found in the calculation of three-field problems with the use of regulators only, and is illustrated in the appendix by a detailed discussion of the two-photon decay of a neutral spin zero meson. It is concluded that cross sections for interactions, for which renormalization is inadequate, can certainly not be calculated in this manner, and that if, in fact, such theories have any meaning, it must be possible to remove the divergences in a more fundamental way.

I. INTRODUCTION

IT has already been shown[1,2] that, at least to fourth order in the coupling constants, a finite S-matrix can be obtained by renormalization for the combined interactions of nucleons, photons, and charged spin zero mesons with (pseudo) scalar coupling. For any interaction involving mesons it is necessary to introduce a direct interaction between four mesons in order to cancel the divergences arising from scattering of mesons by mesons.[3] No additional contact term is required for the above three-field mixture where the mesons are charged. The problem is complicated in higher orders by secondary infinities from the contact interaction[1] and the "overlapping" of divergences.[4] However, these problems have now been solved in detail by Salam[5] for the interactions of the separate pairs of fields, and there is reason to believe that the S-matrix for the above charged meson mixture is also finite to any order after renormalization.

In view of the very definite experimental evidence[6] for neutral spin zero mesons, it is of interest to consider what modifications are required if neutral mesons are included in the above mixture with (pseudo) scalar coupling.[7] It is found that the number of possible types of primitive divergent is again strictly limited. For pseudoscalar mesons it is necessary to introduce two extra contact terms coupling four mesons, and for scalar mesons three more contact terms coupling three mesons. No divergences of any new form can ever appear in the calculations requiring the introduction of still further contact terms.

The difficulties of secondary infinities from the four-meson contact terms are the same as in the charged meson mixture. The three-meson terms are particularly innocuous in this respect, giving rise to only one divergent self-energy graph.[8] Thus, the introduction of neutral spin zero mesons with (pseudo) scalar coupling introduces no essentially new difficulty into the three-field renormalization problem, and it is again probable that a finite S-matrix can be defined up to any order.

The method of renormalization can certainly not be applied if pseudovector coupling is assumed.[3] It is here shown, further, that it is not even possible to define a finite S-matrix for this coupling by the formal use of regulators[8,10] in a manner which is both self-consistent and consistent with the renormalization of the pseudoscalar coupling. This is discussed in relation to the three-field calculations of Ozaki, Onenda, and Sasaki[11] and of Fukuda, Miyamoto, and Hayakawa[12] (to be referred to as OOS and FMH, respectively). These authors applied regulators, formally, to both pseudoscalar and pseudovector coupling and found "ambiguities" in their results for meson decay life times. These calculations can now be separated into those which are equivalent to renormalization (and thus have a reasonable theoretical basis) and those which are definitely inconsistent with it and quite without foundation. This point is illustrated in the appendix, where the two-photon decay of a neutral pseudoscalar meson is considered in detail. For this process the two possible couplings are equivalent to lowest order, and regularization must not disturb this equivalence. With this

[1] P. T. Matthews, Phys. Rev. **80**, 292 (1950). It is hoped to publish elsewhere a more detailed account of this work.
[2] A. Salam, Phys. Rev. **79**, 910 (1950).
[3] P. T. Matthews, Phil. Mag. **41**, 185 (1950); Phys. Rev. **80**, 292 (1950). F. Rohrlich, Phys. Rev. **80**, 666 (1950).
[4] F. J. Dyson, Phys. Rev. **76**, 1736 (1949), §VII.
[5] A. Salam (to be published). Salam has treated the case when the contact interaction just cancels the divergences and no "real" contact interaction is allowed for.
[6] Steinberger, Panofsky, and Steller, Phys. Rev. **78**, 802 (1950). References to further experimental evidence are given in this paper.
[7] Particular calculations have been made in this frame work by K. M. Case, Phys. Rev. **76**, 1 (1949), and K. A. Brueckner, Phys. Rev. **79**, 641 (1950).
[8] J. C. Ward, Phys. Rev. **79**, 406 (1950).
[9] W. Pauli and F. Villars, Revs. Modern Phys. **21**, 434 (1949).
[10] J. Steinberger, Phys. Rev. **76**, 1180 (1949).
[11] Ozaki, Onenda, and Sasaki, Prog. Theor. Phys. **4**, 524 (1949); **5**, 25, 165, 373 (1950). Also Y. Katayama, Prog. Theor. Phys. **5**, 272 (1950).
[12] H. Fukuda and Y. Miyamoto, Prog. Theor. Phys. **4**, 347, 392 (1949). Fukuda, Miyamoto, and Hayakawa, Prog. Theor. Phys. **5**, 283, 352 (1950). Also a joint paper by Tomonaga, *et al.*, Prog. Theor. Phys. **4**, 477 (1949).

condition, there are two ways in which regulators can be applied. One of these is rejected because it would not lead to a finite S-matrix for the pseudovector coupling and the other because it removes finite gauge invariant terms, in contradiction to the renormalization of the pseudoscalar coupling.

II. RENORMALIZATION

The hamiltonian for the three-field mixture with the addition of neutral pseudoscalar mesons with pseudoscalar coupling is the same as that considered in reference 1 with the addition of a term H_4, where

$$H_4=i\bar{\psi}\gamma_5(g_1\tau_P+g_2\tau_N)\psi\phi', \tag{1}$$

and ϕ' is the neutral meson potential ($\phi'(x)$ real). (Scalar mesons are obtained by replacing $(\gamma_5)_{\alpha\beta}$ by $-i\delta_{\alpha\beta}$.)

This introduces two new types of vertex with one neutral meson line and either two neutron or two proton lines (to be referred to as neutron and proton vertices, respectively).

If the number of external neutral meson lines is E_m', the condition for primitive divergents is found by Dyson's[4] method to be

$$\tfrac{3}{2}E_n+E_p+E_m+E_m'<5. \tag{2}$$

Any graph with $E_n=E_m=0$, and E_p odd, is excluded by Furry's theorem.[13] The only remaining new primitive divergents (apart from self-energy and vertex parts to be considered below) are (i) $E_p=1$, $E_m'=1$, $E_m=2$; (ii) $E_p=2$, $E_m'=1$; (iii) $E_p=2$, $E_m'=2$; (iv) $E_m'=3$; (v) $E_m'=1$, $E_m=2$; (vi) $E_m'=4$; (vii) $E_m'=2$, $E_m=2$.

Graphs of type (i) are at most logarithmically divergent; but from considerations of invariance the whole expression is a vector. Since the leading term cannot be a vector, it must vanish identically and the contribution from such graphs is convergent.

Graphs of type (ii) give the decay of a neutral meson into two photons. This process has been observed[6] and has been considered in low orders by Steinberger,[10] by Fukuda and Miyamoto,[12] and by OOS.[11] From considerations of invariance the integral must be expressible in the form (k_1 and k_2 are momentum vectors of the photons)

$$D\delta_{\mu\nu}+(k_{1\lambda}k_{2\lambda}-k_{1\mu}k_{2\nu})E+k_{1\mu}k_{2\nu}F \\ +\epsilon_{\mu\nu\sigma\rho}k_{1\sigma}k_{2\rho}G+\text{conv. integral},$$

where D may be infinite, but E, F, and G are finite constants; but for gauge invariance to be satisfied D must be zero,[14] (The terms in E, F, and G have been chosen to satisfy gauge invariance), and the integral converges.

Type (iii) is another possible real process which is potentially logarithmically divergent. The leading term $A\delta_{\mu\nu}$ can be separated off by putting the photon momenta zero and the meson momenta equal and satisfying the free field equation. For gauge invariance A is identically zero,[15] and again all integrals from such graphs converge.

If the neutral mesons are pseudoscalar, graphs of types (iv) or (v) are excluded by a "Lorentz invariant" type of selection rule as introduced by FMH.[16] No such argument is applicable for scalar mesons and in this case genuine divergences occur. These must be cancelled by the introduction of two more direct interaction terms,

$$\chi_1\phi'^2+\chi_2\phi^*\phi\phi',$$

where χ_1 and χ_2 are infinite constants, so chosen as to cancel the infinite contributions from the graphs, and leave a finite matrix element in agreement with the experimental value, given by the scattering of mesons in an external meson field. The only secondary divergence introduced by the inclusion of the χ-terms is a single self-energy part.[8] The infinite terms may be absorbed in the mass and "charge" renormalizations *after* the cancellation of the infinities from the three meson parts of the χ-terms.

The last two types, (vi) and (vii), are new forms for the scattering of mesons by mesons, which give rise to genuine divergences. They must be cancelled by the introduction of direct interactions $\lambda_1\phi^*\phi\phi^2$ and $\lambda_2\phi^4$, where the infinite constants λ can be chosen to give agreement with experiment.[17] They introduce difficulties of secondary infinities similar to those for separate pairs of fields.[5]

It remains to be seen what renormalizations of the coupling constants are necessary to remove infinities from self-energy and vertex parts. The proton and neutron self-energy parts are each modified by virtual neutral mesons. The charged meson vertex parts are also modified, but from any such part with the proton entering (τ_- vertex) a corresponding part with the neutron entering (τ_+ vertex) can be obtained by reversing all arrows in the graph. Thus, the same infinities are associated with both τ_+ and τ_- vertices. Since with both such vertices are associated half a proton and half a neutron line, the same renormalization is applicable to both, as required by the single coupling constant f.

For renormalization, the neutron vertex of a neutral meson is associated with a neutron line, the proton vertex with a proton line. Further, there is no one-to-one correspondence between neutron vertex parts and proton vertex parts. The possibility that these two discrepancies cancel, leading to the same infinite con-

[13] W. Furry, Phys. Rev. **51**, 125 (1937).

[14] For scalar mesons D does not vanish on account of γ-factors, but from symmetry considerations employed by Schwinger for the photon self-energy. J. Schwinger, Phys. Rev. **6**, 790 (1949).

[15] This can also be proved by the method due to Ward, since $A\delta_{\mu\nu}$ can be expressed as the integral of a double derivative of a neutral meson self-energy. J. C. Ward, Phys. Rev. **77**, 293 (1950).

[16] An explicit proof due to F. J. Dyson is to be published in a paper by A. Salam.

[17] The constant is taken to be $\lambda=\lambda'+\delta\lambda(\lambda', e, f, g)$ where λ' is independent of e, f, and g and chosen to fit experiment, and $\delta\lambda$ is chosen to cancel divergences.

stants for both vertices, can be ruled out by considering the terms dependent on e^3. Thus different renormalizations are required for the two constants g_1 and g_2.[18]

Summarizing, to obtain a finite S-matrix by renormalization for the interaction of nucleons, photons, and charged spinless mesons with (pseudo) scalar coupling the interaction must involve the three constants e, f, and λ. If the mesons are pseudoscalar and neutral pseudoscalar mesons are also included, it is necessary to introduce the constants e, f, g_1, g_2, λ, λ_1, and λ_2. If all the mesons are scalar, then the additional constants χ_1 and χ_2 are also certainly necessary for a finite theory. The renormalized value of all these constants can (theoretically) be determined by experiment.

With this scheme a finite S-matrix can certainly be obtained by renormalization to fourth order in the "charges" e, f, and g. In higher orders the problem is complicated by the overlapping of divergences[4] and the secondary infinities arising from the contact terms.[1] A general proof has not yet been given that renormalization can be carried out consistently to any order. However, it has been shown here that at no stage can divergences of a new form appear in the theory, involving the necessity of introducing any additional constants.

Finally we remark that it would be possible to include the electron-positron field coupled to the electromagnetic field with the same renormalization of the constant e.[19] It would also be possible to add neutral vector mesons with vector coupling and to remove all additional divergences by a renormalization of the single new coupling constant.[20] If any other type of particle or coupling were included, Dyson's method sets no limit on the possible types of primitive divergent[21] and renormalization certainly fails to define a finite S-matrix. (We have not considered here the possibility of mixing meson fields with relations between the coupling constants.)

III. REGULARIZATION AND "AMBIGUITIES"

The clear distinction between meson theories for which renormalization is effective and those for which it is not provides a criterion for settling the "ambiguities" which have been met by OOS[11] and by FMH[12] in the calculation of meson decay lifetimes.

In applying renormalization, the theory is always set up in gauge invariant form; and the condition that the resulting S-matrix elements must be gauge invariant is used to *define* the values of certain integrals, which would otherwise be ambiguous owing to the singularities of the Δ-functions at the origin. A detailed evaluation of these integrals is then correct only if it yields a result consistent with this definition. In practice, it is often found that the required result is obtained because the γ-factors of potentially divergent terms vanish identically (as for the scattering of light-by-light); but in other cases the correct result is only derived by making full use of the symmetry properties of the Δ-functions inherent in their general definitions.[22] This has been illustrated by the calculations of the photon self-energy by Schwinger[14] and Wentzel.[23] "Making full use of symmetry properties" is not a very well-defined mathematical process in momentum space, and in order to make the procedure more precise the ambiguous integrals can be defined by the regulators of Pauli and Villars.[9] This is a purely formal procedure in agreement with renormalization for any theory to which renormalization is applicable.

Now the procedure of regularization has been extended by Steinberger[10] to determine a finite S-matrix for *any* of the standard meson interactions by imposing just six conditions on the subsidiary fictitious masses which are introduced. However, these extended theories are purely formal, as demonstrated by Pais and Uhlenbeck;[24] and there is really no reason to believe them to be correct. Renormalization, on the other hand, has a sound (though not rigorous) theoretical basis and for electrodynamics is in very good agreement with experiment. Thus, it would seem that if a conflict should arise between a renormalized and a regularized theory, it is certainly the latter which should either be modified or possibly discarded

This is precisely the situation with the pseudoscalar and pseudovector interactions of pseudoscalar mesons. The former can be renormalized; the latter is finite only when regularized; but the two theories can be shown to be equivalent for certain effects in low orders.[25] If the coupling constants are taken to be the same for both couplings, the equivalence theorem, when it is valid, has the form

$$[pv] = -2\kappa_0[ps], \tag{3}$$

where $[ps]$ and $[pv]$ are the S-matrix elements and κ_0 is the nucleon reciprocal Compton wavelength. The difficulty arises because of the term κ_0 in Eq. (3). If the equivalence theorem is to be maintained, one must either

(A) apply Steinberger's conditions to $\kappa_0[ps]$ and $[pv]$

or

(B) apply Steinberger's conditions to $[ps]$ and $[pv]/\kappa_0$.

These alternatives were suggested by OOS,[11] who have calculated according to (A); but this is not equivalent

[18] If electromagnetic effects are excluded, the interaction of nucleons with both charged and neutral spin zero mesons can be expressed in Kemmer's symmetric form with a single coupling constant g and one λ- and one χ-term; but this breaks down when the photon field is included. N. Kemmer, Proc. Cambridge Phil. Soc. **34**, 354 (1938).

[19] A particular calculation with this combination of fields has been made by M. N. Rosenbluth, Phys. Rev. **79**, 615 (1950).

[20] P. T. Matthews, Phys. Rev. **76**, 1254 (1949).

[21] P. T. Matthews, Phil. Mag. **41**, 185 (1950).

[22] J. Schwinger, Phys. Rev. **75**, 1439 (1948).

[23] G. Wentzel, Phys. Rev. **74**, 1070 (1948).

[24] A. Pais and G. E. Uhlenbeck, Phys. Rev. **79**, 145 (1950).

[25] F. J. Dyson, Phys. Rev. **73**, 929 (1948). K. M. Case, Phys. Rev. **76**, 14 (1949).

to the renormalization of the pseudoscalar coupling and is ruled out by the criterion developed above. (It has the effect of dropping finite and gauge invariant terms through the new condition $\Sigma C_i/\kappa_i=0$ on $[ps]$.)

Alternative (B) is equally unsatisfactory because, when applied in general to the pseudovector coupling, it will not give a finite S matrix (since effectively the condition $\Sigma C_i=0$ has now been removed).

There remains the third possibility of abandoning the equivalence theorem and applying Steinberger's conditions to both $[ps]$ and $[pv]$. This is the procedure which has been followed by FMH,[12] but it is equally objectionable as (A) or (B) because the equivalence theorem is based on the evaluation of integrals by using just those symmetry properties of the Δ-functions which have given the correct values (that is, in accordance with gauge invariance) for renormalized theories. It is quite unreasonable to accept this method of calculation in one case and reject it in another.

Thus, we can say that when renormalization is applicable, it leads to unique results. There is no way consistent with renormalization of extending the formal procedure of regularization to theories to which renormalization is not applicable. The only self-consistent application of regularization to all theories, (A), is incompatible with renormalization and has the effect of removing finite and gauge invariant terms.

We conclude that a formal extension of regularization definitely fails for interactions which cannot be renormalized If, in fact, such theories have any physical significance, it must be possible to remove the divergences from the S-matrix in a more fundamental way.

The author is indebted to Professor J. R. Oppenheimer for several helpful discussions, and also for extending to him the hospitality of the Institute for Advanced Study, where this work was done.

APPENDIX

The decay of a neutral pseudoscalar meson into two photons (k_1, μ) and (k_2, ν) is here discussed in detail. For pseudovector coupling the matrix element is

$$[pv]=(-i/2\hbar c)^3\int dx_1dx_2dx_3 Tr[\gamma_5\gamma_\rho S_F(x_1-x_2) \times\gamma_\mu S_F(x_2-x_3)\gamma_\nu S_F(x_3-x_1)]A_\mu(x_2)A_\nu(x_3)d\phi(x_1)/dx_{1\rho}. \quad (4)$$

Integration by parts with respect to x_1 and use of the relation

$$\gamma_\mu\partial S_F(x)/\partial x_\mu=\kappa_0 S_F(x)-2i\delta(x), \quad (5)$$

yields

$$[pv]=-2\kappa_0[ps]+2i(-i/2\hbar c)^3\int dx_2dx_3 \times\{Tr[\gamma_5\gamma_\mu S_F(x_1-x_2)\gamma_\nu S_F(x_3-x_1)] +Tr[\gamma_5 S_F(x_1-x_2)\gamma_\mu S_F(x_2-x_3)\gamma_\nu]\}. \quad (6)$$

For the equivalence theorem to be valid for this problem, it must be shown that the terms arising from the δ-function in Eq. (5) vanish. (In Case's[25] proof of the equivalence theorem it is assumed tacitly that the nucleons are free and these terms are not considered.) Using the symmetry property, $\Delta_F(x)=\Delta_F(-x)$ and noticing that only the γ-dependent terms of the S_F factors give a non-zero trace,

$$Tr[\gamma_5\gamma_\mu S_F(x_1-x_2)\gamma_\nu S_F(x_3-x_1)] =-Tr[\gamma_5\gamma_\mu\gamma_\alpha\gamma_\nu\gamma_\beta]\partial\Delta_F(x_1-x_2)\partial\Delta_F(x_1-x_3)/\partial x_{1\alpha}\partial x_{1\beta}. \quad (7)$$

This can be shown to vanish identically by interchanging the suffixes α and β. The final term vanishes similarly, thus proving the validity of the equivalence theorem for this effect. (Similar proofs have been given OOS[10] and FMH.[11])

The physically significant term $[ps]$ has been calculated by Steinberger.[10] It is potentially logarithmically divergent, but is in fact, absolutely convergent in accordance with gauge invariance.

It is of interest to consider the two vanishing terms in momentum space, because it is through them that the so called "ambiguities" arise. The first is easily shown to be proportional to

$$\int d^4p\frac{Tr[\gamma_5\gamma_\alpha\gamma_\beta\gamma_\mu\gamma_\nu]p_\beta k_{2\alpha}}{[(p+k_2/2)^2+\kappa_0^2][(p-k_2/2)^2+\kappa_0^2]^2} \quad (8)$$

which is the form given by Steinberger.[10] Using Feynman's identity[26]

$$1/ab=\int_0^1 dx/[(a-b)x+b], \quad (9)$$

and making the transformation

$$p=q+k(\tfrac{1}{2}-x),$$

the integral reduces to

$$-\tfrac{1}{2}k_{2\alpha}k_{1\beta}\int d^4q\int_0^1 dx(2x-1)/[k_1^2(x^2-x)-q^2-\kappa_0^2]^3, \quad (10)$$

which vanishes identically when integrated over x, in accordance with calculation in configuration space. A similar calculation shows that the third term also vanishes. Thus, $[ps]$ is the unique result given by renormalization, consistent with gauge invariance and the equivalence theorem.

The same result would have been obtained for pseudoscalar coupling by regularization, but it is not possible to introduce regulators for pseudoscalar and pseudovector coupling without inconsistences. Alternative (A), used by OOS,[11] would remove finite and gauge invariant terms from $[ps]$. Alternative (B) would give the above result for this effect but would not, in general, give a finite S-matrix for pseudovector coupling.[27] The other possibility is to apply Steinberger's conditions separately to pseudoscalar and pseudovector coupling so that the same integrals are evaluated differently for the two cases. This was done by Steinberger[10] and FMH,[12] both stressing the inconsistency of their method. (These calculations are in agreement, however, with renormalization for pseudoscalar coupling.)[28]

---

[26] R. P. Feynman, Phys. Rev. **76**, 769 (1949).

[27] Note that (B) is really not even sufficient for the present problem, because the condition $\Sigma C_i=0$ on $[pv]$ (excluded by (B)), is required to make the integral in Eq. (6) definitely zero, if no symmetry arguments are used and one relies on regulators alone to evaluate ambiguous integrals.

[28] After the completion of this work, a method of calculation equivalent to a much more fundamental introduction of regulators was given by Schwinger. In its application to the meson—two-photon decay problem Schwinger, in effect, regularized according to (B). As stated in the text, this does not, in general, lead to a finite S-matrix for pseudovector coupling, because one of the required conditions is missing. This shows itself in Schwinger's calculation in that the "regulators" operate effectively on the partial derivative of $[pv]$ and the integrated terms [corresponding exactly to the integral in Eq. (6)], must be removed by what is essentially a symmetry argument as described in footnote 27 (J. Schwinger, Physics Seminar, Institute for Advanced Study, Princeton, October 17, 1950).

The Nuclear Spins and Quadrupole Moments of Stable Germanium Isotopes*

J. M. Mays† and C. H. Townes
Columbia University, New York, New York

(Received November 24, 1950)

Analysis of the hyperfine structure of spectral lines arising from the $J=0\rightarrow1$ rotational transition of GeH_3Cl allows the assignment of zero spin to the nuclei of Ge^{70}, Ge^{72}, Ge^{74}, and Ge^{76}, and a spin of 9/2 to Ge^{73}. The nuclear quadrupole moment of Ge^{73} is determined to be $(-0.2\pm0.1)\times10^{-24}$ cm².

I. INTRODUCTION

In earlier measurements[1] of the $J=2\rightarrow3$ rotational transition of GeH_3Cl the hyperfine structure of the lines due to molecules containing Ge^{73} indicated a sizable nuclear quadrupole moment for this isotope. Hyperfine structure of this transition (near 26,000 Mc/sec) is rather complex because both Ge^{73} and the Cl nuclei show quadrupole coupling, and spectra for $K=0$, 1, and 2 are superimposed. Consequently, the considerably simpler transition $J=0\rightarrow1$ in the 9000-Mc/sec region was studied in order to obtain the Ge^{73} spin and quadrupole coupling. The results obtained and methods used are described here more fully than in a previous brief report.[2]

II. PROCEDURE

Absorption lines due to the $J=0\rightarrow1$ transition were plotted by a recording Stark spectrometer. A curve for the various germanium isotopes in GeH_3Cl^{35} is shown in Fig. 1. The three hyperfine lines of all even isotopes are due to the Cl^{35} nuclear quadrupole. For Ge^{73}, the hyperfine structure is partly due to the Ge^{73} quadrupole, and is more complex. Although Ge^{73} is somewhat more abundant than Ge^{76}, only a few lines due to Ge^{73} are visible in Fig. 1, because of the complexity of hyperfine structure for this isotope. A greater amplification than that of Fig. 1 is necessary to make most of the $Ge^{73}H_3Cl$ lines visible.

Frequencies of the Ge^{73} lines were obtained from values of the rotational and quadrupole coupling constants for the even Ge isotopes measured in the $J=2\rightarrow3$ transition and by assuming the spectrometer sweep to be linear over small frequency changes. A number of measurements of each $Ge^{72}H_3Cl^{35}$ and $Ge^{72}H_3Cl^{37}$ line were thus obtained and averaged.

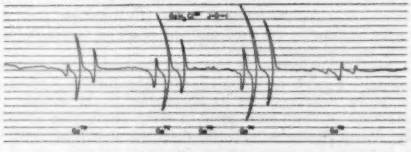

FIG. 1. A recording of the $J=0\rightarrow1$ GeH_3Cl^{35} spectrum. Each even isotope of Ge gives a triplet due to the Cl^{35} quadrupole coupling. Spectrum for the Ge^{72} isotope is very much more complex because of the Ge^{73} quadrupole. Although Ge^{73} is as abundant as Ge^{76}, most of the Ge^{73} lines are too small to be seen well with the amplification used in this trace.

In addition to the frequencies for the two sets of Ge^{73} lines, the quadrupole coupling constants eqQ for Cl^{35} and Cl^{37} were known from measurements on molecules with even germanium isotopes to be -46 and -36 Mc/sec. The spin of Ge^{73} is of course half-integral, and greater than 1/2, since there are obviously effects due to its quadrupole moment. A preliminary examination of the general spacing of hyperfine structure lines and positions of the more intense lines indicated that the quadrupole coupling of Ge^{73} was probably 2 or 3 times larger than that of Cl^{35} or Cl^{37}, and of the same sign; i.e., negative.

Taking $(eqQ)_{Ge^{73}}=a$ and $(eqQ)_{Cl}=b$, the theoretical quadrupole pattern of the $J=1$, $K=0$ level for the each of the spins 3/2, 5/2, 7/2, 9/2, and 11/2 for values of a/b ranging from 2 to 3 was calculated.[3] The calculations were somewhat laborious, since for each assignment of I and a/b two second- and two third-order secular equations must be solved. However, because the $J=0$ level is unsplit by quadrupole coupling, the splitting of the spectral line depends only on the splitting of the $J=1$, $K=0$ level. In addition, theoretical relative intensities are easily obtained, being simply given by $2F+1$, where F is the total angular momentum. With

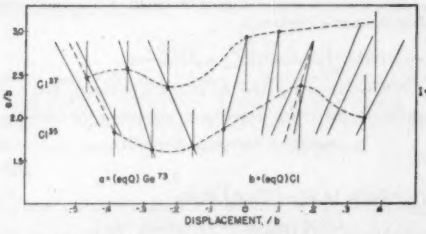

FIG. 2. Ge^{73} spin assumed to be 7/2. Comparison of observed frequencies (vertical lines) for the $Ge^{72}H_3Cl^{35}$ and $Ge^{72}H_3Cl^{37}$ $J=0\rightarrow1$ transition with theoretical frequencies (slanted lines) for various values of Ge^{73} quadrupole coupling. Agreement between theory and experiment should be indicated by intersection of vertical and slanted lines at one horizontal level for each Cl isotope, or by dashed lines being straight. The ratio of ordinates of these dashed lines should be the ratio of quadrupole couplings of the Cl isotopes, or 1.27. Agreement is clearly unsatisfactory for the assumed spin of 7/2.

* Work supported jointly by the Signal Corps and ONR.

† Eastman Kodak Fellow, 1949–50. Present address, Department of Chemistry, Harvard University, Cambridge, Massachusetts.

[1] Dailey, Mays, and Townes, Phys. Rev. **76**, 136 (1949).

[2] Townes, Mays, and Dailey, Phys. Rev. **76**, 700 (1949).

[3] J. Bardeen and C. H. Townes, Phys. Rev. **73**, 97 (1948).

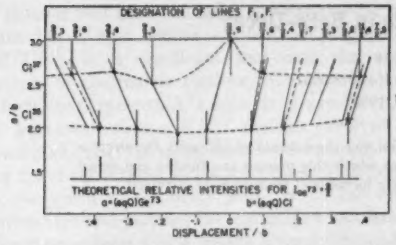

FIG. 3. Same as Fig. 2, but with the Ge^{73} spin assumed to be 9/2. Fit of experimental and theoretical lines gives dashed lines with correct ratio of ordinates and satisfactorily straight. The worst deviation, the 11/2, 5 transition of Cl^{37}, was overlaid by a foreign line and hence inaccurately measured.

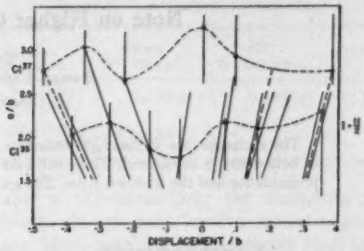

FIG. 4. Same as Fig. 2, but with the Ge^{73} spin assumed to be 11/2. The fit is unsatisfactory.

a/b as ordinate and the displacement of quadrupole components in terms of b as abscissa the calculated results were plotted for each value of I. On each of the graphs (Figs. 2, 3, and 4) the experimentally determined displacements of components for $Ge^{73}H_3Cl^{35}$ and $Ge^{73}H_3Cl^{37}$ in terms of the appropriate value of b were drawn as vertical lines. These displacements are with respect to the predicted position of the rotational transition without hyperfine structure. Clearly, on the graph for the correct value of I the experimental lines for $Ge^{73}H_3Cl^{35}$ should intersect the theoretical curves along a horizontal line corresponding to the actual ratio a/b_{35}. The lines for $Ge^{73}H_3Cl^{37}$ should intersect the theoretical curves in another horizontal line corresponding to a/b_{37}. The ratio $(a/b_{37})/(a/b_{35})$ should, of course, equal the known ratio b_{35}/b_{37}.

III. RESULTS

For spins 3/2, 5/2, 7/2, and 11/2, the conditions described above were definitely not fulfilled. For $I=9/2$, a very much better correlation was obtained as shown in Fig. 3. Deviations from the theoretical pattern for $I=9/2$ are within experimental error. Agreement is best for $Ge^{73}H_3Cl^{35}$, since the Cl^{35} lines are three times as intense as those for Cl^{37} and hence more accurately measured. The 11/2, 5 line of Cl^{37} was subject to a particularly large error because it was obscured by an excited state line of $Ge^{72}H_3Cl^{37}$. On this basis the spin 9/2 is assigned to Ge^{73}.

The theoretical relative intensities are also shown in Fig. 3. Dotted lines indicate centers of gravity of lines. Because the spectral lines often fell close together, some lines were wholly or partially obscured by the Stark components of adjoining lines, and some close pairs of lines were not resolved. Thus, the relative intensities could not be measured accurately. However, the general pattern of intensities agreed with the theoretical. In addition to determination of the Ge^{73} spin, Fig. 3 allows an evaluation of a/b; and, hence, the Ge^{73} quadrupole coupling constant as -95 ± 3 Mc/sec.

An estimate of the value of Q for Ge^{73} can be made on the basis of the assignment of 45 percent ionic character to the Ge—Cl bond,[1] by use of the theory of Townes and Dailey.[4] In the single and double bond structures the three p-orbitals of the Ge atom are assumed to be equally populated by valence electrons and thus not to contribute to q. The ionic structure $H_3Ge^+Cl^-$, however, corresponds to a deficiency of 0.75 p-electrons if tetrahedral hybridization is assumed; and thus, q for Ge should be 0.34 of that for GeII. This latter quantity can be calculated approximately from the known doublet separation[5] $\Delta\nu=1768$ cm^{-1} for GeII by means of the formula

$$q=2l(l+1)e\Delta\nu/Z_i Ra^2a_0^3(l+\tfrac{1}{2})(2l+3)(2l-1),$$

where Z_i is the effective "unscreened" value of Z defined by Landé, which for p-electrons can usually be taken as the atomic number minus four; R is the Rydberg constant and a is the fine structure constant. Using this formula and the value $-95/0.34$ for eqQ of GeII, a value of $Q=-0.2\times10^{-24}$ cm^2 is obtained. Because of the uncertainties in the GeH_3Cl structure and the various approximations used,[4] the limits of error are given as $\pm0.1\times10^{-24}$ cm^2.

The spin of 9/2 for Ge^{73} fits in rather well with present theories of nuclear shell structure. Ge^{73}, which has 41 neutrons and an even number of protons, has the same spin as Cb^{93}, which has 41 protons and an even number of neutrons. This case is the heaviest pair of nuclei in which the neutron and proton shells are known to fill in the same order. The fact that Ge^{73} is the lightest nucleus with a known spin of 9/2 fits very well into the nuclear shell scheme of Mayer,[6] where the first neutron or proton which goes into the $5g_{9/2}$ shell is the 41st.

No evidence of a quadrupole moment for the even isotopes of Ge was observed. A rough calculation based on the observed line widths and the splitting to be expected for various spin values shows that the quadrupole moments of these nuclei must be less than 1/30 of the Ge^{73} quadrupole moment or $Q<0.007\times10^{-24}$ cm^2. This appears to be very good evidence that the spins of the even Ge isotopes are zero, since then no quadrupole moment is observable.

[4] C. H. Townes and B. P. Dailey, J. Chem. Phys. 17, 782 (1949).
[5] R. F. Bacher and S. Goudsmit, *Atomic Energy States* (McGraw-Hill Book Company, Inc., New York, 1932).
[6] M. Goeppert-Mayer, Phys. Rev. 75, 1969 (1949).

Note on Higher Order Effects in Beta-Decay*

EUGEN MERZBACHER†
Harvard University, Cambridge, Massachusetts
(Received November 16, 1950)

The exchange of a virtual light quantum between an electron and the nucleus which emits the electron in beta-decay is considered. The conditions are deduced under which this process can modify the decay probabilities and the selection rules. The special case of "strictly forbidden" transitions is discussed.

I. INTRODUCTION

IN radiation processes, conservation of angular momentum and parity gives rise to selection rules which, given the initial and final states of the radiating system, restrict the angular momentum and parity carried away by the radiation field. Generally, if the wavelength λ of the emitted radiation is large compared with the linear dimensions R of the radiating system, only the radiation of minimum angular momentum compatible with the selection rules is quantitatively significant, corresponding essentially to the first nonvanishing term in a "multipole" expansion whose successive terms decrease in the ratio R/λ. In beta-decay, where R is the nuclear radius and λ the wavelength of the electron, R/λ never exceeds 0.1.

If the first nonvanishing term in the matrix element is proportional to $(R/\lambda)^n$, the beta-decay is said to be nth forbidden. The relations between the selection rules and the corresponding degree of forbiddenness are well known, as is the fact that these relations are the same whether plane or coulomb wave functions are employed for the electron.[1] However, it is conceivable that angular momentum might be transferred from the nucleus to the electron by the electromagnetic radiation field as an intermediary. The subject of this note is the correction to be made to the decay probabilities as well as modifications of the selection rules by considering the effect of the second order electromagnetic interaction between the nucleus and the electron.

II. THEORY

The matrix element for this process, emission, and subsequent reabsorption of a virtual light quantum, is proportional to the fine structure constant as well as to the ratio between the nucleon velocity and the velocity of light. However, if light quanta of very short wavelength ($\sim R$) contribute substantially to the transfer of energy and angular momentum to the electron, then it appears possible that the small factors $e^2/\hbar c = 1/137$ and $v/c \sim 1/10$ might be compensated by large contributions to the integrals. Thus, under conditions to be deduced in this paper, strong selection rules for the beta-decay could conceivably be circumvented by the effect of a combination of processes which in the language of conventional perturbation theory may be described as follows:

(1) Emission of a light quantum from the nucleus which goes to an excited state and subsequently, in the transition to its final state, emits an electron and a neutrino. The electron reabsorbs the light quantum.

(2) Emission of a light quantum from the nucleus which goes to an excited state. A pair is created in the vacuum by the light quantum; the positron is absorbed by the nucleus which, under simultaneous neutrino emission, makes a transition to the final state.

(3) A pair and a light quantum are created in the vacuum. The light quantum is absorbed by the nucleus, raising it to an excited level. From there the nucleus goes to the final state by absorbing the positron and emitting a neutrino.

(Strictly speaking, one might need to substitute *antineutrino* for *neutrino*.)

There are, correspondingly, three similar processes involving the excited states of the final rather than the initial nucleus; however, for an estimate of the orders of magnitude of the decay probabilities it is sufficient to exhibit the analysis of processes 1 to 3, the other transitions being analogous.

The processes described are of the second order as far as the interaction with the electromagnetic field is concerned, and all involve the emission and subsequent reabsorption of a virtual light quantum. The term "detour transition" will be employed hereafter to characterize these processes, in contrast with the ordinary "direct" beta-decay without electromagnetic interaction. A special case of a detour transition has been considered before but only with regard to the shape of the energy spectrum which arises if the detour process predominates over the direct transition.[2]

Appreciable amounts of energy can be transferred in this indirect way to the electron only if there is a pronounced tendency for the interaction between the electron and the light quantum to take place well outside, but within the distance of a Compton wavelength λ_e from the nucleus. The ratio $\lambda_e/R \approx 250A^{-\frac{1}{3}}$ characterizes the relative sizes of the regions of electromagnetic and beta-interaction of the electron and must clearly play a decisive role in the comparison of the direct with the detour transition. The matrix element of the latter is restricted by conservation laws in such

* Summary of a Ph.D. thesis (Harvard University, June, 1950).
† Now at the Institute for Advanced Study, Princeton, New Jersey.
[1] The article by E. J. Konopinski, Revs. Modern Phys. 15, 209 (1943), reviews the theory of beta-decay and contains references to most of the earlier work.
[2] H. J. Lipkin, Phys. Rev. 76, 567 (1949).

a manner that for a change of nuclear angular momentum by L this matrix element is proportional to $(R/\lambda)^{L-1}$. It is significant that only the numerical factors in the matrix element, but not the power in which the parameter R/λ appears, depend on the kind of beta-interaction and the parities involved in the transition. Since the situation is fundamentally different for direct transitions, where the degree of forbiddenness is, for given L, decidedly sensitive to the choice of interaction and parities, the comparison of detour with direct transitions yields results strongly dependent on the detailed assumptions made about the transition.

These results are summarized in Table I, where a distinction is made between three types of interaction. Fermi interactions comprise the scalar and vector types, GT (Gamow-Teller) refers to the tensor and pseudovector interactions, and the pseudoscalar case stands alone. The transitions L even (no) and L odd (yes) are classified as belonging to "group A," while the transitions L odd (no) and L even (yes) are labeled by B. Column D indicates the degree of forbiddenness of the direct transition. An estimate for the relative importance of the detour as compared to the direct transition is obtained from the ratio of their contributions to the total decay probability. Disregarding interference effects, we denote these contributions by $\Omega^{(2)}$ and $\Omega^{(0)}$, respectively. The columns headed by $\Omega^{(2)}/\Omega^{(0)}\sim$ in Table I list the dependence of this ratio on the disintegration energy W_0 (assumed to be large) and on λ_c/R. (When the decay energy is small, W_0 must be replaced by (W_0-1)[1].) The qualitative conclusions from this behavior are as follows. Only in the case of group B transitions and Fermi interaction or group A transitions and pseudoscalar interaction is a strong competition between the detour and the direct processes possible. On the other hand, for group B transitions with either GT- or pseudoscalar interaction, the contribution of the higher order process is negligible. The remaining two cases (group A transition with Fermi or GT-interaction) are of a nature intermediate between these two extremes. The antisymmetrical "Critchfield" interaction behaves, as far as the questions treated here are concerned, like a GT-interaction, since the pseudovector interaction is one of its three components.

The fact that the detour transition is least important when a GT-interaction is applied follows from the explicit spin dependence introduced in the lowest order by such an interaction. This spin dependence causes GT selection rules to be less stringent than any other type of selection rule for the direct transition. The intervening electromagnetic interaction has essentially the effect of supplying an additional factor γ in the matrix element; but since the five types of interaction represent all products of Dirac matrices, no selection rules more liberal than those for GT-interaction can ever be obtained in this manner. In other words, the spin flip which was available for satisfying the conservation of angular momentum has already been achieved by using a GT-interaction; the remaining angular momentum change must involve orbital angular momentum. More quantitative statements must be based on the evaluation of the matrix elements.

TABLE I. Classification of interactions.

Group	Parity change	L	Fermi D	Fermi $\Omega^{(2)}/\Omega^{(0)}\sim$	GT D	GT $\Omega^{(2)}/\Omega^{(0)}\sim$	Pseudoscalar D	Pseudoscalar $\Omega^{(2)}/\Omega^{(0)}\sim$
A	no / yes	even / odd	L	$(\lambda_c/RW_0)^2$	L	$(\lambda_c/RW_0)^2$	$L+1$	$(\lambda_c/RW_0)^4$
B	no / yes	odd / even	$L+1$	$(\lambda_c/RW_0)^4$	$L-1$	1	L	1

The calculation will be outlined only briefly here.[3] The combined effective matrix element for the three second-order processes described above is

$$H_{eff}=\frac{g\alpha}{8\pi^2}\sum_m\int(d\mathbf{k})\int(d\mathbf{x})\bar{\Psi}_f\exp[i(\mathbf{k}-\mathbf{P}-\boldsymbol{\pi})\cdot\mathbf{x}]$$
$$\times T\Psi_m\int(d\mathbf{x}')\bar{\Psi}_m'\exp(i\mathbf{k}\cdot\mathbf{x}')\boldsymbol{\Gamma}_\perp\Psi_i'\bar{u}\gamma$$
$$\times\left[\frac{-i\boldsymbol{\gamma}\cdot(\mathbf{P}-\mathbf{k})+\kappa-\beta\tau}{(m+\tau+P_0)\tau(\mathbf{P}\cdot\mathbf{k}-P_0^2-P_0\tau)}\right.$$
$$\left.-\frac{-i\boldsymbol{\gamma}\cdot(\mathbf{P}-\mathbf{k})+\kappa+\beta(P_0-k)}{(m+k)k(\mathbf{P}\cdot\mathbf{k}-P_0k)}\right]Tv. \quad (1)$$

$\alpha=e^2/4\pi\hbar c$ ($\cong 1/137$),

g is the beta-decay interaction constant ($\cong 10^{-48}$ erg-cm^3),

$\hbar\mathbf{k}$ is the momentum of the virtual light quantum,

$\hbar\mathbf{P}$, $\hbar\boldsymbol{\pi}$ are the momenta of the electron and neutrino, respectively,

$\hbar cP_0$ is the energy of the electron,

$\hbar cm$ is the energy excess of the intermediate nuclear state over the initial energy,

$1/\kappa$ is the Compton wavelength of the electron,

$\tau=[(\mathbf{P}-\mathbf{k})^2+\kappa^2]^{\frac{1}{2}}$ is the energy of the virtual electron in the intermediate state,

$\boldsymbol{\gamma}(=i\alpha\beta)$ and β are the conventional Dirac matrices,

$\boldsymbol{\Gamma}_\perp$ is the component perpendicular to $\mathbf{k}$ of the vector $\boldsymbol{\Gamma}=\mathbf{v}/c$, where $\mathbf{v}$ is the nucleon velocity vector,

T is the interaction matrix, with $\cdots T\cdots T\cdots$ forming a scalar,

Ψ_i, Ψ_m, Ψ_f are the initial, intermediate, and final nuclear wave functions. The sum in Eq. (1) is to be carried out over all intermediate states.

The electron and neutrino wave functions were assumed to be of the forms $u(P)\exp(i\mathbf{P}\cdot\mathbf{x})$ and $v(\pi)\exp(i\boldsymbol{\pi}\cdot\mathbf{x})$, with u and v being spinors. A bar denotes the adjoint wave function. (All exponential time factors have been omitted.) The general conclusions presented here are hardly affected by the coulomb force, which was neglected throughout, particularly since the radiative correction is more pronounced for light than for heavy nuclei.

The basis of the approximations used in the evaluation of the matrix element is the observation, already mentioned, that an appreciable probability for the

[3] Details are contained in the thesis on which this paper is based, see reference 1.

transfer of angular momentum from the nucleus to the electron via the light quantum can be expected only if the major contribution to the **k**-integral stems from photons whose wavelength is comparable to the nuclear dimensions ($kx\sim 1$). The momenta of the final electron and neutrino, on the other hand, do not exceed several mc; i.e., P and π are considerably smaller than the effective k. Hence, one can neglect $\mathbf{P}$ and $\boldsymbol{\pi}$ in the exponential.

At the same time, the expression contained in the brackets [ ] of (1) is appropriately expanded in terms of P/k. The only terms needed in this expansion are the powers of $(\mathbf{P}\cdot\mathbf{k}/k^2)$. A further simplifying assumption concerns the relative magnitude of the most effective nuclear excitation energy and the most effective k. The assumption $m/k\ll 1$ is physically justified on the ground that even light quanta with wavelengths as short as the nuclear dimensions can, owing to the large mass of a nucleon, excite no more than a few of the lowest nuclear energy levels. (A more precise formulation of the conditions implied can be given if an expansion in terms of m/k is made.) With these assumptions, the summation over the intermediate states of the nucleus can finally be carried out. The first nonvanishing term in the effective matrix element is found to be:

$$H_{eff}=\frac{g\alpha}{4\pi^2}\int(d\mathbf{k})\int(d\mathbf{x})\bar{\Psi}_f\exp(i\mathbf{k}\cdot\mathbf{R})\times T_a\Gamma_{bL}\Psi_i\left(\frac{\mathbf{P}}{k}\right)^{L-1}\frac{P_{L-1}(\mathbf{P},\mathbf{k})}{k^3}\bar{u}\gamma\times\left[\frac{i\boldsymbol{\gamma}\cdot\mathbf{k}}{k}(\pi)^{\frac{1}{2}}\frac{\Gamma(L)}{\Gamma(L-\frac{1}{2})}-\beta\frac{L-\frac{1}{2}}{L}\right]Tv, \quad (2)$$

where $P_L(\mathbf{P},\mathbf{k})$ is the legendre polynomial of order L of the cosine of the angle between $\mathbf{P}$ and $\mathbf{k}$, a and b refer to two different nucleons, and $\mathbf{R}=\mathbf{x}_a-\mathbf{x}_b$. L is the total change of angular momentum of the nucleus. (2) holds for given L, whether parity changes or not. Depending on the parities, however, the contribution from one or the other terms in the square bracket of Eq. (2) vanishes identically, thus providing another reason for the different behavior of the groups A and B which were distinguished in Table I.

As an illustrative example we consider a group B transition with scalar (Fermi) interaction. Carrying out the integration over **k**-space, one finds to a good approximation:[4]

$$H_{eff}\approx\frac{g\alpha i^L}{8L[1.3\cdots(2L-3)]}\int(d\mathbf{x})\bar{\Psi}_f P_{L-1}(\mathbf{P},\mathbf{R})\times\left(\frac{\mathbf{R}}{R}\times\boldsymbol{\Gamma}\right)_-\Psi_i(\mathbf{P}R)^{L-1}u\sigma_+v, \quad (3)$$

[4] Following R. E. Marshak, Phys. Rev. **61**, 431 (1942), we have chosen the magnetic quantum number of the initial state equal to its maximum value.

where the subscripts + and − are defined by

$$A_+=(A_x+iA_y)/(2)^{\frac{1}{2}},\quad A_-=(A_x-iA_y)/(2)^{\frac{1}{2}}.$$

As a special case, we now apply (3) to the transition $L=2$ (yes) which belongs to group B. For two limiting cases the total transition probability $\Omega^{(2)}$ for the detour process per unit time ($=\hbar/mc^2=1.28\times10^{-21}$ sec) can be given compactly; we are primarily interested in the ratio between $\Omega^{(2)}$ and $\Omega^{(0)}$, the probability per unit time for the direct transition:

$$\Omega^{(2)}/\Omega^{(0)}\approx 0.15\alpha^2(\lambda_c/R)^4(\Gamma^2/W_0^4)\quad\text{for}\quad W_0\gg 1, \quad (4)$$

and

$$\Omega^{(2)}/\Omega^{(0)}\approx 13\alpha^2(\lambda_c/R)^4[\Gamma^2/(W_0-1)^2]\ \text{for}\ W_0-1\ll 1. \quad (5)$$

λ_c is the Compton wavelength of the electron, R the radius of the nucleus, W_0 the total available energy (in units mc^2), and Γ^2 a nuclear parameter whose value $\sim(v/c)^2$ lies between 0.01 and 0.1.

For medium-sized nuclei ($A\sim 65$) and $W_0>4$, the ratio $\Omega^{(2)}/\Omega^{(0)}$ is less than 0.1. On the other hand, for a light nucleus (say $A=8$) one finds for $W_0\gg 1$,

$$\Omega^{(2)}/\Omega^{(0)}\cong 2200\Gamma^2/W_0^4,$$

TABLE II. Selection rules for the strictly forbidden direct transitions.

Interaction	i	f	Parity change
Scalar	even	0	yes
	odd	0	no
Vector	0	0	yes
Tensor	—	—	—
Pseudovector	0	0	no
Pseudoscalar	even	0	no
	odd	0	yes

which is of the order of unity. For light nuclei and $(W_0-1)\ll 1$, the ratio $\Omega^{(2)}/\Omega^{(0)}$ can easily become much greater than unity. It is thus concluded that the radiative corrections in this case can be appreciable for light nuclei and a small energy release.

These and similar calculations which have been carried out for the other cases confirm the statements made above and incorporated in Table I. When corrections to the direct transition probabilities are actually to be computed, one must, of course, take interference terms into account. (Incidentally, in the case $L=2$ (yes), Fermi interaction, the interference terms are zero.) Clearly, in view of the considerable uncertainties in the evaluation of nuclear matrix elements, comparison with experiment would be relatively unambiguous only when the detour process prevails strongly over the direct transition. The special case of "strictly" forbidden transitions, which cannot proceed directly at all but *must* be of a complex nature, is of particular interest provided, of course, that the beta-decay interaction is of a type which gives rise to such selection rules. The selection rules for the strictly forbidden direct transi-

tions are summarized in Table II under the assumption, made only for definiteness, that the spin, i, of the initial nucleus exceeds or equals the spin, f, of the final nucleus. If $i<f$, one need only multiply the half-life deduced for $i'=f$, $f'=i$ by $(2i+1)/(2f+1)$. Owing to the summation over all intermediate states, there are no such selection rules for the complete detour process.

With the possibility of practical applications in mind, we choose as an example of a transition which is strictly forbidden when the interaction is of the scalar type, the case $L=1$, $f=0$, no parity change. According to the classification of Table I, this is a Case B, Fermi; hence, Eq. (3) is applicable and reduces for this special case to

$$H_{eff}=\frac{g\alpha}{8}\int\bar{\Psi}_f\left(\frac{\mathbf{R}}{R}\times\boldsymbol{\Gamma}\right)_-\Psi_i\vec{u}\sigma_+\vec{v}. \tag{6}$$

Summing $|H_{eff}|^2$ over all final states we find for the transition probability per unit time and per unit energy interval

$$(G^2\alpha^2/128\pi^3)|M|^2(W^2-1)^{\frac{1}{2}}W(W_0-W)^2, \tag{7}$$

where

$$M=\int\bar{\Psi}_f(\mathbf{R}/R\times\boldsymbol{\Gamma})_-\Psi_i.$$

With $G\cong 5\times10^{-12}$ the half-life is roughly

$$t=2.5\times10^9/f|M|^2\text{ sec}=80/f|M|^2\text{ years}. \tag{8}$$

The quantity $|M|^2$ can be estimated by the averaging process described by Greuling,[5] and is found to range between 1/200 and 1/20. Hence, the ft-value for this transition is of the order of 10^{11} or 10^{12}.

For a total energy release of 2 Mev ($W_0=4$) we can compare our results with those of Longmire[6] who calculated the half-lives of nuclei decaying by simultaneous $\beta-\gamma$ emission. For this value of W_0, the half-life for the detour process is computed to be less than 10^3 years, which is shorter by a factor of at least 10^5 than the value found by Longmire. Hence, in the case of a strictly forbidden transition the nucleus is more likely to decay by the second-order process involving a virtual light quantum than by the first-order process with the emission of a γ-ray. The large number of intermediate states available to the virtual light quantum is the cause of this behavior.

The decay of C^{14} into N^{14} is presumably a transition of the type $i=0\rightarrow f=1$, no parity change ($W_0=1.29$). The spin values have been measured, and the statement about parity is a theoretical prediction of nuclear theory. If the scalar interaction is assumed to be valid, this transition is of the strictly forbidden type considered above. Under these assumptions a half-life of $\sim10^5$ years is calculated. This is considerably longer than the observed value of $\sim$6000 years, thus indicating that the conspicuously long half-life of C^{14} can hardly be explained by the assumption that the interaction is scalar.

Even if better agreement were obtained in this case, there would still remain the problem[1,7] of reconciling the well-known "allowedness" of the $He^6\rightarrow Li^6$ decay with a strictly forbidden $C^{14}\rightarrow N^{14}$ process. γ-rays not being observed, both transitions should be of the same nature ($0\rightarrow1$, no) and the difference in the half-lives should be accounted for by the difference in W_0. Always assuming that He^6 has no spin, these considerations (and another estimate carried out for $Be^{10}\rightarrow B^{10}$) support the considerable evidence previously accumulated by many authors that the scalar interaction (alone) cannot account for the β-decay, that GT selection rules are probably the ones operative in nature, and that the length of the half-life of C^{14} is to be explained on the basis of the particular structure of the nuclei involved which makes the decay strongly, but not strictly forbidden.[8]

I wish to express my gratitude to Professor Julian Schwinger for suggesting this problem and for much help in the course of the work. I also wish to thank Professor Robert Oppenheimer for several useful suggestions. During the work, the author was the recipient of a Charles W. Holtzer scholarship from Harvard University and a grant from the Leopold Schepp Foundation of New York.

[5] E. Greuling, Phys. Rev. **61**, 568 (1942).
[6] C. L. Longmire, Phys. Rev. **75**, 15 (1949).
[7] J. R. Oppenheimer, Phys. Rev. **59**, 908 (1941).
[8] R. Bouchez, Compt. rend. **230**, 440 (1950).

Covariant Transformation Law for the Field Equations*

JACK HELLER
Syracuse University, Syracuse, New York and Polytechnic Institute of Brooklyn, Brooklyn, New York
(Received September 11, 1950)

Ordinarily, the existence of Bianchi identities is proven on the strength of the transformation properties of the lagrangian of the theory. In this paper, nothing is assumed concerning the lagrangian, except that the field equations themselves are covariant with respect to general coordinate transformations. It is then shown that at least the coefficients of the second-order derivatives in the field equations satisfy the usual relationships. Furthermore, a very weak restriction on the transformation law of the field equations is sufficient to derive conservation laws that hold even in the presence of matter.

I. INTRODUCTION

IN his first paper on covariant field theories, Bergmann[1] introduced the field equations as the Euler-Lagrange equations of a variational principle. If the lagrangian is designated by L and if L is a function of the field variables y_A and their first derivatives with respect to the coordinates, $y_{A,\rho}$, the field equations will take the form

$$L^A \equiv \partial^A L - (\partial^{A\rho} L)_{,\rho} = 0, \quad \partial^A L = \partial L/\partial y_A, \quad \partial^{A\rho} L = \partial L/\partial y_{A,\rho}. \tag{1.1}$$

In a physical theory, the field equations must be covariant; i.e., if they are satisfied in one permissible coordinate system, they must automatically be satisfied in every permissible system. For a completely covariant theory, the permissible coordinate systems include all those which can be transformed into each other with a nonvanishing jacobian. To assure this covariance, it was assumed in I that the lagrangian would, in the face of an infinitesimal coordinate transformation, transform as

$$\delta L = Q^{\rho}{}_{,\rho}. \tag{1.2}$$

The field variables themselves were to obey a homogeneous linear transformation law, whose infinitesimal form is denoted by

$$\bar{\delta} y_A = F^{B\mu}{}_{A\nu} \xi^{\nu}{}_{,\mu} y_B - y_{A,\rho} \xi^{\rho}. \tag{1.3}$$

The condition (1.2) is sufficient to assure not only covariance of the field equations, but also the formulation of the algebraic relationships between the canonical momenta (I-5.6) and the construction of the "strong" conservation laws (I-3.11). In this paper we shall investigate whether the conditions necessary for the formulation of the algebraic relationships between the canonical momenta and the construction of the "strong" conservation laws are not independent of the assumption (1.2). It turns out that covariance of the field equations (1.1) alone suffices for the algebraic constraints. For the "strong" conservation laws we must assume a particular transformation law for the field equations.

* This work was given partial support by the ONR under a contract with Syracuse University.

[1] P. Bergmann, Phys. Rev. **75**, 680–685 (1949). Referred to hereafter as I. Formulas in I are referred to by symbols such as (I-5.6).

II. TRANSFORMATION LAW OF THE FIELD EQUATIONS

If condition (1.2) is satisfied, the expressions L^A transform according to the equation

$$\bar{\delta} L^B = -F^{B\mu}{}_{A\nu} \xi^{\nu}{}_{,\mu} L^A - (L^B \xi^{\rho})_{,\rho}. \tag{2.1}$$

If we merely wish to assume that the expressions L^A transform in accordance with some linear, homogeneous transformation law, then it appears reasonable to start with an infinitesimal transformation law of the form

$$\bar{\delta} L^B = -G^{B\mu}{}_{A\nu} \xi^{\nu}{}_{,\mu} L^A - (L^B \xi_{\mu})_{,\rho} + H^{B\mu}{}_{A\nu} L^A{}_{,\mu} \xi^{\nu}, \tag{2.2}$$

where the $G^{B\mu}{}_{A\nu}$ and $H^{B\mu}{}_{A\nu}$ are constant coefficients as yet undetermined. The law (2.2) was chosen as the most general linear homogeneous transformation law with the correct order of differentiation.

The requirement of group character immediately leads to restrictions on the transformation coefficients. By forming the commutator of two arbitrary, infinitesimal transformations ξ^{ν} and ξ'^{μ}, we find the two conditions

$$G^{C\nu}{}_{A\mu} G^{B\sigma}{}_{C\rho} - G^{C\sigma}{}_{A\rho} G^{B\nu}{}_{C\mu} = \delta^{\nu}{}_{\rho} G^{B\sigma}{}_{A\mu} - \delta^{\sigma}{}_{\mu} G^{B\nu}{}_{A\rho} \tag{2.3}$$

and

$$H^{B\mu}{}_{A\nu} = 0. \tag{2.4}$$

III. IDENTITIES

We can obtain the complete conditions satisfied by the transformation law of the field equations by forming $\bar{\delta} L^A$ (the infinitesimal change in L^A) as specified functions of the field variables and their first and second derivatives, and by equating the resulting expression to the right-hand side of (2.2), taking into account the restrictions already obtained in (2.3) and (2.4). On both sides of the equation we shall have terms containing as factors ξ^{μ} and their first, second, and third derivatives. These functions and their derivatives which generate the infinitesimal coordinate transformation are completely arbitrary at one point of space-time, except that the higher derivatives must satisfy the usual symmetry relations

$$\xi^{\alpha}{}_{,\mu\nu} = \xi^{\alpha}{}_{,\nu\mu}, \tag{3.1}$$

etc. Since, however, the transformation law for L^A must come out the same, whether we obtain it through

the use of Eq. (2.2) or by the lengthy, straightforward calculation, the coefficients of the arbitrary functions and their various derivatives on the left must equal the corresponding coefficients on the right. By carrying out this computation, the following three sets of necessary identities were obtained:

$$F^{C\beta}{}_{B\alpha}\partial^{B\mu\nu}L^A\cdot y_C+F^{C\mu}{}_{B\alpha}\partial^{B\nu\beta}L^A\cdot y_C + F^{C\nu}{}_{B\alpha}\partial^{B\beta\mu}L^A\cdot y_C=0, \quad (3.2)$$

$$F^{C\beta}{}_{B\alpha}(\partial^{B\mu}L^A\cdot y_C+2\partial^{B\mu\nu}L^A\cdot y_{C,\nu})-\partial^{B\mu\beta}L^A\cdot y_{B,\alpha} + F^{C\mu}{}_{B\alpha}(\partial^{B\beta}L^A\cdot y_C+2\partial^{B\beta\nu}L^A\cdot y_{C,\nu}) - \partial^{B\beta\nu}L^A\cdot y_{B,\alpha}=0, \quad (3.3)$$

$$F^{C\beta}{}_{B\alpha}(\partial^{B}L^A\cdot y_C+\partial^{B\mu}L^A\cdot y^{\cdot}_{C,\mu}+\partial^{B\mu\nu}L^A\cdot y_{C,\mu\nu}) + \delta^{\beta}{}_{\alpha}L^A-\partial^{B\beta}L^A\cdot y_{B,\alpha}-2\partial^{B\beta\nu}L^A\cdot y_{B,\alpha\nu} + G^{AB}{}_{B\alpha}L^B=0. \quad (3.4)$$

These three sets contain all the restrictions on the form of covariant Euler-Lagrange equations and their transformation laws. While it appeared to be very difficult to get the information contained in Eqs. (3.3) and (3.4) into a readily usable form, Eqs. (3.2) are identical with Eq. (I-3.6). Since it is these conditions which are necessary for the formulation of the algebraic relationships between the canonical momenta, (I-5.6), the further development of a theory with the more general transformation law (2.2) could be carried out along the same lines as one with the special law (2.1).

IV. FORMATION OF FURTHER IDENTITIES BY THE USE OF THE COMMUTATOR

Identities can be obtained in a different form [though contained in Eqs. (3.2), (3.3), (3.4)] if we form $(\bar\delta_1\bar\delta_2-\bar\delta_2\bar\delta_1)L^A$ in two different ways and equate the results. First, we can easily verify that

$$\bar\delta_1 L=L^A\bar\delta_1 y_A+(\partial^{A\rho}L\cdot\bar\delta_1 y_A)_{,\rho}. \quad (4.1)$$

From this relation we form

$$\bar\delta_2\bar\delta_1 L=(\bar\delta_1\bar\delta_2-\bar\delta_2\bar\delta_1)L = L^A(\bar\delta_1\bar\delta_2-\bar\delta_2\bar\delta_1)y_A+[\partial^{A\rho}L\cdot(\bar\delta_1\bar\delta_2-\bar\delta_2\bar\delta_1)y_A]_{,\rho}. \quad (4.2)$$

We can also form the transformation $\bar\delta_1$ of $\bar\delta_2$ directly:

$$\bar\delta_1(\bar\delta_2 L)=\bar\delta_1[L^A\bar\delta_2 y_A+(\partial^{A\rho}L\cdot\bar\delta_2 y_A)_{,\rho}] = \bar\delta_1 L^A\cdot\bar\delta_2 y_A+L^A\bar\delta_1\bar\delta_2 y_A+[\bar\delta_1(\partial^{A\rho}L\cdot\bar\delta_2 y_A)]_{,\rho}. \quad (4.3)$$

Forming the commutator from (4.3) and equating the result to the expression (4.2), we obtain

$$\bar\delta_1 L^A\cdot\bar\delta_2 y_A-\bar\delta_2 L^A\cdot\bar\delta_1 y_A + [\bar\delta_1(\partial^{A\alpha}L)\cdot\bar\delta_2 y_A-\bar\delta_2(\partial^{A\alpha}L)\cdot\bar\delta_1 y_A]_{,\alpha}=0. \quad (4.4)$$

The last term in this expression is a complete divergence, and hence the first two terms must also be a complete divergence. Writing out these first two terms and using (2.2) and (1.3), we can arrange them into an expression of the form $A_\mu\xi^\mu{}_2+B^\nu{}_\mu\xi^\mu{}_{2,\nu}$, where the coefficients A_μ and $B^\nu{}_\mu$ are themselves functions of the field variables, the coordinate variations $\xi^\alpha{}_1$, and their derivatives. This expression will be a complete divergence only if A_μ equals $B^\nu{}_{\mu,\nu}$. Since the $\xi^\alpha{}_1$ and their derivatives are arbitrary, except for symmetry of higher derivatives, at any one point of space-time, the coefficients of $\xi^\alpha{}_1$ and its derivatives must vanish identically. Following this straightforward but lengthy calculation, we find the following identities (the first being the coefficient of $\xi^\alpha{}_1$ and the others of the successive derivatives):

$$(F^{B\beta}{}_{A\kappa}y_B L^A{}_{,\iota}+G^{B\beta}{}_{A\kappa}y_{B,\iota}L^A+\delta^{\beta}{}_{\iota}y_{A,\kappa}L^A)_{,\beta}=0, \quad (4.5)$$

$$(G^{C\alpha}{}_{A\iota}F^{B\beta}{}_{C\kappa}-G^{C\beta}{}_{A\kappa}F^{B\alpha}{}_{C\iota}+\delta^{\alpha}{}_{\iota}F^{B\beta}{}_{A\kappa} - \delta^{\beta}{}_{\kappa}F^{B\alpha}{}_{A\iota})(y_B L^A)_{,\beta}+2\{F^{B\alpha}{}_{A\iota}y_B L^A{}_{,\kappa} + G^{B\alpha}{}_{A\iota}y_{B,\kappa}L^A+\delta^{\alpha}{}_{\kappa}y_{C,\iota}L^C\}_{(\iota\kappa)}\equiv 0, \quad (4.6)$$

and

$$\{y_C L^B F^{C\beta}{}_{A\kappa}(G^{A\alpha}{}_{B\iota}+\delta^A{}_B\delta^{\alpha}{}_{\iota})\}^{(\alpha\beta)}{}_{[\iota\kappa]}=0. \quad (4.7)$$

In these three equations, the symmetrization or antisymmetrization with respect to certain indices is indicated by the symbols $\{\ \}^{(\alpha\beta)}$ and $\{\ \}^{[\alpha\beta]}$, respectively.

In these three sets of identities, if we let $G^{A\rho}{}_{C\nu}=F^{A\rho}{}_{C\nu}$, we find that (4.7) is satisfied identically, while (4.5) and (4.6) yield the contracted Bianchi identities. When $F^{A\rho}{}_{C\nu}\neq G^{A\rho}{}_{C\nu}$, (4.5), (4.6), and (4.7) are all together 210 identities, which may, however, possess some mutual algebraic dependence.

V. CONSERVATION LAWS

In order to form "strong" conservation laws, we must find sixteen functions whose divergence is identically zero whether the field equations are satisfied or not. The sixteen functions

$$t^{\rho}{}_{\iota}=\delta^{\rho}{}_{\iota}L-y_{A,\iota}\partial^{A\rho}L \quad (5.1)$$

have zero divergences when the field equations are satisfied, for

$$t^{\rho}{}_{\iota,\rho}\equiv y_{A,\iota}L^A. \quad (5.2)$$

In the presence of matter the field equations are not equal to zero; but

$$L^A=P^A, \quad (5.3)$$

where P^A is representative of the distribution of matter in the field. When $P^A\neq 0$, we must subtract from (5.1) a function whose divergence will cancel the expression $y_{A,\iota}L^A$ or $y_{A,\iota}P^A$. We shall construct such a function by using the identities that can be established in the formalism. With no restrictions on $F^{A\alpha}{}_{B\beta}$ and $G^{A\alpha}{}_{B\beta}$, it appears impossible to form such expressions. However, with a relation between $F^{A\alpha}{}_{B\beta}$ and $G^{A\alpha}{}_{B\beta}$, it is possible to form sixteen functions whose divergence is always zero.

From (4.6), contracting on κ and α and solving for $y_{A,\iota}L^A$, we obtain

$$5y_{C,\iota}L^C+(F^{B\rho}{}_{A\iota}y_B L^A{}_{,\iota}+G^{B\rho}{}_{A\iota}y_{B,\iota}L^A) + (F^{B\rho}{}_{A\iota}y_B L^A{}_{,\rho}+G^{B\rho}{}_{A\iota}y_{B,\rho}L^A) + (G^{C\rho}{}_{A\iota}F^{B\rho}{}_{C\nu}-G^{C\rho}{}_{A\nu}F^{B\rho}{}_{C\iota})(y_B L^A)_{,\rho}\equiv 0. \quad (5.4)$$

We note that the last term on the right is a divergence, but the others are not unless

$$G^{B\alpha}{}_{A;\alpha}=F^{B\alpha}{}_{A;\alpha}. \tag{5.5}$$

In that case, we can form the sixteen functions

$$T^{\rho}{}_{\iota}=l^{\rho}{}_{\iota}+F^{B\rho}{}_{A;\iota}L^{A}y_{B}, \tag{5.6}$$

whose divergence is identically zero whether the L^A vanish or are equal to P_A. This expression is identical with (I-3.11).

The author would like to express his appreciation to Dr. Peter G. Bergmann for the suggestion of and the helpful discussions in connection with this problem.

PHYSICAL REVIEW VOLUME 81, NUMBER 6 MARCH 15, 1951

The Mass of S^{35} from Microwave Spectroscopy*

TUNIS WENTINK, JR.,† WALTER S. KOSKI,‡ AND VICTOR W. COHEN
Brookhaven National Laboratory, Upton, New York

(Received November 30, 1950)

The $J=1\rightarrow2$ rotational absorption transition in OCS has been observed for the molecules containing S^{35} and S^{34}. From the frequencies, the frequency differences, and the previously known frequencies of S^{34}, S^{33}, and S^{32} we have evaluated the mass difference ratios $(S^{35}-S^{33})/(S^{34}-S^{32})$ and $(S^{35}-S^{33})/(S^{33}-S^{32})$. From these values and values of the stable S masses two independent values of the $(S^{35}-S^{32})$ mass differences are calculated to be 2.99844 ± 0.00042 and 2.99770 ± 0.00048, respectively.

I. INTRODUCTION

WE have remeasured[1] the frequencies of the $J=1\rightarrow2$ molecular rotational absorption transitions of OCS containing S^{32}, S^{33}, S^{34}, and S^{35} for the purpose of determining the mass of S^{35} and of evaluating the nuclear quadrupole interaction to a higher accuracy.

II. METHOD

Our apparatus, somewhat similar to various other K-band spectroscopes described in the literature,[2,3] is illustrated schematically in Fig. 1. It utilizes 100-kc/sec Stark effect modulation and for maximum sensitivity a phase-sensitive detector at the output. Our frequencies were measured by means of variable microwave frequency markers obtained from a frequency standard somewhat similar to those used in other laboratories.[4] Figure 2 shows a schematic arrangement of the system. The basis of our measurements is a General Radio 100-kc/sec crystal-controlled secondary frequency standard calibrated against Radio Station WWV.

As shown below in Eq. (3) the mass of S^{35} can be expressed in terms of frequency differences and ratios. In determining such differences small systematic errors, such as are caused by delays in the spectroscope amplifier, tend to cancel out of differences and ratios of nearly equal frequencies.

Because of the electric quadrupole moment of the odd S isotopes, the $J=1\rightarrow2$ transition is split into several components which are only partially resolved.[1] From the shape of the pattern one can infer the nuclear spin, while for the magnitude of the separations one may evaluate the quadrupole coupling constant.[5]

The significant spectral frequency referred to in the Eqs. (2) and (3) are those of the center of gravity of the $J=1\rightarrow2$ group of lines for one isotopic molecule. The displacement of the strong central line can be evaluated from the quadrupole coupling constant.[5]

Table I contains a summary of our data on S^{35} along with comparable results for the stable isotopes as measured by Geschwind and Gunther-Mohr.[6]

By taking the ratio of the intervals between the upper and lower minor components and the central one for S^{35} one gets a value of 1.48, which is in excellent agreement with the theoretical ratio of 1.46 for a nuclear spin of $\frac{3}{2}$. Clearly, the sign of the quadrupole moment of S^{35} is opposite that of S^{33}, since the patterns are inverted with respect to each other.[7] The value of the quadrupole constant is 20.5 ± 0.2 Mc/sec. Townes and Dailey[8] have made a rough calculation of the molecular electric field gradient in OCS to evaluate the electric quadrupole moment of S^{33}. Using their figures, we get a value of 0.06×10^{-24} cm^2 for the electric quadrupole moment of S^{35}, which is considered to be good to within a factor of 2.

As a result of the quadrupole interaction, the strong central line is shifted by 0.440 ± 0.003 Mc/sec down in frequency. For the most reliable value of the OCS^{34} frequency we took the value of the OCS^{34} frequency

* Research carried out under contract with the AEC.

† Now at the Graduate School, Cornell University, Ithaca, New York.
‡ Permanent address: Chemistry Department, Johns Hopkins University, Baltimore, Maryland.

[1] Cohen, Koski, and Wentink, Phys. Rev. **76**, 703 (1949).
[2] McAfee, Hughes, and Wilson, Rev. Sci. Instr. **20**, 821 (1949).
[3] Strandberg, Wentink, and Kuhl, Phys. Rev. **75**, 270 (1949).
[4] C. G. Montgomery, *Technique of Microwave Measurements*, Vol. 11 of Radiation Laboratory Series (McGraw-Hill Book Company, Inc., New York, 1947), Chapter 6.
[5] J. Bardeen and C. H. Townes, Phys. Rev. **73**, 97 (1948).
[6] S. Geschwind and R. Gunther-Mohr, private communication in advance of publication.
[7] C. H. Townes and S. Geschwind, Phys. Rev. **74**, 626 (1948).
[8] C. H. Townes and B. P. Dailey, J. Chem. Phys. **17**, 782 (1949).

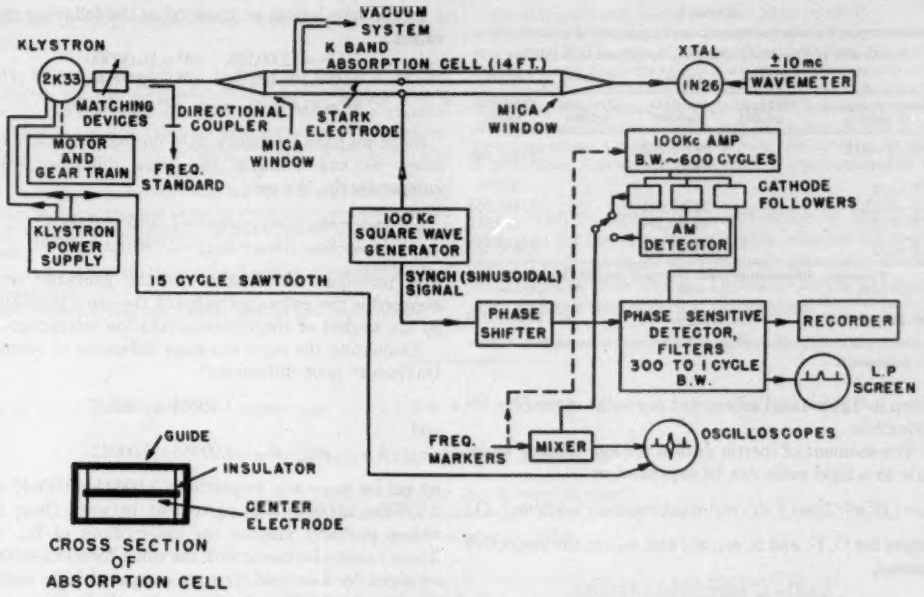

FIG. 1. Block diagram of microwave spectroscope.

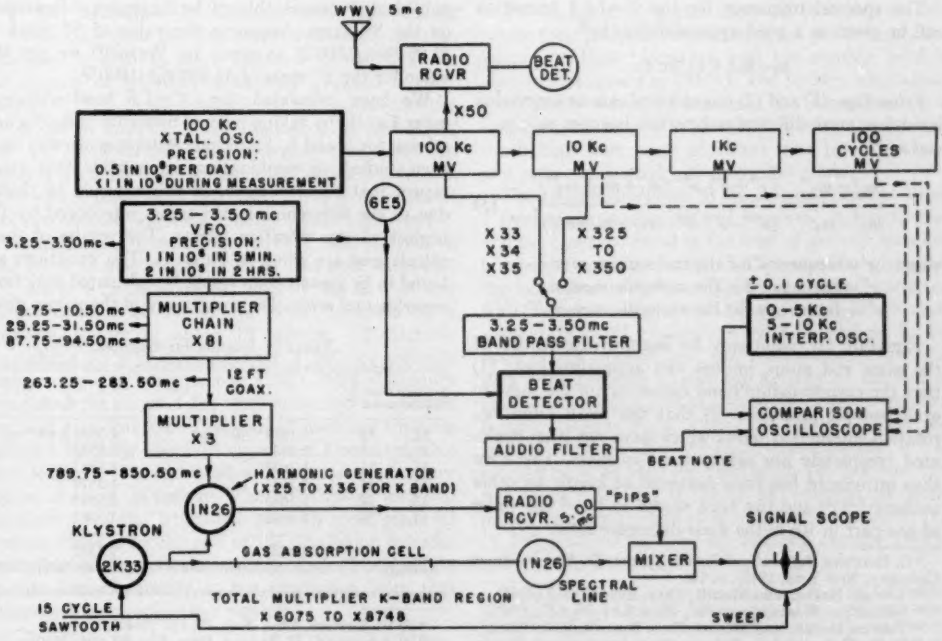

FIG. 2. Block diagram of the microwave frequency standard.

TABLE I.

Frequencies and frequency differences for isotopic OCS (Mc/sec)				
	OCS^{32} [a]	OCS^{33} [a]	OCS^{34} [a]	OCS^{35}
Center of gravity of pattern	24325.921 ±0.002	24019.641 ±0.004	23731.299 ±0.003	23457.403 ±0.011
$F=1/2\rightarrow3/2$		24012.292		23462.343
$5/2\rightarrow5/2$		24012.974		
$1/2\rightarrow1/2$				
$3/2\rightarrow5/2$		24019.641		23456.963
$5/2\rightarrow7/2$		24020.264		±0.011
$3/2\rightarrow3/2$		24025.467		23453.323
Frequency differences between centers of gravity (Mc/sec)				
$(\nu^{32}-\nu^{33})$ [a]		$(\nu^{33}-\nu^{34})$ [a]		$(\nu^{34}-\nu^{35})$
306.280±0.005		594.622±0.004		273.896±0.010

[a] Reference 6.

given in Table I and subtracted our value of the $S^{34}-S^{35}$ difference.

The moment of inertia I_0 of a triatomic linear molecule as a rigid rotor can be expressed as

$$I_0=[\Pi(m)/\Sigma(m)][(l_1^2/m_3)+(l_2^2/m_1)+(l_1+l_2)^2/m_2] \quad (1)$$

where for O, C, and S, m_1, m_2, and m_3 are the respective masses,

l_1 = O−C internuclear distance,
l_2 = C−S internuclear distance,
$\Pi(m)=m_1m_2m_3$, $\Sigma(m)=m_1+m_2+m_3$.

The spectral frequency for the $J\rightarrow J+1$ transition will be given to a good approximation by[9]

$$\nu_0=h(J+1)/4\pi^2I_0. \quad (2)$$

From Eqs. (1) and (2) one can evaluate an expression involving mass differences between isotopes m_3', m_3'' and m_3''':

$$\frac{m_3'-m_3''}{m_3'-m_3'''}=\frac{(\nu''-\nu')}{(\nu'''-\nu')}\frac{\nu'''}{\nu''}\frac{(m_1+m_2+m_3'')}{(m_1+m_2+m_3')}, \quad (3)$$

where ν' = frequency for the molecule $m_1m_2m_3'$,
ν'' = frequency for the molecule $m_1m_2m_3''$,
ν''' = frequency for the molecule $m_1m_2m_3'''$.

Equation (3), valid only for isotopic substitution of the same end atom, implies two approximations: (1) that the corresponding bond distances are the same in each isotopic molecule, (2) that the small vibration-rotation interaction terms which have not been evaluated completely are proportional to mass. The error thus introduced has been discussed at length by other authors[3,7,10–13] and has been shown to be of the order of one part in 10^4 in the mass difference ratio.

[9] G. Herzberg, *Infrared and Raman Spectra* (D. Van Nostrand Company, New York, 1947), p. 14.
[10] Townes, Holden, and Merritt, Phys. Rev. **72**, 513 (1947).
[11] Strandberg, Wentink, and Hill, Phys. Rev. **75**, 827 (1949).
[12] Townes, Holden, and Merritt, Phys. Rev. **74**, 1113 (1948).
[13] D. R. Bianco and A. Roberts, unpublished report, Physics Department, State University of Iowa.

In our calculations we have taken the following mass values:

$C^{12}=12.00386$, $O^{16}=16.00000$;
$S^{32}=31.98199$, $S^{33}=32.98168$;
$S^{34}=33.97890$ and $S^{35}=34.98006$.

Since we have frequency data on four isotopic molecules, we can evaluate two mass difference ratios independently. We get

$$(m_{35}-m_{32})/(m_{34}-m_{32})=1.50155\pm0.00015,$$
$$(m_{35}-m_{32})/(m_{33}-m_{32})=2.99881\pm0.00030.$$

The principal contribution to the probable errors assigned is the estimated value of the error introduced by the neglect of the vibration-rotation interaction.

Evaluating the $m_{35}-m_{32}$ mass difference in terms of Davison's[14] mass differences

$$m_{34}-m_{32}=1.99691\pm0.00037$$

and

$$m_{33}-m_{32}=0.99963\pm0.00012,$$

we get for $m_{35}-m_{32}$, respectively 2.99844±0.00042 and 2.99770±0.00048. The agreement between these two values partially justifies the assumptions of Eq. (1). These values also check with the value 2.99818±0.00045 as given by Low and Townes computed from nuclear reaction data.[15] The absolute value of the S^{35} mass is dependent upon the absolute value of S^{32}. Since there has been some question concerning the accuracy of the published S^{32} masses, this will be the principal limitation on the S^{35} mass. Assuming the value of S^{32} mass of 31.98199±0.00021 as given by Penfold[16] we get the value for the S^{35} mass of 34.98006±0.00038.

We have calculated the OC−CS bond distances using Eq. (1) by taking pairs of moments of inertia and solving for l_1 and l_2. Since four isotopic molecules have been studied, six combinations are possible. One would expect that the differences in values would be chiefly due to the differences in the errors introduced by the neglect of the vibration effects. The results of these calculations are given in Table II. The variations are found to be greater than would be calculated only from experimental error. The consistency of the values given

TABLE II. Internuclear distances.

Isotopic combination used		C−O	C−S
32,	33	1.1634×10^{-8} cm	1.5584×10^{-8} cm
32,	35	1.1636	1.5583
33,	35	1.1638	1.5582
32,	34	1.1641	1.5579
33,	34	1.1648	1.5573
34,	35	1.1626	1.5591
Average		1.1637 mean deviation 0.0005	1.5582 mean deviation 0.0004

[14] P. W. Davison, Phys. Rev. **75**, 757 (1949).
[15] W. Low and C. H. Townes, Phys. Rev. **80**, 608 (1950).
[16] A. S. Penfold, Phys. Rev. **80**, 116 (1950).

serve as a very rough check that use of Eq. (1) is justified.

The S^{35} was furnished by the AEC Isotopes Branch in the form of $H_2S^{35}O_4$ with only about one-half percent of the S present being S^{35}. Considerable effort was spent in working out a chemical process for converting the small total amount of sulfur (approx. $\frac{1}{4}$ mg) into OCS without reducing the ratio of S^{35} to S^{32}. Our procedure was essentially as follows:

(1) precipitating the $SO_4^{=}$ with $Ba(OH)_2$ in a Pt test tube and removing the supernatant liquid by centrifuging and decantation;

(2) reducing the dried $BaSO_4$ to BaS at 900°C in an H_2 atmosphere;

(3) adding I_2 and HCl in an alcohol solution in excess to produce elementary S;

(4) carefully drying the S under vacuum and then distilling it;

(5) adding CO and baking for about 16 hr at 450°C.

The total gas pressure in the absorption cell of the spectroscope was about 120μ. In spite of the low S^{35} concentration, the central OCS^{35} line was distinctly visible in an oscilloscope presentation of the output of the 100-kc amplifier. The satellite lines were observed and measured by cooling the guide with dry ice, using a 1-cycle sweep, a phase-sensitive detector, and an oscilloscope with a long persistent screen. Graphical records were also obtained by using a gear-driven Klystron, a phase-sensitive detector, and an ink recorder.

We wish to express our appreciation to Mr. James Sharman for his valuable assistance with the electronic circuits and especially the frequency standard. We also wish to thank Miss Theresa Danielson for her assistance with some of the numerical calculations.

PHYSICAL REVIEW VOLUME 81, NUMBER 6 MARCH 15, 1951

Photo-Activation of Bismuth*

NATHAN SUGARMAN AND ROBERT PETERS
Institute for Nuclear Studies, University of Chicago, Chicago, Illinois
(Received November 10, 1950)

Work is reported on nonfission activities produced in bismuth under irradiation with photons of 48- and 86-Mev maximum energies. The results are similar to those obtained by bombardment with high energy particles in that many particles are emitted.

THE activation of bismuth with high energy photons from the University of Chicago betatron has been reported to result in fission[1] as well as in the production of activities tentatively assigned to Bi^{204} and Bi^{206}. This paper reports some nonfission activities produced in bismuth under irradiation by photons of 48- and 86-Mev maximum energies. The results in general resemble those obtained by bombardment with high energy particles in that many particles (spallation) are also emitted when high energy photons are used.

Two procedures were followed. (1) Bismuth foils of one gram in weight and 2 cm^2 in area were irradiated for about 4 hr and counted directly on an Eck and Krebs counter of 30 mg/cm^2 wall thickness at a geometry factor of about 15 percent. (2) Aliquots containing 15 g of bismuth from a 500 ml solution, prepared by dissolving in conc. HNO_3 150 g of bismuth irradiated for about 4 hr, were subjected to analysis for lead and thallium. The isolated lead and thallium samples weighing about 15 mg and of 2-cm^2 area were counted on a thin end-window counter at a geometry factor of about 20 percent. The isolations of lead and thallium from the irradiated bismuth were made at various times after the end of the irradiation in order to distinguish between the activity of a lead or thallium species formed directly in the irradiation from that descended from radioactive parents.

The radioactive species observed in irradiated bismuth, their probable assignments, the nuclear reactions leading to their formation, and the activity level of each species appear in Table I. The 86-Mev irradiations were performed at 55 cm from the target and at a radiation intensity of about 2400 r/min; the 48-Mev irradiations were made at 55 cm from the target and at a radiation intensity of about 900 r/min.

The assignments given to the radioactivities in Table I were made on the basis of reported[2] radioactivities and the observed trend in the level of activity with the number of emitted particles. The reactions given for the individual activities of Table I are those consistent with the mass assignments and are written in the most elementary way for balance of mass and charge. In the cases of the isolated lead and thallium activities, the data were analyzed to give the activity at the end of irradiation of the parent as well as the daughter activity formed independently. Thus, for example, from the activity of 68-min Pb^{201m} formed independently, it was found that at 86 Mev the yield of the $(\gamma, 4np)$ reaction was about 1/50 that of the $(\gamma, 5n)$ reaction, as determined from the activity of 68-min Pb^{201m} formed by the $(\gamma, 5n)$ reaction followed by electron capture (designated e.c. in Table I).

* This work was supported in part by a grant from the AEC.
[1] N. Sugarman, Phys. Rev. **79**, 532 (1950).

[2] Templeton, Howland, and Perlman, Phys. Rev. **72**, 766 (1947); G. T. Seaborg and I. Perlman, Revs. Modern Phys. **20**, 585 (1948); H. M. Neumann and I. Perlman, Phys. Rev. **78**, 191 (1950); Way, Fano, Scott, and Thew, "Nuclear Data," Circular of the National Bureau of Standards 499, September 1, 1950.

TABLE I. Radioactivities observed in photo-activation of bismuth.

86 Mev					48 Mev				
Observed half-life	Probable assignment[a]	Reaction	A^{∞} per gram Bi[b] (c/m)	Normalized activities[b]	Observed half-life	Probable assignment[a]	Reaction	A^{∞} per gram Bi[b] (c/m)	Normalized activities[b]
Experimental conditions: foil irradiation and counting of unseparated sample									
6.1 day	6.4-day Bi^{206}	$(\gamma, 3n)$	7650	100	6.5 day	6.4-day Bi^{206}	$(\gamma, 3n)$	3600	100
14 day	~14-day Bi^{205}	$(\gamma, 4n)$	2360[c]	30.8					
11.4 hr	12-hr Bi^{204}	$(\gamma, 5n)$	3200	41.8	12 hr	12-hr Bi^{204}	$(\gamma, 5n)$	122	3.4
80 min	90-min Bi^{202}	$(\gamma, 7n)$	820	10.7	90 min[c]	90-min Bi^{202}	$(\gamma, 7n)$	<7	<0.2
Experimental conditions: chemical separation of indicated fraction from 15 g Bi Pb fraction (average of 2 experiments)									
60–69 min	68-min Pb^{204m}	$(\gamma, 5n)$, e.c.	7800[d]	41.8	70–80 min	68-min Pb^{204m}	$(\gamma, 5n)$, e.c.	264[d]	3.4
		$(\gamma, 4np)$	170	0.9			$(\gamma, 4np)$	8	0.1
50–52 hr	52-hr Pb^{203}	$(\gamma, 6n)$, e.c.	1430	7.7	52 hr[c]	52-hr Pb^{203}	$(\gamma, 6n)$, e.c.	<8	<0.1
		$(\gamma, 5np)$	<260	<1.4					
7–8 hr	8-hr Pb^{201}	$(\gamma, 8n)$, e.c.	170	0.9					
		$(\gamma, 7np)$	<80	<0.4					
Tl fraction (average of 2 experiments)									
72 hr	72-hr Tl^{201}	$(\gamma, 8n)$, e.c. $(\gamma, 7np)$, e.c.	45	0.9	4.6 min[e, f]	4.8-min Tl^{207} 4.2-min Tl^{206}	$(\gamma, 2p)$ $(\gamma, 2pn)$	<8	<0.1
		$(\gamma, 6n2p)$	30	0.6					
7 hr	7-hr Tl^{199}	$(\gamma, 10n)$, e.c. $(\gamma, 9np)$, e.c. $(\gamma, 8n2p)$	11	0.2					

[a] Species identification based upon the arguments given in the publications of reference 2 and this paper.
[b] Activities measured at a geometry factor of about 15 percent and uncorrected for counting efficiencies of the individual species.
[c] Estimated long-lived activity from decay curve.
[d] Activity of 68-min Pb^{204m} multiplied by 25 to correct for branching ratio[3] of 12-hr Bi^{204} to 68-min Pb^{204m}.
[e] Component was not observed; limiting activity estimated.
[f] Individual experiment, 10-min irradiation; yield obtained by comparison with monitor foil.

The decay curves of the separated thallium fractions from irradiations at 86 Mev were resolved into a 7-hr and a 72-hr activity. The activity levels were low; thus the analyses are somewhat uncertain. The results show about equal yields for the formation of 72-hr Tl^{201} from parent decay and from direct formation.

A comparison of the 86-Mev and 48-Mev activation experiments shows that at the lower energy the yield of the $(\gamma, 5n)$ reaction is lowered about 12-fold relative to the $(\gamma, 3n)$ reaction, and there is no evidence for reactions involving more than 5 particles. This comparison is independent of the counting efficiencies of the individual species which decay, in the main, by electron capture accompanied by γ-rays and conversion electrons.

The "normalized activities" columns of Table I give the yields for the individual activities normalized to a value of 100 for the saturation activity of 6.4-day Bi^{206} per gram of bismuth. Although the activity values have not been corrected for counting efficiencies, which may vary appreciably for different species, it is interesting to note that the yields drop sharply with increasing number of emitted particles, and that the emission of neutrons appears to be the favored process.

The yield of the fission process is considerably lower than the combined yields of the other nuclear processes observed in bismuth. In two experiments at 86 Mev, the ratio of the saturation activity of Bi^{208}, obtained from the activity of 52-hr Pb^{203}, to that of the fission product 5.3-hr Ag^{113} was found to be 200. The ratio of the yield of Bi^{208} to the yield of fission is given by the ratio of the fission yield of the β^- emitter Ag^{113} to the counting efficiency of the complex decay process in Pb^{203}, multiplied by 200. If it is assumed that the fission yield of Ag^{113} is of the same order of magnitude as the counting efficiency of Pb^{203}; and if the counting efficiencies of the other observed radioactivities are assumed equal, then the ratio of the combined yield of nuclear processes observed [starting at the $(\gamma, 3n)$ reaction] to the fission process is about 4000. At 48 Mev the fission process is still observed to occur, although in lowered yield. The relative yield for fission at 48 Mev to 86 Mev is about tenfold lower than the relative yield of the $(\gamma, 3n)$ reaction at the same energies.

Work is continuing on the measurement of the absolute yields and the energies of the photons responsible for the observed reactions.

The authors gratefully acknowledge the assistance of Mr. C. R. McKinney and members of the Betatron Group in these experiments.

Observations on Lithium and Beryllium Nuclei Ejected from Heavy Nuclei by High Energy Particles

LUIS MARQUEZ* AND I. PERLMAN
Radiation Laboratory and Department of Chemistry,† University of California, Berkeley, California
(Received December 1, 1950)

The yields of Be^7 produced by 335-Mev protons on nuclei of different atomic number have been determined and found to decrease with increasing atomic number. Reactions are described in which the irradiation of an element with protons or alpha-particles results in products higher by three in atomic number. These reactions are interpreted tentatively as second-order processes in which the initial step is the production of high energy lithium nuclei, which in turn cause nuclear reactions of the type (Li,xn). From the observed over-all yields, deductions are made as to the cross sections for the separate steps.

I. INTRODUCTION

THE conditions and mechanisms by which nuclear fragments of mass number greater than four are ejected from heavy nuclei are beginning to receive consideration. The fission of elements in the region of uranium is a special reaction which does not fall into the category under discussion.

The appearance of "hammer" tracks in photographic emulsions struck by cosmic rays is an indication that Li^8 can be produced in a nuclear disintegration. Under better controlled conditions of projectile energy, Li^8 has been observed with high energy protons and deuterons on a variety of gases[1] and with 26.7-Mev x-rays in a photographic emulsion.[2] Evidence that a wide variety of reactions can take place with medium-light elements in which aggregates of nucleons are split off has been obtained by Batzel and Seaborg.[3] How such reactions differ from heavy element fission is not clear; but there probably are differences stemming from the fact that they are endoergic, while heavy element fission is strongly exoergic.

There is also mounting evidence from cosmic-ray studies[4–8] that a variety of charged fragments may be ejected from nuclei and that some of these may have kinetic energies of the order of 100 Mev. The mechanism by which a complex of nucleons can be given such high kinetic energy is not understood. The phenomenon appears to be not unlike that which is the subject matter of the present studies. The question of cross section for such reactions is probably a crucial point in the consideration of the mechanism, but at this stage no significant data are available.‡

The present studies were introduced by some observations of abnormal charge increase in nuclear reactions. It was found that if bismuth (element 83) is irradiated with high energy deuterons, isotopes of astatine (element 85) are produced.[9] It was suggested that high energy deuterons eject alpha-particles from the bismuth, which in turn react with bismuth by well-known reactions of the type (α,n) to produce astatine. Subsequently, other reactions have been observed in which irradiation with alpha-particles resulted in products with an increase of *three* in atomic number. In such a case it would be inferred that a second-order reaction has occurred with *lithium* nuclei formed in the primary reaction.

The present report deals partly with reactions of this type in which it was found that an increase of three in atomic number could be obtained with high energy alpha-particles or protons. The energy of the projectile, rather than its type, is most important in determining the yield. Measurements have also been made on the yields of Be^7 produced in high energy nuclear encounters as this nucleus is one of the few of this size which can be identified.

II. Be^7 FORMATION

The lightest nucleus above helium which can be identified by its radioactive properties is Be^7, which was chosen for investigation of conditions for production of such fragments. The disadvantage in the use of Be^7 for this purpose is its low sensitivity for detection because of the relatively long half-life (52.9 days)[10] and low counting efficiency (one gamma-ray of 0.48 Mev in 10 disintegrations).[11,12]

---

* Now at the Institute for Nuclear Studies, University of Chicago, Chicago, Illinois.

† This work was performed under the auspices of the AEC.

[1] S. C. Wright, Phys. Rev. **77**, 742 (1950).

[2] C. H. Millar and A. G. W. Cameron, Phys. Rev. **79**, 182 (1950).

[3] R. E. Batzel and G. T. Seaborg, Phys. Rev. **79**, 528 (1950).

[4] C. F. Powell and G. P. S. Occhialini, *Nuclear Physics in Photographs* (Oxford University Press, London, 1947).

[5] A. Bonetti and C. Dilworth, Phil. Mag. **40**, 585 (1949).

[6] S. O. C. Sörenson, Phil. Mag. **40**, 947 (1949).

[7] P. E. Hodgson and D. H. Perkins, Nature **163**, 439 (1949).

[8] J. B. Harding, Nature **163**, 440 (1949).

‡ *Note added in proof:* A recent paper by D. H. Perkins [Proc. Roy. Soc. (London) **203**, 399 (1950)] describes extensiveo bservations on the emission of heavy fragments in cosmic-ray stars. The author has identified fragments with charges up to ten units and has found them to have energies in excess of that which would result from coulombic repulsion. The present paper contains deductions in agreement with Perkins' observations and others cited, as is the conclusion that a simple evaporation model cannot explain such high particle energies.

[9] D. H. Templeton and I. Perlman, Abstracts of Papers (Meeting of Am. Chem. Soc., Portland, Oregon, September 13–17, 1948), pp. 55–60.

[10] E. Segrè and C. E. Wiegand, Phys. Rev. **75**, 39 (1949).

[11] R. M. Williamson and H. T. Richards, Phys. Rev. **76**, 614 (1949).

[12] C. M. Turner, Phys. Rev. **76**, 148 (1949).

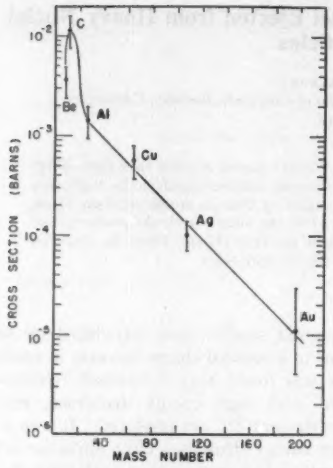

FIG. 1. Yield of Be^7 with 335-Mev protons.

(A) Methods

Beryllium, carbon, aluminum, copper, silver, and gold were irradiated with protons of 335-Mev incident energy. Stacks of foils, 2×4 cm, were used and aligned so that the circulating proton beam penetrated in the direction of the 2-cm dimension. The beam traversing the different targets was therefore degraded in energy by different amounts; for example, the energy range in aluminum was 335–320 Mev, in silver 335–290 Mev, and in gold 335–270 Mev. The accuracy of the cross sections determined and the inferences drawn are not such as to warrant corrections for energy loss nor for attenuation of the beam through nuclear reactions, which becomes appreciable for the heavier elements. The foils were held in place against a copper block and the two foils closest to the block were discarded to avoid contamination from recoil atoms originating in the holder. In some cases thin aluminum foils were wrapped around the target foils to serve as a beam monitor, since Na^{24} from the reaction $Al^{27}(p,3pn)Na^{24}$ is known to be produced with 0.010-barn cross section with protons in the energy range 100–350 Mev.[13]

After irradiation for one to five hours, the targets were worked up and the beryllium fraction isolated with a known weight of added beryllium used to check the yield. In the case of the carbon target, extremely high purity graphite was used; and since no conflicting activities were produced, there were no chemical separations made.

From the aluminum target the only conflicting long-lived isotope produced is Na^{22}. The target was dissolved in HCl, diluted to about 1 liter, some sodium and 10 mg of Be(II) added, and the mixed aluminum and beryllium hydroxides precipitated with ammonia. The precipitate was washed, dissolved in dilute HCl, and the process repeated twice. Only Be^7 could be detected after this treatment.

The Be^7 was separated from the copper, silver, and gold targets by the use of its amphoteric properties. The targets were dissolved in suitable acids, 10–30 mg of Be(II) carrier added and precipitated with ammonia from the copper and silver or, in the case of the gold target, the gold was extracted into ethyl acetate. The resulting beryllium concentrates were dissolved in dilute acids, and sulfide-insoluble substances removed by precipitating a mixture of sulfide-insoluble carriers. Several precipitations were then made from sodium hydroxide solution with iron and other hydroxide insoluble substances used as scavangers. Beryllium is soluble in sodium hydroxide solution. Finally, beryllium as the basic acetate was extracted several times into chloroform in the manner described by McMillan.[14]

(B) Identification of Be^7

Since the radiation from Be^7 consists solely of a gamma-ray of 0.48 Mev, the absence of electrons as well as decay with proper half-life and the distinctive chemistry were used as criteria for the purity of the Be^7. In all cases except that of the gold target it was possible to show that the gamma-rays had the proper half-thickness in lead. The activity isolated from the gold target had but six counts per minute, and positive identification could not be made, especially since there were some shorter lived impurities which had to be resolved.

(C) Cross Sections

The means of monitoring the beam were different for the different targets. For the beryllium target, aluminum foils were used and the Na^{24} measured as already mentioned. The amount of Na^{24} also served to monitor the beam for the aluminum target. For the carbon target, the yield of C^{11} was used according to the excitation curve of Peterson,[15] which shows a cross section of 0.040–0.050 barn in the energy range 350–200 Mev for the reaction $C^{12}(p,pn)C^{11}$. The annihilation radiation of the C^{11} positrons was also used to calibrate the efficiency of the counter for the Be^7 gamma-rays making the assumption that the counting efficiencies for the 0.48-Mev and 0.51-Mev gamma-rays would be the same.

The cross section for the copper target was determined with the yield of Cu^{64} used as a monitor, which has been shown to be 0.025 barn for 340-Mev protons.[16] For the silver target, the yield of 8.2-day Ag^{106} was determined in a separate irradiation with an aluminum monitor, after which it served as a monitor. The gold

[13] P. C. Stevenson and R. L. Folger (private communication).

[14] E. M. McMillan, Phys. Rev. **72**, 591 (1947).

[15] Aamodt, Peterson, and Phillips (University of California Radiation Laboratory Unclassified Report UCRL-526, November, 1949) (unpublished).

[16] R. Batzel and G. T. Seaborg (private communication).

targets were handled similarly, yields being based on an arbitrary point on the decay curve of the gold fraction two days after irradiation. The reason for the secondary monitoring for the copper, silver, and gold targets was to eliminate introduction of Be^7 into the target from the aluminum monitor by recoil.

As mentioned, the counting efficiency of the Be^7 gamma-ray was determined by calibrating the counter against annihilation radiation of C^{11}. For the argon-chlorine Geiger tubes used in these studies, the efficiency was found to be 0.65 percent. Finally, to calculate the cross sections for production of Be^7, the yield of 0.48-Mev gamma-rays was taken to be 1 in 10 disintegrations.[11,12] The errors in cross section include those from counting statistics, counter efficiency calibration, chemical yields, and uncertainties in monitor effectiveness. We estimate that the combined uncertainties are some 30 to 40 percent for the targets other than gold, while the yield obtained from the gold is probably reliable only within a factor of two or three.

The yields of Be^7 from 335-Mev protons are plotted in Fig. 1 against the mass number of the target. The general decrease in yield with increase in atomic number or mass number is apparent and amounts to a factor of 1000 between carbon and gold. It is highly probable that Be^7 results from a different process in the different targets. From carbon, one may visualize Be^7 as the residue from spallation reactions of the type, $C^{12}(p,pan)Be^7$; but, from the heavier nuclei, the Be^7 must be considered as the ejected fragment.

On the basis that the turning point in principal mode of formation might be reached at aluminum between formation of Be^7 as an ejected fragment or as a spallation residue, several spallation products of aluminum were examined. The yields are shown in Table I for 335-Mev protons on aluminum. Since the yields decrease in the expected manner and that of Be^7 is slightly below C^{11}, it is not unlikely that at least part of the Be^7 arises as a spallation residue.

Returning to Fig. 1, it is noted that the yield of Be^7 from a beryllium target (Be^9) is lower than that from a carbon target (C^{12}). Without further study it is not possible to give an explanation. One factor which could contribute to a low yield of Be^7 from Be^9 is the following. It may be assumed that the most important form of excitation in the reaction is the creation of an excited state of Be^9, since the incoming proton will not stay in the nucleus. After this, Be^7 would be reached by evaporation of two neutrons. The first step would result in an excited state of Be^8 from which dissociation into two alpha-particles would compete with further neutron evaporation.

III. ABNORMAL CHARGE INCREASE

In irradiations of tin with ~350-Mev alpha-particles and protons, it has been observed that iodine activities are produced, which means that an increase of three in atomic number has taken place. The iodine activities

TABLE I. Yields of products from irradiation of aluminum with 335-Mev protons.

Nucleus	Yield (barn)
Na^{24}	1.0×10^{-2}
Na^{22}	1.2×10^{-2}
F^{18}	5.5×10^{-3}
C^{11}	1.9×10^{-3}
Be^7	1.4×10^{-3}

were identified[17] as the new neutron-deficient isotopes I^{120}, I^{121}, I^{123}, as well as previously known I^{124} and I^{126}; therefore, none could have come from β^- decay processes. It was also possible to rule out fairly conclusively impurities in the tin as the source of the iodine. The most likely explanation is that the iodine nuclei result from second-order reactions in which lithium nuclei are postulated to be ejected from tin, and these in turn transmute other tin nuclei into iodine. The implications of the yields obtained will be discussed.

(A) Methods

The tin targets were irradiated in the circulating beam of the cyclotron for periods of one to eight hours. After irradiation, the targets were placed in a distilling flask with 10 mg of I^- and 30 cc of H_2SO_4. Upon heating, the tin was dissolved and the iodine was distilled over, probably as hydrogen iodide, and was trapped either in ice-cold solution of sulfur dioxide or in sodium hydroxide solution. The solution in either case was acidified with sulfuric acid and the iodide oxidized to iodine with excess nitrite and distilled as iodine into sodium hydroxide solution. Upon acidification the iodine was extracted into carbon tetrachloride. After removal of the iodine from the carbon tetrachloride with sulfur dioxide solution or sodium hydroxide, the extraction cycle was repeated three times. The iodine was finally isolated as silver iodide, which was weighed to determine the chemical yield.

The iodine activities were resolved by following the decay curves and using the counting efficiencies previously estimated,[17] the yields were calculated. From the longer irradiations, it was possible to identify with a spectrometer the conversion electron line of I^{123}, the positron spectrum of I^{124}, and the β^- spectrum of I^{126}.

TABLE II. Cross sections for formation of iodine activities from high energy particles on tin.

Isotope	350-Mev protons (barn)	350-Mev alphas (barn)
30-min I^{120}	0.5×10^{-6}	0.9×10^{-6}
1.8-hr I^{121}	0.1×10^{-6}	1.1×10^{-6}
13-hr I^{123}	0.7×10^{-6}	1.3×10^{-6}
4.5-day I^{124}	0.4×10^{-6}	0.4×10^{-6}
13-day I^{126}	0.6×10^{-6}	0.1×10^{-6}
Total	2.3×10^{-6}	3.8×10^{-6}

[17] L. Marquez and I. Perlman, Phys. Rev. 78, 189 (1950).

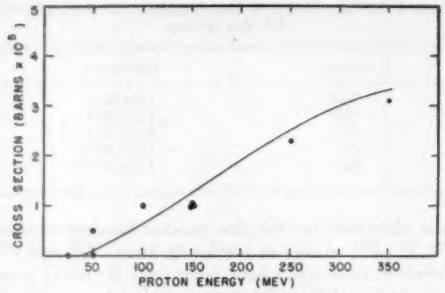

FIG. 2. Excitation function for protons (total iodine cross section).

(B) Yields of Iodine from Tin

Table II shows cross sections for the several iodine activities resulting from high energy protons and alpha-particles on tin. The difficulties of accurate resolution of the different species were considerable and no great confidence can be had in any particular value. Probably comparison of the sums of the several cross sections is more meaningful. It is seen that the total yield with alpha-particles is somewhat greater than with protons but not significantly so. It may be mentioned that 4-min I^{122} and 56-day I^{125} probably were formed also, but the one was not detected because of its short half-life and the other because of its long half-life and low counting efficiency.

In order to see how the yields of iodine activities varied with particle energy, excitation functions were determined for both protons and alpha-particles and are shown in Figs. 2 and 3. The values for energies below 100 Mev became quite uncertain because of low activities, and at about 25 Mev no iodine could be detected. The threshold of detection appeared to be at about 50 to 60 Mev.

The possible role of impurities in the tin as the source of the iodine activities can best be discussed at this point. Spectroscopic examination of the tin showed only traces of the elements lead, copper, iron, arsenic, antimony, bismuth, and silver, each of which was estimated to be present to the extent of less than 5 ppm. Since the formation of iodine with 350-Mev alpha-particles was found to have a cross section of $\sim 10^{-5}$ barn, antimony is ruled out as a source of the iodine. The actual cross sections expected from antimony are at least 100 times lower than would be required. Furthermore, it would not be possible to explain the similar yields for protons and alpha-particles. Tellurium cannot be ruled out quite so conclusively from the chemical analysis, because the limits of detection are poor. However, if tellurium were present, the trends of the excitation curves are the opposite of what would be expected. Also, I^{130} and I^{131} would be formed, and when a low resolution beta-ray spectrometer was used, their spectra were not encountered. Elements of higher atomic number than iodine were ruled out by an analysis for barium radioactivities. Barium activity would be encountered in higher yield than iodine, yet an upper limit for its formation cross section could be set at 10^{-6} barn and it is probably much lower. The iodine activities could not arise from thorium or uranium through fission, since the wrong iodine isotopes are found; and, in any case, very low limits could be set for the presence of these elements from the inability to detect alpha-radioactivity which would be found in high yield from spallation products. Iodine itself as an impurity in the tin was eliminated from consideration by chemical analysis which showed that less than 10 ppm were present. From the yields of comparable reactions to form light antimony isotopes from an antimony target,[18] the iodine would have had to be present to an extent at least ten times greater than the upper limit measured.

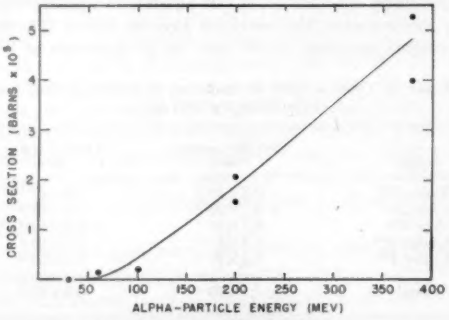

FIG. 3. Excitation function for alphas (total iodine cross section).

IV. DISCUSSION

The explanation for the observed reaction products by means of second-order reactions involving lithium nuclei demands examination with regard to expected and observed yields. The mechanism is in qualitative agreement with the features observed; that is, it accounts for the particular iodine isotopes found, the increase in yield with increase in projectile energy, and the fact that the activities and their yields are nearly the same whether alpha-particles or protons are used. That lithium nuclei can be ejected in high energy nuclear reactions is also inferred from the proof that specific nuclei Li^8 and Be^7 are formed. The objective is then to piece together conditions for each stem of the two-step process which could give the observed over-all results.

There are three important parameters that enter into the determination of the over-all yield, for none of which do we have values: (1) the cross section (σ_{Li}) for the production of lithium nuclei, (2) the energy distribution of the lithium nuclei, and (3) the cross section for the formation of iodine isotopes from lithium nuclei

[18] M. Lindner and I. Perlman, Phys. Rev. 78, 499 (1950).

on tin. The energy distribution for the lithium nuclei (item 2) is of great importance, not only in its effect on the cross section for producing iodine from tin, but also as it determines the ranges of the lithium nuclei in the tin.

The first simplifying assumption made is that regarding the cross section of the lithium reactions with tin to give iodine. It is assumed that all lithium nuclei which enter tin nuclei result in iodine isotopes; that is, all three protons which enter remain. This assumption is probably not seriously in error, because it is known that for alpha-particles in the proper energy range, reactions of the type (α,xn) are most prominent in medium-heavy and heavy nuclei. Recently, it has been shown that (C^{12},xn) reactions occur[19,20] with appreciable cross section, which means that six protons entering a nucleus can all remain. We shall then assume that the cross section for the formation of iodine isotopes is nearly the same as the penetration cross section for lithium into tin given by the formula:

$$\sigma=\pi R^2(1-B/E),$$

where B is the potential barrier height (taken to be 30 Mev), E is the energy of the lithium ion ($E>B$), and πR^2 is the geometric cross section of tin (1.7×10^{-24} cm^2). The total cross section for the production of iodine isotopes (σ_I) is estimated from the measured values for full energy protons or alpha-particles to be 4×10^{-29} cm^2 (Table II).

The cross section for formation of lithium nuclei in the primary reaction can then be calculated for various assumed values of monoenergetic lithium ions of energy ϵ:

$$\sigma_{Li}=\sigma_I\Big/\left[\pi R^2\int_{E=B}^{E=\epsilon}n(1-B/E)dx\right],$$

in which n is the number of tin nuclei per cm^3 and x is the distance traveled by the lithium ions. The relation between E and x was obtained from the theory of the interaction of heavy ions with matter, and the integrations were performed numerically. Some typical results

[19] Miller, Hamilton, Putnam, Haymond, and Rossi, Phys. Rev. **80**, 486 (1950).

[20] Ghiorso, Thompson, Street, and Seaborg, Phys. Rev. **81**, 154 (1951).

TABLE III. Relation between calculated cross section and energy of lithium nuclei.

ϵ(Mev)	36	40	50	80	120	200
σ_{Li}(barn)	3.0	1.2	0.3	5×10^{-2}	2×10^{-2}	5×10^{-3}

are shown in Table III, from which it is seen that the cross sections are surprisingly high, and only those seem to be reasonable which assume that the lithium ions are ejected with high energy, say, 80 Mev or higher. Even if it is assumed that the effective energy of the lithium ions is 80 Mev, the resulting cross section is 0.05 barn, which is 500 times greater than that observed for the formation of Be^7 from silver. The differences in yields for these two cases would have to be reconciled by the arguments that in the one case the sum of a number of lithium isotopes is compared with the single isotope, Be^7, and the greater charge of beryllium as compared with lithium should make its ejection more difficult.

If the deduction that the lithium nuclei are ejected with high kinetic energy should be borne out by some form of direct measurement, it would seem to be impossible to explain this phenomenon through a compound nucleus model. Instead, one must assume that such fragments are ejected before the excitation energy is distributed in order that they may carry away a large fraction of the available energy. Indeed, it is probable that when energy of the order of 200 Mev is evenly distributed throughout a medium heavy nucleus, a fragment containing three protons would compete very poorly in evaporation probability with particles such as protons, and especially neutrons. Qualitatively, these arguments are restatements of the picture given by Serber[21] for high energy nuclear reactions. The cosmic-ray work already cited in which charged particles of high energy are expelled from nuclei may be concerned with the same process, although neither the nature of the exciting particle nor cross sections are known which would be necessary to make comparisons.

We wish to thank Mr. James T. Vale and the other members of the 184-inch cyclotron operating group for making the irradiations.

[21] R. Serber, Phys. Rev. **72**, 1114 (1947).

Long-Lived Bi^{207} and Energy Levels of Pb^{207}

H. M. NEUMANN* AND I. PERLMAN
Radiation Laboratory and Department of Chemistry,† University of California, Berkeley, California
(Received November 30, 1950)

The long-lived isotope of bismuth, Bi^{207}, has been prepared by deuteron irradiation of lead and from the alpha-decay of At^{211}. From the genetic relationship with At^{211}, the half-life is estimated as 50 years. The conversion electron spectrum has been determined and is discussed in terms of the energy states of Pb^{207}. Further evidence on these states has been obtained from the discovery of three rare alpha-groups in the decay of Po^{211} of energies 6.90, 6.57, and 6.34 Mev, which are compared with the main group at 7.43 Mev.

I. INTRODUCTION

THE region of naturally occurring bismuth isotopes lies in the range from Bi^{209} to Bi^{214}, but isotopes down to Bi^{198} have been produced by cyclotron irradiations.[1-3] Two isotopes, Bi^{207} and Bi^{208}, have never been reported although sought for[1,4] and have been presumed to be either long-lived or very short-lived, probably the former. The present report deals with the properties of Bi^{207} produced under more favorable conditions by two methods previously tried: the deuteron irradiation of lead[1] and the alpha-decay[4] of At^{211}.

This nucleus, Bi^{207}, decays by electron capture; and its gamma-ray spectrum is of particular interest in indicating energy levels of Pb^{207}. The lowest lying energy levels of lead isotopes seem to be widely spaced as indicated, for example, by the well-known lowest excited state of Pb^{208} at 2.62 Mev and by other data from radioactive decay processes.[5]

Other measurements of energy states of Pb^{207} have been obtained in the present studies by observation of multiple alpha-groups in the decay of Po^{211}, which is best obtained without conflicting alpha-activities by preparing its electron capture parent At^{211}. Also included in this report are some observations on the failure to find any activity from Bi^{208} which can be explained in terms of the energy states of Pb^{208}.

II. Bi^{207} FROM THE ALPHA-DECAY OF At^{211}

The 7.5-hr isotope At^{211} decays 40 percent by emission of a 5.89-Mev alpha-particle[6] and 60 percent by electron capture to give Po^{211}(AcC′), which in turn decays with a 7.43-Mev alpha-particle. Because of the short half-life of Po^{211} (estimated to be several milliseconds), it cannot be dissociated from its parent, so that At^{211} appears to decay with two alpha-groups widely separated in energy. The alpha-decay of Po^{211} results in stable Pb^{207} and the alpha-branching of At^{211} produces Bi^{207}, which should be unstable toward decay by electron capture to Pb^{207}.

Four large sources of At^{211} (each $\sim 10^9$ disintegrations/min) were prepared by bombarding four thick target samples of metallic bismuth with 38-Mev helium ions. Under these conditions roughly equivalent amounts of At^{210} and At^{211} are formed. The presence of At^{210} does not interfere with the measurements to be made. The astatine was separated from each target by volatilizing it from the molten target onto a cooled silver disk.

Two of the silver plates were used for counting purposes without further purification of the astatine. The alpha-decay of these samples showed a 7.2-hour decay (At^{211}), followed by the longer-lived Po^{210} which arises from the electron capture decay of At^{210}. The decay of the At^{210} gamma-ray was measured with a Geiger-Müller counter using a 1008-mg/cm^2 Pb absorber to eliminate x-rays from both At^{210} and At^{211}, and a half-life of 8.0 hr was observed. The residual activity remaining after complete decay of the astatine isotopes was determined with a Geiger-Müller counter, the sample being covered with just sufficient aluminum to absorb the Po^{210} alpha-particles. This residual activity showed one component of 6.4-day half-life (apparently Bi^{206} from the alpha-decay of At^{210}), and a second long-lived component (Bi^{207} from the alpha-decay of At^{211}).

Sufficient activity was available to determine absorption curves in aluminum and beryllium of both of these activities. The absorption properties of the 6.4-day activity were found to be similar to those reported[1] for Bi^{206}. The absorption curve for the long-lived Bi^{207} activity is shown in Fig. 1, resolved into its several components. Curve "O" is the unresolved aluminum absorption curve, while curve "A" is that of the electromagnetic radiation obtained by filtering out the electrons with 475 mg cm^{-2} of beryllium. Curve "A" was then resolved into curve "B," which includes the K x-rays and gamma-rays, and curve "C," the L x-rays. Correction was made in these curves for the absorption of the L x-rays by the beryllium. Finally, curve "D" represents the electrons.

On other samples of Bi^{207} prepared in another manner beta-ray spectrometer measurements were made and further detailed discussion of the decay characteristics

* Present address: Department of Chemistry, Northwestern University, Evanston, Illinois.
† This work was performed under the auspices of the AEC.
[1] Templeton, Howland, and Perlman, Phys. Rev. **72**, 766 (1947).
[2] H. M. Neumann and I. Perlman, Phys. Rev. **78**, 191 (1950).
[3] D. G. Karraker and D. H. Templeton, Phys. Rev. **81**, 510 (1951).
[4] E. L. Kelly and E. Segrè, Phys. Rev. **75**, 999 (1949).
[5] Sunyar, Alburger, Friedlander, Goldhaber, and Scharff-Goldhaber, Phys. Rev. **78**, 326 (1950); **79**, 181 (1950); D. E. Alburger, Brookhaven National Laboratory Report BNL-64 (July, 1950).
[6] Corson, Mackenzie, and Segrè, Phys. Rev. **58**, 672 (1940).

of Bi^{207} will be referred to the following section, where these data are treated.

The two remaining astatine samples were dissolved after the initial volatilization separation, and further purification was effected consisting of carrying on tellurium during reduction with SO_2, and extractions into isopropyl ether. An aliquot was then counted to determine the amount of astatine present. When the decay of astatine was complete, bismuth carrier was added, bismuth and polonium fractions isolated, and the bismuth fraction carefully purified to eliminate the possibility of contamination by other elements. The activity of the bismuth fraction was followed with a Geiger counter and showed both the 6.4-day and long-lived components, each with the characteristics as noted in the chemically unseparated decay products of the astatine.

The half-life of Bi^{207} may be determined by measuring the activity which results from the decay of a known quantity of its parent, At^{211}. However, one encounters here the usual difficulty of estimating the counting efficiency for nuclei which decay by electron capture. In estimating the counting efficiency of Bi^{207} we have assumed that each electron capture decay event produces one L x-ray and that in addition each conversion electron is accompanied by an L x-ray. The Auger coefficient for L x-rays in this region is taken to be 0.5 and the counting efficiency of the x-rays has been shown to be about 3 percent in the counters employed. With these assumptions and estimations, the actual disintegration rate can be determined; and, therefore, the half-life of Bi^{207} can be calculated from the activities of At^{211} and the Bi^{207} daughter. The value so obtained is 50 years.

The counting rate of Bi^{207} without absorbers is largely that of the hard electrons. From the curves of Fig. 1 it can be shown that hard electrons are found in about 15 percent of the disintegrations and that the over-all counting efficiency without absorbers is about 1 count for 6 disintegrations.

Another sample of Bi^{207} prepared in a different manner was followed for decay over a period of 33 months. The minimum half-life, estimated from the counting data which indicated no significant decay, was 40 years. This means that the counting efficiency for Bi^{207} cannot be much lower than that estimated (15 percent) which corresponds with a 50-year half-life since the half-life decreases with the counting efficiency.

III. Bi^{207} FROM DEUTERONS ON LEAD

Bombardment of a thick lead target with 18-Mev deuterons should produce in various amounts all of the bismuth isotopes in the mass range 203 to 209. With the exception of Bi^{207} and Bi^{208}, all of these isotopes had been identified previously, and the longest-lived of these[9] is 14.5-day Bi^{205}.

In August, 1946, a thick lead target was bombarded with 18-Mev deuterons, and in November, 1947, the remaining bismuth activity was separated by J. J. Howland of this laboratory. The sample has shown no decay in the past 33 months, and from the counting statistics we could set a lower limit of 40 years for the half-life as mentioned above.

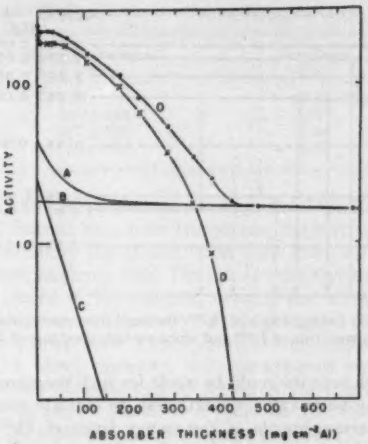

FIG. 1. Aluminum absorption curves for Bi^{207}. The components are: O, the unresolved curve; A, x-rays and γ-rays; B, K x-rays and γ-rays; C, L x-rays; D, electrons. See text for method of resolution.

The aluminum absorption characteristics for this activity were identical to those of Bi^{207} shown in Fig. 1. It is also significant that the ratio of electrons to L x-rays is the same in both samples, since if Bi^{208} contributed to the activity, an increased number of x-rays would be expected over those present in the pure Bi^{207} sample. (See discussion below on properties of Bi^{208}.) The long-lived activity formed in deuteron bombardment of lead is then essentially all Bi^{207}.

Sufficient activity from the deuteron bombardment of lead was available for use in a beta-ray spectrometer, and twelve conversion lines were observed. It is assumed that all of these lines belong to Bi^{207}; further arguments against attributing any of the electron radioactivity to Bi^{208} will be given below. The beta-ray spectrometer was a 255°-shaped magnetic field instrument operated with a resolution of 1.5 percent. The conversion lines, their assignments and relative intensities are shown in Table I. The absorption curve of Fig. 1 is consistent with these data, since it shows a major electron component at about 1 Mev and the tail of a soft component. The conversion lines around 500 kev are not sufficiently abundant to show up in the curve, and the hardest electrons are also in low abundance and blend with the electromagnetic radiation. The last four electrons listed in Table I were in too low abundance for us to have observed the L conversion lines.

There is no unique decay scheme which can be deduced from these data. It would be helpful to have the photo-electron spectrum from the uncoverted gamma-rays and their abundances, but not nearly

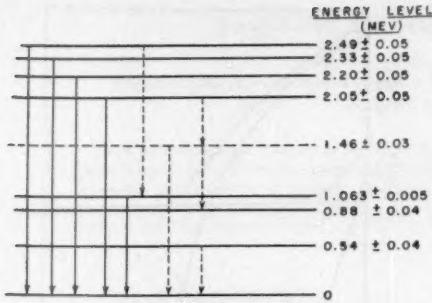

FIG. 2. Energy levels of Pb^{207}. Deduced from conversion electron spectrum of Bi^{207} and alpha-particle spectrum of Po^{211}.

enough activity could be made for such measurements. It may be of value, nevertheless, to indicate some possible arrangements of the energy levels of Pb^{207}, particularly since some independent data are available to aid in selections; and this has been done in Fig. 2. There is, of course, no way of deducing from the conversion electron spectrum the total electron capture decay energy even if the excited states of Pb^{207} resulting from the electron capture are as shown in Fig. 2. As a result, we do not know how much the decay energy exceeds 2.49 Mev, the energy of the hardest gamma-ray. The reasons for the energy level scheme as shown in Fig. 2 will be given after some further data are discussed which were obtained from the alpha-decay of Po^{211}.

It is readily apparent that the electron capture decay of Bi^{207} is highly forbidden. This is not surprising, as the spin of Pb^{207} is known to be $\frac{1}{2}$, and the spin of Bi^{207} would be expected to be the same as that of Bi^{209}, 9/2.

IV. ALPHA-DECAY OF Po^{211}

While about 40 percent of the At^{211} disintegrations are alpha-decay processes going to Bi^{207}, the remainder form Po^{211} by electron capture.[6] Being short-lived (estimated half-life several milliseconds), the Po^{211} exists in equilibrium with its parent and decays with the half-life of the latter. Some At^{211}, free from At^{210}, was

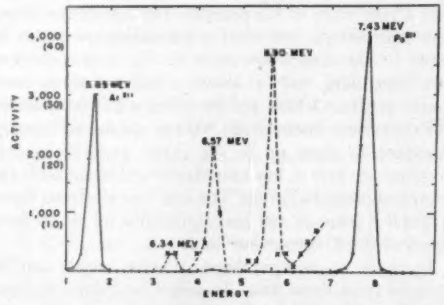

FIG. 3. Alpha-particle pulse analysis of At^{211}-Po^{211}. Broken-line portion of curve is on 100-fold expanded ordinate scale.

prepared by bombardment of a thin bismuth target with 25-Mev helium ions. A sample was collected by volatilization onto a platinum disk and examined with an alpha-particle pulse analyzer.[7] In addition to the alpha-particles of 5.89 Mev from At^{211} and 7.43 Mev from Po^{211}, three additional groups of low abundance were observed. These results are shown in Fig. 3, in which the groups in question are shown with a 100-fold expanded ordinate scale over that for the main groups. The low abundance groups are believed to be short range groups from Po^{211} for which the observed abundances and energies are given in Table II. The alpha-energies of At^{211} and of the Po^{211} ground-state transition served as standards to determine the energies of the short-range groups.

The branching of At^{211} decay is, from these experiments, 40.9±0.5 percent by alpha-emission and 59.1 ±0.5 percent by electron capture.

The principal piece of evidence that the three new alpha-groups are low energy groups of Po^{211} comes from their association with At^{211} and decay with the proper

TABLE I. Conversion electrons from Bi^{207}.

Electron energy (Mev)	Assignment	γ-ray energy (Mev)	Relative intensity of electron
0.049	K or L	0.137 or 0.064	0.11
0.062	Auger electrons		0.05
0.477	K	0.565	0.07
0.551	L		0.008
0.975	K	1.063	0.37
1.050	L		0.08
1.37	K	1.46	0.011
1.46	L		0.004
1.96	K	2.05	0.0014
2.11	K	2.20	0.0005
2.24	K	2.33	0.0014
2.40	K	2.49	0.0016

half-life. It is also of interest to examine whether or not the abundances of the several groups conform with what would be expected from alpha-decay theory. The test should not be expected to give close agreement, since it has been shown[8] that nuclei with odd nucleons will be characterized by prohibited alpha-decay which varies from one nucleus to another. Figure 4 shows the curve calculated[9] for the *half-life–decay energy* relationship for *even-even* polonium isotopes making the assumption of normal nuclear radii as previously[9] defined. Po^{211} would be expected to lie above the curve on two counts: (1) forbidden alpha-decay because of the odd nucleon, and (2) there is reason to believe that the nuclear radius is abnormally low. The half-life for Po^{211} has been estimated[10] to be 5 msec; but this is close to the half-life expected if there were no prohibition of alpha-decay,

[7] Ghiorso, Jaffey, Robinson, and Weissbourd, *The Transuranium Elements: Research Papers* (McGraw-Hill Book Company, Inc., New York, 1949), Paper No. 16.8, National Nuclear Energy Series, Plutonium Project Record, Vol. 14B.

[8] Perlman, Ghiorso, and Seaborg, Phys. Rev. 77, 26 (1950).

[9] I. Perlman and T. J. Ypsilantis, Phys. Rev. 79, 30 (1950).

[10] Curie, *et al.*, Revs. Modern Phys. 3, 427 (1931).

and we are inclined to estimate it as 50 msec or longer. From this the partial half-lives for the low energy groups are calculated from their abundances and plotted in Fig. 4. It may be seen that the relationships for these groups are not out of line with their assignment to short range groups of Po^{211}.

The energies of these alpha-groups of Po^{211} have an obvious bearing on the energy levels of Pb^{207}.

V. ENERGY LEVELS OF Pb^{207}

The three low energy alpha-groups from Po^{211} establish three of the energy levels of the daughter nucleus Pb^{207}. After the measured particle energies were converted into decay energies by adding the daughter nucleus recoil energy, differences from the ground-state transition gave the following levels for Pb^{207}: 0.54 $\pm$0.04, 0.88$\pm$0.04, and 1.11$\pm$0.06 Mev. In Table I, which shows the conversion electron lines from the decay of Bi^{207}, two of the gamma-rays can be seen to agree with two of these levels; but there are no conversion lines which correspond directly to the 0.88-Mev level. It is, of course, possible that those events which reach the 0.88-Mev level are either rare or that the degree of internal conversion of the gamma-ray is too low for detection. That this state does exist is known from the beta-decay of AcC″ (Tl^{207}) in which a gamma-ray of 870 kev in low abundance has been reported.[11]

Other levels and transitions indicated in Fig. 2 were derived from the conversion electrons of the Bi^{207} decay. To aid in the construction of the energy level diagram it is advantageous to estimate the decay energy of Bi^{207}. The basis of the estimation is the following decay cycle:

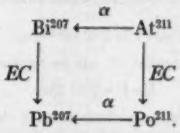

The alpha-decay energies of At^{211} and Po^{211} are known to be 6.0 Mev and 7.6 Mev, respectively. We shall estimate the electron capture decay energy of At^{211} using the empirical correlations of Thompson,[12] which gives 0.8 Mev as the decay energy corresponding to the measured half-life. From these values, the decay energy of Bi^{207} may be seen to be 2.4 Mev. Great reliance cannot be placed in this estimation, and it will be noted (Fig. 2) that a gamma-ray of greater energy (2.49 Mev) has been observed. However, the estimation is probably good enough to show that the hard gamma-rays cannot be in cascade and, therefore, they must lie in some such fashion as is shown in Fig. 2.

The broken lines in the diagram indicate alternative levels and transitions. For example, it is not necessary to assume a level at 1.46 Mev, since the same gamma-ray energy can be obtained between two other known levels. Similarly, the gamma-ray of 0.565 Mev can result from at least three transitions; but a state about this far above the ground state must exist, according to the alpha-decay data. The soft gamma-rays have not been placed in the diagram, because the energies are not known unambiguously. It is probable that the lowest excited state is that obtained from alpha-decay at 0.54 Mev; therefore, soft gamma-rays represent transitions between excited states. If there were any low lying excited states, it is probable that the corresponding alpha-groups would have been seen.

The apparent absence of low lying energy states of lead isotopes is explained by the assumption of a "closed shell" of 82 protons; and there is also, no doubt, a contribution from the neutron shell in this region closed with 126 neutrons. The lowest excited state of Pb^{204} is probably 374 kev above the ground state with a metastable state 905 kev above it.[5] Measurements of alpha-radioactivity of Po^{210} would indicate that the lowest lying excited state of Pb^{206} is 800 kev above the ground state, and this receives some support by the absence of gamma-radiation in the β^- decay of Tl^{206}. Of the other stable lead isotopes, the levels of Pb^{207} are discussed in this paper, while Pb^{208} is thought to have its lowest excited state at 2.62 Mev.

TABLE II. Abundances of alpha-particle groups from Po^{211}.

Alpha-particle energy (Mev)	Abundance (percent)
7.43	98.88
6.90±0.04	0.57
6.57±0.04	0.48
6.34±0.06	0.07

VI. PREDICTED PROPERTIES OF Bi^{209}

In the preparation of Bi^{207} with deuterons on lead it would be expected that Bi^{208} would be formed in comparable quantities. Nevertheless, we have attributed all of the electrons observed in the preparation to Bi^{207} as a result of considerations already given and some which follow.

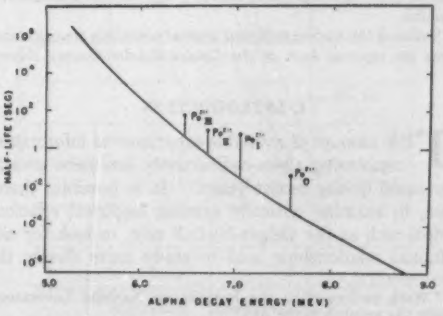

FIG. 4. Alpha-energy–half-life relationship for Po^{211} groups. Solid line is theoretical curve for even-even polonium nuclei on the assumption of normal nuclear radii.

[11] J. Surugue, J. phys. radium 7, 145 (1946).
[12] S. G. Thompson, Phys. Rev. 76, 319 (1949).

There is no decay cycle comparable to that used for Bi^{207} which has enough known components to permit estimation of the decay energy of Bi^{208}. However, in this case, some neutron binding energies are known which permit the closing of another cycle:

$$\begin{array}{ccc} Bi^{208}+n & \longrightarrow & Bi^{209} \\ EC \downarrow & & \uparrow \beta^- \\ Pb^{208}+n & \longrightarrow & Pb^{209}. \end{array}$$

The β^- decay energy of Pb^{209} is known to be 0.70 Mev, and the neutron binding energies in Bi^{209} and in Pb^{209} have been measured although there are some uncertainties in the values. These binding energies from several sources have been discussed[13] and the principal uncertainty pertinent to the present discussion is the choice for the binding energy of the $Pb^{208-209}$ neutron between the limits 3.87 Mev and approximately 400 kev higher. If the higher value is selected, the electron capture energy for Bi^{208} becomes 2.3 Mev, while if the lower value is accepted, the decay energy is 2.7 Mev. From detailed work on the gamma-ray spectra of the natural radioactivities it is known that the lowest excited state of Pb^{208} is 2.62 Mev. It is seen, therefore, that the electron capture decay of Bi^{208} either cannot go to an excited state of Pb^{208} or can do so with very low decay energy. A search for the 2.62-Mev gamma-ray in the Bi^{207}, Bi^{208} mixture did not yield any positive results. As a result, we are probably justified in considering that all electrons of energy above the Auger electron region belong to Bi^{207} and that the only electromagnetic radiation from the decay of Bi^{208} is x-rays. We have made the tacit assumption in this discussion that Bi^{208} is long-lived, but obviously there is no direct evidence on this point.

We wish to thank Mr. C. I. Browne and Mr. G. D. O'Kelley for their aid in determining the electron spectra reported here, and Mr. A. Ghiorso for the alpha-particle pulse analyses.

[13] Huizenga, Magnusson, Simpson, and Winslow, Phys. Rev. 79, 908 (1950).

PHYSICAL REVIEW VOLUME 81, NUMBER 6 MARCH 15, 1951

On the Systematics of Even-Even Alpha-Emitters

IRVING KAPLAN
Brookhaven National Laboratory, Upton, New York*
(Received September 25, 1950)

The systematics of even–even alpha-emitters are studied. Empirical relationships are found, of the form

$$\log\lambda = a + b/v, \quad Z \text{ constant},$$

for values of $Z=84$, 86, 88, 90, 92, and 94. For these cases, the relationships found represent a more precise empirical correlation of alpha-energy and disintegration constant than does the Geiger-Nuttall rule. Relationships of the form

$$\log\lambda = A + B/v, \quad (A-2Z) \text{ constant},$$

exist for members of different partial radioactive series and are related to the disintegration schemes of the thorium and uranium families.

Values of the nuclear radii and internal potentials are calculated from the rigorous form of the Gamow-Condon-Gurney theory. The radii of "normal" even-even alpha-emitters can be presented by

$$r_0 = 1.57A^{\frac{1}{3}}\times 10^{-13} \text{ cm},$$

while the internal potential, U, can be represented by

$$E-U=0.52 \text{ Mev}.$$

The latter relationship is an indication of the approximate constancy, for the different nuclei, of the logarithmic derivative of the radial wave function at the boundary of the nucleus.

The empirical relations $\log\lambda = a + b/v$, Z constant, are compared with theory; and the significance of the comparison is discussed.

The values of the half-lives of Th^{224}, Ra^{220}, and Em^{216} are predicted.

The isotopes of polonium and emanation, which show departures from "normal behavior," are considered.

I. INTRODUCTION

THE amount of available experimental information concerning alpha-radioactivity has been greatly increased during recent years.[1,2] It is possible, therefore, to examine critically existing empirical relationships, such as the Geiger-Nuttall rule, to look for additional relationships, and to study more closely the validity of the Gamow-Condon-Gurney theory of alpha-decay. Although several investigations of the systematics of alpha-radioactivity have been made,[3–7] the present treatment is based on a somewhat different approach from that of any of the others.

The present study is limited to the ground state transitions of even-even alpha-emitting nuclides in

* Work performed at the Brookhaven National Laboratory, under the auspices of the AEC.

[1] G. T. Seaborg and I. Perlman, Revs. Modern Phys. 20, 585 (1948).

[2] Perlman, Ghiorso, and Seaborg, Phys. Rev. 77, 26 (1950).

[3] A. Berthelot, J. phys. radium 3, 52 (1942).

[4] S. Biswas and A. P. Patro, Indian J. Phys. 22, 539 (1948).

[5] S. Biswas, Phys. Rev. 75, 530 (1949).

[6] S. Biswas, Indian J. Phys. 23, 51 (1949).

[7] I. Perlman and T. J. Ypsilantis, Phys. Rev. 79, 30 (1950).

order to avoid complications introduced by the spin changes involved either in transitions to excited states, or in transitions of even proton-odd neutron, or odd proton-odd neutron nuclei. In Sec. II, some relationships will be obtained from the experimental data. In Sec. III, the rigorous form of the Gamow-Condon-Gurney theory will be used to calculate the values of the nuclear radii and the internal potentials. These values will then be used to obtain theoretical expressions which can be compared with some of the empirical relationships of Sec. II. In Sec. IV, some of the correlations obtained in the earlier sections will be used to predict the values of the half-lives of Th^{224}, Ra^{220}, and Em^{216}. In Sec. V, a group of nuclides consisting of Em^{212} and the even-even nuclides of polonium of atomic weight 210 or less will be considered separately because,

TABLE I. Alpha-radioactivity data. Even-even nuclides.

Parent nucleus	Alpha-energy (Mev)	Alpha-half-life (sec)	$\log_{10}$ (disintegration constant) ($\log\lambda$)	Alpha-velocity (10^9 cm/sec)
$_{96}Cm^{242}$	6.18	1.30×10^{7}	−7.242	1.740
$_{96}Cm^{240}$	6.37	2.59×10^{6}	−6.572	1.767
$_{94}Pu^{240}$	5.20	1.89×10^{11}	−11.437	1.596
$_{94}Pu^{238}$	5.60	2.90×10^{9}	−9.622	1.657
$_{94}Pu^{236}$	5.85	8.55×10^{7}	−8.090	1.694
$_{94}Pu^{234}$	6.26	8.64×10^{6}	−6.097	1.752
$_{92}U^{238}$	4.25	1.42×10^{17}	−17.312	1.444
$_{92}U^{234}$	4.84	7.40×10^{12}	−13.029	1.540
$_{92}U^{232}$	5.40	2.21×10^{9}	−9.504	1.628
$_{92}U^{230}$	5.96	1.80×10^{6}	−6.416	1.710
$_{92}U^{228}$	6.83	7.2×10^{2}	−3.017	1.830
$_{90}Th^{232}$	4.05	4.38×10^{17}	−17.801	1.410
$_{90}Th^{230}$ (o)	4.76	3.15×10^{12}	−12.658	1.513
$_{90}Th^{228}$ (o)	5.52	8.19×10^{7}	−8.072	1.646
$_{90}Th^{226}$	6.41	1.85×10^{3}	−3.426	1.773
$_{88}Ra^{226}$ (o)	4.88	5.61×10^{10}	−10.907	1.547
$_{88}Ra^{224}$	5.78	3.14×10^{5}	−5.656	1.685
$_{88}Ra^{222}$	6.62	3.8×10^{1}	−1.745	1.802
$_{86}Em^{222}$	5.59	3.31×10^{5}	−5.678	1.657
$_{86}Em^{220}$	6.39	5.45×10^{1}	−1.896	1.772
$_{86}Em^{218}$	7.25	1.90×10^{-2}	1.562	1.886
$_{84}Po^{218}$	6.12	1.83×10^{2}	−2.421	1.733
$_{84}Po^{216}$	6.89	1.58×10^{-1}	0.643	1.839
$_{84}Po^{214}$	7.83	1.50×10^{-4}	3.666	1.961
$_{84}Po^{212}$	8.95	3.0×10^{-7}	6.364	2.096

as has been shown by Seaborg and his collaborators,[2,7] these nuclei show departures from "normal" behavior which are probably explainable in terms of shells in nuclear structure.

II. EMPIRICAL RELATIONSHIPS

The data used in the present study are the alpha-energies and alpha-half-lives given by Seaborg and Perlman[1] and Perlman, Ghiorso, and Seaborg[2] for the ground-state transitions of even-even nuclei. For convenience, the basic data are given in Table I together with useful derived quantities.

Following the convention of Perlman, Ghiorso, and Seaborg, the term "alpha-energy" is used to denote the total energy of the transition between ground states. It

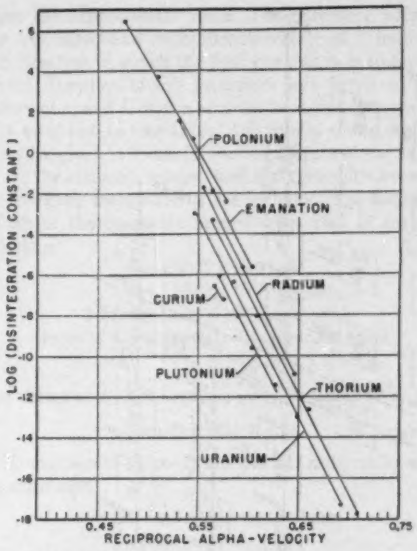

FIG. 1. Logarithm of the disintegration constant *vs* reciprocal of the velocity for constant Z. Disintegration constant, λ, in sec^{-1}; velocity in units of 10^9 cm/sec.

is the sum of the kinetic energies of the alpha-particle and the recoil nucleus. The "alpha-velocity" is the velocity of the alpha-particle relative to the product

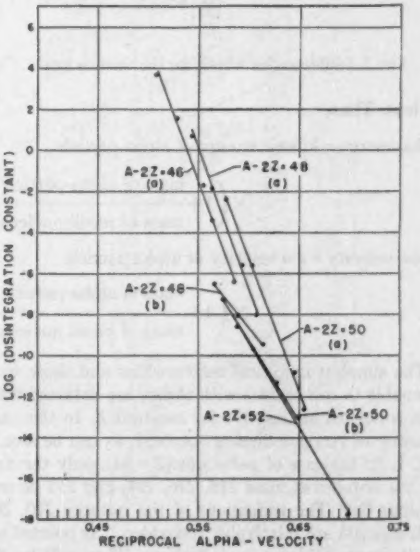

FIG. 2. Logarithm of the disintegration constant *vs* reciprocal of the velocity, for constant $A-2Z$. Disintegration constant, λ, in sec^{-1}; velocity in units of 10^9 cm/sec.

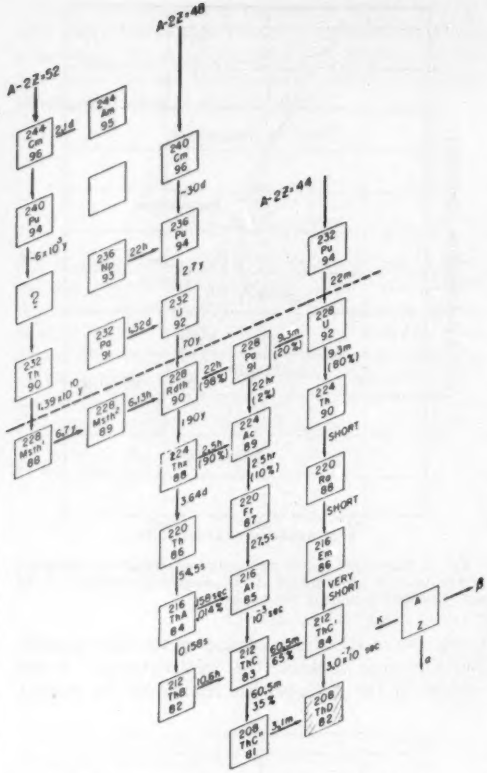

FIG. 3. Disintegration scheme for the thorium family.

nucleus. Thus,

$$\text{alpha-energy} = \text{kinetic energy of alpha-particle} \times\left(1+\frac{\text{mass of alpha-particle}}{\text{mass of recoil nucleus}}\right),$$

$$\text{alpha-velocity} = v = \text{velocity of alpha-particle} \times\left(1+\frac{\text{mass of alpha-particle}}{\text{mass of recoil nucleus}}\right).$$

The simplest empirical relationships and those most amenable to comparison with theory are obtained when $\log\lambda$ is plotted against $1/v$ for constant Z. In this case, a family of straight lines is obtained, as can be seen in Fig. 1. In the case of polonium ($Z=84$), only the data for the isotopes of mass 218, 216, 214, and 212 lie on a straight line. The transitions of the isotopes 210, 208, 206, and 204 are relatively "forbidden," as pointed out by Perlman, Ghiorso, and Seaborg. They will be discussed in Sec. V.

The equations of the straight lines, obtained by the method of least squares, are ($\log\lambda \equiv \log_{10}\lambda$)

$$\begin{aligned}
&(Z=84)\ \log\lambda = 48.17-87.50/v,\\
&(Z=86)\ \log\lambda = 54.05-99.02/v,\\
&(Z=88)\ \log\lambda = 53.92-100.33/v,\\
&(Z=90)\ \log\lambda = 50.55-96.32/v,\\
&(Z=92)\ \log\lambda = 51.24-98.95/v,\\
&(Z=94)\ \log\lambda = 49.18-97.02/v.
\end{aligned} \tag{1}$$

In Eq. (1), and in all similar equations, the velocity is expressed in units of 10^9 cm/sec, and λ is in sec^{-1}.

These empirical relations constitute a more precise, yet simple, form of the Geiger-Nuttal rule, which has been previously expressed in the following forms:[8]

$$\log\lambda = a + b\log R, \tag{2}$$

where R is the range of the α-particle, and a and b are constants for the members of a radioactive series;

$$\log\lambda = c + dv^n, \tag{3}$$

where v is the velocity of the α-particle, c and d are constants for the members of a radioactive series, and $n=1$ or 2. The data of Table I do not yield straight lines for $\log\lambda$ *vs* v or v^2, for constant Z.

The "constants" which appear in Eqs. (1) are functions of $(Z-2)$ and r_0, the atomic number and radius of the product nucleus, respectively. The Gamow theory makes possible the calculation of the radii, and a comparison between theory and experiment will be made later.

When $\log\lambda$ is plotted against $1/v$ for different values of the neutron excess (Fig. 2), straight lines are obtained for members of different partial radioactive series. Thus, for $A-2Z=48$, the points for Th^{228}, Ra^{224}, Em^{220}, and Po^{216} fall on line (a), while the points corresponding to Cm^{240}, Pu^{236}, and U^{232} fall on line (b). Similarly, in the case $A-2Z=50$, the points corresponding to Th^{230}, Ra^{226}, Em^{222}, and Po^{218} fall on line (a), while those for Cm^{242}, Pu^{238}, and U^{234} fall on line (b). For $A-2Z=52$, only the line corresponding to Cm^{244}, Pu^{240}, and Th^{232} is found. In the case $A-2Z=46$, the points for U^{230}, Th^{226}, Ra^{222}, Em^{218}, and Po^{214} fall on the line (a). The data are insufficient to form the (b) line in this case. In the case $A-2Z=44$, there are not yet enough experimental results to justify a plot of this kind.

On comparison of these results with Figs. 3 and 4, which represent the thorium and uranium families, it becomes apparent that the partial series starting with Th^{230}, U^{230}, Th^{228}, and U^{228} are characterized by straight lines given by $\log\lambda = A+B/v$, with $A\sim 72$ and $B\sim -135$. The partial series consisting of isotopes of mass number 232 or greater are characterized by $A\sim 30$ or 35 and $B\sim -70$. In all cases, the relative instability with respect to alpha-decay increases as the nuclides move away from the dotted lines of Figs. 3 and 4. The relative stability of nuclei of mass numbers 230 and 232 has been pointed out by Perlman, Ghiorso, and Seaborg (reference 2,

[8] Rutherford, Chadwick, and Ellis, *Radiations from Radioactive Substances* (The Macmillan Company, New York, 1930), p. 176.

Fig. 4) and is related to the shape of the nuclear energy surface in the heavy element region.

It will be seen later that the slopes of the $\log\lambda$ vs $1/v$ lines as obtained from the Gamow theory agree much better with the lines for constant Z than with those for constant $A-2Z$, indicating once again that the Geiger-Nuttall rule in the form used in the present report can be interpreted as applying to the isotopes of a given element in a more simple and direct way than to the members of a radioactive series.

III. THEORETICAL CONSIDERATIONS

The results of the Gamow-Condon-Gurney one-particle theory of alpha-radioactivity in its most rigorous form can be expressed in the form of two equations which reduce, for the case of zero spin change (ground states of even-even nuclei), to[9]

$$\lambda=\frac{2V}{r_0}\frac{\mu^2\tan\alpha_0}{\mu^2+\tan^2\alpha_0}\exp\left[-\frac{4\epsilon^2Z'}{\hbar v}(\alpha_0-\sin\alpha_0\cos\alpha_0)\right], \quad (4)$$

$$\mu=-\tan\alpha_0\tan(\mu k r_0), \quad (5)$$

where v = alpha-velocity as previously defined $=(2E/m)^{\frac{1}{2}}$, r_0 = "radius" of the product nucleus, m = reduced mass of the system, $\mu=(1-U/E)^{\frac{1}{2}}$, U = constant potential of the alpha-particle within the nucleus, α_0 = arc cos $[mv^2r_0/4\epsilon^2Z']^{\frac{1}{2}}$, $Z'=Z-2$ = charge of the product nucleus, ϵ = unit electrical charge, $k=mv/\hbar=(2mE)^{\frac{1}{2}}/\hbar$.

Equations (4) and (5) connect the four quantities λ, E, r_0, and U. In the usual procedure, the experimental values of λ and E are used to find r_0 and U. Now, r_0 can be considered to be the radius of interaction of the product nucleus and an alpha-particle with respect to alpha-decay. The potential U, which always turns out to be positive, can be regarded either as a repulsive potential tending to eject an alpha-particle from the nucleus against the coulomb barrier, or merely as a parameter whose physical significance is obscure. In the latter case the result of the numerical evaluation of U can be regarded, not as a determination of an energy level, but rather as a step in the implicit elimination of U to give one equation connecting E and λ. The rigorous expressions (4) and (5) have generally been approximated by simpler forms, either to avoid mathematical complexities in the derivation or to simplify the numerical calculations. However, the availability of a large amount of experimental data seems to make the more rigorous calculations desirable in the hope that the values obtained for the "nuclear radii" may be more significant or that some light may be thrown on the physical significance of the potential U.

The iterative procedure adopted for the solution of Eqs. (4) and (5) consisted in guessing a value of r_0, solving Eq. (5) for μ and then calculating λ from Eq. (4). An incorrect guess results in a value of λ different from the experimental value. The difference between the calculated and experimental values of λ indicates the direction in which the first guess at r_0 is to be corrected. Iteration of this procedure was found to give values of r_0 and U which resulted in satisfactory values of λ after two to four trials. The results of the calculations are given in Table II. For completeness, the values of U, the coulomb energy, and the difference between the coulomb energy and U are included. The following values of the constants needed were used in the calculations:

$$\epsilon=4.8025\times10^{-10}\text{ esu},$$
$$\hbar=1.0543\times10^{-27}\text{ erg-sec},$$
$$1\text{ Mev}=1.602\times10^{-6}\text{ ergs},$$
$$\text{mass of alpha-particle}=4.004\text{ mass units}=6.6442\times10^{-24}\text{ g}.$$

The values of E, λ, v used are given in Table I.

The Nuclear Radii

The calculated values of the nuclear radii conform to the expression

$$r_0=(1.57\pm0.015)A^{\frac{1}{3}}\times10^{-13}\text{ cm}, \quad (6)$$

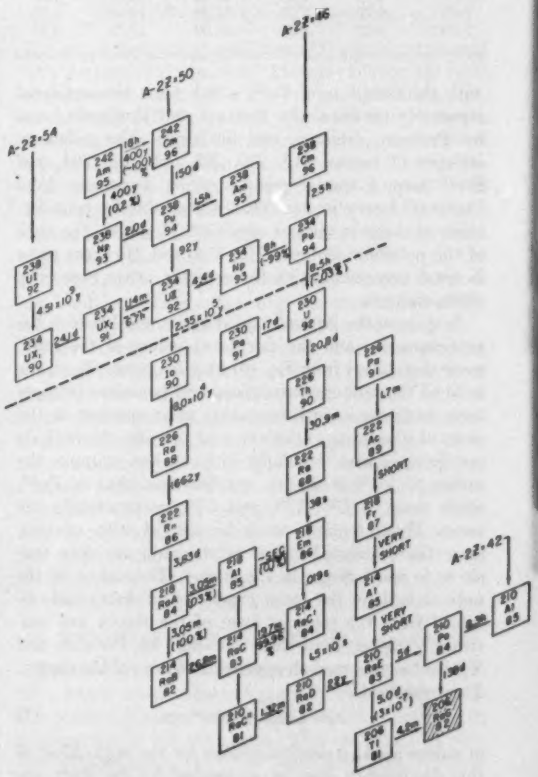

FIG. 4. Disintegration scheme for the uranium family.

[9] M. A. Preston, Phys. Rev. 71, 865 (1947); see this paper for further references.

TABLE II. Nuclear radii and internal potentials from alpha-decay data.

Parent nucleus	Radius of product nucleus (10^{-13} cm)	Internal potential U (Mev)	Coulomb energy (Mev)	$\frac{2Ze^2}{r_1}-U$ (Mev)	$R=r_0A^{\frac{1}{3}}$ (10^{-13} cm)
$_{96}Cm^{242}$	9.61	5.67	28.16	22.49	1.55
Cm^{240}	9.48	5.84	28.55	22.80	1.53
$_{94}Pu^{240}$	9.86	4.71	26.87	22.16	1.60
Pu^{238}	9.48	5.07	27.94	22.31	1.54
Pu^{236}	9.57	5.33	27.68	22.35	1.56
Pu^{234}	9.54	5.74	27.76	21.92	1.56
$_{92}U^{238}$	9.81	3.76	26.42	22.66	1.59
U^{234}	9.65	4.33	26.85	22.52	1.57
U^{232}	9.61	4.89	26.97	22.08	1.57
U^{230}	9.64	5.45	26.88	21.43	1.58
U^{228}	9.31	6.29	27.84	21.55	1.53
$_{90}Th^{232}$	9.79	3.55	25.88	22.33	1.60
Th^{230}	9.52	4.23	26.61	22.38	1.56
Th^{228}	9.43	4.99	26.86	21.87	1.55
Th^{226}	9.56	5.89	26.50	20.61	1.58
$_{88}Ra^{226}$	9.41	4.35	26.31	21.96	1.55
Ra^{224}	9.46	5.25	26.17	20.92	1.57
Ra^{222}	9.55	6.14	25.92	19.78	1.59
$_{86}Em^{222}$	9.43	5.06	25.65	20.59	1.57
Em^{220}	9.47	5.86	25.54	19.68	1.58
Em^{218}	9.60	6.74	25.19	18.45	1.60
$_{84}Po^{218}$	9.33	5.58	25.31	19.73	1.56
Po^{216}	9.28	6.35	25.44	19.09	1.56
Po^{214}	9.27	7.28	25.46	18.18	1.56
Po^{212}	9.05	8.38	26.09	17.71	1.53

with the exception of Po^{212}, which must be considered separately (as shown by Perlman and Ypsilantis,[7] and by Perlman, Ghiorso, and Seaborg[2]). The polonium isotopes of masses 212, 210, 208, 206, and 204, and Em^{212} form a special group showing departures from "normal" heavy nuclear radii explainable by consideration of shells in nuclear structure. However, the radii of the polonium isotopes 218, 216, and 214 seem to be in good agreement with those of the other even-even alpha-emitters.

In spite of the generally good agreement between the expression (6) and the calculated values of the radii, some departures from Eq. (6) may be noted. Thus, the radii of the radium, emanation, and polonium isotopes seem to decrease with increasing mass number; in the cases of plutonium, uranium, and thorium the radii do not quite increase regularly with $A^{\frac{1}{3}}$. For example, the radius of Pu^{238} is slightly smaller than that of Pu^{236}, while those of U^{234}, U^{232}, and U^{230} are practically the same. These remarks must be viewed with caution, since the calculated values of the radii are very sensitive to small errors in the energy. The values of the radii (based on the same experimental data) and obtained from the rigorous form of the theory are consistently higher than those obtained by Perlman and Ypsilantis, who used an approximate form of the theory. They obtained

$$r_0=1.48A^{\frac{1}{3}}\times10^{-13}\text{ cm}, \tag{7}$$

or values about 6 percent smaller for the radii. Most of this discrepancy can be accounted for by their approximations.

Present[10] has calculated corrections to the nuclear radius arising from the neutron excess $(A-2Z)$, from the electrostatic repulsion of the protons, and from the surface tension forces. He obtained the expression:

$$r_0=r_0^*A^{\frac{1}{3}}[1+0.08(A-2Z)^2A^{-2}-0.3A^{-\frac{1}{3}}+0.010Z^2A^{-4/3}]. \tag{8}$$

On the basis of this expression and the values of the radii from alpha-decay, the average value of r_0^* for the alpha-emitters of Table I is found to be

$$r_0^*=(1.50\pm0.015)\times10^{-13}\text{ cm}.$$

The Internal Potential U

The calculated values of U are plotted as a function of E in Fig. 5. The results can be represented by the expression

$$E(\text{Mev})=0.52(\pm0.013)+U; \tag{9}$$

i.e., the value of the alpha-energy exceeds that of the internal potential by the constant amount 0.52 Mev (with an average deviation of 0.013 Mev).

In view of the absence of an adequate theory of nuclear structure, the physical significance of the values of U is not understood. The difference $E-U$ appears in the Gamow-Condon-Gurney theory in the expression $\mu=(1-U/E)^{\frac{1}{2}}$. The calculated values of μ and r_0 are such that

$$\mu kr_0=2.986\pm0.005. \tag{10}$$

From these last two expressions it follows that

$$E-U=(2.99)^2\hbar^2/2mr_0^2. \tag{11}$$

If we take $r_0=1.57A^{\frac{1}{3}}\times10^{-13}$, and use $A^{\frac{1}{3}}\approx6.1$ and $m\approx6.53\times10^{-24}$ g,

$$E-U=0.52\text{ Mev}. \tag{12}$$

The significance of the results expressed by Eqs. (9), (10), and (11) has been pointed out by Professor G.

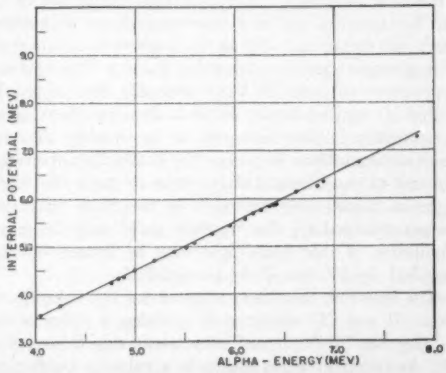

FIG. 5. Internal potential vs alpha-energy.

[10] R. D. Present, Phys. Rev. 60, 28 (1941).

Breit (personal communication). In Eq. (11), the value 2.99 is an approximation to π, so that Eq. (11) can be written as

$$E-U\approx\pi^2\hbar^2/2mr_0^2. \tag{13}$$

Equations (10) and (13) mean, in the case of a rectangular potential, that r times the radial part of the nuclear wave function is a sine function with phase almost equal to π at the nuclear boundary. The logarithmic derivative of the radial factor is determined by the behavior of the wave function as it enters the coulomb barrier. The large height of the coulomb barrier makes the logarithmic derivative numerically large but negative, since the general view of a quasi-stationary state requires a rapid decrease of the function in the barrier. This implies that the phase of the sine curve differs very little from π and is somewhat smaller than π. The fact that the quantity μkr_0 is very nearly constant is an indication of the approximate constancy, for the different nuclei, of the logarithmic derivative of the radial wave function at the boundary.

The log λ *vs* $1/v$ Relationship

In Sec. I it has been shown that if logλ is plotted against $1/v$ for constant Z, a family of straight lines results. These lines can be represented by the empirical equations (1). In this section, these equations will be compared with the predictions of the Gamow-Condon-Gurney theory. According to this theory, for zero spin change, logλ and v are related by the equation[9]

$$\log\lambda=\log\left[\frac{2v}{r_0}\frac{\mu^2\tan\alpha_0}{\mu^2+\tan^2\alpha_0}\right]-\frac{4\epsilon^2z'}{\hbar LV}(\alpha_0-\sin\alpha_0\cos\alpha_0), \tag{14}$$

where

$$\alpha_0=\arccos(mv^2r_0/4\epsilon^2z')^{\frac{1}{2}}.$$

The expression $(\alpha_0-\sin\alpha_0\cos\alpha_0)$ can be expanded in powers of the parameter $mv^2r_0/4\epsilon^2z'$, yielding

$$\log\lambda=\log\left[\frac{2v}{r_0}\frac{\mu^2\tan\alpha_0}{\mu+\tan^2\alpha_0}\right]-\frac{4\epsilon^2z'}{\hbar Lv}$$

$$+\frac{8\epsilon}{\hbar L}(mr_0z')^{\frac{1}{2}}\left[1-\frac{1}{6}\frac{mv^2r_0}{4\epsilon^2z'}+\frac{1}{20}\left(\frac{mv^2r_0}{4\epsilon^2z'}\right)^2-\cdots\right], \tag{15}$$

where $L=2.3026=\log_e(10)$.

If the calculated values of r_0 and μ (Table II) are inserted into Eq. (15), it is found that the first and third terms on the right-hand side vary relatively slightly for a given value of Z, so that it is possible to represent logλ for the even-even isotopes of a given element by the equation

$$\log\lambda=a+b/v,$$

where a is the average value, for the isotopes of a given element, of the first and third terms on the right-hand side of Eq. (15) and

$$-b=4\epsilon^2Z'/\hbar L; \tag{16}$$

TABLE III. Comparison of the empirical and theoretical logλ *vs* $1/v$ relationships.

Value of Z'	Ratio: $\frac{\text{coefficient of } 1/v \text{ in empirical equation}}{\text{coefficient of } 1/v \text{ in theoretical equation}}$
$Z=84,\ Z'=82$	0.896
$Z=86,\ Z'=84$	0.987
$Z=88,\ Z'=86$	0.977
$Z=90,\ Z'=88$	0.917
$Z=92,\ Z'=90$	0.921
$Z=94,\ Z'=92$	0.883

i.e., the slope of the logλ *vs* $1/v$ line is proportional to Z' and is independent of r_0 and U. Thus, a comparison of the slopes of the experimental and theoretical logλ *vs* $1/v$ lines for constant Z should provide a reasonably good basis for the comparison of theory and experiment.

The theoretical expressions, derived as described above, are:

$$\begin{aligned}
&(Z=84,\ Z'=82)\ \log\lambda=53.54-97.71/v,\\
&(Z=86,\ Z'=84)\ \log\lambda=54.82-100.30/v,\\
&(Z=88,\ Z'=86)\ \log\lambda=55.38-102.68/v,\\
&(Z=90,\ Z'=88)\ \log\lambda=56.13-105.07/v,\\
&(Z=92,\ Z'=90)\ \log\lambda=56.54-107.46/v,\\
&(Z=94,\ Z'=92)\ \log\lambda=57.07-109.85/v.
\end{aligned} \tag{17}$$

The set of theoretical equations (17) can be compared with the empirical equations (1) by calculating the ratio of the coefficients of $1/v$ in the two sets of relationships, as in Table III. In general, the agreement between theory and experiment for the even-even alpha-emitters is good. It must be pointed out, however, that the $1/v$ term represents the major contribution of the effect of the barrier penetrability and is independent of the nuclear model used. The agreement between theory and experiment, therefore, testifies to the validity of the quantum-mechanical treatment of the barrier, but does not imply anything concerning the correctness of the one-body model of the nucleus used in the theory.

Some discrepancies still remain. For example, the slopes of the experimental lines are not strictly proportional to the atomic number of the product nucleus. Some of this disagreement may be due to experimental errors in the determination of the alpha-energy. Or, it may be necessary to revise the theory in a fundamental manner in order to take into account the probability of formation of an alpha-particle within a nucleus, which may in turn affect our ideas about the penetration of the coulomb barrier. The latter possibility is likely, particularly in view of the work of Seaborg and his co-workers on the even-odd and odd-odd alpha-emitters.

IV. THE PREDICTION OF UNKNOWN HALF-LIVES

The usefulness of the empirical correlations found in the present report depends partially on the success of the prediction of unknown experimental quantities. In examination of the even-even alpha-emitters it is seen that in three cases, Th^{234}, Ra^{220}, and Em^{216}, the half-lives are given as "short," "short," and "very short," respec-

TABLE IV. Predicted values of unknown half-lives.

	Parent nucleus Th^{224}	Parent nucleus Ra^{220}	Parent nucleus Em^{216}
Method (a): Extrapolation of $\log\lambda$ vs $1/v$			
$1/v$	0.527	0.517	0.498
$\log\lambda$	0.04	2.06	4.77
$\lambda(\text{sec}^{-1})$	1.1	1.2×10^{2}	5.9×10^{4}
$T_{\frac{1}{2}}$(sec)	0.6	6×10^{-3}	1.1×10^{-5}
r_0(cm)	9.55×10^{-13}	9.65×10^{-13}	9.75×10^{-13}
Method (b): Application of $U=E-0.52$ Mev			
E(Mev)	7.33	7.63	8.95
U	6.81	7.11	8.42
$\log\lambda$	0.06	1.87	4.38
$\lambda(\text{sec}^{-1})$	1.2	7.4×10^{1}	2.4×10^{4}
$T_{\frac{1}{2}}$(sec)	0.6	9.4×10^{-3}	2.9×10^{-5}
r_0(cm)	9.50×10^{-13}	9.51×10^{-13}	9.49×10^{-13}

tively.[1] The alpha-energies in the three cases are, including the energy of the recoil nucleus: 7.33 Mev, 7.63 Mev, and 8.95 Mev, respectively. Quantitative predictions of the half-lives can be made by at least two independent methods: (a) by extrapolation of the $\log\lambda$ vs $1/v$ curves, for $Z=90$, 88, and 86; (b) by using $U=E-0.52$ Mev, together with Eqs. (4) and (5).

The results obtained by the use of the two methods are given in Table IV. Thus, the predicted half-life of Th^{224} is 0.6 sec by both methods; for Ra^{220} the predicted values of the half-life are 6×10^{-3} or 9.4×10^{-3} sec; for Em^{216} the results are 1.1×10^{-5} or 2.9×10^{-5} sec. In the cases of Ra^{220} and Em^{216} it is possible to choose between the two predictions by means of the following considerations: the radii of the product nuclei were calculated from the predicted value of λ and the experimental value of E with the aid of Eqs. (4) and (5).

The values of the radii which follow from the predictions of λ by method (b) are more nearly consistent with the general trend of the radii of Table II than are those which follow from method (a). On this basis, it would seem that the predicted values most consistent with other properties of the even-even alpha-emitters are those obtained by method (b).

V. THE EXCEPTIONAL ISOTOPES OF POLONIUM AND EMANATION

According to Perlman, Ghiorso, and Seaborg,[2] the polonium isotopes and Em^{212} form a special group of even-even alpha-emitters whose properties are quite different from those of the other even-even nuclei. These exceptional nuclides have been discussed in considerable detail by Seaborg and his colleagues[2-4] and will, therefore, be touched on only briefly in this report. It will be recalled that for Po^{218}, Po^{216}, Po^{214}, and Po^{212}, the plot of

TABLE V. Exceptional even-even alpha-emitters.

Isotope	Alpha-energy (Mev)	Alpha-disintegration constant (sec^{-1})	Product radius ($r_0\times10^{13}$)	$E-U$ (Mev)	Departure factor	$R=r_0A^{\frac{1}{3}}$ $\times10^{13}$ cm
Po^{218}	6.12	3.79×10^{-3}	9.33	0.54	···	1.56
Po^{216}	6.89	4.39	9.28	0.54	···	1.56
Po^{214}	7.83	4.63×10^{3}	9.27	0.55	···	1.56
Po^{212}	8.95	2.61×10^{6}	9.05	0.57	···	1.53
Po^{210}	5.40	5.81×10^{-8}	8.42	0.66	30	1.43
Po^{208}	5.24	7.33×10^{-9}	8.43	0.65	30	1.43
(Po^{206}	5.3	8.91×10^{-6}	8.87	0.60	6(?)	1.51)
Po^{204}	5.45	8.8×10^{-8}	8.31	0.68	50	1.42
Em^{212}	6.30	5.02×10^{-4}	8.83	0.61	10	1.49

$\log\lambda$ vs $1/v$ gives a good straight line. The situation is not the case for Po^{210}, Po^{208}, Po^{206}, and Po^{204}. Also, the nuclide Em^{212} does not fall on the line determined by Em^{222}, Em^{220}, and Em^{218}. The alpha-transitions of these exceptional isotopes are relatively "forbidden," in the sense that the corresponding alpha-energies are low and the half-lives long, as compared with the "normal" isotopes. The rigorous alpha-decay theory has been applied to those exceptional isotopes and the results of the calculations are given in Table V. All of the polonium isotopes are included although the deviations from normal for Po^{218}, Po^{216}, and Po^{214} are doubtful. The "departure factor" is defined by Perlman, Ghiorso, and Seaborg as the factor by which the measured half-life is greater than the value for the same Z and E taken off curves defined by even-even nuclides.

The values of the radii of the products of the alpha-decay of Po^{218}, Po^{216}, and Po^{214} do not differ significantly from those of the "normal" even-even alpha-emitters for which $R=1.57$. In Po^{212} there is evidence of some shrinkage, while for Po^{210}, Po^{208}, and Po^{204} the shrinkage is considerable. The isotope Po^{206} seems to indicate less shrinkage of the nuclear radius. However, the absence of a second decimal figure may indicate an experimental error of the order of 1 to 2 percent. Since the value of the radius is quite sensitive to errors in the energy, this may correspond to an error of several percent in the value of R. In any case, the deviations of r_0 and $E-U$ from the "normal" values are consistent with the values of the departure factors. Similar conclusions hold for Em^{212}. The values of $(E-U)$ for the "exceptional" isotopes of polonium indicate a slightly different behavior of the logarithmic derivative of the radial wave function from that of the "normal" cases.

The author wishes to express his appreciation for the interest and helpful suggestions of Professor Gregory Breit and for the benefit of many discussions with Dr. Melville Clark, Jr.

Determination of the Number of Neutrons Associated with the Stoppage of Negative μ-Mesons in Lead*

GERHART GROETZINGER,† MARTIN J. BERGER, AND GORDON W. MCCLURE‡
Institute for Nuclear Studies, University of Chicago, Chicago, Illinois

(Received October 4, 1950)

Negative mesons (at sea level and therefore assumed to be μ-mesons) were focused onto a lead absorber by means of a magnetic cosmic-ray spectrometer. The number of μ-mesons which stopped in the absorber was determined with an anticoincidence arrangement. Neutrons issuing from the lead absorber were registered during intervals of from 5 to 135 μsec after each such stoppage by a counting system consisting of enriched-BF_3 counters surrounded by 8 cm of paraffin, whose efficiency was measured with the help of a calibrated Na-Be source of $\approx$1-Mev photo-neutrons.

For 5500 stopped μ-mesons, the average number of neutrons emitted per μ-meson stoppage was found to be 1.96 ± 0.72. This result is consistent with the assumption that a neutrino (or light neutral meson) is emitted in the interaction between a μ-meson and a nucleon.

I. INTRODUCTION

IN a previous paper[1] we described an experiment, carried out at sea level, in which the emission of neutrons following the capture of negative μ-mesons in lead was found. The capture of mesons as the initiating event for neutron emission was established through the use of a G-M counter spectrometer capable of discriminating against all particles except negative mesons. The number of neutrons emitted per captured meson was given as roughly two. Shortly before the publication of this paper Sard *et al.*[2] had reported the emission of neutrons following the stoppage of charged penetrating radiation for which the negative meson component was held to be responsible. In a later paper[3] the number of neutrons per captured μ-meson was stated to be most likely two to three, and certainly smaller than five.

The purpose of the present experiment was to determine the neutron multiplicity with greater accuracy than in our preliminary experiment, using the same cosmic-ray spectrometer, but an improved arrangement for counting neutrons. The hard component of the cosmic radiation at sea level contains a considerable number of slow protons;[4,5] furthermore, locally produced penetrating showers are accompanied by many neutrons.[6] Even after the phenomenon of neutron emission subsequent to μ-meson capture had been established, it was therefore essential to continue the use of the spectrometer in order to obtain the correct number of stopped mesons and the neutrons associated with them.

The number of neutrons emitted per μ-meson capture provides significant information concerning the interaction between μ-mesons and nucleons. Marshak and Bethe[7] proposed the interaction

$$(\mu^-\text{meson})+(\text{proton})=(\text{neutron}),$$

while Sakata[8] proposed the interaction

$$(\mu^-\text{meson})+(\text{proton})=(\text{neutron})+(\text{neutrino}).$$

It follows from the conservation of energy and momentum that if a neutrino is emitted, it will carry away most of the energy made available by the disappearance of the rest mass of the μ-meson (108 Mev). Tiomno and Wheeler,[9] and Rosenbluth[10] showed, on the basis of the free particle model of the nucleus, that the most probable excitation energy given to the nucleus in this case will be $\sim$15 Mev, and the maximum energy $\sim$22 Mev. It was pointed out further[9] that if a light neutral meson were emitted instead of a neutrino, or if the binding of the nucleons were taken into account, the energy given to the nucleus would be somewhat, but not much, smaller. Under the most favorable assumptions the emission of an average number of between one and two neutrons could be expected. Taketani and Sasaki,[11] on the other hand, come to the conclusion that the nuclear excitation energy would be 6 Mev for large Z and approximately 14 Mev for small Z.

If no neutrino is emitted, enough energy is available for the emission of a larger number of neutrons. A small number of fast nucleons will be emitted within a very short time ($\approx10^{-21}$ sec) after the absorption of the μ-meson, taking with them a considerable fraction of the energy. The residual energy is distributed among the remaining nucleons, some of which will eventually evaporate. Table I gives the approximate numbers of neutrons expected to evaporate from a lead nucleus

* This research was supported in part by the joint program of the ONR and AEC.

† Now at the Lewis Laboratory, NACA, Cleveland, Ohio.

‡ Now at the Bartol Research Foundation, Swarthmore, Pennsylvania.

[1] G. Groetzinger and G. W. McClure, Phys. Rev. **74**, 341 (1948). G. W. McClure and G. Groetzinger, Phys. Rev. **75**, 340 (1949).

[2] Sard, Ittner, Conforto, and Crouch, Phys. Rev. **74**, 97 (1948).

[3] Sard, Conforto, and Crouch, Phys. Rev. **76**, 1134 (1949).

[4] Merkle, Goldwasser, and Brode, Phys. Rev. **78**, 92 (1950).

[5] G. W. McClure, dissertation (University of Chicago), unpublished.

[6] Cocconi, Cocconi-Tongiorgi, and Greisen, Phys. Rev. **74**, 1867 (1948).

[7] R. E. Marshak and H. A. Bethe, Phys. Rev. **72**, 508 (1947).

[8] S. Sakata and T. Inoue, Prog. Theor. Phys. **1**, 143 (1946). Taketani, Nakamura, Ono, and Sasaki, Phys. Rev. **76**, 60 (1949).

[9] J. Tiomno and J. A. Wheeler, Revs. Modern Phys. **21**, 153 (1949).

[10] M. N. Rosenbluth, Phys. Rev. **75**, 532 (1949).

[11] M. Taketani and M. Sasaki, Phys. Rev. **76**, 852 (1949).

TABLE I. Number and energy of evaporated neutrons as a function of the excitation energy.

Residual excitation (Mev)	% of the meson mass	Number of neutrons	Neutron energies (Mev)
32.4	30	3	2.7–1.6
27	25	2	2.5–1.6
21.6	20	2	2.2–1.6
16.2	15	1	1.9
13.5	12.5	1	1.8

for several moderate excitation energies. In making this estimate, it was assumed that because of the large coulomb barrier no charged particles are emitted. The relation between excitation energy U and temperature T was taken to be

$$U=T^2A/12,$$

where A is the atomic number of the nucleus. The numerical factor 12 was found by Le Couteur[12] to be consistent with the characteristics of evaporation stars (silver and bromine) as observed in photographic emulsions.

On the basis of the Marshak-Bethe type of interaction one would expect charged particles to be evaporated at least from light and medium nuclei after the capture of a μ-meson. But according to many authors[13] μ-mesons do not produce stars in photographic emulsion, or if so, only in a small fraction of the cases [(10±10) percent].[14] Experiments with a cloud chamber,[15] a crystal counter,[16] and an ionization chamber[5] have shown that the emission of charged particles subsequent to the capture of μ-mesons in lead, silver chloride, and argon, respectively is at best a very rare event.

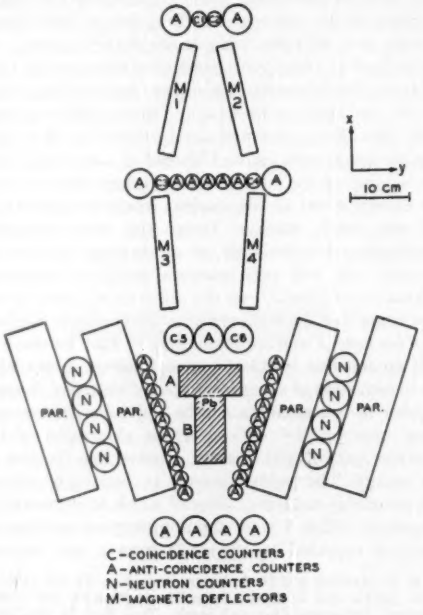

FIG. 1. Schematic diagram of the apparatus.

II. EXPERIMENTAL PROCEDURE

(A) Description of the Equipment

A schematic diagram of the apparatus is shown in Fig. 1. The upper part consists of a magnetic double spectrometer able to select mesons of either charge. The two top counters C_1 and C_2 are connected in parallel and form one spectrometer in coincidence with the counters C_3 and C_5, and a second spectrometer in coincidence with C_4 and C_6. The selection of the mesons with respect to charge (and energy) is provided by their deflection in the magnetized iron plates M_1, M_2, M_3, and M_4, which have a height of 20 cm, a thickness of 3 cm, and a length of 60 cm. The plates M_1 and M_2, and the plates M_3 and M_4, respectively, represent parts of two separate closed magnetic circuits, the field strengths in the plates M_1 to M_4 being approximately 18,000 gauss. The counters A are in anticoincidence with counters C_1 to C_6. The anticoincidence counters have the purpose of reducing the number of counts due to mesons not stopped in the lead absorber (Pb). All of the counters have a diameter of one or two inches as indicated in the figure, and an effective length of 50 cm. This is also the length of the lead absorber. Neutrons are recorded by a counting system consisting of two sections arranged symmetrically with respect to the magnetic spectrometer. Each section contains four proportional counters with a two-inch diameter and an effective length of 50 cm, filled with 0.39 atmos of enriched boron trifluoride (96 percent B^{10}).[17] The counters are sandwiched between layers of paraffin 8 cm thick, which extend in length a few inches beyond the counters.

Coincidences corresponding to the traversal of either a positive or a negative meson (depending on the direction of the magnetic field) through one of the spectrometers which was not accompanied by the discharge of one of the anticoincidence counters were recorded in the course of the experiment as well as discharges of the neutron counters from 5 to 135 μsec after these events.

(B) Determination of the Number of Stopped Mesons

For the determination of the number of mesons stopped in the lead block (Pb) the neutron counting

[12] K. J. Le Couteur, Proc. Phys. Soc. (London) **63A**, 259 (1950).
[13] D. H. Perkins, Phil. Mag. **40**, 601 (1949).
[14] C. F. Powell, *Cosmic Radiation* (Interscience Publishers, New York, 1949).
[15] W. Y. Chang, Revs. Modern Phys. **21**, 166 (1949).
[16] H. G. Voorhies and J. C. Street, Phys. Rev. **76**, 1100 (1949).
[17] The enriched BF_3 was obtained from the Isotope Division of the AEC. The counters were made by Mrs. N. Wood.

arrangement was removed and a second layer of anticoincidence counters installed around the lead absorber to make the anticoincidence arrangement more efficient. Counting rates were determined with and without the lead absorber in the position indicated in the figure. After making a minor correction to account for the fact that the solid angle subtended by the spectrometer was not entirely covered by anticoincidence counters, the number of mesons stopped during the experiment (2557 hours) was found to be 5500. The error in this determination is negligible compared with that of the number of neutrons connected with the stoppage of these mesons.

(C) Determination of the Number of Neutrons

The number of discharges of the BF_3 counters observed in 2557 hours with the telescope collecting negative mesons was 67. The expected number of chance counts during this period was 7.4. With the magnetic field reversed one count was observed during a period of 705 hours, while the expected number of chance counts was 2.3. It is thus apparent that the telescope was properly selective. The number of recorded neutrons caused by the stoppage of negative mesons was therefore 59.6 ($\pm$9.7 percent probable error).

To determine from this number the number of neutrons originating in the lead absorber due to the stopping of negative mesons, it is necessary to estimate the efficiency of neutron counting. This calibration involves the determination of (i) the efficiency $\epsilon(x, y, z)$ of counting with an appropriate neutron source placed at various positions from which neutrons due to μ-meson capture can originate, (ii) the spatial distribution $f(x, y, z)$ of the sources of the neutrons in the course of the experiment (stopped μ-mesons), and (iii) the mean life T of the neutrons in the counting arrangement, which must be known to take into account the fact that neutrons are counted only during the period from 5 to 135 μsec after the stoppage of a meson. The over-all efficiency, η, can then be expressed, in terms of these quantities, as follows:

$$\eta=[\exp(-5/T)-\exp(-135/T)] \times \int \epsilon(x, y, z) f(x, y, z) dV. \quad (1)$$

The integration is to be carried out over the region occupied by the lead absorber.

(i) The spectrometer has already been used in another investigation, in the course of which the probability of the transmission of a meson was determined as a function of the energy.[18] Although the meson spectrum in the energy range in question is rather flat, the transmission probability is such that the majority of the mesons coming to a stop in the lead absorber will do so in its lower part (part B in Fig. 1). With the lead absorber removed, a calibrated Na-Be photoneutron source was placed at several locations inside the space occupied by Part B of the absorber in the course of the experiments. The source was of known strength to within $\pm$20 percent and yielded monoenergetic neutrons of about 1 Mev energy.[19]

Numerous additional measurements were made with a Ra-Be neutron source in various positions. It was found that in spite of the different distribution of neutron energies, the dependence of the counting efficiency on the position of the source was approximately the same as for the Na-Be source. Thus, most of the relative efficiency measurements (and also periodic checks of the efficiency during the course of the experiment) could be made with the Ra-Be source, which was a great convenience, because the Na-Be photoneutron source decayed rapidly and gave off intense gamma-radiation. The description of the measurements is facilitated by the introduction of a cartesian coordinate system, with its (x-y) plane as indicated in Fig. 1. The variations of the counting efficiency in the x- and y-directions, in the region occupied during the experiment by part B of the lead absorber, were found to be quite small; and the only significant variations occurred in the z-direction, along which $\bar{\epsilon}(z)$ (averaged with respect to x and y), was determined at intervals of 5 cm.

(ii) The x- and y-dimensions of part B of the absorber are small compared with the path length of a meson through the telescope. Moreover, the counting efficiency $\epsilon(x, y, z)$ is essentially a function of z only. It is thus sufficient to consider the spatial distribution $f(x, y, z)$ of the stopped μ-mesons as a function of z only. The probability $f(z)$ can be obtained by simple geometric considerations. Let a (=50 cm) be the extension of the lead absorber (and of the effective length of the coincidence counters) in the z-direction, and let b be the length of the projection on the (x-y) plane of the path of a meson through the spectrometer, the length being measured from one of the top counters to a point P inside part B of the lead absorber at which the meson comes to a stop. Actually, there is a probability distribution of the length b; but, as has been pointed out before, the relative change in b due to variations of P in B, etc., is small, so that it is permissible to take a mean value for b (=70 cm). In Fig. 2, the rectangle $ABCD$ represents the approximate surface on which a meson traverses the spectrometer, the surface here being developed onto a plane. In this plane the path is rectilinear, if one neglects scattering. A particle incident at Q, at a distance ζ from A, and with an angle of incidence ϕ, will reach the line $\overline{CD}$ at P, at a distance z from C. We note that $\overline{AB}=a$, $\overline{AC}=b$, and $z=\zeta+b\tan\phi$. The spectrometer records essentially only mesons whose paths, before entry into the spectrometer,

[18] G. Groetzinger and G. W. McClure, Phys. Rev. **77**, 777 (1950).

[19] This energy is somewhat lower than that of the neutrons to be expected in the evaporation following the capture of a meson in lead (Table I).

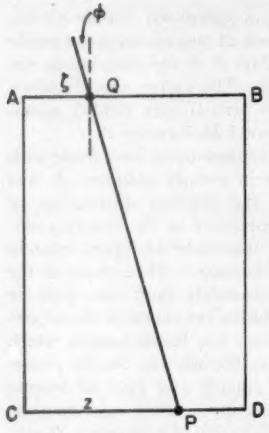

FIG. 2. Diagram illustrating the derivation of Eq. (3).

lie in two planes inclined 17° to the vertical (x-z) plane. Thus the distribution of the angles of incidence will be not much different from the zenith angle distribution, and we take it here to be proportional to $\cos^2\phi$. Since each point of incidence Q between A and B is equally likely, the joint frequency distribution of ϕ and ζ is $\text{const}\cdot\cos^2\phi d\phi d\zeta$. Let $F(z,\zeta)dzd\zeta$ be the joint frequency distribution of z and ζ. Then

$$F(z,\zeta)dzd\zeta = \text{const}\cdot\cos^2[\tan^{-1}\{(z-\zeta)/b\}]\frac{\partial(\phi,\zeta)}{\partial(z,\zeta)}dzd\zeta. \quad (2)$$

Evaluating the jacobian and integrating with respect to ζ from zero to a, one obtains

$$f(z)dz=\left[\int_0^a F(z,\zeta)d\zeta\right]dz$$

$$=\text{const}dz\int_0^a [1+(z-\zeta)^2/b^2]^{-1}\times\cos^2[\tan^{-1}\{(z-\zeta)/b\}]d\zeta. \quad (3)$$

(iii) An approximate estimate was made of the mean life T of the neutrons in the counting system. With a Ra-Be source placed at the position of the lead absorber, it was found that the removal of either section of the counting system reduced the number of counts recorded by the other section by only three percent. Thus there was scarcely any reflection of neutrons from one section to the other, and it was permissible to base the estimate of the mean life on the consideration of one section only. Fifty percent of the volume of the gap between the two paraffin blocks of each section was occupied by neutron counters, so that the mean neutron absorption cross section of the entire gap could be assumed to be approximately one-half of that inside the counters. With[20] $\sigma v=1.6\times10^{-16}$, σ being the absorption cross section and v the thermal neutron velocity, one finds $T\approx230$ μsec. This is not very different from the value of T in an infinite medium of paraffin (180–200 μsec). We felt justified, therefore, in considering for the purpose of this approximate calculation a solid paraffin block 21 cm thick instead of two slabs 8 cm thick separated by a 5-cm gap containing the BF_3 counters. Rainwater and Havens,[21] who used neutrons which impinged on paraffin blocks with energies of a few Mev, give the mean life of these neutrons to be 45 and 100 μsec for paraffin thickness of 3.2 cm and 6.8 cm, respectively. These data can be fitted to the empirical expression

$$T(s)=190(1-e^{-0.095s}) \quad (4)$$

from which it follows that $T(21\text{ cm})\approx164$ μsec, and $A=[\exp(-5/T)-\exp(-135/T)]=0.53$. A variation of 15 percent in $T(21\text{ cm})$ will entail a variation of 10 percent in A.

Putting into expression (1) the empirical function $\epsilon(z)$, and the function $f(z)$ (calculated by numerical integration from (3) and normalized to unity), and using the value $A=0.53$, one obtains for the over-all efficiency η a value of 5.5×10^{-3}. Thus, the total number of neutrons emitted was 10,800. The most important error in the calibration arises from the uncertainty of the strength of the Na-Be photo-neutron source (≈20 percent). Altogether we would estimate the total probable error in the number of neutrons to be about 35 percent.

It should be pointed out that our equipment had a relatively very low efficiency for counting neutrons with energies in excess of, say, 25 Mev, so that very fast neutrons, which might be expected to emerge from the nucleus prior to the evaporation process, if the Marshak-Bethe type of interaction were the correct one, would not have been observed.

III. RESULTS AND DISCUSSION

According to the results of Sec. II, 5500 μ-mesons produced 10,800±4100 neutrons, i.e., the multiplicity was 1.96±0.72. This is consistent with the Sakata-interaction (assuming that the energy transfer to the nucleus takes place as calculated by Tiomno and Wheeler, and by Rosenbluth). Agreement with the Marshak-Bethe theory, on the other hand, can perhaps only be brought about by making the somewhat unlikely assumption that at least three-quarters of the rest energy of the μ-meson is carried off by fast nucleons.

We are indebted to Mr. Jack Aron for his help with the construction and operation of the equipment, and to Dr. Wattenberg and Mr. Eggler of the Argonne National Laboratory for providing us with the calibrated photo-neutron source.

[20] *The Science and Engineering of Nuclear Power* (Addison-Wesley Press, Inc., Cambridge, 1947), Vol. 1, Appendix C, p. 387.
[21] J. Rainwater and W. W. Havens, Phys. Rev. **70**, 136 (1946).

High Energy Photo-Nuclear Reactions*

KARL STRAUCH†
Radiation Laboratory and Department of Physics, University of California, Berkeley, California
(Received October 30, 1950)

Transition curves in lead of the photons responsible for various nuclear reactions have been obtained using 322-Mev bremsstrahlung from the Berkeley synchrotron. The area under these curves or "track length" determines an effective photon energy. The integrated cross sections of the reactions $C^{12}(\gamma,n)C^{11}$ and $Cu^{63}(\gamma,n)Cu^{62}$ are found to be 0.090 and 0.76 Mev-barn, respectively. Relative yields of various reactions from Zn have been measured, and relative cross sections have been calculated from these and the effective photon energies. A lower limit of 1.4 Mev-barns is obtained for the total cross section for photon absorption by the Zn nucleus, and 30 Mev is found for a lower limit to the average photon energy absorbed by the same nucleus. These results are discussed with respect to the proposed theories for nuclear photon absorption.

I. INTRODUCTION

WITH the development of high energy electron accelerators, x-ray beams have become available which contain photons energetic enough to produce multiple nuclear disintegrations. It is of interest to know the energies of the photons responsible and the cross sections for various reactions. These two quantities are difficult to obtain because of the continuous energy spectrum of the available bremsstrahlung. Baldwin and Klaiber[1] used the 100-Mev General Electric betatron to obtain excitation curves for the reactions $C^{12}(\gamma,n)C^{11}$, $Cu^{63}(\gamma,n)Cu^{62}$, U(γ, fission), and Th(γ, fission) by measuring the yield as a function of the electron beam energy and normalizing the beam intensity with the help of the calculated energy response of a monitor. Their results show a very narrow peak for the energy distribution of the photons responsible for the reaction under study, hereafter called "effective photons." McElhinney *et al.*[2] have obtained partial excitation functions for the reactions $Ta^{181}(\gamma,n)Ta^{180}$ and $Cu^{63}(\gamma,n)Cu^{62}$ by a similar method using the 21-Mev Illinois betatron. They find a greater spread in energy of the cross section peaks than do Baldwin and Klaiber; however, the "effective photons" are still well grouped around an average value. Similar results have recently been reported by Johns *et al.*[3]

The conclusion that no very high energy quanta participate in these reactions is verified by the absolute cross-section measurements on C by Lawson and Perlman,[4] who obtain the same values with 50-Mev and 100-Mev bremsstrahlung. In addition, the relative yields of several reactions on many elements as obtained by Perlman and Friedlander[5] are found to be the same when measured with the 50-Mev and 100-Mev betatron beam.

With the completion of the Berkeley 322-Mev synchrotron, another approach to this problem became possible. By studying the intensity variation in an absorber, such as lead, of those photons responsible for a given nuclear reaction, it is possible to determine a mean energy value for these photons and to gain some information on their energy spread. This method will be studied and applied to several photo-nuclear reactions in Sec. II of this paper, and some relative and absolute cross-section measurements will be described in Sec. III. The required theoretical calculations from the cascade shower theory are reported by L. Eyges in an accompanying paper.[6]

II. TRANSITION CURVES

(A) Method

As the synchrotron beam passes through an absorber, its energy spectrum is changed by cascade processes: lower energy photons multiply, higher energy photons disappear. To study this transformation, detectors sensitive to various photon energies are required; these are available in the form of photo-nuclear reactions from different target nuclei. As we have just seen, there is good evidence that the energies of the photons responsible for such reactions are grouped in a narrow interval. The reaction is determined by the known target and product nuclei; the latter are identified by their radioactivities.

The amount of target activity is proportional to the number of photons responsible for the production of the radioactive product nucleus; thus, by placing identical targets at various depths in a lead absorber and comparing the induced activity, the density of "effective photons" is measured as a function of absorber thickness. The resulting curves are similar to the transition curves or Rossi curves obtained in cosmic-ray work except that here the transformation in lead of a selected energy band of x-rays is being studied.[7]

We are primarily interested in the effective photon

* This work was sponsored by the AEC.
† Now at Harvard University, Cambridge, Massachusetts.
[1] G. C. Baldwin and G. S. Klaiber, Phys. Rev. **70**, 259 (1946); **71**, 3 (1947); **73**, 1156 (1948).
[2] McElhinney, Hanson, Becker, Duffield, and Diven, Phys. Rev. **75**, 542 (1949).
[3] Johns, Katz, Douglas, and Haslam, Phys. Rev. **80**, 1062 (1950).
[4] J. L. Lawson and M. L. Perlman, Phys. Rev. **74**, 1190 (1948).
[5] M. L. Perlman and G. Friedlander, Phys. Rev. **74**, 442 (1948); **75**, 989 (1949).
[6] L. Eyges, Phys. Rev. **81**, 981 (1951).
[7] In an attempt to measure threshold energies, Baldwin and Klaiber (reference 1) have reported two such curves taken with the 100-Mev betatron beam.

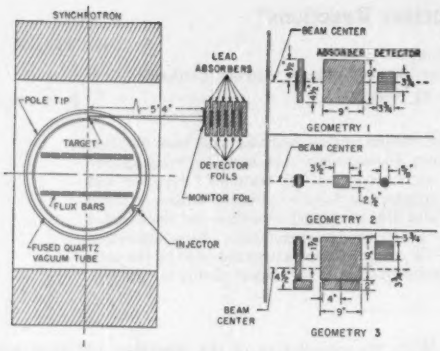

FIG. 1. Position of absorber stack with respect to the synchrotron and various geometries used in the experiment.

energy W_e responsible for various reactions; Eyges[6] shows that this can best be obtained from the area under the corresponding transition curve or its "track length." In the case of lead he obtains a simple analytic expression for W_e which is applied to the track length of the curves observed in this work. Some information on the accuracy of shower theory calculations in the energy region under consideration is also gained. This feature is examined in detail by Eyges.[6]

(B) Experimental Apparatus and Procedure

In the normal setup, hereafter designated as Geometry 1, a stack of lead absorbers 9×9 in. in area was placed at 5¼ ft from the synchrotron Pt target (Fig. 1). The lead was of commercial grade and the measured surface density was divided by 6.5 g/cm² to obtain the thickness in radiation lengths.[8] Foils of the target material had an area of 3¾×3¾ in. and a thickness from 0.040 to 0.75 g/cm², determined by the activity required for counting purposes. The foils were mounted on thin cardboard holders and then placed behind various thicknesses of lead. The whole stack was centered on the beam by the use of a telescope.

When a transition curve was measured for photons producing a short half-life such as Cu^{62}(10.1 min), a monitor foil was placed in front of the absorber stack and one or two foils placed inside during a run. At larger depths the induced activity becomes small; to be able to use longer bombardments, the monitor foil was then placed inside the stack at a previously measured position. If a longer half-life resulted from the reaction under study, e.g., Zn^{62} (9.5 hr), a complete set of 24 foils was placed inside the absorber stack during the irradiation.

After bombardment the foils were rolled into cylinders having a diameter of ⅞ in., placed over Eck and Krebs thin-walled glass Geiger counters, and their activities compared. The consecutive interchange of samples compensated for the different counter efficiencies. In some cases, such as with Zn detectors, several half-lives are produced. Decay curves were then taken for each sample and the different product activities separated. The irradiation time depends, of course, on the half-life and the yield of the product activity, but it was in general of the same order as the half-life. A 2-mil Cu foil of standard size gives about 8000 counts per minute when placed in a 130 R/min beam as measured behind ½-in. lead at 1 meter from the target.

At the position of the lead stack the synchrotron beam has a width of about 1 in. between half-intensity points; at 2 in. from the axis, the beam is down to three percent of its value at the axis. These results were obtained by comparing the activity of irradiated ¼-in. diameter disks placed at various distances from the beam axis. The dimensions of Geometry 1 were so chosen as to include as much of the incident photon flux as was practicable. Possible effects of scattering on the transition curves taken with this geometry will be examined in the following section.

The relative foil activity was determined as a function of lead thickness in radiation lengths by normalizing the activity of the first foil to unity in all cases.

(C) Influence of Geometry

As the x-ray beam passes through the lead stack, it spreads in a lateral direction owing primarily to multiple scattering of electrons. The quantitative interpretation of the transition curves depends on the applicability of one-dimensional shower theory; this means that all the scattered photons must be detected.

The transition curve for the photons effective in the reaction $Cu^{63}(\gamma,n)Cu^{62}$ as obtained with Geometry 1 is shown by Curve 1 in Fig. 2. This transition curve was used to study the possible influence of scattering, since it arises from lower energy photons for which such effects are expected to be most pronounced. The following tests were carried out.

(1) The transition curve was also taken using lead absorbers of area 2½×3½ in. and detector disks of 1⅜ in. diameter; this is Geometry 2 in Fig. 1. Standard end-window Victoreen tubes were used to compare the activities. The results as shown by Curve 2 in Fig. 2 lie from five to ten percent below the results obtained with Geometry 1. If we consider the difference in dimensions between the two geometries, such a small difference in results indicates that scattering effects are not very important at these photon energies.

(2) The transition curves for photons effective in the

[8] The value of 5.9 g/cm² given by B. Rossi and K. Greisen [Revs. Modern Phys. 13, 240 (1941)] for the radiation length in Pb was increased by 10 percent for the following reason. The pair production cross-section measurements of J. L. Lawson [Phys. Rev. 75, 433 (1949)] and R. L. Walker [Phys. Rev. 76, 527 (1949)] give results 10 percent lower than the theoretical calculations of W. Heitler [*The Quantum Theory of Radiation* (Oxford University Press, Oxford, 1944)]. Since bremsstrahlung and pair production are inverse processes to which the principle of detailed balancing applies, it is reasonable to assume that the radiation cross section is also 10 percent smaller than the theoretical values given by Heitler.

reaction $C^{12}(\gamma,n)C^{11}$ obtained with Geometries 1 and 2 are identical. This is not surprising, since the average energy of the photons responsible for this reaction is higher than for the previous one, and scattering is less important.

(3) To estimate the influence of the portion of the beam not usually effective, Geometry 3 (Fig. 1) was used; here monitor and detector foils are placed above their normal position so that only about 1 percent of the total beam is caught. The results are shown by Curve 3 of Fig. 2. If scattering outside Geometry 1 is important, more "effective photons" will scatter into Geometry 3 than out of it, resulting in a higher maximum than obtained under normal conditions. This is not observed; on the contrary, the peak is smaller as one would expect if it were primarily due to the outer edges of the synchrotron beam (there are proportionally fewer high energy photons in the outside portion of the beam). At larger depths Curve 3 appears to decrease less than normal. This is mainly due to neutron background which becomes appreciable at these low intensities. The transition curve obtained with Geometry 1 can be corrected using Curve 3 for the effect of the portion of the beam missing the detectors. Such corrections amount to one percent of the relative intensity which is smaller than other sources of error.

(4) To test for possible backscattering effects, Cu detector foils were placed at various positions in Geometry 1 with and without lead backing. No significant difference in relative activity was observed.

(5) To determine whether the size of the beam had any influence on the shape of the transition curve, various collimators were used to cut the beam size down to $\frac{1}{4}$-in. diameter. No change in peak height was observed.

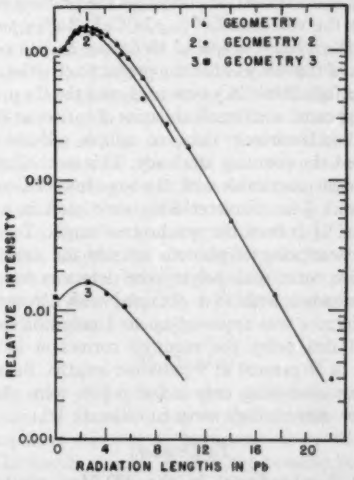

FIG. 2. Influence of geometry on transition curve in Pb of x-rays causing the reaction $Cu^{63}(\gamma,n)Cu^{62}$.

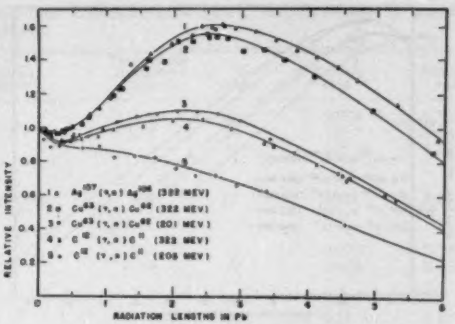

FIG. 3. Beginning of transition curves of x-rays responsible for several (γ,n) reactions.

The results of these tests indicate that the transition curves taken with Geometry 1 are not affected by the dimensions chosen. This means that the one-dimensional shower theory can be applied.

The activity of the samples could also be produced by secondary electrons and neutrons present in the stack. The small cross sections for electron disintegrations measured by Laughlin *et al.*[9] show such contamination to be negligible, while the neutron background can be estimated from the behavior of the transition curves at larger absorber depths. The absorption coefficient for neutrons in Pb (about 0.1 per radiation length) is smaller than for photons. At large depths of lead, neutrons would be primarily responsible for the observed activities. In the curves reported here[10] the final absorption indicates small neutron background. It may be noted that the track length is quite insensitive to the behavior of the transition curves at large depths.

(D) Results

Ag, Cu, and C Detectors

Short bombardments of silver, copper, and polystyrene detectors result in activities produced primarily by (γ,n) processes: $Ag^{107}(\gamma,n)Ag^{106}$, 24 min (counting was started after the 2.3-min activity of Ag^{108} had died out); $Cu^{63}(\gamma,n)Cu^{62}$, 10.1 min; $C^{12}(\gamma,n)C^{11}$, 20 min. In the first two cases these activities are also produced by $(\gamma,3n)$ reactions; the results reported in Sec. III indicate such contributions to be three percent or less. The transition curves for the photons effective in these three (γ,n) reactions as taken with Geometry 1 are shown in Figs. 3 and 4. In the case of Cu and C detectors, curves were obtained with bremsstrahlung with a maximum photon energy of about 200 Mev in addition to the 322-Mev maximum energy.

[9] Laughlin, Skaggs, Hanson, and Orlin, Phys. Rev. 73, 1223 (1948).

[10] The transition curve for the photons effective in the reaction $Al^{27}(\gamma,2pn)Na^{24}$ indicated a relatively large neutron background and therefore is not reported. In this case the reaction cross section for x-rays is small, while the cross section for $Al^{27}(n,\alpha)$ is large.

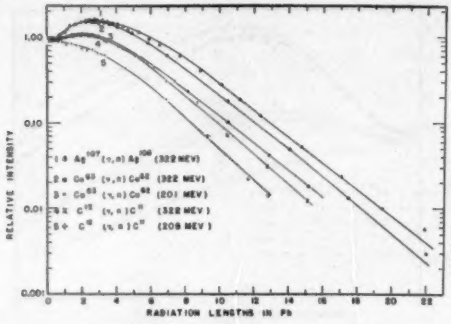

FIG. 4. Semilogarithmic plot of transition curves of x-rays responsible for several (γ,n) reactions.

The five curves show the same characteristic features. As the synchrotron beam penetrates the lead stack, photons are absorbed. In the energy region of interest, the absorption is primarily due to pair production. The absorption of the "effective photons" originally present in the beam produces the initial dip of the transition curves. Some of the electrons produced by photons of energy much higher than W_e are responsible for the production of "effective photons" in one or more steps. This multiplication results in a rise or at least a levelling off of the transition curves. For a given beam energy, the rise is largest for the reaction with the lowest threshold (Ag). For a given detector the rise is smallest when the lower energy beam is used. At large depths multiplication of "effective photons" stops and an exponential absorption is approached. The slowest absorption is observed with the lowest threshold detector. The final slopes of the curves for the same detectors but different beam energies are the same within experimental error. Some of these features will be examined in greater detail in Sec. II(E).

The values of W_e as obtained from the track length of these transition curves are given in Table II. The agreement with the results of McElhinney *et al.*[2] and Katz *et al.*[3] is good, but the results appear to be lower than would be expected from the excitation curves of Baldwin and Klaiber.[1] The ratio of the track lengths of the transition curves for "effective photons" of a given energy obtained with beams of different maximum photon energy is predicted accurately by shower theory, since most approximations cancel out [Eq. (9) of reference 6]. Theoretical and experimental results are presented in Table I; the agreement is satisfactory.

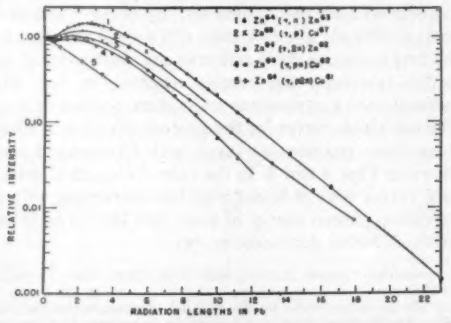

FIG. 5. Semilogarithmic plot of transition curves of x-rays responsible for several reactions from Zn taken with 322-Mev bremsstrahlung.

Long bombardments of Cu detectors allow the observation of the 12.8-hr product of the reaction $Cu^{65}(\gamma,n)Cu^{64}$. A few points of the corresponding transition curve were obtained and W_e estimated by comparison with the complete curves for (γ,n) processes.

Zn Detectors

Figure 5 shows transition curves for the photons causing several reactions from Zn and the corresponding values of W_e are given in Table II. The curves for the quanta responsible for the (γ,n), $(\gamma,2n)$, and (γ,pn) processes from Zn^{64} were obtained with Geometry 1. The observed activities have contributions of less than 10 percent from other Zn isotopes as seen in Sec. III. To obtain the transition curves for the photons responsible for the reactions $Zn^{64}(\gamma,p2n)Cu^{61}$, $Zn^{66}(\gamma,pn)Cu^{64}$, and $Zn^{68}(\gamma,p)Cu^{67}$, a special technique had to be used because of the low yield of the product activities. Thick detector foils (0.096 in.) were used, and the Cu products were separated with small amounts of carrier at the end of the bombardment; thus, no sample self-absorption decreased the counting efficiency. This method did not prove to be practicable with the large foils of Geometry 1; instead, $\frac{7}{8}$-in. diameter disks were used in a stack placed at $2\frac{1}{2}$ ft from the synchrotron target. To correct for the scattering of photons outside the detectors a transition curve with polystyrene detectors was taken and compared with that obtained with Geometry 1. No difference was apparent up to 3 radiation lengths. Beyond this point the required correction increased rapidly to 56 percent at 9 radiation lengths. Because of this large scattering only a few points were obtained for these curves; they serve to estimate W_e.

TABLE I. Experimental and theoretical track length ratios for 322-Mev and 200-Mev bremsstrahlung.

Reaction	Beam energy (Mev)	Observed track length	Ratio Exp.	Ratio Theor.
$C^{12}(\gamma,n)C^{11}$	322	6.43	1.44	1.50
	205±5	4.48		
$Cu^{63}(\gamma,n)Cu^{62}$	322	10.0	1.51	1.55
	201±5	6.63		

Ta Detectors

Short bombardment in the 322-Mev synchrotron beam of Ta metal produces a new 70-min half-life

TABLE II. Effective photon energy W_e, relative yields, and integrated cross sections for some nuclear reactions induced by 322-Mev bremsstrahlung.

Reaction	Product half-life	Product β-particles and energy (Mev)[a]	Track length (radiation length)	W_e (Mev)	Relative yield	Relative σ_{int}
$C^{12}(\gamma,n)C^{11}$	20 min.	β^+ 0.99	6.4	27	0.074	0.12
$Cu^{63}(\gamma,n)Cu^{62}$	10.1 min	β^+ 2.92[b]	10.0	18	1.0	1.0
$Cu^{65}(\gamma,n)Cu^{64}$	12.8 hr	β^+ 0.64 (15%) β^- 0.57 (31%) K (54%)		19[d]	1.2	1.3
$Zn^{64}(\gamma,n)Zn^{63}$	38 min	β^+ 0.47 (1%); 1.40 (7%); 2.36 (85%) K (7%)	9.3	19	0.83	0.89
$Zn^{66}(\gamma,p)Cu^{65}$	63 hr	β^- 0.56	7.2	24	0.070	0.097
$Zn^{64}(\gamma,2n)Zn^{62}$	9.5 hr	β^+ 0.66 (10%)[b] K (90%)	5.9	29	0.039	0.067
$Zn^{64}(\gamma,pn)Cu^{62}$	10.1 min	see above	5.5	30	0.21	0.37
$Zn^{66}(\gamma,pn)Cu^{61}$	12.8 hr	see above		30[d]	0.11	0.19
$Zn^{66}(\gamma,3n)Zn^{63}$	38 min	see above			0.029	
$Zn^{64}(\gamma,p2n)Cu^{61}$	3.4 hr	β^+ 1.20 (63%); 0.55 (2.5%); 0.26 (0.03%)[c] K (34%)	2.9[d]	57[d]	0.045	0.17
$Zn^{67}(\gamma,4n)Zn^{63}$	38 min	see above			<0.02	
$Zn^{68}(\gamma,p3n)Cu^{62}$	10 min	see above			0.033	
$Zn^{68}(\gamma,p4n)Cu^{61}$	3.4 hr	see above			0.014	
$Ag^{107}(\gamma,n)Ag^{106}$	24 min	β^+ 2.0 Mev	10.9	16		
$Ta^{181}(\gamma,n)Ta^{180}$	8 hr	$K_{16^{-1}}$	9.3	19		
$Ta^{181}(\gamma,2p\cdots)$ rare earth	70 min	?	2.5	68		
Pb$(\gamma,?)$	hours	?	2.2	78		
Pb$(\gamma,?)$	days	?	2.9	57		
$Bi^{209}(\gamma,?)$	hours	?	2.2	78		

[a] Unless otherwise stated, values taken from G. T. Seaborg and I. Perlman, Revs. Modern Phys. 20, 585 (1948).
[b] R. W. Hayward, Phys. Rev. 79, 541 (1950).
[c] Owen, Cook, and Owen, Phys. Rev. 78, 686 (1950).
[d] Only a few points were obtained for the transition curve, and W_e estimated by comparison with complete curves.

besides the 8-hr activity due to $Ta^{181}(\gamma,n)Ta^{180}$. Chemical separations[11] have shown the short half-life to be associated with a rare earth; it is thus formed by the ejection of at least two charges. A few points of the transition curve of the photons responsible for this new activity are shown in Fig. 6. The high effective photon energy (Table II) obtained by assuming a straight line absorption curve, explains the absence of previous observation.

Long irradiation of Ta produces in addition several activities with a half-life of the order of days. These could not be separated from the 8-hr activity under the conditions of this experiment. Thus the transition curve shown in Fig. 6 is not produced by photons responsible only for the (γ,n) reaction, but also by quanta of higher energy. This is shown clearly by a comparison of its shape with the curve for the (γ,n) reaction in Cu. For absorber thicknesses of less than 5 radiation lengths, the Cu curve lies higher than that for Ta, the reverse being true beyond that point. It is expected, therefore, that $W_e = 19$ Mev, as obtained from the track length, is too high.

Bi Detectors

Disks of Bi of $2\frac{1}{4}$-inch diameter were used as detectors in Geometry 1 and many activities with half-lives ranging from minutes to days were observed after a three-hr bombardment. It was not possible to resolve the decay curves into the various known half-lives in this region of the periodic table. The transition curve obtained at the end of the irradiation is shown in Fig. 6 and corresponds to very high energy photons. Two hours after the end of the bombardment, the transition curve became less steep, indicating that lower energy photons were producing the longer half-lives. The low activity of the samples when the effect become appreciable precluded quantitative observation.

Pb Detectors

When Pb is irradiated with the 322-Mev beam, many activities appear besides the expected Tl^{206} (4 min) and

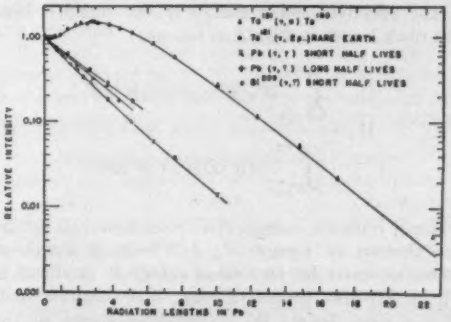

FIG. 6. Semilogarithmic plot of transition curves of x-rays responsible for several reactions from Ta, Pb, and Bi taken with 322-Mev bremsstrahlung.

[11] The author is indebted to Dr. G. Wilkinson for carrying out this separation.

Tl^{207} (5 min). As in the case of Bi, the decay curves could not be resolved into half-lives known in this region. The curve shown in Fig. 6 for the "short half-lives" was taken 1 hour after the end of the bombardment and represents the relative sample activity for a period of 8 hr. After that time it began to rise slowly and the transition curve marked "long half-lives" was taken 36 hours after the end of the bombardment. The energies of the responsible photons as given in Table II represent lower limits only, owing to the large neutron background in this case.

Further work, especially chemical separations, is being planned in the case of Bi and Pb to establish the origin of the new activities. It does not appear to be impossible that they are at least partially produced by photo-fission.[12]

(E) Discussion

The transition curves presented here are caused by photons grouped in a certain energy range. What features of the curves are most energy-sensitive? In the region under consideration, high energy photons are absorbed more rapidly than low energy quanta. The initial drop thus corresponds to the absorption of the photons participating in the reaction, averaged over the incident spectrum. It is difficult to measure this drop accurately, since it is quite small (see Fig. 3). As can be seen from Fig. 1 of reference 6, the experimental points check the theoretical curves calculated for W_e in the case of Cu and C, showing no large contributions to these reactions from high energy photons.

The slope of the transition curves at large absorber depths should correspond to the lowest energy photon participating in the reaction. This again is difficult to measure accurately owing to the low sample activity in this region. Also, contamination by neutron background is difficult to separate from the photon induced activity. The final slopes, before these effects become appreciable, correspond to 15 Mev and 18 Mev in the case of Cu and C detectors, in reasonable agreement with the known thresholds[2] of 10.9 Mev and 18.7 Mev.

The effective photon energy W_e as obtained from the track length is defined as follows:

$$W_e=\frac{\int_{W_{\min}}^{W_0} W\sigma(W)Z(W)N(W)dW}{\int_{W_{\min}}^{W_0} \sigma(W)Z(W)N(W)dW}, \qquad (1)$$

where W = photon energy; $\sigma(W)$ = reaction cross section for photons of energy W; $Z(W)$ = track length of transition curve for photons of energy W produced in Pb by 322-Mev bremsstrahlung; W_0 = quantum limit of the x-ray beam; $W_{\min}$ = threshold energy of the reaction; $N(W)$ = number of photons of energy W present in the incident beam.

If the energies of the photons responsible for a given reaction are grouped around an average value, as is believed to be the case for the reaction studied here, the value of W_e is close to the average energy, as is shown in detail by Eyges.[6]

The main advantages of the track length method of determining the average energy, W_e, of the photons responsible for certain nuclear reactions are as follows. (1) No beam monitor with an accurately known energy dependence is required. (2) For long half-lives, only one bombardment is needed to obtain the effective energy. This is important, since the irradiation times are of the order of a half-life. (3) For short half-lives, few bombardments are needed to obtain a fair value for W_e. This is useful in the case of new activities.

The principal disadvantage of the method comes from the absence of detailed information on the shape of the excitation functions.

III. INTEGRATED REACTION CROSS SECTION AND RELATIVE YIELDS

(A) Method

When a target is placed in the synchrotron beam, the number of reactions n per unit time of bombardment is given by:

$$n=N\int_{W_{\min}}^{W_0}\sigma(W)q(W)dW, \qquad (2)$$

where N = number of target nuclei per unit area, and $q(W)$ = number of photons of energy W incident on the target per unit time. The other symbols have the same meaning as in Eq. (1). This integrand will now be expressed in terms of quantities that can be calculated or measured.

The energy spectrum of the synchrotron beam as calculated for 322-Mev electrons incident normally on a 0.020-in. platinum target is shown in Fig. 7. The ordinate represents a function $f(W)$ given by the equation

$$q(W)dW=kf(W)dW/W. \qquad (3)$$

The numerical value of the constant k is equal to U, the energy incident on the target per unit time, as can be seen as follows. The numerical value of the ordinate of Fig. 7 has been so chosen that the area under the curve is unity. This means that

$$U=\int_0^{322} Wq(W)dW=k\int_0^{322} f(W)dW=k.$$

The variation of $f(W)$ with energy takes into account the deviation of the beam spectrum as calculated for the Berkeley synchrotron from the expression dW/W.

[12] Evidence for photo-fission in Bi has been reported recently by N. Sugarman, Phys. Rev. **79**, 532 (1950).

Equation (3) now becomes:

$$n = NU \int_{W_{min}}^{W_0} [\sigma(W) f(W)/W] dW. \quad (4)$$

If $\sigma(W)$ has an appreciable value only near the effective energy W_e this can be written

$$n = NU[f(W_e)/W_e] \int_{W_{min}}^{W_0} \sigma(W) dW$$
$$= NU[f(W_e)/W_e]\sigma_{int}. \quad (5)$$

To obtain the integrated cross section σ_{int} of a reaction, it is thus necessary to measure n, U, and W_e. The transition curve method is well suited to obtain this last quantity.

In practice, the yield y_1 of a reaction 1 is often measured with respect to the yield y_2 of a reaction 2. The relative cross section can then be calculated using

$$\sigma_1/\sigma_2 = W_e^1 f(W_e^2) y_1 / W_e^2 f(W_e^1) y_2. \quad (6)$$

(B) Integrated Cross Section

σ_{int} has been measured for the reactions $C^{12}(\gamma,n)C^{11}$ and $Cu^{63}(\gamma,n)Cu^{62}$, and the results as calculated with Eq. (5) are given in Table III. The values of W_e as obtained from the transition curves were used.

The energy incident on the target per unit time was measured by a method developed by Blocker, Kenney, and Panofsky which is described in detail elsewhere.[13] Only the procedure as applied to this particular problem will be outlined. The setup consists of a monitor ionization chamber, a two-inch collimator, and a large ionization chamber of known geometry placed in the beam, respectively, at 4, $4\frac{3}{4}$, and $5\frac{3}{4}$ ft from the platinum target. A thin polystyrene sample holder was situated on the front face of the large chamber so that sample disks could be irradiated under repeatable geometrical conditions.

The monitor chamber was calibrated[14] against the beam energy passing through the selected target area by the use of Pb, Cu, and Al disks of the same ($\frac{7}{8}$-in.) diameter and containing the same number of electrons. The taking of Pb−Al and Pb−Cu ionization current differences eliminates effects due to background and Compton electrons. It is then possible to calculate[13] the energy passing through the target area per unit current in the monitor ionization chamber. Cu and C disks of $\frac{7}{8}$-in. diameter were then irradiated in the standard area. U is obtained from the integrated beam as measured by the calibrated monitor chamber. The number of reactions n per unit time of bombardment is calculated by the usual method from the number of counts obtained by placing the sample under an end-window Geiger counter. Beam intensity variation, length of bombardment, decay during and after irradiation, sample self-absorption, and counter efficiency[15] are all taken into account.

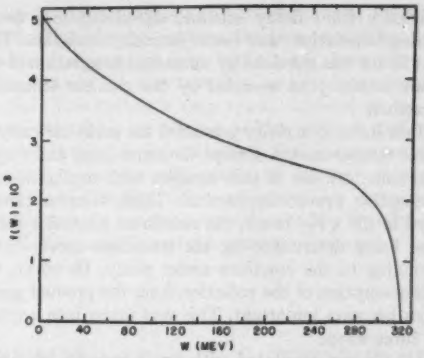

FIG. 7. Theoretical bremsstrahlung spectrum from the Berkeley synchrotron. The function $f(W)$ is defined by Eq. (3). The ordinate scale is chosen to normalize the area under the curve to unity.

The accuracy of the values of σ_{int} is estimated to be 25 percent. The result for the $Cu^{63}(\gamma,n)Cu^{62}$ reaction is in good agreement with the value reported by Johns *et al.*[3] (0.70 Mev-barn with 25-Mev betatron). The integrated cross section for $C^{12}(\gamma,n)C^{11}$ is lower than the value obtained by Lawson and Perlman (0.15 Mev-barn with 100-Mev betatron), but the discrepancy does not lie outside of the estimated errors.

(C) Relative Yields

It is of interest to know the relative yield of several photo-nuclear reactions starting from one element. Zn was chosen for such a study because of the relatively convenient half-lives and known decay schemes of several product nuclei. The results are summarized in Table II and represent the average of two or more measurements. Where W_e is known, the relative cross sections are calculated using Eq. (6). The yield of the reaction $Cu^{63}(\gamma,n)Cu^{62}$ is taken to be unity, since the yield of the 10.1-min activity of Cu^{62} was usually used as a reference.

To obtain the relative yield of reactions leading to different product nuclei, the activities as extrapolated to the end of the bombardment were used after the following factors had been taken into account: counting

TABLE III. Integrated reaction cross sections.

Reaction	W_e(Mev)	σ_{int}(Mev-barn)
$C^{12}(\gamma,n)C^{11}$	27	0.090
$Cu^{63}(\gamma,n)Cu^{62}$	18	0.76

[13] Blocker, Kenney, and Panofsky, Phys. Rev. **79**, 419 (1950).

[14] The author is indebted to W. Blocker and R. Kenney for this calibration.

[15] The absolute β-standard used consists of a thin U_3O_8 deposit covered with an Al foil. The calibration by coincidence methods was made by L. Aamodt. The Cu and C disks and the U_3O_8 deposit were of approximately equal sizes.

efficiency from decay scheme, self-absorption, decay during irradiation, and beam intensity variation. This last factor was obtained by numerical integration of the beam intensity as recorded by the monitor ionization chamber.

Low induced activity presented the main difficulty in these measurements. Except for some (γ,n) and (γ,pn) reactions, the use of thin samples with negligible self-absorption proved impractical. Thick samples can be used in the x-ray beam, the maximum allowable thickness being determined by the transition curves corresponding to the reactions under study. However, the self-absorption of the radiation from the product nuclei then becomes important. This was taken into account in three ways.

(1) Cu was separated with small amounts of carrier after bombardment of thick $ZnSO_4$ samples; the activity of the resulting thin Cu sample was followed to obtain the relative yields of Cu^{61}, Cu^{64}, and Cu^{67} with respect to Cu^{62}.

(2) Isotopically enriched samples[16] of ZnO were used to obtain the yields of Cu^{61}, Cu^{62}, and Zn^{63} from the various Zn isotopes by counting samples of identical thickness and area.

(3) Since Zn^{62} decays 90 percent by K-capture and the counter efficiency for x-rays is very low, nearly the same radiation is counted from Zn^{62} and Cu^{62}. The relative yield can therefore be obtained from a thick sample.

The uncertainty of the given results varies with the different reactions, but is estimated to be less than 30 percent.

(D) Summary

A lower limit to the total integrated cross section $\sigma_{\text{int}}{}^{\text{tot}}$ for photon absorption by the Zn nucleus can be estimated from the results summarized in Table II since $\sigma_{\text{int}}{}^{\text{tot}}=\sum\sigma_{\text{int}}$. This sum should be extended over all possible reactions to give the correct value. Adding the integrated cross sections, for the (γ,n), $(\gamma,2n)$, (γ,p), (γ,pn), and $(\gamma,p2n)$ reactions, a value of 1.2 Mev-barns is obtained. The relative yields, but not W_e, are known for the $(\gamma,3n)$, $(\gamma,p3n)$, and $(\gamma,p4n)$ processes. By estimating the corresponding effective photon energies from the number of ejected nucleons, an additional contribution of about 0.2 Mev-barn is obtained. The fact that not all of the observed reactions started from the same Zn isotope should not greatly affect this result since the excited nuclei were all of the even-even type. Thus we obtain

$$\sigma_{\text{int}}{}^{\text{tot}}\geqslant 1.4 \text{ Mev-barn}.$$

In a similar manner a lower limit for the mean energy $\bar{W}$ for photon absorption can be estimated using $\bar{W}=\sum\sigma_{\text{int}}W_e/\sum\sigma_{\text{int}}$. The result is

$$\bar{W}\geqslant 30 \text{ Mev}.$$

[16] Supplied by the Carbide and Carbon Chemicals Corporation.

It should be noted that the relative yields of the (γ,n) reactions observed with 322-Mev bremsstrahlung agree well within experimental errors with the G. E. results obtained with 100-Mev and 50-Mev betatron beams.

IV. CONCLUSIONS

From the results reported in this paper it is apparent that the (γ,n) process is the dominant mode of decay of the x-ray excited Zn nucleus. However, other reactions contribute at least an equal amount to the total absorption cross section. It thus seems that the photon absorption curve has a broad maximum around 20 Mev, tailing off slowly at higher energies.

In a recent paper Levinger and Bethe[17] show from quite general sum rule considerations that photon absorption by dipole transitions leads to a reasonable total absorption cross section if exchange forces are included. The results reported here agree well with their calculations, since the value of x (the fraction of the n–p interaction due to exchange force) obtained from $\sigma_{\text{int}}{}^{\text{tot}}=1.4$ Mev-barn and $\bar{W}=30$ Mev is of the correct order of magnitude.

Goldhaber and Teller[18] have proposed a more specific model for nuclear dipole absorption in which all protons move together against all neutrons. This leads to sharp resonance absorption and scattering. The importance of processes resulting in the ejection of more than one nucleon seems to indicate that at least some other process for higher energy photon absorption must exist.

The decay of the compound nucleus Zn^{64} when excited by different methods is of interest. Ghoshal[19] has obtained this compound nucleus by α-particle bombardment of Ni and proton bombardment of Cu, while in this paper the excitation with x-rays has been described. The cross section for formation of the compound nucleus depends, of course, on the method of excitation; but the decay might be independent of this factor if the nucleus has lost all "memory" of its origin. Ghoshal finds the peak of the (α,n) reaction at 20 Mev, the peaks of the $(\alpha,2n)$ and (α,pn) processes at 31 Mev. The values of W_e for the reaction (γ,n), $(\gamma,2n)$, and (γ,pn) are 19 Mev, 29 Mev, and 30 Mev, respectively. This close agreement is not surprising, since the α-particle binding energy is small. In addition Ghoshal finds that the yield of the (α or p,pn) reaction is four times larger than the yield of the (α or p,$2n$) process. The relative yield of 5.5 of the corresponding x-ray induced reactions is quite similar considering that peak and integrated cross sections are being compared. It thus appears that the decay of a 30-Mev excited Zn nucleus does not depend on its method of excitation.

Levinthal and Silverman[20] have obtained energy and angular distributions of protons emitted by several elements irradiated in the synchrotron beam. They find a relatively large number of high energy protons which

[17] J. S. Levinger and H. A. Bethe, Phys. Rev. 78, 115 (1950).
[18] M. Goldhaber and E. Teller, Phys. Rev. 74, 1046 (1948).
[19] S. Ghoshal, Phys. Rev. 80, 939 (1950).
[20] C. Levinthal and A. Silverman (to be published).

would not be expected according to the statistical theory, and these protons show an asymmetrical angular distribution. This indicates that the (γ,ϕ) reaction is not necessarily produced by photons grouped in a narrow interval around W_e. This should be noticeable from the shape of the transition curve corresponding to the (γ,ϕ) reaction. It is unfortunate that the accuracy obtained in this case does not warrant any conclusions along this line.

It is a pleasure to thank Professor A. C. Helmholz, under whose guidance this work was carried out, for many helpful suggestions and assistance, and Professor E. McMillan for his constructive interest and support. Several conversations with Professor R. Serber on the interpretation of the transition curves proved very fruitful. The author is very much indebted to Dr. L. Eyges for taking an interest in this problem and performing the required calculations. Mr. J. Rose assisted in some of the measurements and his help is much appreciated. Finally, this work would not have been possible without the fine cooperation of Mr. W. Gibbins, Mr. G. McFarland, and the synchrotron crew.

PHYSICAL REVIEW VOLUME 81, NUMBER 6 MARCH 15, 1951

Effective Photon Energies of High Energy Photo-Nuclear Reactions*

LEONARD EYGES
Radiation Laboratory, Department of Physics, University of California, Berkeley, California
(Received October 30, 1950)

An attempt has been made to use shower theory to evaluate the effective energies of the photo-nuclear reactions measured by Strauch. It seems that these energies can be determined most accurately from the area under the transition curve, the so-called "track length." A theoretical formula for the track length is discussed. The shape of the transition curve at small thicknesses can also be calculated quite accurately and serves as a rough check on the effective energies as derived from the track length. A comparison with experiment of the theoretical shape of the whole transition curve is given; and, as one would expect, the agreement is not very good.

I. INTRODUCTION

IN this paper we try to use shower theory to evaluate some of Strauch's[1] results on high energy photo-nuclear reactions. As Strauch has described, the cross sections for these reactions have more or less sharp maxima for some photon energy. For most of our calculations it will be adequate to assume that the width at this maximum is very small; i.e., that the reactions take place for only one photon energy, which we shall call W_e, the "effective energy." The effect of this approximation is discussed later. If it were easy to make accurate calculations with present shower theory, there would be no problem; one would simply calculate shower curves for various energies W_e, and for some value of W_e would obtain a fit with the experimental curve. For the energies in which we are interested, however, around 20 Mev, it is well known that shower theory cannot be relied upon to predict an accurate cascade curve, mainly because the cross sections for pair production and bremsstrahlung vary considerably over the range of energies of interest, which is from about 20 to 300 Mev. We must look, therefore, to some quantity that can be calculated more accurately than can the shape of the entire transition curve and yet one that gives us the information we desire.

It is clear that one does not really need to know the whole transition curve in order to find the energy to which it corresponds. If we consider transition curves corresponding to different energies, but to the same initial conditions, then at any thickness there is a unique correlation between the energy and the height of the curve. Thus, any one point on the transition curve determines the energy, in principle. Of course, this is no real help, for if we could calculate an arbitrary point accurately, we could calculate the detailed shape. There is a particular point on the transition curve however, which can be calculated rather more accurately than can any other point; namely, the height of the maximum. The reason is, as Rossi and Greisen[2] have pointed out, that at the maximum of the shower one can take into account approximately the variation of the pair production cross section with energy. This enhances the accuracy considerably. Thus, if the shower curve corresponding to an energy W_e shows a maximum, one might hope to determine W_e by the position and height of the maximum. Therein lies the difficulty. Although some of Strauch's curves have a maximum, those corresponding to higher energies do not. We must find a different method if we wish it to be universally applicable.

For very large thicknesses multiplication becomes

* This work was performed under the auspices of the AEC.
[1] K. Strauch, Phys. Rev. 81, 973 (1950).
[2] B. Rossi and K. Greisen, Revs. Modern Phys. 13, 274 (1941).

unimportant, and the "shower" curves simply become the exponential absorption curve of photons[3] of energy W_ϵ. One might hope to determine the absorption coefficient from the slope of the experimental curve and from this to get the energy W_ϵ. There is no difficulty in principle with this idea; in practice one must go to such large thicknesses before pure absorption sets in that the intensity becomes impractically small.

The beginning of Strauch's shower curves have a characteristic shape. There is a drop at very small thicknesses owing to the absorption of photons of energy W_ϵ; multiplication soon sets in, however, and the curve becomes less steep and may even rise again. The initial slope is entirely due to self-absorption; and this slope, in principle, determines the energy. Unfortunately, this slope is very difficult to measure with any accuracy. On the other hand, one might hope that since the first part of the shower curve, up to perhaps a half-radiation length, is mainly an absorption curve, multiplication processes being secondary, one might be able to calculate this multiplication with sufficient accuracy to predict the behavior of the beginning of the curve with reasonable accuracy. This expectation is fulfilled. One can calculate the shower curve to almost a radiation length with considerable accuracy. Unfortunately, there is an experimental limitation. It is difficult to get good statistics on the beginning part of the curve. Therefore, one cannot obtain a very accurate value for W_ϵ in this manner.

Finally, it is possible to determine the effective energy W_ϵ from the area under the transition curve, the so-called "track length." This quantity has the advantage that one can take the variation of the pair production cross section with energy into account, just as in the calculation of the height at the maximum. Moreover, it has an advantage over the latter quantity: although not all of Strauch's transition curves have a maximum, all have an area. It is the track length which we have mainly used in calculating W_ϵ, although we have also used the initial behavior of the shower curve, up to almost a radiation length, as a rough check.

The remainder of this paper is in four parts: in Sec. II we have calculated the photon spectrum to be expected from the synchrotron target; in Sec. III we have calculated the track length as a function of energy, and applied our formula to Strauch's results; in Sec. IV we have calculated the detailed shape of the curves at their beginning; finally, in Sec. V, we have calculated, as best we could, the detailed shape of the transition curves, neither expecting nor getting very good agreement, with experiment.

For convenient reference, we give here the usual shower equations, using the notation of Rossi and Greisen unless otherwise indicated.

$$\frac{\partial\pi(E,t)}{\partial t}=2\int_0^1\gamma\left(\frac{E}{u},t\right)\psi\left(\frac{E}{u},u\right)\frac{du}{u}-\int_0^1\pi(E,t)\phi(E,v)dv+\int_0^1\frac{1}{1-v}\pi\left(\frac{E}{1-v},t\right)\phi\left(\frac{E}{1-v},v\right)dv+\epsilon\frac{\partial\pi(E,t)}{\partial E},\quad(1a)$$

$$\frac{\partial\gamma(W,t)}{\partial t}=\int_0^1\pi\left(\frac{W}{v},t\right)\phi\left(\frac{W}{v},v\right)\frac{dv}{v}-\sigma(W)\gamma(W,t).\quad(1b)$$

Here $\pi(E,t)$ is the number of electrons of energy E at thickness t and $\gamma(W,t)$ is the same for photons. $\psi(W,u)$ is the probability per radiation length that a photon of energy W produce a pair, one particle of which has fractional energy u. $\phi(E,v)$ is the probability per radiation length that an electron of energy E emit a photon with fractional energy v. The usual shower theory deals with high energies where ψ and ϕ are functions of u and v only; but for our purposes, keeping the dependence on W and E explicit facilitates discussion. ϵ in the above equations is the critical energy, and thicknesses are measured in radiation units. We also depart slightly from Rossi and Greisen by letting $\sigma(W)$ be the *total* absorption coefficient for photons of energy W. This will be discussed later. If we call $\sigma_c(W)$ the absorption coefficient for the Compton effect and $\sigma_p(W)$ that due to pair production, then

$$\sigma(W)=\sigma_p(W)+\sigma_c(W).$$

II. PHOTON SPECTRUM FROM THE TARGET

The 322-Mev electrons from the beam of the synchrotron are allowed to fall on a target of Pt, 0.020 in. thick, producing the beam of photons used in the experiment. If the target were infinitely thin, the distribution of photon energies W whould be given by $\phi(E_0,v)$, where $E_0=322$ Mev and $v=W/E_0$. Actually, the finite thickness of the target introduces a correction, which we shall calculate in this section. First, we make explicit an assumption inherent in our use of the function $\phi(E_0,v)$. This function gives the energy distribution of the photons produced by an electron of energy E_0, integrated over the angles between the electron and the photon directions. At first sight, one might think that the appropriate function for our purposes should be the energy distribution of photons produced in essentially the same direction as the electron. In passing through the target, however, the electrons are multiply scattered; and in the present geometry the effect of these

[3] If we take the finite width of the reaction cross sections into account, the shower curve at large thicknesses really becomes the absorption curve of the photons of lowest energy that can produce the reaction.

deviations arising from scattering will be taken care of to a good approximation[4] by using the integrated function $\phi(E_0, v)$.

We can find the photon spectrum by simply putting into the shower equations a power series expansion corresponding to the correct initial conditions, i.e.,

$$\pi(E_0, E, t)=\delta(E_0-E)+P(E_0, E)t+\cdots,$$
$$\gamma(E_0, W, t)=Q(E_0, W)t+R(E_0, W)t^2+\cdots.$$

Equating to zero various powers of t in the shower equation, the unknown functions P, Q, and R are found in succession as easily evaluable integrals. $Q(E_0, W)$ comes out to be just $\phi(E_0, v)$, as it must. If we use the the approximate expression $\phi(E_0, v)\approx 1/v$ to calculate the small correction term $R(E_0, W)$, we obtain

$$R(E_0, W)=-\tfrac{1}{2}[\sigma(W)-\ln(1-W/E_0)].$$

Thus our corrected spectrum from the target is

$$\phi(E_0, v)-\tfrac{1}{2}t\{\sigma(W)-\ln(1-v)\}. \qquad (2)$$

This corrected spectrum is plotted in Fig. 7 of Strauch's paper.[1] The physical interpretation of this spectrum is clear. For v small, $\ln(1-v)\approx 0$ and the important term in the correction is just the absorption of photons in the target. The correction term $-\frac{1}{2}\sigma(W)t$ represents this self-absorption. For large v the term in $\ln(1-v)$ is important. This term *diminishes* the number of high energy photons. This represents a double radiation process: there is an overwhelmingly probability for emitting a low energy quantum in which the energy of the electron is diminished below 322 Mev; therefore, it can no longer emit a quantum with this upper limit. Thus the effect of the finite target thickness is to diminish appreciably the number of very high energy photons.

After leaving the target, the beam must pass through a quartz donut about $\frac{3}{4}$ in. thick. The main effect of this on energies above 18 Mev is to reduce the intensity uniformly, since the absorption coefficient is small and varies slowly with energy in this region. We therefore neglect this correction.

III. THE TRACK LENGTH

The most accurate calculation of the track length of photons to date is the numerical work by Richards and Nordheim[5] in which collision loss of the electrons and the Compton effect are taken into account, as well as the variation with energy of the radiation and pair production cross sections. These are not very convenient for our purpose, however, since they are made for a single incident photon. To apply them to the present problem, one would need to integrate their results numerically over the photon spectrum emerging from the synchrotron. Moreover, aside from the labor involved, there is the difficulty that Richards and Nordheim's results hold only when the single incident photon has an energy much larger than the energy W_s of the photons which one is considering; in these circumstances it is not clear how to carry out the integration over the photon beam from the synchrotron, since, of course, it contains photons with energies arbitrarily close to W_s.

Fortunately, the photon energies with which we have to deal are always greater than about 17 Mev; i.e., about two and a half times the critical energy in lead. In this case, it is possible to make a slight adaptation of the formulas for the track length in Rossi and Greisen so that they apply with considerable accuracy. Before we do this, there is a somewhat peculiar feature of the usual track length formulas, which we should consider. For the sake of discussion, suppose we are interested in the track length of photons of energy W, due to an initial spectrum which goes as $1/W$ up to some maximum energy W_0. Now, following Nordheim and Hebb[6] the track length of photons of energy W, due to an arbitrary initial spectrum $\gamma(W_0, W, 0)$ is

$$Z(W_0, W)=\frac{1}{\sigma\cdot 2\pi i}\int_{s-i\infty}^{s+i\infty}\frac{A(s)M(s, 0)W^{-(s+1)}}{[A(s)-B(s)C(s)/\sigma]}ds, \qquad (3)$$

where

$$M(s, 0)=\int_0^\infty W^s\gamma(W_0, W, 0)dW.$$

For a $1/W$ spectrum up to W_0, $M(s, 0)=W_0^s/s$; and we therefore have

$$Z(W_0, W)=\frac{1}{\sigma W\cdot 2\pi i}\int_{s-i\infty}^{s+i\infty}\frac{A(s)}{[A(s)-B(s)C(s)/\sigma]}\frac{e^{sy}}{s}ds, \qquad (4)$$

where $y=\ln(W_0/W)$ and the integration path is to the right of all the singularities of the integrand. Here $A(s)$, $B(s)$, $C(s)$ are defined as by Rossi and Greisen.[2,7] Now the integrand of (4) has simple poles at $s=1, -2.6, -3.6\cdots$. If we evaluate the residues at these poles and divide the result by the initial spectrum dW/W to get the track length relative to the number of photons at $t=0$, we find

$$Z_{\text{rel}}(W_0, W)=\frac{1}{\sigma}\left[0.437\frac{W_0}{W}-0.02\left(\frac{W}{W_0}\right)^{2.6}-0.005\left(\frac{W}{W_0}\right)^{3.6}+\cdots\right]. \qquad (5)$$

Now it is clear that (5) becomes invalid[8] when W approaches W_0. The relative number of photons of energy W, when W is very close to W_0, will be given by $e^{-\sigma t}$, since there will be essentially no multiplication.

[4] L. I. Schiff, Phys. Rev. **70**, 87 (1946).
[5] J. Richards and L. Nordheim, Phys. Rev. **74**, 1106 (1948).
[6] L. W. Nordheim and M. H. Hebb, Phys. Rev. **56**, 494 (1939).
[7] Note that $B(s)$ as defined in reference 2 has a factor σ in it so that the integrand in (4) is really independent of σ.
[8] This was called to my attention by Dr. Strauch.

Hence, Z_{rel} will be just $1/\sigma$; and for smaller W where there is multiplication Z_{rel} must be greater than $1/\sigma$. This condition fails to hold for (5) when $W\approx 0.41W_0$. It is not clear why (5) is incorrect for $W\sim W_0$, when (4) is almost certainly correct. It may be that the integrand in (4) has singularities off the real axis, although Nordheim and Hebb have made a search near $s=1$, and we also have made a rather perfunctory search, without finding any. We are concerned with this point, not because we want to use a formula like (5) for W close to W_0—in Strauch's experiments W/W_0 is always fairly small—but we really would like to know whether (5) can be considered to be correct for W/W_0 small, where the higher order terms are negligible. This is not obvious, since the fact that (5) breaks down for $W\sim W_0$ throws suspicion on it.

Some light can be shed on this question in the following way. If one uses the Carlson-Oppenheimer[9] approximation to the shower equations, it is easy to show that this is equivalent to using

$$A(s)=2s/(s+1),\quad B(s)=2\sigma/(s+1),\quad C(s)=1/s.$$

Then

$$Z_{rel}(W_0, W)=\frac{1}{\sigma\cdot 2\pi i}\int_{\delta-i\infty}^{\delta+i\infty}\frac{se^{ys}}{s^2-1}ds$$

$$=\frac{0.500}{\sigma}\left(\frac{W_0}{W}+\frac{W}{W_0}\right). \qquad (6)$$

This is a most reasonable result, since Z_{rel} as given by (6) is always greater than $1/\sigma$ and approaches $1/\sigma$ as W approaches W_0. Unfortunately, Eq. (6), however reasonable in appearance, cannot really be trusted for W close to W_0, since the Carlson-Oppenheimer approximation is not very good in this region. For smaller values of W, Eq. (6) shows that Z_{rel} is proportional to W_0/W with a correction term of order $(W/W_0)^2$, which is small. This is probably a trustworthy qualitative conclusion in general, since the Carlson-Oppenheimer approximation is not bad for $W\ll W_0$.

We have also tried to check (5) in the following manner. We have calculated the shower curve as a function of thickness for various values of $y=\ln(W_0/W)$ and integrated these numerically to find the track length; we have used an expansion in powers of t for small t and the usual saddle point method for larger t. This method gives reasonable results; e.g., as W approaches W_0 the relative track length approaches $1/\sigma$. The major difficulty is that it is not very accurate, since the saddle point method can be off by 10 or 15 percent for the smaller values of y and t. We have corrected for the inaccuracies of the saddle point method as best we could by comparison of the answers which it gives with the quite accurate results given by the power series in t. for those values of t for which one can get an answer by both methods. Comparison of our answers for Z_{rel} by this method with (5) makes it appear that (5) is correct for $y=3$, is a few percent low for $y=2$, about 30 percent low for $y=1$, and, of course, off by a factor 1/0.41 for $y=0$. We have done the same sort of calculation for an initial spectrum

$$1/W[(4/3)(1-W/W_0)+0.38(W/W_0)^2],$$

which is a rough approximation to the spectrum from the synchrotron, and find that the formula corresponding to (5) is more accurate than for the $1/W$ spectrum, being off, for example, only by a few percent for $y=1$. All in all, then, it seems clear that although formulas like (5) are not correct for W close to W_0, they are probably valid for $W\ll W_0$.

Now we turn to the real problem of interest, that of calculating as accurately as possible the track length of photons using the initial spectrum given by (2). We are interested in energies from about 17 Mev up. Energy loss of electrons by ionization is not negligible in this range; but, as Rossi and Greisen[2] have shown, one can correct for this by using an asymptotic expansion in powers of ϵ/W. The variation with energy of the pair production cross section can also be included in the manner indicated by Rossi and Greisen,[10] i.e., by writing

$$\psi(W, u)du=\sigma_p(W)du \qquad (7)$$

and considering that the unknown function in the shower equations for the track length is not $Z(W_0, W)$ but $\sigma_p(W)\cdot Z(W_0, W)$. The above approximation for $\psi(W, u)$ means that the pair spectrum is taken to be flat; i.e., that the probability for the production of an electron of any energy is independent of energy. This is a quite good approximation in the range 18 to 322 Mev. The variation of the radiation cross section with energy can be included by taking some average expression appropriate to the region 18 to 322 Mev. The expression we have chosen is

$$\phi(v)=\frac{1}{v}\left[\frac{4}{3}-(1-v)+\frac{3}{4}v^3\right]. \qquad (8)$$

Reference to Rossi and Greisen will show that this seems to be a reasonable approximation except for v close to unity, where $\phi(v)$ is relatively small anyway.

If one carries out the calculations according to the above sketch, using the boundary condition that the incident spectrum is that given by (2) he obtains

$$Z(W_0, W)=0.346W_0/\sigma_p(W)\cdot W^2\cdot\nu(\epsilon/W), \qquad (9)$$

where

$$\nu(\epsilon/W)=1+0.71(\epsilon/W)-0.32(\epsilon/W)^2+0.41(\epsilon/W)^3+\cdots.$$

We have not included the dubious negative powers of W_0/W which one gets from the evaluation of (4) at the poles on the negative real axis, since the discussion at the beginning of this section implies that they are

[9] J. F. Carlson and J. R. Oppenheimer, Phys. Rev. **51**, 220 (1937).

[10] See reference 2, p. 293.

negligible for the energies which interest us. The factor 0.346 appears in (9) instead of the usual 0.437 for two reasons. First, $M(1,0)$, as evaluated by numerical integration of the spectrum given by (2), turns out to be $0.816\,W_0/W$ instead of W_0/W as before. Second, we have used the $A(s)$, $B(s)$, and $C(s)$ corresponding to the $\phi(v)$ and $\psi(u)$ given above instead of those calculated with the usual asymptotic $\phi(v)$ and $\psi(u)$, as by Rossi and Greisen. This alters the residue at $s=1$. This change is rather insensitive to the choice of $\phi(v)$. For example, if we use the $A(s)$ corresponding to $v\phi(v)=(4/3)(1-v)+v^2$ and to $(4/3)(1-v)+\frac{1}{2}v^2$, the factor 0.346 changes to 0.355 and 0.330, respectively. Thus, using the average $\phi(v)$ given by (8) introduces only a small error.

At the lowest energies for which we wish to use (9) the cross section for Compton effect is about 15 percent of that for pair production, and is therefore not negligible. To take this into account accurately one would need to supplement Eqs. (1) by a term describing the production of electrons with energy greater than W in the Compton effect, and a term describing the photons with energy greater than W that get an energy W in a Compton scattering. This is difficult and we shall not attempt it, since the effect of these terms is probably small anyway. In addition to these effects the Compton effect acts to absorb the photons of energy W in which we are interested. One takes this into account roughly in the following manner. One replaces $\sigma_p(W)$ in (7) by $\sigma(W)$ and as mentioned before uses the total absorption coefficient $\sigma(W)$ in (1b). A glance at Eq. (1b) shows that this means that we take the absorption of photons of energy W into account correctly, but that we falsify the spectrum of electrons with energy greater than W, since replacing $\sigma_p(W)$ by $\sigma(W)$ makes the pair cross section too large. But a photon of 18 Mev is produced on the average by an electron of, say, twice that energy, where the Compton effect is very small anyway, so that it doesn't matter that we have allowed $\psi(W,u)$ to include the Compton effect. Also, and this is probably a stronger argument, we have checked (9) by comparison of the analogous formula for a single incident photon with the numerical results of Richards and Nordheim and found agreement within five percent from 14 Mev up, if we use $\sigma(W)$ and not $\sigma_p(W)$.

In evaluating the experiments, one wants not the track length given by (9), but $Z_{\rm rel}(W_0,W)$, the track length relative to the number of photons initially present in dW.

If we use the notation

$$\gamma(W_0,W,0)=f(W_0,W)/W$$

and make the change from $\sigma_p(W)$ to $\sigma(W)$ just mentioned, the relative track length is given by

$$Z_{\rm rel}(W_0,W)=0.346W_0/\sigma(W)W\nu(\epsilon/W)f(W_0,W). \quad (10)$$

In applying (10), as Strauch has explained, we have increased the radiation length by 10 percent over the value given by Rossi and Greisen and have decreased the pair production cross section per cm by 10 percent. It is obviously difficult to estimate the error in (10); but if forced to guess we would say that it is probably good to 15 percent at 17 Mev, and perhaps 10 percent at twice this energy. As was discussed earlier in this section, (10) must break down for $W\sim W_0$; but if we can extrapolate from our previous results, it should still be reasonably accurate for $W/W_0<\frac{1}{2}$.

As Strauch has noted, a kind of internal check on the experiments and theory can be had by carrying out an experiment on a given element with two different maximum energies W_{01} and W_{02} of the photon beam. The ratio of the relative track lengths is then

$$\frac{Z_{\rm rel}(W_{01},W)}{Z_{\rm rel}(W_{02},W)}=\frac{W_{01}f(W_{02},W)}{W_{02}f(W_{01},W)}. \quad (11)$$

This theoretical expression for the ratio should be quite accurate, since most of the approximations involved in the derivation of (10) effectively cancel in forming it. Equation (11) has been checked for the two reactions $Cu^{63}(\gamma,n)Cu^{62}$ and $C^{12}(\gamma,n)C^{11}$, which were carried out at maximum energies of 322 and about 200 Mev. The results are given in Table I of Strauch's paper.[1]

IV. SMALL THICKNESSES

If we wish to find the shape of the transition curve for small thickness, an expansion in powers of t suggests itself. As we have seen, the transition curve must drop at the very beginning, since absorption of the photons in the incident beam is a first-order effect proportional to t, and the production of photons is at least of second order. This suggests the use of an expansion of the form

$$\gamma(W_0,W,t)=e^{-\sigma(W)t}[\gamma(W_0,W,0)+K(W_0,W)t+L(W_0,W)t^2+\cdots], \quad (12a)$$

$$\pi(W_0,E,t)=[M(W_0,E)t+N(W_0,E)t^2+\cdots]. \quad (12b)$$

This expansion obviously satisfies the boundary conditions. The factor $e^{-\sigma(W)t}$ in (12a), of course, represents the absorption of photons of energy W initially in the beam and the coefficients $K(W_0,W)$, $L(W_0,W)$, etc. describe their subsequent multiplication.

These functions can be found by putting (12a) and (12b) into the shower equations (1) and equating to zero successive powers of t. The functions then come out to be simple, but sometimes tedious integrals. Alternately, one can find, in much the same manner, the Mellin transforms of the shower equations as a series in t and can then invert this transform, evaluating the complex integrals that result by the method of residues. Both methods, lead to the same result, of course, which we first write down and then discuss. As before, the quantity of interest is not $\gamma(W_0,W,t)$ but

$$\gamma_{\rm rel}(W_0,W,t)=\gamma(W_0,W,t)/\gamma(W_0,W,0).$$

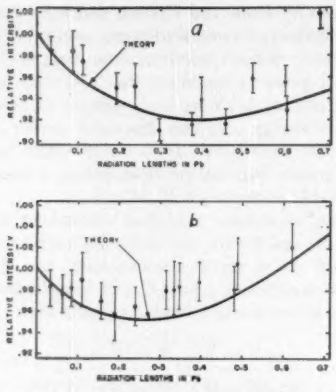

FIG. 1. (a) Relative intensity in Pb of photons causing $C^{12}(\gamma,n)C^{11}$. (b) Relative intensity of Pb of photons causing $Cu^{63}(\gamma,n)Cu^{62}$.

Our results are

$$\gamma_{rel}(W_0, W, t) = e^{-\bar{\sigma}(W)t}\left[1+\frac{\bar{\sigma}_p F(y)t^2}{f(W_0,W)}+\frac{G(y)t^3}{3f(W_0,W)}+\cdots\right], \quad (13)$$

where

$$y=\ln(W_0/W), \quad \bar{\sigma}_p=\sigma_p[(W_0W)^{\frac{1}{2}}],$$

$$F(y)=(16/9)(3e^{-y}-3+y+\tfrac{1}{2}y^2e^{-y}+2ye^{-y}) +1.8(\tfrac{1}{2}+\tfrac{1}{2}e^{-2y}-ye^{-y}-e^{-2y}) +0.45(e^{-y}-e^{-2y}-ye^{-2y}),$$

$$G(y)=\bar{\sigma}^2(y-1+e^{-y})-\bar{\sigma}H(y)-\bar{\sigma}(\epsilon/W_0)(e^y-1),$$

$$H(y)=1.645-\sum_{n=1}^{\infty}(e^{-ny}/n^2)+(1-e^{-y})\ln(1-e^{-y})-ye^{-y}.$$

The following approximations have been used in calculating the above result. As an analytic approximation to the initial spectrum, we have used

$$W\gamma(W_0, W, 0)=\left[\frac{4}{3}\left(1-\frac{W}{W_0}\right)+0.6\frac{W^2}{W_0^2}\right].$$

In calculating the term in t^2, we have used, as for the track length, $v\phi(v)=(4/3)(1-v)+\frac{2}{4}v^2$, and $\psi(W,u)du=\text{const}\cdot du$. In calculating the small term in t^3, we have, for simplicity, used $\phi(v)=1/v$. In terms in t^2 and t^3 describing the multiplication, there is the factor $\sigma_p[(W_0W)^{\frac{1}{2}}]$. This enters in the following way. Multiplication takes place because electrons of some average energy between W_0 and W are created and then radiate photons of energy W; for this average energy we have chosen the geometrical mean of W_0 and W; hence, the pair production cross section at this energy is $\sigma_p[(W_0W)^{\frac{1}{2}}]$. We have checked this approximation by writing $\sigma_p(W)$ as a linear function of $\ln(W)$, which is a fair representation in the energy range of interest here, and then calculating the coefficient of t^2 using the initial spectrum $\gamma(W_0, W, 0)=1/W$, and the approximation $\phi(v)=1/v$. One can then carry out the integrations and it turns out that to a very close approximation one gets the same results for the coefficient of t^2 as if he had started from the beginning with the average value $\sigma_p[(W_0W)^{\frac{1}{2}}]$.

For $W=W_0$ it is clear that (13) must become $e^{-\sigma(W)t}$, since there can no longer be any multiplication. Thus, for this case ($y=0$), $F(y)$, and $G(y)$ must vanish. This provides a useful check on the calculations. In the terms in t^2 there enters a correction due to collision loss. This correction diverges as W goes to zero, but for $W>\epsilon$ it is probably correct.

We have used the above formula to calculate the beginning shapes of the transition curves for the reactions $Cu^{63}(\gamma,n)Cu^{62}$ and $C^{12}(\gamma,n)C^{11}$, using for the respective "resonance" energies the values 18 Mev and 27 Mev derived from the track length. The results are shown in Fig. 1. The experiments, of course, do not give very reliable results at these thicknesses, since one is trying to measure changes in intensity of the order of a few percent and very long counting periods are needed to get good statistical accuracy. Within the experimental errors, however, the theory seems to give fair agreement. If anything, the theoretical curve seems to be too low. The theoretical curves would be raised if one assumed that the effective energies were somewhat lower than 18 and 27 Mev, but the poor accuracy of the experiments does not justify this.

One should note that the expansions given above are quite accurate where they apply. This is because the main phenomenon at small thicknesses is simply the absorption of original photons and one knows accurately this absorption coefficient. The shower theory enters, of course, in giving the coefficients $F(y)$, etc. for the higher order terms, but it turns out that these are not at all sensitive to the approximate expression for the cross sections one chooses for radiation and pair production.

V. MISCELLANY

We have also calculated as best we could, the detailed shape of the transition curves for the $Cu^{63}(\gamma,n)Cu^{62}$ and $C^{12}(\gamma,n)C^{11}$ reactions using the usual saddle point method. As in the calculation of the track lengths, one can take some reasonable average value for the radiation cross section and can take into account the ionization loss by using the asymptotic expansions as given by Rossi and Greisen. One cannot take into account the variation of the pair production cross section, however, in even the approximate way in which it was done in calculating the track length. Since the pair production varies by almost a factor of two between maximum and minimum energies with which we deal, i.e., between 322 and 18 Mev, considerable uncertainty is introduced into

the results. Nonetheless, we thought it might be of some interest to present them.

Since one cannot take into account the variation of the absorption cross section $\sigma(W)$ with energy, he must choose some average value in carrying out the calculations. The question arises as to what is the most reasonable value. We have chosen to use $\sigma(W_e)$ for the following reasons. This value is roughly correct for the track length and, for the same reasons that apply there, for the maximum of the shower curve; also, for very large thicknesses, the cascade curve approaches a pure absorption curve with absorption coefficient $\sigma(W_e)$.

The saddle point method leads to the following expression

$$\gamma_{rel}(W_0, W, t) = \frac{1}{(2\pi)^{\frac{1}{2}}} \frac{H_2(s) \exp[\lambda_1(s)t] M(s, 0)}{f(W_0, W)[\nu_1(s, \epsilon/W) \cdot W]^s [\lambda_1''(s)t + 1/s^2]^{\frac{1}{2}}}, \quad (14)$$

where

$$t = (1/s - y)/\lambda_1'(s).$$

Here, the functions $\lambda_1(s)$, $H_2(s)$, and $\nu_1(s, \epsilon/W)$ are defined in terms of $A(s)$, $B(s)$, and $C(s)$ as by Rossi and Greisen; but in the actual calculation of the latter functions we have used $\psi(u)du = \sigma(W_e)du$ and the $\phi(v)$ given by (8). $M(s, 0)$ is calculated numerically from the curve in Fig. 7 of Strauch's paper. Using the above expression, we have calculated the transition curves for the reactions $Cu^{63}(\gamma, n)Cu^{62}$ and $C^{12}(\gamma, n)C^{11}$. The curves are shown in Fig. 2. Whether the agreement is better or worse than one should expect is a moot equation. The agreement for Cu with a resonance energy of 18 Mev is not as good as that for C for which the resonance energy is 27 Mev. This is not implausible qualitatively, since the various approximations involved in taking average cross sections and neglecting Compton effect are somewhat more serious at 18 than at 27 Mev. One might perhaps have expected better agreement at the maximum, for the reasons given in the introduction.

It may be, however, that the errors in the saddle point method are not negligible. It is altogether possible that the saddle point method gives too low a value by perhaps 10 percent near the maximum; if this is true, the shower theory proper is in better agreement with the experiment than evaluation by the saddle point method would seem to imply.

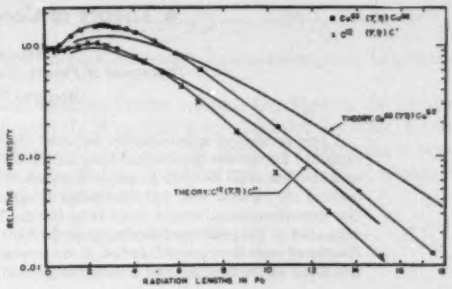

FIG. 2. Relative intensity in Pb of photons causing $Cu^{63}(\gamma, n)Cu^{62}$ and $C^{12}(\gamma, n)C^{11}$.

In all the work thus far, we have assumed that the (γ, n) cross sections are infinitely sharp, i.e., if we call $\Sigma(W)$ the cross section as a function of energy, that $\Sigma(W) = \delta(W - W_e)$, where W_e ist he "resonance" energy. What then is the effect of the finite width? Suppose for illustration that $\Sigma(W)$ is constant, and has a square shape centered about a value W_e, and with width Δ, i.e.,

$$\Sigma(W) = \text{constant}, \quad W_e - \tfrac{1}{2}\Delta < W < W_e + \tfrac{1}{2}\Delta,$$
$$\Sigma(W) = 0 \text{ otherwise.}$$

It is then easy to see, e.g., that if $\frac{1}{2}\Delta \ll W_e$, Eq. (9) is replaced approximately by the following relation:

$$Z_{rel}(W_0, W_e) = \frac{0.346 W_0 (1 + \Delta^2/6W_e^2)}{\sigma(W_e) W_e \cdot f(W_0, W_e) \nu(\epsilon/W_e)}. \quad (15)$$

The effect of the finite width is quite small. For example, if $W_e = 20$, $\Delta = 10$, this effect increases Z_{rel} by about four percent. One can see also that the effect of the finite width varies with depth in the shower. The spectrum of photons goes as $1/W^{s+1}$, where s is 0 at the beginning of the shower, is unity at the maximum, and increases slowly with thickness thereafter. Thus, the effect of the finite width in raising the shower curve increases slowly with thickness. Taking it into account would therefore slightly increase the discrepancy between experiment and theory shown in Fig. 2.

I should like to thank Professor Robert Serber for several interesting discussions and helpful suggestions.

A Theory of Cooperative Phenomena

RYOICHI KIKUCHI*
Department of Physics, University of Tokyo, Tokyo, Japan
(Received November 6, 1950)

A new method of approximation for order-disorder phenomena is developed. In Sec. A, the method is explained for the one-dimensional Ising lattice. Sections B and C cover the approximations already known, such as those of Bethe (Sec. B) and of Kramers-Wannier (Sec. C), which are shown to be derived as special cases of the method with suitable choices of variables. In Sec. D, an improved treatment is explained for the three-dimensional simple cubic Ising lattice. This approximation is found to agree with the rigorous expansion of the partition function up to the fourth moment by Kirkwood's moment method, so far as the disordered state is concerned. In Sec. E the general formula for the entropy is given. In Sec. H an improved treatment of the face-centered lattice (Ising model) is given.

I. INTRODUCTION

WE shall develop a new method of approximation to the entropy of an order-disorder system. It gives, by suitable choices of the variables, the approximations already known, such as that of Bethe,[1] and the "variation method" derived by Kramers and Wannier.[2] Our improved treatment for a simple cubic lattice has been tested by comparison with the rigorous expansion of the partition function by Kirkwood's method of moments,[3] and is found to agree with his expansion up to the fourth moment, so far as the disordered state is concerned.

Though most of the two-dimensional problems have been solved,[4] the new approach for the three-dimensional problems seems to be worthwhile, especially at the present stage of the theory when the theory is confronted with formidable mathematical difficulties and various new approximations[5–8] are still being reported.

II. SIMPLE LATTICES

A. Linear Ising Lattice

We call a linear lattice composed of M lattice points a *system*, and consider an *ensemble* which contains L systems as illustrated in Fig. 1. The totality of the kth lattice points (one from each of the L systems, marked with black circles) will be called the *set* of kth lattice point, and the *set* of the kth bond will mean the whole of the bonds marked with heavy lines in the figure.

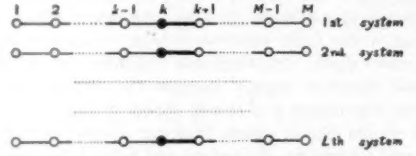

FIG. 1. An *ensemble* of linear lattices.

The probability of appearance of a bond having one of the configurations shown in the left column of Table I is denoted by y_i as shown in the second column.[9] Without loss of generality, configurations $(+\ -)$ and $(-\ +)$ can be assumed to have the same probability of appearance due to their symmetry. β_i indicates the number of different configurations having the same probability. y_i's are normalized by the equation

$$\sum_{i=1}^{3}\beta_i y_i = 1. \qquad \text{(A.1)}$$

We say that "the set of the kth bond has *right distribution of spin*" or, briefly, "the kth bond has *r.d.*", when, among the L bonds belonging to the set of heavy lines in Fig. 1, y_1L bonds have the configuration $(+\ +)$, y_2L have $(+\ -)$, y_2L have $(-\ +)$, and y_3L have $(-\ -)$. We show in Table II, which can be derived from

TABLE I. Probabilities of appearance of configurations of a bond.

Bond	Prob.	β_i*	ε_i**
⊕—⊕	y_1	1	$-\varepsilon$
⊕—⊖ ⊖—⊕	y_2	2	$+\varepsilon$
⊖—⊖	y_3	1	$-\varepsilon$

* β_i indicates the number of different configurations having the same probability.
** ε_i denotes the energy per bond.

[9] We shall call a bond a *basic figure* for Sec. A, as the configurations of a bond are chosen as variables upon which the whole theory of Sec. A is constructed.

* Present address: Gates and Crellin Laboratories, California Institute of Technology, Pasadena, California.
[1] H. A. Bethe, Proc. Roy. Soc. (London) **A150**, 552 (1935).
[2] H. A. Kramers and G. H. Wannier, Phys. Rev. **60**, 252, 263 (1941).
[3] H. A. Bethe and J. G. Kirkwood, J. Chem. Phys. **7**, 578 (1939).
[4] L. Onsager, Phys. Rev. **65**, 117 (1944); B. Kaufman, Phys. Rev. **76**, 1232 (1949); G. H. Wannier, Phys. Rev. **79**, 357 (1950).
[5] Yin-Yuan Li, J. Chem. Phys. **17**, 447 (1949); Phys. Rev. **76**, 972 (1949). C. N. Yang, J. Chem. Phys. **13**, 66 (1945); C. N. Yang and Y.-Y. Li, Chinese J. Phys. **7**, 59 (1947).
[6] D. ter Haar and B. Martin, Phys. Rev. **77**, 721 (1950).
[7] T. L. Hill, J. Chem. Phys. **18**, 988 (1950).
[8] J. M. Cowley, Phys. Rev. **77**, 669 (1950).

TABLE II. Probabilities of appearance of spins.

Spin	Probability
+	$x_1=y_1+y_2$
−	$x_2=y_2+y_3$

Table I, the probability x_i of a lattice point having the respective spin.

Similarly to the bonds, we say that "(the set of) the kth lattice points has right distribution of spins," when, among the L lattice points belonging to the set of black circles in Fig. 1, x_1L have (+) spins, and x_2L, (−) spins. When the set of a bond has r.d., each of the end points of the bond naturally has r.d.

Analogously to the treatment by means of the eigenvalue problems,[4] we fill up the lattice points one by one from an end. In Fig. 2, we assume that each bond on the left side of B has been put with r.d., and we are going to fill up the point A. What will be the number of ways of putting a spin on A so that the bond $B-A$ has r.d.?

As the set of the lattice point B is assumed to have r.d., x_1L lattice points among the set have (+) spins and x_2L, (−) spins. Among the first x_1L points, we can select y_1L at random, so that for these y_1L, we put (+) spins on A and for the remaining y_2L, (−) spins on A, making y_1L bonds having the configuration (+ +) and y_2L bonds having the configuration (+ −) among the set of the bond $B-A$. In this process, the number of ways of putting x_1L spins on A is

$$g_1=(x_1L)!/[(y_1L)!(y_2L)!]. \tag{A.2}$$

For the remaining x_2L of the set of the point B having (−) spins, we can pick up y_2L at random in order to make $y_2L(-+)$'s and $y_3L(--)$'s. The number of ways of making this selection is

$$g_2=(x_2L)!/[(y_2L)!(y_3L)!]. \tag{A.3}$$

Thus, the number G_L of ways of putting a spin on A so that $B-A$ has r.d. becomes finally

$$G_L=g_1g_2=\prod_{i=1}^{2}(x_iL)!\Big/\prod_{i=1}^{3}(y_iL)!^{\beta_i}. \tag{A.4}$$

We introduce the abbreviated expression "to put (a spin on) *A with reference to B*," meaning "to put a spin on A so that the bond $B-A$ has r.d., provided B has had r.d." The words in the parenthesis might sometimes be omitted. And at the same time, for simplicity's sake, we put

$$\begin{aligned}\prod_{i=1}^{2}(x_iL)!&\equiv X_L\equiv\{\text{Point}\}_L,\\ \prod_{i=1}^{3}(y_iL)!^{\beta_i}&\equiv Y_L\equiv\{\text{Bond}\}_L.\end{aligned} \tag{A.5}$$

The notations on the right-hand sides are conveniently used when we briefly compose G_L. That is, the number of ways G_L of putting a spin on a lattice point A with reference to the adjacent point B, completing a bond $B-A$, so that the bond has r.d., is calculated schematically as follows:

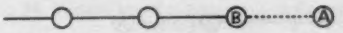

FIG. 2. An intermediate stage of constructing a linear Ising lattice.

$$G_L=\frac{\{\text{the part already filled}\}_L}{\{\text{the whole to be completed}\}_L}=\frac{\{\text{Point } B\}_L}{\{\text{Bond } BA\}_L}=\frac{X_L}{Y_L}. \tag{A.6}$$

As the number of ways of filling any lattice point is equally G_L, the number required to complete a system filling M lattice points is $(G_L)^M$ for an ensemble. The number of ways for one system G is given by the Lth root of $(G_L)^M$, and when we apply Stirling's formula and the condition (A.1), the entropy S for a system becomes

$$\begin{aligned}S&=k\ln G=k(M/L)\ln G_L\\&=k(M/L)[\textstyle\sum x_iL\ln(x_iL)-\sum\beta_iy_iL\ln(y_iL)]\\&=kM\Big[\sum_{i=1}^{2}x_i\ln x_i-\sum_{i=1}^{3}\beta_iy_i\ln y_i\Big].\end{aligned} \tag{A.7}$$

The total energy for a system is easily calculated, and combining it with (A.7), we can formulate the free energy, whose minimum gives the equilibrium state. Thus proceeding, we can verify that the well-known solution for linear Ising lattice[4] can be attained, of which the details are omitted here.

B. Bethe's Approximation (Two-Dimensional Square Lattice)

In this case also, we choose a bond as a basic figure, and the y_i's in Table I and the x_i's in Table II are sufficient to represent the variables. The entropy of the system is formulated when we calculate the number of ways of putting a spin on the point A in Fig. 3, so that the bonds $B-A$ and $C-A$ have r.d., respectively, assuming that every bond in the part of solid lines has had r.d. This number can be calculated in three steps:

(i) The number of ways of putting a spin on A with reference to B so that $B-A$ has r.d., independent of the bond $C-A$, is as follows (see (A.2)–(A.6)):

$$g=\{\text{Point } B\}_L/\{\text{Bond } BA\}_L=X_L/Y_L. \tag{B.1}$$

(ii) Thus, the bond $B-A$ has had r.d., but the distribution of the bond $C-A$ is not known. We will correct the latter. This correction cannot be done perfectly, but as a best approximation, following the idea of Takagi,[10] we can multiply (B.1) by the proba-

[10] Y. Takagi, Proc. Phys. Math. Soc. Japan 23, 44 (1941).

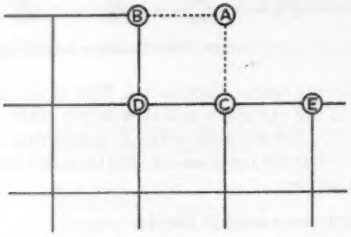

FIG. 3. An intermediate stage of constructing a two-dimensional square lattice.

bility that the bond $C-A$ has r.d. after the step (i). This probability Γ is

$$\Gamma=\frac{\{\text{Point } C\}_L}{\{\text{Bond } AC\}_L}\div\frac{L!}{\{\text{Point } A\}_L}=\frac{X_L{}^2}{Y_L L!}, \tag{B.2}$$

TABLE III. Probabilities of appearance of configurations of a square.

Square	Prob.	γ_i*
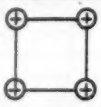	z_1	1
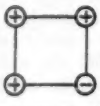 etc.	z_2	4
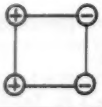 etc.	z_3	4
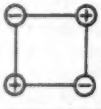 etc.	z_4	2
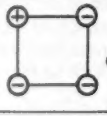 etc.	z_5	4
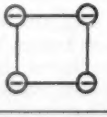	z_6	1

* γ_i is the number of different configurations having the same probability.

because, in the step (i), we have put a spin on A independently of C, which is identical with having calculated the number of ways of putting a spin on A as

$$L!/[(x_1L)!(x_2L)!]=L!/X_L, \tag{B.3}$$

so far as the bond $C-A$ is concerned; whereas the correct number of ways of putting a spin on A so that the bond $C-A$ has r.d. is, analogously to (B.1) or (A.6), expressed by

$$\{\text{Point } C\}_L/\{\text{Bond } CA\}_L.$$

(iii) Multiplying g and Γ, we get the approximate number of ways G_L of putting a spin on A so that both bonds $B-A$ and $C-A$ have r.d.:

$$G_L=g\Gamma=X_L{}^3/(Y_L{}^3L!), \tag{B.4}$$

which can easily be proved to coincide with the formula derived by Takagi,[10] which is identical with Bethe's first approximation.[1]

Moreover, for other types of lattices also, the y_i's and x_i's are sufficient to give Bethe's approximation. Generally, for the lattice with coordination number 2ω, the number of ways of constructing a system $(G_L)^{M/L}$ is easily shown to be approximated[11] by

$$(G_L)^{M/L}=[X_L{}^{2\omega-1}/(Y_L{}^{\omega}L!{}^{\omega-1})]^{M/L},$$

giving Bethe's approximation.

C. The Kramers-Wannier Approximation (Two-Dimensional Square Lattice)

(C1) *Free Energy*

To improve the approximation, we choose a square as a basic figure, and use as variables the probabilities of appearance z_i's of configurations of a "square" shown in the left column of Table III. From this table, we derive Table IV, which gives the probabilities of appearance w_i's of configurations of an "angle." Just as was mentioned above concerning Table I, the configurations interchangeable by symmetry operations, say,

$$\begin{pmatrix}+&+\\+&-\end{pmatrix},\quad \begin{pmatrix}+&-\\+&+\end{pmatrix},\quad \begin{pmatrix}-&+\\+&+\end{pmatrix}\quad\text{and}\quad \begin{pmatrix}+&+\\-&+\end{pmatrix}$$

are naturally assumed to appear with the same probability. The γ_i's and δ_i's denote the numbers of different configurations with the same probability. The concepts of *set*, *r.d.*, and *with reference to* are extended for the new variables, but no explanation seems to be necessary.

Extending Eq. (A.5), we define

$$\prod_{i=1}^{6}(z_iL)!{}^{\gamma_i}\equiv Z_L\equiv\{\text{Square}\}_L, \tag{C1.1}$$

$$\prod_{i=1}^{6}(w_iL)!{}^{\delta_i}\equiv W_L\equiv\{\text{Angle}\}_L. \tag{C1.2}$$

We also use the y_i's of Table I and the x_i's of Table II.

[11] Except for the case $2\omega=3$.

The entropy of a system is obtained when we calculate the number of ways of putting a spin on A in Fig. 3, so that both the square $ABDC$ and the angle ACE have r.d., provided that every square and every angle in the part drawn with solid lines have had r.d.

To calculate this number, we proceed in three steps, just as in Sec. B:

(i) The number of ways of putting a spin on A with reference to the angle BDC, so that the square $ABDC$ has r.d. independent of the angle ACE, is given, using the rule (A.6),

$$g=\{\text{Angle } BDC\}_L/\{\text{Square } ABDC\}_L=W_L/Z_L. \quad \text{(C1.3)}$$

(ii) The correction factor for the angle ACE to have r.d. is, (see Eq. (B.2)),

$$\Gamma=\frac{\{\text{Bond } CE\}_L}{\{\text{Angle } ACE\}_L}\div\frac{\{\text{Point } C\}_L}{\{\text{Bond } AC\}_L}=\frac{Y_L^2}{W_L X_L}. \quad \text{(C1.4)}$$

(iii) Multiplying g and Γ, we obtain the approximate number desired:

$$G_L=g\Gamma=Y_L^2/(X_L Z_L). \quad \text{(C1.5)}$$

It should be noted that W_L does not appear in the final result. This fact was to be anticipated at the outset; the details will be stated in Sec. E2.

From Eq. (C1.5), we obtain the entropy S of a system composed of M lattice points:

$$S=k(M/L)\ln G_L$$
$$=kM[2\sum\beta_i y_i\ln y_i-\sum x_i\ln x_i-\sum\gamma_i z_i\ln z_i]. \quad \text{(C1.6)}$$

Next, the energy of a system is composed rigorously as follows: when we denote the energy between the same spins by $-\epsilon$, and that between the different spins by $+\epsilon$, each bond has the energy represented by ϵ_i in Table I. As the total number of bonds in a system composed of M lattice points is $2M$, the energy E of a system is given by

$$E=2M\sum_{i=1}^{3}\epsilon_i\beta_i y_i=2M\epsilon(2y_2-y_1-y_3). \quad \text{(C1.7)}$$

Therefore, combining Eqs. (C1.7) and (C1.6), we obtain the free energy μ per lattice point:

$$\mu=(E-ST)/M$$
$$=2\epsilon(4y_2-1)$$
$$-kT[2\sum\beta_i y_i\ln y_i-\sum x_i\ln x_i-\sum\gamma_i z_i\ln z_i]. \quad \text{(C1.8)}$$

(C2) *Fundamental Equations*

Before minimizing μ, we determine the independent variables. Because of Eq. (A.1), the x_i's in Table II satisfy the normalization equation:

$$x_1+x_2=1. \quad \text{(C2.1)}$$

The y_i's in Table I and z_i's in Table III are geometrically connected by the relations:

$$\begin{cases} y_1=z_1+2z_2+z_3, \\ y_2=z_2+z_3+z_4+z_5, \\ y_3=z_3+2z_5+z_6. \end{cases} \quad \text{(C2.2)}$$

Taking Eqs. (C2.1) and (C2.2) into account, we use for the independent variables, y_2, z_3, z_4, ξ_1 and ξ_3, among which the last two are defined by

$$\xi_1\equiv x_1-x_2, \quad \text{(C2.3)}$$

$$\xi_2\equiv z_2-z_4. \quad \text{(C2.4)}$$

Dependent variables are expressed by linear combinations of independent ones; e.g.,

$$2z_1=1+\xi_1-4y_2+2z_4-2\xi_2. \quad \text{(C2.5)}$$

These relations are summarized in Table V, in which the quantities except 1 in the upper row, are the independent variables. ξ_1 and ξ_2 are conveniently

TABLE IV. Probabilities of appearance of configurations of an angle.

Angle	Prob.	δ_i^*
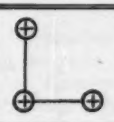	w_1	1
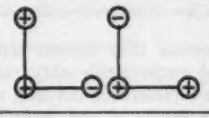	w_2	2
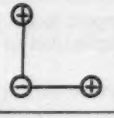	w_3	1
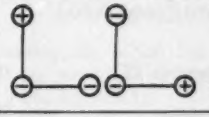	w_4	2
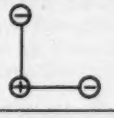	w_5	1
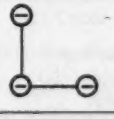	w_6	1

* δ_i is the number of different configurations having the same probability.

TABLE V. Relations between the dependent variables (on the left column) and the independent ones (on the upper row except 1). The meaning of this table is, for example, $2y_3=1-\xi_1-2y_3$.

	1	ξ_1	y_3	z_3	z_4	ξ_2
$2x_1$	1	1				
$2x_2$	1	−1				
$2y_1$	1	1	−2			
$2y_2$	1	−1	−2			
$2z_1$	1	1	−4		2	−2
$2z_2$			1	−1	−1	1
$2z_5$			1	−1	−1	−1
$2z_6$	1	−1	−4		2	2

chosen as independent because they become zero for the disordered state, and consequently they can be interpreted as parameters representing the long range order of the usual terminology.

Differentiating Eq. (C1.8) with respect to the independent variables, and putting the derivatives to zero, we get the fundamental equations:

$$\partial\mu/\partial\xi_1=0: \quad (x_1/x_2)(y_3/y_1)^2(z_1/z_6)=1, \tag{C2.6}$$
$$\partial\mu/\partial y_2=0: \quad H^4=[y_3^2/(y_1y_3)][(z_1z_6)/(z_3z_5)]$$

where

$$H\equiv\exp(\epsilon/kT), \tag{C2.7}$$

$$\partial\mu/\partial z_3=0: \qquad z_3^3=z_3z_5, \tag{C2.8}$$

$$\partial\mu/\partial z_4=0: \qquad (z_3z_5)^2=z_4^2z_1z_6, \tag{C2.9}$$

$$\partial\mu/\partial\xi_2=0: \qquad (z_2/z_5)^2=z_1/z_6. \tag{C2.10}$$

When μ is minimum, we can simplify Eq. (C1.8) as follows:

$$\begin{aligned}\mu=\mu&-\xi_1(\partial\mu/\partial\xi_1)-y_2(\partial\mu/\partial y_2)-z_3(\partial\mu/\partial z_3)\\&-z_4(\partial\mu/\partial z_4)-\xi_2(\partial\mu/\partial\xi_2)\\=-2\epsilon&+kT(\tfrac{1}{2}\ln x_1+\tfrac{1}{2}\ln x_2-\ln y_1-\ln y_3\\&+\tfrac{1}{2}\ln z_1+\tfrac{1}{2}\ln z_6),\end{aligned} \tag{C2.11}$$

or defining λ by the relation

$$\lambda\equiv\exp(-\mu/kT) \tag{C2.12}$$

and combining Eq. (C2.11) with Eq. (C2.6), we have

$$\lambda=H^2y_1^2/(x_1z_1). \tag{C2.13}$$

(C3) *Disordered State*

The disordered state is defined by

$$\xi_1=\xi_2=0, \tag{C3.1}$$

TABLE VI. Relations between the dependent variables (y_1, y_2, and z_1) and the independent ones (z_3 and z_4) for the disordered state. The meaning of this table is the same as Table V.

	1	z_3	z_4
y_1	$\frac{1}{2}$	−3	−1
y_2		3	1
z_1	$\frac{1}{2}$	−6	−1

which gives, from Table V,

$$\begin{cases} x_1=x_2=\tfrac{1}{2} & \text{(C3.2)}\\ y_1=y_2=\tfrac{1}{2}-y_3 & \text{(C3.3)}\\ z_1=z_6=\tfrac{1}{2}-2y_3+z_4 & \text{(C3.4)}\\ z_2=z_5=\tfrac{1}{2}(y_3-z_3-z_4). & \text{(C3.5)}\end{cases}$$

Equations (C2.6) and (C2.10) becoming identities, the fundamental equations reduce to the following, for the determination of the three independent variables, y_3, z_3, and z_4:

$$\begin{cases} H^2=(y_3z_3)/(y_1z_4), & \text{(C3.6)}\\ z_3=z_3, & \text{(C3.7)}\\ z_2^2=z_1z_4. & \text{(C3.8)}\end{cases}$$

On substitution of Eq. (C3.7) into Eq. (C3.5), we have

$$y_3=3z_3+z_4. \tag{C3.9}$$

We can now derive Table VI, which gives the relation between the independent variables z_3 and z_4 and the dependent ones y_1, y_2, and z_1, which appear in Eqs. (C3.6) and (C3.8).

Using Table VI, we can solve Eqs. (C3.6) and (C3.8) easily for z_3 and z_4, finding the results:

$$\begin{cases} z_3=(3H^2-1)(3-H^2)/[16H^2(6-H^2-H^{-2})]. & \text{(C3.10)}\\ z_4=(3-H^2)^2/[16H^2(6-H^2-H^{-2})]. & \text{(C3.11)}\end{cases}$$

Combining Eqs. (C3.10) and (C3.11) with Eqs. (C3.9), (C3.6), and (C2.13), we get, finally,

$$\lambda=8[6-H^2-H^{-2}]^{-1}=2[1-\sinh^2(\epsilon/kT)]^{-1}, \tag{C3.12}$$

which is identical with Eq. (90) of Kramers-Wannier's paper,[2] in which ϵ/kT is denoted by K, and λ has the same meaning as our λ.

(C4) *The Transition Temperature, T_t*

As the general properties of the second-order phase change, each of ξ_1 and ξ_2 indicating the long-range order has two non-zero values with equal absolute magnitude and different signs below the transition temperature. Therefore, at T_t, $d\xi_1/dT$ and $d\xi_2/dT$ become infinite, but a certain combination of them remains finite. At the same time, it should be noted that at T_t the variables satisfy the equations for the disordered state treated in Sec. C3. Hence, we can determine the value of the second-order transition temperature using the solution for the disordered state.

By differentiation of Eqs. (C2.6) and (C2.10) at T_t, we have:

$$\begin{cases} \dfrac{d\xi_1}{d\xi_2}=\dfrac{2}{z_6}\Big/\left\{2-\dfrac{2}{y_1}+\dfrac{1}{z_6}\right\}, & \text{(C4.1)}\\ \dfrac{d\xi_1}{d\xi_2}=\left\{\dfrac{2}{z_1}+\dfrac{2}{z_2}\right\}\Big/\dfrac{1}{z_1}. & \text{(C4.2)}\end{cases}$$

Equating the right-hand sides of Eqs. (C4.1) and (C4.2), we get

$$(1/z_1+z_3)-(2/y_1)+2=0. \tag{C4.3}$$

This is the equation to be added to determine T_t.

Using the formulas (C3.10) and (C3.11), we transform Eq. (C4.3) into an equation for H, the solution of which gives the value for the transition temperature:

$$H_t^2=[5+(17)^{\frac{1}{2}}]/4, \tag{C4.4}$$

which coincides with Eq. (92) of Kramers and Wannier.[3]

(C5) *The Ordered State*

For the ordered state, we must solve Eqs. (C2.6)–(C2.10) without any special conditions such as Eq. (C3.1). Generally speaking, these simultaneous algebraic equations for many variables can be reduced to a single algebraic equation for one variable. Therefore, in every case we can solve the problem if we resort to the numerical calculation of a higher order algebraic equation. This might be counted among the merits of our method. In the present case we can solve the problem analytically as we fortunately get a quadratic equation.

For the sake of convenience, we add Eq. (C2.13) to the fundamental equations and solve the six simultaneous equations for the six variables, ξ_1, y_2, z_3, z_4, ξ_3, and λ. Omitting the detailed accounts of the process of transformations, we list the results at once. The reduced single algebraic equation is

$$(\lambda H^6)^2-(H^8+8H^4-11)(\lambda H^6)+8H^{12}-12H^8+6H^4-1=0. \tag{C5.1}$$

The six independent variables are connected with λ by the following relations:

$$\begin{aligned}
&\xi_1=\xi_3\theta,\\
&z_3=y_2+z_4(1-\theta),\\
&\xi_3^2=z_4[2-8y_2-\theta(\theta-4)z_4],\\
&z_4=r(\theta r-\Lambda+1)^{-1},\\
&2y_2=1-(\theta r-\Lambda+1)^{-1},\\
&\theta^2(\theta-2)(\Lambda+1)r+[(H^4-2)\theta\Lambda+H^4-(\theta+1)]=0,\\
&\Lambda=-(a\theta+c)/\{\theta(a\theta+b)\}.
\end{aligned} \tag{C5.2}$$

$$1-\frac{H^2}{\lambda}=\frac{2H^4a\theta+(a+b)(2H^4-1)-d}{(2H^4-1)[(b+d)\theta+c(2H^4-1)]},$$

$$\begin{aligned}
&a=H^8-6H^4+1,\\
&b=3H^8+2H^4-1,\\
&c=(H^4-1)^2(2H^4-1),\\
&d=H^{16}-8H^{12}+10H^8-4H^4+1.
\end{aligned}$$

The solution of Eq. (C5.1) is

$$\lambda=[H^8+8H^4-11+(H^4-5)^{\frac{1}{2}}(H^4-1)^{\frac{1}{2}}]/(2H^6). \tag{C5.3}$$

The plus sign has been adopted before the root, so that at the transition temperature, when we insert Eq. (C4.4) into H_t^2, Eq. (C5.3) gives the same value for λ as that calculated from the disordered formula (C3.12):

$$\lambda_t=[9-(17)^{\frac{1}{2}}]/2. \tag{C5.4}$$

Thus, the problem has been solved completely.

Next we show that our results are identical with those of Kramers and Wannier. They found the following results:[11a]

$$\lambda=H^2+(1+H^2z)(1-z^2)/[H^4(H^2-H^{-2})], \tag{C5.5}$$

where z is a root of[11b]

$$[1+2zH^{-2}+z^2]^2=(H^2-H^{-2})^2z. \tag{C5.6}$$

We found that Eq. (C5.6) can be factorized as

$$[H^2z^2+(H^4+1)z+H^4]\times[H^4z^2-H^2(H^4-3)z+1]=0. \tag{C5.7}$$

Adopting the second factor we can simplify Eq. (C5.5), obtaining

$$z=(H^8+2-\lambda H^6)/[H^2(H^4-5)]. \tag{C5.8}$$

On inserting Eq. (C5.8) into the last factor of Eq. (C5.7), we obtain an equation for λ which proves nothing but Eq. (C5.1).

Therefore, our approximation described in Sec. C is identical throughout all temperatures with that explained by Kramers and Wannier under the name of the "variation method."

D. An Improved Treatment for the Simple Cubic Lattice (Ising Model)

(D1) *Free Energy and Fundamental Equations*

The shortest way to improve Bethe's approximation for the simple cubic lattice is to take a square as a basic figure, adopting the z_i's in Table III as variables. The w_i's in Table IV, the y_i's in Table I, and the x_i's in Table II are also used. The concepts of *set*, *r.d.*, and *with reference to* are extended to the three-dimensional lattice.

The entropy of a system is obtained when we calculate the number of ways of putting a spin on the point A in Fig. 4, so that all of the squares and angles containing A have r.d., provided every square and every angle in the part drawn with solid lines have had r.d. This number of ways is calculated in the following seven steps:

(i) The number of ways G_1 of putting a spin on A with reference to the angle FGB, so that the square $AFGB$ has r.d., is (see Eq. (C1.3)):

$$G_1=\{\text{Angle } FGB\}_L/\{\text{Square } AFGB\}_L=W_L/X_L.$$

(ii) The correction between A and $D-C$: so far as the face $ABDC$ is concerned, by the process (i), we

[11a] Reference 2, Eq. (91b).
[11b] Reference 2, Eq. (91a).

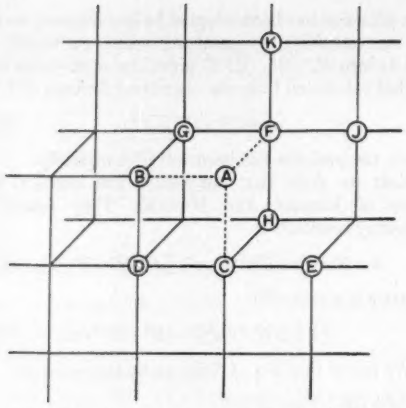

FIG. 4. An intermediate stage of constructing a simple cubic lattice.

have put A with reference to only B, while ideally we have to put A with reference to the angle BDC. Therefore, the correction factor Γ_1 becomes

$$\Gamma_1=\frac{\{\text{Angle } BDC\}_L}{\{\text{Square } ABDC\}_L}\div\frac{\{\text{Point } B\}_L}{\{\text{Bond } BA\}_L}=\frac{W_LY_L}{Z_LX_L}.$$

(iii) The correction between A and H: considering the fact that, so far as the face $ACHF$ is concerned, we must put A with reference to the angle CHF, the correction factor Γ_2 must be

$$\Gamma_2=\frac{\{\text{Angle } CHF\}_L}{\{\text{Square } ACHF\}_L}\div\left[\frac{\{\text{Point } F\}_L}{\{\text{Bond } AF\}_L}\times\frac{\{\text{Point } C\}_L}{\{\text{Bond } AC\}_L}\div\frac{L!}{\{\text{Point } A\}_L}\right]$$
$$=(W_LY_L{}^3L!)/(Z_LX_L{}^3),$$

where the factor in the square brackets is derived by the following considerations. So far as this face is concerned, we have put $A-F$ with reference to F in the process (i), and in the process (ii) we have corrected between A and C, i.e., have multiplied the factor,

$$[\{\text{Point } C\}_L/\{\text{Bond } AC\}_L]\div[L!/\{\text{Point } A\}_L].$$

(iv) The correction between A and E: just as in Sec. C1 (ii), the correction factor Γ_3 becomes

$$\Gamma_3=\frac{\{\text{Bond } CE\}_L}{\{\text{Angle } ACE\}_L}\div\frac{\{\text{Point } C\}_L}{\{\text{Bond } AC\}_L}=\frac{Y_L{}^2}{W_LX_L}.$$

(v) The correction between A and J: following (iv) gives

$$\Gamma_4=\frac{\{\text{Bond } FJ\}_L}{\{\text{Angle } AFJ\}_L}\div\frac{\{\text{Point } F\}_L}{\{\text{Bond } FA\}_L}=\frac{Y_L{}^2}{W_LX_L}.$$

(vi) The correction between A and K: following (iv) gives

$$\Gamma_5=\frac{\{\text{Bond } FK\}_L}{\{\text{Angle } AFK\}_L}\div\frac{\{\text{Point } F\}_L}{\{\text{Bond } FA\}_L}=\frac{Y_L{}^2}{W_LX_L}.$$

(vii) Therefore, the number of ways G_L of putting a spin on A is

$$G_L=G_1\prod_{i=1}^{5}\Gamma_i=Y_L{}^9L!/(Z_L{}^3X_L{}^7). \qquad \text{(D1.1)}$$

Hence, the entropy for a system with M lattice points is

$$S=k(M/L)\ \ln G_L$$
$$=kM[9\textstyle\sum\beta_iy_i\ \ln y_i-7\sum x_i\ \ln x_i-3\sum\gamma_iz_i\ \ln z_i]. \qquad \text{(D1.2)}$$

Next, considering that the total number of bonds for a system is $3M$, and following Eq. (C1.7), we have the energy for a system as

$$E=3M\sum_{i=1}^{3}\epsilon_i\beta_iy_i=3M\epsilon(4y_2-1), \qquad \text{(D1.3)}$$

where ϵ_i is given in Table I.

Differentiating the free energy μ per lattice point

$$\mu=(E-TS)/M, \qquad \text{(D1.4)}$$

with respect to the independent variables shown in Table V, and setting the derivatives equal to zero, we get the following fundamental equations:

$$\partial\mu/\partial\xi_1=0: \quad (x_1/x_2)^7(y_2/y_1)^9(z_1/z_6)^3=1 \qquad \text{(D1.5)}$$

$$\partial\mu/\partial y_2=0: \quad H^4=[y_2{}^2/(y_1y_3)]^3[z_1z_6/(z_2z_5)]^3, \qquad \text{(D1.6)}$$

where

$$H\equiv\exp(\epsilon/kT)$$

$$\partial\mu/\partial z_3=0: \quad z_3{}^2=z_2z_5 \qquad \text{(D1.7)}$$

$$\partial\mu/\partial z_4=0: \quad z_2{}^2z_6{}^2=z_4{}^2z_1z_6 \qquad \text{(D1.8)}$$

$$\partial\mu/\partial\xi_2=0: \quad (z_2/z_5)^2=z_1/z_6. \qquad \text{(D1.9)}$$

(D2) *The Disordered State*

Just as in Sec. C3 of the two-dimensional case, the relations (C3.1)–(C3.5) hold, Eqs. (D1.5) and (D1.9) becoming identities. The fundamental equations reduce to the following for the determination of the three independent variables y_2, z_3, and z_4:

$$\begin{cases} H^2=(y_2/y_1)^3(z_1/z_2)^2, & \text{(D2.1)} \\ z_3=z_2, & \text{(D2.2)} \\ z_2{}^2=z_1z_4. & \text{(D2.3)} \end{cases}$$

Inserting Eq. (D2.2) into Eq. (C3.5), we get Eq. (C3.9). Hence, Table VI holds, where z_3 and z_4 are the independent variables, and are determined by the following relations derived from Eqs. (D2.1) and (D2.3):

$$H^2[\tfrac{1}{2}-3z_3-z_4]^3z_4{}^2=(3z_3+z_4)^3z_3{}^3, \qquad \text{(D2.4)}$$

$$2z_3{}^3+12z_4z_3+z_4(2z_4-1)=0. \qquad \text{(D2.5)}$$

Putting

$$\varphi \equiv z_2/z_4, \tag{D2.6}$$

we have, from Eq. (D2.5),

$$z_4=[2(\varphi^2+6\varphi+1)]^{-1}. \tag{D2.7}$$

Inserting Eqs. (D2.6) and (D2.7) into Eq. (D2.4), we get

$$H^2=[(3\varphi+1)/(\varphi+3)]^3/\varphi. \tag{D2.8}$$

Thus, the disordered state has been solved with a parameter φ. The other variables are expressed through φ as follows:

$$\begin{cases} y_1=(\varphi^2+3\varphi)z_4, \\ y_2=(3\varphi+1)z_4, \\ z_1=\varphi^2 z_4, \\ z_3=\varphi z_4. \end{cases} \tag{D2.9}$$

Here we add a few remarks on the region of existence of the solution for the disordered state. Equation (D2.8) gives the H^2 *vs* φ curve shown schematically in Fig. 5. By the physical considerations, $\varphi \equiv z_2/z_4$ must be equal to unity when $H^2=1$, because we have the perfectly disordered state as T tends to infinity. Hence, the point P is realized. Moreover, taking into account the fact that the hatched portion cannot be realized, we can conclude that the part PQ drawn with the heavy curve corresponds to the real state, where the maximum point Q is easily shown to have the abscissa

$$\varphi_Q=\tfrac{1}{3}[7+(40)^{\frac{1}{2}}]\doteqdot 4.4415. \tag{D2.10}$$

The part QR corresponds to the unstable state, the specific heat becoming negative as explained in the following section.

The situation that the solution for the disordered state cannot be extended as far as $T=0$ occurs in the Kramers-Wannier case also. Equation (C3.12) is the solution for the disordered state, but does not hold for H large enough, as λ must be positive.

(D3) *Specific Heat for the Disordered State*

The specific heat c per spin is defined by the following:

$$c/k=(1/kM)dE/dT=12dy_2/d\tau, \tag{D3.1}$$

where we put

$$\tau \equiv kT/\epsilon. \tag{D3.2}$$

Using the relations derived in the previous section, we get the desired result:

$$\frac{c}{k}=-\frac{12}{\tau^2}\frac{\varphi(\varphi+3)(3\varphi+1)(3\varphi^2+2\varphi+3)}{(\varphi^2+6\varphi+1)^3(3\varphi^2-14\varphi+3)}. \tag{D3.3}$$

As mentioned in the previous section, c becomes negative for $\varphi > \varphi_Q$, because φ_Q is a root of[12]

$$3\varphi^2-14\varphi+3=0. \tag{D3.4}$$

[12] As we shall see in the following section, the state corresponding to φ_Q is not realized. Hence, the specific heat always remain finite.

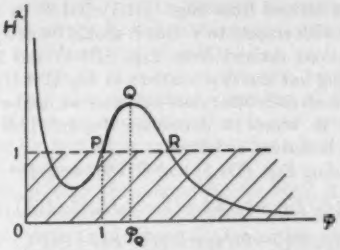

FIG. 5. H^2 *vs* φ of the equation (D2.8). In the curve, the part outside the portion PQ is not realized.

Combining Eqs. (D2.8) and (D3.3), we obtain the specific heat *vs* temperature curve, which is shown in Fig. 6 by the solid curve for $\tau > 4.610$.

(D4) *The Transition Temperature, T_t*

We can determine T_t following the method explained in Sec. C4. Differentiating Eqs. (D1.5) and (D1.9) and using the relation $\xi_1=\xi_2=0$, we get

$$\frac{d\xi_1}{d\xi_2}=\frac{6}{z_1}\Big/\left\{14-\frac{9}{y_1}+\frac{3}{z_1}\right\}=\left\{\frac{2}{z_1}+\frac{2}{z_2}\right\}\Big/\frac{1}{z_1}. \tag{D4.1}$$

Transforming the right-hand equation, and inserting Eqs. (D2.7) and (D2.9), we get

$$\varphi(\varphi-3)(\varphi-5)=0, \tag{D4.2}$$

of which the solution corresponding to a stable state is

$$\varphi_t=3, \tag{D4.3}$$

since all of the part other than $1<\varphi<\varphi_Q$ is not realized, as is explained by Fig. 5. Equation (D4.3) is the value corresponding to T_t. Inserting Eq. (D4.3) into Eq. (D2.8), we get

$$\begin{aligned} H_t^2&=125/81\doteqdot 1.5432, \\ 1/\tau_t&\doteqdot 0.21693, \\ \tau_t=kT_t/\epsilon&\doteqdot 4.6097. \end{aligned} \tag{D4.4}$$

The last value is to be compared with that of Bethe's second approximation[1]

$$kT_t/\epsilon \doteqdot 4.744.$$

Inserting Eq. (D4.3) into Eq. (D3.3), we obtain the value for the specific heat c_+ at T_t on the higher temperature side:

$$c_+/k \doteqdot 0.389. \tag{D4.5}$$

(D5) *The Specific Heat c_- at T_t on the Low Temperature Side*

To solve the ordered state is not easy, but the specific heat c_- at T_t on the low temperature side can be obtained without difficulty. Simply speaking, c_- is derived when we insert into Eq. (D3.1) the value of $dy_2/d\tau$ at T_t determined from the five simultaneous

equations derived from Eqs. (D1.5)–(D1.9) by differentiation with respect to τ. But it should be noted that the equations derived from Eqs. (D1.5) and (D1.9) are nothing but the two relations in Eq. (D4.1), being dependent on each other; and therefore we need another equation in order to determine $dy_2/d\tau$. This extra equation is derived as follows.

Expanding Eqs. (D1.5) and (D1.9), we get

$$\begin{cases} \xi_2/\xi_1=[\zeta_2/2(\zeta_1+\zeta_2)][1+(1-2\xi_2/\xi_1)(\xi_2/\zeta_2)^2], & \text{(D5.1)} \\ \xi_2/\xi_1=(\zeta_1/6)[7-(9/\eta)+3/\zeta_1]+B\xi_1^2+O(\xi^4), & \text{(D5.2)} \end{cases}$$

with

$$\begin{aligned} B=(7/6)\zeta_1[&5-(27/\eta)+(36/\eta^2)-12/\eta^3] \\ &+\tfrac{3}{2}(1-2\xi_2/\xi_1)[7-(21/\eta)+12/\eta^2] \\ &+(1/2\zeta_1)(1-2\xi_2/\xi_1)^2[7-9/\eta] \\ &+(1/6\zeta_1^2)(1-2\xi_2/\xi_1)^3, \end{aligned} \quad \text{(D5.3)}$$

where we put

$$\begin{cases} \eta\equiv 1-2y_2, \\ \zeta_1\equiv 1-4y_2+2z_4, \\ \zeta_2\equiv y_2-z_3-z_4. \end{cases} \quad \text{(D5.4)}$$

Equating the right-hand sides of Eqs. (D5.1) and (D5.2), we get

$$\Psi+A\xi_2^2+O(\xi^4)=0, \quad \text{(D5.5)}$$

where

$$\begin{aligned} \Psi&=(\zeta_1/6)[7-(9/\eta)+3/(\zeta_1+\zeta_2)] \\ A&=-[1/2\zeta_2(\zeta_1+\zeta_2)](1-2\xi_2/\xi_1)+B\cdot(\xi_1/\xi_2)^2. \end{aligned} \quad \text{(D5.6)}$$

Differentiating Eq. (D5.5) with respect to τ and assuming[13] that $d\xi_2^2/d\tau$ is finite and $dO(\xi^4)/d\tau$ can be set equal to zero at T_t, we get

$$\frac{dy_2}{d\tau}+3\frac{dz_3}{d\tau}-3\frac{dz_4}{d\tau}+\frac{1514}{1323}\cdot 28\xi_2\frac{d\xi_2}{d\tau}=0, \quad \text{(D5.7)}$$

where we have utilized the following relation derived from Eq. (D4.1) at T_t:

$$d\xi_1/d\xi_2=8. \quad \text{(D5.8)}$$

Equation (D5.7) is used as the additional equation to determine $dy_2/d\tau$ other than the three derived from Eqs. (D1.6)–(D1.8) by differentiation and insertion of the value at T_t:

$$\begin{cases} 42\dfrac{dy_2}{d\tau}-45\dfrac{dz_3}{d\tau}-75\dfrac{dz_4}{d\tau}+5\left(28\xi_2\dfrac{d\xi_2}{d\tau}\right)=\dfrac{135}{112}\left(\dfrac{2}{\tau_t}\right)^2, \\ 3\dfrac{dy_2}{d\tau}-9\dfrac{dz_3}{d\tau}-3\dfrac{dz_4}{d\tau}-28\xi_2\dfrac{d\xi_2}{d\tau}=0, \\ 5\dfrac{dy_2}{d\tau}-3\dfrac{dz_3}{d\tau}-13\dfrac{dz_4}{d\tau}+28\xi_2\dfrac{d\xi_2}{d\tau}=0. \end{cases} \quad \text{(D5.9)}$$

We can solve for $dy_2/d\tau$ from Eqs. (D5.7) and (D5.9) and, inserting it into Eq. (D3.1), we get

$$\frac{c_-}{k}=\frac{39285}{2548}\left(\frac{2}{\tau_t}\right)^2\doteqdot 2.902. \quad \text{(D5.10)}$$

(D6) *The Ordered State*

The equations for the ordered state (D1.5)–(D1.9) can be solved numerically. Putting

$$\theta\equiv\xi_1/\xi_2, \quad \text{(D6.1)}$$

we can derive, from Eqs. (D1.7), (D1.8), and (D1.9),

$$\begin{aligned} z_3&=y_2+z_4(1-\theta), \\ \xi_2^2&=z_4[2-8y_2-\theta(\theta-4)z_4], \\ 2y_2&=z_4[2\theta+\{2(\theta^2-z_4^{-1})\}^{\frac{1}{2}}]. \end{aligned} \quad \text{(D6.2)}$$

Assigning a value for θ, we can determine z_4 from Eq. (D1.5) by trial and error. The equations are solved by this process, Eq. (D1.6) being used to determine H.

We derive the specific heat from Eq. (D3.1), inserting the value $dy_2/d\tau$ obtained from Eqs. (D1.5)–(D1.9) by differentiation with respect to τ. The relation between the specific heat and the temperature for the ordered state is shown in Fig. 6 by the solid curve for $\tau<4.610$. In the same figure we illustrated the first and the second approximations by Bethe[1] for comparison.

(D7) *Discussion and Comparison with the Rigorous Expansion*

On the basis of the above analysis, we wish to infer the range of existence of the correct transition temperature. We put two hypotheses induced from the known results:

"So far as this scheme of the variational method is used,

(i) the approximate transition temperature is higher than the correct one, and

(ii) the value of the specific heat for the disordered state is smaller than the correct one corresponding to the same temperature."

Of these two, (i) was noticed by Kramers and Wannier without proof.[2] No verification exists for (ii) either; but if we accept these hypotheses, we can conclude the range for the true transition temperature τ_c:

$$\tau_Q=4.2221<\tau_c<4.6097, \quad \text{(D7.1)}$$

because, at $\varphi=\varphi_Q$ which corresponds to τ_Q, the specific heat for the disordered state becomes infinite. Equation (D7.1) does not contradict the prediction by Oguchi,[14]

$$0.21<1/\tau_c<0.24. \quad \text{(D7.2)}$$

Next, we compare our result of this section with the rigorous expansion of the partition function. We expand physical quantities of the disordered state in powers of the reciprocal temperature. Expanding for $K\equiv 1/\tau$ from

[13] This assumption is verified from Eqs. (D5.7) and (D5.9).

[14] T. Oguchi, Busseiron-Kenkyu (Japanese) **22**, 26 (1950).

Eq. (D2.8) and inserting the expansion into Eq. (D1.3), we get

$$-E/(M\epsilon)=3K+11K^3+(422/5)K^5+O(K^7). \quad \text{(D7.3)}$$

Kirkwood's moment method, which gives the correct expansion,[3] when retained up to the fourth moment, gives

$$-E/(M\epsilon)=-3+3K+11K^3, \quad \text{(D7.4)}$$

where the term (-3) comes in because of the different choice of the zero point of energy. Comparing Eq. (D7.3) with Eq. (D7.4), we know that our approximation in this section is valid up to the fourth moment of Kirkwood's method so far as the disordered state is concerned. For the ordered state, however, we could not transform our results into forms to be compared with Kirkwood's, owing to the complexity of the equations.

It is interesting to compare Eq. (D7.3) with the rigorous expansion derived by Oguchi[14,15]

$$-E/(M\epsilon)=3K+11K^3+(542/5)K^5+(123547/105)K^7+\cdots. \quad \text{(D7.5)}$$

Our Eq. (D7.3) deviates at the coefficient of K^5.

It may be of interest to mention here our further attempt at an approximation. When we take a cubic cell as a basic figure, we get the following expansion:

$$-E/(M\epsilon)=3K+11K^3+(542/5)K^5+(121027/105)K^7+O(K^9), \quad \text{(D7.6)}$$

which is correct up to the coefficient of K^5 and is to be compared with ter Haar and Martin's result,[6] which is the extension of Kramers-Wannier's "variation method" to the three-dimensional case:

$$-E/(M\epsilon)=3K+11K^3+(542/5)K^5+(107587/105)K^7+\cdots. \quad \text{(D7.7)}$$

Equation (D7.6) seems to be a better approximation than is Eq. (D7.7). Our cubic-cell approximation gives the transition temperature

$$\tau_c \fallingdotseq 4.5810. \quad \text{(D7.8)}$$

As the method explained in Sec. D is one of approximations, the value for the transition temperature Eq. (D4.4) and those for the specific heat Eqs. (D4.5), (D5.10) do not have rigorous meaning beyond the fourth moment of Kirkwood's method.

E. General Discussion Concerning the Method

(E1) *The Relation between our Free Energy and the Rigorous Partition Function*

The rigorous partition function for a system can be expressed as follows:

$$\exp(-F/kT)=\sum_i G(E_i)\exp(-E_i/kT), \quad \text{(E1.1)}$$

where F is the free energy, E_i is a total energy of the system, and $G(E_i)$ is the number of configurations having the energy E_i. Our mathematical problem is to find the functional form of $G(E_i)$.

In the methods explained in the previous sections, we got only the approximate function $G(E_i)$. The origin of the approximation lies in the method of counting the number of ways of putting a lattice point. We will examine each case.

In Sec. B, after the process (i), the bond $B-A$ has r.d.; but even after the correction (ii), $C-A$ does not have r.d. perfectly, because the correction cannot be made completely with the knowledge of the y_i's only.

In Sec. C1, after the process (i), the square $ABDC$ has r.d. (provided the angle BDC has had r.d.); but even after the correction (ii), the angle ACE does not have r.d. perfectly. So we can say that in Sec. C, every bond has r.d. rigorously, but any angle or any square has r.d. only approximately. In other words, in Sec. C the correlation between two neighboring lattice points (e.g., A and B in Fig. 3) is fully considered, but the correlation between points situated diagonally in a square (e.g., A and D in Fig. 3) is only partially considered, and the correlation between two points farther apart is completely neglected.

Generally,[16] the larger the basic figure becomes, the farther the correlation reaches and the better the approximation becomes.

(E2) *The Rigorous Formula for the Entropy*

In order to make the approximation clearer and at the same time to suggest the procedure for reaching the rigorous solution, we derive the general formula for

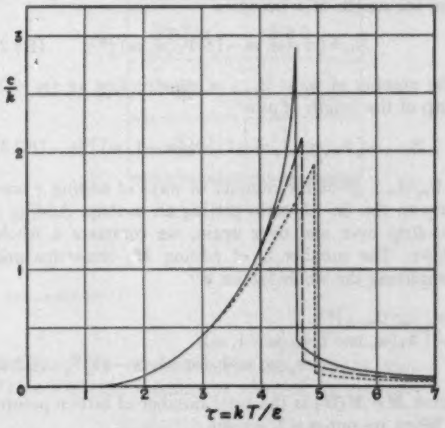

FIG. 6. The specific heat c per lattice point for the simple cubic Ising lattice plotted against $\tau=kT/\epsilon$. ---------- Bethe's first approximation. — — — — Bethe's second approximation. ———— This paper.

[14] T. Oguchi, private communication.

[16] The increase in the number of lattice sites does not necessarily result in a better approximation. Yin-Yuan Li reports the same situation in reference 5. The intrinsic meaning is not yet clear.

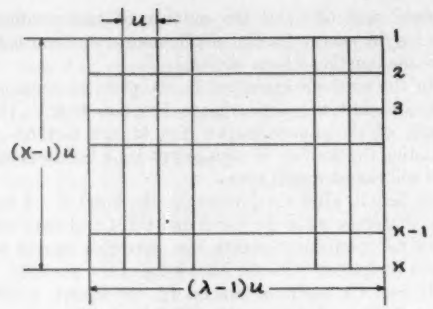

FIG. 7. A rectangle having the width $(\kappa-1)u$ and the length $(\lambda-1)u$.

the entropy. We explain it for the two-dimensional square lattice as an example.

Let us consider a rectangle having the width $(\kappa-1)u$ and the length $(\lambda-1)u$ as shown in Fig. 7, where u is the lattice constant. On each of the $\kappa\lambda$ lattice points, we put (+) or (−) spin, obtaining various configurations of the rectangle. We denote the probability of appearance of a configuration by $x_{\kappa\lambda,i}$ $(i=1, 2, \cdots, 2^{\kappa\lambda})$ and for brevity's sake we put

$$\prod_{\substack{i \\ \text{all configurations}}} (x_{\kappa\lambda,i}L)!\equiv\Phi_L(\kappa,\lambda). \tag{E2.1}$$

We take as a basic figure a square with $\kappa=\lambda=m$. Following the method in Sec. A, the number of ways Ω_m of constructing a strip with the width $(m-1)u$[16a] and the length M_1u becomes[17]

$$\Omega_m=[\Phi_L(m, m-1)/\Phi_L(m, m)]^{M_1}. \tag{E2.2}$$

The number of ways Ω_{m-1} of constructing an $(m-1)$-strip of the length M_1u is[17]

$$\Omega_{m-1}=[\Phi_L(m-1, m-1)/\Phi_L(m-1, m)]^{M_1}. \tag{E2.3}$$

Ω_m/Ω_{m-1} gives the number of ways of adding a one-strip to the $(m-1)$-strip getting an m-strip. Adding a one-strip over and over again, we complete a whole lattice. The number G of adding M_2 one-strips and completing the whole lattice is[17]

$$\begin{aligned} G&=[\Omega_m/\Omega_{m-1}]^{M_2} \\ &=[\Phi_L(m, m-1)\Phi_L(m-1, m)/ \\ &\qquad \Phi_L(m, m)\Phi_L(m-1, m-1)]^M, \end{aligned} \tag{E2.4}$$

where $M=M_1M_2$ is the total number of lattice points.

When we put $m=2$, we get

$$G=[Y_L^2/X_LZ_L]^M, \tag{E2.5}$$

which is identical with the Mth power of G_L defined in Eq. (C1.5).

The approximation in this method of counting the number of ways originates in the fact that we substituted Ω_m, which is calculated for a separate m-strip, for the number of ways of constructing an m-strip which lies in the whole lattice plane and closely connected with other strips.

Equation (E2.4) gives the approximate formula for the entropy $S_2(m)$ for a system[18]

$$\begin{aligned} S_2(m)&=(k/L)\ln G \\ &=-k(M/L)[\{\ln\Phi_L(m, m)-\ln\Phi_L(m, m-1)\} \\ &\quad -\{\ln\Phi_L(m-1, m)-\ln\Phi_L(m-1, m-1)\}], \end{aligned} \tag{E2.6}$$

which can be simplified as[18]

$$S_2(m)=-k(M/L)[\Delta_\kappa\Delta_\lambda\ln\Phi_L(\kappa,\lambda)]_{\kappa=\lambda=m}, \tag{E2.7}$$

where Δ_κ is the notation for the difference:

$$\Delta_\kappa f(\kappa)\equiv f(\kappa)-f(\kappa-1). \tag{E2.8}$$

The rigorous entropy S_2 for a system of the two-dimensional square lattice is the limiting case of $S_2(m)$:

$$S_2=\lim_{m\to\infty} S_2(m). \tag{E2.9}$$

For the case of the three-dimensional cubic lattice, we choose a cube of edge mu as a basic figure. For a rectangular parallelepiped having edges $(\kappa-1)u$, $(\lambda-1)u$, and $(\mu-1)u$, we denote the probability of appearance of a configuration by $x_{\kappa\lambda\mu,i}$ $(i=1, 2, \cdots, 2^{\kappa\lambda\mu})$, and we introduce Φ_L as follows:

$$\prod_{\substack{i \\ \text{all configurations}}} (x_{\kappa\lambda\mu,i}L)!\equiv\Phi_L(\kappa,\lambda,\mu). \tag{E2.10}$$

Then proceeding just as for the two-dimensional case, we find the approximate formula for the entropy of a system[18]

$$S_3(m)=-k(M/L)[\Delta_\kappa\Delta_\lambda\Delta_\mu\ln\Phi_L(\kappa,\lambda,\mu)]_{\kappa=\lambda=\mu=m}, \tag{E2.11}$$

and the rigorous formula of the entropy S_3 for a system is expressed by

$$S_3=\lim_{m\to\infty} S_3(m). \tag{E2.12}$$

When we put $m=2$, we get a case in which a cube is the basic figure to which we referred at the end of Sec. D7. In every case, no matter what the lattice form and the basic figure, we can obtain the formula of entropy following the method explained in this section, but the details are omitted here.

[16a] We shall call such a strip an m-strip following Kramers and Wannier (reference 2), as there lie m lattice points transversely.

[17] We neglect the end effect, assuming that M_1 and M_2 are very large numbers.

[18] L is canceled out of this formula when we apply the Stirling formula.

TABLE VII. Probabilities of appearance of configurations of (a) a tetrahedron, (b) a triangle, (c) a bond, and (d) a lattice point.

Tetrahedron	Prob.	α_i^*
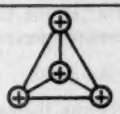	x_1	1
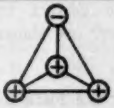 etc.	x_2	4
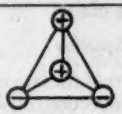 etc.	x_3	6
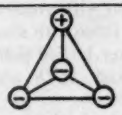 etc.	x_4	4
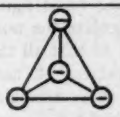	x_5	1

(a)

Triangle	Prob.	β_i^*
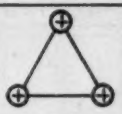	y_1	1
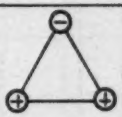 etc.	y_2	3
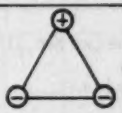 etc.	y_3	3
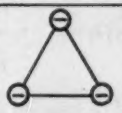	y_4	1

(b)

Bond	Prob.	γ_i^*	ε_i^{**}
⊕—⊕	z_1	1	$-\varepsilon$
⊕—⊖	z_2	2	ε
⊖—⊖	z_3	1	$-\varepsilon$

(c)

Spin	Prob.
⊕	w_1
⊖	w_2

(d)

* α_i, β_i and γ_i indicate the number of different configurations having the same probability.
** ε is the energy per bond.

III. FACE-CENTERED LATTICES (ISING MODEL)

F. Variables

The probabilities of appearance of a group of lattice points having some configurations are taken as variables, as shown in Table VII (a)–(d).

These variables are subject to the normalizations:

$$\sum_{i=1}^{5}\alpha_i x_i=\sum_{i=1}^{4}\beta_i y_i=\sum_{i=1}^{3}\gamma_i z_i=\sum_{i=1}^{2}w_i=1, \qquad \text{(F.1)}$$

and they are connected by the relations shown in Table VIII, the meaning of which is, for example,

$$2x_1=1+\xi_1-4z_2-2\xi_2+2x_3, \qquad \text{(F.2)}$$

where ξ_1 and ξ_2 are defined by

$$\begin{cases}\xi_1=w_1-w_2,\\ \xi_2=y_2-y_3,\end{cases} \qquad \text{(F.3)}$$

which represent the long-range orders.

TABLE VIII. The relations between the dependent variables (on the left column) and the independent ones (on the upper row except 1). The meaning of this table is, for example, $2z_1=1+\xi_1-2z_2$.

	1	ξ_1	z_2	ξ_2	x_3
$2w_1$	1	1			
$2w_2$	1	−1			
$2z_1$	1	1	−2		
$2z_2$	1	−1	−2		
$2y_1$	1	1	−3	−1	
$2y_2$			1	1	
$2y_3$			1	−1	
$2y_4$	1	−1	−3	1	
$2x_1$	1	1	−4	−2	2
$2x_2$			1	1	−2
$2x_4$			1	−1	−2
$2x_5$	1	−1	−4	2	2

We adopt the simplified expressions (see Sec. II):

$$X_L\equiv\prod_{i=1}^{5}(x_iL)!^{\alpha_i}=\{\text{Tetrahedron}\}_L,$$
$$Y_L=\prod_{i=1}^{4}(y_iL)!^{\beta_i}=\{\text{Triangle}\}_L,$$
$$Z_L=\prod_{i=1}^{3}(z_iL)!^{\gamma_i}=\{\text{Bond}\}_L, \tag{F.4}$$
$$W_L\equiv\prod_{i=1}^{2}(w_iL)!=\{\text{Point}\}_L.$$

As stated at the end of Sec. IIB, we can obtain Bethe's approximation when we adopt the z_i's and w_i's as variables,[19] for both the two-dimensional triangular lattice and the three-dimensional face-centered lattice. We consider better approximations in the following sections. As the method and the terminologies are the same in the following as in Sec. II, no explanation will be repeated except when necessary.

G. Two-Dimensional Triangular Lattice (Ising Model)

As the exact solution of this case has been already obtained,[4,20] we report only the results of our calculation for comparison.

We choose a triangle as the basic figure, and adopt the y_i's, z_i's, and w_i's as variables. The number of ways of putting A in Fig. 8, so that the triangles ABC and ACD have r.d., provided every triangle in the part drawn with solid lines has had r.d., is expressed by

$$G_L=\frac{\{\text{Bond }BC\}_L}{\{\text{Triangle }ABC\}_L}\times\left[\frac{\{\text{Bond }CD\}_L}{\{\text{Triangle }ACD\}_L}\div\frac{\{\text{Point }C\}_L}{\{\text{Bond }AC\}_L}\right]$$
$$=Z_L{}^3/(Y_L{}^3W_L). \tag{G.1}$$

Constructing the entropy from (G.1) and minimizing the free energy, we get for the transition temperature

$$\tau_t\equiv kT_t/\epsilon=\tfrac{1}{2}\ln(5/3)\doteqdot 3.9153, \tag{G.2}$$

and for the specific heat c_+ and c_- at the transition temperature on the higher and lower temperature sides

$$c_+/k\doteqdot 0.734 \quad\text{and}\quad c_-/k\doteqdot 3.486. \tag{G.3}$$

The c *vs* τ curve is shown in Fig. 9 by the solid line. Bethe's approximation and the correct transition temperature obtained by Wannier[21] are shown in the same figure for comparison.

H. An Improved Treatment for the Face-Centered Cubic Lattice (Ising Model)

(H1) *Fundamental Equation*

Figure 10 illustrates the structure of the face-centered cubic lattice viewed from the direction of a body-diagonal. The lattice points shown with greater circles are on a lattice plane higher than those with small ones. Capital letters indicate the higher lattice points and small letters, the lower. *Afge* and *ACDf* are tetrahedrons.

We adopt a tetrahedron as the basic figure. The entropy is obtained when we calculate the number of ways, G_L, of putting a spin on A so that all the tetrahedrons and the triangles containing A have r.d., provided every tetrahedron and every triangle in the part drawn with solid lines have had r.d.

G_L is shown to be

$$G_L=\frac{\{\text{Triangle }feg\}_L}{\{\text{Tetrahedron }Afeg\}_L}\times\left[\frac{\{\text{Triangle }CDf\}_L}{\{\text{Tetrahedron }ACDf\}_L}\div\frac{\{\text{Point }f\}_L}{\{\text{Bond }Af\}_L}\right]$$
$$\times\left[\frac{\{\text{Bond }BC\}_L}{\{\text{Triangle }ABC\}_L}\div\frac{\{\text{Point }C\}_L}{\{\text{Bond }AC\}_L}\right]$$
$$\times\left[\frac{\{\text{Bone }Be\}_L}{\{\text{Triangle }ABe\}_L}\div\left(\frac{\{\text{Point }e\}_L}{\{\text{Bond }Ae\}_L}\times\frac{\{\text{Point }B\}_L}{\{\text{Bond }AB\}_L}\div\frac{L!}{\{\text{Point }A\}_L}\right)\right]$$
$$=(Z_L{}^6L!)/(X_L{}^3W_L{}^5). \tag{H1.1}$$

Hence, the entropy S of a system with M lattice points is

$$S=k(M/L)\ln G_L$$
$$=kM[6\textstyle\sum\gamma_iz_i\ln z_i-2\sum\alpha_ix_i\ln x_i-5\sum w_i\ln w_i]. \tag{H1.2}$$

For the system, the total number of bonds being $6M$,

[19] The notation is different in this Section from that of Sec. II.
[20] G. F. Newell, Phys. Rev. **79**, 876 (1950); K. Husimi and I. Syozi, Prog. Theor. Phys. **5**, 177 (1950); I. Syozi, Prog. Theor. Phys. **5**, 341 (1950).
[21] G. H. Wannier, Revs. Modern Phys. **17**, 50 (1945).

the energy E becomes

$$E=6M\sum_{i=1}^{3}\gamma_i\epsilon_i z_i=6M\epsilon(4z_2-1). \tag{H1.3}$$

When we minimize the free energy μ per lattice point,

$$\mu=(E-TS)/M \tag{H1.4}$$

referring to Table VIII, we get the fundamental equations:

$$\partial\mu/\partial\xi_1=0: \quad (w_2/w_1)^6(z_1/z_3)^6(x_3/x_1)^2=1, \tag{H1.5}$$
$$\partial\mu/\partial z_2=0: \quad H^{12}=[z_2^2/(z_1z_3)]^6[(x_1x_3)/(x_2x_4)]^6,$$

where

$$H\equiv\exp(\epsilon/kT), \tag{H1.6}$$

$$\partial\mu/\partial\xi_2=0: \quad (x_1/x_3)(x_4/x_2)^2=1, \tag{H1.7}$$

$$\partial\mu/\partial x_3=0: \quad (x_3x_4)^4=x_1x_3^6x_2. \tag{H1.8}$$

(H2) *Disordered State*

In this case

$$\xi_1=\xi_2=0, \tag{H2.1}$$

resulting in

$$\begin{cases} w_1=w_2=\frac{1}{2}, \\ z_1=z_3=\frac{1}{2}-z_2, \\ x_1=x_3=\frac{1}{2}-2z_2+x_2, \\ x_2=x_4=\frac{1}{2}z_2-x_2. \end{cases} \tag{H2.2}$$

Equations (H1.5) and (H1.7) become identities and Eqs. (H1.6) and (H1.8) are simplified to

$$H^6=(z_2/z_1)^3(x_1/x_2)^3, \tag{H2.3}$$
$$x_2^4=x_1x_3^3. \tag{H2.4}$$

Introducing a parameter φ defined by

$$\varphi\equiv x_2/x_3, \tag{H2.5}$$

we can solve the equations, finding the results:

$$\begin{cases} x_2=z_2\varphi/[2(\varphi+1)], \\ z_1=z_2(\varphi^3-\varphi^2+\varphi+1)/2, \\ z_3=1/(\varphi^3-\varphi^2+\varphi+3), \end{cases} \tag{H2.6}$$

and

$$H^2=2\varphi^2/(\varphi^3-\varphi^2+\varphi+1). \tag{H2.7}$$

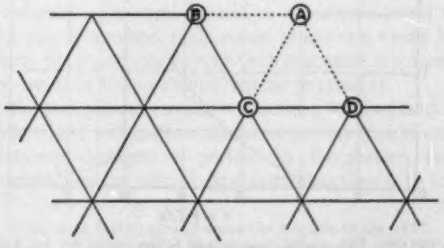

FIG. 8. An intermediate stage of constructing a two-dimensional triangular lattice.

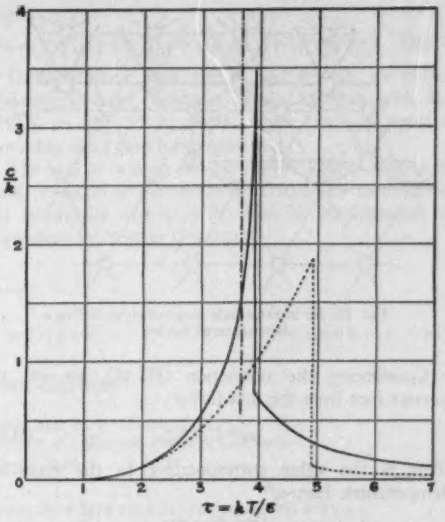

FIG. 9. The specific heat c per lattice point for the two-dimensional triangular lattice (Ising model) plotted against $\tau=kT/\epsilon$. ---------- Bethe's approximation. ———— This paper. — — — — — The correct transition temperature by Wannier.

The specific heat c per spin becomes

$$c/k=24dz_2/d\tau$$
$$=\frac{48\varphi(\varphi^3-\varphi^2+\varphi+1)(3\varphi^2-2\varphi+1)}{\tau^2(-\varphi^3+\varphi+2)(\varphi^3-\varphi^2+\varphi+3)^2}, \tag{H2.8}$$

where

$$\tau\equiv kT/\epsilon. \tag{H2.9}$$

The equation

$$\varphi^3-\varphi-2=0 \tag{H2.10}$$

has one real root

$$\varphi_1\doteq 1.5214. \tag{H2.11}$$

Therefore, c becomes negative for

$$\varphi>1.5214. \tag{H2.12}$$

(H3) *The Transition Temperature, T_t*

Differentiating Eqs. (H1.5) and (H1.7) and inserting Eqs. (H2.1) and (H2.2), we get

$$\frac{d\xi_1}{d\xi_2}=\frac{2}{x_1}\Big/\left\{5-\frac{3}{z_1}+\frac{1}{x_1}\right\}=\left\{\frac{2}{x_1}+\frac{2}{x_2}\right\}\Big/\frac{1}{x_1}. \tag{H3.1}$$

Using Eq. (H2.6), we get from the right-hand side equation,

$$[\Phi(\varphi)-2][\Phi(\varphi)-3]=0, \tag{H3.2}$$

where

$$\Phi(\varphi)\equiv\varphi^3-\varphi^2+\varphi. \tag{H3.3}$$

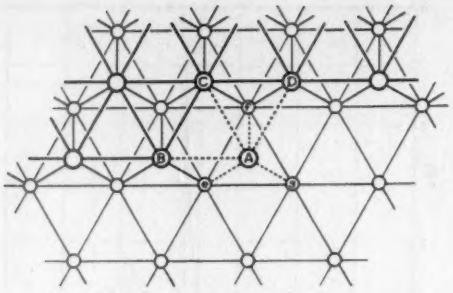

FIG. 10. An intermediate stage of constructing a face-centered lattice.

Considering the restriction (H2.12), we get the correct root from the first factor:

$$\varphi_t \doteqdot 1.3532. \tag{H3.7}$$

This is the value corresponding to the transition temperature. Hence,[22]

$$\begin{cases} H_t^2 \doteqdot 1.221, \\ \tau_t \doteqdot 10.025. \end{cases} \tag{H3.8}$$

The specific heat c_+ at T_t on the higher temperature side is obtained from Eq. (H2.8):

$$c_+/k \doteqdot 0.335\ 5. \tag{H3.9}$$

Equations (H3.8) are to be compared with the results of Bethe's approximation:

$$\begin{cases} H_t^2 = 1.2. \\ \tau_t \doteqdot 10.970. \end{cases} \tag{H3.10}$$

Following the discussion of Sec. IID7, we infer that the correct transition temperature τ_c would be in the range

$$\tau_1 \doteqdot 9.239 < \tau_c < 10.025,$$

where τ_1 corresponds to the value of φ_1 (H2.11), and at τ_1 the specific heat for the disordered state becomes infinite.

(H4) *The Specific Heat c_- at T_t on the Low Temperature Side*

Following the idea explained in Sec. IID5, and equating the formulas for ξ_2/ξ_1 obtained from Eqs. (H1.5) and (H1.7), we get

$$\Psi + A\xi_1^2 + O(\xi^4) = 0, \tag{H4.1}$$

where

$$\begin{aligned} \Psi &= \{5-(6/\zeta)+[2/(\eta_1+\eta_2)]\}\eta_1/4, \\ A &= (5\eta_1/4)[2-(12/\zeta)+(15/\zeta^2)-4/\zeta^3] \\ &\quad +(5/2)(1-2\theta)[2-(6/\zeta)+3/\zeta^2] \\ &\quad +(1/4\eta_1)(1-2\theta)^2(5-6/\zeta) \\ &\quad -[(1-2\theta)\theta^2/2\eta_2(\eta_1+\eta_2)], \end{aligned} \tag{H4.2}$$

and

$$\begin{cases} \zeta = 1-2z_2 \\ \eta_1 = 1-4z_2+2x_3 \\ \eta_2 = z_2-2x_3 \\ \theta = \xi_2/\xi_1. \end{cases} \tag{H4.3}$$

Differentiating Eqs. (H4.1), (H1.6), and (H1.8) with respect to τ, and inserting the value at T_t, we get

$$5(dz_2/d\tau)+[(675-187\alpha)/144\alpha]d\xi_1^2/d\tau = 0, \tag{H4.4}$$

$$10(5\alpha^2-6\alpha+5)\frac{dz_2}{d\tau} - 80\alpha^2\frac{dx_3}{d\tau} + \frac{25}{24}(\alpha^2-1)\frac{d\xi_1^2}{d\tau} = \frac{12}{\tau_t^2}(\alpha^2-1), \tag{H4.5}$$

$$-4(dz_2/d\tau)+(3\alpha+5)dx_3/d\tau = 0, \tag{H4.6}$$

with

$$\alpha \equiv \varphi_t + 1 \doteqdot 2.3532. \tag{H4.7}$$

Solving for $dz_2/d\tau$ from Eqs. (H4.4)–(H4.6), we get the specific heat c_- at T_t on the low temperature side:

$$\frac{c_-}{k} = \frac{(3\alpha+5)(675-187\alpha)}{(3\alpha-5)(675-187\alpha)-15\alpha(3\alpha+5)} \frac{144}{25\tau_t^2} \doteqdot 2.7888. \tag{H4.8}$$

(H5) *The Ordered State*

Equations (H1.5)–(H1.8) can be solved numerically. Putting

$$\begin{cases} \psi \equiv x_2/x_4, \\ q \equiv x_4/x_3, \end{cases} \tag{H5.1}$$

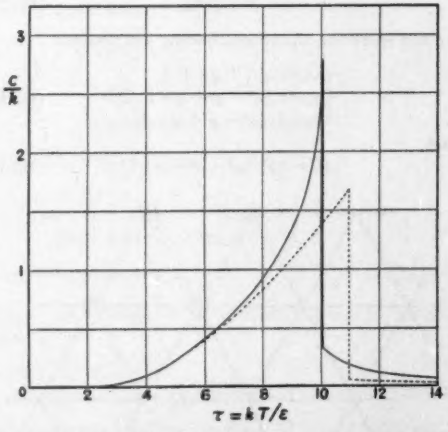

FIG. 11. The specific heat c per lattice point for the face-centered cubic lattice (Ising model) plotted against $\tau = kT/\epsilon$. - - - - - - - - Bethe's approximation. ———— This paper.

[22] The value 10.026 0 for τ_t reported earlier [Ryoichi Kikuchi, Phys. Rev. 79, 718 (1950)] has been revised by later calculations.

we get the equation

$$\left\{\frac{3+(3+\psi)q+\psi q^4}{3+(1+3\psi)q+\psi^3 q^4}\right\}^5\left\{\frac{1+2\psi q+\psi^3 q^4}{1+2q+\psi q^4}\right\}^8=\psi^4, \quad \text{(H5.2)}$$

which determines q for an assigned value of ψ.

Other variables are expressed with ψ and q:

$$H^4=[2+(\psi+1)q]^3 q^4\psi^2 (1+2\psi q+\psi^3 q^4)^{-1}(1+2q+\psi q^4)^{-1}, \quad \text{(H5.3)}$$

and

$$s_0=[2+(\psi+1)q]/[6+4(\psi+1)q+(\psi^2+\psi)q^4]. \quad \text{(H5.4)}$$

Differentiating Eqs. (H5.3) and (H5.4), we obtain the specific heat, which is shown together with Eq. (H2.8) in Fig. 11 by solid curves. Bethe's result is drawn in the figure for comparison.

The author wishes to express his hearty thanks to Prof. T. Sakai of University of Tokyo and members of his laboratory especially to Mr. N. Hashitsume for their deep interest in this work.

PHYSICAL REVIEW VOLUME 81, NUMBER 6 MARCH 15, 1951

Photo-Mesons from Carbon*

J. M. Peterson, W. S. Gilbert, and R. S. White
Radiation Laboratory, Department of Physics, University of California, Berkeley, California

(Received November 27, 1950)

Photons from the Berkeley 322-Mev electron synchrotron have been used to produce mesons from a carbon target. These mesons have been observed with nuclear emulsions at angles of 45°, 90°, and 135° to the photon beam. The ratio of the number of π^- to π^+ mesons produced is 1.29±0.22, 1.30±0.12, and 1.34±0.20, respectively, at each of the above angles. The energy spectra and the differential cross sections of π-mesons at each of these angles have been obtained. The total cross section for the production of π-mesons is $4.0\pm1.6\times10^{-28}$ cm² per nucleus per "equivalent quantum." The number of "equivalent quanta," Q, is defined as the total energy in the beam divided by the maximum photon energy. The cross section for production of μ-meson pairs at the target is estimated to be less than 2 percent of the cross section for π-meson production.

I. INTRODUCTION

THE production of mesons by photons was definitely established for the first time when they were observed in the x-ray beam of the 322-Mev electron synchrotron at the University of California Radiation Laboratory by McMillan and Peterson[1] in January, 1949. Carbon was the first pure target material to be bombarded by the x-ray beam for the production of mesons.[2] Carbon was chosen because of its relatively low atomic number and its ready availability and ease of fabrication. The background is due largely to electrons, positrons, and photons which are produced and scattered in the target material and which tend to fog the nuclear emulsions used as detectors in this experiment. Since the electron pair production cross section varies as the second power of the atomic number, while meson production varies by about the two-thirds power,[3] the background is reduced by use of as low an atomic number as possible.

For pure photon-nucleon interactions the ideal targets to bombard with photons are either protons or neutrons. Ordinary hydrogen is perfect for the former, and deuterium is the nearest experimental approach to the latter. Experiments using hydrogen have been performed by Cook[4] and by Steinberger and Bishop.[5] An experiment with deuterium is now in progress.

Although it was realized that with a carbon target one might not get a true picture of a pure photon-nucleon interaction because of possible distortion by the other nucleons in a carbon nucleus, it was felt that one might get a first approximation. Also, if distortion by the neighboring nucleons were important, it could be measured by comparison of the negative and positive meson spectra from carbon with those from hydrogen and deuterium. Furthermore, the energy spectra and the ratio of negative to positive mesons from carbon are each of interest in themselves.

An exploratory experiment[2] using a line target of carbon had given a rough energy spectrum of mesons emitted near 90° to the beam direction in the laboratory system. It had indicated that the angular distribution of mesons was approximately spherically symmetric, at least in the region near 90°, and also that more π^- mesons are produced than π^+ mesons by a ratio of 1.7±0.2. The present experiment was designed to display more fully the angular and energy spectra of mesons produced in carbon by x-rays generated by 322-Mev electrons.

* This work was performed under the auspices of the AEC.
[1] E. M. McMillan and J. M. Peterson, Science **109**, 438 (1949).
[2] McMillan, Peterson, and White, Science **110**, 579 (1950).
[3] R. F. Mozley, Phys. Rev. **80**, 493 (1950).
[4] L. J. Cook (private communication).
[5] J. Steinberger and A. S. Bishop, Phys. Rev. **78**, 494 (1950).

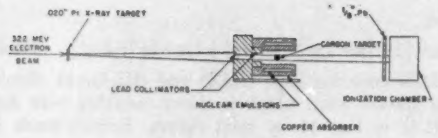

FIG. 1. Schematic drawing showing the essential experimental components.

II. EXPERIMENTAL METHOD

The x-rays were produced by letting the 322±5-Mev electron beam strike a 0.020-inch platinum target placed on the inner side of the accelerating tube. The resultant bremsstrahlung beam emerged from the machine in a narrow cone whose full width at half-intensity was 0.0135 radian (0.77°). At 55 inches from the platinum target the beam was collimated by a tapered hole in a lead block six inches thick, as is illustrated in Fig. 1. The collimating hole was 0.50 inch in diameter at the entrance end and was part of a cone whose apex was at the platinum target. This primary collimator defined by geometry a cone of x-rays whose full width was 0.0091 radian (0.52°). Directly behind the primary collimator was the secondary collimator, a three-inch thickness of lead in which there was a cylindrical hole just slightly larger than the geometrically defined beam. The purpose of the secondary collimator was to shield the detection equipment from the spray of electrons, positrons, and secondary photons produced in the walls of the primary collimator. Cross-section views of the collimator, target, and detector assembly are shown in Fig. 2.

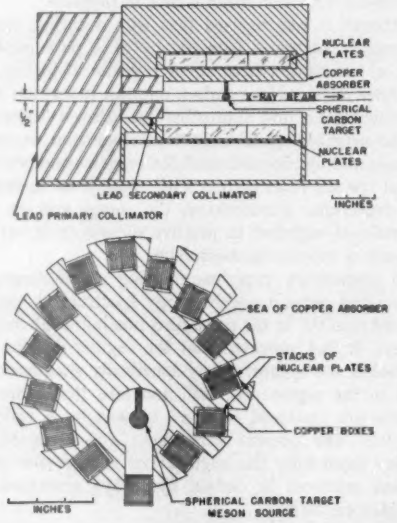

FIG. 2. (A) Drawing of a longitudinal view of the collimator-target-detector assembly. (B) Drawing of a cross-sectional view of the target-detector assembly.

The diameter of the carbon sphere was 0.620 inch, just equal to the diameter of the diverging x-ray beam at that point. That the beam size was accurately determined by the geometry was confirmed by photographic film measurements. The carbon target was surrounded by a large cylinder of copper, in which were imbedded stacks of nuclear emulsion plates. Mesons emitted from the carbon were slowed down and stopped throughout a large volume of the copper, and the imbedded emulsions served to sample the meson density at various points. Both the energies and angles of the emitted mesons were determined by the positions of the meson-endings relative to the target, to within uncertainties due to scattering and to the finite size of the target.

The intensity of the x-ray beam was practically constant as it traversed the carbon target. The part of the beam which traversed the diameter of the carbon was attenuated by only 3.5 percent. Some 15 feet beyond the carbon target the x-ray beam struck a large ionization chamber which served as the monitor in this experiment. The considerations which went into the design of the component parts of the experiment are discussed in greater detail in the following sections.

(A) Detectors

At the time of the bombardment, the emulsion method was the only reliable method for the detection of both π^- and π^+ mesons, although successful electronic techniques had been developed for the detection of π^+ mesons.[6,7] Furthermore, the emulsion method allows one to collect, at no extra cost, other interesting data, such as, for example, the energy and angular distributions of μ^+ mesons. The Ilford type C-2 emulsion was chosen because its sensitivity was felt to be optimum for the identification of meson tracks and yet great enough to allow easy recognition of relatively faint μ^+ tracks at the end of the π^+ tracks. Electrons passing through this emulsion leave developable grains at only a relatively few points along its path, so few that an electron track cannot normally be recognized. These grains form a single-grain background in the emulsions and were the determining factor in the amount of exposure which could be used in this experiment. The emulsions used were nominally 100 microns in thickness.

(B) Absorbers

Since the meson density drops off as the inverse square of the distance from a point target, a relatively dense material such as copper or lead was desirable as the absorbing material. The rms angle of multiple coulomb scattering, from its initial direction to the point where a meson is first detected in the emulsion, can be up to 47° for a lead absorber and up to 26° for

[6] Alvarez, Longacre, Ogren, and Thomas, Phys. Rev. 77, 752 (1950).
[7] J. Steinberger and A. S. Bishop, Phys. Rev. 78, 493 (1950).

copper. Since most of the scattering takes place in the last part of the meson's trajectory, which usually is in glass, the rms angle of scattering for a typical meson is 24° for a lead absorber and 18° for copper. Because of its greater stopping power per unit thickness, and also because of its smaller scattering, copper was selected for the absorber material.

Since the scattering in the copper absorber is fairly large, it was decided to use completely poor geometry in the meson detection system. The large copper cylinder surrounding the carbon target, as shown in Fig. 2, satisfies this condition.

Throughout the experiment the distribution in ϕ, the azimuthal angle about the x-ray beam axis, is treated as constant because the x-ray beam is unpolarized.

As is indicated in Fig. 2 there were 14 slots in the outer edge of the copper cylinder cut radial to the x-ray beam axis. In these slots were placed copper boxes containing stacks of nuclear plates. Each box had space for 3 stacks of plates placed end to end, each stack containing about 14 plates. The plates were so oriented that the planes of the emulsions were approximately radial. Only the central 6 plates were selected for scanning. This geometry and selection of plates allowed one to calculate the fraction of each meson's range which was in copper, and the fraction in glass and emulsion. In addition, the removal of a portion of the detectors at several times during a run allowed a variety of exposures under well-controlled conditions and was economical with respect to synchrotron operating time. The difference in copper absorber thickness between consecutive plate positions was $\frac{1}{4}$ inch. Since the stopping power of an inch of the glass used was just slightly greater than $\frac{1}{4}$ inch of copper in this energy range, the whole meson energy spectrum could be observed above a minimum energy determined by self-absorption in the carbon target.

(C) Target

The small spherical target was chosen as an approximation to a point source so as to afford sufficient angular resolution in the detection of the mesons. Also, this shape allows the source to have the same appearance and characteristics in all directions of observation.

The size of the carbon target was determined by the minimum detectable meson energy which was compatible with a reasonable exposure time. With the 0.620-inch diameter carbon target used, the minimum energy was 12.5 Mev.

The angular resolution of this experiment was determined not only by the scattering in the absorbing materials, but also by the angular width of the meson source as seen from the detector and by the width of the detector as seen from the source. In most cases the width of the scanned areas of emulsion was about equal to the width of the meson source, so that these two sources of angular width have approximately equal effects. The rms value of this angular width from both sources varied from about $\pm 5.6°$ to $\pm 1.9°$ over the energy range at $\theta = 90°$ and about $\pm 3.9°$ to $\pm 1.6°$ at 45° and at 135°. Because of multiple coulomb scattering the angle between the direction of the meson as it leaves the target and the line drawn from the end point of the meson to the target can be up to 5°. Combining these angular uncertainties one finds that the total root mean square angular uncertainties are about $\pm 7°$ at $\theta = 90°$ and about $\pm 6°$ at 45° and 135°. The scattering calculations were made using the method developed by Foldy.[8]

The energy resolution can be affected by several factors: thickness of the target, scattering in the absorber, widths of the target and of the scanned areas, and straggling due to energy loss fluctuations. At 90° the only important factor is target thickness, and the rms energy uncertainty is a maximum of ± 4.0 Mev at the lowest energy observed and when calculated for the middle points of the various plates varies from ± 2.8 Mev down to ± 1.2 Mev at the highest energy observed. At 45° and 135° the edge of the copper absorber is at an angle of 45° to the meson trajectory; and, as a result, uncertainties due to scattering in the absorber and to widths of the target and scanned areas also become important. The resultant total rms energy uncertainty at 45° and 135°, again calculated for the middle points of the plates, is a maximum of ± 7.0 Mev at a meson energy of 150 Mev and decreases to ± 3.0 Mev at 33 Mev, the nominal energy at the middle of the plates of the first box.

(D) Exposures

Three sets of plates were removed from the apparatus and replaced with blank plates during the exposure run. These removals occurred at exposures of 2.4, 4.8, and 9.6×10^{11} "equivalent quanta." The number of "equivalent quanta," Q, is defined as the total energy in the beam divided by the maximum photon energy. The middle exposure was about optimum. Most of the plates scanned were from this batch. The exposure was limited by the darkening of the leading edges of the plates in the box with no absorber, even though this box was about twice as far from the target as the box in the next higher energy interval.

(E) Examination of the Emulsions

The emulsions were scanned for meson endings with standard microscopes of from 250- to 900-power magnification. All together, about 84 square centimeters of emulsion were scanned.

Meson track endings in Ilford C-2 emulsions have in general two characteristics by which they can be recognized. One is a large amount of small angle scattering over the last one or two hundred microns of the track length. The other is a relatively fast change

[8] L. L. Foldy, Phys. Rev. 75, 311 (1949).

of grain density over the last 100 microns of the track length. In addition, some types of mesons have characteristic track endings which make identification easier. It is known from data on magnetically sorted π^- mesons that about 73±2 percent of the π^- mesons which stop in Ilford C-2 emulsions have one or more observable tracks leaving the meson ending.[9] These mesons are labelled σ-mesons (star mesons). Any meson track with no observable track leaving its ending is called a ρ-meson. As several thousand π^- meson endings in emulsions have been observed without conclusive evidence of a π-μ-ending,[10] one can draw the conclusion that a π^- meson is almost always captured before having time to decay. Therefore, any π-μ-decay observed in the emulsion must certainly have been initiated by a π^+ meson. From work with magnetically sorted π^+ mesons it has been observed that more than 99 percent of the π^+ mesons decay into μ^+ mesons.[11,†]

The characteristics of the track endings of μ^- mesons are not so well known. From observations with cosmic-ray mesons, Chang[12] has found no certain stars at the end of over 50 μ^- mesons. Other observers,[13] using artificially produced mesons, have found some 28 events in emulsions thought to be the endings of μ^- mesons. Of these, 26 are ρ-endings, and two are σ-types. These two σ-endings could have been due to π^- meson contamination.‡

The track ending of a μ^+ meson is always a ρ-type because it can only decay spontaneously.[14] Ilford C-2 emulsions are not sensitive enough to detect electron tracks.

The types of track endings of the four kinds of mesons can be summarized in Table I.

There is the possibility that π-μ-ending, with the μ^+ track of less than 100 microns in length, might be confused with a σ_1-ending whose one prong is a lightly ionizing track. However, in a study of 65 σ_1-endings in emulsions exposed to magnetically sorted π^- mesons, it was found that most of the σ_1-endings with fast prongs had also recognizable "clubs," i.e., blobs of grains at the meson endings presumably caused by recoil of the residual nuclei. It is known that π-μ-endings do not exhibit such "clubs." From these data one can deduce that only about one percent of all σ-endings are confusable with π-μ-endings, provided one examines these tracks for "clubs."

TABLE I. Types of meson track endings.

Kind of meson	Types of endings
π^-	σ_n, ρ (n=1, 2, 3, ··· =number of prongs)
μ^-	ρ
π^+	π-μ
μ^+	ρ

From the discussion above, one can interpret the various meson track endings in the following way.

(a) The number of π^- mesons is equal to 1/0.73 of the total number of σ-meson endings.

(b) The number of π^+ mesons is equal to the number of π-μ-endings.

(c) The ρ-endings are made up of 0.27 of the π^- meson endings, and also of μ^+ endings from the π-μ-decay processes. Since the range of the μ^+ meson is only about 600 microns, there should be, on the average, as many μ^+ endings as π^+ endings in any sample volume. However, not as many of the μ^+ endings will be recognized, partly because, being emitted isotropically from the end of π^+ mesons, many of them will be traveling at unfavorable angles for observation, whereas most of the π^+ mesons are parallel to the plane of the emulsion. Also, since the μ^+ track on the end of a π^+ track acts like a label, the μ^+ ending is harder to recognize, especially if short, as it has no such label. The number of μ-mesons, if any, either negative or positive, emitted from the carbon target is very small. A previous experiment put an upper limit on the cross section for the production of pairs of μ-mesons as 0.02±0.02 of the cross section for the production of π^+ mesons and π^- mesons.[15] This experiment allows a similar estimate to be made, as will be shown later. Only a negligible number of μ-mesons are expected from π-μ-decay processes in flight.

Mesons endings which occur very near either surface of the emulsion are in danger of misinterpretation by an observer because lightly ionizing tracks might leave the emulsion without being recognized. To avoid these misinterpretations only meson endings 3 microns or greater from either surface after development were used in the calculations. This 3-micron criterion was established by plotting the frequency of each type of meson *versus* the distance to the nearest surface, as is shown in Fig. 3. Since the 100-micron emulsion is only about 40 microns in thickness after development, the above criterion removes about 15 percent of the available emulsion volume.

The reliable observation of mesons in emulsions requires considerable experience. The absolute efficiency for the recognition of mesons by the five observers who worked on this experiment was determined by duplicate scanning of certain areas of the emulsion. All had efficiencies of greater than 90 percent for the recognition of σ- and π-μ-endings and greater than 80 percent for the recognition of ρ-endings. As another means for the comparison of the observers and the minimization of

[9] F. L. Adelman and S. B. Jones, Science **111**, 226 (1950).
[10] University of California Radiation Laboratory Film Group, private communication.
[11] F. M. Smith, private communication.
† *Note added in proof:* H. L. Friedman and J. Rainwater, Bull. Am. Phys. Soc. **26**, No. 1, 47 (1951).
[12] W. Y. Chang, Revs. Modern Phys. **21**, 166 (1949).
[13] S. B. Jones and R. S. White, Phys. Rev. **81** (to be published).
‡ *Note added in proof:* George and Evans, Proc. Phys. Soc. (London), 64 (1951), find that 8.7±1.7 percent of the μ^- mesons captured in emulsion form stars.
[14] Leighton, Anderson, and Seriff, Phys. Rev. **75**, 1136 (1949).
[15] McMillan, Peterson, and White, unpublished data.

their differences, each area of emulsion to be scanned was divided into three parallel sections, which were generally scanned by three different observers. The results of the three sections were then plotted separately and found to be consistent within the limits of random sampling. After demonstrating in this way that no significant errors would be caused by individual observer differences, the data were collected irrespective of observer.

III. ANALYSIS OF DATA

(A) Minus-Plus Ratio

The ratio of the number of π^- mesons to the number of π^+ mesons produced in a certain meson energy range is, simply,

$$[\pi^-]/[\pi^+]=1.37[\sigma]/[\pi\text{-}\mu],$$

where $[\sigma]$ and $[\pi\text{-}\mu]$ represent the numbers of σ- and π-μ-endings, respectively, found in a volume of emulsion corresponding to the energy in question.

There is another analytical method for the determination of the minus-plus ratio, which is a less reliable method but is of interest in indicating experimental consistency. The method is developed as follows. The number of π^- mesons is again taken as 1.37σ. Since only π-mesons are emitted from the target, the difference between the total number of mesons, T, including ρ-types, and the number of π^- mesons, is due to π^+ and μ^+ mesons. Taking $[\pi^+]=[\mu^+]$, it follows that

$$\left(\frac{[\pi^-]}{[\pi^+]}\right)_{\text{alternate}}=\frac{1.37[\sigma]}{\frac{1}{2}(T-1.37[\sigma])}=\frac{2}{0.73(T/[\sigma])-1}.$$

(B) Energy Spectrum

For a point source emitting $(d^2N_0(E,\theta)/dEd\Omega)$ π-mesons per unit beam exposure per Mev per steradian at polar angle, θ, and with kinetic energy, E, it can be easily shown that

$$\langle d^2N_0(E,\theta)/dEd\Omega\rangle_{Av}=\frac{n}{Q}\frac{1}{\left[\frac{1}{R^2}\frac{dE}{dR}\right]_{Av}},$$

where n is the number of mesons ending per unit volume of the emulsion, Q is the number of "equivalent quanta," R is the distance from detector to source, and dE/dR is the rate of energy loss in the emulsion evaluated at the energy E. Since these quantities may vary over a large detection volume element, the indicated average must be taken over the detector.

One possible effect that might distort the emission spectrum as measured in this way is π-μ-decay in flight; however, the time of flight[16–19] in the air between the carbon target and the absorbing medium plus the slow-down time in the absorber is so short that only about 3 percent of the π-mesons decay before coming to rest.§

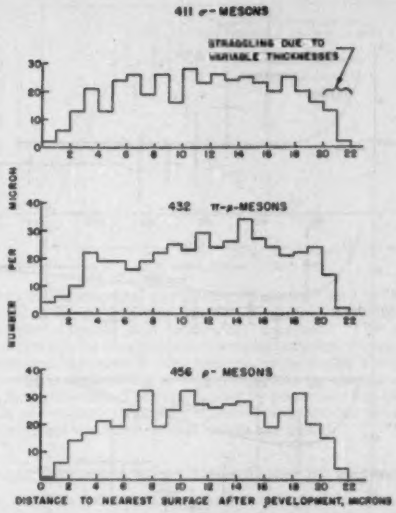

FIG. 3. Depth distributions of the three types of mesons found. Data from all angles are included.

Another distorting effect is the nuclear scattering and absorption of the mesons while traversing the absorber. Indications are that the nuclear absorption cross section for mesons of energies greater than 150 Mev may be as great as a nuclear area,[20] in which case the absorption could be as much as 30 percent. Information on low energy mesons of about 30 Mev indicates that the nuclear absorption cross section may be somewhat smaller than a nuclear area but that the nuclear scattering cross section may be of the order of a nuclear area.[21] The nuclear scatters of large angles would cause mesons of energy, E, to be detected at a position in the emulsions which corresponds to a smaller energy.||

The measured emission spectrum could be distorted also if the approximation of a point source were not valid. However, calculations show that the point source approximation was justified for the target used.

In order to find out whether any of the mesons observed might have come from sources other than the

[16] J. R. Richardson, Phys. Rev. 74, 1720 (1948).
[17] E. Martinelli and W. Panofsky, Phys. Rev. 77, 465 (1950).
[18] Kraushaar, Thomas, and Henri, Phys. Rev. 78, 486 (1950).
[19] Chamberlain, Mozley, Steinberger, and Wiegand, Phys. Rev. 79, 394 (1950).

§ *Note added in proof:* The value of reference 19 was used in our calculations. The value of the half-life of π^+ mesons, recently measured by Jakobson and Schulz (Phys. Rev., to be published) agrees with that of reference 19. Also in agreement is the value for π^- mesons which was measured by Lederman, Bernardini, Booth, and Tinlot, Bull. Am. Phys. Soc. 26, No. 1, 48 (1951).

[20] Camerini, Fowler, Lock, and Muirhead, Phil. Mag. 41, 413 (1950).

[21] H. Bradner and B. Rankin, Phys. Rev. 80, 916 (1950).

|| *Note added in proof:* Data from Bernardini, Booth, Lederman, and Tinlot, Phys. Rev. 80, 924 (1950), indicate that the total cross section for nuclear interaction of 30- to 50-Mev π^- mesons is very nearly equal to a nuclear area.

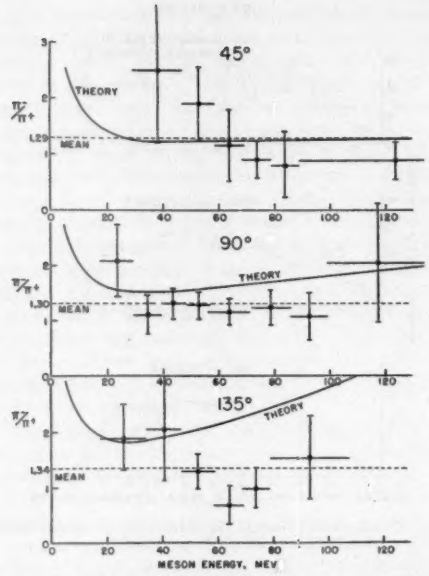

FIG. 4. Plots of the experimental minus-plus ratio against meson energy for three angles of emission. The theoretical curve is for the case in which the neutron-photon interaction is negligible; the coulomb effect of a distributed charge is included.

carbon target a blank run was made, i.e., a run identical with the main run except that the carbon target was omitted. No mesons at all were found in areas which in the main run would have yielded about 130 mesons.

(C) Cross Section

If one assumes the existence of some functional relationship between E, θ, and k, where k is the energy of the photon creating the meson of energy E at angle θ, he can relate the emission spectrum to the differential cross section by the formula

$$d\sigma(k,\theta)/d\Omega=[d^2N_0(E,\theta)/dEd\Omega](\partial E/\partial k)_\theta[1/Vn_i\bar{N}(k)],$$

where:

$\bar{N}$ = the integrated number of photons of energy k per Mev per unit beam exposure per square centimeter of beam area averaged over the volume, V, of the carbon target,

$d\sigma(k,\theta)/d\Omega$ = cross section for the production of mesons per steradian at angle θ by a photon of energy, k, in cm² per nucleus,

n_i = the numerical density of target atoms in cm^{-3}.

However, the correct model by which to calculate $(\partial E/\partial k)_\theta$ is not known, so that the above cross section was not computed. A cross section which can be computed without reference to any particular collision model is the mean cross section per steradian averaged over the x-ray energy spectrum. Integrating the meson spectrum we get:

$$d\langle\bar{\sigma}(\theta)\rangle/d\Omega=(dN_0(\theta)/d\Omega)(1/Qn_iV),$$

where $dN_0(\theta)/d\Omega$ is the total number of mesons per steradian emitted at angle θ. The integrated number of photons, Q, per unit beam exposure per square cm of area, as used here, is not clear cut. As a first approximation, for a bremsstrahlung beam one can write $\bar{N}(k)=A/k$, so that

$$Q=A\ln(k_2/k_1),$$

where k_1 and k_2 are the minimum and maximum effective photon energies, respectively.

Another method which avoids the approximation in the $1/k$ spectrum and a knowledge of the threshold is to define the number of "equivalent quanta" as the total energy in the beam divided by the maximum photon energy. Then

$$Q=(1/k_{\max})\int_0^{k_{\max}}k\bar{N}(k)dk.$$

If the actual bremsstrahlung spectrum has the shape $\bar{N}(k)=A/k$, this definition defines the total number of "equivalent quanta" as the constant, A.

From the ionization chamber, which was calibrated by Blocker, Kenney, and Panofsky[22] by a method previously reported by them,[23] the total energy of the beam was obtained. From this energy measurement and the maximum photon energy of 322 Mev, the number of "equivalent quanta" was found.

The total cross section, $\bar{\sigma}_i$, can now be obtained by integration of the differential spectrum over all angular space:

$$\bar{\sigma}_i=2\pi\int_0^\pi(d\bar{\sigma}(\theta)/d\Omega)\sin\theta d\theta.$$

$d\bar{\sigma}(\theta)/d\Omega$ was measured at 3 angles, 45°, 90°, and 135°, so that extrapolation was necessary below 45° and above 135°. Fortunately, however, the $\sin\theta$ factor minimizes the effect of errors in these regions.

TABLE II. Over-all minus-plus ratio *versus* angle of emission.

Angle	Experimental ratio	Weighted theoretical ratio	Mean energy (Mev)	Experimental ratio (alternate method)
45°	1.29±0.22	1.25	70	1.60
90°	1.30±0.12	1.62	56	1.60
135°	1.34±0.20	2.12	54	1.32

[22] Blocker, Kenney, and Panofsky, private communication.
[23] Blocker, Kenney, and Panofsky, Phys. Rev. **79**, 419 (1950).

IV. RESULTS

(A) Minus-Plus Ratio

The ratios of the number of π^- mesons to the number of π^+ mesons in each energy interval for the three values of the angle θ are shown in Fig. 4. (All of the statistical uncertainties given in this paper are standard deviations.) The theoretical ratio for photon-nucleon collisions, as determined by Brueckner and Goldberger,[24,25] for the case in which the nucleon interacts only in the proton state is plotted in the same figure. The coulomb effect of distributed charge has also been included.

Since, at each of the three angles observed, the experimental data are statistically consistent with a constant value of the minus-plus ratio as a function of energy, the data were combined to determine the over-all minus-plus ratio at each angle. These values are given in Table II, along with the mean theoretical values found by weighting the theoretical value at each energy interval with the number of mesons found in

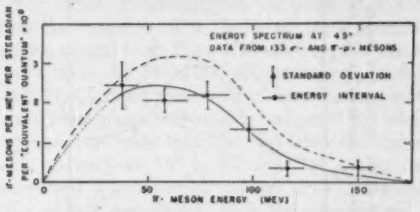
ENERGY SPECTRUM AT 45°
DATA FROM 133 π⁻ AND π⁺-μ⁻ MESONS
STANDARD DEVIATION
ENERGY INTERVAL
π-MESONS PER MEV PER STERADIAN PER "EQUIVALENT QUANTUM" ×10⁸
π- MESON ENERGY (MEV)

FIG. 5. Experimental energy spectrum of π^- and π^+ mesons emitted at 45° to the beam direction in units of 10^{-8} meson per Mev per steradian per "equivalent quantum." The smooth curve through the data has been drawn for purposes of integration. The dotted line below 30 Mev has been extrapolated. The dashed curve shows the emission spectrum corrected for nuclear absorption in the absorber. The cross section for absorption was assumed to be one nuclear area.

that interval. The mean energy determined similarly is also listed. The alternate, less reliable, method of computing the minus-plus ratio, discussed in Sec. III(A), which uses the total number of mesons, was applied also to the data for the purpose of comparing the methods. It should be added that if one plots and integrates the negative and positive energy spectra separately and thus obtains the minus-plus ratios, the results agree well with those obtained by consideration of the ratio to be independent of energy.¶

The experimental ratio appears to be independent of angle, as well as energy, whereas the theoretical ratio

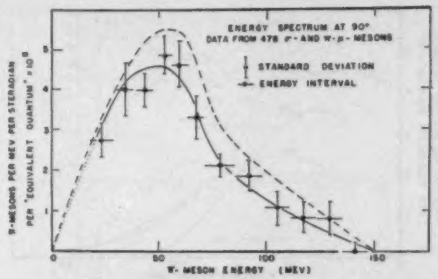
ENERGY SPECTRUM AT 90°
DATA FROM 478 π⁻ AND π⁻-μ⁻ MESONS
STANDARD DEVIATION
ENERGY INTERVAL
π-MESONS PER MEV PER STERADIAN PER "EQUIVALENT QUANTUM" ×10⁸
π- MESON ENERGY (MEV)

FIG. 6. Experimental energy spectrum of π^- and π^+ mesons emitted at 90° to the beam direction in units of 10^{-8} meson per Mev per steradian per "equivalent quantum." The smooth curve through the data has been drawn for purposes of integration. The dotted line below 30 Mev has been extrapolated. The dashed curve shows the emission spectrum corrected for nuclear absorption in the absorber. The cross section for absorption was assumed to be one nuclear area. Thei ndicated error for the point with zero ordinate was taken as that due to one meson.

is not. This result might be explained by scattering of the mesons before they escape the carbon nuclei in which they are formed. This effect would make all characteristics of the emission spectrum isotropic. However, this explanation does not hold, as the experimental energy spectra do depend on angle of emission. Another possible explanation, as indicated in Brueckner's analysis,[25] is that the assumption of negligible photon interaction with the nucleon in the neutron state is not valid, but that the neutron does interact with electromagnetic field of the photon through its magnetic moment and does play an appreciable part in the process.

A previous experiment[2] gave an over-all ratio of 1.7 ± 0.2 at an angle of 90°. That experiment differed from the present one chiefly in two respects; (1) a line target was used, and (2) the angular resolution was only about $\pm45°$. The discrepancy between the old and new results is slightly greater than that allowed by the statistical errors; however, the new result is believed

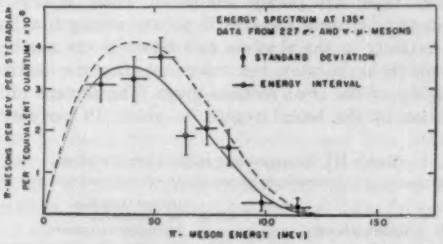
ENERGY SPECTRUM AT 135°
DATA FROM 227 π⁻ AND π⁻-μ⁻ MESONS
STANDARD DEVIATION
ENERGY INTERVAL
π-MESONS PER MEV PER STERADIAN PER "EQUIVALENT QUANTUM" ×10⁸
π- MESON ENERGY (MEV)

FIG. 7. Experimental energy spectrum of π^- and π^+ mesons emitted at 135° to the beam direction in units of 10^{-8} meson per Mev per steradian per "equivalent quantum." The smooth curve through the data has been drawn for purposes of integration. The dotted line below 30 Mev has been extrapolated. The dashed curve shows the emission spectrum corrected for nuclear absorption in the absorber. The cross section for absorption was assumed to be one nuclear area.

[24] K. A. Brueckner and M. L. Goldberger, Phys. Rev. **76**, 1725 (1949).

[25] K. A. Brueckner, Phys. Rev. **79**, 641 (1950).

¶ *Note added in proof:* Camac, Corson, Littauer, Shapiro, Silverman, Wilson, and Woodward (Bull. Am. Phys. Soc. **26**, No. 1, 48 (1951)) give a preliminary measurement for the ratio of π^- to π^+ mesons produced from carbon in the energy interval 60 to 75 Mev. This value is 1.1 ± 0.2. From the plots of Fig. 4 it can be seen that the agreement is excellent, especially for the same energy interval.

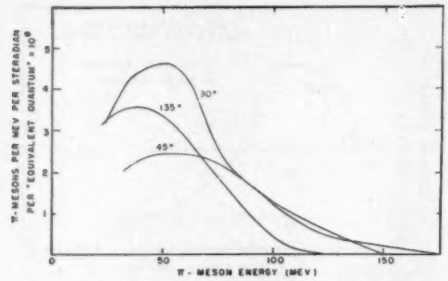

FIG. 8. An intercomparison of the three energy spectra. These are the curves which were not corrected for nuclear absorption.

to be the more reliable, because of the greater experience of the observers.

(B) Energy Spectra and Cross Sections

The spectra of π-mesons emitted from the carbon target were computed from the data using the total number of π-mesons, both positive and negative, at each energy interval. That is, it was assumed that the minus-plus ratio was independent of energy, as indicated in the last section. If one actually plots the negative and positive spectra separately, no statistically significant distinction appears in their relative shapes.

The emission spectra for 45°, 90°, and 135° are shown in Figs. 5, 6, and 7, respectively. Smooth curves were drawn through the experimental points and extrapolated to zero energy for the purpose of obtaining the total number of mesons emitted at each direction. The dashed curves show the emission spectra corrected for nuclear absorption in the absorbers. A cross section of one nuclear area, as calculated from 90-Mev neutron cross-section experiments,[26] was assumed. In Fig. 8 the three smooth curves are drawn together for the purpose of intercomparison of the three spectra.

Integrals of the spectra lead to values of the average cross section per steradian listed in Table III. The errors listed are purely statistical. There is also a systematic error of about ±35 percent arising from an uncertainty in the absolute calibration of the number of quanta in the beam, but it does not affect the relative validity of the cross sections given. The present calibration of the beam is good to about 10 percent;[22] however, at the time the carbon exposures were made, the monitoring technique was not as reliable as it is at present.

TABLE III. Average cross sections per steradian.

Emission angle	$d\bar{\sigma}/d\Omega$ cm² per steradian per nucleus per "equivalent quantum"
45°	$2.52\pm0.22\times10^{-29}$
90°	$3.87\pm0.18\times10^{-29}$
135°	$2.82\pm0.19\times10^{-29}$

[26] Cook, McMillan, Peterson, and Sewell, Phys. Rev. 75, 7 (1949).

The lack of a strong forward peak, which would be predicted by classical electromagnetic theory if the interaction were that of an electric dipole effect, has already been pointed out[5] in a study of π^+ mesons produced by photons on hydrogen. The binding apparently plays a role in the shape of the energy spectrum of carbon, as results at 90° indicate that the hydrogen spectrum is considerably flatter than that for carbon.

The effect of the binding of the nucleons is evidenced most strongly in the magnitude of the cross section. Comparison of these results at 90° with those of Cook's[4] results from the liquid hydrogen shows that the cross section per proton in the carbon nucleus for the production of π^+ mesons from carbon is only about $\frac{1}{3}$ that from hydrogen. This result checks a previous result of Steinberger and Bishop.[5]

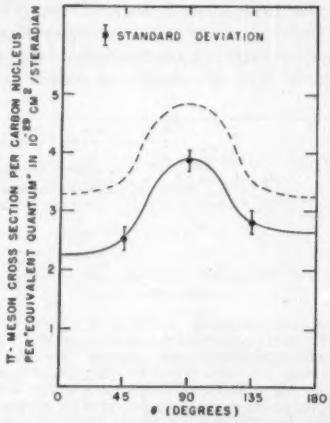

FIG. 9. Average π-meson cross section per carbon nucleus per "equivalent quantum" in units of 10^{-29} cm² per steradian. The smooth curve was drawn for the purpose of integration. The dashed curve shows the cross section corrected for nuclear absorption in the absorber. The cross section for absorption was assumed to be one nuclear area.

The cross-section figures per steradian listed in Table II are also plotted in Fig. 9. The smooth curve in the figure was drawn in to obtain the total average cross section integrated over all angles. The resultant figure is 4.0×10^{-28} cm² per nucleus per "equivalent quantum." If the effect of nuclear absorption of the absorbers were included, again assuming an absorption cross section of one nuclear area, the total cross section for production of mesons would be increased by 30 percent. The total uncertainty in the cross section is due largely to the uncertainty in the absolute calibration of the beam in terms of the monitor used and is estimated to be about ±40 percent.

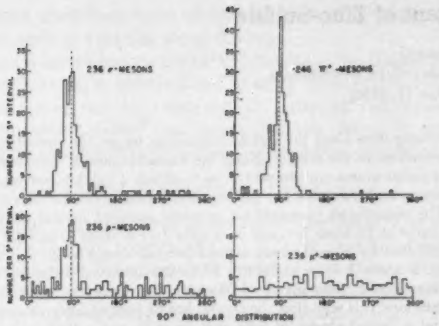

FIG. 10. Angular distributions of the mesons found at 90°. The abscissa is the angle from the beam direction.

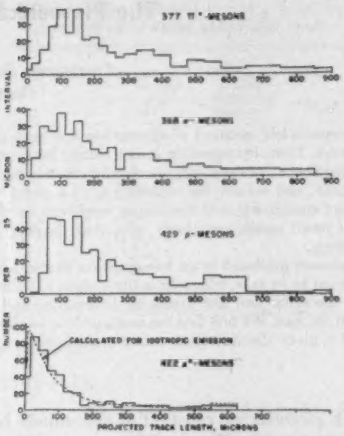

FIG. 11. Distributions in projected track length in emulsion for four types of mesons. Data from all angles included. The track length measurements are estimated to be accurate to within 10 percent.

(C) Internal Consistencies

The angular distributions of the mesons found at the emission angle of 90° are plotted in Fig. 10. The angle of each meson is measured at the point at which it enters the emulsion. The projected track lengths in emulsion ranged from 25 to 4000 microns, but the bulk of them lay in the 100 to 200 micron interval, as shown in Fig. 11. Choosing mesons which end near the middle of the various plates with residual ranges of 200 microns as typical, one finds that the calculated rms angle of scatter varies from 14° to 21° over the energy range covered and is in the neighborhood of 18°, where most of the mesons were found. Both the σ-meson and the π-μ-meson plots of Fig. 10 give half-widths of 17.5° at half-amplitude, in good agreement with the calculated amount of multiple scattering.

The distribution of the angles at which the μ^+ mesons leave the end of the π^+ mesons, measured with respect to the beam direction, is clearly isotropic within the statistics involved. That the μ^+ mesons are isotropic also with respect to the angle to the normal to the emulsion plane is shown by the track length distribution of the μ^+ mesons in Fig. 11. The smooth curve is that calculated for isotropic emission from points uniformly distributed throughout the scanned volume.

The plot of the angular distribution of the ρ-mesons is clearly composite, being composed of a peak at 90° due to π^- mesons which do not make stars and a flat background due to μ^+ mesons whose beginnings are not observed. One can find the fraction of π^- mesons which do not form stars by comparing the number of mesons under the hump of the ρ-meson plot, after subtracting off the flat background, with the number of σ-mesons on the plot above. This fraction turns out to be 0.31 $\pm$0.07, the error being purely statistical. This value compares well with the value 0.27$\pm$0.02 found by Adelman and Jones[9] with magnetically sorted negative mesons. The angular width of this hump is again about 17.5°.

If μ-mesons were formed in the target, they would appear as ρ-mesons in the plates and would contribute to the hump in the ρ-meson angular distribution. If the value 0.27 is used as the real fraction of the π^- mesons which did not form visible stars, one can again use the number of ρ-mesons in the hump to determine an upper limit on the cross section for the production of μ-mesons. By subtracting from this group of ρ-mesons 0.27 times the total number of π^- mesons, as determined by the number of σ-mesons in the same angular range, one obtains a residual number of ρ-mesons, possibly attributable to μ-mesons from the target. Assuming that the μ-mesons are produced in pairs, one arrives at an upper limit to the ratio of the cross section for μ-meson production to that for π-meson production. This value is 0.02$\pm$0.02; the error is statistical.

The angular plots for emission angles of 45° and 135° correspond very well with those obtained at 90° but are less conclusive, as fewer mesons were counted there.

It is a pleasure to acknowledge the continued guidance and support of Professor E. M. McMillan. We wish to thank Mrs. Edith Goodwin and Mrs. Hazel Gaffey for help in the microscope work, Dr. H. Bradner, Dr. E. Gardner, and co-workers for the use of the facilities of the Radiation Laboratory Film Program and for many helpful discussions, Mr. W. Salsig for mechanical design, and Mr. W. D. Gibbins and the other members of the synchrotron crew for cooperation in making the exposures.

The Piezoelectric Constant of Zinc-Sulfide*

B. D. SAKSENA†
Pennsylvania State College, State College, Pennsylvania
(Received September 13, 1950)

The piezoelectric constant of zinc-sulfide has been calculated in two ways. First, by regarding it as a purely ionic crystal and considering that all of the atoms are equally effective in producing the moment, and second, by regarding it as a purely covalent crystal and considering only the nearest neighbors. In the former case, the result agrees completely with that obtained by Born and Bormann.

The moment produced in an homogeneous elastic deformation is considered to be $ze\Delta r$, where Δr is the variation of the distance between the sulfur and zinc atoms on deformation and ze is the charge on the ions. We first find the moments due to all the sulfur atoms at a given distance from a zinc atom in the crystal. Resolving these along the axes and summing, we get the piezoelectric equations of the crystal. Next, the moments due to various sets of sulfur atoms are summed so as to obtain a quickly converging result, and from this the piezoelectric constant can be obtained. The piezoelectric constant for a purely covalent crystal (formal charge on Zn atom 2−, and on S atom 2+) is found to be 5.4×10^4 and that for a purely ionic crystal (formal charge on Zn 2+ and on S atom 2−) -15.8×10^4. Since the observed value of the piezoelectric constant (-4.20×10^4) lies between these two extremes, it is seen that the crystal has 67 percent ionic character and a formal charge of 0.68 unit on zinc and −0.68 unit on sulfur.

THE piezoelectric constant of zinc-sulfide has been calculated by Born and Bormann[1] on the basis of the lattice theory. It is proposed to calculate it here by an alternative method used by the author[2] for α-quartz, which enables us to calculate the piezoelectric constant directly from the structure of the crystal.

The Si−O bonds in α-quartz were considered to be largely covalent because of the large value of the Si−O force-constant,[3–5] namely, 5.0×10^5 dynes/cm and the high values of dissociation energy[6] (184 kcal) and the hardness (7.0) of the crystal. The forces between the silicon and oxygen atoms are therefore of a short range character; i.e., the forces between the nearest neighbors are large in comparison with those between the next nearest ones. It was therefore supposed that in the case of α-quartz the nearest neighbors alone would be effective in determining the moment, and the polarization was computed on this basis. The supposition appears to be well justified, since there is good agreement between the observed and calculated values.[2,7] For a purely ionic crystal, since the forces between the neighbors are weak and those between the next nearest are not negligible, the piezoelectric moment would have to be computed by considering all of the atoms.

Zinc-sulfide is considered to be partly homopolar and partly ionic.[8] It may be expected that the force per unit displacement between the zinc and sulfur atoms is much smaller than that between the silicon and oxygen atoms in quartz; and this is, indeed, indicated by its smaller hardness (4.0) and dissociation energy[9] (97 kcal) and greater compressibility (-38×10^{-12} cm²/dyne). We have, therefore, computed its moment in two ways: firstly, by considering it as a purely ionic crystal, and secondly, by regarding it as a purely covalent crystal and considering only the nearest neighbors. The results obtained in the first case are identical with those obtained by Born.

Zinc-sulfide is a cubic crystal, the side of the unit cell, a, being 5.427A, and the closest distance between the zinc and sulfur atoms equal to 2.35A. There are four zinc and four sulfur atoms in the unit cell, the zinc atoms being at the corners and face-centers of the unit cell, and the sulfur atoms at points $(\frac{1}{4},\frac{1}{4},\frac{1}{4})$, $(\frac{1}{4},\frac{3}{4},\frac{3}{4})$, $(\frac{3}{4},\frac{1}{4},\frac{3}{4})$, and $(\frac{3}{4},\frac{3}{4},\frac{1}{4})$. There is only one piezoelectric constant, e_{14}, given by the equations:

$$p_x=e_{14}u_{yz},\quad p_y=e_{14}u_{zx},\quad p_z=e_{14}u_{xy},\qquad(1)$$

where p_x, p_y, p_z are the components of the electric moments along the axes, and u_{yz}, u_{zx}, and u_{xy} are the strain components.

For finding the moments we suppose that a homogeneous elastic deformation acts on the crystal, and that the axes of the crystal are also the axes of the strain so that they remain unchanged after the strain. In an elastic deformation, the distances between the zinc and sulfur atoms would be altered. For a purely ionic crystal, we can assume that each zinc atom carries a charge of +2 units, and a sulfur atom a charge of −2 units. The electrical moment produced by a change in the distance, r, between a zinc and a sulfur atom would be $2e\Delta r$. If Δr is considered to be positive, there would be a motion of the positive charge away from the negative charge, so that the moment would be directed from the sulfur to the zinc atom along the line joining them. The direction cosines of the moment can be obtained by subtracting the coordinates of the

* This research was carried out under contract N6onr-269 Task V of the ONR.
† Visiting Research Associate. Now at the National Research Council, Ottawa, Canada.
[1] M. Born and E. Bormann, Ann. phys. **62**, 218 (1920).
[2] B. D. Saksena, Proc. Indian Acad. Sci. **28**, 423 (1948).
[3] B. D. Saksena, Proc. Indian Acad. Sci. **16**, 270 (1942).
[4] J. Barriol, J. phys. radium **7**, 209 (1946).
[5] Matossi, J. Chem. Phys. **17**, 679 (1949).
[6] Alfred G. Gaydon, *Dissociation Energies and Spectra of Diatomic Molecules* (Chapman and Hall, Ltd., London, 1947), p. 214.
[7] B. D. Saksena, Proc. Indian Acad. Sci. A. **28**, 437 (1948).
[8] L. Pauling, *Nature of the Chemical Bond* (Cornell University Press, Ithaca, New York, 1940), pp. 6, 178.
[9] Reference 6, p. 216.

sulfur atom from those of the zinc atom. The moments can then be resolved along the axes.

In a homogeneous elastic deformation, the change in the distance, r, between two points P and Q caused by the strain can be expressed in terms of the strain components. Love[10] has shown that the change in the length of a line PQ after strain is given by the expression:

$$\Delta r = r(l^2u_{xx}+m^2u_{yy}+n^2u_{zz}+lmu_{xy}+mnu_{yz}+lnu_{zx}), \quad (2)$$

where r is the length of a line PQ before strain, l, m, n are its direction cosines, and u_{xx}, u_{xy}, etc., are the strain components. If we associate P with a zinc atom and Q with a sulfur atom, the resolved parts of the moments along the axes due to the elastic deformation would be given by the expressions:

$$p_x = 2e\Delta r \cdot l, \quad p_y = 2e\Delta r \cdot m, \quad p_z = 2e\Delta r \cdot n. \quad (3)$$

In order to obtain the piezoelectric moment for the crystal, we should first find the moments due to all the sulfur atoms at a given zinc atom. We consider the zinc atom P which lies at the origin (0, 0, 0) of our unit cell, and find the moments $2e\Delta r$ due to all the sulfur atoms at the same distance r from P in the crystal. These can be resolved along the axes as indicated in Eqs. (3) and summed. In this way we obtain the piezoelectric equations as given in Eqs. (1). The next step is to add the moments due to various sets of sulfur atoms at different distances from P so as to obtain a quickly converging result. This has been possible by using a method similar to that described by Slater[11] for finding the Madelung constant for NaCl. Knowing the moment due to all of the sulfur atoms at any zinc atom, we can easily determine the piezoelectric moment for the unit-cell; and from this we can obtain the value of the piezoelectric constant by dividing by the volume of the unit cell.

We must first find all the sulfur atoms which surround the zinc atom (0, 0, 0). It is easy to show that these are situated at points $(n_1a/4; n_2a/4; n_3a/4)$, where n_1, n_2, n_3 are any three numbers selected from the set 1, −3, 5, −7, 9, −11, 13, −15, etc. The distance from the origin to any point is $(n_1^2+n_2^2+n_3^2)^{\frac{1}{2}} \cdot a/4$. The number of sulfur atoms at this distance can be determined easily. If n_1, n_2, n_3 are all different, there are six ways of arranging them, and since each can be positive or negative, there are eight possible combinations of signs giving 48 terms. But, since the product of n_1, n_2, n_3 must be either positive or negative, we have only 24 points. If two indices are equal, we have 12 points; and if all are equal, we have only 4 points.

If, therefore, we have a group of four points for which the moments act along the directions whose direction-cosines are $(-l, -m, -n)$, $(-l, m, n)$, $(l, -m, n)$, and $(l, m, -n)$, the resolved parts of moments along the axes will be given by

$$p_x = -(2e)(4rlmn)u_{yz}, \quad \text{with similar terms for } p_y \text{ and } p_z. \quad (4)$$

Relation (4) can be easily verified with the help of relations (2) and (3). Since we are finding the moments at the zinc atom at the origin (0, 0, 0), we can express the values of l, m, and n in terms of n_1, n_2, and n_3. These are, without regard to their signs,

$$l = n_1/(n_1^2+n_2^2+n_3^2)^{\frac{1}{2}}, \quad m = n_2/(n_1^2+n_2^2+n_3^2)^{\frac{1}{2}}, \quad n = n_3/(n_1^2+n_2^2+n_3^2)^{\frac{1}{2}}.$$

Since $r = (n_1^2+n_2^2+n_3^2)^{\frac{1}{2}} \cdot a/4$, expression (4) now becomes

$$p_x = -4n_1n_2n_3(2ea)u_{yz}/4(n_1^2+n_2^2+n_3^2) \quad (5)$$

with similar terms for p_y and p_z.

Let us now consider s sulfur atoms (where s is a multiple of four) at distance r from the zinc atom at the origin. Since the direction cosines of the moments due to these atoms can be arranged in groups of four of the type considered above, the moments along the axes due to the s sulfur atoms at distance r from the origin is given by

$$p_x = -sn_1n_2n_3(2ea)u_{yz}/4(n_1^2+n_2^2+n_3^2) \quad (6)$$

with similar terms for p_y and p_z. The values of the quantity g given by the expression $-\frac{1}{4}s(n_1n_2n_3)/(n_1^2+n_2^2+n_3^2)$ are tabulated in Table I for different values of n_1, n_2, n_3. It may be seen that the sign of the moment changes for different values of n_1, n_2, and n_3, since the sign of the product $n_1n_2n_3$ also changes. Table I can be extended to include higher values of n_1, n_2, and n_3.

To find the resolved parts of the moments along the axes resulting from all of the sulfur atoms at different distances from the zinc atom at the origin, or in other words, to obtain the value of the quantity, g, for the crystal, we adopt the following procedure which gives a quickly converging result. We consider the zinc atom $P(0, 0, 0)$ inside a cube whose side extends from $-\frac{1}{2}na$ to $\frac{1}{2}na$ along the three axes of the crystal. All points with all three indices (n_1, n_2, n_3) equal to n lie at the

TABLE I. Values of the moments resulting from neighboring groups of sulfur atoms at any zinc atom.

Values of n_1	n_2	n_3	Distance r from the zinc atom at the origin	Number s of sulfur atoms at distance r	$-\frac{1}{4}s\frac{(n_1n_2n_3)}{(n_1^2+n_2^2+n_3^2)}$
1	1	1	$(3)^{\frac{1}{2}} \cdot a/4$	4	−1/3
−3	1	1	$(11)^{\frac{1}{2}} \cdot a/4$	12	9/11
−3	−3	1	$(19)^{\frac{1}{2}} \cdot a/4$	12	−27/19
−3	−3	−3	$(27)^{\frac{1}{2}} \cdot a/4$	4	1
1	5	1	$(27)^{\frac{1}{2}} \cdot a/4$	12	−15/27
1	5	−3	$(35)^{\frac{1}{2}} \cdot a/4$	24	18/7
1	5	5	$(51)^{\frac{1}{2}} \cdot a/4$	12	−25/17
−3	5	−3	$(43)^{\frac{1}{2}} \cdot a/4$	12	−135/43
−3	5	5	$(59)^{\frac{1}{2}} \cdot a/4$	12	225/59
5	5	5	$(75)^{\frac{1}{2}} \cdot a/4$	4	−5/3

[10] A. E. H. Love, *Mathematical Theory of Elasticity* (Dover Publications, New York, 1944), pp. 38, 39.

[11] John C. Slater, *Introduction of Chemical Physics* (McGraw-Hill Book Company, Inc., London and New York, 1939), p. 229.

TABLE II. Variation of moment with cell dimensions.

n	Total number of sulfur atoms	Total moment
1	4	−0.0416666
3	32	−0.1545964
5	108	−0.1206254
7	256	−0.1217672
9	500	−0.1215307
11	864	−0.1216475

corners of the cube, those with two indices equal to n lie at the edges of this cube, and those with one index equal to n lie in the faces of this cube, while the remaining points, with indices all different from n, are wholly within the cube. Their contributions are therefore $\frac{1}{8}$, $\frac{1}{4}$, $\frac{1}{2}$, and 1, respectively.

In this way we have calculated moments for all values of n up to 11. The results are given in Table II. It is thus seen that the result rapidly converges to −0.1216. This quantity multiplied by $(2ea)$ gives the resolved part of the moment from all the sulfur atoms in the crystal at any zinc atom.

Similarly, the resolved part of the moment arising from all of the zinc atoms at any sulfur atom would be the same. The total moment is, however, not doubled and remains the same, since each ion is counted twice, once when the zinc atom was at the origin and secondly when the sulfur atom was at the origin. Since there are four zinc and four sulfur atoms in the unit-cell, the piezoelectric moment along the axes would be multiplied by four; i.e., $-4(0.1216)2ea$. The piezoelectric constant e_{14}, being equal to the moment per unit volume, is given by $e_{14}=-0.9728ea/a^3=-0.9728e/a^2$. Since $e=4.77\times10^{-10}$, and $a=5.427\times10^{-8}$ cm, we get $e_{14}=-15.8\times10^4$. If, however, the charge on the ion is ze instead of $2e$ we have

$$e_{14}=-7.9z\times10^4. \tag{7}$$

We can now consider the moments arising from the nearest neighbors only. If ze is the charge on the ion, then from Table I, the resolved part of the moment from four sulfur atoms at any zinc atom is $-\frac{1}{2}\times\frac{1}{4}(zea)$, and proceeding in the manner described in the previous previous paragraph we get

$$e_{14}=-2.7z\times10^4. \tag{8}$$

If zinc-sulfide were perfectly covalent, there would be a formal charge of 2− on zinc and 2+ on sulfur.[9] The value of e_{14} for a purely covalent crystal is therefore $+5.4\times10^4$, while that for a purely ionic crystal has been shown to be -15.8×10^4. According to Cady[12] the best experimental value of e_{14} is -4.2×10^4, which lies between the two extremes.

We can, therefore, roughly estimate the proportion of the ionic to the covalent character in the following manner. The charge on a zinc atom for a 100 percent ionic crystal is +2 units and for a 100 percent covalent character it is −2 units. If, therefore, the crystal has x percent ionic and $100-x$ percent covalent character, the formal charge may be assumed to be

$$z=4a-2, \quad \text{where} \quad a=x/100. \tag{9}$$

Similarly the value of e_{14} for a 100 percent ionic character $(a=1)$ is -15.8×10^4 and for a 100 percent covalent character $(a=0)+5.4\times10^4$. Therefore, for a crystal which is x percent ionic and $100-x$ percent covalent, and has a formal charge of z units, the piezoelectric constant e_{14} is given by

$$e_{14}=-7.9az-2.7(1-a)z. \tag{10}$$

Using Eqs. (9) and (10) it is possible to obtain z for any value of e_{14}. Since the observed value of the latter is -4.2×10^4, we get $a=0.67$ and $z=0.68$. This shows that the atoms have 67 percent ionic character, and that the formal charge on zinc is 0.68 unit. This appears to be a quite reasonable conclusion for, according to Pauling, also, the bonds have enough ionic character. Relation (10) has been plotted graphically in Fig. 1. It appears that the piezoelectric constant is zero when the ionic character is 50 percent and then diminishes rapidly towards −15.8 as the ionic character increases. Since the ionic character may be supposed to increase with the increase of temperature, the value of e_{14} would diminish (towards higher negative value) on heating the crystal. Further, if the crystal be considered to be 100 percent ionic at its melting point (1020°C), it can be seen by a linear intrapolation that even at the absolute zero of temperature the value of e_{14} would have an appreciable negative value (about −0.7).

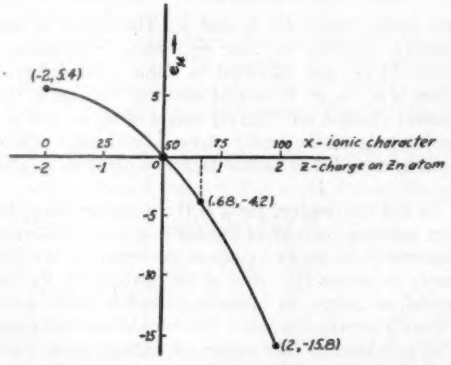

FIG. 1. Dependence of the piezoelectric constant on the ionic character.

The results obtained for the purely ionic crystal are identical with those of Born. The second relation in expressions (5) of Born and Bormann reduces to $e_{14}=-7.6z\times10^4$, which is identical with our expression (7). Expression (3) of their paper, which has been quoted in later literature also,[13] does not contain z, the

[12] Walter G. Cady, *Piezo-Electricity* (McGraw-Hill Book Company, Inc., London and New York, 1946), p. 229.

[13] Reference 12, p. 743.

charge on the ion. The value of e_{14} calculated from this expression[14] is -23×10^4. From relation (7) derived in the present paper we find that for a purely ionic crystal $z=2$, and $e_{14}=-15.8\times10^4$. This at first sight appears to be a discrepancy; but since the second relation in expressions (5) of Born is identical with our expression (7), it only means that the value 6.5 of $k-k_0$, which has been used to calculate e_{14} from expression (3) of Born, would give a value of z which is 23/15.8 (or 1.5) times 2. This is also verified with the help of the first relation in expressions (5) of Born which gives a relation between z and $k-k_0$, and we find $z=3.03$. The value of $k-k_0$ (6.5) needs to be revised.

[14] Herzfeld, *Handbuch der Experimental Physik* (VII), Teil 2, p. 341.

PHYSICAL REVIEW VOLUME 81, NUMBER 6 MARCH 15, 1951

A Note on the Ground State in Antiferromagnetics

J. M. LUTTINGER
Department of Physics, University of Wisconsin, Madison, Wisconsin
(Received October 19, 1950)

The lowest state of an antiferromagnetic substance is investigated by using the Ising model for the spins. By means of a method of Luttinger and Tisza it is found possible to derive earlier results of Anderson very simply.

I. INTRODUCTION

RECENT neutron diffraction experiments of Shull on antiferromagnetics have been interpreted by Anderson[1] in terms of a model in which spins interact with not only their nearest neighbors, but also with their next-nearest neighbors. Néel[2] had already introduced such a model to explain the large ratios of the "paramagnetic" Curie temperature θ to the actual transition temperature T_c. The basic point of improvement in Anderson's version is the finding of configurations of the spins which give lower energies than the ones which were used by Néel. The existence of these configurations has two effects: (1) the θ/T_c ratios are increased, and are more in conformity with experiment; (2) the configurations predicted seem to be just those found by Shull in his neutron diffraction experiments. Anderson chose the configurations he did largely on the basis of plausibility and intuition, and the question arises as to whether or not these are really the configurations of lowest energy. It is the purpose of this paper to show in a systematic and rigorous manner that this is indeed the case. The technique used is a generalization of a method developed by Luttinger and Tisza,[3] and applied by them to the case of dipole interactions in crystals. The present problem is simpler, however, and allows of a much more complete solution.

II. GENERAL METHOD

The model used is essentially that of Ising,[4] in which each quantum mechanical spin is replaced by a scalar "spin" which can take the values ±1. It is assumed that there is an interaction energy $\gamma(\geq0)$ between nearest neighbors (NN) and interaction energy $\alpha(\geq0)$ between next-nearest neighbors (NNN). In this case the energy may be written

$$E=\tfrac{1}{2}[\gamma\sum_j\mu_j\sum_{i=NN\text{ of }j}\mu_i+\alpha\sum_j\mu_j\sum_{i=NNN\text{ of }j}\mu_i], \quad (1)$$

where $\mu_j=\pm1$ (or $\mu_j^2=1$). For a given arrangement of spins (i.e., a given set of values of μ_j) it is very easy to calculate the energy of the array. One can also ask what the arrangement of spins on the lattice points must be so that E is a minimum. Now the expression for E is a quadratic form in the spins μ_j, and were it not for the complexity of the constraining conditions $\mu_j^2=1$, it would be a simple matter to find its minimum. We can replace (just as in reference 3) the "strong conditions" $\mu_j^2=1$ by the "weak" conditions

$$\textstyle\sum_j\mu_j^2=N, \quad (2a)$$

where N is the number of spins present. This equation follows (by addition) from the strong conditions, but is, of course, considerably less stringent. If we minimize E under the condition (2a) and find that our solution also satisfies the strong condition, then we will have solved the problem. The essence of our method is that this proves to be the case. The minimization of Eq. (1) under the condition (2a) is, of course, a standard problem in the theory of quadratic forms. The solution is given by the lowest eigenvalue of the matrix of the quadratic form.[5] Our problem is then to find the smallest eigenvalue of Eq. (1) for the case of simple cubic (S.C.), body centered cubic (B.C.) and face centered cubic

[1] P. W. Anderson, Phys. Rev. 79, 705 (1950). The reference to Shull's work is also to be found in this paper. A very clear summary of Anderson's work is to be found in J. H. Van Vleck, Report to the Grenoble Conference, Grenoble, 1950.
[2] L. Néel, Ann. physique 3, 137 (1948).
[3] J. M. Luttinger and L. Tisza, Phys. Rev. 70, 954 (1946).
[4] G. Ising, Z. Physik 31, 253 (1925).
[5] Courant-Hilbert, *Methoden der Mathematischen Physik* (Verlag J. Springer, Berlin, 1931), Vol. I, p. 26.

(F.C.). The S.C. case does not, so far as we know, have a realization in nature, but it forms a simple introduction to the techniques employed here.

III. THE SIMPLE CUBIC CASE

If we introduce a matrix E_{ij} defined by

$$E=\tfrac{1}{2}\sum_{i,j} E_{ij}\mu_i\mu_j, \tag{3a}$$

then our problem is to find the lowest eigenvalue of the matrix $\|E_{ij}\|$. It proves to be convenient (just as in the theory of fourier series) to allow complex values for the spins μ_j. Any array occurring in nature will, of course, have real μ_j; and these will be built up of superpositions of arrays with complex elements. With this in mind we redefine the weak condition as

$$\sum_j \mu_j^*\mu_j=N, \tag{2b}$$

and the energy as

$$E=\tfrac{1}{2}\sum_{i,j} E_{ij}\mu_i^*\mu_j. \tag{3b}$$

Just as in the case of the normal coordinates of a solid, we have translational symmetry in our energy matrix $\|E_{ij}\|$; and, therefore, the characteristic vectors (or basic arrays, as we shall call them here) must be of the form[6]

$$\mu_{l_1l_2l_3}=e^{i(\kappa_1 l_1+\kappa_2 l_2+\kappa_3 l_3)}=\exp[i(\boldsymbol{\kappa}\cdot\mathbf{l})]. \tag{4}$$

Here l_1, l_2, l_3 are integers which define a point in the crystal lattice, $\kappa_i=(2\pi/L)n_i$, the n_i being integers $-\frac{1}{2}L\leq n_i\leq+\frac{1}{2}L$, and $L^3=N$. We have assumed a periodic boundary condition, but it is easy to see that this involves no loss in generality. This result can be verified directly by substitution. Let us call an array of the form (4) $\mathbf{Z}_\kappa$. Then any array may be written (finite fourier series)

$$\boldsymbol{\mu}=\sum_\kappa c_\kappa\mathbf{Z}_\kappa$$

or

$$\mu_{l_1l_2l_3}=\sum_\kappa c_\kappa e^{i(\kappa_1 l_1+\kappa_2 l_2+\kappa_3 l_3)}.$$

Now the nearest neighbors to l_1, l_2, l_3 are given by $(l_1\pm1, l_2, l_3)$, $(l_1, l_2\pm1, l_3)$, $(l_1, l_2, l_3\pm1)$ and the next-nearest neighbors are given by $(l_1, l_2\pm1, l_3\pm1)$, $(l_1\pm1, l_2, l_3\pm1)$, $(l_1\pm1, l_2\pm1, l_3)$. Therefore, the expression (3b) reduces to

$$\begin{aligned}E=\tfrac{1}{2}\sum_{\kappa,\kappa'}\sum_{l_1l_2l_3}&\exp[i(\boldsymbol{\kappa}-\boldsymbol{\kappa}')\cdot\mathbf{l}]c_\kappa c_{\kappa'}^*\\ &\times[\gamma(e^{i\kappa_1'}+e^{-i\kappa_1'}+e^{i\kappa_2'}+e^{-i\kappa_2'}+e^{i\kappa_3'}+e^{-i\kappa_3})\\ &+\alpha(e^{i(\kappa_1'+\kappa_2')}+e^{-i(\kappa_1'+\kappa_2')}+e^{i(\kappa_1'-\kappa_2')}\\ &+e^{-i(\kappa_1'-\kappa_2')}+e^{i(\kappa_1'+\kappa_3')}+e^{-i(\kappa_1'+\kappa_3')}\\ &+e^{i(\kappa_1'-\kappa_3')}+e^{-i(\kappa_1'-\kappa_3')}+e^{i(\kappa_2'+\kappa_3')}\\ &+e^{-i(\kappa_2'+\kappa_3')}+e^{i(\kappa_2'-\kappa_3')}+e^{-i(\kappa_2'-\kappa_3')})].\end{aligned}$$

However,

$$\sum_{l_1l_2l_3}\exp[i(\boldsymbol{\kappa}-\boldsymbol{\kappa}')\cdot\mathbf{l}]=N\delta_{\kappa\kappa'};$$

and, therefore,

$$\begin{aligned}E=N\sum_\kappa[&\gamma(\cos\kappa_1+\cos\kappa_2+\cos\kappa_3)+2\alpha(\cos\kappa_1\cos\kappa_2\\ &+\cos\kappa_2\cos\kappa_3+\cos\kappa_3\cos\kappa_1)]|c_\kappa|^2.\end{aligned} \tag{5}$$

This shows that the energy is now diagonal, and that the eigenvalues are

$$\begin{aligned}E(\boldsymbol{\kappa})=N\gamma[&(\cos\kappa_1+\cos\kappa_2+\cos\kappa_3)\\ &+2r(\cos\kappa_1\cos\kappa_2+\cos\kappa_2\cos\kappa_3+\cos\kappa_3\cos\kappa_1)],\end{aligned}$$

where $r=\alpha/\gamma$, the ratio of next-nearest to nearest neighbor interaction. Writing the energy in units of $N\gamma$ as $\epsilon(\boldsymbol{\kappa})$ we have, finally,

$$\begin{aligned}\epsilon(\boldsymbol{\kappa})=&\cos\kappa_1+\cos\kappa_2+\cos\kappa_3\\ &+2r(\cos\kappa_1\cos\kappa_2+\cos\kappa_2\cos\kappa_3+\cos\kappa_3\cos\kappa_1).\end{aligned} \tag{6}$$

We now must seek the minimum value of Eq. (6) as a function of κ. It can easily be shown that for $r<\frac{1}{4}$ this minimum is given by $\cos\kappa_1=\cos\kappa_2=\cos\kappa_3=-1$, while for $r>\frac{1}{4}$ the lowest state is given by two of the cosines being -1 and the other being $+1$ (for example, $\cos\kappa_1=\cos\kappa_2=-1$, $\cos\kappa_3=+1$). For $r<\frac{1}{4}$, the configuration is given by

$$\mu_{l_1l_2l_3}=(-)^{l_1+l_2+l_3},\quad \mu^2_{l_1l_2l_3}=1,$$

so that the strong condition is satisfied. The configuration consists in each spin being surrounded by six antiparallel neighbors. For $r>\frac{1}{4}$, the configuration is given by (for example)

$$\mu_{l_1l_2l_3}=(-)^{l_1+l_2},\quad \mu^2_{l_1l_2l_3}=1,$$

so that the strong condition is once again satisfied. The configuration consists of rows of spins along the z axis, each of which is surrounded by four antiparallel rows of spins.

IV. THE BODY CENTERED CASE

In treating the B.C. case it is convenient to introduce the concept of the field F_l at a lattice point $\mathbf{l}$,

$$F_l\equiv-[\gamma\sum_{NN\text{ to }l}\mu_{l'}+\alpha\sum_{NNN\text{ to }l}\mu_{l'}].$$

With this definition the energy (3b) becomes

$$E=-\tfrac{1}{2}\sum_l\mu_l^*F_l.$$

Since F_l is a linear function of the $\mu_{l'}$'s, we can introduce vector notation (in N space) and write

$$\mathbf{F}=\begin{pmatrix}F_1\\F_2\\\cdot\\\cdot\\\cdot\\F_N\end{pmatrix}=\begin{pmatrix}\mathfrak{F}_{11}\cdots\mathfrak{F}_{1N}\\\cdot\quad\cdot\\\cdot\quad\cdot\\\cdot\quad\cdot\\\mathfrak{F}_{N1}\cdots\mathfrak{F}_{NN}\end{pmatrix}\begin{pmatrix}\mu_1\\\mu_2\\\cdot\\\cdot\\\cdot\\\mu_N\end{pmatrix}=\mathfrak{F}\boldsymbol{\mu}.$$

[6] F. Seitz, *Modern Theory of Solids* (McGraw-Hill Book Company, Inc., New York, 1940), p. 125.

The characteristic vectors of the energy will then be the characteristic vectors of the matrix $\mathfrak{F}$, i.e.,

$$\mathfrak{F}\psi = f\psi. \tag{7}$$

That is, the characteristic vectors (or basic arrays, as we have called them) have the property that the field at any point in the lattice is proportional to the spin at that point.

Now let us call the array on the lattice points **A**, that on the body centers **B**. We shall use the notation

$$\psi = \begin{pmatrix} \mathbf{A} \\ \mathbf{B} \end{pmatrix}$$

to characterize the array completely. From our previous argument on translational symmetry it follows once again that

$$A_l = \rho_1 \exp[i(\kappa\cdot\mathbf{l})], \quad B_l = \rho_2 \exp[i(\kappa\cdot\mathbf{l})].$$

Such an array will have for the field at a lattice point $\mathbf{l}$

$$F_l(\text{l.p.}) = -\exp[i(\kappa\cdot\mathbf{l})][\rho_2\gamma(1+\epsilon^{-i\alpha_1})(1+\epsilon^{-i\alpha_2})(1+\epsilon^{-i\alpha_3}) + \rho_1\alpha(\epsilon^{i\alpha_1}+\epsilon^{-i\alpha_1}+\epsilon^{i\alpha_2}+\epsilon^{-i\alpha_2}+\epsilon^{i\alpha_3}+\epsilon^{-i\alpha_3})],$$

while the field at the body center $\mathbf{l}$ will be

$$F_l(\text{B.C.}) = -\exp[i(\kappa\cdot\mathbf{l})][\rho_1\gamma(1+\epsilon^{i\alpha_1})(1+\epsilon^{i\alpha_2})(1+\epsilon^{i\alpha_3}) + \rho_2\alpha(\epsilon^{i\alpha_1}+\epsilon^{-i\alpha_1}+\epsilon^{i\alpha_2}+\epsilon^{-i\alpha_2}+\epsilon^{i\alpha_3}+\epsilon^{-i\alpha_3})].$$

The characteristic value equation reads

$$F_l(\text{l.p.}) = f\rho_1 \exp[i(\kappa\cdot\mathbf{l})],$$
$$F_l(\text{B.C.}) = f\rho_2 \exp[i(\kappa\cdot\mathbf{l})],$$

or

$$\begin{aligned} &\rho_1\lambda + \rho_2\nu = f\rho_1, \quad \rho_1\nu^* + \rho_2\lambda = f\rho_2, \\ &\lambda \equiv -2\alpha(\cos\kappa_1+\cos\kappa_2+\cos\kappa_3), \\ &\nu \equiv -\gamma(1+\epsilon^{-i\alpha_1})(1+\epsilon^{-i\alpha_2})(1+\epsilon^{-i\alpha_3}). \end{aligned} \tag{8}$$

These equations can be solved directly. It is possible, however, to write down the solution at once, as the following considerations show. Let $\mathbf{T}$ be the operation (translation) which moves the lattice points up to their nearest adjoining body centers. Then

$$\mathbf{T}\begin{bmatrix} \rho_1 \exp[i(\kappa\cdot\mathbf{l})] \\ \rho_2 \exp[i(\kappa\cdot\mathbf{l})] \end{bmatrix} = \begin{bmatrix} \rho_2\epsilon^{-i(\alpha_1+\alpha_2+\alpha_3)} \exp[i(\kappa\cdot\mathbf{l})] \\ \rho_1 \exp[i(\kappa\cdot\mathbf{l})] \end{bmatrix}. \tag{9}$$

However, this translation is merely a renaming of lattice points and body centers; and, therefore, the new array must also be (apart from a factor) the same basic array. Therefore,

$$\mathbf{T}\begin{bmatrix} \rho_1 \exp[i(\kappa\cdot\mathbf{l})] \\ \rho_2 \exp[i(\kappa\cdot\mathbf{l})] \end{bmatrix} = p\begin{bmatrix} \rho_1 \exp[i(\kappa\cdot\mathbf{l})] \\ \rho_2 \exp[i(\kappa\cdot\mathbf{l})] \end{bmatrix}, \tag{10}$$

where p is a scalar factor. Using Eqs. (9) and (10) we then obtain

$$\rho_2\epsilon^{-i(\alpha_1+\alpha_2+\alpha_3)} = p\rho_1, \quad \rho_1 = p\rho_2$$

or

$$p^2 = \epsilon^{-i(\alpha_1+\alpha_2+\alpha_3)}, \quad p = \pm\epsilon^{-\frac{1}{2}i(\alpha_1+\alpha_2+\alpha_3)}.$$

If we take $\rho_1 = 1$, we then obtain

$$\rho_2 = \pm\epsilon^{\frac{1}{2}i(\alpha_1+\alpha_2+\alpha_3)},$$

which give us the two required solutions of Eq. (8). That these are really solutions can be verified easily by direct substitution in Eq. (8). The corresponding characteristic values are

$$f_\pm = -[2\alpha(\cos\kappa_1+\cos\kappa_2+\cos\kappa_3) \pm 8\gamma\cos\tfrac{1}{2}\kappa_1\cos\tfrac{1}{2}\kappa_2\cos\tfrac{1}{2}\kappa_3]. \tag{11}$$

Since $-\pi \le \kappa_i \le \pi$, $\cos(\frac{1}{2}\kappa_i) \ge 0$; and, therefore,

$$f_- \ge f_+, \quad E_\pm = -\tfrac{1}{2}Nf_\pm, \quad E_+ \ge E_-.$$

In looking for the lowest state we need only consider E_-.

$$E_- = N\gamma[r(\cos\kappa_1+\cos\kappa_2+\cos\kappa_3) - 4\cos\tfrac{1}{2}\kappa_1\cos\tfrac{1}{2}\kappa_2\cos\tfrac{1}{2}\kappa_3].$$

Defining for convenience $\epsilon = E_-/N\gamma$

$$\epsilon = r(\cos\kappa_1+\cos\kappa_2+\cos\kappa_3) - 4\cos\tfrac{1}{2}\kappa_1\cos\tfrac{1}{2}\kappa_2\cos\tfrac{1}{2}\kappa_3, \tag{12}$$

we have only to find the minimum value of ϵ. Once again, it is a matter of elementary calculus to show that for $r < \frac{3}{4}$ the minimum is given by $\kappa_i = 0$ and the corresponding energy is $\epsilon = 3r - 4$. This means that we have a uniform arrangement of spins on the lattice points and a uniform (but oppositely directed) arrangement on the body centers. The strong conditions are clearly satisfied, since $\mu^2(\text{l.p.}) = 1$, $\mu^2(\text{B.C.}) = +1$. For $r > \frac{3}{4}$ the situation is a little more complicated. The lowest arrangement is given by $\kappa_i = \pm\pi$, and the corresponding energy is $\epsilon = -3r$. However, at first glance the characteristic vectors seem to be complex. For example

$$\mu_l^- = \begin{bmatrix} 1 \\ i \end{bmatrix}(-)^{l_1+l_2+l_3}, \quad \kappa_i = \pi.$$

The situation is easily remedied by noticing that in this case $E_- = E_+(\cos\frac{1}{2}\pi = 0)$, so that there is a degeneracy. When degeneracy is present, we can take a linear combination of the two characteristic vectors; and it is once more a characteristic vector with the same characteristic value. Now,

$$\mu_l^+ = \begin{bmatrix} 1 \\ -i \end{bmatrix}(-)^{l_1+l_2+l_3},$$

so that by building

$$\frac{\mu_l^+ + \mu_l^-}{2} \pm \frac{\mu_l^- - \mu_l^+}{2i} = \begin{bmatrix} 1 \\ \pm 1 \end{bmatrix}(-)^{l_1+l_2+l_3},$$

we get basic arrays which are real and which satisfy the strong conditions. Because of this degeneracy, we see that the spin array at the lattice points is completely uncorrelated with the array at the body centers, a result which has already been noticed by Anderson.

V. THE FACE CENTERED CASE

We shall not give the details for this case, but merely indicate the methods and results. If we split the array into its four components and write

$$\psi=\begin{bmatrix}\psi\ (\text{l.p.})\\ \psi\ (xz\ \text{face})\\ \psi\ (xy\ \text{face})\\ \psi\ (yz\ \text{face})\end{bmatrix},$$

then the translation group gives us

$$\mu_l=\begin{bmatrix}\rho_1\\ \rho_2\\ \rho_3\\ \rho_4\end{bmatrix}\exp[i(\kappa\cdot\mathbf{l})].$$

Further, just as in the body centered case, we can apply translation operators which translate the various component lattices into each other. The conditions derived from the requirements of invariance under these translations are enough to determine the form of the characteristic vectors completely. There are four types

$$\mu_l^{(1)}=\begin{bmatrix}1\\ e^{\frac{1}{2}i(\alpha_1+\alpha_2)}\\ e^{\frac{1}{2}i(\alpha_2+\alpha_3)}\\ e^{\frac{1}{2}i(\alpha_3+\alpha_1)}\end{bmatrix}\exp[i(\kappa\cdot\mathbf{l})],$$

$$\mu_l^{(2)}=\begin{bmatrix}1\\ e^{\frac{1}{2}i(\alpha_1+\alpha_2)}\\ -e^{\frac{1}{2}i(\alpha_2+\alpha_3)}\\ -e^{\frac{1}{2}i(\alpha_3+\alpha_1)}\end{bmatrix}\exp[i(\kappa\cdot\mathbf{l})],$$

$$\mu_l^{(3)}=\begin{bmatrix}1\\ -e^{\frac{1}{2}i(\alpha_1+\alpha_2)}\\ e^{\frac{1}{2}i(\alpha_2+\alpha_3)}\\ -e^{\frac{1}{2}i(\alpha_3+\alpha_1)}\end{bmatrix}\exp[i(\kappa\cdot\mathbf{l})],$$

$$\mu_l^{(4)}=\begin{bmatrix}1\\ -e^{\frac{1}{2}i(\alpha_1+\alpha_2)}\\ -e^{\frac{1}{2}i(\alpha_2+\alpha_3)}\\ e^{\frac{1}{2}i(\alpha_3+\alpha_1)}\end{bmatrix}\exp[i(\kappa\cdot\mathbf{l})].$$

The corresponding energies are

$$E_1=N\gamma[r(\cos\kappa_1+\cos\kappa_2+\cos\kappa_3)+2(\cos\tfrac{1}{2}\kappa_1\cos\tfrac{1}{2}\kappa_2+\cos\tfrac{1}{2}\kappa_2\cos\tfrac{1}{2}\kappa_3+\cos\tfrac{1}{2}\kappa_3\cos\tfrac{1}{2}\kappa_1)],$$

$$E_2=N\gamma[r(\cos\kappa_1+\cos\kappa_2+\cos\kappa_3)+2(-\cos\tfrac{1}{2}\kappa_1\cos\tfrac{1}{2}\kappa_2-\cos\tfrac{1}{2}\kappa_2\cos\tfrac{1}{2}\kappa_3+\cos\tfrac{1}{2}\kappa_3\cos\tfrac{1}{2}\kappa_1)],$$

$$E_3=N\gamma[r(\cos\kappa_1+\cos\kappa_2+\cos\kappa_3)+2(\cos\tfrac{1}{2}\kappa_1\cos\tfrac{1}{2}\kappa_2-\cos\tfrac{1}{2}\kappa_2\cos\tfrac{1}{2}\kappa_3-\cos\tfrac{1}{2}\kappa_3\cos\tfrac{1}{2}\kappa_1)],$$

$$E_4=N\gamma[r(\cos\kappa_1+\cos\kappa_2+\cos\kappa_3)+2(-\cos\tfrac{1}{2}\kappa_1\cos\tfrac{1}{2}\kappa_2+\cos\tfrac{1}{2}\kappa_2\cos\tfrac{1}{2}\kappa_3-\cos\tfrac{1}{2}\kappa_3\cos\tfrac{1}{2}\kappa_1)].$$

Since $\cos\kappa_i/2\geq 0$, it is clear that E_2, E_3, $E_4\leq E_1$. Therefore, we can ignore E_1. By symmetry, it makes no difference which of the three remaining E's we choose. Let us take E_2, and define

$$\epsilon=E_2/N\gamma=r(\cos\kappa_1+\cos\kappa_2+\cos\kappa_3)+2(-\cos\tfrac{1}{2}\kappa_1\cos\tfrac{1}{2}\kappa_2-\cos\tfrac{1}{2}\kappa_2\cos\tfrac{1}{2}\kappa_3+\cos\tfrac{1}{2}\kappa_3\cos\tfrac{1}{2}\kappa_1).$$

The finding of the minimum of this expression is as always fairly straightforward. We find for $r>\frac{1}{2}$ that the configuration with $\kappa_i=\pm\pi$ is that of minimum energy. We can choose as our array, any of the arrays

$$\mu_l=\begin{bmatrix}1\\ \pm 1\\ \pm 1\\ \pm 1\end{bmatrix}(-)^{l_1+l_2+l_3}$$

because of the degeneracy in the energy values. Clearly, these satisfy the strong conditions, and show that (for $r>\frac{1}{2}$) there is no correlation between the order in the different faces. As in the body centered case, there are slight complications for $r<\frac{1}{2}$. The complex arrays which minimize the energy are $\kappa_1=\kappa_2=0$, $\kappa_3=\pm\pi$ (or similar arrays with 1, 2, 3 permuted). This gives basic arrays of the type

$$\mu_l^{(3)}=\begin{bmatrix}1\\ \pm i\\ -1\\ \mp i\end{bmatrix}(-)^{l_3},\quad \mu_l^{(4)}=\begin{bmatrix}1\\ \mp i\\ -1\\ \pm i\end{bmatrix}(-)^{l_3}.$$

By combining these properly it is easy to see that we can construct basic arrays of the form

$$\begin{bmatrix}1\\ 1\\ -1\\ -1\end{bmatrix}(-)^{l_3}\quad\text{and}\quad\begin{bmatrix}1\\ -1\\ -1\\ 1\end{bmatrix}(-)^{l_3},$$

which satisfy the strong conditions. As Anderson has already noted, the existence of this degeneracy shows that the spins are correlated only in planes. That is, the lattice points and xy face are correlated, as are the yz and zx faces, but they are not correlated with each other.

Interaction of Slow Electrons and Surface Films of Ionic Crystals

HAROLD JACOBS AND DIETRICH DOBIESCHEK
Thermionics Branch, Evans Signal Laboratory, Belmar, New Jersey
(Received August 14, 1950)

A study has been made of the interactions of slow electrons and thin films of potassium chloride evaporated on a nickel target. Experimental diodes were made up which contained a rotating anode, an oxide coated cathode, and a potassium chloride source. The ionic crystal was evaporated to the anode and the anode rotated to the place where the oxide coated cathode faced the alkali chloride deposit. Since electrical charges on the potassium chloride could enhance or lower the current from the cathode, a method was set up whereby the accumulation and release of charging could be studied. It was found that electrons could be trapped in the potassium chloride film and released by bombarding electrons at a critical kinetic energy. The energy of the electrons needed to release the trapped electrons was found to be very near the same energy required by photons, as described by Hilsch and Pohl in their work on F' centers in potassium chloride. It was concluded that the electron affinity of evaporated films of potassium chloride must be very small; i.e., <0.5 ev.

Another factor which the experiments brought out was that, at critical kinetic energies, the bombarding electrons caused dissociation of the film of compound coating the anode. It was found that when the electrons attained an energy equivalent to the heat of formation of the potassium chloride, decomposition of the alkali chloride occurred. This agrees with previous studies on oxides and points out that the same equivalence of electron energy and heat of formation holds for ionic crystals, such as potassium chloride, as holds for thin films of oxides.

I. INTRODUCTION

IN recent optical investigations of potassium chloride with a stoichiometric excess of potassium, it was found that at characteristic wavelengths of light, an absorption of photons and a simultaneous increase in the electrical conductivity of the material occurred. This selective photo-conductivity was thought to occur when the energy of the light was sufficient to free an electron from a trapped state. In potassium chloride, there was observed to be associated with excess potassium in the material an energy trap of about 2.3 ev. This type of trap was called an F center. Another type of trap, less sharp in definition, and showing a maximum absorption of light near 1.7 ev, was also observed. This lower energy trap was called an F' center. A description of these experiments can be found in the writings of Seitz,[1] Hilsch and Pohl,[2] and others.

In the following experiments, a method was developed in which the absorption of electrons by potassium chloride could be studied. The problems involved were first, to determine whether electron energy traps in surface films of potassium chloride could be detected by selective absorption of bombarding electrons, and second, to determine whether the energies at which electrons are absorbed would correspond to the energies of light absorption, as reported by Hilsch and Pohl.

Another question of interest is the mechanism of the decomposition of compounds upon electron bombardment. In the work of Headrick and Lederer,[3] and Jacobs,[4] it was proposed that surface films of oxides would decompose when bombarding electrons achieved a kinetic energy equivalent to the heat of formation of the oxide. This suggestion has not been tested quantitatively for ionic crystals such as potassium chloride. It was hoped that, by means of the following experiments, the energies of bombarding electrons required for decomposition of potassium chloride could be determined.

[1] F. Seitz, *Modern Theory of Solids* (McGraw-Hill Book Company, Inc., New York, 1940), pp. 558 to 575.
[2] R. Hilsch and R. W. Pohl, Z. Physik **59**, 812 (1930).
[3] L. B. Headrick and E. A. Lederer, Phys. Rev. **50**, 1094 (1936).
[4] H. Jacobs, J. Appl. Phys. **17**, 596 (1946).

II. EXPERIMENTAL METHOD

In order to detect the absorption of bombarding electrons, the following technique was used. Experimental tubes were constructed in which thin films of KCl could be evaporated upon the anode. The anode film could be rotated to a position very close to an oxide coated cathode operating at reduced temperatures (Fig. 1). The film was then bombarded by increasing the anode potential in 0.5 volt increments. At each voltage and current increase, a waiting period of a constant time was used. During this waiting period, at characteristic anode potentials, no change in cathode current took place. However, at other characteristic potentials (i.e., near 1.0 volt and 2.5 volts), it was sometimes observed that the cathode current would

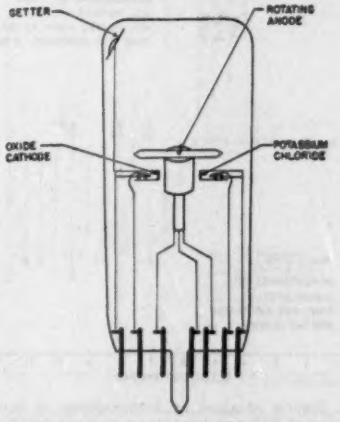

FIG. 1. Experimental tube.

drift upward, very slowly, until a new equilibrium current was reached. This drift upward in cathode current at critical energies was used as the means of determining the energies at which bombarding electrons were absorbed. As will be later demonstrated, the interpretation of the drift upward is as follows: In the KCl film there were assumed to be many F and F' centers in which electrons were trapped, especially since there was a source of electron emission close by (the heated oxide cathode). As the anode potential was increased, the bombarding electrons had a greater kinetic energy. At a critical kinetic energy, the bombarding electrons had sufficient energy to remove the bound electrons from their traps (i.e., as by an ionization process). This, in turn, left the surface of the KCl film with a slightly greater positive charge than the metal part of the anode. The increasing positive charge at the KCl surface could then cause an increase in cathode current until a new equilibrium was reached. To summarize the situation, in the case of rising emission, the interpretation we have used is that the rising emission is due to positive charging caused by the absorption of the energy of bombarding electrons.

In further increasing the anode potential, and thus the electron kinetic energy, another type of phenomena was observed and utilized. When the kinetic energy of the bombarding electrons reached the region of 4.5 ev to 5.0 ev, a very rapid falling emission was observed together with a relatively permanent deterioration of the cathode emission properties. Only by means of long and continued heating could the cathode regain its emission capabilities after the 4.5 ev to 5.0 ev bombardment of KCl films. This was interpreted as follows. When the kinetic energy of the electron attained the energy equivalent to the heat of formation of KCl (i.e., 4.5 ev) the KCl decomposed, releasing chlorine gas. The chlorine then combined with the free barium in the cathode, causing relatively permanent low emission.

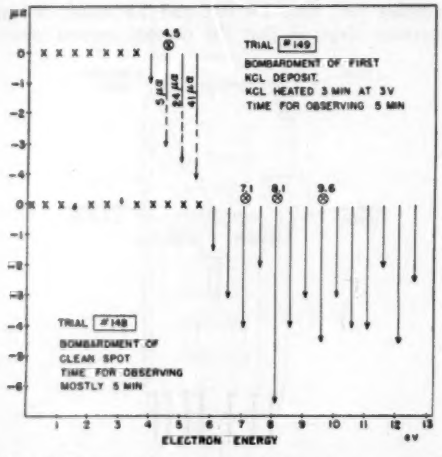

FIG. 2. Spectra obtained by bombardment of successively thicker layers of KCl contaminants on anode (tube 15). Change in cathode current *vs* electron energy.

Measurements could be made at still higher energies, if the waiting periods were kept small, to prevent complete deterioration of the cathode emission. At higher energies it was found that there were peaks of decomposition at various characteristic energies. For instance, for KCl there were peaks of decomposition at 5.0 ev, 7.0 ev, 9.0 ev, and 16.5 ev. This indicates that some sort of selective process occurs where the rates of decomposition increase at critical energies.

As to further details of the method, the design of the tube utilizing a rotating anode helped keep contaminations to a minimum. In addition, it was found that the energies of interaction were independent of thickness and current over a considerable range. Films were built up in successively thicker layers and measurements made following the deposition. Sometimes measurements were repeated several times before additional depositions. The oxide cathode was run at about 500°C during measurements, and currents used were in the order of 3 to 50 μamp. Small corrections were made in each case to obtain true electron energies instead of anode potential readings. Best results were obtained from films deposited on a clear portion of the anode, which was composed of high purity nickel. The estimated thicknesses of the KCl films were roughly 10^{-7} to 10^{-5} cm.

III. DATA

For the case of each experimental diode a run was made of cathode current *versus* anode potential. The anode potential was raised in 0.5 volt intervals with a waiting period of a constant time at each step (i.e., 5, 10, or 30 min). The drift in current, at a particular voltage, during the constant time interval, was then recorded. In Fig. 2 we see some representative graphs obtained in this process. The ordinate of the graph represents the amount and direction of cathode current drift during a waiting period of five minutes. The abscissa indicates the energy of the electrons during the waiting period. In trial #148 for instance, when bombarding the clear portion of the anode, there was very little drifting in the five-minute waiting periods until about 6 ev. Starting at 6 ev there was a tendency for falling emission at each half-volt interval. The indications here are that even a clear portion of the anode has some contamination. In trial #149, a very thin layer of KCl was evaporated over the clear portion of the anode and then rotated in front of the cathode. We see no rising or falling current up to 4.0 to 4.5 ev. However, at 4.0 volts there was a change in cathode current, a decrease of one microampere during the five-minute waiting period. When the electron energy was increased to 4.5 ev, a 5-μamp decrease in cathode current was noticed during the five-minute waiting

interval. The very strong slumping probably started in the region of 4.5 ev.

In Fig. 3, trial #150, additional KCl was evaporated on the anode and measurements made. At 0.5 ev a rising cathode current was noticed during the five-minute waiting period, the rise in current being 2.5 μamp. Another peak in rising was recorded at 2.0 ev. The change in current in five minutes was one μamp, with the current rising. At 4.5 ev a slumping of 1.5 μamp was noticed in two minutes. In trial #151, we have a repetition of trial #150, and in trial #152 there is recorded the change of current as a function of energy, with a five-minute waiting period, for another deposit. In these trials we notice the following, which was found to be generally true in the experiments. At 0.5 ev, 1.0 ev, and 1.5 ev, the change in current during the five-minute waiting period indicated a rising emission. At an energy near 2.5 ev we sometimes obtained slumping emission, but the energy at which the drifting occurred has usually been constant. The amount of rising emission at the lower energies was found to be somewhat dependent on the thickness of the KCl, although the energy for interactions was not. It can also be seen that the energy for the heavy slumping is about 4.5 ev to 5.0 ev. This too was found to be independent of thickness over a considerable range.

If the rising current near 1.0 ev indicates a positive charging of the KCl due to ionization by bombarding electrons, there exists an indication that nearly the same energy is required by an electron to ionize an F' center as is required by a photon. The changes in cathode current caused by 2.5 ev electrons were relatively smaller in magnitude and more often resulted in a decrease in cathode current. This disturbance corresponds to the absorption of 2.3 ev photons by F centers. The large slumping emission at about 4.5 ev corresponds to the heat of formation of KCl (about 4.5 ev). The 4.5 ev slumping demonstrates that, for KCl, the principle is valid that a bombarding electron with energy equal to the heat of formation of the compound will cause the KCl to decompose.

IV. FURTHER DISCUSSION

The experiments described above can provide us with some quantitative estimates which are useful in testing the hypothesis made in the introduction of this writing. Let us assume that, in equilibrium, there must be electrons trapped in the KCl. These electrons may be described as being in such states as an F center or an F' center. Most recent thinking on the subject indicates that for F centers the electrons are trapped in vacancies in the lattice caused by the missing electronegative element, such as chlorine. F' centers are the result of two electrons trapped in the vacant lattice position. In addition, it is likely that the trapped electrons are in the F' state because of the presence of a nearby heated cathode, which would provide an excess of electrons. Suppose electrons should fall on the film of material, their energies being sufficient to release the trapped electrons from their F' state. A charge would then develop such that there would be a slightly more positive potential on the surface of the KCl than on the surface of the metal. This would affect the emission current in the diode. To calculate the density of surface charges required for an increase of one electron volt applied to the incoming electrons, we can assume a thickness of 10^{-5} cm of KCl.

Using the following relationship:

$$V_2 - V_1 = (4\pi\sigma/K)a, \tag{1}$$

where

$\sigma = N_0 e$, e = electron charge $= 4.8\times10^{-10}$

N_0 = No. of surface charges on the KCl layer/cm^2,

K = dielectric constant $\cong 5$,

a = thickness of KCl layer, the distance from the surface of the KCl to the base metal of the anode, 10^{-5} cm,

$V_2 e - V_1 e = (4\pi N_0 e^2/K)a$,

$N_0 = K\times1.6\times10^{-12}/4\pi e^2 a = 2.8\times10^{11}$, and

$V_2 e - V_1 e = 1$ electron volt $= 1.6\times10^{-12}$ erg.

This means, if we have 2.8×10^{11} traps on the surface and they are all charged positively, a difference in potential of one volt will appear from the base metal to the surface of the KCl, and the electron stream will behave as though an additional volt were applied.

If we assume that these surface traps occupy a thickness of 10^{-8} cm, a concentration of traps per unit volume would be $\cong 2.8\times10^{19}$. Actually, in our experi-

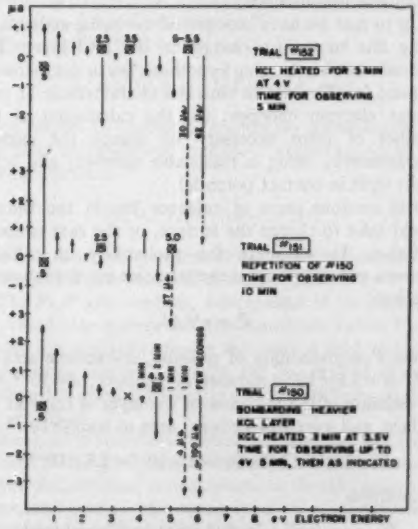
TRIAL #152
KCL HEATED FOR 5 MIN AT 4 V
TIME FOR OBSERVING 5 MIN
TRIAL #151
REPETITION OF #150
TIME FOR OBSERVING 10 MIN
TRIAL #150
BOMBARDING HEAVIER KCL LAYER
KCL HEATED 3 MIN AT 3.5 EV
TIME FOR OBSERVING UP TO 4V 5 MIN, THEN AS INDICATED
ELECTRON ENERGY

FIG. 3. Spectra obtained by bombardment of successively thicker layers of KCl contaminant on anode (tube 15). Change in cathode current vs electron energy.

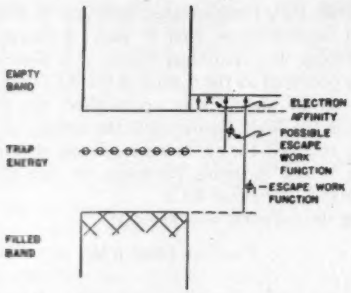

FIG. 4. Schematic energy-level diagram of an insulator. The zero of potential is assumed to be slightly above the bottom of the empty band. The work function for inserting an electron is much smaller than removing an electron from the filled band or from the traps. (From Seitz, reference 1, page 400.)

ments differences corresponding to 0.1 volt were estimated by the effect on the cathode emission, which would place the trap density at about 10^{13}/cc, an entirely reasonable number. The number of traps on the surface would be 2.8×10^{10}/cm² under the conditions of our experiment. The estimate of charging at 0.1 volt was based on measuring the effect on the cathode current–anode voltage characteristic. This characteristic shows that a slight increase in anode potential causes a slight increase in emission current. By observing the rising emission, and the tube emission characteristic, the potential change on the anode could be estimated and 0.1 volt was usually found. The value of 0.1 volt checks well with a shift in contact potential, which was also observed.

Up to now we have interpreted the rising emission as being due to surface charges in the KCl layer. The evidence for the charging hypothesis lies in the following factors: (a) The rise in emission characteristic at particular electron energies; (b) the calculation of the number of traps necessary to change the current characteristic, being a reasonable number; and (c) a slight shift in contact potential.

Still another piece of evidence lies in the time it would take to charge the surface, or the rate of rising emission. To calculate the probability of collision between one electron and the traps, we use the following relation:

$$P_c = \sigma N A d, \tag{2}$$

where P_c = probability of collision, A = surface area = 1 cm², $N = 2.8\times10^{15}$ = number of traps/cc, $d = 10^{-8}$ cm, an estimate of the thickness of the layer of traps at the surface, and σ = cross-sectional area of trap[5] $\cong 10^{-15}$.

$$P_c = 10^{-15}\times2.8\times10^{13}\times1\times10^{-8} = 2.8\times10^{-6}.$$

In addition,

$$50\ \mu\text{amp/cm}^2 = 3\times10^{14}\ \text{particles/second/cm}^2.$$

This means, that if $P_c = 2.8\times10^{-6}$, and 3×10^{14} particles/sec/cm² (50 μamp/cm²) strike the surface, then there are $\cong10^{10}$ collisions per second, initially.

At the surface of the KCl, that is, to a depth of 10^{-8} cm, the number of non-ionized traps is 2.8×10^{10}. As the surface is bombarded by electrons with sufficient energy for ionization of the traps, the number of non-ionized traps decreases as follows:

$$dn/dt = -\alpha n, \tag{3}$$

where n = number of F' centers in a non-ionized state at the surface of the KCl/cm², and t = time in seconds.

It has been shown that $dn/dt \cong -10^{10}$, initially, and $n = 2.8\times10^{10}$, initially. Solving for α, we find $\alpha = 1/2.8$.

The fraction of traps which has not been ionized is given in the following relation:

$$n/N_0 = \epsilon^{-\alpha t}, \tag{4}$$

where N_0 = initial number of traps/cm² = 2.8×10^{10}, t = time in seconds, and $\alpha = 1/2.8$.

Thus in 2.8 sec, 63.2 percent of the traps have been ionized, and in 11.2 sec, 98.2 percent of the traps have been ionized and charged positively.

In practice it was found that the time for charging was in the order of 60 sec before a new equilibrium was reached. Hence, the rate of charging is a fourth piece of evidence which quantitatively points to the rising emission at critical energies being due to the release of electrons from trapped states near the surface.

V. CONCLUSIONS

(a) The decomposition of KCl films upon electron bombardment occurs in a similar manner to that of oxide films. When the kinetic energy of the electron approaches the heat of formation of the chloride, the compound decomposes, liberating chlorine. This process occurs at 4.5 to 5.0 electron volts.

(b) The traps in potassium chloride can be detected by electrical methods. At critical voltages a slight positive charging of the surface has been noted, which can be attributed to the emptying of the traps. The energies of electron absorption are nearly equal to the energies of photon absorption. However, the electron absorption is primarily a surface effect while the photon absorption is a volume effect. It is of interest to note that there is an equivalence of energy when comparing electrons and photons in their interaction with these materials. From the band scheme point of view this could only occur if the electron affinity were very small (Fig. 4).

In the band scheme, the electron would be accelerated by an energy X as it entered the material. The difference in the optical and electron energies for the same transition would be equal to X. Since the electron and optical energies are almost equivalent, X must be smaller than 0.5 volt for the case of films of KCl evaporated in vacuum.

Acknowledgment should be made to Dr. J. E. Gorham and to Mr. G. R. Kilgore for their aid during the preparation of this work.

[5] Mott and Gurney, *Electronic Processes in Ionic Crystals* (Oxford University Press, London, 1948), p. 131.

Conservation Laws in the General Theory of Relativity with Electromagnetic Field*

HENRY ZATZKIS
Departments of Mathematics and Physics, Syracuse University, Syracuse, New York

(Received November 13, 1950)

The principal result of this paper is the reformulation of the so-called strong conservation laws of the general theory of relativity with electromagnetic field, resulting in relationships between closed two-dimensional surface integrals in ordinary three-dimensional space. This formulation is particularly useful if particles are represented as singularities of the field because it obviates the necessity for an examination of the detailed structure of the singularities themselves. This method has been used for determining the total energy (or mass) in a domain containing a Schwarzschild singularity. It turns out that the value of this energy depends on the choice of coordinate system unless the energy density is integrated over all of space, in which case the integral converges toward the expected value. In future papers the method of closed surface integrals will be applied to the rigorous treatment of the problem of motion.

I. INTRODUCTION

IN a series of papers[1-3] it has been shown that any covariant field theory that can be derived from a variational principle (least action principle) contains four differential identities between the field equations, which in relativity are known as the contracted Bianchi identities. As a result, the customary expression for the energy-momentum densities, which has a vanishing divergence in the event that the field equations are satisfied ("weak" conservation laws), can be supplemented by additional terms, vanishing when the field equations are satisfied, so that the divergence of the new expression vanishes identically even when the field equations are not satisfied ("strong" conservation laws).

In this paper, we shall show that, as a result of the strong conservation laws, there exists a set of components with three indices of which the supplemented energy-momentum densities are the divergences. The existence of these new quantities is equivalent to the strong conservation laws themselves. With their help, the total energy or linear momentum contained in a three-dimensional spatial domain can be expressed as a surface integral over the closed two-dimensional surface of the domain. We shall determine the explicit form of the three-indexed quantities for the theory of relativity with an electromagnetic field, and we shall then apply these expressions to the determination of the energy contained in a sphere at the center of which is located a point charge (a Schwarzschild singularity with electric charge). We shall find that, as long as the radius of the sphere is finite, the rigorous expression depends on the choice of coordinate system, a result which highlights the fact that in relativity energy and momentum do not have an invariant significance. If the radius of the sphere is permitted to increase to infinity, the total energy converges toward the expected value, the mass multiplied by c^2, regardless of the coordinate system chosen.

* This work was carried out under contract with the ONR. This paper incorporates the major results of a doctorate thesis submitted to the Graduate School, Syracuse University.

[1] P. G. Bergmann, Phys. Rev. 75, 680 (1949).

[2] P. G. Bergmann and J. H. M. Brunings, Revs. Modern Phys. 21, 480 (1948).

[3] Bergmann, Penfield, Schiller, and Zatzkis, Phys. Rev. 80, 81 (1950).

II. MATHEMATICAL BACKGROUND

It is assumed that the field equations can be derived from a variational principle of the form

$$\delta I=0, \tag{1}$$

$$I=\int_V L(y_A; y_{A,\mu})d^4x, \tag{2}$$

where, as usual, $y_{A,\mu}$ is short for

$$y_{A,\mu}=\partial y_A/\partial x^\mu \quad (A=1, \cdots N;\ \mu=1\cdots 4).$$

The variations of the N field variables y_A are arbitrary except that they must remain confined to the interior of the four-dimensional domain V.

The resulting field equations are

$$L^A\equiv(\partial L/\partial y_A)-(\partial L/\partial y_{A,\rho}),_\rho=0. \tag{3}$$

With respect to finitesimal coordinate transformations, the field variables will transform according to a law having the form

$$\bar\delta y_A=F_{A\rho}{}^{B\nu}\xi^\rho,_\nu y_B-y_{A,\rho}\xi^\rho. \tag{4}$$

The four functions ξ^ρ represent the infinitesimal changes of the coordinate values of a fixed world point.

The $F_{A\rho}{}^{B\nu}$ are numbers, independent of the choice of the coordinate system and the coordinate values themselves, but characteristic for the type of field variables representing the field. Finally, the $\bar\delta y_A$ are the changes produced in the field variables y_A as functions of their arguments x^ρ.

Being an infinitesimal transformation law, Eq. (4) is subject to the group requirement that the commutator of two infinitesimal transformations should again be a transformation of the same type. This condition is represented by the condition on the F

$$F_{A\rho}{}^{C\nu}F_{C\rho}{}^{B\sigma}-F_{A\rho}{}^{C\sigma}F_{C\rho}{}^{B\nu}=\delta_\rho{}^\nu F_{A\rho}{}^{B\sigma}-\delta_\rho{}^\sigma F_{A\rho}{}^{B\nu}. \tag{5}$$

The general covariance of the field equations is assured if the lagrangian transforms merely by adding a complete divergence under an infinitesimal coordinate transformation.

An immediate consequence of the required covariance of the field equations is the existence of four differential identities between their left-hand sides L^A,

$$(F^{B\rho}{}_{A\sigma}y_B L^A)_{,\rho}+y_{A,\mu}L^A\equiv 0. \tag{6}$$

In the general theory of relativity these identities are known as the contracted Bianchi identities.

III. WEAK AND STRONG CONSERVATION LAWS

If the field equations are satisfied, there exist sixteen quantities $t_\sigma{}^\rho$:

$$t_\sigma{}^\rho=L\delta_\sigma{}^\rho-y_{A,\sigma}\partial L/\partial y_{A,\rho}, \tag{7}$$

functions of the field variables and their first derivatives only, which satisfy four ordinary (not covariant) divergence relationships:

$$t^\rho{}_{\sigma,\rho}=0. \tag{8}$$

A remark is here in order as to how we shall represent the presence of matter. In the absence of detailed knowledge of the structure of matter, we shall either describe it by a set of N continuous and differentiable functions R^A (as is done in hydrodynamics), or else by singularities in the field.

If we adopt the first alternative, then the field equations are (analogous to the poisson equation)

$$L^A=R^A. \tag{9}$$

The right-hand side of Eq. (8) no longer vanishes, but we obtain instead

$$t^\rho{}_{\sigma,\rho}=y_{A,\sigma}R^A=y_{A,\sigma}L^A. \tag{10}$$

Because of the existence of the differential identities, Eq. (6), this right-hand side can also be given the form of a divergence. Equation (10) may be written in the form

$$T^\rho{}_{\sigma,\rho}\equiv 0, \tag{11}$$

where $T_\sigma{}^\mu$ are the expressions

$$T^\rho{}_\sigma=\delta^\rho{}_\sigma L-y_{A,\sigma}(\partial L/\partial y_{A,\rho})+F^{B\rho}{}_{A\sigma}L^A y_B. \tag{12}$$

Equations (11) with Eq. (12) represent the "strong" conservation laws. Of course, they go over into the "weak" form, Eq. (8), if the field equations (3) are satisfied.

IV. THE SURFACE INTEGRALS

We shall utilize the strong conservation laws to obtain for the "energy" and the "linear momentum" contained within a three-dimensional region a representation by two-dimensional surface integrals. By so so doing we can avoid the necessity for a penetration into singular regions (if we represent matter in the form of singularities of the field).

From the existence of the strong conservation laws

$$T^\rho{}_{\sigma,\rho}\equiv 0, \tag{11}$$

we can infer the existence of certain functions $U_\sigma{}^{[\rho\tau]}$, which are antisymmetric in the indices ρ and τ, such that

$$T^\rho{}_\sigma=U^{[\rho\tau]}{}_{\sigma,\tau}. \tag{13}$$

The quantities $U^{[\rho\tau]}{}_\sigma$ are not determined uniquely by the requirement (13). We can always add to them other quantities whose integrals over any closed surface vanish identically; i.e., we can set

$$\bar{U}^{[\rho\tau]}{}_\sigma=U^{[\rho\tau]}{}_\sigma+V^{[\rho\tau\omega]}{}_{\sigma,\omega}, \tag{14}$$

where $V^{[\rho\tau\omega]}{}_\sigma$ is completely antisymmetric in the three upper indices ρ, τ, and ω, but otherwise is arbitrary. Then,

$$V^{[\rho\tau\omega]}{}_{\sigma,\omega\rho}\equiv 0. \tag{15}$$

Such quantities $V^{[\rho\tau\omega]}{}_\sigma$ are not difficult to construct. If we start with a completely arbitrary field $Z_{\tau\omega}$, then

$$V^{\rho\tau\omega}{}_\sigma=\delta^{\rho\tau\omega\alpha}Z_{\tau\omega}. \tag{16}$$

However, this generalization of the quantities $U^{[\rho\tau]}{}_\sigma$ has no effect on the values of the surface integrals, since the integrals of the additional terms vanish over any closed surface.

We shall rewrite the divergence Eq. (11) by separating the spatial and time components. Latin indices will denote space coordinates and 4 denotes time.

$$T^\rho{}_{\sigma,\rho}=T^4{}_{\sigma,4}+T^\tau{}_{\sigma,\tau}\equiv 0. \tag{17}$$

Now assume "particles" to be defined by isolated three-dimensional regions where the field equations of empty space are not satisfied. Consider a closed two-dimensional surface enclosing such a region in ordinary three-dimensional space. We integrate Eq. (17) over that region and obtain by means of the gauss theorem

$$(d/dt)\int\int\int T_\sigma{}^4 d^3x+\oint\oint T_\sigma{}^\tau n_\tau dS=0. \tag{18}$$

But, since we have

$$\int\int\int T^4{}_\sigma d^3x=\int\int\int U^{[4\alpha]}{}_{\sigma,\alpha}d^3x$$

$$=\oint\oint U^{[4\alpha]}{}_\sigma n_\alpha dS, \tag{19}$$

we finally obtain four conservation laws:

$$(d/dt)\oint\oint U^{[4\sigma]}{}_{\sigma}n_{\sigma}dS+\oint\oint T^{\nu}{}_{\sigma}n_{\sigma}dS=0,\qquad(\sigma=1,2,3,4),\quad(20)$$

which contains surface integrals only. The quantities $T^{\nu}{}_{\sigma}$ in Eq. (20) play the role of flux vectors or "Poynting vectors" across the two-dimensional surface.

In those regions where the field equations are satisfied, the $T^{\nu}{}_{\sigma}$ go over into the much simpler expressions $t^{\nu}{}_{\sigma}$. Thus the four conservation laws, Eq. (20), assume the form

$$(d/dt)\oint\oint U^{[4\sigma]}{}_{\sigma}n_{\sigma}dS+\oint\oint t^{\nu}{}_{\sigma}n_{\sigma}dS=0.\quad(21)$$

The four quantities which are conserved are, therefore,

$$P_{\nu}=\oint\oint U^{[4\nu]}n_{\sigma}dS,\quad(22)$$

P_{ν}="linear momenta," P_4="energy" (or "mass").

In general, the values of the surface integrals, given by Eqs. (22), will depend on the surface chosen, if matter is represented by a density distribution. A sufficient requirement that the surface integrals are independent of the surface chosen would be that

$$t^{\nu}{}_{\sigma,\nu}=0,\quad(23)$$

or

$$U^{[4\sigma]}{}_{,\sigma}=0;\quad(24)$$

but this condition is ordinarily not satisfied; hence, empty space will in general have an energy and linear momentum density.

V. THE SURFACE INTEGRALS IN THE GENERAL THEORY OF RELATIVITY

We shall now derive the explicit expressions for the quantities $U^{[\sigma\tau]}{}_{\sigma}$ in the general theory of relativity for the case of combined gravitational and electromagnetic fields. We start with the defining Eq. (12). In our case the lagrangian L is the sum of two terms

$$L=L_{\text{grav}}+L_{\text{el}}=L_1+L_2,\quad(25)$$

with

$$L_1=(c^3/16\pi\kappa)(-g)^{\frac{1}{2}}g^{\mu\nu}(\Gamma^{\sigma}{}_{\mu\sigma}\Gamma^{\rho}{}_{\mu\nu}-\Gamma^{\sigma}{}_{\mu\rho}\Gamma^{\rho}{}_{\nu\sigma})$$
$$=(c^3/16\pi\kappa)\Lambda^{(\alpha\beta)\rho,\,(\gamma\delta)\sigma}g_{\alpha\beta,\rho}g_{\gamma\delta,\sigma},\quad(26)$$

and

$$L_2=-(-g)^{\frac{1}{2}}\Phi_{\mu}\Phi^{\mu\nu}/16\pi c=-Y^{\mu\rho,\,\nu\sigma}\Phi_{\mu,\rho}\Phi_{\nu,\sigma}/16\pi c,\quad(27)$$

where

$$F^{(\gamma\delta)\rho}{}_{(\alpha\beta)\sigma}=F_{\text{grav}}{}^{B\rho}{}_{A\sigma}=-\tfrac{1}{2}(\delta^{\gamma}{}_{\alpha}\delta^{\rho}{}_{\beta}\delta^{\delta}{}_{\sigma}+\delta^{\gamma}{}_{\beta}\delta^{\delta}{}_{\alpha}\delta^{\rho}{}_{\sigma}$$
$$+\delta^{\delta}{}_{\beta}\delta^{\rho}{}_{\alpha}\delta^{\gamma}{}_{\sigma}+\delta^{\delta}{}_{\alpha}\delta^{\rho}{}_{\beta}\delta^{\gamma}{}_{\sigma}),\quad(28a)$$

$$F^{\gamma\rho}{}_{\mu\sigma}=F_{\text{el}}{}^{B\rho}{}_{A\sigma}=-\delta^{\rho}{}_{\mu}\delta^{\gamma}{}_{\sigma},\quad(28b)$$

and the coefficients of the quadratic forms are

$$\Lambda^{(\alpha\beta)\rho,\,(\gamma\delta)\sigma}=\tfrac{1}{2}(-g)^{\frac{1}{2}}\{g^{\alpha\beta}(g^{\gamma\rho}g^{\delta\sigma}+g^{\delta\rho}g^{\gamma\sigma})$$
$$+g^{\gamma\delta}(g^{\alpha\rho}g^{\beta\sigma}+g^{\alpha\sigma}g^{\beta\rho})$$
$$+g^{\rho\sigma}(g^{\alpha\gamma}g^{\beta\delta}+g^{\beta\gamma}g^{\alpha\delta}-2g^{\alpha\beta}g^{\gamma\delta})$$
$$-g^{\alpha\sigma}(g^{\beta\gamma}g^{\delta\rho}+g^{\beta\delta}g^{\gamma\rho})-g^{\beta\sigma}(g^{\alpha\gamma}g^{\delta\rho}+g^{\alpha\delta}g^{\gamma\rho})\},\quad(29a)$$

and

$$Y^{\mu\rho,\,\nu\sigma}=2(-g)^{\frac{1}{2}}(g^{\mu\nu}g^{\rho\sigma}-g^{\mu\sigma}g^{\rho\nu}).\quad(29b)$$

Making the indicated substitutions in Eq. (12), one obtains

$$T^{\nu}{}_{\sigma}=A^{[\nu\tau]}{}_{\sigma,\tau}-((-g)^{\frac{1}{2}}\Phi^{[\nu\tau]})_{,\tau}/4\pi c,\quad(30)$$

where

$$A^{[\nu\tau]}{}_{\sigma}=(c^3/32\pi\kappa)(-g)^{\frac{1}{2}}[g_{\omega\lambda,\,\sigma}-g_{\omega\sigma,\,\lambda}]$$
$$\cdot[\delta^{\nu}{}_{\sigma}(g^{\tau\rho}g^{\omega\lambda}-g^{\tau\lambda}g^{\omega\rho})+\delta^{\tau}{}_{\sigma}(g^{\nu\lambda}g^{\omega\rho}-g^{\nu\rho}g^{\omega\lambda})$$
$$+\delta^{\omega}{}_{\sigma}(g^{\nu\rho}g^{\tau\lambda}-g^{\nu\lambda}g^{\tau\rho})].\quad(31)$$

This expression has already been derived by Freud.[4] And thus we finally obtain the following expressions for the quantities $U^{[\nu\tau]}{}_{\sigma}$:

$$U^{[\nu\tau]}{}_{\sigma}=A^{[\nu\tau]}{}_{\sigma}-(-g)^{\frac{1}{2}}\Phi_{\sigma}\Phi^{[\nu\tau]}/4\pi c.\quad(32)$$

In particular, we obtain

$$U^{[4m]}{}_{4}=(c^3/32\pi\kappa)(-g)^{\frac{1}{2}}(g_{\alpha\sigma,\,\rho}-g_{\alpha\rho,\,\sigma})g^{\alpha\rho}g^{\sigma\sigma}$$
$$-[(-g)^{\frac{1}{2}}/4\pi c]\Phi_4\Phi^{[4m]},\quad(33a)$$

$$U^{[4m]}{}_{\tau}=(c^3/32\pi\kappa)(-g)^{\frac{1}{2}}[(g_{\tau\sigma,\,\rho}-g_{\tau\rho,\,\sigma})\delta^{m}{}_{\tau}g^{\tau\rho}g^{4\sigma}$$
$$+(g_{\tau\sigma,\,\rho}-g_{\tau\rho,\,\sigma})g^{4\rho}g^{m\sigma}]-[(-g)^{\frac{1}{2}}/4\pi c]\Phi_{\tau}\Phi^{[4m]}.\quad(33b)$$

VI. THE SCHWARZSCHILD SINGULARITY

In order to illustrate the preceding developments we shall compute P_4 for a spherically symmetric charged mass point at rest, the so-called Schwarzschild singularity. The solution of the field equations, in quasi-cartesian coordinates, is[5]

$$g_{44}=1-(2\kappa m/rc^2)+\kappa e^2/r^2c^4,\quad(34a)$$

$$g_{4\sigma}=0,\quad(34b)$$

$$g_{\tau\sigma}=(1/c^2)[-\delta_{\tau\sigma}+(g_{44}-1)\xi^{\tau}\xi^{\sigma}/g_{44}r^2],\quad(34c)$$

$$\Phi_4=-c\epsilon/r.\quad(34d)$$

On making the indicated substitutions one obtains

$$P_4=mc^2-3\epsilon^2/2r.\quad(35)$$

Equation (35) shows that *in this coordinate system* the purely gravitational field does not contribute to the

[4] Ph. von Freud, Ann. Math. **40**, 417 (1939).

[5] P. G. Bergmann, *Introduction to the Theory of Relativity* (Prentice-Hall, Inc., New York, 1946), p. 204.

field energy. The gravitational mass (and energy) resides entirely at the position of the singularity. However, when P_4 is computed for the purely gravitational field by the use of "isotropic" coordinates,[6] one obtains

$$P_4=mc^2(1-\kappa m/2rc^2). \quad (36)$$

[6] R. C. Tolman, *Relativity, Thermodynamics and Cosmology* (Clarendon Press, Oxford, England, 1934), Eq. (82.14), p. 205.

By a mere change of the coordinate system we have achieved a field in which part of the gravitational mass resides in the field. Only if viewed from an infinite distance does P_4 yield the total mass, m, of the singularity.

The author wishes to express his sincere gratitude to Professor Peter Bergmann, who suggested this problem

PHYSICAL REVIEW VOLUME 81, NUMBER 6 MARCH 15, 1951

Electron Loss Cross Sections for Hydrogen Atoms Passing through Hydrogen Gas

J. H. MONTAGUE
Department of Physics and Institute for Nuclear Studies, University of Chicago, Chicago, Illinois
(Received November 7, 1950)

Measurements have been made of the electron loss cross section in hydrogen gas for hydrogen atoms moving with kinetic energies between 45 kev and 329 kev. At these two limiting energies the values of the cross section were $6.6_8\times10^{-17}$ cm^2 and $2.2_1\times10^{-17}$ cm^2, respectively, with an error of plus or minus 10 percent. Between 120 kev and 329 kev the cross section was found to vary approximately as E^n, where E is the kinetic energy of the atom, and n is -0.70 ± 0.05.

I. INTRODUCTION

STUDIES of electron capture and loss by light ions passing through matter are of interest for a more complete understanding of the phenomena themselves, and are necessary for an interpretation of experimental range-energy curves at low energies. Furthermore, they are of interest in that they play an important role in the stopping of fission fragments, where the charge of the fragment plays an important part.

General surveys of the work done on capture and loss have been given by Knipp and Teller[1] and by Bohr.[2] Previous experimental investigations have been made using either hydrogen canal rays,[3-6] or high energy alpha-particles from radioactive sources.[7-9] Consequently, for particle energies of from 25 kev to about one Mev few data are available. Recently, Hall[10] has helped to fill this gap by his study of the ratio of the charged to neutral component in hydrogen ion beams of energies between twenty and four hundred kev passing through metallic media. The present paper gives values of the electron loss cross section in hydrogen for hydrogen atomic beams with energies in about the same range.

In this experiment a collimated beam of protons was passed through a thin aluminized-nitrocellulose window into an electron-exchange chamber, which could be evacuated to a pressure at which the mean free path for collision was more than ten times the diameter. The beam emerging from the window consisted of both a charged and a neutral component, owing to capture and loss processes taking place in the window material. The charged particles were deflected away by a magnetic field in which the electron-exchange chamber was situated; the neutral particles, however, continued across the chamber and into a detector.

When hydrogen gas at low pressure was introduced into the chamber, some of the moving atoms in the neutral beam lost their planetary electron in collisions with the hydrogen atoms in the gas, and were then deflected by the magnetic field so that they no longer entered the detector. Assuming that all neutral particles which undergo a charge change will fail to enter the detector (this assumption will be examined more critically later), it is clear that the number of particles $N(p)$ arriving at the detector when the electron-exchange chamber is filled with hydrogen gas at a pressure p millimeters of mercury is given by

$$(p)\equiv N(p)/N(0)=\exp(-N(p)\sigma_i d) =\exp[(-19.21\times10^{18}p\sigma_i d)/T], \quad (1)$$

where $N(0)$ is the number of particles entering the detector when the chamber is evacuated, $n(p)$ is the number of atoms per cc in the gas, T is the absolute temperature of the gas, d is the path length for the moving particles (i.e., the distance from the entrance window to the detector), and σ_i is the electron loss cross section per atom of hydrogen for atoms of the energy under consideration.

[1] J. Knipp and E. Teller, Phys. Rev. **59**, 659 (1941).
[2] N. Bohr, *The Penetration of Atomic Particles through Matter* (Det. Kgl. Danske Videnskabernes Selskab, 1948).
[3] E. Ruchardt, Ann. Physik **71**, 377 (1923).
[4] A. Ruttenauer, Z. Physik **4**, 267 (1921).
[5] H. Bartels, Ann. Physik **13**, 373 (1932).
[6] H. Meyer, Ann. Physik **30**, 635 (1937).
[7] E. Rutherford, Phil. Mag. **47**, 277 (1924).
[8] P. Kapitza, Proc. Roy. Soc. (London) **106**, 602 (1924).
[9] G. Henderson, Proc. Roy. Soc. (London) **109**, 157 (1925).
[10] T. Hall, Phys. Rev. **79**, 504 (1950).

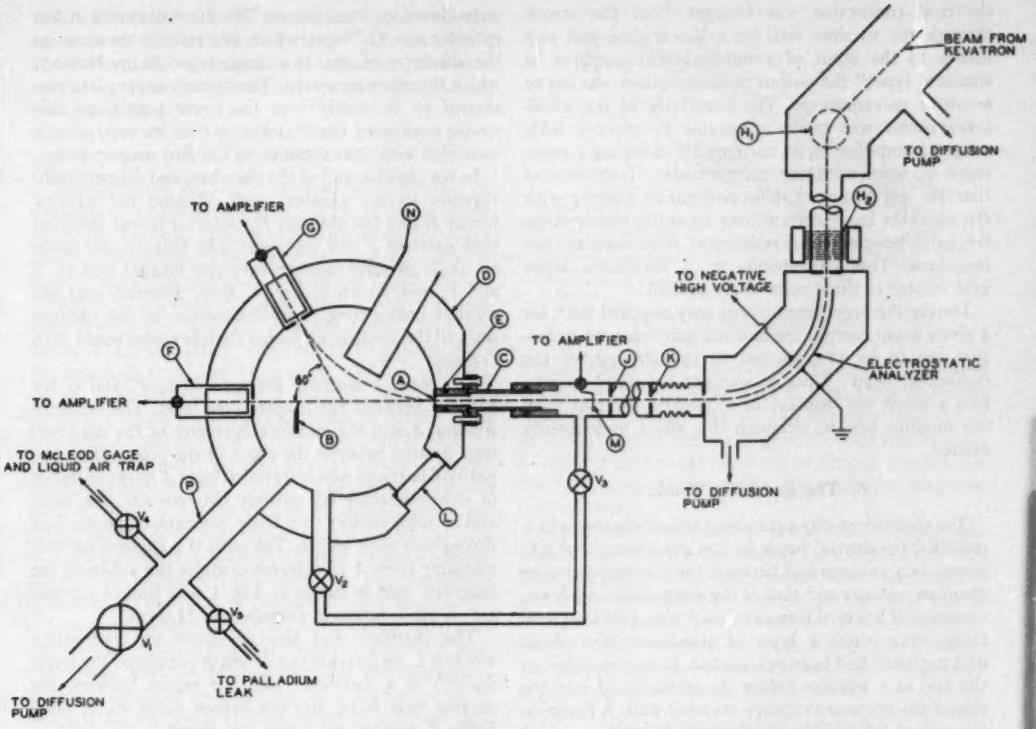

FIG. 1. Apparatus, schematic.

II. DESCRIPTION OF THE APPARATUS

Figure 1 is a schematic diagram of the experimental arrangement; the items labeled by letters in the figure will be identified and referred to in the following paragraphs.

(A) Production and Collimation of the Proton Beam

The source of energetic hydrogen ions was the University of Chicago 400-kev Cockcroft-Walton accelerator, or kevatron, which is described elsewhere.[11–13] The kevatron beam was first analyzed by the vertical magnetic field H_1 (Fig. 1) and the selected component (either the proton beam or the molecular-hydrogen-ion beam) directed down a 1.28-meter tube to the entrance of an electrostatic analyzer. Accurate positioning of the beam was accomplished by adjustments of the magnetic field H_1 and of the weak horizontal magnetic field H_2. The purpose of the electrostatic analyzer was to provide an accurate estimate of the beam energy in terms of the potential difference between the deflecting plates necessary to bend the beam around the analyzer and into the collimating assembly. This analyzer was one which has been described previously in the literature;[12,14] for this experiment it was calibrated against another electrostatic analyzer used in this laboratory, the construction and calibration of which have been given elsewhere.[15]

After leaving the electrostatic analyzer, the ion beam passed into the collimating assembly. This consisted of two circular brass diaphragms, J and K, with openings 0.158 cm in diameter, separated by 13.33 cm. The collimating tube was connected to the output of the analyzer by a flexible coupling for ease in alignment. From the collimator the beam travelled a distance of about 10 cm to the entrance window A, and through it into the electron-exchange chamber. An insulated monel wire screen M of 34 percent transmission was located just beyond the final collimating diaphragm and was used to collect a portion of the beam for monitoring purposes. The amount of beam so collected was usually between 0.05×10^{-3} and 1×10^{-3} μamp. An

[11] Allison, del Rosario, Hinton, and Wilcox, Phys. Rev. **71**, 139 (1947).
[12] L. del Rosario, Phys. Rev. **74**, 305 (1948).
[13] A. H. Morrish, Phys. Rev. **76**, 1653 (1949).
[14] Allison, Skaggs, and Smith, Phys. Rev. **57**, 550 (1940).
[15] Allison, Frankel, Hall, Montague, Morrish, and Warshaw, Rev. Sci. Instr. **20**, 735 (1949).

electrical connection was brought from the screen through the vacuum wall by a Kovar-glass seal and thence to the input of a direct-current amplifier of standard type;[16] the output of the amplifier was fed to a mirror galvanometer. The sensitivity of the whole arrangement was easily adjustable to cover a wide range of amplifier input currents by changing a resistance in series with the galvanometer. Tests showed that the galvanometer deflection varied linearly with the amplifier input current over its entire usable range for galvanometer series-resistances from zero to two megohms. This corresponds to a maximum input grid-voltage of three volts above ground.

During the experiment it was only required that, for a given beam energy, the monitor galvanometer deflection should be proportional to the strength of the collimated beam. Thus, it was not necessary to take into account the emission of secondary electrons from the monitor screen, although this effect undoubtedly existed.

(B) The Entrance Window

The aluminized-nitrocellulose entrance window, which provided the neutral beam for the experiment and also served as a vacuum seal between the electron-exchange chamber vacuum and that of the electrostatic analyzer, consisted of a film of nitrocellulose,[17] about 0.01 mg/cm² thick, over which a layer of aluminum (also about 0.01 mg/cm²) had been evaporated. It was mounted on the end of a window holder, E, which fitted into the side of the electron-exchange chamber wall. A flange on the end of the window holder opposite that on which the window was mounted bolted to a sliding coupling C, which facilitated the changing of windows. Since the windows were very fragile, a bypass line (between valves V_2 and V_3 in Fig. 1) was provided in order to eliminate pressure differences across the window during evacuations.

The aluminum coating on the window was in electrical contact with the window holder and prevented the building up of charge on the window as the beam passed through it. At first, windows without such conducting aluminum layers were used and it was found that they quickly broke when bombarded by a beam, even when their thickness was as high as 0.03 mg/cm². The aluminum prevented such breakages, however, and some of the foils coated with it have lasted as long as seventy-five hours under the proton beam.

(C) The Electron-Exchange Chamber

The electron-exchange chamber was a hollow cylinder of bronze, 3.17 cm high, the top and bottom of which were closed by brass plates. The inner diameter of the cylinder was 12.70 cm, which was exactly the same as the diameter of the two magnet pole-faces between which the chamber rested. The bottom cover plate was shaped to fit snugly over the lower pole face; this device positioned the chamber so that its vertical axis coincided with that common to the two magnet poles.

In the circular wall of the chamber, and diametrically opposite to one another, were situated the window holder E and the detector F. Detector G was identical with detector F and was located so that its axis made an angle of sixty degrees with the mutual axis of E and F, and shown in Fig. 1. Both detectors and the window holder were easily removable, as the vacuum seals to the electron-exchange chamber were made with O-rings.

The plane containing the axes of E, F, and G lay halfway between the magnet pole faces. The entrance window A and the entrance apertures of the detectors were located between the edges of the poles. Thus, the paths of particles which travelled from A to the entrance of either detector lay entirely between the pole faces and so were subject to a fairly constant magnetic field throughout their length. The path of a charged particle traveling from A to detector G under the action of the magnetic field is shown in Fig. 1 as a broken circular arc; it has a radius of curvature of 11.0 cm.

The chamber wall also contained an observation window L, an internal can N which permitted the introduction of a fluxmeter into the region between the magnet pole faces, and the bypass valve V_3. A brass baffle B was located inside the chamber, as shown in Fig. 1, at a distance of 0.1 cm from the common axis of F and E, and 3.25 cm from the entrance to F. Its purpose, which will be explained more fully later, was to lessen the effect of scattering in the entrance window upon the experimental measurements.

Evacuation of the chamber, and the introduction of hydrogen gas into it, was accomplished through the manifold P, which is shown very schematically in Fig. 1. The manifold was connected by a large sylphon vacuum valve V_1 to a liquid-nitrogen trap and an oil diffusion pump which evacuated the electron-exchange chamber to better than 10^{-4} mm Hg. Valve V_4 leads to a second liquid-nitrogen trap and a McLeod gauge, which was used to measure the gas pressure in the electron-exchange chamber. Hydrogen gas was let in through valve V_5 from a palladium leak. This method both purified the gas and allowed it to be let in slowly. In practice the leak was allowed to run continuously, and when sufficient hydrogen gas was in the deflection chamber, the valve V_5 was closed.

When valves V_1 and V_5 were closed, the McLeod gauge indicated a pressure rise of 4×10^{-4} mm Hg/hour in the electron-exchange chamber; this rise rate was practically independent of whether or not the cold trap was used. During the experiment the chamber was

[16] The circuit is given on the data sheet for the Raytheon CK5697/CK570 electrometer triode, published by the Raytheon Manufacturing Company, Newton, Massachusetts.

[17] The nitrocellulose films were prepared from Zapon Aquanite-A Lacquer by a standard technique.

never left closed off for more than fifteen minutes before re-evacuation. Since hydrogen pressures above 1×10^{-2} mm Hg were used in the chamber, the effect on the measured cross sections of such a leakage rate was negligible.

(D) The Detectors

The detectors were of a type which measured the strength of a proton or atomic beam in terms of the secondary electron current produced when the beam struck a beryllium-copper collector plate.[18] A cutaway view of one of the detectors is shown in Fig. 2. For the detection of particles the collector plate U was connected with one used for monitor current and was biased 67.5 v negatively with respect to ground. Since the long axis of U was oriented at 10.0° to the horizontal, the direction of the resulting electric field between U and the grounded electrode W (whose lower face was parallel to plate U, and separated from it by 0.32 cm) was nearly parallel to that of the magnetic field around the detector. Thus, all secondary electrons emitted when a moving proton or neutral atom impinged on the beryllium-copper were pulled to W and so gave an effective positive current to the collector plate. The magnetic field restricted any horizontal motion of the electrons to tight spirals and thus served to trap them between U and W. It should be noted that the internal geometry of the detector was such that any beam particle passing through the detector's entrance aperture and moving in a horizontal path would strike the plate U. The entrance aperture used in the present measurements was 0.32 cm high by 0.147 cm wide. The detector itself was of 2.22 cm diameter and 9.8 cm over-all length.

It was found that, for a given beam current entering the detector, the detector response was independent of the negative bias voltage applied to the collector plate for voltages in the range from forty-five volts to above three hundred volts. Thus, with the −67.5-v bias used in this experiment the detector was operating well within its saturation region. As regards other properties of the detector it should be noted that each loss cross section was completely measured at a constant value of the magnetic field. Thus, it was only necessary to show that the detector response is directly proportional to the number of ions or atoms striking the surface per second, and that a correction can be experimentally made for any effect of the hydrogen gas, when admitted, on the detector sensitivity. The investigation of these points is described in a later section of this paper.

(E) The Magnetic Field

The magnetic field was generated by an electromagnet, the current supply for which was a 110-v dc generator-ac motor set used only for this purpose.

[18] Beryllium-copper was chosen because of its high electron multiplication. J. S. Allen, Rev. Sci. Instr. 18, 739 (1947).

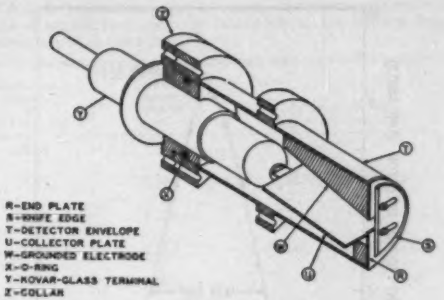

FIG. 2. Cutaway view of detector.

Fields as high as 10^4 gauss could be obtained, and were measured approximately with a generating fluxmeter which fitted into the can N. The fluxmeter was driven by a synchronous motor and gave readings reproducible to about 3 percent. It was used as a rough monitor for the field, and also for indicating when the magnetic field was zero.

It was found necessary to shield the collimator and adjacent parts from the magnet's leakage flux, which was quite intense. Since the window holder was enclosed by the electron-exchange chamber wall, it could not be externally shielded. It was made of Armco iron, however, in order to provide as much shielding as possible. The sliding coupling C was also made of Armco, so as to give some extra shielding.

III. EXPERIMENTAL METHODS

(A) Measurement of Proton Energy after the Entrance Window

Measurements were first made of the deflecting magnet currents necessary to bend protons of various energies into the sixty-degree detector G. For this work the entrance window W was removed and the electron-exchange chamber was evacuated to less than 2×10^{-4} mm Hg pressure. The proton energies were determined with the electrostatic analyzer, and the magnet current corresponding to the peak detector-current was read several times. Independent trials were found to agree within better than 2 percent. Hysteresis effects were taken into account by zeroing the magnetic field before each trial with the aid of the generating fluxmeter, and by never decreasing the magnet current during a measurement (these precautions were observed throughout the experiment).

The apparatus could now be used as a magnetic energy-analyzer for determining the energy of the protons after they had passed through the entrance window; such a measurement was made before each cross-section determination. A profile of normalized detector current r_G *versus* magnet current was taken with the electron-exchange chamber evacuated to less than 2×10^{-4} mm Hg. The quantity r_G is here defined

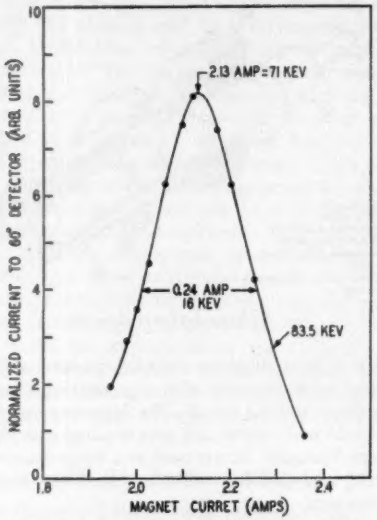

FIG. 3. Plot of 60° detector current *versus* magnet current for a 167-kev molecular hydrogen-ion beam incident on the window. The peak gives a mean energy of 71 kev after the window.

as the ratio of the sixty-degree detector current to the monitor current. From the magnet current at the peak of the profile the energy of the protons on leaving the window was determined.

A typical profile is shown in Fig. 3; the particles incident on the window were molecular-hydrogen ions of 167-kev energy, each of which was equivalent, for purposes of this experiment, to two protons of 83.5-kev energy. The peak of the profile was at 2.13 amp, which gives a proton energy of 71 kev after the window. The width of the profile at half-maximum corresponds to about 16 kev in energy, or 23 percent of the average energy. Not all of this width is due to energy straggling, however; a considerable part is due to angular deviations caused by scattering in the window as is evidenced by the fact that some particles entered the detector at magnet currents greater than the one (marked with an arrow) corresponding to the incident proton energy of 83.5 kev. The relative energy-widths at half-maximum of these profiles are listed in Table II. No correction has been made for the effect of scattering. It will be seen that the relative widths decrease with increasing beam energy, as might be expected.

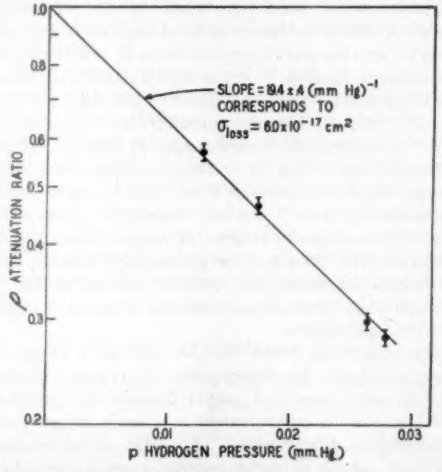

FIG. 4. Attenuation curve at the 0° detector for a 71-kev atomic-hydrogen beam. The magnetic field bends 71-kev protons with a radius of curvature of 5.6 cm.

From these data on the proton kinetic energies before and after the entrance window, energy losses in the window for protons of various incident energies could be estimated. Since no attempt was made to make the windows identical to one another, the losses varied somewhat from window to window. They were always, however, of a reasonable order of magnitude, when compared with those calculated from the data of Warshaw.[19] The actual losses varied from 8 to 15 kv in the various foils used; they are listed in the last column of Table II.

(B) Measurement of Loss Cross Section

To determine the loss cross section it was necessary to measure the attenuation ratio ρ, which is defined in Eq. (1). If we define $r(p)$ as the normalized current to the zero-degree detector (i.e., the ratio of simultaneous readings of detector-galvanometer deflection and monitor-galvanometer deflection) at hydrogen pressure p, then, clearly

$$\rho(p)=r(p)/r(0), \tag{2}$$

where $r(0)$ is the value of r at zero hydrogen pressure. As used in this discussion, the term "zero hydrogen pressure" means a total pressure in the electron-exchange chamber of less than 0.2 micron, so that the hydrogen atom's mean free path for electron loss is greater than ten times the distance between entrance window and the detector.

For the loss cross-section measurement the magnetic field was adjusted to a suitable value, which was never less than that required to bend the protons leaving the window into the 60° detector (a radius of curvature of 11.0 cm). Valve V_1 was opened and the electron-exchange chamber evacuated to a pressure of less than 0.2 micron. At least four measurements of $r(0)$ were taken and averaged. Valve V_1 was then closed and the chamber was filled with hydrogen gas to a desired pressure, generally in the range from five to eighty microns. The gas was assumed to be approximately at room temperature, since a calculation showed that

[19] S. D. Warshaw, Phys. Rev. **76**, 1759 (1949).

temperature equilibrium between the chamber walls and the initially hot gas should be reached in considerably less than one second. At least five measurements of r were made and averaged, and at the same time the gas pressure was read with the McLeod gauge. Finally, V_1 was reopened and $r(0)$ measured again. The value of $\rho(p)$ was calculated by dividing $r(p)$ by the average of the two values of $r(0)$ taken before and after the determination of $r(p)$. This was done in order to take some account of changes (rarely more than five percent) which occurred in successive readings of $r(0)$

At a given beam energy the quantity ρ was determined for at least three hydrogen pressures. A plot was then made of $\log_{10}\rho$ *versus* hydrogen pressure p. From Eq. (1) it can be seen that such a plot should result in a straight line passing through the point ($\rho=1$, $p=0$), and of slope s given by

$$s=\sigma_i d/(1.191\times10^{-19}T) \qquad (3)$$

per mm Hg. Generally, the experimental points fell closely on such a line. In any case the slope of the best line through the points which also passed through ($\rho=1$, $p=0$) was determined; and from it the uncorrected value of the loss cross section, σ_i'', was calculated.

One of these "attenuation" curves, i.e., plots of attenuation ratio *versus* hydrogen pressure, is given in Fig. 4. The curve is for a 71-kev neutral beam; during the measurement the magnetic field was set so that 71-kev protons were deflected with a radius of curvature, a, of 5.6 cm. Table I shows how the points for Fig. 4 were calculated from the measured values of the normalized detector current r. The data are entered in the table in the order in which the experimental measurements were made. Note that $r(0)$ stays fairly constant throughout; this behavior was typical of most of the runs. At the bottom of the table the calculation of the uncorrected cross section σ_i'' is shown, and corrections for the change of detector sensitivity with hydrogen pressure and for finite detector slit width (these corrections will be discussed immediately) are added to σ_i'' to give the corrected loss cross section σ_i.

It should be mentioned that, because the kevatron did not focus well at low voltages, atomic beams of kinetic energies less than 90 kev per particle were generally obtained from the kevatron's molecular-ion beam. The molecular ions decompose in the window and each gives two particles having half the energy of the original molecule. Preliminary measurements showed that, within experimental error, no difference could be observed between the cross section determined for atoms coming from the kevatron's proton beam, and that measured for atoms of the same energy but obtained from molecular ions.

TABLE I. Attenuation ratios at various hydrogen pressures for a 71-kev atomic beam and the calculation of the electron loss cross section from these data.[a]

Hydrogen pressure p 10^{-2} mm Hg	Normalized detector current r	Attenuation ratio $\rho(p)=r(p)/\text{mean } r(0)$
<0.02	1.152	
2.64	0.347	0.347/1.165=0.298
<0.02	1.178	
2.80	0.333	0.333/1.178=0.283
<0.02	1.177	
1.74	0.549	0.549/1.180=0.465
<0.02	1.183	
1.28	0.667	0.667/1.173=0.569
<0.02	1.163	

Calculation of the loss cross section:
s = slope of straight line in Fig. 4 = 19.4±0.4 mm^{-1} Hg,
T = room temperature = 297°K,
a = radius of curvature of 71-kev protons in magnetic field = 5.6 cm,
σ_i'' = uncorrected loss cross section = $(1.191/12.70)\cdot10^{-19}Ts$ = $(5.40\pm0.12)\cdot10^{-17}$ cm²,
$\sigma_i'=\sigma_i''+0.16\times10^{-17}$ cm² = 5.56×10^{-17} cm²,
σ_i = corrected loss cross section = $\sigma_i'(1+0.0284a^4)$ = $(5.95\pm0.14)\cdot10^{-17}$ cm².

[a] The data are presented in the order in which they were determined experimentally. They are the data used in plotting Fig. 4.

(C) Corrections to Be Applied to the Cross Sections

(a) *Correction for the Variation of Detector Sensitivity with Hydrogen Pressure*

If the quantity σ_i'' calculated from the slope of one of the attenuation curves is to be interpreted as the true loss cross section (neglecting the correction for slit width), then the following two conditions must be satisfied:

(i) the detector sensitivity (i.e., the galvanometer deflection per particle entering the detector) must be independent of the strength of the beam, and

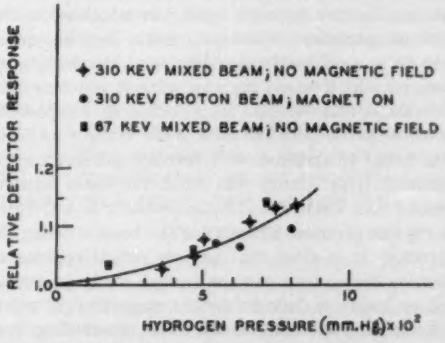

FIG. 5. Variation of detector response with hydrogen pressure.

(ii) the detector sensitivity must be independent of the hydrogen pressure in the detector.

Variations of detector sensitivity with magnetic field, bias voltage on the collecting plate, etc., will not put σ_l'' in error, since these quantities were kept constant during a cross-section measurement.

For the zero-degree detector, operated with its collector at -67.5 v with respect to ground, condition (i) is almost certainly met. Provided that the kevatron beam was sufficiently defocused so that no portions of it had high local intensities, the currents to detector and monitor were found to vary together quite consistently. Condition (ii) was not satisfied, however. Figure 5 shows the variation of detector sensitivity with hydrogen pressure when the 67.5-volt negative bias was used on the collector plate. The ordinate is the relative detector response and is defined as the ratio of the detector sensitivity at hydrogen pressure p to that at hydrogen pressure zero. The points indicated by crosses and by squares were taken with zero magnetic field across the electron-exchange chamber so that both protons and neutral atoms (i.e., a "mixed" beam) entered the detector. Because the magnetic field was zero, loss processes no longer affected the normalized detector current r appreciably, so any observed change in r must be due to a change in detector sensitivity. Thus, the relative detector response at hydrogen pressure p was here measured as the ratio $r(p)/r(0)$. It will be noticed that the relative detector response increases slightly with increasing hydrogen pressure and that at a given hydrogen pressure it is essentially independent of the energy of the incoming protons. This last fact indicates that Rutherford scattering of the beam particles by the hydrogen nuclei in the chamber was negligible—if it were not, one would expect the relative detector response to decrease with decreasing proton energy.

The points indicated by circles on the graph were taken on the 60° detector into which a 305-kev proton beam was being deflected by the magnetic field; the relative detector response again was calculated as the ratio of normalized detector currents. The behavior is seen to be very nearly the same as at the zero-degree detector with a mixed beam entering it and zero field. This shows that the effect is approximately independent of the magnetic field. The slope of the 60° detector curve was found to decrease with decreasing beam energy, however. This change was small for beam energies greater than 200 kev, and it can probably be attributed to capture processes attenuating the beam entering the detector. It is clear that protons which capture an electron during their passage through the hydrogen gas will no longer be deflected by the magnetic field and so will miss the 60° detector slit. Since the capture cross section decreases with a high negative power of the proton energy,[20] the attenuation due to capture processes should do likewise.

From the preceding paragraphs it may be seen that, when a detector is used with its collector plate biased 67.5 v negatively, its response varies slightly with hydrogen pressure; but this behavior is effectively independent of the beam energy and the magnetic field strength. Such a variation is explainable, for the positive slope of the curve in Fig. 5 could be due to ionization of the gas in the detector by incoming protons or atoms or by secondary electrons. The change of detector response with hydrogen pressure was found to correspond to a "cross section" of about -0.16×10^{-17} cm^2. Thus, to take this behavior into account, $(0.16\pm0.05)\times10^{-17}$ cm^2 was added to the uncorrected loss cross section σ_l'', i.e.,

$$\sigma_l' = \sigma_l'' + (0.16\pm0.05)\times10^{-17}\ \text{cm}^2 \qquad (4)$$

where σ_l' is the cross section corrected for detector response changes.

(b) *Correction for Slit Width*

If the angular aperture defined by the zero-degree detector's entrance slit had been infinitesimally small, all neutral particles which had lost their planetary electron before entering the slit would have been prevented from entering by the magnetic field. For a slit of width w, however, particles changing charge at a distance from the detector of less than b will not be deflected enough by the magnetic field to miss the slit, and will therefore be detected. The distance b clearly depends upon the horizontal displacement of the particle from the detector axis; its average value is given approximately by

$$(b)_{\text{av}} = (1/w)\int_0^w (2ax)^{\frac{1}{2}}dx = \tfrac{2}{3}(2aw)^{\frac{1}{2}}, \qquad (5)$$

where a is the radius of curvature with which the charged particles are deflected by the magnetic field. This means that the path length between the entrance window and the detector is effectively shortened by a distance b, and so the observed cross section is too small. The true cross section σ_l is given by

$$\sigma_l = \sigma_l'(1+0.0284a^{\frac{1}{2}}). \qquad (6)$$

In the derivation of this formula it has been assumed that the secondary-electron emission of beryllium-copper is the same for protons and hydrogen atoms at the same energy,[21] and that it is sufficiently large so

[20] N. Bohr, reference 2, pp. 111 ff.

[21] H. W. Berry [Phys. Rev. 74, 848 (1948)] has found that the secondary electron emission of tantalum is about fifty percent higher when it is bombarded by neutral helium atoms than when the incident particles are helium ions of the same energy. The energies in his work were less than four kev. If, in the present case, the secondary electron emission of beryllium-copper is greater for incident hydrogen atoms than for incident hydrogen ions of the same energy, the correction factor given in Eq. (6) would be too large.

that no account need be taken of the current brought to the collector plate by the positive ions resulting from neutral atoms which have changed charge but still enter the detector.

(c) The Effect of Scattering in the Entrance Window

Scattering in the entrance window was found to put the observed cross section considerably in error, at least at low proton energies. Neutral particles scattered in the direction away from the 60° detector can be bent into the zero-degree detector by the magnetic field if they change charge at the proper spot. They thus cause the observed cross section to be too low, and a little consideration shows that the effect can be quite large. The purpose of the baffle B (Fig. 1) was to prevent such particles from entering the detector. The mere introduction of the baffle increased the observed cross sections at some energies by as much as 50 percent, even when the same magnetic field was used in both determinations. Note that the baffle was placed sufficiently far (3.2 cm) from the detector so that no neutral changing charge on the knife edge could enter the detector if the magnetic field was not less than that which bends the protons with 11.0-cm radius of curvature.

As the magnetic field is increased, charged particles are removed more effectively from the neutral beam, and the error introduced by scattering becomes smaller. Thus, one would expect the observed cross section to increase with magnetic field. This effect was indeed found at lower beam energies. It was, however, always possible to reach a point at which further increases in the field strength no longer affected the observed cross section, within experimental error. The value of σ_i on such a plateau was then taken as the true loss cross section for the energy in question. At higher beam energies (this includes all but the two lowest energies for which a cross section measurement is given) the measured cross section was found to be essentially independent of the magnetic field, owing to the decrease in scattering with increasing energy. This independence is illustrated in Fig. 6 for atomic beams of two different energies. The abcissas in the figure are the radii of curvature through which a proton beam of energy equal to that of the atomic beam in question (71 kev for curve A and 123 kev for curve B) would be deflected by the applied magnetic field in which the cross-section measurement was made. These radii of curvature are plotted on a reciprocal scale, so that the magnetic field increases linearly toward the right. Note, however, that the magnetic field at a given radius of curvature is not the same for both curves A and B.

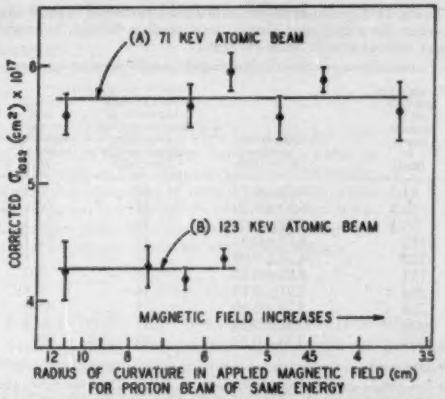
(A) 71 KEV ATOMIC BEAM
(B) 123 KEV ATOMIC BEAM
CORRECTED σ_{obs} (cm²) x 10¹⁷
6
5
4
MAGNETIC FIELD INCREASES
12 10 8 6 5 45 4 35
RADIUS OF CURVATURE IN APPLIED MAGNETIC FIELD (cm)
FOR PROTON BEAM OF SAME ENERGY

FIG. 6. Plot showing the measured cross section's independence of the magnetic field strength.

(D) Sources of Error

The limits of error indicated in Table II for the measured cross sections were estimated from the scatter of points on the attenuation curves, and on the curves of cross section *versus* magnetic field. They thus take into account errors due to inhomogeneity of the beam and to fluctuation of experimental conditions, reading errors, etc. These errors are essentially random. There are also, however, several sources of systematic error, of which the following are probably the most important.

(i) *Corrections applied to the cross section:* These corrections might be an error because of invalid assumptions made in calculating them. Since the corrections are usually about 10 percent of the measured cross section, the error in the cross section due to such invalid assumptions could hardly amount to more than 5 percent.

(ii) *McLeod gauge calibration:* The McLeod gauge was calibrated by measuring the volumes of its bulb and capillary. The experimental error in the calibration was less than one percent. Since an error in the gauge calibration affects all the measured cross sections by the same percentage, this means that the systematic error in the results due to McLeod gauge calibration errors is less than one percent.

(iii) *Energy straggling in the entrance window:* This effect was considerable at low beam energy, and because of it measurements at energies less than 45 kev were not considered reliable. It decreases fairly rapidly as the energy increases, however, and so should introduce a systematic error which decreases with increasing energy. For a given cross-section measurement this error is probably not greater than the difference between the measured cross section and the cross section (read from the curve in Fig. 7) for an atomic beam equal in energy to the proton beam incident on the entrance window. When this criterion is used, it is estimated that the straggling could not put any of the quoted cross sections in error by more than 5 percent.

IV. RESULTS

The experimental values of the electron loss cross section at various atomic beam energies are given in Table II, and are plotted as a function of beam energy in Fig. 7. The limits of error on the absolute values of the cross section are estimated to be plus or minus 10 percent. (The errors indicated in the table represent

TABLE II. Experimental values of the electron loss cross section per atom for a hydrogen atomic beam passing through hydrogen gas at various atomic beam energies.

Energy per particle in H atomic beam E (kev)	Loss cross section (10^{-17} cm^2)	Relative energy-width at half-maximum of detector current vs monitor current profile[a] (percent)	Energy loss in the entrance window (kev)
44.5	6.68±0.23	32	9.2
50.8	6.42±0.20	37	16
70.5	5.72±0.22	23	13.5
112	4.71±0.11	15	8.3
123	4.26±0.09	15	8.5
153	3.80±0.10	14	7.0
204	3.21±0.12	16	9.8
263	2.78±0.10	9	11.0
305	2.38±0.13	11	13.8
321	2.25±0.12	11	23

[a] The values are determined as shown in Fig. 3. They are larger than the width due to energy straggling alone, since they are uncorrected for angular deviations produced by scattering in the entrance window.

random error only and do not include the systematic errors which were discussed previously.) However, the relative values are probably good within 5 percent, as evidenced by the smooth curve on which the points lie in Fig. 7. No results are presented for energies less than 45 kev because of the excessive energy straggling in the foil which occurred at such energies.

Figure 7 is a logarithmic plot of the electron loss cross section *versus* beam energy. Between particle energies of 120 kev and 330 kev, the experimental points may be seen to lie approximately on a straight line, of slope -0.70 ± 0.05. Therefore,

$$\sigma_l \sim E^{-(0.70\pm0.05)}, \quad 120 \text{ kev} < E < 330 \text{ kev}, \qquad (7)$$

where E is the hydrogen atom energy.

Bartels[5] gives values of the mean free path for electron capture and of the equilibrium ratio of the charged to neutral component for hydrogen ion beams of energy less than 35 kev passing through hydrogen gas. From the first of these quantities σ_c, the electron capture cross section, can be calculated; the second is equal to σ_l/σ_c. Values of the loss cross section have been computed from these data, and are plotted as circles on Fig. 7.

Meyer,[6] using the same method as Bartels, has given values of σ_l for hydrogen atoms of energies between 35 kev and 150 kev passing through hydrogen gas. The cross sections range from 13×10^{-17} cm^2 at 35 kev to 20×10^{-17} cm^2 at 150 kev with indicated errors of about 15 percent. Such values disagree both with the present data and with those of Bartels. In particular, it hardly seems possible that the dependence of σ_l on energy that has been obtained from the present work could be so radically in error.

In evaluating the present results it should be noted that the method used by Meyer and by Bartels does not allow either cross section to be measured directly; their loss cross-section values are calculated from data directly concerned with the ratio of charged ions to neutral atoms in a beam. The advantage of the present method is that it provides a direct measurement of the loss cross section.

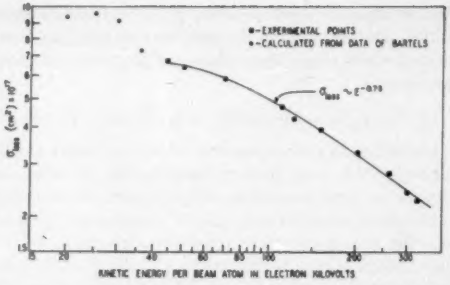
●-EXPERIMENTAL POINTS
•-CALCULATED FROM DATA OF BARTELS
$\sigma_{loss} \sim E^{-0.70}$
σ_{loss} (cm^2) ×10^{17}
KINETIC ENERGY PER BEAM ATOM IN ELECTRON KILOVOLTS

FIG. 7. Logarithmic plot of the electron loss cross section per hydrogen atom for a hydrogen atomic beam passing through hydrogen gas, as a function of beam energy.

Bohr[21] has derived the following expression for σ_l in terms of particle energy:

$$\sigma_l = 4\pi a_0^2 z_1^{-2}(z_2^2+z_2)(E_0/E), \qquad (8)$$
$$E \gg E_0,$$
$$z_1, z_2 \text{ small},$$

where $a_0=\hbar^2/\mu e^2$ is the Bohr radius, z_1 is the atomic number of the moving particle, and z_2 the atomic number of the substance penetrated. E_0 is that energy at which the particle's velocity is equal to the velocity of an electron in the first Bohr orbit; it equals 24.8 kev for a hydrogen atom. For hydrogen atoms moving through gas, Eq. (8) reduces to

$$\sigma_l = 8\pi a_0^2(E/E_0). \qquad (9)$$
$$E \gg E_0$$

For $E=245$ kev, Eq. (9) gives $\sigma_l=8.0\times10^{-17}$ cm^2, which is to be compared with 2.8×10^{-17} cm^2 from the present data. In making the comparison it should be remembered that, for 245-kev hydrogen atoms, $E\sim10E_0$. This is hardly a case of $E\gg E_0$, which is the range of validity of Eq. (9). Equation (9) also predicts that $\sigma_l\sim E^{-1}$, which is not far removed from the experimental result of Eq. (7).

Even though Eq. (8) is not valid at low energies, it might well give a fairly accurate prediction of the dependence of σ_l on z_1 and z_2. Thus, for hydrogen atoms passing through helium ($z_2=2$), cross sections 2.5 times as large as the ones here measured might be expected. It seems important to investigate these points in future work.

The author wishes to thank Professor Samuel K. Allison for suggesting this problem, for extending the facilities of his laboratory, and especially for his constant advice and encouragement, without which this work would not have been completed. Grateful acknowledgment is also made of the invaluable assistance of Mr. Fred Ribe, and of the help of Messrs. David Bushnell, Richard Carlson, Harvey Casson, Herbert Kanner, and Allan Morrish.

[21] N. Bohr, reference 2, p. 109, formula (4.2.3).

Calculations of Surface Energy for a Free-Electron Metal

H. B. HUNTINGTON
Department of Physics, Rensselaer Polytechnic Institute, Troy, New York
(Received February 23, 1950)

The surface energy of a free-electron metal is calculated using a square-cut barrier placed so that there is no net charge on the surface. The result is nearly independent of barrier height but leads to a value for surface tension less than half that observed for most molten metals. For sodium a self-consistent surface barrier, first developed by Bardeen, is also used in numerical computation of surface energy. The value so obtained is about half that resulting from the use of the square-cut barrier. Previous theoretical treatments of this problem have generally predicted surface energies larger than observed. The opposite result in this case appears to result from the requirement that the surface be maintained electrically neutral.

I. INTRODUCTION

THERE have been several previous treatments[1] of the surface energy for a metal using the free-electron model. Of particular interest is the work of Brager and Schuchowitzky[2] who used a free-electron model with infinite potential barrier at the geometrical surface of the metal. (By geometrical surface is meant that surface which just contains the last layer of atomic cells.) They found a contribution to the energy proportional to the surface which they identified with the surface energy. When compared with the experimentally measured values for the surface energies of molten metals, this term was too large by a factor of two or three but varied proportionally in going from one metal to the next.

A good critical review of the preceding literature on this subject has been contributed by Skapski.[3] He criticizes in particular the notion that free electrons give metals a higher surface energy than is found for other solids or liquids. In fact, in terms of the free energy per surface atom the values for the monovalent metals are lower in comparison with their cohesive energy than those usually found in other materials. On the basis that the same forces which give rise to volume cohesion are also responsible for surface energy, Skapski shows that a very simple semi-empirical calculation can predict the surface energy quite satisfactorily.

Recently Huang and Wyllie[4,*] have used a free-electron model with barrier of finite height at the geometrical surface of the metal. This method gives results in better agreement with experiment than those of Brager and Schuchowitzky, as they turn out to be only about $\frac{2}{3}$ the experimental values. The height of the barrier is in each case dictated by the known cohesive energy, and this choice serves to interrelate directly volume and surface forces. Their treatment has the following defect, that by fixing the position and height of the square barrier simultaneously, one cannot be certain that charge will be conserved; i.e., that the negative charge outside the geometrical surface will equal the electronic charge missing inside the surface. In fact it can be seen from Eq. (2) that to conserve charge with a square-cut barrier at the geometrical surface would require that the height of the barrier be just at the Fermi level. This would be equivalent to postulating a zero work function. As we shall see, the requirement that charge be conserved greatly decreases the surface energy.

II. SQUARE-CUT BARRIER POTENTIAL

In order to express the electron wave functions in a simple analytic form in the region of the surface one chooses a square-potential barrier[5] of height $(\hbar p)^2/2m$ at $x=a$. The geometrical surface of the metal is taken to be the plane $x=0$. Negative values of x refer to the metal interior. For rectangular specimens with dimensions L_1, L_2, L_3 the electronic wave functions can be written in the form of standing waves,

$$\psi=2/(L_2L_3)^{\frac{1}{2}}\sin k_y y \sin k_z z\,\phi(x) \qquad (1)$$

where, for

$$x\leq a,\quad \phi(x)=-(2/L)^{\frac{1}{2}}\sin(k_x\xi-\gamma)$$
$$x\geq a,\quad \phi(x)=(2/L)^{\frac{1}{2}}\sin\gamma\exp\{-(p^2-k_x^2)^{\frac{1}{2}}\xi\}.$$

with $\xi=x-a$ and $\sin\gamma=k_x/p$. The allowed values for k_y and k_z are positive multiples of π/L_2 and π/L_3 respectively. By virtue of the phase shift at the surface under consideration $k_x=(n_x\pi-\gamma)/(L_1+a)$.

The requirement that charge be conserved prevents the independent choice of a and p. Their interrelationship can be expressed analytically:

$$\tfrac{2}{3}k_m^3a=\tfrac{1}{4}\pi k_m^2+(\tfrac{1}{2}p^2-k_m^2)\sin^{-1}(k_m/p)-\tfrac{1}{2}k_m(p^2-k_m^2)^{\frac{1}{2}}, \qquad (2)$$

where k_m refers to the electrons on the Fermi surface, so that $k_m^3/3\pi^2=n$, the density of electronic charge. In Fig. 1 the barrier height is plotted in units of the Sommerfeld bandwidth against the displacement of the barrier in units of r_s with $4\pi r_s^3/3=1/n$.

[1] D. V. Gogate and D. S. Kothari, Phil. Mag. **20**, 1136 (1935); A Samoilovich, Acta Physicochimica (U.S.S.R.) **20**, 97 (1945); S. Dorfman, Compt. rend. **41**, 386 (1943).

[2] A. Brager and A. Schuchowitzky, Acta Physicochimica **21**, 13 (1946).

[3] A. S. Skapski, J. Chem. Phys. **16**, 386, 389 (1948).

[4] K. Huang and G. Wyllie, Proc. Phys. Soc. (London) **62**, 180 (1949).

[*] *Note added in proof:*—In recent correspondence Mr. Wyllie has pointed out that charge is conserved by their method within the Fermi-Thomas approximation. The approximation, however, appears to be inadequate to treat a step-function potential.

[5] This treatment is based on that of J. Bardeen, Phys. Rev. **49**, 653 (1936).

To calculate the surface energy of this model one may find the energy required to split a block of dimensions $(2L_1, L_2, L_3)$ in half. One half of this term then gives ΔE, the energy associated with one newly formed surface. (The results are of course independent of where the break is made.) The total energy of the electrons in the unsplit block is given by the sum,

$$\frac{\hbar^2}{2m}\sum_{\text{spin}}\sum_{n_x}\sum_{n_y}\sum_{n_z}\left\{\left(\frac{n_x\pi}{2L}\right)^2+\left(\frac{n_y\pi}{L}\right)^2+\left(\frac{n_z\pi}{L}\right)^2\right\},$$

where the summations are over all positive values of the n's for which the summand does not exceed k_m^2. After splitting, the energy is made up of two such expressions but only the terms involving k_x^2 contribute to the change in energy. After summing over spins and integrating over k_y and k_z one obtains for total increase

$$2\Delta E=\frac{L_2L_3\hbar^2}{4\pi m}\left[2\sum_{n_x=1}^{k_mL_1/\pi}\left(\frac{n_x\pi-\gamma}{L_1+a}\right)\left\{k_m^2-\left(\frac{n_x\pi}{L_1}\right)^2\right\}-\sum_{n_x=1}^{2k_mL_1/\pi}\left(\frac{n_x\pi}{2L}\right)^2\left\{k_m^2-\left(\frac{n_x\pi}{2L_1}\right)^2\right\}\right] \quad (3)$$

$$=\frac{\hbar^2}{2m}\frac{L_1L_2L_3}{\pi^2}\int_0^{k_m}\frac{k_x}{L_1}\times\left(\frac{\pi}{2}-2\gamma-2k_xa\right)(k_m^2-k_x^2)dk_x \quad (3a)$$

$$=\frac{3n\hbar^2L_2L_3}{2m}\left[\frac{\pi k_m}{8}-\frac{4}{15}k_m^3a-\frac{k_m}{2}\left\{1-\left(\frac{p}{k_m}\right)^2+\frac{3}{8}\left(\frac{p}{k_m}\right)^4\right\}\sin^{-1}\frac{k_m}{p}-\frac{3}{8}k_m(p^2-k_m^2)^{\frac{1}{2}}\left\{\frac{1}{k_m}-\frac{p^2}{2k_m^3}\right\}\right]. \quad (3b)$$

The first term of (3b) inside the square brackets corresponds to that given by Brager and Schuchowitzky[2] using a slightly different approach. It would be the sole contribution for an infinite barrier at the geometrical surface. From Eq. (2) one can substitute for a and obtain for the energy per unit surface,

$$\frac{\Delta E}{L_2L_3}=\frac{3n\hbar^2}{4m}\left[\frac{\pi k_m}{40}-\frac{k_m}{10}\sin^{-1}\frac{k_m}{p}\left\{1-3\left(\frac{p}{k_m}\right)^2+\frac{15}{8}\left(\frac{p}{k_m}\right)^4\right\}-\frac{k_m}{4}(p^2-k_m^2)^{\frac{1}{2}}\left\{\frac{7}{k_m}-\frac{15p^2}{2k_m^3}\right\}\right]. \quad (4)$$

In Fig. 1 there is also shown the dependence of surface energy on the barrier position, a, as found from Eqs. (2) and (4). It is rather encouraging to notice that the total variation of this quantity is little more than 10

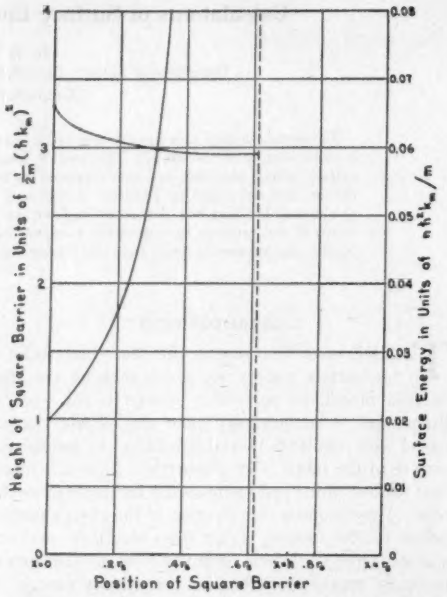

FIG. 1. The height of the square-cut barrier in units of $(\hbar k_m)^2/2m$ is plotted against its position where x is measured in units of r_s. Vertical line is the asymptote for infinite barrier. The nearly horizontal curve is the plot of surface energy in units of $n\hbar^2k_m/m$ as a function of barrier position.

percent for the complete range of possible values for barrier height and barrier position. One might be tempted to argue from this that for the purpose of calculating surface energy all barriers which conserve charge give essentially the same result and it is unnecessary to seek a self-consistent solution. In the next section it will be shown to what extent this is borne out.

The surface energy term just evaluated amounts to nearly one-fourth the Brager and Schuchowitzky term. It has already been pointed out[2] that such a term, varying as $\Omega^{-4/3}$, where Ω is the atomic volume, follows fairly well the variations of surface tension from one molten metal to another. As the original was too large by a factor between 2 and 3, the present result lies in the neighborhood of 60 percent of the experimental values. Unfortunately most of the considerations which have been omitted in this comparison tend to increase the discrepancy.

III. SELF-CONSISTENT SOLUTION FOR SODIUM

The actual surface barrier is known to be of the image type rather than square-cut. For sodium there exist the self-consistent solutions developed by Bardeen[5] for his treatment of work functions and dipole layers. In this section the result is given of a calculation of surface energy based on these solutions.[6]

[6] H. B. Huntington, Phys. Rev. 75, 1627A (1949).

In Bardeen's work the variation of the exchange potential with the total momentum of the electron causes the form of the barrier potential to depend on the value of $|k|$ of the electron. Besides the exchange potentials there is an electrostatic contribution to the barrier from the dipole layer which is the same for all electrons. Though the exchange curves could be read with sufficient accuracy from the figures of Bardeen's article, it was found necessary to obtain the electrostatic potential by integrating the poisson equation using the final self-consistent charge distribution (see Fig. 2a). There was need to have this potential fairly well-defined since it had a shallow minimum in the region where the electronic density had nearly reached full value, and therefore influenced the wave functions critically. It was found on integrating these functions numerically that the phase shifts caused by the barrier depended mainly on k_z and barely at all on $|k|$. It can be shown that the different curves for the exchange potential can be approximately superimposed by vertical displacements for the region over which the wave functions have appreciable applitude. In Fig. 2b is shown the complete potential used for $|k|=0.8k_m$, which is very nearly correct for any other value of $|k|$. As a result the integrations over k_y and k_z can be performed immediately in the calculation of the surface energy.

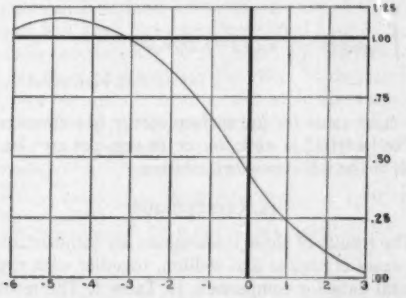

FIG. 2 (a). Charge density distribution at surface. Charge density is normalized to unity at interior of metal. Position x is measured in Bohr units. (From Bardeen.)

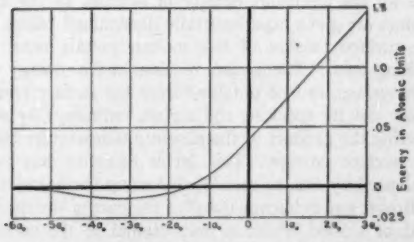

FIG. 2 (b). Typical potential curve. Potential is in atomic units and includes both electrostatic and exchange contributions. Former is cause of shallow trough inside metal. Exchange contribution ($k=0.8k_m$) is magnified slightly to include correlation effect.

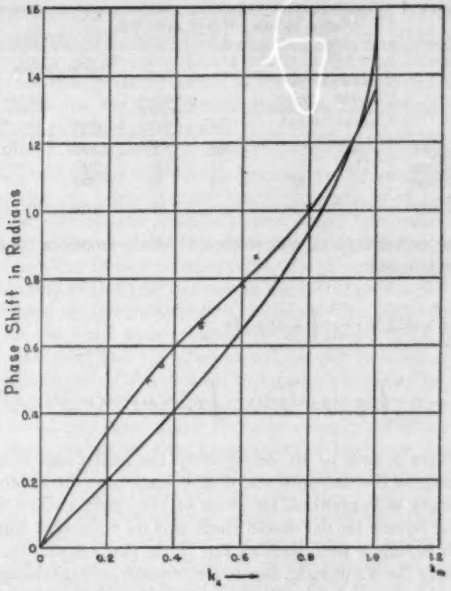

FIG. 3. Phase shifts in radians as function of k_z. ● for $k/k_m=1.0$, × for $k/k_m=0.8$, ○ for $k/k_m=0.6$. Curve through points is graph of Eq. (6). Lower curve gives phase shift for square barrier at geometrical surface.

In an equation analogous to Eq. (3a) one obtains:

$$\Delta E=(\hbar^2L_xL_y/2m)\int_0^{k_m}(\tfrac{1}{4}\pi-\gamma)(k_m^2-k_z^2)k_z\,dk_z, \quad (5)$$

where the γ are phase shifts in the standing electron waves as caused by the average barrier ($|k|=0.8k_m$). The dependence of γ on k_z is shown by the points plotted on Fig. 3. Different symbols indicate results obtained from curves for different values of $|k|$. It can be seen that γ depends principally on k_z. This dependence can be fitted by the analytic expression,

$$\gamma=k_zr_s[0.66+0.7\{0.8-(k_z/k_m)\}^2] \quad (6)$$

and the curved line through these points is the plot of this expression. The other line in Fig. 3 gives for comparison the phase shifts for the case of the square barrier placed at the geometrical surface. Though the two curves do not differ too markedly, the surface energy term obtained by evaluating Eq. (5) with the help of expression (6) is 0.023 in units of $n\hbar^2k_m/m$, or about 40 percent of the result previously given for the square barrier (see Fig. 1). This comes about because the surface energy term is obtained by subtracting two quantities of nearly equal magnitudes.

In any energy calculation involving self-consistent wave functions one must avoid counting electron interactions twice by subtracting one-half of the change in

TABLE I. Comparison of calculation with measured surface tension values (units of dyne/cm).

	Surface energy			Surface tension (exp.)		
	Square-cut barrier	Self-consistent barrier	$-TS_A$[4]	Surface tension (calc.)	Liquid	Solid (reference 9)
Copper	860	—	−360	500	1100	1370
Sodium	170	—	− 34	136	290	—
Sodium	—	88	− 34	54	290	—

the self-energy of the electrons which amounts to a contribution,

$$\frac{1}{2}\int \rho_i\phi(\rho_i)d\tau-\frac{1}{2}\int \rho_f\phi(\rho_f)d\tau$$

$$=-\frac{1}{2}\int(\rho_i-\rho_f)\phi(\rho_i)d\tau-\int\rho_f[\phi(\rho_f)-\phi(\rho_i)]d\tau, \quad (7)$$

where ρ_i and ρ_f are respectively the initial and final electron distributions and $\phi(\rho)$ in each case the appropriate self-potential. (Because of the crude nature of the square barrier model there was no consistent way to include a term such as Eq. (7) in that calculation.) Here the ϕ's include, beside electrostatic, also exchange and correlation contributions. Since the initial situation refers to a uniform value for ρ_i and ϕ, i.e., no surface, it follows the first term on the right of Eq. (7) vanishes as a result of the conservation of charge.

It is not correct, however, to take $\phi(\rho_f)-\phi(\rho_i)$ to be just the barrier potential at the surface, ϕ_b. As formulated here the barrier potential arises only from mutual interactions of the electrons, namely the surface dipole layer and the changes in the exchange and correlation potential caused by the introduction of the surface. It does not include, however, the change in the electronic coulomb interaction. In the Wigner-Seitz method[7] the coulomb interaction potential arises from the electronic distribution in the same atomic polyhedron as the field point. The charge outside of this polyhedron is neutralized by the coulomb potentials of the outside ions. In the approximation of uniform electronic distribution the coulomb interaction potential can be written:

$$V_e(r)=3e/2r_s-er^2/2r_s^3,$$

where r is measured from the center of the atomic polyhedron. The average value of this potential is $1.2e/r_s$. It follows that

$$\phi(\rho_f)-\phi(\rho_i)=\phi_b+\Delta V_e, \quad (8)$$

where ΔV_e is the change in the coulomb potential caused by the surface.

A fundamental difficulty in treating V_e in a unique manner arises because this potential is developed from the concept of the atomic polyhedron, whereas our present model has dispensed with the polyhedra in the postulation of a geometrically plane surface. Some arbitrariness is, therefore, involved in the following procedure for establishing ΔV_e. This procedure was to assume that $V_e(x)$ remains unchanged at its average value, $1.2e/r_s$, in the region inside the geometrical surface ($x\leq 0$). Outside the surface, $x>0$, it is assumed that the electrostatic interaction potential is that arising from a uniform charge distribution in the atomic polyhedron nearest to the field point. By appropriate averaging, this potential is expressed as a function of x only. Accordingly the resulting function becomes

$$V_e(x)=(2/s_0^2)\int_0^\infty V_e(r)sds,$$

where $r^2=(x+\frac{1}{2}d)^2+s^2$, d is the distance between atomic planes parallel to the surface and s_0^2d equals the volume of the atomic polyhedron. For $r<r_s$, $V_e(r)=3e/2r_s-er^2/2r_s^3$ and for $r>r_s$, $V_e(r)=e/r$.

By this somewhat arbitrary procedure, one can express as a function of x,

$$\phi(\rho_f)-\phi(\rho_i)=\phi_b+V_e(x)-1.2e/r_s,$$

where ϕ_b stands for the barrier potential. Direct evaluation gives

$$-\frac{1}{2}\int\rho_f\phi_b d\tau-\frac{1}{2}\int\rho_f(V_e-1.2e/r_s)d\tau$$

$$=(-0.034+0.043)n\hbar^2k_m/m.$$

The final value for the surface energy of sodium turns out to be 0.032 in $n\hbar^2k_m/m$, or 88 ergs per cm², on the basis of the self-consistent solution.

IV. CONCLUSION

The results of these calculations are summarized for the cases of copper and sodium, together with experimental data for comparison, in Table I. The result of the square barrier calculation can be applied directly to any metal since it varies as the 4/3 power of the electronic density. The self-consistent barrier is specialized for the electronic density of sodium. In the fifth column are given experimentally determined values for the surface tension of the molten metals near the melting point.[8] The surface tension, or free energy per unit surface, can be obtained from the surface energy (more strictly speaking the surface enthalpy) by subtracting the product of the absolute temperature times the surface entropy. This latter quantity has been evaluated by Huang and Wyllie[4] using the calculation of Brager and Schuchowitzky[9] of the part of the specific heat of a solid which is proportional to the surface.

[7] F. Seitz, *Modern Theory of Solids* (McGraw-Hill Book Company, Inc., New York, 1940), Chapter X.

[8] For more extensive listings of this quantity see references 2 or 4.

[9] A. Brager and A. Schuchowitzky, Acta Physicochemica **21**, 1001 (1946).

Their results are given in column 3 and combined with the tabulations in the preceding columns in column 4 for comparison with the data from the molten metals. Reliable measurements of surface tension for solids are difficult to find but recently Udin, Shaler, and Wulff[10] have employed the technique of observing the elongation and contraction of fine wires under small loads at high temperatures to obtain an apparently quite reliable value for the surface tension of copper. Their value for this quantity just above the melting point is given in column 6 of Table I.

It is evident from a comparison of columns 4 and 5 in Table I that in all cases the calculations give values considerably smaller than the experiments. Of the quantities which a more complete theory might have included there does not appear to be any which would readily remove the discrepancy. (a) A consideration of the short range repulsive forces between ions would lower still more the calculated values, though this term is not large. (b) The calculations are strictly for a solid metal and the experimental evidence is for the most part taken on molten metals but the evidence of the measurements on copper indicate that surface tension is larger in the solid than in the liquid phase (as seems rather sensible intuitively). (c) Surface energy calculated here applies to the freshly cleaved surface. Surface tension measurements refer to equilibrated, or partially equilibrated, surfaces where the density of the surface layer has been reduced. Since the lowered surface density corresponds to a more thermodynamically stable state, this also has the effect of decreasing the surface energy. (d) In this calculation the surface has been assumed to be geometrically plane, which is a valid approximation for the close-packed surfaces. Smoluchowski[11] has shown for tungsten that the energy differences between crystal surfaces should be quite appreciable. The inclusion of surface planes, other than closest packed, would alter results in the right direction but it appears unlikely the correction would be large since for the equilibrated specimen surfaces of low energy would predominate.

To summarize the results of this investigation. It would appear that surface tensions for metals as calculated on a free-electron model for surfaces of closest packing are less than half those found experimentally for molten metals. This discrepancy is in the opposite direction from that reported by the more recent treatments of this problem, where the investigators did not insist on the conservation of charge. The replacement of the usual square barrier by one shown to be self-consistent had the effect of still further increasing the discrepancy. It is difficult to surmise what may be the cause of the present disagreement. It should be remembered that these values for surface energy are obtained from the rather close cancellation of two large terms. Small errors in evaluation or uncertain assumptions, usually physically satisfactory, may play a part. It may be that the free-electron model is simply too crude for this problem and to improve the results one must take into account the periodicity of the metallic potential field. The presence of the surface disturbs the charge distribution as far back as the position of the centers of the first layer of atoms. The interaction of this modulation of wave functions in the neighborhood of the ionic core, which one overlooks in the free-electron model, could possibly be important in determining the surface energy.

The author wishes to express his appreciation to Mr. G. Wyllie for stimulating correspondence. He is indebted to Mr. Nieh Tsung-li for assistance in the numerical integration of the wave functions in the self-consistent field.

[10] Udin, Schaler, and Wulff, Met. Trans. A. I. M. E. 186 (February, 1949).
[11] R. Smoluchowski, Phys. Rev. 60, 661 (1944).

A Direct Determination of the Magnetic Moment of the Protons in Units of the Nuclear Magneton*†

C. D. JEFFRIES
Stanford University, Stanford, California††
(Received November 10, 1950)

A direct measurement of the proton magnetic moment in units of the nuclear magneton has been made, using the method of Alvarez and Bloch. The experiment consists of comparison of the nuclear magnetic resonance frequency of protons with the orbital frequency of protons revolving in the same homogeneous field. The resonance frequency of protons in water has been measured by the method of nuclear induction; the orbital frequency has been measured by a special device: a small decelerating cyclotron operated at an odd multiple of the fundamental cyclotron frequency.

The device has been operated in a field of about 5300 gauss at all odd multiples from the first to the eleventh, with a corresponding range of the dee frequency between 8.1 and 89 Mc/sec. As expected, the sharpness of the cyclotron resonance was observed to greatly increase at the higher multiples; besides this advantage for obtaining high accuracy, the comparison of the results at different multiples also furnished an important check on the reliability of the measurements.

An approximate theory for the shape of the cyclotron resonance curves has been developed, and its qualitative agreement with the observations has been established. The perturbing effects of extraneous electric and magnetic fields have been investigated, both theoretically and experimentally, and found to be negligible. With the smallest relative half-width of resonance about 1/10,000, which was observed at the higher multiples, and guided by the interpretation of the resonance shape, the magnetic moment of the proton has been found to be 2.7924 ± 0.0002 nuclear magnetons.

I. INTRODUCTION

THROUGH the development of new experimental methods it has been possible, in recent years, to achieve relative measurements of nuclear magnetic moments, with high accuracy. They are based on the comparison of resonance frequencies, and the magnetic moment of the proton has been chosen as the common standard to which other moments are referred. This choice has been motivated by convenience as well as by the basic significance of the proton moment. Nevertheless, there remains the problem of measuring the proton moment μ_p itself with comparable accuracy in terms of the natural unit of nuclear magnetic moments, the "nuclear magneton" $\mu_n=eh/4\pi Mc=\mu_B m/M$ (e=elementary charge, c=velocity of light, h=Planck's constant, M=mass of proton, m=mass of electron, μ_B=Bohr magneton).

Starting with the first measurement by Stern and Frisch,[1] the proton moment has been redetermined repeatedly with increasing accuracy by atomic and molecular beam experiments.[2–4] In these experiments, however, it is not directly the ratio μ_p/μ_n which is measured, but μ_p is either obtained in absolute units or in units of the magnetic moment of the electron. Applying the necessary radiative corrections to the latter, the most accurate value obtained in this way was given by Taub and Kusch[5] as $\mu_p=2.7935\mu_n$.

A method for determining directly nuclear magnetic moments in units of the nuclear magneton was described several years ago by Alvarez and Bloch;[6] it is based on the comparison of the nuclear resonance frequency with the orbital frequency of protons revolving in a magnetic field. Through the recent developments, which allow convenient and precise measurements of nuclear resonance frequencies,[7,8] this method is now capable of high accuracy. By a modification, consisting in the comparison of the nuclear resonance frequency of protons with the orbital frequency of *electrons*, Purcell and Gardner[9] have thus been able to obtain a direct determination of the proton magnetic moment in units of the *Bohr magneton*.

Correspondingly, it is the aim of the experiment reported here, and briefly published earlier,[10] to compare the proton resonance frequency, observed by nuclear induction, with the orbital frequency of *protons* in the same magnetic field and thus to obtain directly the proton magnetic moment in units of the *nuclear magneton*. In conjunction with the measurement of Purcell and Gardner it can also be considered as a new method for determining the mass ratio of the proton to the electron.

While this experiment has been in progress, a similar one based on the same principle has been carried out by Hipple, Sommer, and Thomas[11] to determine the value of the Faraday. In their apparatus, the "omegatron," protons are accelerated by an essentially homogeneous oscillating electric field, and they are trapped in an

* This paper is based on a dissertation submitted to the Department of Physics and the Committee on Graduate Study of Stanford University in partial fulfillment of the requirements for the degree of Doctor of Philosophy.

† Assisted by the joint program of the AEC and ONR.

†† Present address: Physikalisches Institut der Universität Zürich, Zürich, Switzerland.

[1] R. Frisch and O. Stern, Z. Physik **85**, 4 (1933).

[2] Rabi, Kellogg, and Zacharias, Phys. Rev. **46**, 157, 163 (1934).

[3] S. Millman and P. Kusch, Phys. Rev. **60**, 91 (1941).

[4] Kellogg, Rabi, Ramsey, and Zacharias, Phys. Rev. **56**, 728 (1939).

[5] H. Taub and P. Kusch, Phys. Rev. **75**, 1481 (1949).

[6] L. W. Alvarez and F. Bloch, Phys. Rev. **57**, 111 (1940).

[7] Purcell, Torrey, and Pound, Phys. Rev. **69**, 37 (1946); Bloembergen, Purcell, and Pound, Phys. Rev. **73**, 679 (1948).

[8] Bloch, Hansen, and Packard, Phys. Rev. **69**, 127 (1946); and Phys. Rev. **70**, 474 (1946); F. Bloch, Phys. Rev. **70**, 460 (1946).

[9] J. H. Gardner and E. M. Purcell, Phys. Rev. **76**, 1262 (1949).

[10] F. Bloch and C. D. Jeffries, Phys. Rev. **80**, 305 (1950).

[11] Hipple, Sommer, and Thomas, Phys. Rev. **76**, 1877 (1949) and Phys. Rev. **80**, 487 (1950).

electric dc potential. Compared with ours, this arrangement has the advantage that it avoids the difficulties of injection; also, up to the present time, it has yielded resonance widths about 3 times smaller than those obtained by our device. On the other hand, the omegatron involves certain perturbations due to space charges and it precludes the feature of operation at higher multiples of the orbital frequency, of which our decelerating cyclotron is capable. For these reasons, as well as for the mutual checking of results obtained by the two different methods, it seemed to us well worth while to develop our technique further.

II. METHOD

As suggested by Alvarez and Bloch,[6] the problem of measuring μ_p/μ_n can be solved by a method of high inherent accuracy based on the measurement of a frequency ratio; by observing both the nuclear resonance frequency ν_N of protons in a magnetic field H' and the orbital frequency ν_R of protons revolving in a magnetic field H, we have

$$\nu_N=2\mu_p H'/h, \quad \nu_R=eH/2\pi Mc \tag{1}$$

and, therefore,

$$H\nu_N/H'\nu_R=\mu_p/(eh/4\pi Mc)=\mu_p/\mu_n. \tag{2}$$

Thus, by performing both experiments in the same homogeneous magnetic field, we may take $H=H'$ in Eq. (2) and μ_p/μ_n is then given directly as the ratio of two frequencies to an accuracy determined, in principle, by the bandwidths of the two resonance phenomena involved; i.e., by the number of coherent cycles in an observation.

We have used the method of nuclear induction both to measure ν_N to within a few parts in 10^5 and to make the magnetic field homogeneous to comparable accuracy. The accuracy of the present experiment hinges then on the determination of ν_R, which we have measured to about one part in 10^4. To obtain this accuracy it is not possible to determine ν_R by measuring the resonant frequency of a conventional accelerating cyclotron because the resonance bandwidth is broadened too much by the magnetic focusing, by a limitation in the number of revolutions due to gas scattering, and by relativistic mass variation. Actually, to be able to apply Eq. (2) with high accuracy, the following requirements are necessary:

(1) The field H must be highly homogeneous over the entire proton orbit. The possibility of magnetic focusing is thus excluded, and some other means must be provided to prevent loss of the protons after many revolutions. We have utilized the electric phase focusing property of cyclotron dees, while in the "omegatron,"[11] loss of protons is prevented by "trapping" them in an electric potential well.

(2) The gas pressure must be sufficiently low in order that collisions do not seriously limit the number of revolutions. This was achieved by operating a cyclotron in an inverse or decelerating fashion, in which the protons are formed in an external arc-source and brought into the dees through several stages of differential pumping—thus maintaining a low pressure in the dee cavity. Essentially, the protons traverse a conventional cyclotron trajectory in the backward direction and are detected by a probe near the center of the dees. This arrangement introduces the problems of injection, but it has other important advantages which will be discussed shortly.

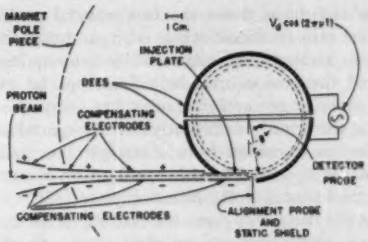

FIG. 1. Schematic arrangement of the decelerating cyclotron. Protons are injected into the dees at a radius r_0 and are decelerated by the dee voltage $V_d\cos(2\pi\nu t)$, where $\nu\cong n\nu_R=neH/2\pi Mc$ and n is an odd integer.

(3) The relativistic mass variation of a proton throughout its orbit must be negligible. This limits the proton energy eV to the order of magnitude of 10^4 electron volts, where the mass variation is $\Delta M/M \cong eV/Mc^2\cong 10^{-5}$. Gas scattering is greater here than at higher energies; on the other hand, the radius of the orbit is conveniently small, which is a practical advantage for having the magnetic field homogeneous over its extension.

(4) Besides the above requirements it is important for high precision that perturbations of the frequency ν_R, due to extraneous electric and magnetic fields, be very small; this problem will be discussed later.

Guided by the above considerations we have constructed a small decelerating cyclotron as shown schematically in Fig. 1. The dees are 4.25 cm in radius, 1.65 cm wide, and are in a homogeneous field of about 5300 gauss, provided by a magnet with pole pieces of 13 cm radius. A beam of protons with energy $eV_0=2\times 10^4$ electron volts is continuously injected tangentially into the dees, and resonance is determined by observing the frequency of the applied sinusoidal dee voltage at which the protons spiral sufficiently inward to strike a detector probe near the center of the dees. An incoming proton is directed along a straight path towards the dee periphery by means of a compensating field E_0, which compensates the Lorentz force on the proton and is provided by suitable compensating electrodes (Fig. 1). Without this compensation a proton entering from the outside into the gap of the magnet would be deflected away by the fringing field; the compensation must be effective up to the end of the injection plate (Fig. 1), where there is a transition from the straight line path to a spiral inside the dees.

This transition raises the fundamental problem of injection into an almost stable orbit, and this difficulty is, in our arrangement, expressed by two requirements: (1) that the proton orbit be a finely spaced spiral in order that a large number of revolutions can take place; (2) that the orbit be sufficiently coarsely spaced initially to afford a transition from a straight line path to a circular path, such that an entering proton clears the finite thickness d of the injection plate (Fig. 1) which shields the dee cavity from the field E_0. With an initial radius r_0 and energy eV_0 a proton must, in the first revolution, lose energy by an amount $eV=2eV_0d/r_0$; otherwise it will strike the injection plate and be lost. This limits the minimum amplitude of the dee voltage to $V_c=V_0d/r_0$. Because of construction difficulties, the smallest practical value of d/r_0 is about 10^{-2}. Therefore, the amplitude of the dee voltage must be about one percent of the initial voltage, which would seem to allow only about $N=V_0/2V_c=50$ revolutions with a corresponding resonance bandwidth[12] of about $1/2\pi N=1/300$.

We have solved the injection problem and actually achieved a very considerable reduction in the resonance bandwidth, and a corresponding gain in accuracy, by extending the operation of the cyclotron from the frequency ν_R of Eq. (1) to a frequency $n\nu_R$, where $n=3$, 5, 7, 9, or 11. The reduction in bandwidth is due to two circumstances; in the first place, operation of the dees at the nth multiple of ν_R will, for a given number of revolutions of a proton, reduce the observed resonance bandwidth by a factor n, since resonance conditions require a proportionally more critical timing between the dee oscillation and the rotation of the proton. In the second place, transit time effects permit an increase in the number of revolutions required for a proton to reach the probe at a given position. In fact, as the spiral orbit of a proton shrinks, it travels ever more slowly through the dee gap, so that the net decelerating action of the oscillating dee field during transit is more and more reduced. This effect is evidently the more pronounced the smaller the radius and the higher the dee frequency. The proton thus approaches the detector probe in an increasingly finely spaced spiral, which in our arrangement may easily contain 500 revolutions. The practical upper frequency limit is reached when the transit time effect becomes appreciable even at the initial radius r_0, consequently requiring a higher dee voltage for injection. Because of this limitation and also because of decreased focusing action for large n, we have been able to operate the present apparatus only up to the 11th multiple of ν_R, where we have observed resonance bandwidths of about one part in 10^4. However, except for increased technical difficulties, there is no reason why, in an apparatus of modified design, the method cannot be extended to appreciably higher multiple frequencies and correspondingly greater accuracies.

It should be pointed out that the transit time effect, which is advantageous for our experiment, actually prevents multiple frequency operation of an accelerating cyclotron where the protons are introduced at zero radius, so that dee fields at a multiple of the resonance frequency ν_R are ineffective in starting the protons into a spiral orbit.

Without actually carrying them out, we have also considered two alternative injection schemes which do not involve multiple frequencies: (1) If the dee voltage is kept at a very low voltage V' and at a frequency near ν_R, the occasional application of a pulse of approximate duration $1/\nu_R$ and with an amplitude $V>V_0d/r_0$ will inject protons and allow them to spiral down to the detector probe in a large number of revolutions. This will allow resonance bandwidths of the order of magnitude of $V'/\pi V_0$, which in principle can be made as small as other factors, such as decrease of focusing, will allow. The main disadvantage of this scheme is that the duty cycle of the proton current and, correspondingly, the magnitude of the detector probe current suffer a reduction proportional to the number of revolutions in the orbit. (2) The dees may be separated into two concentric parts: an outer split ring driven at relatively high voltages to allow injection, and a pair of inner dees at low voltage to allow many revolutions to take place. Apart from its technical difficulty, the disadvantage of this scheme lies in the complicated analysis of the orbits in the transition region.

A. Analysis of Decelerating Cyclotron

It is essential for a precise measurement like the one presented here that, beyond the qualitative aspects, the principal features be understood in a quantitative manner, so that proper functioning of the apparatus and correct interpretation of the results may be obtained. In our experiment it is particularly important to analyse the motion of the protons and thereby to gain insight into the shape of the observed resonance curves. No attempt will be made to give a rigorous solution to the problem of the cyclotron motion of a particle in a pair of dees. Instead, a number of approximations will be made which are more or less justified in a theory which merely purports to analyse the principal features and determine the resonance frequency to within about $\frac{1}{4}$ of the resonance bandwidth.

First, we approximate the dees by a two dimensional set of infinite plates shown in cross section in Fig. 2. This approximation neglects the end effects due to the side walls of the dees; it is assumed further, and is well justified by the actual dimensions of our apparatus, that the gap separating the two dees is small compared to the dee width b. Secondly, we neglect the curving of the orbits due to the field H during the transition of the protons from one dee into the other. This means that b

[12] It is shown later that the resonance bandwidth is about $1/2\pi N$, where N is the number of revolutions at exact resonance of a proton crossing the gap at the instant of maximum dee voltage.

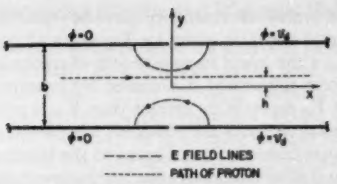

FIG. 2. Cross section of the electrode configuration used in approximating the dees in the calculations. The gap separating the dees is taken to be zero. The field H is in the y direction.

is considered to be sufficiently small compared to the radius of the orbit.[13]

Consider the effect of the electric field on a proton in transit through the plates in the x-direction with an energy very large compared to the dee voltage v_d in which case the path may be approximated by a straight line $y=h$. The lens focusing action due to the change in the proton velocity will be negligible. However, if v_d varies sinusoidally with time as the proton crosses the gap, it will be subject to phase focusing; i.e., it will receive a net transverse momentum either toward or away from the median plane, depending on the phase of the voltage. v_d must be positive for deceleration, and a proton will be focused if v_d is increasing in time when it passes the point $x=0$, and defocused if v_d is decreasing. The converse is true in a conventional accelerating cyclotron in which v_d is negative.

As shown in Appendix A, the approximate radial and transverse motion of a proton in dees of width b and radius R is given for $b \ll r < (R-b)$ by the differential equations:

$$\frac{V_0}{r_0^2}\frac{dr}{dN} = -\frac{V_d}{r}\frac{\cosh(ny/r)}{\cosh(nb/2r)}\cos\delta, \tag{3}$$

$$\frac{M\pi\nu^2}{n^2}\frac{d^2y}{dN^2} = \frac{eV_d}{r}\frac{\sinh(ny/r)}{\cosh(nb/2r)}\sin\delta, \tag{4}$$

where r=radius of the proton orbit, y=displacement from the median plane of the dees, N=number of revolutions, V_d=amplitude of dee voltage, ν=frequency of dee voltage, n=an odd integer $\cong \nu/\nu_R$, δ=phase of dee voltage when the proton is midway between the two dees, and eV_0=proton energy at the radius r_0. δ may be expressed as a function of N and $\Delta\nu=\nu-n\nu_R$, so that

$$\begin{matrix}\sin\\ \cos\end{matrix}\left[\delta\right] = \begin{matrix}\sin\\ \cos\end{matrix}\left[\delta_0+(2\pi N\Delta\nu/\nu_R)\right], \tag{5}$$

where δ_0 is the initial value of δ at $N=0$.

From the form of Eq. (4) it is evident that the transverse motion is either concave or convex toward the median plane, depending on the sign of $\sin\delta$; i.e., there is phase focusing for negative $\sin\delta$ and defocusing for positive $\sin\delta$. In the case of focusing, the motion consists of oscillations about the median plane, which are sinusoidal for small amplitudes, i.e., for $ny \ll r$. Under typical conditions of the transverse oscillation is small compared to ν_R.

Since we are interested in orbits containing many revolutions, protons for which $\sin\delta$ is positive even during a small portion of the orbit are defocused enough to strike the dees and do not reach the detector probe. The probe current is therefore almost entirely due to protons for which $\sin\delta$ is always negative and for which the amplitude of transverse oscillation remains less than $b/2$. The exact analysis of the transverse oscillation is a complex problem, the solution of which is not essential for our present purpose and will not be attempted. It can be stated, however, that the amplitude of oscillation is the greater, the larger the initial transverse proton velocity, the smaller $\sin\delta$, and the smaller the dee voltage. It can be seen further from Eq. (4) that for small values of y and large values of r/b, the focusing action starts to improve for increasing n, but becomes less effective if n becomes either too large or r too small. For $n=9$ or 11, and for the actual dimensions used in the present experiment, the focusing action continuously decreases with decreasing radius.

In the special case of exact resonance for protons in the median plane, i.e., for $\Delta\nu=0$, $y=0$, a solution of the radial motion can be obtained easily by integration of Eq. (3). This is done in Appendix A, where we have calculated for various values of n the number of revolutions N_0 necessary for a proton with initial radius r_0 to reach radius r, assuming that the phase δ is always zero, i.e., that the proton always crosses the dee gap when the voltage is at its maximum; this will be the case if the initial phase δ_0 is zero and the dee voltage is at the exact resonance frequency $n\nu_R$. With the radius of the dees only 0.4 cm larger than the initial radius $r_0=3.85$ cm, the neglect of the end effects made in this calculation is not strictly justified. In the beginning of the orbit, i.e., for r close to r_0, the side walls of the dees produce a shielding effect near the gap, and this will somewhat reduce N_0 from the values shown in Fig. 3. Nevertheless, this graph clearly shows the transit time effect; the higher the value of n, the more rapidly N_0 increases with decreasing radius.

For protons in the median plane it is possible to calculate the approximate shape of the resonance curve, i.e., the detector probe current as a function of the dee frequency ν near the resonance frequency $n\nu_R$. Although the results cannot be applied rigorously to the observed curves, they serve as a useful guide in the proper determination of the dee frequency at which exact resonance occurs.

Both the magnitude and the frequency dependence of the probe current are functions of the dee voltage. As was explained earlier in this section, no protons will be injected into the dees unless the dee voltage has an

[13] Our approach to the problem is similar to that of R. Wilson [Phys. Rev. 53, 408 (1938)] and of M. Rose [Phys. Rev. 53, 392 (1938)] in their analyses of an accelerating cyclotron.

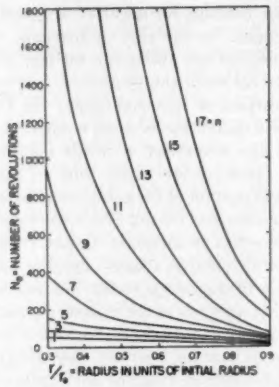

FIG. 3. The number of revolutions N_0 [Eq. (9A), Appendix A] which a proton in the median plane must make, starting from the radius r_0, in order to reach a radius r with a dee voltage $V_d=200$ volts peak at a frequency $n\nu_R$. The rapid increase in N_0 with decreasing radius for large n is due to the transit time effect. The phase δ is taken to be always zero, i.e., the proton encounters the peak dee voltage each time it crosses the dee gap. The constants have been chosen to correspond to the present experiment: $V_0=20$ kilovolts, $r_0=3.8$ cm, $b=1.65$ cm. N_0 may be calculated for any other dee voltage by using the relation $N_0 \propto 1/V_d$.

amplitude V_d at least as great as V_c, the cut-off value necessary for a proton to just clear the injection plate after one revolution. For $V_d=V_c$ only those protons immediately adjacent to the injection plate will enter; furthermore, they must pass through the dee gap when the voltage is at its maximum, i.e., their initial phase must be $\delta_0=0$.

If, for the moment, any focusing or defocusing action is disregarded, a proton will reach the detector probe at a radius r provided that the dee frequency ν is sufficiently near the resonance frequency $n\nu_R$ so that the phase δ remains within the values $-\pi/2$ and $+\pi/2$; i.e., the spiral orbit must continue to shrink by deceleration and must not start to expand by acceleration before the detector probe is reached. In the limiting case $V_d=V_c$, a vanishingly small probe current could be expected with a uniform and symmetric distribution around the frequency $n\nu_R$; the relative half width of this rectangular resonance curve is shown in Appendix B to be

$$\Delta\nu^*/n\nu_R=1/2\pi nN_0. \tag{6}$$

The preceding disregard of focusing and defocusing effects is, however, quite unrealistic. Even protons moving very closely in the median plane will rapidly be lost as soon as defocusing occurs, i.e., essentially as soon as the phase δ becomes positive, whereas for negative values of δ and consequent focusing, the protons will indeed reach the probe if the dee frequency is sufficiently near the resonance frequency. For $V_d=V_c$, the initial phase δ_0 is zero, and the phase δ becomes positive for $\Delta\nu=\nu-n\nu_R>0$; this requires that the previously discussed symmetric resonance curve be replaced by one whose total width is given by Eq. (6) and which lies entirely on the lower frequency side of resonance.

The next refinement is obtained by considering dee voltages V_d appreciably greater than V_c, in which case finite probe currents are obtained, since even entering protons not immediately adjacent to the injection plate will clear it after the first revolution; however, the initial phase angle δ_0 is now not required to be zero. Resonance curves are calculated in Appendix B and plotted in Fig. 4 for this case, still assuming that the focusing condition $-\pi/2<\delta<0$ is necessary and sufficient for a proton to reach the probe. The discontinuities in the slope are due to this assumption; a more detailed and rather complex analysis of the transverse motion would be necessary to avoid this assumption and to obtain continuous curves which, of course, are observed experimentally.

The plots in Fig. 4 are given for various dee voltages; the current amplitudes have been normalized to unity, and the widths are given in units of $\Delta\nu_c^*$, which is defined by Eq. (6) for a dee voltage of V_c. If the obvious discontinuities in these curves are smoothed out, they agree qualitatively with the experimentally observed resonance curves—the chief discrepancy being that, for the higher values of n, the experimental curves are somewhat wider. This discrepancy arises because Fig. 4 is based on the assumption that the protons stay very nearly in the median plane. This is not a realistic assumption, particularly at the higher multiple frequencies, where the focusing action decreases and the protons oscillate with appreciable amplitude about the median plane. As is evident from the factor $\cosh(ny/r)$ of Eq. (3), this means that these protons take fewer revolutions to reach the detector probe than do those in the median plane, with the result that the resonance is correspondingly broadened.

Although the previous analysis is not sufficient for an exact calculation of resonance curves, it contains, nevertheless, most of their essential features. Particularly for V_d in the vicinity of V_c, it represents rather faithfully the position of the point P in Fig. 4 where the current on the high frequency side goes to zero; it is shown in Appendix B that this point lies at $\Delta\nu=\Delta\nu_c^*[(V_d/V_c)^2-1]^{\frac{1}{2}}$. As pointed out above, for V_d close to V_c, the initial phase δ_0 must be close to zero and for dee frequencies slightly less than $n\nu_R$, the protons will be very nearly always focused throughout their orbit in contrast to the case of dee frequencies slightly higher than $n\nu_R$, where the protons will be very nearly always defocused and lost. Therefore, independent of the details of transverse motion, the point P (Fig. 4) approaches, to a good approximation, the resonance frequency $n\nu_R$ as the dee voltage approaches the cut-off value V_c. It is principally this fact which allows us to derive the value of ν_R within about $\frac{1}{8}$ of the line width; in the absence of any theory the total width of the resonance curves would have to be considered as experimental error.

B. Perturbing Electric and Magnetic Fields

It is essential to investigate the effects of perturbing fields, particularly since a radial electric field will evidently cause a shift in the resonance frequency. Consider the case of a proton revolving in a circular orbit of radius r, and frequency ν_R in a magnetic field H which is in the z direction. The superposition of a small radial electric field E_r will appear to the proton as an additional magnetic field $\Delta H=-cE_r/2\pi r\nu_R$ and the fractional decrease in orbital frequency will be $\Delta\nu_R/\nu_R=\Delta H/H=-(E_r/E_0)\cdot(r_0/r)$, where $E_0=v_0H/c$ is the electric field necessary to cancel the Lorentz force due to the magnetic field H on the proton so that it would travel in a straight line with a velocity $v_0=r_0 2\pi\nu_R$. Actually, this is the electric field between the compensating electrodes (Fig. 1) and r_0 is the radius of injection. Taking $E_0=11{,}000$ volts/cm and $r_0/r=5$, one finds that a radial field of 0.01 volt/cm will cause a frequency error of one part in 2×10^5.

A similar expression for the frequency shift has been obtained by a perturbation calculation in which the radial and tangential components of a general perturbing electric field as seen by the proton were expressed as fourier series in the polar angle θ. From this calculation it is found that the only form of general field which will cause a frequency shift is one in which the radial component averaged over θ does not vanish. If this average is $\bar{E}_r$, then the fractional frequency shift is $\Delta\nu_R/\nu_R=-(\bar{E}_r/E_0)(r_0/r)$.

This perturbing field $\bar{E}_r$ may have several sources: (1) between the compensating electrodes there exists a strong dc field which fringes slightly into the dee cavity; (2) space charges may cause a small dc field; (3) the dees themselves produce rf fields which may partly contribute to $\bar{E}_r$; (4) the distortions of the field in the dees, due to the detector probe, may cause frequency shifts. It is believed that all of these sources of frequency error have been made negligible in the present experiment, as the following discussion will show.

The field from the compensating electrodes is shielded from the dee cavity by the injection plate (Fig. 1) and the alignment probe, which can be moved into a position where it acts as a shield. When this shield is moved down into the region of least shielding, a fan-shaped dc fringe field is admitted into the dee cavity, which causes a decrease in the resonance frequency of about one part in 6×10^5. This observed shift is in agreement with a calculation based on the measurement of the fan-shaped field of a two-dimensional model shaped like the cross section of Fig. 1. However, as the shield is moved upward into the effective shielding region, the frequency is observed to increase and then to remain stationary even as the shield is moved farther in. Thus, if the shield is beyond a certain position, the leakage field is made negligible, so that further shielding has no effect on the resonance frequency.

A calculation of the space-charge field of the protons themselves is difficult, owing to the uncertainty in the charge distribution. However, a crude calculation of this effect shows that there will be a radial electric field of the order of magnitude of $E_r\sim10^{-3}$ volt/cm, so that one expects a negligible frequency error. This expectation was confirmed by the observed experimental fact that a change in the entering proton current by a factor of 10 has no other effect than to change proportionally the magnitude of the detector probe currents without affecting their frequency dependence.

Likewise the charge produced by ionization of the gas in the dees has a negligible effect on the resonance frequency. At an air pressure of 10^{-4} mm Hg there is a probability of only 10^{-1} that a proton will produce one ion pair along a path consisting of 10^9 revolutions. The electrons will very rapidly leave the dee cavity, while the positive ions may have a lifetime at most about $\frac{1}{10}$ that of an orbital proton. Again, it is experimentally observed that a change of the gas pressure in the dee chamber by a factor of 10 has no effect on the frequency dependence of the probe current, which proves that space charges due to ionization are likewise negligible.

The cyclotron dees produce a perturbing electric field with primarily a θ-component which decelerates the protons. Because of the geometrical symmetry of the dees, the r-component averages to zero in one cycle and hence produces no frequency shift. However, any geometrical asymmetries of the dee configuration will cause a frequency shift.

The only essential asymmetry in the present arrangement is the detector probe (Fig. 1), which has been placed along a radius at $\theta=25°$ for structural reasons. Radio-frequency field lines terminate on this probe and the radial field component does not average to zero around a circle as it would do if the probe were at $\theta=0$. An upper limit to the frequency error, caused by the detector probe, has been estimated in the following manner: A two-dimensional electrostatic problem has been solved[14] in which the dees are represented by an

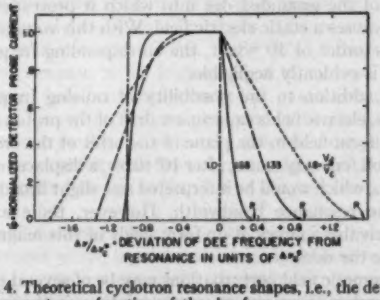

FIG. 4. Theoretical cyclotron resonance shapes, i.e., the detector probe current as a function of the dee frequency ν expressed in terms of $\Delta\nu/\Delta\nu_c^*$, where $\Delta\nu=\nu-n\nu_R$ and $\Delta\nu_c^*$ is the half width for a dee voltage $V_d=V_c$ given by Eq. (6). The curves plotted are from Eqs. (13A), (14A), and (15A) of Appendix B with the current normalized to unity at maximum amplitude.

[14] I am indebted to Mr. K. Trigger for having carried out this calculation.

infinite split cylinder and the probe by an infinite wire at a radius $r=0.4r_0$. With the top semi-cylinder at a potential of V_d volts and the wire and lower semi-cylinder at zero volts, the radial component of the field $E_r'=V_d f(\theta)$ along a circle of radius $r=0.5r_0$ has been calculated. This is an upper limit calculation because the shielding effect of the top and bottom of the dees is neglected. For resonance at the nth multiple the dee voltage is $V_d\cos(2\pi n\nu_R t)$, and the perturbing electric field will be

$$\bar{E}_r=\int_0^{2\pi} E_r'\cos n\theta d\theta.$$

Taking $V_d=200$ volts, one finds for $n=7$, $\Delta\nu_R/\nu_R=+1/4500$; for $n=9$, $\Delta\nu_R/\nu_R=+1/600{,}000$; for $n>11$, $\Delta\nu_R/\nu_R$ is extremely small.

These values are in essential agreement with the experimental results; the resonance frequency is observed to be the same for the 9th and 11th multiples, but at the 7th multiple it is increased by about one part in 1.5×10^4. Thus we conclude that the detector probe effect is negligible at the 9th and higher multiples. This fact was verified further by an experiment in which a dummy detector probe identical to the actual detector probe was installed in the dees at an angle $\theta=-25°$ and at a slightly smaller radius than the actual detector. This removed the geometrical asymmetry but still allowed the spiraling protons to strike the actual detector first. It was observed that at the 9th multiple the presence or absence of the dummy probe did not change the resonance frequency under otherwise identical operating conditions, whereas at the 7th multiple, the addition of the dummy probe caused the resonance frequency to decrease by about one part in 1.5×10^4, and thus to agree with the 9th and 11th multiples. Hence, by the use of a dummy probe the perturbing effect of the detector probe can be canceled for all dee frequencies. Another effect of the detector probe is due to the fact that, in collecting protons, it reaches a voltage slightly above that of the grounded dee into which it protrudes and thus causes a static electric field. With this voltage only of the order of 10^{-3} volt, the corresponding frequency shift is evidently negligible.

In addition to the possibility of causing frequency shifts, electric fields can cause a drift of the proton orbit. A uniform field in the plane of the orbit of the order of 0.1 volt/cm may cause, after 10^3 turns, a displacement of $0.05r_0$, which would be interpreted as a slight broadening of the resonance bandwidth. However, there are no conceivable sources of uniform fields of this magnitude inside the dees.

Magnetic field perturbations may be of several types: (1) random or consistent space variations in the field H; (2) radio-frequency fields produced both by displacement currents and by real currents flowing in the dees; (3) the field produced by the proton current. This latter field is utterly negligible, being of the order of 10^{-9} gauss for the proton currents used in this experiment.

A space variation of the field by an amount $\Delta H/H$ within the area of the proton orbit will evidently set a lower limit to the resonance bandwidth by the amount $\Delta\nu_R/\nu_R\sim\Delta H/H$. If this variation is random, the proton orbit will not be particularly affected, but a consistent variation due to a tilt of the pole pieces will cause a drift of the orbit; this drift may be estimated as follows. A proton revolving in a circular orbit of radius r and frequency ν_R in a field H in the z direction may be considered as a system with a magnetic moment $\mu_s=e2\pi\nu_R r^2/2c$. If the field H increases slightly in the x direction at a constant rate dH/dx, this will produce on the system a force $F_x=\mu_s dH/dx$ and result in a drift with uniform velocity v such that the Lorentz force F_x' on the drifting system will be equal and opposite to F_x. With $\mathbf{F}'=(\mathbf{v}\times\mathbf{H})e/c$ one obtains thus $F_x'=-Hev_y/c=-\mu_s dH/dx$, and for the drift velocity $v_y=(er^2/2Mc)(dH/dx)$. In N revolutions the center of the orbit will therefore drift a distance $y=rN\Delta H/H$, where $\Delta H/H=(r/H)(dH/dx)$.

As described in Sec. III, the magnetic field in the interior of the dees has been made quite uniform, the maximum variation over the distance r_0 being $\Delta H/H=\pm1/25{,}000$. Because of the transit time effect, most of the orbit revolutions occur at a radius which is considerably smaller than the initial radius r_0 and at a consequently smaller value of $\Delta H/H$. It is estimated that under typical experimental conditions the magnetic field inhomogeneities limit the resonance bandwidth to about one part in 7×10^4; actually, other factors limit the observed bandwidths to several times this value.

From Fig. 7 it can be seen that the field non-uniformity consists chiefly of a consistent tilt. Taking $r_0/2$ as an average value of r, for which $\Delta H/H\simeq1/50{,}000$, one calculates a drift distance in 10^3 revolutions of $y=10^{-2}r_0$. Thus, this drift will have a negligible effect on the mechanics of the orbital motion as previously discussed.

If the dee voltage is $V_d\cos(2\pi n\nu_R t)$, then the magnetic field H_d produced by the displacement current is of the order of magnitude $H_d\simeq2\pi n\nu_R V_d/c$ and has components which are parallel to the field H. At the higher multiples the rapid oscillations of H_d will result in an effective perturbing field $\bar{H}_d$ which is decreased by approximately a factor $1/n$. Thus, a reasonable estimate of the frequency error due to displacement currents is $\Delta\nu_R/\nu_R=\bar{H}_d/H=eV_d/Mc^2=1/(3\times10^6)$ for a typical dee voltage.

The real rf currents flowing in the dees and lead wires may produce a field having components parallel to the field H. With symmetrical dee geometry and lead wires, this field, from the viewpoint of the proton, averages to zero in one revolution. Thus, the symmetry of the dee geometry in the present experiment removes the possibility of frequency errors due to rf dee currents. However, the dee leads are somewhat asymmetric, but a calculation has shown that this causes a maximum frequency error of one part in 3×10^5.

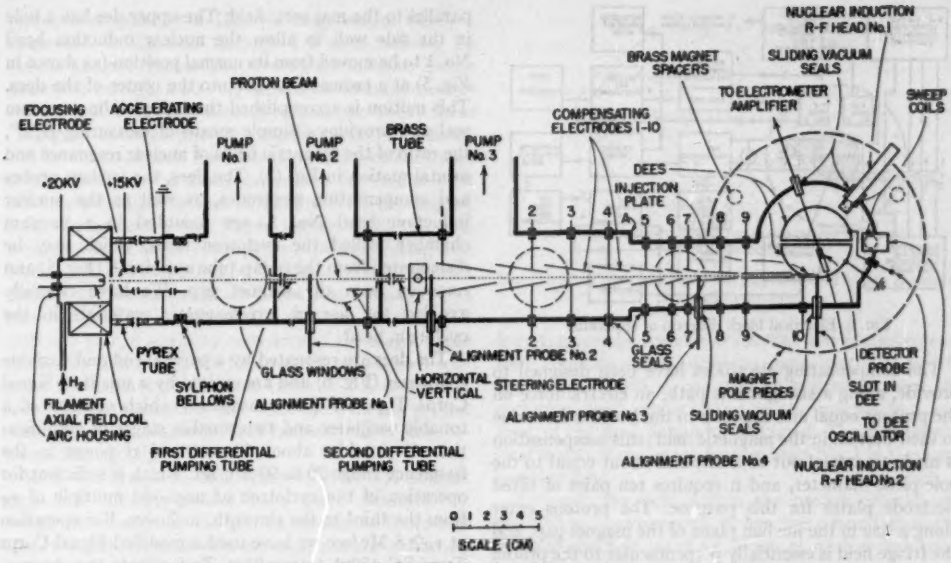

FIG. 5. Detailed drawing of apparatus.

III. DESCRIPTION OF APPARATUS

A detailed scale drawing of our apparatus is given in Fig. 5, and an electrical block diagram in Fig. 6. The operation in reference to this drawing is, very briefly, this: protons from the arc source are accelerated to 20 kv; they pass through the differential pumping stages and enter into the field of the magnet, where the Lorentz force on them is cancelled by the electric field of the compensating electrodes; finally the protons enter the dees where they are decelerated by the dee voltage until they strike the detector probe near the center.

The arc source is of conventional design, utilizing an axial magnetic field of several hundred gauss to enhance the ionization of hydrogen gas, which enters through a palladium leak, by collision with electrons from a hot tantalum filament. With the filament at 50 v below the arc housing, the arc current is about ½ amp. Protons are pulled through a 1 mm hole in the arc housing by a cylindrical focusing electrode at an adjustable potential of about 5 kv below the arc housing. Coaxial with this electrode is a second accelerating electrode at a fixed potential of 20 kv below the arc housing. These electrodes constitute a proton gun which produces a proton beam of 1 μamp. about 3 mm in diameter. The proton gun is aligned with respect to the rest of the apparatus by means of a sylphon bellows.

The gas pressure in the arc is normally about 10^{-2} mm Hg and about 10^{-4} mm Hg in the region of the accelerating electrode, which is evacuated by pump No. 1. In order to maintain considerably lower pressures in the dee cavity, it has been necessary to employ differential pumping; the collimated proton beam from the gun passes through the first differential pumping tube into an intermediate region evacuated by pump No. 2, whereby the gas pressure is reduced to about 3×10^{-6} mm Hg without appreciable reduction in the beam current; the process is repeated with a second differential pumping tube, allowing an ultimate gas pressure of about 5×10^{-7} mm Hg in the region containing the dees, which is evacuated by pump No. 3. The pressure in this region is limited by outgassing and small leaks, and is independent of the pressure in the arc source.

The differential pumping tubes have a diameter of 3 mm and are 8 cm long. The pumps are 4-inch metal oil diffusion pumps equipped with cold vapor traps containing solid CO_2 or liquid nitrogen. All pressures have been measured with D.P.I. Type VG-1A ionization gauges. Because of the high speed of the pumps, little difficulty has been experienced in maintaining the vacuum. Except for a Pyrex glass pipe in the proton gun, the vacuum system is constructed of brass or copper, the joints being made with rubber gaskets. Electrical leads are brought through either Kovar or platinized glass seals.

In addition to the detector probe in the dees, there are four probes which, together with horizontal and vertical steering electrodes, are used to properly align the proton beam. All these probes operate through sliding vacuum seals of the Wilson type. Both the alignment probes and the ends of the differential pumping tubes are coated with a fluorescent substance and are visible through glass windows; this facilitates alignment and makes it possible to observe the shape of the beam.

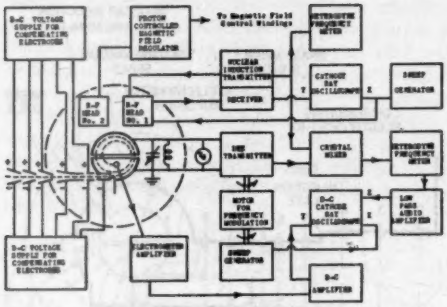

FIG. 6. Electrical block diagram of apparatus.

The compensating electrodes have been designed to provide, along a straight-line path, an electric force on the protons equal and opposite to the Lorentz force due to their motion in the magnetic field; this compensation is made to extend out to a distance about equal to the pole-piece diameter, and it requires ten pairs of tilted electrode plates for this purpose. The protons enter along a line in the median plane of the magnet gap, and the fringe field is essentially perpendicular to the proton path. By measuring the magnetic field with a flip coil, it has been possible to graphically determine the arrangement and shape of the ten pairs of tilted plates which will give an electric field perpendicular to the magnetic field and vary in magnitude approximately in the same manner along this line. The voltage for each pair of electrodes is balanced to ground, so that the potential along the proton path remains at zero. Each electrode is supplied by a separate voltage divider across a common center-grounded dc supply, whose overall voltage may be varied by a single control. This provides single-control adjustment of the compensating field for any value of the magnet current and also allows for local adjustments. By the help of the alignment probes, it is possible to adjust the relative electrode voltages so that the proton path is essentially a straight line, with a proton current of about 10^{-9} amp at alignment probe No. 4.

The protons enter the lower (grounded) dee tangentially to the injection plate which is attached to it. This plate is 0.25 mm thick and extends over the width of the dee. Together with the alignment probe No. 4, which has also the width of the dee, this plate very effectively shields the interior of the dee cavity from the field of compensating electrode No. 10. The dees are made of 0.16 cm thick copper and have an inside radius of 4.25 cm and an inside width of 1.65 cm. They are centered both radially and axially in the magnet gap. The grounded dee is slotted on one face to admit the detector probe, which is variable in position along a radius at an angle of 65° with respect to the dee gap. This probe is a small copper strip 1 mm wide and 0.1 mm thick, extending over the width of the dee and parallel to the magnetic field. The upper dee has a hole in the side wall to allow the nuclear induction head No. 1 to be moved from its normal position (as shown in Fig. 5) at a radius of 6.7 cm into the center of the dees. This motion is accomplished through a sliding vacuum seal and provides a simple means of measuring H/H', the ratio of the magnetic fields of nuclear resonance and orbital motion in Eq. (2). The dees, the various probes and compensating electrodes, as well as the nuclear induction head No. 1, are mounted in a vacuum chamber, called the cyclotron head, which may be dismounted from the pump tube at point A (Fig. 5) and removed from the magnet gap. We have carefully avoided the use of ferromagnetic materials in the cyclotron head.

The dees are resonated by a parallel coil and variable condenser (Fig. 6) and are excited by a modified Signal Corps Type ARQ-8 transmitter, which consists of a tunable oscillator and two tunable stages of amplification; it provides about 50 watts of rf power in the frequency range 20 to 90 Mc/sec, which is sufficient for operation of the cyclotron at any odd multiple of ν_R from the third to the eleventh, inclusive. For operation at $\nu_R \cong 8$ Mc/sec we have used a modified Signal Corps Type BC 459 A transmitter. To facilitate the observation of resonance, described below, the frequency is varied by a small amount in the neighborhood of $n\nu_R$ by means of a motor driven butterfly condenser at a rate of $\frac{1}{4}$ cycle/sec. The detector probe currents are of the order of magnitude of 10^{-12} amp for the higher multiple frequencies and are amplified by a balanced electrometer circuit,[15] utilizing a pair of Victoreen UX41-A tetrodes. The input resistance of the amplifier is 10^9 ohms; due to the capacitance in the coaxial lead from the probe to the tetrodes, the time constant is limited to about 10^{-2} sec. The time required to sweep through resonance is about one second, which is sufficiently larger than the detector time constant to prevent any appreciable distortion of the resonance shapes.

The nuclear induction apparatus for observing the nuclear resonance of protons consists of a transmitter-receiver unit and the r—f head No. 1 (Fig. 5) and is of the usual design.[6,16,17] The rf head is designed to fit inside a brass tube 1.25 cm in diameter so that it can be moved into the dee cavity. The proton sample, a 0.02-molar solution of $MnSO_4$ in pure H_2O, is cylindrical in shape with a volume of 0.1 cc. The sweep coils are 2.5 cm in diameter and are mounted coaxial with the sample on the outside walls of the cyclotron head.

We have used a single-yoke, air-cooled electromagnet with circular plane pole pieces 26.4 cm in diameter, spaced 4.80 cm apart. There are two coils, requiring 7.2 amp at 60 volts to produce a field of 5300 gauss; within about 0.3 percent, this is the field value at which we have operated throughout the experiments. The magnet

[15] J. A. Victoreen, Proc. Inst. Radio Engrs. 37, 432 (1949).
[16] W. G. Proctor, Phys. Rev. 79, 35 (1950).
[17] M. E. Packard, Rev. Sci. Instr. 19, 435 (1948).

power is supplied by a 125-volt dc generator which is connected to the coils through a 9 ohm resistor. To reduce current fluctuations due to fluctuations in the generator voltage, a 60-volt bank of automobile storage batteries is connected directly across the coils; these "floating" batteries provide a regulation factor of about 100 by virtue of their low internal resistance. The value of the field can be finely controlled by means of a 2000-ohm variable resistor in parallel with the magnet coils. To achieve a still higher constancy of the field value, we have employed a proton-controlled magnetic field regulator as described by Packard.[17] This apparatus obtains its information from the nuclear induction r—f head No. 2 (Fig. 5) and controls a current of about 0.1 amp in a pair of auxiliary coils around the magnet pole pieces. By this means the field can be maintained constant to within 1/200,000 for times of the order of ½ hour. This stabilization has been used in the precise mapping of the magnetic field necessary to obtain extreme homogeneity.

With the cyclotron head removed from the magnet gap, field inhomogeneities have been measured by noting the change in the proton resonance frequency upon the displacement of a movable nuclear induction head from the center of the pole pieces to the point under observation; during this procedure the field is held to a constant value by the regulator described above. By this method it was possible to detect relative field variations down to 1/200,000.

When the magnet coils are energized, there occurs normally a considerable bending of the magnet yoke, which tends to make the pole faces non-parallel. This effect has been prevented to a large extent by the use of two brass spacers (Fig. 5) which are inserted when the field is zero. Further field corrections have been made by ferromagnetic "shims," which were held to the pole faces by thin brass caps; circular rings of 0.01 cm steel shim stock have been used near the edges of the pole faces; nickel, electroplated on brass shim stock to a thickness of about 2×10^{-4} cm, has been used in a trial-and-error process to make the field still more homogeneous in a circle of about 3.9 cm radius, which is the maximum radius of the proton orbit.

In order to obtain consistent reproduction of the magnetic field configuration in this region, it has been found necessary to operate the magnet within a temperature range between 38° and 43°C, and to employ a current cycling procedure whenever the coils are energized; it consists in increasing the current to about 30 percent above its normal value, then decreasing it to normal, repeating the procedure for about five times.

By taking these precautions it has been possible to achieve and maintain a homogeneous field in the region of the dees, which does not vary from the center value by more than 1/25,000. Figure 7 is a plot of the field configuration in terms of the fractional variation from the center value; it is an average of seven independent measurements. The deviation of any one measurement

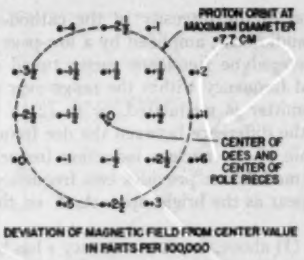
PROTON ORBIT AT MAXIMUM DIAMETER
•7.7 CM
CENTER OF DEES AND CENTER OF POLE PIECES
DEVIATION OF MAGNETIC FIELD FROM CENTER VALUE IN PARTS PER 100,000

FIG. 7. Plot of the variation of the magnetic field within the region of the proton orbits.

from the average is about 1/200,000. The measurements were taken on several different days, spaced as widely apart as a month in one case, during which time the cyclotron head was installed in the magnet gap and most of the final data were obtained. The field in the local region of nuclear induction head No. 1 is also very homogeneous.

Although the field within the proton orbit is reproducibly homogeneous, it has been found that the value of the field, at the position of nuclear induction head No. 1 relative to that at the center, may vary from day to day by as much as 1/20,000, while only a very small variation occurs over a period of a few hours. For this reason we have constructed the nuclear induction head No. 1 to be movable between the normal monitoring position and the dee center, so that the field ratio H/H' of Eq. (2) can be measured directly to high accuracy. In the present experiment a typical value is $H/H'=(1-1/30{,}000)$.

As is shown in the block diagram of Fig. 6, the end result of the overall operation of the apparatus is the oscillographic presentation of the two resonance phenomena involved. The nuclear induction signals are displayed in the usual manner on an oscillograph by superimposing upon the constant field H', by means of the sweep coils (Fig. 5), a 60-cps sinusoidal field of about two gauss and applying a horizontal sinusoidal sweep of the same frequency and adjustable phase; the rf leakage into the receiver coil has been adjusted so that a pure absorption mode is observed.

The cyclotron resonances are observed by a small frequency modulation of the dee transmitter at a rate of ¼ cycle/sec and a sawtooth horizontal sweep of the same rate applied to a DuMont Type 304-H dc oscillograph with a long-persistence screen. The detector probe currents, amplified by the electrometer circuit and a subsequent single-stage dc amplifier, are applied to the vertical plates of this oscillograph. With the horizontal sweep phased to begin (and end) when the dee frequency is a maximum, a trace such as that of Fig. 8 is obtained; it is apparent that resonance is swept through twice, first with the dee frequency decreasing and then with it increasing.

A record of the dee frequency is made on the trace by

modulation of the intensity of the cathode-ray tube with the audio beat, amplified by a low-pass amplifier, from a heterodyne frequency meter tuned either to: (1) a fixed frequency within the range over which the dee transmitter is modulated, or to (2) a frequency which is the difference between the dee frequency and a harmonic of the nuclear induction frequency. This intensity modulation provides two frequency markers which appear as the bright spots A, A′ on the trace of Fig. 8.

In case (1) above, the dee frequency ν has been measured with a Signal Corps Type BC-221 Q heterodyne frequency meter while at the same time ν_N has been measured with a very similar instrument—a Navy Type LM-18 meter. By calibrating both meters with the crystal from only one of them, it is possible to make a relative measurement of ν and ν_N to an accuracy within about 1/50,000, this limitation being set by the reading of the dial.

Case (2) above has been used at the 9th multiple cyclotron frequency to obtain greater accuracy than case (1) affords. As shown in Fig. 6, it requires a mixer tuned on the input to $\nu \cong 9\nu_R$ and to ν_N, and on the output to $\nu'' = \nu - 3\nu_N \cong 9\nu_R - 3\nu_N = \nu'$. The frequency ratio $\mu = \nu_N/\nu_R$ in Eq. (2) can then be written in the form $\mu = 9\nu_N/(\nu' + 3\nu_N)$, and one obtains for the relative error of measurement $\delta\mu/\mu = \pm[\nu'/(\nu' + 3\nu_N)][(\delta\nu'/\nu')^2 + (\delta\nu_N/\nu_N)^2]^{\frac{1}{2}}$. Thus, the accuracy of measurement of the frequencies is made less critical by the factor $\nu'/(\nu' + 3\nu_N) \cong 1/15$. We have used the Signal Corps BC-221Q meter to measure ν'', while at the same time ν_N has been measured with the Navy LM-18 meter. In this case we have calibrated each meter with its own crystal, observing that the crystals do not differ in frequency by more than 1/25,000. This allows a measurement of ν_N/ν_R with an error of only about $\pm 1/250{,}000$.

As is shown in Fig. 8, the frequency markers A, A′ occur on the trace slightly displaced from their true position because of a time delay in the amplifiers. In terms of frequency this displacement corresponds to a shift of about 1/50,000 and can easily be corrected for by moving the markers forward on the photograph until they are at mirror symmetrical positions B, B' on the two halves of the trace. Another advantage of sweeping through resonance both with increasing and decreasing dee frequency, is that it shows the absence of distortion of the two resonance curves because of the observed fact that they are symmetrical about the center of the trace.

FIG. 8. Photograph of a typical cyclotron resonance trace at the 9th multiple of ν_R. The vertical deflection is proportional to the detector probe current; in the horizontal direction, the dee frequency first increases and then decreases, thus sweeping twice through resonance. The two bright spots on the trace at A and A′ are the frequency markers, which are slightly displaced from their true positions B and B′ because of time delay in the amplifiers. The relative width at half maximum amplitude is about 1/9000 for this resonance curve.

IV. MEASUREMENTS AND INTERPRETATION

The following procedure has been used in the operation of the apparatus: First, with the magnet warmed up and the current turned on through the cycling procedure described in Sec. III, the field is adjusted to about 5300 gauss. The proton gun is put into operation and the voltages on the compensating electrodes are so adjusted that a proton beam enters the dees. Next, a measurement of H/H' of Eq. (2) is made by means of the sliding rf head No. 1; during this process the magnetic field is maintained constant either by the proton-controlled field regulator or by manual control of the magnet current, using the nuclear induction signals from rf head No. 2 as a field indicator. Rf head No. 1 is then returned to its normal position just outside the dees and the signals from it are used to observe the exact proton resonance frequency by adjusting the frequency until the traces are symmetrical about their center point. With the receiver adjusted for a pure absorption mode, this is a simple and sensitive method of ascertaining true resonance, as discussed by Jacobsohn and Wangsness.[18] The magnetic field is held to this resonance value either by the field regulator or by fine manual control of the magnet current; the latter method was necessary at the higher dee frequencies, where the regulator was unstable because of insufficient rf shielding from the dee transmitter. The dee transmitter frequency is then set to approximately $n\nu_R$ and varied slightly until resonance curves are observed on the dc oscillograph; the heterodyne frequency meter, which provides the frequency markers, is adjusted to give an intensity marker on the trace near the maximum of the resonance curve. Data are obtained by photographing a single trace (of 4 seconds duration) of the cyclotron resonance curve while at the same time another observer is holding the magnetic field to the value for exact nuclear resonance by means of visual observation of the nuclear induction signals and fine manual magnet current control. Immediately after the photographic exposure the marker frequency and the nuclear induction transmitter frequency are measured. The exposure and frequency measurement take about 10 seconds during which time frequency drifts are negligible and the magnetic field is held constant to within $\pm 1/100{,}000$. After photographing several resonance curves for various dee voltages and detector probe positions, H/H' is again measured and noted to be the same as before.

[18] B. A. Jacobsohn and R. K. Wangsness, Phys. Rev. 73, 942 (1948).

We have observed cyclotron resonance at all odd multiples of ν_R from the 1st to the 11th. The most precise data were obtained at the 9th multiple; minor instrumental difficulties have so far prevented equally useful data at the 11th multiple. The detector probe position has been varied within the range $r/r_0=0.2$ to 0.8, and the dee voltage within the range $V_d=110$ to 350 volts peak. The observed detector probe currents are smaller at the higher multiple frequencies and decrease both as the detector probe is moved to smaller radii and as the dee voltage is decreased. The largest currents observed have been about 10^{-10} amp, and the smallest about 3×10^{-13} amp. The calculated Johnson noise current is about 4×10^{-14} amp; the observed background fluctuation is about twice as large as this value because of rf pickup, microphonics, amplifier drifts, etc. We have observed that a variation of the proton current entering the dees (e.g., by varying the arc filament heating) by a factor of 20 has no effect other than to vary the amplitude of the resonance signals; particularly, there are neither current dependent changes in the signal shape nor frequency shifts.

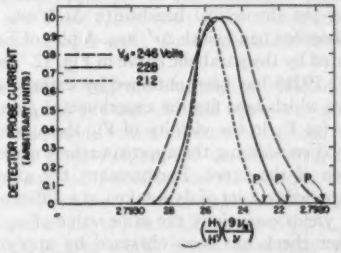

FIG. 9. Observed cyclotron resonance curves (normalized to unit amplitude) at the 9th multiple of ν_R for various dee voltages V_d. In each case the detector probe was at a position $r=0.4r_0$, and the cut-off voltage V_c was observed to be 206 volts. The dee frequency ν is given in terms of $(H/H')(9\nu_N/\nu)$. The points P correspond to the disappearance of the probe current on the high-frequency side.

The gas pressure in the dee chamber, as measured in the manifold to the pump, has been about 10^{-6} mm Hg during most of the measurements. At the 7th and 9th multiples we have varied the pressure in this region from about 5×10^{-7} mm Hg to about 10^{-5} mm Hg. Under otherwise identical operating conditions this variation does not change the shape or resonance frequency of the cyclotron resonance signals. The only pressure effect is a decrease of the signal magnitude; at a pressure of about 2×10^{-5} mm Hg the signals have fallen to the noise level and are no longer observable. This is in rough agreement with an exponential dependence of the current I upon the pressure P (in mm Hg) of the form $I=I_0\exp(-2.6\times10^5P)$ which one obtains for a proton making 500 revolutions at an average radius of 2 cm and taking a total gas kinetic scattering cross section of 1.25×10^{-15} cm^2. In view of this agreement and the experimental fact that neither the resonance frequency nor the bandwidth are pressure dependent, we have not made a detailed analysis of scattering effects. Because of scattering in the plane of the dees, one would expect a pressure broadening of the resonance bandwidth. We have not observed this in the present experiment, evidently because the probability that a proton be scattered sufficiently in the transverse direction to be lost, is considerably greater than the probability that it be scattered sufficiently in the median plane to cause a resonance broadening.

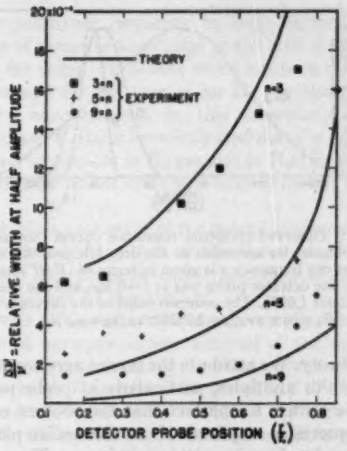

FIG. 10. Comparison of the theoretical and experimental relative widths at half maximum amplitude of cyclotron resonance curves for various detector probe positions. The data have been obtained at the 3rd, 5th, and 9th multiples of ν_R with a fixed dee voltage for each multiple. It was: $V_d/V_c=176/127$, $179/141$, and $247/223$, for the 3rd, 5th and 9th multiples respectively. Using these values of V_d/V_c, the theoretical half width has been obtained from the formulae in Appendix B.

The traces, like that of Fig. 8, are not drawn on the oscillograph in a linear frequency scale because frequency modulation is obtained by rotation of a butterfly condenser. However, the tuning curve of this condenser may be easily measured, and Fig. 9 shows several typical resonance curves for various dee voltages replotted on a linear frequency scale in terms of $(H/H')(n\nu_N/\nu)$. These curves have been normalized to unit amplitude; the actual signal amplitude at the highest dee voltage is about 10 times larger than that at the lowest.

As a first check on the theory of Sec. II we compare the relative width at half maximum amplitude of observed curves like those of Fig. 9, with the corresponding width of theoretical curves like those of Fig. 4. This comparison is given in Fig. 10 as a function of the detector probe position for a fixed dee voltage at the 3rd, 5th, and 9th multiples. The fairly good agreement at the 3rd multiple between the experimental points and the theoretical curve indicates that here the focusing action is sufficient to confine the protons to approximately the median plane of the dees, which was assumed

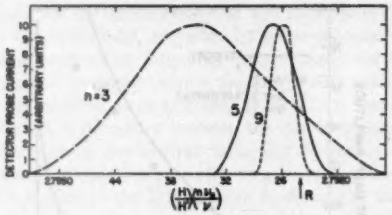

FIG. 11. Observed cyclotron resonance curves (normalized to unit amplitude) for operation at the 3rd, 5th, and 9th multiples of ν_R. The dee frequency ν is given in terms of $(H/H')(n\nu_N/\nu)$. In each case the detector probe was at $r=0.36r_0$ and the dee voltage V_d was about $1.05V_c$. The common point of the curves is approximately at R, where $n\nu_N/\nu=2.7924\cong\nu_N/\nu_R=\mu_p/\mu_n$.

in the theory. We attribute the poorer agreement at the 5th and 9th multiples, particularly at probe positions near the center, to the fact that the protons oscillate with appreciable amplitude about the median plane due to the weaker focusing action in this case. The assumption that they oscillate with increasingly greater amplitude as the radius decreases is supported by the fact that the observed bandwidth is about the same at the 9th multiple for all probe positions less than about $r=0.4r_0$.

The theoretical expectation (Sec. II) that phase focusing causes the resonance point to lie near the higher frequency side of the curves is verified in Fig. 11, which shows observed resonance curves at the 3rd, 5th, and 9th multiples replotted on a linear frequency scale in terms of $(H/H')(n\nu_N/\nu)$. In each case the dee voltage was about 5 percent greater than the cut-off value V_c. A dummy probe was used at the 3rd and 5th multiples to cancel frequency shifts due to the detector probe (Sec. II). The curves are evidently similar in shape, with a corresponding point at the approximate position R, where $(H/H')(n\nu_N/\nu)=2.7924$; interpreting this point as an indication of resonance, the same value may be taken to be the desired ratio μ_p/μ_n.

Although this method of deducing μ_p/μ_n from the data serves indeed as a valuable check, we have used

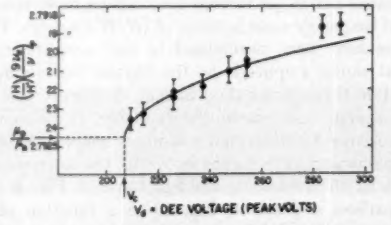

FIG. 12. The variation of observed values of $(H/H')(9\nu_N/\nu)_P$ with the dee voltage V_d for cyclotron operation at the 9th multiple of ν_R, and a detector probe position at $r=0.26r_0$. The solid curve is the expected approximate theoretical behavior and is a plot of Eq. (7) for $n=9$, where $V_c=207$ volts (observed value), $\Delta\nu'/9\nu_R=1/5600$ (observed total resonance bandwidth for $V_d=1.04V_c$), and $\mu_p/\mu_n=2.79245$ (graphically chosen to give a best fit to the experimental points).

the more quantitative procedure of observing the point P on the high frequency side of the resonance curves where the current goes to zero, as a function of the dee voltage at fixed values of n and the detector probe position. This point is indicated in Fig. 9 and corresponds to the point P in the theoretical curves of Fig. 4. The experimental points shown in Fig. 12 are observed values of $(H/H')(n\nu_N/\nu)_P$ corresponding to this point for various dee voltages near the 9th multiple of ν_R with the detector probe at $r=0.26r_0$. As shown in Sec. II, it is theoretically expected that this point approaches the true resonance value as the dee voltage V_d approaches the cut-off value V_c. However, as V_d approaches V_c, the signal amplitude decreases steadily so that a measurement of $(H/H')(n\nu_N/\nu)_P$ is difficult for V_d very near V_c. Therefore, we have extrapolated the data to V_c by using the expression

$$(H/H')(n\nu_N/\nu)_P = \mu_p/\mu_n[1-(\Delta\nu'/n\nu_R)((V_d/V_c)^2-1)^{\frac{1}{2}}], \quad (7)$$

which is obtained from Eq. (17A) (Appendix B) after replacing the theoretical bandwidth $\Delta\nu_c^*/n\nu_R$ by the actual observed bandwidth $\Delta\nu'/n\nu_R$. A plot of Eq. (7) is represented by the parabolic curve in Fig. 12. The value $\mu_p/\mu_n=2.79245$ has been obtained by extrapolation of the curve which best fits the experimental points, particularly for V_d in the vicinity of V_c; the agreement is fairly good considering the approximations made in the derivation of the curve. Furthermore, the above procedure applied to a set of data taken at a different probe position yields essentially the same value of μ_p/μ_n.

Another check has been obtained by applying this same procedure at the 3rd, 5th, and 7th multiples also, with the result in each case that the value of μ_p/μ_n obtained is in good agreement with that for the 9th multiple. This consistency, together with the excellent agreement of this value with the value of $(H/H')(n\nu_N/\nu)$ at point R of Fig. 11, provides assurance that our interpretation of the cyclotron resonance is essentially correct.

V. CALCULATION OF μ_p/μ_n

The value of μ_p/μ_n reported here is based upon a total of 135 individual cyclotron resonance observations, arranged in 17 groups. In each group of data, all the significant experimental parameters are held constant except the dee voltage. For each group $(H/H')(n\nu_N/\nu)_P$ has been plotted *versus* V_d and the parabolic curve of Eq. (7) has been fitted to the experimental points as in Fig. 12 in order to determine μ_p/μ_n. A summary of the data is given in Table I, where the best fitting value of μ_p/μ_n and the graphical fitting error have been determined by making several trials of fitting in each case. The data at the 3rd, 5th, and 7th multiples have been obtained with a dummy probe at $r=0.35r_0$ to prevent frequency shifts.

The average value of μ_p/μ_n from this table is 2.79242, and the mean deviation from this average value is about

1/74,000. This variation is not due to any internal inconsistency in the data, but is the result of statistical errors of measurement, which are estimated to be as follows:

(1) $\pm 1/100{,}000$ due to errors in setting the nuclear induction signal to exact resonance because of inexact adjustment of the receiver to a pure absorption mode.

(2) $\pm 1/100{,}000$ due to drift of the H field during observation of resonance.

(3) $\pm 1/75{,}000$ due to errors in the measurement of H/H'.

(4) $\pm 1/50{,}000$ due to errors in frequency measurements at the 3rd, 5th, and 7th multiples. This error is reduced by a factor 5 at the 9th multiple, as discussed in Sec. III.

(5) $\pm 1/100{,}000$ due to errors in correction of the frequency marker position (see Fig. 8) and correction of the non-linearity of the frequency scale of the traces.

(6) $\pm 1/50{,}000$ due to the average magnetic field inhomogeneity over a proton orbit; this is less than the inhomogeneity across the dee diameter because the transit time effect causes most of the proton revolutions to occur at smaller radii, where the field is more homogeneous.

Since these errors are statistically independent, we take the root of the sum of their squares as an indication of the over-all statistical error of any one measurement; this is $\pm 1/29{,}000$ for the 3rd, 5th, and 7th multiples and $\pm 1/34{,}000$ for the 9th multiple. Reducing these by $1/6^{\frac{1}{2}}$, where 6 is the average number of measurements used in a graphical calculation of μ_p/μ_n, we get about $\pm 1/80{,}000$, which agrees essentially with the statistics of Table I.

In order to obtain a good estimate of the absolute accuracy of our result, we have investigated all conceivable sources of systematic errors:

(1) Possible shifts in the cyclotron resonance frequency due to perturbing electric and magnetic fields have been discussed in detail in Sec. II, where it is shown that such errors are negligible, the total effect being to raise the observed value of μ_p/μ_n by about 1/500,000.

(2) The relativistic proton mass variation is $\Delta M/M = 1/100{,}000$ at an energy of 10 kv, which is approximately the average energy of the protons during their cyclotron orbit.

(3) Magnetic impurities in the movable nuclear induction head may cause an error of at most $+1/200{,}000$ in the measured value of H/H'.

(4) The paramagnetism of the manganese ions dissolved in the proton water sample increases the observed nuclear resonance frequency by a small amount. Using the calculations of Bloembergen and Dickinson[19] we find this to be about 1/400,000 for our 0.02 Molar sample.

(5) The magnetic field due to the electrons surrounding the protons in the water sample reduces the observed nuclear resonance frequency to some extent. In the absence of accurate knowledge of the size of this error we use the value $-1/37{,}000$, which has been calculated by Ramsey[20] for the case of an H_2 gas sample; preliminary measurements in this laboratory by M. Packard and E. Hahn have indicated that the resonance frequency of protons in H_2 gas and in H_2O in the same magnetic field do not differ significantly for our purpose here.

To obtain an estimate of the overall systematic error we take the algebraic sum of the above errors; this is $1/140{,}000$ and tends to make the values of μ_p/μ_n in Table I too low by this amount.

There is still another systematic error, arising from the use of our approximate analysis of the cyclotron resonance curve in locating the point of true resonance on this curve. This error is in the nature of an uncertainty which can only be estimated. In view of the generally fair agreement of the observed data with the approximate theory presented here, we believe that our analysis has not systematically misinterpreted the location of true cyclotron resonance by more than about $\frac{1}{4}$ of the total bandwidth of the resonance curves observed at the higher multiple frequencies; this corresponds to an error of about $\pm 1/14{,}000$. Considering that, compared to this error, all other errors both systematic and statistical are negligible, and using the average of the values in Table I, we can state our final result to be

$$\mu_p = (2.7924 \pm 0.0002)\mu_n. \tag{8}$$

This value is in essential agreement with the latest result reported by Hipple, Thomas, and Sommer,[11] which is

$$\mu_p = (2.79268 \pm 0.00006)\mu_n. \tag{9}$$

With the limits of error of the results of Eqs. (8) and (9) just touching each other, they can still be considered

TABLE I. Summary of data.

Cyclotron frequency multiple n	Detector probe position r/r_0	Number of measurements	Best fit value of μ_p/μ_n	Graphical fitting error in μ_p/μ_n
9	0.50	5	2.79230	±0.00002
9	0.40	7	2.79244	±0.00004
9	0.31	6	2.79238	±0.00006
9	0.26	6	2.79235	±0.00007
9	0.21	3	2.79243	±0.00003
9	0.40	8	2.79245	±0.00004
9	0.31	5	2.79245	±0.00003
9	0.26	11	2.79245	±0.00002
9	0.21	6	2.79245	±0.00003
9	0.40	6	2.79242	±0.00003
9	0.31	5	2.79243	±0.00003
9	0.26	7	2.79243	±0.00002
9	0.21	7	2.79239	±0.00002
7	0.36	22	2.79250	±0.00005
7	0.36	12	2.79250	±0.00005
5	0.36	10	2.79242	±0.00002
3	0.36	9	2.79230	±0.00025

[19] N. Bloembergen and W. C. Dickinson, Phys. Rev. 79, 179 (1950).

[20] N. F. Ramsey, Phys. Rev. 77, 567 (1950).

as a gratifying mutual confirmation. A more severe test will be obtained as soon as the accuracy of our method is somewhat increased. This should be possible by modifications of the present apparatus, now in progress in this laboratory; it is anticipated that appreciably smaller cyclotron resonance bandwidths than reported here can be obtained by changing the dee proportions and extending the operation to still higher multiples of ν_R, as well as by the use of baffle plates in the dees to remove those circulating protons which do not move closely in the median plane and are a source of resonance broadening. This latter scheme requires a new arc-source of protons with a higher current output, which is now under construction. It is also expected that this modified apparatus will be used in the determination of mass ratios of the light ions.

We shall not enter here into a discussion of the relation of our result to the faraday, the mass ratio of proton to electron, and other fundamental constants. These relations have been discussed by DuMond[21] and by Hipple, Sommer, and Thomas.[11]

In conclusion, the author wishes to express his sincere appreciation to Professor F. Bloch for suggesting this experiment and the method of the decelerating cyclotron operated at multiple frequencies, as well as for much help and encouragement throughout the course of the work. It is a pleasure to acknowledge valuable discussions with Professor H. H. Staub on the design of the apparatus, and his very helpful advice during its construction. Thanks are also due to Dr. M. E. Packard for numerous suggestions and to Mr. Kenneth Trigger, Mr. Burton Stuart, Mr. Edward Wright, and Elizabeth Jeffries for their assistance in various phases of the work.

Appendix A

Taking the potential of the electric field of Fig. 2 to be $\Phi(x, y)$ with the boundary conditions $\Phi(+x, \pm b/2)=v_d$ and $\Phi(-x, \pm b/2)=0$, it can be shown that Φ is given by

$$\Phi(x, y)=v_d-\frac{v_d}{\pi}\arctan\left[\frac{\cos(\pi y/b)}{\sinh(\pi x/b)}\right], \tag{1A}$$

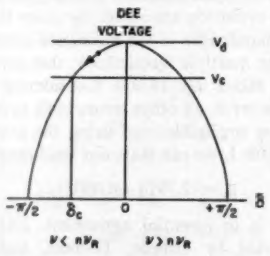

FIG. 13. Diagram of the variation of the dee voltage and its effective phase δ, experienced by a revolving proton in its consecutive passages through the dee gaps. For the case of a dee frequency below resonance, a representative point is indicated with the arrow showing the direction of the variation; for frequencies above resonance, the variation has the opposite direction.

[11] J. W. M. DuMond, Phys. Rev. **77**, 411 (1950).

from which the components of the electric field E are seen to satisfy the relation

$$-E_x+iE_y=v_d/b\cosh(\pi z/b) \tag{2A}$$

where $z=x+iy$. Thus, near the median plane $y=0$, the field E_x drops in a distance $x=b$ to about $\frac{1}{10}$ of its value at the origin.

By taking $v_d=V_d\cos(2\pi\nu t+\delta)$, where δ is the phase angle of the voltage when the proton is at $x=0$, the energy change ΔE and the transverse momentum change ΔP_y of the proton in transit at a constant value of y from $x=-\infty$ to $x=+\infty$ at a velocity $dx/dt=v$ are given by the expression:

$$-\Delta E+iv\Delta P_y=e\int_{-\infty}^{+\infty}(-E_x+iE_y)dx$$
$$=\frac{eV_d}{b}\int_{-\infty}^{+\infty}\frac{\cos[(2\pi\nu x/v)+\delta]}{\cosh(\pi z/b)}dx. \tag{3A}$$

Evaluation[22] of this integral yields:

$$\Delta E=-eV_d\frac{\cosh(2\pi y\nu/v)}{\cosh(\pi b\nu/v)}\cos\delta, \tag{4A}$$

$$\Delta P_y=\frac{eV_d}{v}\frac{\sinh(2\pi y\nu/v)}{\cosh(\pi b\nu/v)}\sin\delta. \tag{5A}$$

Applying these equations to the actual case of a proton revolving in a circular orbit of radius $r=nv/2\pi\nu$ in dees of width b and radius R, and considering that the changes of r and y per revolution are small, so that differences can be replaced by differential quotients, we have

$$\frac{V_0}{r_0^2}\frac{dr}{dN}=-\frac{V_d}{r}\frac{\cosh(ny/r)}{\cosh(nb/2r)}\cos\delta, \tag{6A}$$

$$\frac{M\pi\nu^2}{n^2}\frac{d^2y}{dN^2}=\frac{eV_d}{r}\frac{\sinh(ny/r)}{\cosh(nb/2r)}\sin\delta, \tag{7A}$$

where N is the number of revolutions and eV_0 is the proton energy at a radius r_0. Because of the approximations made, these equations are approximately valid for $b\ll y<(R-b)$.

Taking $\sin\delta=\sin[\delta_0+(2\pi N\Delta\nu/\nu_R)]$ where $\Delta\nu=\nu-n\nu_R$ and δ_0 is the initial phase at $N=0$, we may integrate Eq. (6A) for $y=0$:

$$\sin[\delta_0+(2\pi N\Delta\nu/\nu_R)]-\sin\delta_0$$
$$=-\frac{2\pi\Delta\nu}{\nu_R}\frac{V_0}{r_0^2V_d}\int_{r_0}^{r}r\cosh(nb/2r)dr, \tag{8A}$$

where N is the number of revolutions in the proton orbit between r_0 and r. Taking the special case $\Delta\nu=0$, $\delta_0=0$, we find the expression

$$N(r)\Big|_{\substack{\delta_0=0\\ \Delta\nu=0}}=N_0(r)=\frac{V_0}{r_0^2V_d}\int_r^{r_0}r\cosh(nb/2r)dr \tag{9A}$$

for the number of proton revolutions required to reach a radius r if the proton encounters the maximum dee voltage at each crossing of the gap. This integral can be evaluated from tables,[23] and is plotted in Fig. 3 as a function of r/r_0 with $V_d=200$ volts and n as a parameter; the constants have been chosen to correspond to the present experiment: $V_0=2\times10^4$ volts, $r_0=3.85$ cm, $b=1.65$ cm.

Appendix B

By neglecting focusing effects, an estimate of the resonance bandwidth for protons in the median plane may be obtained, as discussed in Sec. II. For a dee frequency ν slightly less than the resonance frequency $n\nu_R$ a proton will constantly slip in phase with respect to the dee voltage as it spirals in. This is represented in the phase diagram of Fig. 13 by a point moving toward negative δ. At the point where $\delta=-\pi/2$ the proton will have reached a minimum radius r and will be accelerated thereafter. A similar situation prevails at $\delta=+\pi/2$ for $\nu>n\nu_R$. Thus, if we take the initial phase $\delta_0=0$, then $\Delta\nu^*$, the maximum frequency deviation

[22] Bierens de Haan, *Nouvelles Tables D'Integrales Definies* (G. Stechert, New York, 1939), p. 387, No. 14.

[23] *Tables of Sine, Cosine and Exponential Integrals*, Volume I. (Works Progress Administration, New York, 1940).

from resonance for which a proton will just reach the detector probe at r, is obtained by taking $2\pi N\Delta\nu/\nu_R=\pi/2=\delta$ on the left side of Eq. (8A) and by using Eq. (9A), with the result

$$\Delta\nu^*/n\nu_R=1/2\pi nN_0. \tag{10A}$$

This expression may be interpreted as the half width of a symmetrical rectangular resonance curve to be expected under the idealized conditions of a well collimated proton beam and no focusing effects.

A refinement can be made by considering initial phase angles other than $\delta_0=0$ for fixed values of n and N_0. There are three different reasons for which a proton may not reach the detector probe: (1) it may not clear the injection plate; (2) the transition from deceleration to acceleration may take place at a radius larger than that at which the probe is located; (3) the transition from focusing to defocusing may take place before the probe is reached. All three reasons must be taken into account in the following considerations.

If V_e is the minimum dee voltage for injection, then a dee voltage of $V_d>V_e$ will inject protons with initial phases δ_0 for which

$$0\leq|\delta_0|\leq\arccos(V_e/V_d)=\delta_e.$$

Because of phase defocusing, we neglect, in the following discussion, all those with positive δ_0. For a given negative initial phase δ_0, all those protons will clear the injection plate (Fig. 1) for which the distance from the outer surface of the injection plate is less than $\Delta r=(r_0/2V_0)(V_d\cos\delta_0-V_e)$. We shall make the reasonable assumption that the incoming proton beam has a uniform distribution over a small thickness behind the injection plate. Therefore, the total injected beam current per unit initial phase angle will be proportional to the above expression for Δr and, in arbitrary units, can be written as $i(\delta_0)=V_d\cos\delta_0-V_e$. The detector probe current I_p can be obtained by integrating $i(\delta_0)$ over appropriate limits of δ_0. These limits are determined, below, by considering separately the cases of the dee frequency (a) slightly below and (b) slightly above the resonance frequency.

(a) In the case of dee frequencies slightly below resonance, there is a maximum absolute magnitude of the phase δ_0, which we designate by δ_0' and which is the particular value of the initial phase for which a proton will just reach the detector probe. Since the proton will reach its minimum radius when the phase δ has the value $-\pi/2$, one obtains from Eq. (8A) the following expression for determining δ_0':

$$\sin(-\pi/2)-\sin(\delta_0')=2\pi N_0\Delta\nu/\nu_R=\gamma. \tag{11A}$$

For dee frequencies below resonance, γ is evidently negative. Let us consider first the case where $|\delta_0'|<|\delta_e|$; since protons with initial phases beyond δ_0' cannot reach the detector probe, I_p is obtained by integrating $i(\delta_0)$ between the limits $\delta_0=0$ and $\delta_0=-\delta_0'$. If, on the other hand, $|\delta_0'|>|\delta_e|$, then all the injected protons can reach the detector probe, so that one obtains in this case the maximum value of I_p; it is obtained by integrating $i(\delta_0)$ between the limits $\delta_0=0$ and $\delta_0=-\delta_e$. From Eq. (11A) and the definition of δ_e, it may be seen that the condition $|\delta_0'|<|\delta_e|$ corresponds to the condition $\gamma<-[1-(1-\alpha^2)^{\frac{1}{2}}]$ where $\alpha=V_e/V_d$. Furthermore, it is seen from Eq. (11A) that the maximum frequency deviation from resonance for which protons will just reach the detector probe is obtained for $\delta_0'=0$, which corresponds to $\gamma=-1$. Thus for $\gamma<-1$, I_p will be zero.

(b) In the case of dee frequencies slightly above resonance, there is a minimum absolute magnitude of the phase δ_0, which we designate by δ_0'' and which is the particular value of the initial phase for which a proton will just reach the detector probe at the instant at which the phase δ has reached the value zero; for later instances the phase δ will become positive, and the proton will be lost by defocusing. Similar to Eq. (11A), one obtains from Eq. (8A) the following expression for determining δ_0'':

$$\sin(0)-\sin(\delta_0'')=2\pi N_0\Delta\nu/\nu_R=\gamma, \tag{12A}$$

where γ is now positive. Since the maximum value of $|\delta_0|$ is $|\delta_e|$, one obtains I_p by integrating $i(\delta_0)$ between the limits $\delta_0=\delta_0''$ and $\delta_0=\delta_e$. If $|\delta_0''|>|\delta_e|$, no injected protons may reach the detector probe before they are defocused, and I_p will be zero. The condition $|\delta_0''|>|\delta_e|$ corresponds to the condition $\gamma>(1-\alpha^2)^{\frac{1}{2}}$, as may be seen from Eq. (12A) and the definition of δ_e.

Performing the integrations indicated above, one thus obtains the following expressions for the detector probe current I_p:

for $-1<\gamma<-[1-(1-\alpha^2)^{\frac{1}{2}}]$,

$$I_p(\gamma)=V_d[1+\gamma-\alpha\arcsin(1+\gamma)]; \tag{13A}$$

for $-[1-(1-\alpha^2)^{\frac{1}{2}}]<\gamma<0$,

$$I_p=V_d[(1-\alpha^2)^{\frac{1}{2}}-\alpha\arcsin(1-\alpha^2)^{\frac{1}{2}}]; \tag{14A}$$

for $0<\gamma<(1-\alpha^2)^{\frac{1}{2}}$,

$$I_p(\gamma)=V_d[(1-\alpha^2)^{\frac{1}{2}}-\alpha\arcsin(1-\alpha^2)^{\frac{1}{2}}-\gamma+\alpha\arcsin\gamma]. \tag{15A}$$

These results are shown graphically in Fig. 4, in which the normalized detector probe current I_p' has been plotted *versus* γ/α for various values of $\alpha=V_e/V_d$. I_p' has been obtained in each case by dividing I_p by its maximum value, which is given by Eq. (14A). From Eqs. (9A), (10A), and (11A), one obtains

$$\gamma/\alpha=(\Delta\nu/n\nu_R)/(\Delta\nu_e^*/n\nu_R), \tag{16A}$$

where $\Delta\nu_e^*/n\nu_R$ is the half width as defined by Eq. (10A) for a dee voltage V_e and arbitrary values of n and the detector probe position.

From Eq. (15A) it follows that the point P (Fig. 4) where the current goes to zero on the higher frequency side of resonance is given by $\gamma=(1-\alpha^2)^{\frac{1}{2}}$; therefore, according to Eq. (16A), one has at this point $\Delta\nu=\Delta\nu_e^*(\alpha^{-2}-1)^{\frac{1}{2}}$.

As explained in Sec. IV, the experimentally observed resonance curves of Fig. 9 have been plotted in terms of $\mu=(H/H')(n\nu_N/\nu)$ as the abscissa rather than in terms of $\Delta\nu$. If in Fig. 9 the value of μ at point P is designated by $(H/H')(n\nu_N/\nu)_P$, then in correspondence with the above value of $\Delta\nu$, we have

$$\begin{aligned}\Delta\mu&=(H/H')[(\nu_N/\nu_R)-(n\nu_N/\nu)_P]\\&\cong(H/H')(\nu_N/\nu_R)(\Delta\nu_e^*/n\nu_R)(\alpha^{-2}-1)^{\frac{1}{2}},\end{aligned}$$

from which we obtain:

$$\begin{aligned}(H/H')(n\nu_N/\nu)_P&\cong(H/H')(\nu_N/\nu_R)[1-(\Delta\nu_e^*/n\nu_R)(\alpha^{-2}-1)^{\frac{1}{2}}].\end{aligned} \tag{17A}$$

This equation has been plotted in Fig. 12.

Letters to the Editor

PUBLICATION of brief reports of important discoveries in physics may be secured by addressing them to this department. The closing date for this department is five weeks prior to the date of issue. No proof will be sent to the authors. The Board of Editors does not hold itself responsible for the opinions expressed by the correspondents. Communications should not exceed 600 words in length.

Production of μ-Mesons by Gamma-Rays

PETER A. WOLFF
University of California, Berkeley, California
January 15, 1951

IN a recent paper Wentzel[1] has proposed a theory in which the μ-meson field is strongly coupled to the nucleon field by a pair type interaction similar to that used to explain beta-decay. This interaction provides forces between a $\mu-\mu^0$ pair, and the resulting bound state is identified with the π-meson. However, besides coupling π-mesons and nucleons, the pair theory also predicts processes in which the μ-mesons appear in unbound states, one example of such a process being photo-production, for which Wentzel estimates a ratio of $\mu-\mu^0$ production cross section to π-production cross section of 0.1—0.01 at photon energies of 350 Mev. This is about the energy available on the Berkeley synchrotron, and since experiments of Peterson[2] have already placed an upper limit on the number of μ-mesons produced from this machine, it seemed worthwhile to recalculate this ratio more precisely.

The calculations were carried out to the lowest order in the coupling constant using the Feynman-Dyson methods, and, since the theory is not covariant, all matrix elements were evaluated in the rest system of the π-meson and then assumed to transform covariantly on returning to the center-of-mass system. Furthermore, in this problem, the usual plane wave solutions for a pair of μ-mesons in the field are no longer correct, because of the presence of binding forces, so two approximate sets of wave functions were adopted. The first consisted of all plane waves plus the single bound level; the second was the same except that each plane wave was corrected by addition of some of the bound solution, the amount being so chosen that the corrected waves were orthogonal to the bound state. Finally, because of the non-covariance, it was necessary to neglect binding effects in the intermediate states and to treat all intermediate particles as being free.

With these approximations the cross section for the production of a π^+ meson by a γ-ray incident on a proton is

$$\sigma_\pi = \frac{e^2}{2\hbar c}\frac{|U|^2}{Mc^2(Mc^2+\hbar\omega)}\left(\frac{p_\pi}{mc}\right)\left(\frac{mc}{\hbar}\right),$$

where $|U|^2$ is the parameter used by Wentzel, p_π is the momentum of the outgoing meson in the center-of-mass system, and m and M are the masses of the π-meson and nucleon, respectively. For the pair cross section, using the first set of wave functions mentioned above, the following expression was obtained:

$$\sigma_{\mu\mu^0} = \frac{\pi^2 e^2}{\hbar c}\left[\frac{2Mc^2+\hbar\omega}{Mc^2+2\hbar\omega}\right]\left(\frac{\Delta}{Mc^2}\right)^2\frac{\eta^2(\mu c)^2}{\hbar\omega\hbar c(2\pi\hbar)^2},$$

where μ is the mass of the pair meson, η the coupling constant, and Δ the total kinetic energy in the center-of-mass system of the three outgoing particles. A similar calculation using the second set of wave functions yields a formula with the same form, but the numerical coefficient of which is approximately half as great. It should be noted that these expressions were derived under the assumption that outgoing particles were nonrelativistic, and they are, therefore, incorrect for energies far from threshold.

From the cross sections the relative yield of $\mu-\mu^0$ pairs to π's is calculated by integrating over a bremsstrahlen (dE/E) spectrum. For a maximum photon energy of 322 Mev and using the value $|U|^2/\eta^2 = 2.4\pi(\mu c)^2/(2\pi\hbar)^2$ (the numerical factor arises from evaluating the integral called "c" by Wentzel), the relative yield turns out to be 0.11 or 0.06 depending upon which set of wave functions was used. These figures are to be compared with the upper limit $0.04(\pm 0.04)$ given by Peterson from experiments on the synchrotron. Finally, it is interesting to note that the ratio calculated above is virtually independent of nucleon cutoff, depending only on $|U|^2/\eta^2$, which is insensitive to the upper limit placed on the nucleon momenta.

In conclusion, I would like to express my thanks to Professor Robert Serber who has given me much helpful advice and encouragement on this problem.

[1] G. Wentzel, Phys. Rev. 79, 710 (1950).
[2] J. Peterson (to be published).

Disintegrations of Nd^{147} and Pm^{149}

EVANI KONDAIAH
Nobel Institute of Physics, Stockholm, Sweden
January 15, 1951

SLOW neutron bombardment of neodymium yields, among other short half-lives, two activities known to have half-lives of 11 days and of 2 hr. The 11-day period has been assigned to Nd^{147} and the 2-hr activity to Nd^{149} which decays by negatron emission to Pm^{149}.[1] Pm^{149} further decays with a half-life of about 2 days.[1]

"Specpure" Nd_2O_3 was irradiated by slow neutrons in the Harwell pile for 4 weeks, and the resulting activities were studied at this Institute using a β-ray spectrometer.[2] Finely powdered Nd_2O_3 was spread with an average thickness of about 2 mg/cm^2 over an aluminum backing of 2 mg/cm^2. The half-life graph showed two components, one having a value 48 ± 3 hr and another 11.6 ± 0.3 days.

The β-spectrum was taken at several periods of decay. Two electron lines, one at 730 gauss-cm and another at 1007.4 gauss-cm, corresponding to the electron energies 44.9 and 82.6 kev, were found. From their energies and intensities they were identified as the K and L lines of a 90-kev γ-ray. These lines were found to decay with the 11-day period. The 11-day period β-spectrum yielded two components on Fermi analysis. The energies of these two components were found to be 350 ± 8 kev and 780 ± 8 kev.

After taking into account the 11-day β-spectrum, Fermi analysis of the 2-day β-spectrum showed that it consists of a single component having maximum energy 1.05 ± 0.01 Mev.

The γ-spectrum, taken in the same spectrograph using a thick copper capsule and a lead-foil about 20 mg/cm^2 thick, showed 5 photo-electron peaks of different intensities. The first one at 963.6 gauss-cm, corresponding to 76-kev energy, was identified as the L photo-line of a 91.8-kev γ-ray. A small peak at 1752 gauss-cm, corresponding to 221 kev, was taken to be the K line of a 309-kev γ-ray. Another small peak at 2117 gauss-cm, corresponding to 304 kev, was taken to be the K line of a 391-kev γ-ray. The last two lines at 2657 and 2920 gauss-cm, corresponding to 435 kev and 502 kev, respectively, were found to be the K and L photo-lines of a 520-kev γ-ray. All these photo-lines seem to decay with the 11-day period. The first photo-spectrum was taken after about a 3-day decay of the sample, and no γ-ray having the half-life of 2 days was observed. The energies of the γ-rays from the γ-spectrum were found to be 91 ± 1, 309 ± 5, 391 ± 5, and 520 ± 3 kev.

The intensities of the two β-components of the 11-day period were estimated to be about 32 and 65 percent, the harder component being the more intense. Using these estimates and the photo-spectrum, the intensities of the γ-rays were estimated as: 91 kev, 66 percent; 309 kev, 1 percent; 391 kev, 2 percent; 520 kev, 32 percent. The K to L ratio for the 91-kev γ-ray was found to be 6.5 ± 1.5 from the β-spectrum. The conversion coefficient for

the 91-kev γ-ray is approximately 0.9. Comparison with Hebb and Nelson's formulas[3] and Rose's tables,[4] makes it appear that the 91-kev γ-ray is probably a mixture of magnetic dipole and electric quadrupole radiations.

Using Feenberg's curves[5] the comparative half-lives for the β-components were found to be 350 kev (11-day) log (ft)=6.6, 780 kev (11-day) log(ft)=7.4, 1.05 Mev (2-day) log(ft)=6.96. Applying the considerations of Nordheim[6] all these three can be placed in the first forbidden group with a change in parity and a change in spin of 0 or 1.

A probable disintegration scheme for Nd^{147} is suggested in Fig. 1.

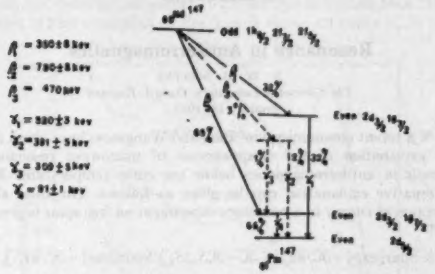

FIG. 1. Probable disintegration scheme for Nd^{147}.

The energies of the γ-rays add up well within the experimental errors mentioned. The β_3-component, having maximum energy of about 470 kev, was not obtained from the Fermi analysis of the 11-day β-spectrum. This is probably due to its low intensity ($\sim$3 percent). However, the possibility that the 391- and 309-kev γ-rays may arise from some impurity of a nearby half-life cannot be entirely ruled out, so these two γ-rays and the corresponding β-ray are shown by broken lines.

Pm^{149} appears to decay by a single β-ray of maximum energy 1.05 Mev. No γ-rays having this period (2 days) were observed.

The term scheme given in Fig. 1 was arrived at from the spin-orbit coupling model of the nucleus.[7,8] A detailed paper describing the experimental details will be published in the *Arkiv för Fysik*.

I wish to convey my sincere thanks to Professor Manne Siegbahn, the director of this institute. My thanks are also due Dr. Kai Siegbahn for kindly supervising this work.

[1] G. T. Seaborg and I. Perlman, Revs. Modern Phys. 20, 585 (1948).
[2] H. Slätis and K. Siegbahn, Arkiv f. Fysik 1, No. 17 (1949).
[3] M. H. Hebb and E. Nelson, Phys. Rev. 58, 486 (1940).
[4] Rose, Goertzel, Spinard, Harr, and Strong, Phys. Rev. 76, 184 (1949).
[5] E. Feenberg and G. L. Trigg, private communication.
[6] L. W. Nordheim, Phys. Rev. 78, 294 (1950).
[7] M. G. Mayer, Phys. Rev. 78, 16 (1950).
[8] Haxel, Jensen, and Suess, Z. Physik 128, 295 (1950).

K^{40} and the Age of the Atmosphere

K. F. CRACKETT
Londonderry Laboratory for Radiochemistry, University of Durham, Durham, England
January 12, 1951

NOW that the decay scheme of K^{40} seems to be rather well established,[1] it is of interest to attempt a calculation of the age of the atmosphere from the amount of this isotope in the earth and the A^{40} content of the atmosphere. Calculations of a similar nature have been made by Poole[2] and Suess[3] using incorrect data.[4] The main difficulties lie in the estimation of (a) the relevant figures for the K^{40} abundance, and (b) the time elapsed since the crust became so well solidified that further additions to the atmosphere have been inappreciable.

With regard to (a) we can take the abundance of ordinary K in the upper crust layers as[5] 2.60 percent, the K^{40} isotopic abundance as[6] 0.0119 percent, the density of the crust as[5] 2.8, and the depth of the K-bearing crust as 4×10^5 cm. This latter figure is admittedly something of a guess.[5] With respect to (b) let us suppose the argon to have been generated from a time t_0 until a time $t=2\times10^9$ yr ago when the crust first began to solidify. Undoubtedly, some argon would have escaped since then, so that we shall derive an upper limit for t_0. Alternatively, if we allow an interval from t_0 to only $t=1\times10^9$ yr ago, we shall obtain a value for t_0 which is perhaps nearer to a lower limit. We then easily derive the relation

$$\frac{\lambda_\sigma}{\lambda_\sigma+\lambda_\beta}(e^{\lambda t_0}-e^{\lambda t})\left(\frac{2.60}{100}\right)(4\times10^5)\left(\frac{0.0119}{100}\right)2.8=76\times13.5\times\frac{1.44}{100}$$

by equating the mass of K^{40} per cm^2 of the earth's surface which has decayed to the actual amount of argon observed.

Using

$$\lambda_\sigma/(\lambda_\sigma+\lambda_\beta)=0.13/1.13, \quad \lambda=5.45\times10^{-10}/\text{yr},$$

we get for the limits of t_0, 3.5×10^9 and 3.1×10^9 yr.

While considerable uncertainty must be attached to these figures, it is perhaps of interest that they agree so well with the age of the earth as calculated by the lead method by Holmes and others.[7]

[1] G. A. Sawyer and M. L. Wiedenbeck, Phys. Rev. 79, 490 (1950).
[2] J. H. J. Poole, Nature 162, 775 (1948).
[3] H. Suess, Phys. Rev. 73, 1209 (1948).
[4] Bleuler and Gabriel, Helv. Phys. Acta 20, 67 (1947).
[5] B. Gutenberg, *Internal Constitution of the Earth* (McGraw-Hill Book Company, Inc., New York, 1939).
[6] A. O. Nier, Phys. Rev. 77, 789 (1950).
[7] Holmes, Nature 157, 680 (1946); 159, 127 (1947); 163, 453 (1949). Houtermans, Naturforsch. 2a, 322 (1947). Bullard, Ver. finn. ge. dät. Inst. 36, 33 (1949).

Radioactive Strontium Produced by Deuteron Bombardment of Rubidium

MICHEL TER-POGOSSIAN AND FRED T. PORTER
Physics Department, Washington University, St. Louis, Missouri
January 15, 1951

THE bombardment of rubidium by protons has been reported[1,2] to produce a strong activity in the chemically separated strontium fraction. These studies[1] disclosed the presence of three activities which were assigned to Sr^{85m} (70-min half-life, gamma-ray and internal conversion electron emission), Sr^{87m} (2.75-hr half-life, gamma-ray and internal conversion electron emission), and Sr^{85} (66-day half-life, K-capture decay and gamma-ray emission). The radiations from these isotopes have been reinvestigated using a 14-cm radius of curvature, uniform field, semicircular magnetic spectrometer.[3]

Radioactive samples were prepared through the bombardment of rubidium chloride with 10-Mev deuterons in the Washington University cyclotron. After bombardment the RbCl was dissolved in water, a small amount of strontium carrier was added in the form of $SrCl_2$, and the strontium precipitated by the addition of Na_2CO_3. This precipitate was washed several times.

A small fraction of one of the separated samples was mounted in a plastic holder, and its decay followed for a period of 140 days. The results indicate a half-life of 65±3 days, in good agreement with the value reported by DuBridge and Marshall.[1]

The secondary electrons ejected from a 50-mg/cm^2 uranium radiator shows K and L shell photo-electron peaks for the 65-day activity, corresponding to a gamma-ray of energy 513±3 kev. This was at first thought to be annihilation radiation. However, an uncovered electron source revealed a relatively strong internal conversion peak whose energy also corresponds to a transition energy of 513 kev. This indicated that at least part of the radiation was really gamma-radiation and not annihilation radiation. The experimental data are shown in Fig. 1.

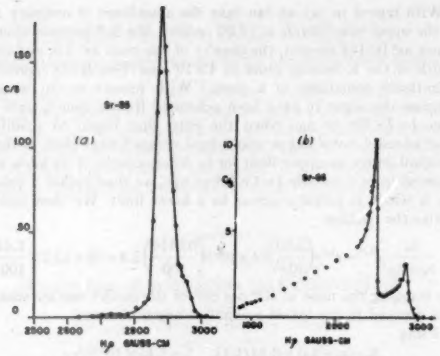

FIG. 1. (a) Internal conversion electron spectrum for the 513-kev gamma-ray from 65-day Sr^{85}. (b) Photo-electron spectrum for the same transition.

To check for the existence of positrons, two scintillation counters were used in coincidence. When separated by an angle of 180° at the source, coincidences between annihilation quanta should be recorded if positrons are present. This method and the apparatus used has been described in an earlier paper.[4] If the electromagnetic radiation is caused by the annihilation of positrons, there should be a sharp peak of coincidences when the two detectors and the source lie in the same straight line.[4] The results for this experiment are shown in Fig. 2. As a reference a known positron

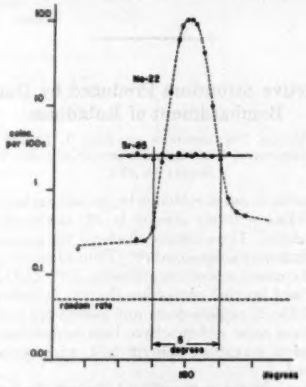

FIG. 2. Results of the experiment showing the absence of annihilation radiation in Sr^{85}. The constant coincidence rate for strontium may be compared to the increase in the coincidence counting rate for Na^{22} when the two detectors are separated by an angle of 180° at the source, this increase being caused by annihilation-annihilation coincidences. From this one deduces that Sr^{85} decays only by orbital electron capture.

emitter (Na^{22}) has been used. Whereas Na^{22} presents a very definite peak when the detectors are situated at an angle of 180° with the source, nothing similar can be observed for the Sr^{85}. Therefore, it can be concluded that the Sr^{85} decays by orbital electron capture without the emission of positrons, and that the 513-kev electromagnetic radiation is true gamma-radiation.

Internal conversion electrons associated with the shorter lived strontium activities were also observed. Internal conversion lines were found which corresponded to transition energies of 152 and 233 kev, and which decayed with a half-life of approximately 70 min. This half-life has previously been attributed[1] to Sr^{85m}. Also, there were internal conversion electron peaks corresponding to K and L shell conversions of a 388-kev transition energy. This appeared to decay with a half-life of about 2¾ hours, and would, therefore, be associated with Sr^{87m}.[1]

The authors wish to thank Dr. C. S. Cook for his advice and interest in the work and Mr. M. Cleland for his help in the annihilation coincidence studies.

* Assisted by the joint program of the ONR and AEC.
[1] L. A. DuBridge and J. Marshall, Phys. Rev. **58**, 7 (1940).
[2] A. C. Helmholz, Phys. Rev. **60**, 415 (1941).
[3] Ter-Pogossian, Cook, Goddard, and Robinson, Phys. Rev. **76**, 909 (1949).
[4] DeBenedetti, Cowan, Konneker, and Primakoff, Phys. Rev. **77**, 205 (1950).

Resonance in Antiferromagnetics

K. W. H. STEVENS
The Clarendon Laboratory, Oxford, England
January 19, 1951

IN a recent communication[1] Bleil and Wangsness have given an explanation of the disappearance of microwave resonance signals in antiferromagnetics below the curie temperature. An alternative explanation can be given as follows. The total absorption of energy in a resonance experiment on free spins is given by[2]

$$K\,\mathrm{Spur}[\exp(-\mathcal{H}/kT)(S_x\mathcal{H}-\mathcal{H}S_x)S_x]/\mathrm{Spur}[\exp(-\mathcal{H}/kT)],$$

where $S_x=\Sigma_i s_x^i$, and K is a numerical constant. In a model in which $\mathcal{H}=g\beta H\Sigma_i s_x^i+\Sigma_{i<j}J_{ij}\mathbf{s}^i\cdot\mathbf{s}^j$, it is found readily that the area reduces to $\frac{1}{4}KH\bar{M}$, where $\bar{M}$ is the magnetic moment of the sample in the field, H. The value of $\bar{M}$ is known to decrease very sharply at the curie temperature as the temperature is lowered, so that the intensity of absorption will decrease correspondingly. In cases where this model can be applied there is no question of the resonance line moving outside the range of microwave experiments, as the exchange energy commutes with the measuring perturbation term, and the line should remain fixed in position. Thus, we prefer to explain the decrease in absorption at the curie temperature as an effect arising from the fact that the system occupies states from which the transition probabilities are small.

[1] D. F. Bleil and R. K. Wangsness, Phys. Rev. **79**, 227 (1950).
[2] M. H. L. Pryce and K. W. H. Stevens, Proc. Phys. Soc. (London) **63**, 36 (1950).

Positron Search in K^{40}

MYRON L. GOOD
Department of Physics, Duke University, Durham, North Carolina*
December 4, 1950

THE gamma-ray of K^{40} is associated with K-capture, because its energy is greater than the beta-ray end-point energy, and its intensity is much less than that of the beta rays.[1-3] The gamma-ray energy is greater than $2m_0c^2$. Under these conditions positron decay is to be expected.

Annihilation quanta from K^{40} were, therefore, sought. The apparatus has been described previously.[4] The only modification was that the K_2CO_3 source was a shell 1¼ in. thick. (See Fig. 1 of reference 4.) The absorber between the crystal and position *II* (which is outside the K_2CO_3 container) was about 7 g/cm². Under these conditions, with a strong Zn^{65} source at position *II*, the curve B (Fig. 1) was obtained. Curve A is a Zn^{65} curve in which position (*I*), which is inside the container, was used, so that scattering effects were minimized. The effect of scattering in curve B is so severe that the beta-shield was changed (to a Pyrex beaker), and the inner support of the K_2CO_3 shell was made thinner. The Zn^{65} source was also made thinner and placed about 3 cm out from the masonite box wall instead of against it as before. These changes resulted in a total absorber thickness of about 4.3 g/cm². Under these conditions the data of curve D (Fig. 1) were obtained. It is

seen that the effect of the scatterer is to raise the low energy side of the peak. The Zn^{65} was removed and the K^{40} distribution observed (curve E). A background of about 10 percent was subtracted. The K^{40} curve shows two partially resolved lines identified with annihilation quanta (0.511 Mev) and with pair production in the crystal followed by escape of the annihilation quantum pair resulting therefrom [1.46−2(0.511)=0.44 Mev]. The latter effect was calculated from the pair cross section for gamma-rays of 1.46 Mev on NaI, the total cross section for 0.511 Mev, and the crystal dimensions. The result is that 1 percent of the area under the K^{40} curve should consist of such a peak. A gaussian curve having this area and the same width as the Zn^{65} positron line was subtracted from the experimental points of the K^{40} curve at 0.44 Mev. The result of this treatment of the data is shown on curve C.

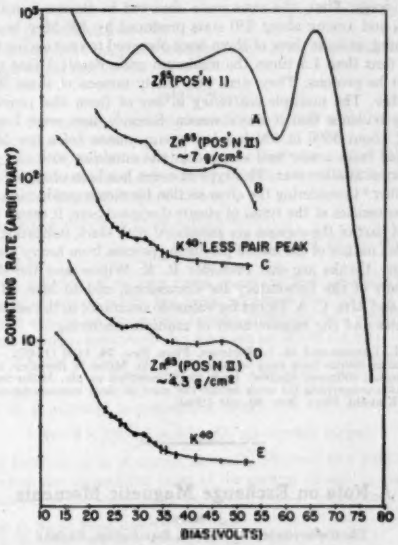

FIG. 1. Differential pulse height distributions. The energy scales are all the same; the relative heights are arbitrary.

It is clear from either curve E or C that there are some annihilation quanta present. By comparison with the Zn^{65} curves, one obtains an apparent (β_+/γ) ratio for K^{40}. This result is 1.6 percent by comparison with curve D, or 1.4 percent with curve B (which the K^{40} data resemble the most). Some of the annihilation quanta must arise from pair production in the lead shield and the sample by the K^{40} gamma-ray, as mentioned by Bell.[5] This effect was calculated roughly and found to be about 40 percent of the observed effect. It is concluded that as many as one positron per hundred gamma-rays may be present. The use of Zn^{65} as a sensitive comparison source was suggested by Bell's earlier work.[6]

The author wishes to express his indebtedness to Drs. Walter M. Nielsen and Henry W. Newson for their cooperation in this work; also to Mr. John Gibbons for assistance in the latter part of the experiment.

* This work was supported in part by a joint contract with the ONR and AEC.

[1] Bell, Weaver, and Cassidy, Phys. Rev. 77, 399 (1950).
[2] D. Alburger, Phys. Rev. 78, 629 (1950).
[3] G. A. Sawyer and M. L. Wiedenbeck, Phys. Rev. 79, 490 (1950).
[4] M. L. Good, Phys. Rev. 81, 891 (1951). Only the doubly cross-hatched outer region as shown in Fig. 1 of this reference was used in the present experiment.
[5] P. R. Bell and J. M. Cassidy, Phys. Rev. 79, 173 (1950).
[6] P. R. Bell and J. M. Cassidy, Phys. Rev. 77, 409 (1950).

Measurement of Semiconductor Impurity Content

CARL N. KLAHR AND L. P. HUNTER
Westinghouse Research Laboratories, East Pittsburgh, Pennsylvania
January 8, 1951

IN investigating the properties of impurity semiconductors, it is desirable to know the impurity concentration. This is useful not only from the viewpoint of theory but as an aid in developing the technology of purifying semiconductors. The measurement of impurity concentration by ordinary means is very difficult, since in a semiconductor it is often less than one part in 10^7 and may be a mixture of chemical impurities and lattice defects. Our purpose is to describe an electrical means of measuring total impurity concentration and to indicate a method for the experimental determination of the effective mass of the current carriers.

The electrical conductivity depends on the total impurity concentration through the mobility factor, which in turn depends on the mean free path of carriers. There are three contributions to the mean free path: ordinary lattice scattering which yields an energy independent mean free path; ionized impurity scattering from ionized donor and acceptor centers; non-ionized impurity scattering from non-ionized centers. The mean free path due to ionized impurities has been discussed by Conwell and Weisskopf[1] and is found to be $l_I=a\epsilon^2$, where ϵ is the energy, and a varies reciprocally with ionized impurity concentration. The non-ionized mean free path has been discussed by Erginsoy[2] and varies as ϵ^4 and reciprocally with concentration of non-ionized centers. With these assumptions we have calculated the Hall constant and the conductivity in the intermediate and low temperature ranges for electronic and hole carriers. The carrier concentrations n_e and n_H can be eliminated between these expressions and the appropriate form of the mass action law.[3] There results a system of curves of mobility *vs* conductivity which at constant temperature would be parametrized by the total impurity content-donor plus acceptor centers. By measuring Hall constant and resistivity of a given sample at a given temperature, its impurity content can be determined from this system of curves.

To simplify the application of this method one can combine low and intermediate temperature measurements of conductivity, σ, and Hall constant, R. Both sets of measurements should be made at sufficiently low temperatures for n_H to be negligible in N-type samples. This can be assured by inspecting graphs of R and σ *vs* T^{-1}. First, the Hall effect should be measured in the exhaustion range at a sufficiently high temperature that impurity scattering is negligible. From it n_e^*, the electron concentration in the exhaustion range, can be determined as $(3\pi/8)(1/R\epsilon)$. At low temperatures, i.e., 10 to 20°K for Ge, we have calculated

$$R\sigma=\mu=A\gamma f(\gamma)/Bn_e^*=AT^{\frac{3}{2}}f(\gamma)/N_I, \tag{1}$$

where

$$\gamma=\frac{\text{average ionized impurity mean free path}}{\text{average non-ionized impurity mean free path}}=B\frac{n_e^*}{N_I}T^{\frac{3}{2}}$$

and

$$N_I=\text{ionized impurity concentration.}$$

$\gamma f(\gamma)$ is a function of γ given in curve a of Fig. 1, while A and B are constants for Ge and which are independent of the impurity content. Once these are determined, the theory permits simple measurement of the impurity content of any sample. The determination of A and B may be carried out as follows:

$$(\partial\mu/\partial T)_{N_I}=(3\mu/2T)[1+\gamma d\ln f(\gamma)/d\gamma], \tag{2}$$

$$(\partial\mu/\partial N_I)_T=-(\mu/N_I)[1+\gamma d\ln f(\gamma)/d\gamma]. \tag{3}$$

$(\partial\mu/\partial T)_{N_I}$ should be measured at low temperatures on one sample, while $(\partial\mu/\partial N_I)_T\approx(\Delta\mu/2\Delta N_P)_T$ could be measured, though probably with difficulty, by adding a known amount of P-type impurity, ΔN_P, to an N-type sample. By measuring $(\partial\mu/\partial T)_{N_I}$, μ, and T, one can calculate γ from Eq. (2) and curve b of Fig. 1. Then N_I can be determined from Eq. (3). The value of B can now be calculated as $B=\gamma N_I/n_e^*T^{\frac{3}{2}}$. From this, A can be calculated from Eq. (1). Once A and B have been determined

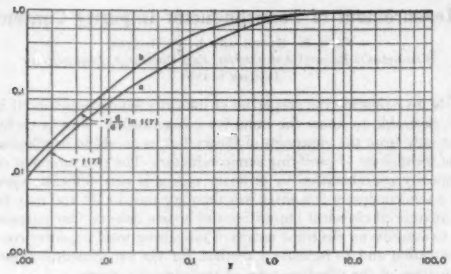

FIG. 1. Functions related to impurity concentration *versus* γ.

for the semiconductor, it is necessary only to measure n_i^* at an intermediate temperature, and T and μ at low temperatures, to obtain N_T. From these data and Eq. (1), one can obtain $\gamma f(\gamma)$, and from Fig. 1, the value of γ can be found. Then, $N_I = Bn_i^* T^{\frac{1}{2}}/\gamma$ and the total impurity content can be calculated as $N_T = N_I + n_i^*$.

A knowledge of A and B should also enable one to calculate the effective mass, m, of the current carrier in Ge and the effective dielectric constant, ρ, in Ge from the equations

$$A = \frac{p^2 k^{\frac{1}{2}}}{4\pi e^2 (2m)^{\frac{1}{2}}} \left[\ln\left(1+\frac{36\rho^3(kT)^3}{N_I^{\frac{1}{3}}\epsilon^4}\right)\right]^{-1},$$

$$B = 20\rho k^3 A/me^2,$$

where k is Boltzmann's constant.

Thus, such experiments allow one, in principle, to measure the total impurity concentration in a semiconductor and also to measure the effective mass and the dielectric constant.

[1] E. Conwell and V. F. Weisskopf, Phys. Rev. 77, 388 (1950).
[2] C. Erginsoy, Phys. Rev. 79, 1013 (1950).
[3] R. H. Fowler, *Statistical Mechanics* (Cambridge University Press, Cambridge, 1936), second edition, p. 398.

The Mechanism of Star Production by Gamma-Rays

SEISHI KIKUCHI
Laboratory of Nuclear Studies, Cornell University, Ithaca, New York
January 20, 1951

THE cross section for star production has been determined with the synchrotron bremsstrahlung beam for maximum energies of 300, 250, 200, and 150 Mev by a comparison of the number of stars produced in a photographic emulsion with the number of radioactive atoms produced in a carbon plate exposed to the beam simultaneously. The spectrum of the bremsstrahlung is assumed to be of the form Q/E, where Q is a constant and E is the quantum energy of a gamma-ray. The cross section, $\sigma(\gamma,n)$, of C^{12} was assumed to have a sharp resonance maximum at 30 Mev and an integrated value 1.48×10^{-25} cm²-Mev, following Lawson and Perlman.[1] The values of the cross section averaged over all types of atoms in the emulsion, except hydrogen, are shown in Table I.[2] Stars with more than two prongs were counted.

The value at 300 Mev was also determined directly from the value of Q as measured by a pair spectrometer by DeWire and Beach of this Laboratory. It was found to be 4.2×10^{-27} cm² with an error of about 30 percent. As an absolute measurement the latter value may be more reliable than is the former. The earlier value[3] of 5×10^{-26} cm², with an error of a factor of 5, was too low. The discrepancy seemed to have come from a rather ambiguous assumption as to the relation of the value of Q with our r-meter readings.

TABLE I. Average cross sections.

Energy (Mev)	300	250	200	150
Cross section (mb) (McMillan)	6.04±0.41	5.63±0.56	2.55±0.19	1.95±0.18

Looking at the results shown in Table I and taking into account the general character of the bremsstrahlung spectrum, it is reasonable to consider that the interaction of a photon with a nucleus, which leads to star production, is mesonic rather than an electromagnetic interaction leading to an ordinary type of photodissociation, when the photon energy is well above the threshold for meson production.

Another, more direct, bit of evidence for a mesonic interaction can be seen in the fact that there are certain cases in which a meson actually emerges from a star. This has been confirmed in two different ways. First, the stars were observed in electron-sensitive plates, and among about 450 stars produced by 300-Mev bremsstrahlung, at least three of them were observed to emit such a thin track (less than 1.5 times the minimum grain density) that they cannot be protons. They were very likely mesons of some 50 to 100 Mev. The multiple scattering of one of them also provided strong evidence that it was a meson. Second, there were 7 cases out of about 3500 in which a low energy meson (of a few Mev) emerged from a star and stopped in the emulsion with the production of another star. This type of event has been observed also by Miller.[3] Considering the cross section for meson production and the frequencies of the types of events discussed here, it seems that a good part of the mesons are associated with stars, indicating the complex nature of the meson producing process from heavy nuclei.

Many thanks are due Professor R. R. Wilson and the other members of the Laboratory for discussions, and to Mrs. M. R. Keck and Mrs. C. A. Lipetz for valuable assistance in the scanning of plates and the measurement of multiple scattering.

[1] J. L. Lawson and M. L. Perlman, Phys. Rev. 74, 1190 (1948).
[2] Similar results have been obtained by R. D. Miller in Berkeley, using a somewhat different method. I am much indebted to Mr. Miller for information concerning his work before the start of these measurements.
[3] S. Kikuchi, Phys. Rev. 80, 492 (1950).

A Note on Exchange Magnetic Moments

G. J. KYNCH
The University of Birmingham, Birmingham, England
January 12, 1951

RECENT papers by Sachs[1] and by Osborn and Foldy[2] have treated the expressions for the exchange currents arising from the exchange forces between nucleons. With two nucleons, 1 and 2, the equation for these currents is

$$\text{div } \mathbf{j}(\mathbf{r}) = V(\boldsymbol{\tau}_1\times\boldsymbol{\tau}_2)_z[\delta(\mathbf{r}-\mathbf{r}_1)-\delta(\mathbf{r}-\mathbf{r}_2)], \qquad (1)$$

where V is a constant proportional to the nuclear potential. The solutions to be found are particular integrals of this equation. Two points may be noted in connection with this equation and the expressions for the exchange moment listed by Osborn and Foldy, and also by Dalitz[3] in a forthcoming note.

The first is that the covariance properties of the expression should include invariance under time reversal. The current vector and the magnetic moment both change sign with time reversal. Now according to Wigner, under time reversal $\tau_x \to \tau_x$, $\tau_y \to -\tau_y$, so that the isotopic spin factor $(\boldsymbol{\tau}_1\times\boldsymbol{\tau}_2)_z$ is antisymmetric under time reversal. Consequently, many expressions listed can be dropped, since apart from the isotopic spin the expression must be symmetric under time reversal; e.g., expressions of the type $(\boldsymbol{\sigma}_1+\boldsymbol{\sigma}_2)\times\mathbf{p}$, $\boldsymbol{\sigma}_1\times\boldsymbol{\sigma}_2$ rather than $\boldsymbol{\sigma}_1\pm\boldsymbol{\sigma}_2$.

The second point is that Eq. (1) is more easily considered following a fourier transformation. If $\mathbf{J}(\mathbf{k})$ is the transform of $\mathbf{j}(\mathbf{r})$, we easily find that

$$k^2\mathbf{J}(\mathbf{k}) = -iV(\boldsymbol{\tau}_1\times\boldsymbol{\tau}_2)_z[\exp(-i\mathbf{k}\cdot\mathbf{r}_1)-\exp(-i\mathbf{k}\cdot\mathbf{r}_2)]\mathbf{k} + \mathbf{k}\times\mathbf{Q}(\mathbf{k}), \qquad (2)$$

where $\mathbf{Q}(\mathbf{k})$ is an arbitrary vector function. Apart from $\mathbf{Q}$, the expression for $\mathbf{J}$ in an expansion in powers of $\mathbf{k}$ is

$$-V(\tau_1\times\tau_2)_s[(r_1-r_2)\cdot\mathbf{k}]\mathbf{k}/k^2.$$

Since $\mathbf{J}(0)$ has a unique value independent of $\mathbf{k}$ it is clear that this term, which is the component of $V(\tau_1\times\tau_2)_s(r_1-r_2)$ in the direction of $\mathbf{k}$, must be supplemented by

$$k^2\mathbf{k}\times\mathbf{Q}_0=-V(\tau_1\times\tau_2)_s[(r_1-r_2)\times\mathbf{k}]\times\mathbf{k},$$

and we obtain finally

$$\mathbf{J}(0)=-V(\tau_1\times\tau_2)_s(r_1-r_2). \tag{3}$$

The importance of this result is seen in the work of Dalitz.

With $\mathbf{Q}=\mathbf{Q}_0+k^2\mathbf{Q}_1$, we can now write

$$\mathbf{J}(\mathbf{k})=V(\tau_1\times\tau_2)_s k^{-2}\{-k^2(r_1-r_2)+i\tfrac{1}{2}\mathbf{k}[(\mathbf{k}\cdot r_1)^2-(\mathbf{k}\cdot r_2)^2]+\cdots\}+\mathbf{k}\times\mathbf{Q}_1(\mathbf{k}), \tag{4}$$

where $\mathbf{Q}_1$ is finite at $k=0$.

The exchange magnetic moment is $\mathbf{m}=\int r\times\mathbf{j}d\tau$, which appears in this formalism as

$$\mathbf{m}=i\,\mathrm{curl}\mathbf{J}(\mathbf{k}), \tag{5}$$

where the operator curl implies differentiation with respect to the components of $\mathbf{k}$.

It is clear that $\mathbf{m}$ only depends on $\mathbf{Q}_1(0)$, the value of $\mathbf{Q}_1$ as $\mathbf{k}\to 0$, which remains a function of the direction of $\mathbf{k}$ though independent of its magnitude. We have

$$\mathbf{m}=i\,\mathrm{curl}[\mathbf{k}\times\mathbf{Q}_1(\mathbf{k})]-V(\tau_1\times\tau_2)_s k^{-2}\times[(\mathbf{k}\cdot r_1)(\mathbf{k}\times r_1)-(\mathbf{k}\cdot r_2)(\mathbf{k}\times r_2)] \tag{6}$$

with $\mathbf{k}\to 0$.

The splitting of $\mathbf{m}$ into parts invariant and otherwise under change of origin, which has been examined by Dalitz, is easily carried out. If we define the Fourier transform in a slightly different manner, relative to the mass center $\mathbf{R}=\frac{1}{2}(r_1+r_2)$,

$$\mathbf{J}=\int\exp[-i\mathbf{k}\cdot(r-\mathbf{R})]\mathbf{j}d\tau$$

and $\mathbf{Q}_1$ is adjusted to correspond, then

$$\mathbf{m}=\mathbf{R}\times\mathbf{J}(0)+i\,\mathrm{curl}(\mathbf{k}\times\mathbf{Q}_1)_{k=0}-(\text{other terms}). \tag{7}$$

This form for $\mathbf{m}$ is, of course, naturally obtained in a field theory in which the expectation value of the current density is normally expanded as the expectation value of a fourier transform.

[1] R. G. Sachs, Phys. Rev. 74, 433 (1948).
[2] R. K. Osborn and L. L. Foldy, Phys. Rev. 79, 795 (1950).
[3] R. Dalitz (to be published).

The Deuteron Quadrupole Moment and the Radiofrequency Spectra of H_2 and D_2 in Low Magnetic Fields*

H. G. Kolsky,† T. E. Phipps, Jr.,‡ N. F. Ramsey, and H. B. Silsbee
Lyman Laboratory of Physics, Harvard University, Cambridge, Massachusetts
January 15, 1951

A MOLECULAR beam apparatus[1,2] of high resolution has been used for the first time to study the rf spectra of H_2 and D_2 in magnetic fields ranging between 1 and 9 gauss. The hamiltonian[3-6] introduced to account for the high field spectra of these molecules has been found to be adequate to account for the present results.

The observed transitions correspond to $(F,m)=(0,0)\leftrightarrow(1,1)$ for D_2 and $(0,0)\leftrightarrow(1,\pm1)$ for H_2. The magnetic field can be evaluated from the separation of the H_2 lines, and, thence, the frequencies corresponding to zero field can be determined by extrapolation. In the usual notation,[3-6] the results are

$$(g_H\mu_H/h)(H_{H_2}'+3H_{H_2}'')=546.39\pm0.10\text{ kc},$$
$$(g_D\mu_N/h)(H_{D_2}'+15S_D)=198.12\pm0.10\text{ kc}.$$

If these values are combined with our previous high field data,[1,2] we obtain improved values of the constants

$$H_{H_2}'=26.726\pm0.050\text{ gauss},\quad H_{H_2}''=33.865\pm0.020\text{ gauss},$$
$$H_{D_2}'=13.44\pm0.06\text{ gauss},\quad S_D=19.308\pm0.008\text{ gauss}.$$

If we assume that the differences in the nuclear moments, zero-point vibrations, and centrifugal stretchings make $H_{D_2}''=1.006\,H_{H_2}''\mu_D/\mu_H$, then we have

$$H_{D_2}'''=86.143\pm0.040\text{ gauss},$$
$$-qQ=(1.2927\pm0.0006)\cdot10^{-2}\text{ cm}^{-1}.$$

From this and from Newell's[6] theoretical value for q, the deuteron quadrupole moment is

$$Q=(2.738\pm0.016)\cdot10^{-27}\text{ cm}^2.$$

Although the method[7] of applying the rf excitation in two separated regions eliminates the first-order effect of inhomogeneities of the magnetic field, two second-order effects may influence low field measurements. First, the relation between transition frequency and field is nonlinear, so that a distinction must be made between the average frequency over the path of a molecule, which is what we observe for any one line, and the average field over the path, which is common to the several lines. Secondly, if, because of the velocity of the molecules, irregularities of the field along the path of the molecules have appreciable Fourier components at any nonzero frequency, a shift in the position of the resonances may result.

The inhomogeneities in our apparatus are rather high. Accordingly, a correction has been applied to the results to compensate for the first effect, and the stated uncertainty includes an allowance for the second. The remaining uncertainty is largely due to variations of the magnetic field with time.

The work is continuing, and a more complete report will be made later.

* This work was assisted by the joint program of the ONR and AEC.
† AEC Fellow.
‡ NRC Fellow.
[1] Kolsky, Phipps, Ramsey, and Silsbee, Phys. Rev. 79, 883 (1950).
[2] Kolsky, Phipps, Ramsey, and Silsbee, Phys. Rev. 80, 483 (1950).
[3] Kellogg, Rabi, Ramsey, and Zacharias, Phys. Rev. 56, 728 (1939).
[4] Kellogg, Rabi, Ramsey, and Zacharias, Phys. Rev. 57, 677 (1940).
[5] N. F. Ramsey, Phys. Rev. 58, 226 (1940).
[6] G. F. Newell, Phys. Rev. 78, 711 (1950).
[7] N. F. Ramsey, Phys. Rev. 78, 695 (1950).

Masses of Al, Si, P, and S Isotopes

Henry T. Motz
Brookhaven National Laboratory, Upton, Long Island, New York*
January 2, 1951

THE mass of S^{32} as derived from mass spectrograph and nuclear reaction data has been in doubt by about 1 mMU for several years. In the course of the compilation of a summary of mass difference data for the region $Z=10$ to $Z=20$, recent results have been made available to the author which increased greatly the accuracy and reliability of the atomic masses around P and S.

Mass spectrograph data are now available for the Al^{27}, Si^{28}, Si^{29}, Si^{30}, and S^{32} isotopes. Owing to relatively inaccurate Q-value determinations, these masses may be considered as isolated from isotopes having masses known to comparable accuracy which fall outside this region. Mass differences between pairs of these five masses are available from Q-values corresponding to ground state transitions. Those mass differences which have a probable error low enough to influence the mass defects are listed in Table I and their relations are shown in Fig. 1. Whole mass units have been neglected in the mass difference values.[1] The recent data of the M.I.T. group are especially important and form the major part of the nuclear reaction data used. A least-squares analysis of the nine observed quantities has been made, and the best fit values found are given in Table I. The data agree well, and a significantly decreased probable error for the mass defects results from the combination of the nine observed quantities. The Al^{28}, P^{31}, and P^{32} mass defects are given as determined from an approximate fit of the observed mass differences with the best fit values. The best fit values

TABLE I. Isotopic mass defects and mass differences.

Quantity	Best fit values (mMU)	Observed value (mMU)	Source
Al^{27}	-10.17 ± 0.06	-10.20 ± 0.08	Mass spectrograph[a]
Si^{28}	-14.19 ± 0.05	-14.19 ± 0.08	Mass spectrograph[b]
Si^{29}	-14.29 ± 0.05	-14.23 ± 0.14	Mass spectrograph[b]
Si^{30}	-16.97 ± 0.06	-17.10 ± 0.15	Mass spectrograph[b]
S^{32}	-17.72 ± 0.05	-17.63 ± 0.09	Mass spectrograph[d,e,f]
Si^{30}–Al^{27}	-6.79^{g}	$-6.79^{g}\pm0.01^{g}$	(d,p) and (d,α)[g]
S^{32}–Si^{30}	-3.43^{g}	$-3.44^{g}\pm0.02^{g}$	(d,p), (d,α), and (β)[g]
Si^{30}–Si^{29}	-2.68	-2.58 ± 0.10	(d,p), (n,γ), and microwave absorption[a,b,i,j]
Si^{29}–Si^{28}	-0.10^{g}	$-0.10^{g}\pm0.02$	(d,p) and (n,γ)[a,b,i,k]
Al^{28}	-9.48 ± 0.06		
P^{31}	-16.35 ± 0.05		
P^{32}	-15.89 ± 0.05		
Constants:	$n=8.971\pm0.007$		$d=14.718\pm0.006$
	$p=8.129\pm0.003$		$\alpha=3.880\pm0.032$
	1 Mev = 1.07407 mMU		

[a] J. Mattauch and H. Ewald, Physik. Z. **44**, 181 (1948).
[b] H. E. Duckworth and R. S. Preston, Phys. Rev. **79**, 402 (1950).
[c] Duckworth, Preston, and Woodcock, Phys. Rev. **79**, 188 (1950).
[d] H. E. Duckworth, private communication (November, 1950).
[e] F. W. Aston, *Mass Spectra and Isotopes* (Longmans, Green and Company, New York, 1941), second edition.
[f] L. G. Smith, Phys. Rev. **81**, 295(A) (1951).
[g] D. M. Van Patter, private communication (November, 1950).
[h] Reference 1.
[i] Kinsey, Bartholomew, and Walker, Phys. Rev. **78**, 481 (1950).
[j] S. Geschwind and R. Gunther-Mohr, private communication (November, 1950).
[k] H. R. Allan and C. A. Wilkinson, Proc. Roy. Soc. (London) **A194**, 131 (1948).

depend on the values of n, p, d, and α, and differences in the current values of α cause a change of about 0.02 mMU in the mass defects.

The value $S^{32}=-19.11\pm0.07$ mMU given by Okuda and Ogata[2] has not been used owing to its large discrepancy with other existing mass spectrograph data. The mass defect of S^{32} given in Table I is consistent with the mass of A^{36} as found by Roberts and

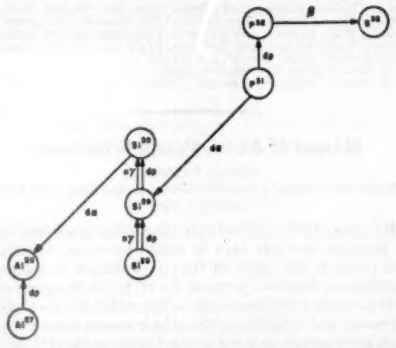

FIG. 1. *Z versus A* diagram illustrating relations of reactions used in the calculation of masses. The arrows refer to the direction of the reaction.

Nier[3] to within 0.3 mMU, which is the probable error of the mass difference value now available. The agreement of these many independent measurements greatly substantiates the recent measurements of S^{32}. Okuda and Ogata's results have been used to varying degrees in most available mass tables. Future data will require an accurate fitting of the mass defects given here with the well-known Ne^{20} and A^{36} masses, but this should cause only a slight variation of the present values. Fourteen other isotopes are linked to the Al to S chain by one or more reactions with errors of about 0.1 to 0.3 mMU. A more complete list of mass defects and source material will be published for the range $Z=10$ to $Z=20$.

* Research carried out under contract with AEC.
[1] H. T. Motz and R. F. Humphreys, Phys. Rev. **80**, 395 (1950).
[2] T. Okuda and K. Ogata, Phys. Rev. **60**, 690 (1941).
[3] T. R. Roberts and A. O. Nier, Phys. Rev. **77**, 746(A) (1950).

Radiations of Nd^{147}

W. S. EMMERICH AND J. D. KURBATOV
The Ohio State University, Columbus, Ohio
January 10, 1951

SPECTROSCOPICALLY pure neodymium was activated with neutrons at the Oak Ridge National Laboratory, and Nd^{147} was studied with a permanent magnet spectrograph, a thick lens beta-spectrometer, and coincidence counters. Several previous investigations of the radiations of Nd^{147} have been reported in the literature, showing in part conflicting results.[1]

In the present study, internal conversion electrons were observed with the spectrograph as listed in Table I.

TABLE I. Internal conversion electrons in Nd^{147}.

Energy of electrons (kev)		Transition energy (kev)
46.0 ± 0.5	*K*	91.3
84.5 ± 1.0	*L*	91.7
89.9 ± 1.0	*M*	91.4
275 ± 3	*K*	320
315 ± 5 (weak)	*L*	322
489 ± 5	*K*	534
528 ± 5	*L*	535

Consistent values for the 91-kev gamma-energy were obtained from internal conversion electrons using binding energies of prometheum. Repeated runs with the same source over a period of time indicated that all three transitions decay with a half-life of about 11 days, corresponding to Nd^{147}.

A Kurie plot of the beta-spectrum, as measured with the beta-spectrometer at four percent resolution, showed a complex spectrum with three components having upper energies of 825, 600, and 380 kev. Exactness of determination of the beta-disintegration of 825 kev is estimated to be ±15 kev. A wider margin of error should be allowed for the lower energy betas, since internal conversion electrons obscure portions of the beta-spectra.

Coincidence measurements, with a resolving time of 5×10^{-7} sec, showed that the 825-kev beta-ray is in coincidence with x-rays and with internal conversion electrons of the 91-kev transition. Beta-electron coincidences were also found between the 600-kev beta-ray and internal conversion electrons of the 320-kev transition. Evidence of gamma-rays in coincidence with betas was obtained. No measurable coincidences could be detected between gamma-rays, between gamma- and x-rays, and among the 38-kev x-rays.

These results allow a tentative establishment of a decay scheme for Nd^{147} with a total energy of disintegration of $\sim$915 kev, in which the three beta-spectra of 825, 600, and 380 kev are followed by the transitions of 91-, 320-, and 534- kev gamma-rays, respectively.

Gamma-rays of 534 kev as well as 38-kev x-rays could be observed by absorption, while the 91-kev transition appears to be largely internally converted.

A full report will be prepared on completion of the work. Grateful acknowledgment is made to The Ohio State University Development Fund for a financial grant making this research possible.

[1] Cork, Shreffler, and Fowler, Phys. Rev. **74**, 240 (1948). C. E. Mandeville and E. Shapiro, Phys. Rev. **79**, 391 (1950).

Electron-Electron Scattering from 0.6 to 1.7 Mev*

LORNE A. PAGE†
Cornell University, Ithaca, New York
January 11, 1951

A MEASUREMENT has been made of the differential cross section for elastic scattering of negative beta-particles by atomic electrons, using a method whereby the two energetic elec-

trons arising from a collision are detected individually in two Geiger-Müller counters connected in coincidence.

Figure 1 (a) shows a plan view of the scattering chamber used. A uniform magnetic field is vertical. Beta-rays from the source, S,

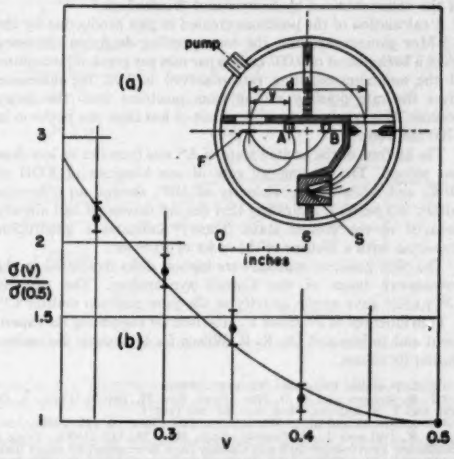

FIG. 1. (a) Plan view of scattering chamber. Shown are beta-emitter, S, scattering foil, F, two movable Geiger-Müller counters, A and B. Fractional energy transfer is given by y/d. (b) Relative differential cross section against fractional energy transfer, v, at fixed incident energy, $E=3.5\ mc^2$. A beryllium scatterer, 4.5 mg/cm², was used. The curve is taken from the Møller formula.

travel in a horizontal plane and strike a scattering foil, F. The two Geiger-Müller counters, A and B, with axes vertical, are movable from left to right in the figure. One counter is situated somewhat above the scattering foil, the other below. Momentum considerations show that to each horizontal setting of counter A, for example, there corresponds a definite horizontal setting of counter B in order for elastic collisions to be recorded. Experimentally, the scattering events appear to be practically elastic, in the sense that an inelasticity of the order of one percent in all events could have been detected. In the interest of obtaining reasonably large solid angles, the counters can be made quite long, because all elastically scattered electrons of given fractional energy transfer are focused in a vertical line at each counter. Fractional energy transfer, v, is related to counter setting by $v=y/d$, where y is the horizontal distance from scattering foil to the nearest counter, and d is the diameter of the circular path of the incident particles.

Using 10 millicuries of $Sr^{90}-Y^{90}$ as beta-emitter, and scattering foils of 0.5 mg/cm² collodion and 4.5 mg/cm² beryllium, results were obtained as follows. Figure 1 (b) shows the variation of measured differential cross section, $\sigma(v)$, with v, at a fixed incident kinetic energy, $E=3.5\ mc^2$ with a total spread of $0.4\ mc^2$. Standard statistical errors are attached. The resolution in v has a width at half-maximum of 0.04. The curve shown has been computed from the formula of Møller[1] for elastic electron-electron scattering. Similar results, not reproduced here, were found at $E=2.3\ mc^2$.

Figure 2 shows the results for absolute differential cross section at $v=0.5$, as a function of incident kinetic energy in units of mc^2. The spread in incident energy for each experimental point is that corresponding to a 12 percent incident momentum spread. The errors shown are statistical only. The experimental error is estimated to be 10 percent standard deviation. Curve A is a plot of Møller's formula. To indicate the effect of the "spin terms" in the Møller expression,[2] a plot is made with these terms arbitrarily suppressed (curve B).

The formula of Møller appears to be verified within the 10 percent experimental error. The result here is not at variance with the results of previous cloud-chamber experiments,[3,4] although for a given incident energy there is essentially no overlap in terms of fractional energy transfer investigated.

It may be of interest to note that an alternative conclusion could be drawn concerning the identity of negative beta-particles

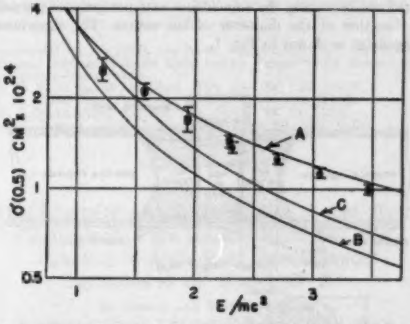

FIG. 2. Absolute differential cross section against incident kinetic energy. Observed cross section, in 10^{-24} cm² per unit fractional energy transfer, is shown as squares for 0.5-mg/cm² collodion scatterer and circles for 4.5-mg/cm² beryllium scatterer. Curve A is the Møller formula, curve B is the Møller formula less the spin terms, and curve C is the Bhabha formula less the virtual annihilation terms.

with atomic electrons.[4,5] In Fig. 2, a third formula, curve C, represents Bhabha's elastic positron-electron scattering formula[7] with the parts arising from virtual annihilation deleted. This pseudo-formula is not far from the Mott formula for coulomb scattering of fast electrons,[8] the latter being of order 10 percent smaller for these energies. The preference shown for the Møller formula would, then, imply that beta-particles are the same as electrons as far as scattering by electrons is concerned.

A detailed account of the experiment is to be published. I am indebted to Professor W. M. Woodward for suggesting the problem and for his active interest and counsel throughout the experiment.

* Based on Ph.D. thesis, Cornell University.
† Now at University of Pittsburgh, Pittsburgh, Pennsylvania.
[1] C. Møller, Ann. Physik 14, 568 (1932).
[2] Mott and Massey, *The Theory of Atomic Collisions* (Clarendon Press, Oxford, 1950), second edition, p. 369.
[3] F. C. Champion, Proc. Roy. Soc. (London) **A137**, 688 (1932).
[4] Groetzinger, Leder, Ribe, and Berger, Phys. Rev. **79**, 454 (1950).
[5] H. R. Crane, Revs. Modern Phys. **20**, 278 (1948).
[6] M. Goldhaber and G. Scharff-Goldhaber, Phys. Rev. **73**, 1472 (1948).
[7] H. J. Bhabha, Proc. Roy. Soc. (London) **A154**, 195 (1936).
[8] N. F. Mott, Proc. Roy. Soc. (London) **A124**, 425 (1929).

The Positron Activity of K^{40}

STIRLING A. COLGATE
Laboratory of Nuclear Studies, Cornell University, Ithaca, New York
December 14, 1950

THE nucleus K^{40} can decay to A^{40} by three processes: (a) orbital electron capture to an excited state of A^{40} with subsequent gamma-emission, (b) electron capture to the ground state of A^{40}, and (c) positron emission. Fireman[1] has calculated the ratio of process (b) to process (c) for various mass differences $K^{40}-A^{40}$. Nier and Roberts'[2] determination of the $Ca^{40}-A^{40}$ mass difference gives a mass difference for $K^{40}-A^{40}$ of $(3.35\pm0.15)\ mc^2$. With this value of the mass difference, Fireman's calculations give the ratio of process (b) to process (c) equal to (0.01, +0.02, −0.005). On the other hand, Sawyer and Wiedenbeck[3] have found the total

electron capture rate [process (a) plus process (b)] to be (13.5±4) percent of the β^- decay rate, and determined the gamma-ray rate to be (12.7±1) percent of the β^- decay. If the gamma-ray is process (a), then there remains a maximum of 5 percent of process (b). If the upper limit of Fireman's ratio is used, there must be less than one positron to 10^3 electrons.[4]

The coincidences of annihilation quanta were looked for with two scintillation counters. The angular correlation was partially determined by noting the coincidence rate per gram of potassium as a function of the diameter of the source. The experimental arrangement is shown in Fig. 1.

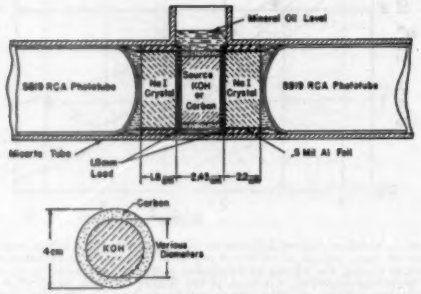

FIG. 1. Experimental arrangement. Typical ring and disk source.

Figure 2 shows the measured counting rates for various source diameters. It is to be noted that the observed potassium coincidence rate (curve I) has a slope opposite to that for the positron detection efficiency (curve II), and, therefore, gives no evidence that the observed coincidence rate from potassium comes from positrons. Furthermore, the potassium curve suggests that the observed coincidence rate arises from the back scattering of the 1.5-Mev gamma-rays. The Compton back scattering of the 1.5-Mev gamma-rays from one NaI crystal to the other would give the observed positive slope of curve I.

The absolute positron detection efficiency was determined by a calculation of the probability for an observation of one of two annihilation quanta in one crystal, and then multiplying this by the observed ratio of the double coincidence rate to the total rate in one crystal for a pure positron source (C^{11}) in the identical geometry. The calculation was checked by using the same solid angles and the corresponding absorption coefficients to find the detection efficiency of the 1.5-Mev gamma-rays of potassium. The gamma-ray activity of potassium, determined by the calculated efficiency and the observed total counting rate, was within 5 percent of the value obtained by Sawyer and Wiedenbeck.[3]

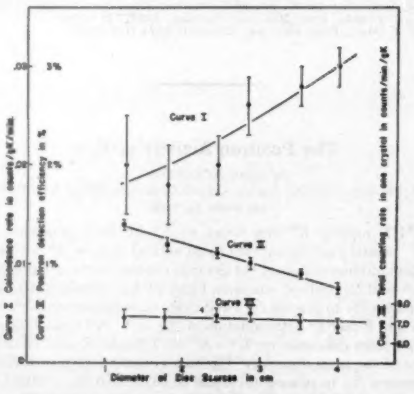

FIG. 2. Counting rates as functions of the source diameter.

A calculation of the positrons created in pair production by the 1.5-Mev gamma-rays and the corresponding detection efficiency gives a background of 0.007 counts per min per gram of potassium. If the minimum counting rate observed is 0.02, the difference gives the rate possibly arising from positrons from the decay process. This results in an upper limit of less than one positron in 1700 electrons.

The lifetime of the excited state of A^{40} was found to be less than one second. The gamma-ray rate of one kilogram of KOH at 20°C, and when boiling violently at 370°, showed no difference within ±5 percent, indicating that the A^{40} driven off had already decayed to the ground state. Theory[5] indicates a quadrupole transition with a lifetime of the order of 10^{-12} sec.

The pure positron sources were carbon disks irradiated in the gamma-ray beam of the Cornell synchrotron. The reaction $C^{12}(\gamma,n)C^{11}$ gave ample activity of the pure positron emitter C^{11}.

I am indebted to Professor P. Morrison for suggesting the experiment and to him and Dr. R. R. Wilson for invaluable discussions during its course.

[1] E. L. Fireman, Phys. Rev. 75, 1447 (1949).
[2] T. R. Roberts and A. O. Nier, Phys. Rev. 79, 198(A) (1940). A. O. Nier and T. R. Roberts, Phys. Rev. 81, 507 (1951).
[3] C. A. Sawyer and M. L. Wiedenbeck, Phys. Rev. 79, 490 (1950).
[4] P. R. Bell and J. M. Cassidy, Phys. Rev. 79, 173 (1950). Using a sintillation spectrometer Bell and Cassidy have determined an upper limit to this ratio of 2×10^{-3}, but this figure cannot be reproduced plausibly from the data presented.
[5] P. Morrison, Phys. Rev., to be published.

The Dielectric Properties of $BaTiO_3$ at Low Temperatures*

WALTER J. MERZ†
Laboratory for Insulation Research, Massachusetts Institute of Technology, Cambridge, Massachusetts

January 22, 1951

BLUNT and Love,[1] using ceramics, measured the dielectric behavior of $BaTiO_3$ at low temperatures. They found a pronounced peak in the dielectric loss at about 70°K, whereas the dielectric constant showed no anomaly down to liquid helium temperatures. Hulm,[2] on the other hand, measured multidomain single crystals and observed a strong increase in the coercive field strength in the region from about 20°K downwards. The increase was so strong that he was unable to polarize the crystals completely and, thus, could not measure the behavior of the electric spontaneous polarization at these very low temperatures.

Since these results were not conclusive, we have measured the dielectric constant and loss of our "single-domain crystals"[3,4] at audiofrequencies, and the hysteresis loop at 60 cps from room temperature down to 4.2°K. The crystal holder, consisting of two spring-loaded silver contacts, was enclosed in a brass chamber serving as a constant volume gas thermometer. The chamber was filled with helium gas and connected to a mercury manometer by a steel capillary.

The results were as follows. The dielectric constant in the direction corresponding to the c axis at room temperature[3] decreases approximately linearly below the last transition near 180°K and reaches a value of about 120 at 4.2°K. We could find no anomaly in the dielectric loss, in contrast to Blunt and Love's measurements; the loss stays about constant and remains small. The coercive field strength, as derived from the hysteresis loops, starts to increase strongly with falling temperature below 90°K. However, our good crystals could be saturated even at helium temperature (Fig. 1) and thus allow measurement of the spontaneous

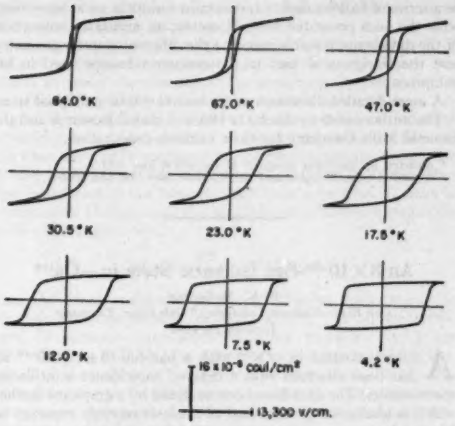

FIG. 1. Hysteresis loops for $BaTiO_3$ at low temperatures.

polarization. This stays almost constant from the 180°K transition down to 4.2°K; its value is of the order of about $P_s \simeq 8.0 \times 10^{-6}$ coulomb/cm². The absolute value changes from sample to sample because of domain formation at the two transition points[3] near 270° and 180°K. In interpreting P_s it must be kept in mind that below the 180°K transition the polar axis points in the (111) direction.[3] The coercive field strength increases strongly from about 250 v/cm at 180°K to almost 10,000 v/cm at 4.2°K (Fig. 2).

These results show that $BaTiO_3$ stays ferroelectric down to liquid helium temperature, and there is no indication that the crystal will change to a nonferroelectric modification. The fact

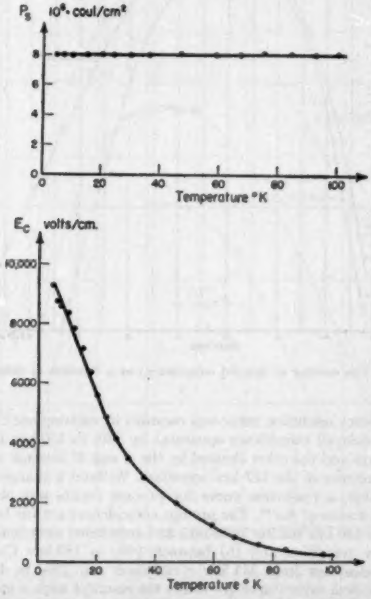

FIG. 2. Spontaneous polarization and coercive field strength vs temperature.

that the coercive field strength increases strongly at low temperatures and that the hysteresis loops become wider and more and more rectangular indicates freezing-in of the domain boundaries. It is of interest to note that $BaTiO_3$, while becoming ferroelectric by a displacive transition similarly to rochelle salt (small specific heat anomaly) and, in contrast to the KH_2PO_4 group, shows no second curie point at which the ferroelectricity disappears as in the case of rochelle salt.

The author is grateful to Professor A. von Hippel for his support during the course of this work.

* Sponsored by the ONR, the Army Signal Corps, and the Air Force.
† Present address, Physics Department, Pennsylvania State College, State College, Pennsylvania.
[1] R. F. Blunt and W. F. Love, Phys. Rev. **76**, 1202 (1949).
[2] J. K. Hulm, Proc. Phys. Soc. (London) **63A**, 1184 (1950).
[3] W. J. Merz, Phys. Rev. **76**, 1221 (1949); **78**, 52 (1950).
[4] M. E. Caspari and W. J. Merz, Phys. Rev. **80**, 1082 (1950).

The Intensity of the Total and of the Hard Component of the Cosmic Radiation as a Function of Altitude at Geomagnetic Latitudes of 28° N and 55° N*

M. VIDALE AND MARCEL SCHEIN
Department of Physics, University of Chicago, Chicago, Illinois
January 22, 1951

THE equipment used in this experiment consisted of four fourfold coincidence counter telescopes (*ABCD, BCDE, BCDF, BCDG*). The counter geometry of the individual telescopes is shown in Fig. 1. Each counter had an outside diameter of 2.54

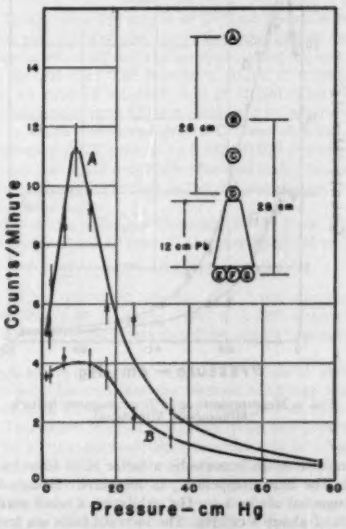

FIG. 1. Measurements at 28°N geomagnetic latitude (Cuba).

cm, a length of 13 cm, and brass walls of 0.078 cm in thickness. A block of 12 cm of lead was interposed between counter *D* and counters *EFG*. Each fourfold coincidence was separately registered on photographic film moved by a clock mechanism.

Through the courtesy of the Office of Naval Research, the first of the two balloon experiments was carried out with the aid of a General Mills balloon launched south of Cuba at a geomagnetic latitude of 28°N. The launching took place from the deck of an

aircraft carrier of the U. S. Navy on November 19, 1949. The balloon rose at the rate of 680 ft/min to a maximum altitude of 93,000 feet corresponding to an atmospheric pressure of 1.2 cm Hg and remained between a pressure of 1.2 and 1.4 cm Hg for several hours. The equipment landed in the ocean and was promptly recovered by a helicopter.

Curves A and B in Fig. 1 give the counting rates obtained during this flight for the fourfold coincidences $ABCD$ and $BCDF$, respectively. Curve A is assumed to give the total vertical flux of the cosmic radiation at 28°N. The maximum in the total radiation occurs at a pressure of 9 cm Hg and represents an increase by a factor of 18 from its value at sea level. Curve B gives the intensity of the cosmic radiation capable of traversing 12 cm of lead (penetrating component). As is evident in Fig. 1, curve B flattens out appreciably above 18 cm Hg pressure and shows a definite drop between 5 and 1 cm Hg. The penetrating component increases by a factor of 8 from its value at sea level to that at the very flat maximum (~9 cm Hg).

The second experiment, in which an identical piece of apparatus was used, was carried out at a geomagnetic latitude of 55°N. For this purpose a General Mills balloon was launched from Minneapolis, Minnesota, on June 6, 1950. The balloon rose at the very slow rate of 311 ft/min to an altitude of 70,000 ft and continued to rise even more slowly (~150 ft/min) until it leveled off for several hours at an altitude of 86,000 ft. This type of flight is particularly valuable for securing accurate counter coincidence data at various atmospheric depths.

The results obtained are shown in Fig. 2. The maximum in the total component occurs at an atmospheric pressure of 5 to 6 cm

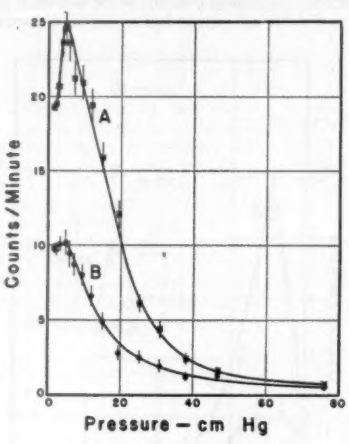

FIG. 2. Measurements at 55°N geomagnetic latitude (Minneapolis, Minnesota).

Hg and represents an increase by a factor of 35 from its value at sea level. The hard component, as measured through 12 cm of lead, flattens out above 5 cm Hg, exhibiting a small maximum at a pressure of about 3 cm Hg. The increase from sea level to the maximum corresponds to a factor of 19.

Comparison of the results obtained at the two latitudes gives a latitude effect of 2.75±0.21 for the hard component at an atmospheric pressure of 1.6 cm Hg. For the total radiation the latitude effect is 1.85 at 9 cm Hg (maximum at 28°N), 3.1 at 5 cm Hg (maximum at 55°N), and 3.85±0.13 at 1.6 cm Hg.

It is of interest to note that the latitude effect of the hard component is smaller than that of the total radiation at the maximum altitude of 85,000 ft.

Winckler[1] has measured the latitude effect of the total radiation in a series of balloon flights and obtains results in good agreement with the ones presented here. However, an accurate comparison of the data is not possible owing to the different counter geometry and the thickness of lead in the counter telescope used in his equipment.

A more detailed discussion of the results will be published later.

The authors wish to thank the Office of Naval Research and the General Mills Company for their valuable cooperation.

* Assisted by the joint program of the ONR and AEC.

[1] Winckler, Stix, Dwight, and Sabin, Phys. Rev. 79, 656 (1950).

An 8×10^{-10}-Sec Isomeric State in $_{76}Os^{186}$

F. K. McGowan
Oak Ridge National Laboratory, Oak Ridge, Tennessee*
January 19, 1951

AN excited state in $_{76}Os^{186}$ with a half-life $(8\pm1)\times10^{-10}$ sec has been observed with a delayed coincidence scintillation spectrometer. The data have been analyzed by a graphical method which is analogous to a method of analysis recently reported by Newton.[1]

Re^{186} (90 hr) is known[2] to decay in 90 percent of its disintegrations by β^- emission into Os^{186}. A 25 percent partial β^- spectrum of 930-kev end point is followed by a 137-kev γ-ray, and the remaining β^- disintegrations lead directly to the ground state. For the 137-kev γ-ray, Metzger and Hill measured $\alpha_K=0.35\pm0.1$ and $N_K/N_L=0.6\pm0.1$.

Curve (1) of Fig. 1 shows the number of coincidences as a function of delay time obtained with a source of Re^{186}. This delayed

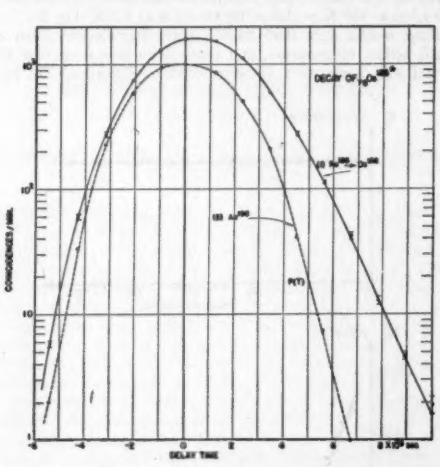

FIG. 1. The number of delayed coincidences as a function of delay time.

coincidence resolution curve was recorded by exciting one channel of the delayed coincidence apparatus by 250- to 450-kev nuclear beta-rays and the other channel by the L and M internal conversion electrons of the 137-kev transition. Without a change in the apparatus, a resolution curve for prompt events was obtained with a source of Au^{198}. The prompt coincidences are (a) between 110- to 150-kev nuclear beta-rays and conversion electrons of the 411-kev transition and (b) between 110- to 150-kev Compton recoil electrons from 411-kev γ-radiation and 250- to 450-kev nuclear beta-rays. Curve (2) shows the result of such a measurement. Since curves (1) and (2) overlap appreciably, the half-life of

Os^{186*} cannot be determined accurately from the slope of curve (1) at a large positive delay time.

Newton[1] has given a general discussion of the evaluation of delayed coincidence experiments. In the ideal experiment one desires to excite one channel of the apparatus by the radiation announcing an excited state in a nucleus and to excite the other channel by the radiation emitted in the decay of the excited state whose lifetime is to be measured. If the excited state has a lifetime much too short to be measured by the coincidence apparatus, one obtains a prompt coincidence curve $P(T)$, where T is the delay time introduced in the delayed coincidence apparatus. If there is a measurable lifetime, one obtains a delayed coincidence resolution curve $F(T, \lambda)$ given by

$$F(T, \lambda) = \int_0^\infty \lambda e^{-\lambda t} P(T-t)dt.$$

Since the energy resolution of the scintillation spectrometer is relatively poor compared to the best magnetic beta-ray spectrometers, the delayed coincidence resolution curve in Fig. 1 for $Re^{186} \rightarrow Os^{186}$ is $F(T, \lambda)$ plus possibly some prompt events not related to the $Re^{186} \rightarrow Os^{186*}$ decay and prompt events due to scattering from one to the other detector. Prompt events from scattering are, of course, greatly reduced in number when the delayed coincidence scintillation spectrometer is used.

Delayed coincidence resolution curves $F(T, \lambda)$ were computed graphically using, for $P(T)$, curve (2) of Fig. 1 and values of λ equal to or near that obtained in the usual way from the slope of curve (1) at a large positive value of T. The prompt curve $P(T)$ represents the response of the apparatus to simultaneous emission of radiation of the same energy that gave curve (1). The computed curves $F(T, \lambda)$ for $T_\frac{1}{2} = (9.0, 8.0, \text{and } 7.0) \times 10^{-10}$ are shown in Fig. 2 and have been normalized to the experimental delayed coincidence resolution curve at $T = 6 \times 10^{-9}$ sec. The agreement between the computed curve for $T_\frac{1}{2} = 8.0 \times 10^{-10}$ sec, and the experimental data is good. The difference between the two curves for $T < 5 \times 10^{-9}$ sec yields a resolution curve of prompt events not related to the $Re^{186} \rightarrow Os^{186*}$ decay; the shape of the resulting residual curve agrees with the experimental resolution curve for prompt events of Fig. 1. It appears that the initial state of the 137-kev γ-ray transition from Os^{186} is metastable with a half-life of 8.0×10^{-10} sec.

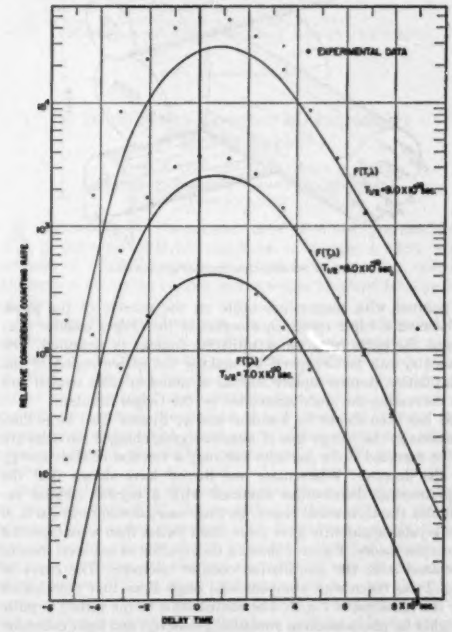

FIG. 2. Comparison of computed delayed coincidence resolution curves $F(T, \lambda)$ for $T_\frac{1}{2} = 9.0$, 8.0, and 7.0×10^{-10} sec with experimental data obtained with a Re^{186} source. The computed curves $F(T, \lambda)$ are normalized to the experimental data at $T = 6 \times 10^{-9}$ sec.

The energy and half-life of this isomeric state suggests that the transition corresponds to forbiddenness $l = 2$. Recently, a few relativistic calculations without screening for L_I shell internal conversion[3] have been completed for $Z = 92$, 84, and 49 for electric and magnetic dipole and electric quadrupole radiation. For a γ-ray energy of 137 kev and $Z = 84$, the computed ratios[4] (N_K/N_{L_I}) for electric dipole, electric quadrupole, and magnetic dipole radiation are 8.5, 2.0, and 19, respectively. Since Metzger and Hill measured $N_K/N_L = 0.6$ for the 137-kev transition in $_{76}Os^{186}$, it appears that electric quadrupole radiation occurs.

* This document is based on work performed for the AEC at Oak Ridge National Laboratory.

[1] T. D. Newton, Phys. Rev. **78**, 490 (1950).

[2] F. R. Metzger and R. D. Hill, Phys. Rev. **81**, 300(A) (1951).

[3] Gellman, Griffith, and Stanley, Phys. Rev. **80**, 866 (1950). Table of L_I shell internal conversion coefficients privately circulated. Computations performed at the Computation Centre, McLennan Laboratory, University of Toronto.

[4] Rose, Goertzel, Spinrad, Harr, and Strong, Phys. Rev. **76**, 1883 (1949). Table of K shell internal conversion coefficients privately circulated.

On the Spin and Magnetic Moment of O^{17}

F. ALDER* AND F. C. YU
Department of Physics, Stanford University,† Stanford, California
January 17, 1951

NUCLEAR induction signals of O^{17} have been observed from H_2O and D_2O and also from some other liquids (methanol, ethanol, and acetic acid) containing oxygen, using the spectrometer described by Proctor.[1] The resonance occurs at a frequency of 5.8 Mc in an external magnetic field of 10,000 gauss. That this resonance originated from O^{17} was confirmed by observing it also in water in which the abundance of O^{17} was enriched from its natural value of 0.037 percent to 0.185 ± 0.006 percent, and by noticing that the signal amplitude observed under the same conditions was increased over that in natural water in proportion to the above abundances.

The ratio of the resonance frequency of O^{17} from H_2O to the resonance frequency of D^2 from D_2O was determined to be

$$\nu(O^{17})/\nu(D^2) = 0.88313 \pm 0.00004. \quad (1)$$

The sign of the magnetic moment of O^{17} was observed to be opposite to that of D^2, i.e. to be negative. A shift of about 1/4000 towards higher frequency was found for the O^{17} resonance from acetic acid.

Although the gyromagnetic ratio of O^{17} is about seven times smaller, it was observed that the thermal relaxation time of O^{17} in pure water is about one-hundred times shorter than that of protons. This short thermal relaxation time can hardly be accounted for by the dipole-dipole interaction. As in other liquids containing nuclei with a finite quadrupole moment, it suggests that the relaxation is due to the interaction with the molecular electric fields and, therefore, that the spin of O^{17} is larger than $\frac{1}{2}$.

According to Bloch's phenomenological theory[2] of nuclear induction, the spin of O^{17} can be determined by comparing its signal amplitude and width with the signal amplitude and width of deuterium whose spin is known, provided that the experimental conditions are so adjusted to achieve the slow passage conditions. If the absorption mode is observed and the amplitude of the sweep field is small compared to the line width of the signal, the signal amplitude recorded by the dc milliammeter will be proportional to

$$nI(I+1)H_0H_1T_2^2\gamma^4\omega_0^2/(1+\gamma^2T_1T_2H_1^2)^\frac{1}{2}, \quad (2)$$

where n is the number of nuclei per unit volume of the sample, I the

spin value, γ the gyromagnetic ratio, ω_0 the resonance frequency, H_s the amplitude of the sweep field, H_1 the half-amplitude of the rf exciting field, and T_1 and T_2 the longitudinal and transversal relaxation times, respectively. Based on the expression (2), the spin determination for O^{17} was carried out with samples of natural water and of O^{17}-enriched water in solutions of either 0.0002-molar concentration of $MnSO_4$ or 0.025-molar concentration of $Fe(NO_3)_3$. A sample of 1.5 percent D_2O in 3-molar concentration of $MnSO_4$ was used for the comparison. In all experiments H_s was chosen as 0.085 gauss and was considerably smaller than the line widths of O^{17} and D^2 signals (about 0.4 gauss) which were mostly due to the field inhomogeneity of the magnet. The dependence of the signal amplitudes of O^{17} and D^2 on the rf field H_1 was found to fit the theoretical expression (2) very well and was used to determine the value T_1T_2. The value of T_2 was given by the measured line width of the signal. Three independent measurements with different samples in different magnetic fields yielded the value 2.44 ± 0.25 for the spin of O^{17}. Considering that the nearest other possible spin values 3/2 and 7/2 are well outside the experimental value, this result indicates that the spin of O^{17} is

$$I(O^{17})=2.5=5/2. \tag{3}$$

In deriving this result it has evidently been assumed that the signal amplitude is, under otherwise identical conditions, proportional to the expression (2). Although there are certainly cases (for example, in the presence of a line structure) where the underlying simplified theory would not hold, it seems experimentally well supported in this case both by the observed line shapes and by the fact that the observed dependence on H_1 of the signal amplitude is in very good agreement with (2).

Because of the large field inhomogeneity over the sample region (about 0.3 gauss) the signals were sufficiently broad for both O^{17} and D^2. In the case of O^{17} the ratio of T_1/T_2 was about 7 for the samples used for the spin determination. It was observed further that the addition of paramagnetic ions does not much affect the thermal relaxation time T_1 of O^{17} nuclei, but that it broadens the line considerably. A 0.001-molar concentration of $MnSO_4$ would give a line width of about 1 gauss for O^{17}, but did not give an appreciable effect on D^2. A further investigation of this abnormal relaxation mechanism of O^{17} in the presence of paramagnetic ions is in progress.

Using the frequency ratio (1), the spin value (3), and the observed negative sign, the value

$$\mu(O^{17})=-1.8928\pm0.00019 \text{ nm} \tag{4}$$

was obtained for the magnetic moment of O^{17}. In deriving the value (4) we have further used the value 2.79245 ± 0.00020 nm for the proton moment recently determined by Bloch and Jeffries[5] and the ratio of the deuteron moment to the proton moment obtained by Levinthal.[4]

The spin value 5/2 with the negative moment approximately equal to the neutron moment assigns a $d_{5/2}$ orbit to the odd neutron of O^{17} as one would expect from the shell model proposed by Mayer[6] and Haxel, Jensen, and Suess.[6] This assignment disagrees with that of Feenberg and Hammack[7] who predicted an $s_{1/2}$ orbit for the ground state of O^{17}.

The authors would like to thank Professor F. Bloch for his valuable comments and constant encouragement throughout this work. Thanks are also due to Mr. Russell Ball at the Radiation Laboratory in Berkeley, California for the loan of the water enriched in O^{17} and to Dr. D. P. Stevenson at the Shell Development Company in Emeryville, California for the mass spectrometric analyses of the abundance of O^{17} in the enriched water.

* Brown Boveri Company Fellow at the University of Basel, Switzerland.
† Assisted by the joint program of the AEC and ONR.

[3] W. G. Proctor, Phys. Rev. 79, 35 (1950).
[5] F. Bloch, Phys. Rev. 70, 460 (1950).
[5] F. Bloch and C. D. Jeffries, Phys. Rev. 80, 305 (1950).
[4] E. C. Levinthal, Phys. Rev. 78, 204 (1950).
[6] M. G. Mayer, Phys. Rev. 78, 16 (1950).
[6] Haxel, Jensen, and Suess, Z. Physik. 128, 295 (1950).
[7] E. Feenberg and K. C. Hammack, Phys. Rev. 75, 1877 (1949).

Scintillation Counting of Cosmic-Ray Particles*

E. P. Ney and D. M. Thon
University of Minnesota, Minneapolis, Minnesota
January 22, 1951

SCINTILLATION counters have the property of producing pulses of amplitude proportional to the energy lost in the scintillator. In order to use scintillators to study the primary heavy nuclei in cosmic rays, we have investigated several experimental arrangements. When a scintillation counter is used as one of the counters in a telescope, the distribution of pulse amplitudes is broadened by the following factors: (a) The statistical fluctuation in energy loss; (*b*) the variation in light collection in the counter; (*c*) the variation in path length through the counter; and (*d*) the statistics of the photo-electrons in the multiplier.

The effect of photo-electron statistics can usually be made very small by good light collection and by the use of a good scintillator. We have found that pyrene dissolved in xylene is a very satisfactory scintillation material. This solution gives pulses with a 5819 multiplier which are about half the size of those from terphenyl in xylene. The fluorescent light from pyrene is light green, however, and suffers negligible absorption in the xylene or in impurities in the xylene. The maximum light output is obtained at a pyrene concentration of 8 g/liter of xylene.

The geometrical arrangement of the scintillation counter is shown in Fig. 1. The multiplier looks into the glass "T" tube which

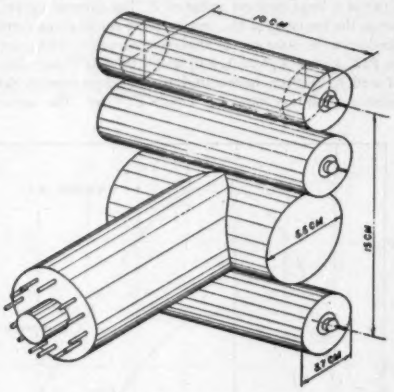

FIG. 1. Scintillation counter geometry.

is painted with magnesium oxide on the outside of the glass. Whenever a triple coincidence occurs in the Geiger counter telescope, the pulse from the scintillation counter is measured. The geometry can be improved by making the active region of the scintillation counter square instead of round in cross section and by decreasing the angle subtended by the Geiger counters.

It has been shown by Landau[1] and by Symon[2] that large fluctuations in the energy loss of monoenergetic charged particles are to be expected if the particles lose only a fraction of their energy in the detector. Whittemore and Street[3] have shown that the experimental distribution obtained with a crystal counter resembles the theoretical curve. In their case, nonuniform parts of the crystal apparently gave more small pulses than were expected from the theory. Figure 2 shows a distribution of sea-level mesons obtained with the scintillation counter telescope. The curve of Fig. 2 was taken with a smaller solid angle than that represented by the telescope of Fig. 1. The contribution to the spread in pulse heights by photo-electron statistics, geometry, and light collection was less than 8 percent. The average energy loss in Fig. 2 corresponds to 9 Mev. The shape and half-width of the distribution agree quite well with the theoretical calculation. Professor Charles

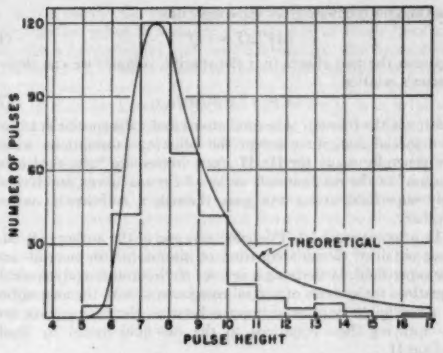

FIG. 2. Theoretical (smooth curve) and experimental pulse distributions.

Critchfield has pointed out to us that because the large pulses come from high energy δ-rays, all of which would not stop in the liquid, the experimental curve should drop off faster on the high energy side than the theoretical curve. The statistics of the data are not good enough to decide this point.

Two types of end-window photo-multipliers are suitable for use in this type of counter; the English Electrical and Musical Industries VX5031 and the R.C.A. 5819. The E.M.I. tube which we used was preferred, because its signal to noise ratio was about 10 times better than that of any of the 5819 tubes which we tried.

We are indebted to Professor Walter Lauer for supplying us with pure pyrene.

* Assisted by the joint program of the ONR and AEC.
[1] L. Landau, J. Phys. U.S.S.R. **8**, 201 (1944).
[2] K. Symon, Ph.D. thesis, Harvard University (1948).
[3] W. L. Whittemore and J. C. Street, Phys. Rev. **76**, 1786 (1949).

A Scintillation Counter Measurement of Heavy Nuclei*

E. P. NEY AND D. M. TRON
University of Minnesota, Minneapolis, Minnesota
January 22, 1951

A SCINTILLATION counter telescope of the type described in the previous letter[1] was flown on October 4, 1950, to an altitude of 105,000 ft on a "Skyhook" balloon. The residual atmosphere above the balloon was less than 10 g/cm² for a period of 5 hr.

The scintillation pulses from the counter were displayed on oscilloscopes in the balloon gondola whenever a coincidence count occurred in the Geiger telescope. Pulse amplitudes over a range of 200 to 1 could be recorded. The oscilloscopes on which the pulses were displayed were photographed continuously, and at one-minute intervals the reading of a Wallace and Tiernan low pressure barometer and a "total count" recorder were also photographed. During the flight approximately 30,000 pulses were recorded.

Because of the stage of development of the scintillation counter at the time of the flight, the resolution of the equipment did not approach the Landau statistical limit. It was not possible, therefore, to resolve adjacent atomic numbers in this flight because of the poor resolution and the fact that at 55°N latitude the cut-off energy imposed by the earth's magnetic field is so low that slow particles of low atomic number can suffer a greater energy loss in the scintillation counter than relativistic particles of higher atomic number.

The energy loss in the scintillation counter is proportional to Z^2/V^2, where Z is the atomic number and V is the particle velocity.

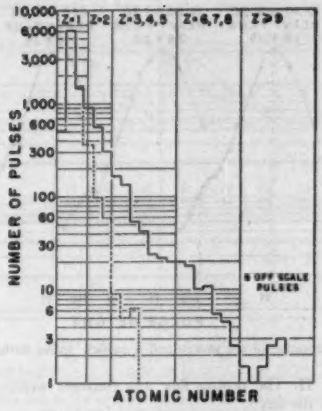

FIG. 1. Atomic number histogram.

A differential pulse amplitude distribution would, therefore, have a scale of abscissas proportional to Z^2. We have changed the scale in Fig. 1 so that we obtain a frequency distribution of pulses as a function of atomic number. The dotted curve in Fig. 1 gives the distribution obtained during the ascent from 500 g/cm² to 100 g/cm². The difference between the curves shows clearly the contribution of multiply charged primaries at the top of the atmosphere. Since one knows the shape of the curve corresponding to singly charged particles, it is possible by successive subtraction to estimate the number of pulses in each interval of atomic number. These results are shown in Table I. The actual number of pulses is included to show the magnitude of the statistical errors.

TABLE I. Measured abundancies of nuclei.

Element	Number of pulses	Flux (particles/cm²-sec-steradian)
H	8740	1.9×10^{-1}
He	1257	2.8×10^{-2}
Li, Be, and B+Stars	387	8.4×10^{-3}
C, N, O+Stars	76	1.6×10^{-3}
$Z\geq9$+Stars	20	4.3×10^{-4}

The total flux of 0.23 parts/cm²-sec-steradian is in reasonable agreement with the results of Winckler and Stroud.[2] The hydrogen-helium ratio of 7 is higher than that previously reported.[3-5] The last three groups in the table must include pulses arising from stars produced by primary protons in the scintillator. Emulsion work leads one to believe that most of these stars would give pulses in the region of the lithium, beryllium, boron group. The energy of such a star would be about 150 Mev. If we assume that all the pulses in the lithium, beryllium, boron region are due to stars, we can calculate the product of $\eta\sigma$, where η is the efficiency of the counter telescope for triggering on a star produced in the scintillator, and σ is the cross section for star production by primary protons. On this assumption, if η is 1, then σ would be half geometric cross section. The abundance of carbon, nitrogen, and oxygen and of $Z\geqq9$ agrees well with the values obtained in photographic plates.[2,4,5] This leads us to believe that stars do not contribute appreciably in this region of pulses.

During the period of the flight there was a variation with time in the frequency of large pulses. This variation seems statistically significant and appears to be further evidence for a change in the flux of heavy nuclei either as a diurnal effect or because of solar activity. At the same time that the heavy nuclei increased, the pulse distribution in the proton—α-particle region indicated the presence of more α-particles. These results are indicated in Fig. 2

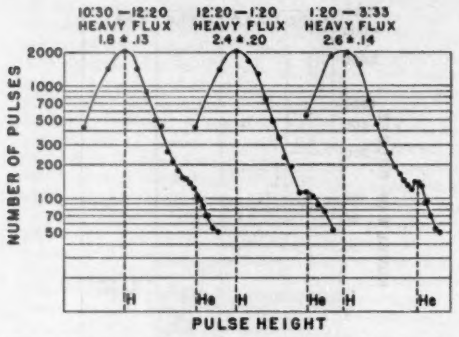

FIG. 2. Distribution of the proton and α-particle pulses during the day.

and Table II. The proton flux was constant within statistics throughout the day.

Further experiments are now in progress with high resolution equipment which will be flown at a latitude of 30° N.

TABLE II. Frequencies of pulses vs time.

Time	Frequency of pulses of magnitude greater than 16 times the average proton pulse (pulses/min)	Frequency of proton pulses (pulses/min)
10:30 to 12:20 A.M.	1.8 ± 0.13	78 ± 0.8
12:20 to 1:20 P.M.	2.4 ± 0.2	76.5 ± 1.4
1:20 to 3:30 P.M.	2.6 ± 0.14	79 ± 0.8

We wish to express our appreciation to Mr. C. B. Moore and Mr. W. Huch of the General Mills Aeronautical Laboratory for their cooperation and assistance.

* Assisted by the joint program of the ONR and AEC.

[1] E. P. Ney and D. M. Thon, Phys. Rev. **81**, 1068 (1951).
[2] J. R. Winckler and W. G. Stroud, Phys. Rev. **76**, 1012 (1949).
[3] Freier, Lofgren, Ney, and Oppenheimer, Phys. Rev. **74**, 1818 (1948).
[4] M. A. Pomerantz and F. L. Hereford, Phys. Rev. **76**, 997 (1949).
[5] H. Bradt and B. Peters, Phys. Rev. **77**, 54 (1950).
[6] P. Freier, Ph.D. thesis, University of Minnesota (1949).

Non-Equilibrium Thermodynamics of Two-Fluid Models

S. R. DE GROOT, L. JANSEN, AND P. MAZUR
Institute for Theoretical Physics, The University, Utrecht, The Netherlands
January 15, 1951

TWO-FLUID models have been proposed for the explanation of the properties of liquid helium II and for superconducting metals.[1] In both cases the existence of two kinds of particles has been assumed: in liquid helium II *normal* (n) and *superfluid* (s) atoms, and in superconducting metals *normal* (n) and *superconductive* (s) electrons. It is supposed that the "chemical reaction" $n \rightleftarrows s$ is possible. In these systems occur further the phenomena of heat conduction, diffusion of electrical conduction, and various cross-effects.

The thermodynamics of irreversible processes, based on the Onsager reciprocal relations,[2] can be used to treat these models mentioned above by means of the general methods, including the entropy balance equation, the phenomenological relations, and the theory of stationary states.[3]

Among the results for helium[4] we note a connection between the fountain effect and the mechano-caloric effect. The fountain effect is the pressure difference, ΔP, which arises in the stationary state when a fixed temperature difference, ΔT, exists between two reservoirs, containing liquid He II, which are connected by a capillary. The mechano-caloric effect is the heat, Q transferred by the unit of mass from one reservoir to the other in the state of fixed ΔP and $\Delta T=0$ (uniform temperature). An application of the Onsager relations gives the connection

$$v\Delta P/\Delta T=-Q^*/T. \tag{1}$$

Between the two effects (v is the specific volume) we can derive Gorter's relation

$$Q^*=-Tx(\partial s/\partial x)_{P,T}, \tag{2}$$

(with x is the fraction of normal atoms and s the specific entropy) as a special case, if we accept the following assumptions, which are generally made for He II: first, immediate "chemical equilibrium" of the reaction $n \rightleftarrows s$ under all circumstances, and second, only superfluid atoms can pass through a sufficiently narrow capillary.

In a recent work,[5] I. Prigogine and one of the authors (P. M.) have obtained Gorter's equation of motion for the normal- and the super-fluid, by deriving a new set of "hydrothermodynamical" equations for systems of several components, with the assumption of a negligible transfer of impulse between the components, and by applying these equations to the two-fluid model by liquid helium II.

For superconductive metals, work is still in progress, but it already can be said that new terms arise in the expression for heat conductivity and probably also in the expression for the thermoelectric homogeneous effect, as compared with the results for ordinary metals.

[1] See e.g., for helium, C. J. Gorter *et al.*, Physica **15**, 285 and 523 (1949); **16**, 113 (1950); for superconductivity, C. J. Gorter and H. B. G. Casimir, Physica **1**, 305 (1934).
[2] L. Onsager, Phys. Rev. **37**, 405 (1931); **38**, 2265 (1931). H. B. G. Casimir, Revs. Modern Phys. **17**, 343 (1945).
[3] S. R. de Groot, *Thermodynamics of Irreversible Processes* (Interscience Publishers, New York, 1951).
[4] de Groot, Jansen, and Mazur, Physica **16**, 421 and 691 (1950).
[5] I. Prigogine and P. Mazur, Physica (to be published).

Field Variation of Superconducting Penetration Depth

J. BARDEEN
Bell Telephone Laboratories, Murray Hill, New Jersey
January 15, 1951

IN a recent article of the same title, Pippard[1] has shown that there is only a small dependence of penetration depth, λ, on the applied magnetic field. Pippard's observations are based on changes of the reactive component of the skin impedance of superconducting tin at 3.2 cm with applied field. The over-all change in λ is no more than 3 percent at the critical field strength. From an application of the Gorter-Casimir two fluid theory, he estimates the size of the regions over which order must exist.

Pippard's argument is briefly as follows. With an increase in applied field, one might expect a decrease in concentration of superconducting electrons near the surface so as to increase the penetration depth and decrease the magnetic energy. The fact that this occurs only to a small degree indicates that the size of the regions over which order exists and which must be considered as a unit in the transition must be at least as large as 10^{-4} cm. The very sharp resistance transition in pure tin is given as further evidence of an order existing over regions of this size. This result appeared to be difficult to reconcile with observations on thin films[2,3] and on colloidal mercury[4] that there is very little change in transition temperature with dimensions, even when the film thickness or particle size is as small as 5×10^{-6} cm; i.e., less than the penetration depth.

These apparently contradictory results both follow from the lattice-vibration theory[5] of superconductivity and may be taken as evidence that the general approach, which is the one anticipated by London, is along the correct lines. London[6] had previously shown that the phenomenological equations follow if it is assumed that the wave functions of the electrons are not changed very much by the magnetic field. The fact that the penetration depth is independent of field is good evidence that the wave functions are not altered; for if they were, one would expect the penetration to change.

In our theory, the wave functions, Ψ_k, of the superconducting electrons are taken to be linear combinations of Bloch functions, ψ_k, which have energies near the Fermi surface. One consequence of a very small effective mass of the superconducting electrons is that the wave functions are not altered very much by an applied field, so that the London equations follow. We wish to point out here as a second consequence that the wave functions must extend over distances of at least 10^{-4} cm, in accord with Pippard's results. A small effective mass corresponds to the fact that it takes considerable energy to confine the wave function to a small region, as would be required to change the concentration near the surface. A localized superconducting electron can be described by a wave function of the form $U(x)\Psi_k(x)$, where $U(x)$ represents the envelope and Ψ_k extends through the crystal with uniform amplitude. The effective mass can be used to estimate the energy change which comes from the variation of $U(x)$. To confine the wave function to a distance $\pi/\Delta k$ requires an energy of the order of

$$\Delta E = \hbar^2(\Delta k)^2/2m_s,$$

where m_s is the effective mass. We have shown that $m_s \sim 10^{-4}$ m, so that $\Delta E \sim 5\times10^{-16}$ erg for $\Delta k \sim 10^4$ cm^{-1}. This corresponds to thermal energy for a few degrees absolute and is the order of the magnetic energy, $H_c^2/8\pi$, per superconducting electron.

In case the size of the wave function is limited by the dimensions of the crystal, as it is in thin films and in colloidal particles, one can take $U(x)$=constant. The Bloch functions of the normal metal from which the linear combinations are formed are localized and satisfy the boundary conditions at the surface. No additional energy is required to localize the electrons in the superconducting state. As the dimensions are made smaller there are fewer terms in the sum over the Bloch states. One would not expect much change in transition temperature as long as the number of terms is sufficient to give a good approximation to the integral obtained as a limit for large volumes.

There is some question concerning the wavelengths of the vibrational waves which interact most strongly with the electrons. The low energies involved in the transition suggest that perhaps long wavelengths are most important. The fact that there is little change in T_c for dimensions of 5×10^{-4} cm shows that the important wavelengths are no more than, say, one-tenth of this, or less than 5×10^{-7} cm. If *all* wavelengths are involved, there are around 10 terms in the sum for a volume of 10^{-18} cm^3, so that one might, in any case, expect changes in T_c for dimensions of $\sim10^{-6}$ cm or less.[7] A measurement of the way in which T_c changes with film thickness or particle sizes hould provide information about the important vibrational wavelengths.

The application of the effective mass concept to the calculation of the surface energy between normal and superconducting phases will be given in a subsequent communication.

[1] A. B. Pippard, Proc. Roy. Soc. (London) **A203**, 210 (1950).
[2] A. I. Shalkinov, Nature **142**, 74 (1938).
[3] E. T. S. Appleyard and A. D. Misener, Nature **142**, 474 (1938); Appleyard, Bristow, and Misener, Proc. Roy. Soc. (London) **A172**, 540 (1939).
[4] D. Shoenberg, Proc. Roy. Soc. (London) **A175**, 49 (1940).
[5] J. Bardeen, Phys. Rev. **79**, 167 (1950); **80**, 567 (1950); **81**, 469 (1951). H. Fröhlich, Phys. Rev. **79**, 845 (1950) has developed a theory along somewhat similar lines.
[6] F. London, Proc. Roy. Soc. (London) **A152**, 24 (1935); Phys. Rev. **74**, 562 (1948).
[7] J. Bardeen, Phys. Rev. **79**, 167 (1950). The estimate given there of $\sim10^{-6}$ cm for the size of the wave function is incorrect, because no account was taken of the increase in the number of interactions with increase in volume.

Magic Numbers and the Missing Elements Technetium and Promethium

HANS E. SUESS
Institute for Nuclear Studies, University of Chicago, Chicago, Illinois
January 15, 1951

IN order to find an explanation for the absence of β-stable isotopes of the elements Tc and Pm,[1-9] a more general abnormality in the region following the closing of the 50- and 82-neutron shell should be taken into consideration. This abnormality can be recognized from the differences of the binding energies of pairs of isobars as found from β-decay schemes. These show that

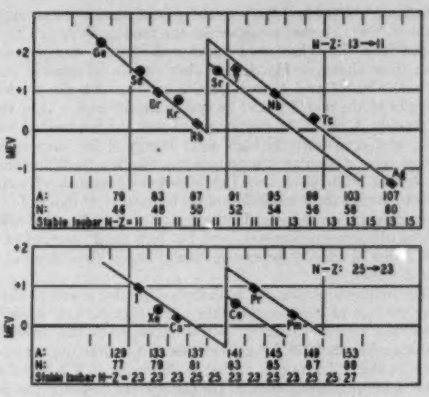

FIG. 1. Differences in the binding energies of the ground states of isobars as derived from beta-decay schemes.

in these regions the binding energies of the even Z, odd N nuclei (in their ground states) do not lie on the same energy surface as those of the odd Z, even N nuclei.

To illustrate this, the β-decay energies for nuclei with a given isotopic number $I=N-Z$ may be plotted *versus* $A=N+Z$. Figure 1 shows such plots for $I=13$ and $I=23$ as examples. Following the general rule of the equivalence of odd N and odd Z nuclei with respect to their binding energies, both kinds of odd mass numbered nuclei with $N<50$ or 82 lie close to a common line intersecting the zero line of decay energy at a point where the isobar stability changes to the next higher value of I. After the filling of the 50- and 82-neutron shell, an upward shift in the β^- decay energies occurs equivalent to the drop in the binding energy of the last neutron. This shift is somewhat larger, however, for the odd Z than for the odd N nuclei, indicating that the drop is not equal for paired and for unpaired neutrons. The general trend in this region can be represented by two different lines: the lower one representing the trend in the decay energies of the odd N, the higher one that of the odd Z nuclei. Thus, for a given I, the isobars with odd numbers of neutrons become stable at a lower mass number than those with an odd number of protons. This difference is large enough to cause the β-instability of all nuclei with a certain odd number of protons, incidentally those of $Z=43$ and 61.

In Fig. 1 the value for Zr^{88} is omitted, because it seems uncertain whether the low decay energy as reported by Steinberg and

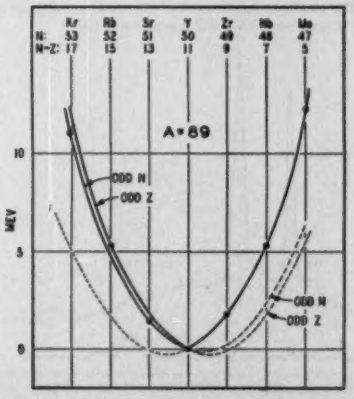

FIG. 2. Energy parabolas for mass number 89, illustrating the proposed split in the energy surface for odd N and odd Z nuclei in the region $N>50$.

Glendenin[4] (0.06 Mev) leads to the ground state or to an excited state of Nb[93]. Further evidence for the proposed rule can be obtained from the behavior of nuclei with isotopic numbers other than those shown in Fig. 1. One finds that in all cases of nuclei with $N>50>Z$ and N somewhat larger than 82, the β^- decay energies of the odd Z nuclei lie systematically higher than those of the odd N nuclei. It may be noted that the unexpected instability and comparatively high decay energy of In^{115} fit well into this picture. A similar, but presumably smaller, "split" seems to occur at $N>126$, though the lack of β-decay data makes it impossible to predict the β-instability of the isotopes of At (85) or Fr (87) from β-decay systematics. In the region of $N>28$ and $Z<40$ a similar abnormality seems to hold, but here the β^- energies of the odd N nuclei seem to be systematically higher than those of the odd Z nuclei.

The proposed picture can be described in other words by saying that the line of maximum stability (the Gamow line) is shifted towards a region of smaller neutron excess when the number of neutrons exceeds 50 or 82 but that this shift is larger for the odd Z than for the odd N nuclei, so that in the region of $N>50>Z$ and for N somewhat larger than 82 the Gamow line is split in two lines referring to odd Z and odd N nuclei, respectively (Fig. 2).

The numerical values for the lowering of the binding energies of the last neutron at $N=50$ and 82 as derived from Fig. 1 are as follows (in Mev):

N:	50	82
paired neutron:	2.4	2.0
unpaired neutron:	1.8	1.3.

These figures are in good agreement with the first estimate made by Mayer[2] of about 2 Mev for all cases.

There are several possible ways of explaining these abnormalities, but it seems premature to the writer to give any one of them final preference. Thanks are due to Maria Mayer for extensive discussions of these possibilities.

[1] H. Jensen, Naturwissenschaften **26**, 381 (1938).
[2] M. G. Mayer, Phys. Rev. **74**, 235 (1948).
[3] L. Kowarski, Phys. Rev. **78**, 477 (1950).
[4] E. R. Steinberg and L. E. Glendenin, Phys. Rev. **78**, 624 (1950).

On the Radioactivity of Hf^{181} and Hf^{175}

ARNE HEDGRAN AND SIGVARD THULIN
Nobel Institute of Physics, Stockholm, Sweden
January 15, 1951

SINCE the interpretation of the measurements on n-irradiated Hf has been shown to be complicated because of the presence of different activities,[1,2] we have separated electromagnetically the Hf isotopes of a pile-irradiated sample. Besides the known activity of Hf^{181} there was also one corresponding to mass number 175, amounting to about 2.5 percent of the total activity as measured by a G-M counter with a 2.2 mg/cm² window.

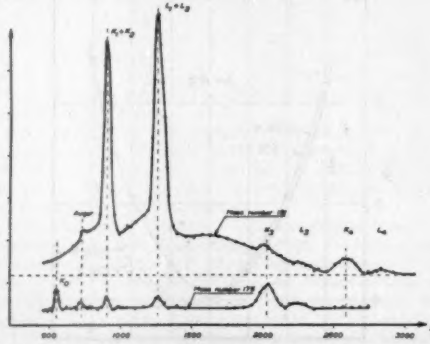

FIG. 1. β-spectra of the separated mass numbers 181 and 175 isotopes. The intensities are not drawn to the same scale.

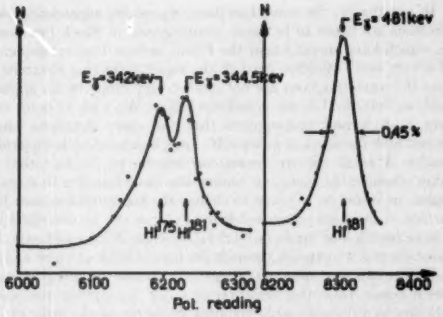

FIG. 2. The high energy photo-lines of unseparated Hf.

The separated isotopes, collected on 2.5 mg Al/cm², were used as samples for β-spectrometer investigations, the results of which are shown in Fig. 1. The letters K_1, $K_2\cdots L_1$, $L_2\cdots$ indicate the K and L conversion lines of the well-known γ-rays of energies 132, 135, 345, and 481 kev, respectively. Because of the presence of small amounts of the strong mass 181 activity in mass 175 source this spectrum also contains the two intense lines of Hf^{181}, but this will not affect the interpretation of the measurements.

The activity of mass number 175 is no doubt due to Hf^{175} which decays by K-capture to Lu^{175}, having two K conversion lines of energies 26 and 279 kev. A comparison of the two β-spectra shows that there must be two different γ-lines of about 345 kev, one in each isotope. Thus our measurements confirm the results of Cork *et al.*[1]

In order to resolve the two 345-kev γ-rays in an unseparated sample, it was investigated in a high resolution β-spectrometer. Figure 2 shows on the left the photo-electron lines from a 0.7 mg/cm³ uranium converter. The energies of the corresponding γ-rays are 342.2 and 344.9 kev, and they are of almost the same intensity.[3] On the right of Fig. 2 the high energy photo-line is shown for comparison.

Since only about half of the 345-kev radiation belongs to Ta^{181}, it would appear that the intensity of the 135-kev radiation was too high to be accounted for by the term scheme and the intensity data given by Chu and Wiedenbeck.[4] Therefore, some measurements were made to determine the intensity ratios in the decay.

From the β-spectrum in Fig. 1. we find $(NK_1+NK_2)/N_\beta=0.32$ and $(NL_1+NL_2+N_M)/N_\beta=0.36$. These values are considerably less than those given in reference 4.

From a measurement in the high resolution β-spectrometer we find $NK_1:NK_2=2:1$, and $NK_2:NL_2\approx 8:1$. From the secondary electron spectrum (Fig. 2) we estimate, taking account of the variation of the photo cross section, the intensity ratio $\gamma_{345}:\gamma_{481}\approx 1:8$.

Measurements of the photo-electron lines in gold of the unconverted 132- and 135-kev radiations indicate an intensity ratio of roughly 5:1. From this we conclude that the 135-kev ray is very highly converted, with almost all of the conversion taking place in the K shell. This means that the intensity of this radiation is much lower than one would expect from previous β-spectrometric investigations. We estimate it to be about 20 percent of the intensity of the 132-kev radiation. Although our determination of the intensity of the 345-kev radiation belonging to the decay of Hf^{181} ($\approx$12 percent of the 481-kev radiation) is still somewhat lower than this, we cannot place any significance on this difference because of the uncertainty of some of our intensity comparisons, and we conclude that in spite of the complexity shown in the activity of n-irradiated Hf the term scheme given originally by Chu and Wiedenbeck is probably correct.

[1] Cork, Stoddard, Rutledge, Branyan, and Le Blanc, Phys. Rev. **78**, 299 (1950).
[2] M. Deutsch and A. Hedgran, Phys. Rev. **79**, 400 (1950).
[3] All measurements were made at the same time, about one month after an irradiation of 4 weeks duration in the Harwell pile.
[4] K. Chu and M. Wiedenbeck, Phys. Rev. **75**, 226 (1949).